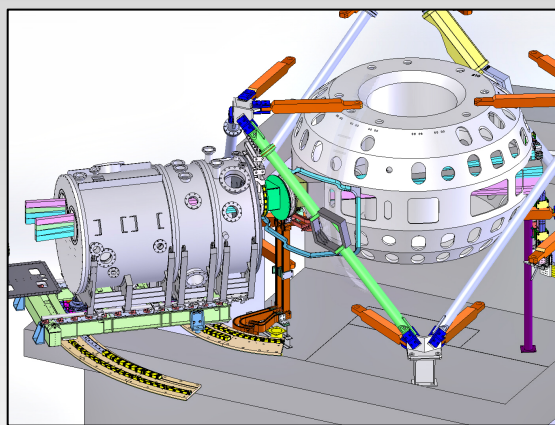
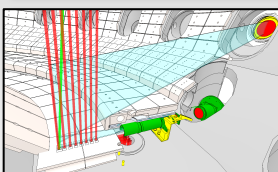
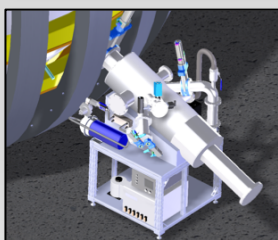
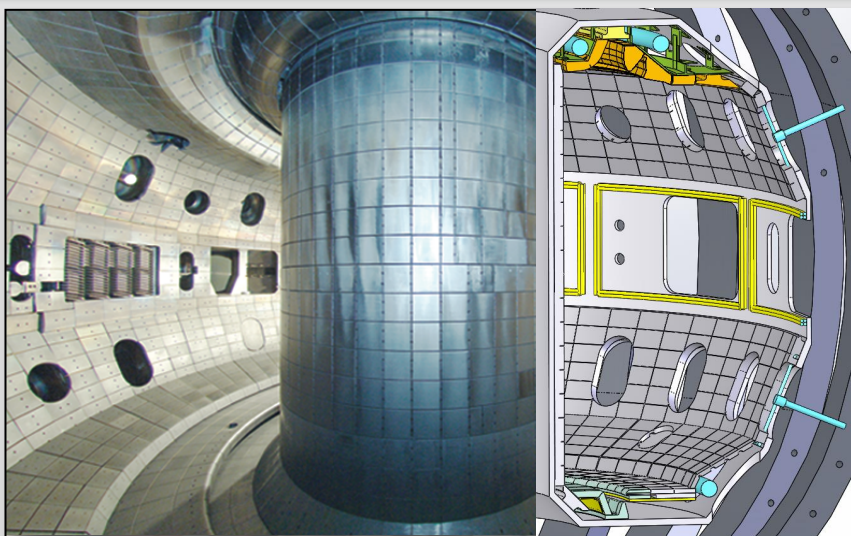
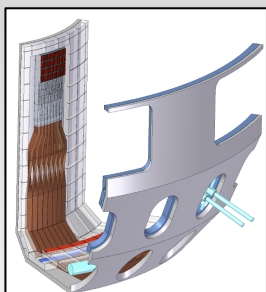
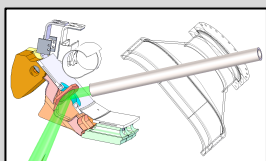
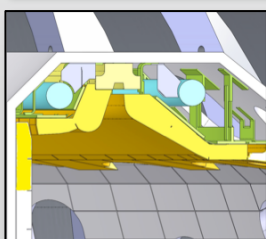


# THE DIII-D NATIONAL FUSION PROGRAM FIVE-YEAR PLAN 2019-2024



January 2018



## TABLE OF CONTENTS

<b>1.</b>	<b>PROGRAM MISSION, STRATEGY, UPGRADES AND IMPACT.....</b>	<b>1-1</b>
1.1	Overview and Background .....	1-1
1.2	Mission and Strategy.....	1-3
1.3	Accomplishments of the DIII-D Program in the 2014-2018 Period.....	1-8
1.4	DIII-D Research Plan Addressing the Needs of Fusion Energy.....	1-13
1.5	DIII-D Facility Capabilities and Proposed Improvements .....	1-21
1.6	DIII-D Facility Operations.....	1-25
1.7	DIII-D Team .....	1-26
1.8	National and International Leadership.....	1-28
1.9	Benefits and Impact of Research .....	1-28
<b>2.</b>	<b>SCIENTIFIC BASIS FOR A BURNING PLASMA CORE .....</b>	<b>2-1</b>
2.1	Robust Plasma Scenarios for Future Reactors .....	2-6
2.1.1	Inductive Scenarios and Basis for $Q=10$ in ITER.....	2-11
2.1.2	Fully Non-inductive Scenarios for Steady-State Fusion.....	2-23
2.2	Disruption Control .....	2-38
2.2.1	Safely Quenching the Fusion Plasma (Disruption Mitigation).....	2-40
2.2.2	Core Stability Control for Disruption-Free Operation.....	2-53
2.2.3	Plasma Control.....	2-64
2.3	Burning Plasma Physics.....	2-75
2.3.1	Turbulence and Transport .....	2-78
2.3.2	Rotation Generation and Momentum Transport .....	2-92
2.3.3	Energetic Particles .....	2-105
2.3.4	Heating and Current-Drive Physics .....	2-117
<b>3.</b>	<b>SCIENTIFIC BASIS FOR A FUSION BOUNDARY SOLUTION .....</b>	<b>3-1</b>
3.1	Divertor Development and Integration .....	3-5
3.1.1	Divertor Closure.....	3-7
3.1.2	Magnetic Configuration .....	3-16
3.2	Model Validation for Boundary Plasma Solutions .....	3-27
3.2.1	Divertor Dissipation.....	3-30
3.2.2	SOL and Divertor Particle Transport .....	3-39
3.2.3	SOL and Divertor Radial Transport.....	3-50
3.3	Advanced Materials Evaluation.....	3-57
3.3.1	Understanding Material Migration and Mitigation.....	3-60
3.3.2	Surface Evolution Science .....	3-71
3.3.3	Evaluation of Reactor-Relevant Materials.....	3-80
<b>4.</b>	<b>PHYSICS OF INTEGRATION OF CORE AND BOUNDARY SOLUTIONS.....</b>	<b>4-1</b>
4.1	Pedestal and ELMS.....	4-4

4.1.1	ELM Control.....	4-7
4.1.2	Pedestal Structure, Fueling, and Transport.....	4-19
4.1.3	L-H Physics.....	4-31
<b>4.2</b>	<b>CORE-EDGE.....</b>	<b>4-41</b>
4.2.1	Compatibility of the Fusion Core with Reactor Relevant Wall Materials .....	4-45
4.2.2	Plasma Shape and Boundary Configuration .....	4-57
4.2.3	Integrated Power and Particle Control.....	4-69
<b>5.</b>	<b>THE DIII-D NATIONAL FUSION FACILITY – OPERATION AND ENHANCEMENTS.....</b>	<b>5-1</b>
5.1	Operations and Maintenance.....	5-6
5.2	Sustaining Engineering .....	5-9
5.3	Facility Capability Improvements.....	5-11
5.3.1	EC System Power Upgrade.....	5-13
5.3.2	Co-Counter NB-30 Degrees (CCNB30).....	5-17
5.3.3	Raise NBI Energy (Power Increase and Pulse Extension).....	5-20
5.3.4	Divertor Upgrade .....	5-21
5.3.5	Advanced 3D Coils.....	5-23
5.3.6	Power Supplies for 3D Coils and PF Shaping Coils.....	5-25
5.3.7	First Wall/Divertor.....	5-26
5.3.8	Fueling and Disruption Mitigators.....	5-28
5.3.9	Helicon Current Drive.....	5-28
5.3.10	High-Field-Side Lower Hybrid.....	5-30
5.3.11	Conformal Wall .....	5-32
<b>6.</b>	<b>DIAGNOSTICS – PLASMA MEASUREMENTS.....</b>	<b>6-1</b>
6.1	Diagnostics for Robust Plasma Scenarios in Future Reactors.....	6-6
6.2	Measurements for Transient Control .....	6-8
6.3	Burning Plasma Science Research.....	6-10
6.4	Measurement Needs for Boundary Model Validation, Divertor Development and Integration .....	6-13
6.5	Advanced Materials Evaluation.....	6-18
6.6	Integrate Development of Diagnostics for Burning Plasma Experiments.....	6-21
6.7	Specific Diagnostic Refurbishments.....	6-22
<b>7.</b>	<b>COMPUTER SYSTEMS AND SCIENCE .....</b>	<b>7-1</b>
7.1	Overview.....	7-1
7.2	DIII-D Experiment Support.....	7-2
7.2.1	Plasma Control System.....	7-2
7.2.2	Data Acquisition .....	7-4
7.2.3	DIII-D Control Room .....	7-5
7.3	Computer Infrastructure.....	7-6

7.3.1	Data Storage.....	7-6
7.3.2	Computational Systems .....	7-8
7.3.3	Networking .....	7-9
7.4	Data Analysis and Remote participation.....	7-10
7.4.1	Analysis Infrastructure.....	7-10
7.4.2	Web Technology.....	7-13
7.4.3	Remote Participation.....	7-14
7.5	Cybersecurity .....	7-15
7.5.1	Training.....	7-15
7.5.2	Privilege Access Management.....	7-16
7.5.3	Patch Management.....	7-16
7.5.4	Continuous Monitoring.....	7-16
<b>8.</b>	<b>THE COLLABORATIVE NATIONAL PROGRAM.....</b>	<b>8-1</b>
8.1	Scope of the DIII-D Fusion Program.....	8-2
8.1.1	The DIII-D National Team .....	8-3
8.1.2	International Collaborations.....	8-4
8.2	National Leadership Role and Program Linkages .....	8-5
8.2.1	DIII-D Research in Support of ITER.....	8-7
8.2.2	DIII-D Support for the US Burning Plasma Organization.....	8-8
8.2.3	DIII-D Research and US Theory Program.....	8-9
8.2.4	Role of DIII-D Research for Enabling Technologies, Contributions, and Needs.....	8-13
8.2.5	Collaboration with other US Fusion Experiments .....	8-16
8.2.6	Collaborations with the Transport Task Force and the Broader Science Community .....	8-18
8.3	University Participation: Training Scientists for Fusion Research in the ITER Era .....	8-19
8.3.1	Opportunities for Training Students .....	8-21
8.3.2	Opportunities for Post-Doctoral Fellowships .....	8-22
8.3.3	Opportunities for Expanded University Partnerships .....	8-28
<b>9.</b>	<b>INTERNATIONAL PARTNERSHIPS.....</b>	<b>9-1</b>
9.1	Collaboration with Other Tokamak Facilities.....	9-3
9.1.1	EAST.....	9-5
9.1.2	KSTAR .....	9-6
9.1.3	QST/JT-60U/JT-60SA .....	9-6
9.1.4	EFDA-JET .....	9-7
9.1.5	ASDEX-U .....	9-8
9.1.6	MAST .....	9-8
9.1.7	ADITYA/SST-1 .....	9-9
9.1.8	Other Fusion Devices.....	9-9
9.2	International Tokamak Physics Activity.....	9-9
9.3	International Cooperative Agreements .....	9-11

9.4	International Investment in DIII-D .....	9-11
9.5	Web Access to the DIII-D Facility .....	9-13
<b>10.</b>	<b>DIII-D GOVERNANCE .....</b>	<b>10-1</b>
10.1	Roles and Responsibilities .....	10-1
10.2	Program planning .....	10-5
10.3	Funding of Research on DIII-D .....	10-7
10.4	Reporting DIII-D Program Activities .....	10-8
10.5	Safety .....	10-8
10.6	Management of the Collaborative National Team.....	10-9
10.6.1	General Principles of Collaboration.....	10-9
10.6.2	Documents Governing Active Collaborations .....	10-11
10.6.3	Approval Process for Project Activities.....	10-11
10.6.4	Budget Planning for DIII-D Projects .....	10-11
10.6.5	Program Reporting.....	10-12
<b>11.</b>	<b>ACCOMPLISHMENTS AND HISTORY OF THE DIII-D PROGRAM .....</b>	<b>11-1</b>
11.1	Overview.....	11-1
11.2	DIII D Accomplishments .....	11-1
11.3	Scientific Accomplishments during the Current Cooperative Agreement 2014–2019 and Projections to 2019-2024 .....	11-3
11.4	Facility Operation and Development.....	11-11
11.5	History of the DIII D Program.....	11-16
11.6	The US Fusion Program Commits to Burning Plasmas.....	11-18
11.7	Continuity of the DIII D Mission.....	11-20
<b>12.</b>	<b>BIBLIOGRAPHY .....</b>	<b>12-1</b>
12.1	Publications for FY13 .....	12-1
12.2	Publications for FY14 .....	12-4
12.3	Publications for FY15 .....	12-8
12.4	Publications for FY16.....	12-14
12.5	Publications for FY17 .....	12-20

## LIST OF FIGURES

Fig. 1-1.	Overview of DIII-D research program elements.....	1-7
Fig. 1-2.	M3D-C1 simulations of an EHO.....	1-9
Fig. 1-3.	Comparison of measured 2D density and temperature with simulation.....	1-10
Fig. 1-4.	Demonstration of ELM suppression in steady-state hybrid plasma.....	1-12
Fig. 1-5.	Access to high-pedestal Super H-mode.....	1-13
Fig. 1-6.	Timeline for transients research.....	1-15
Fig. 1-7.	Timeline for burning plasma physics research.....	1-16
Fig. 1-8.	Timeline for steady-state scenario research.....	1-17
Fig. 1-9.	Timeline for divertor research.....	1-19
Fig. 1-10.	Timeline for PMI research.....	1-20
Fig. 1-11.	Timeline for core-edge research.....	1-20
Fig. 1-12.	Timeline for major hardware upgrades in DIII-D five-year plan.....	1-21
Fig. 1-13.	Active collaborations with the DIII-D Program.....	1-26
Fig. 2-1.	Simulations of fully non-inductive plasmas in a compact net-electric advanced tokamak pilot plant with 4m radius, 7T, and $\eta_{th}=\eta_{CD}=0.4$ . Auxiliary heating and current drive is adjusted to ensure each point is fully non-inductive.....	2-5
Fig. 2-2.	Summary of steady-state scenario concepts being studied on DIII D.....	2-9
Fig. 2-3.	Primary goals to be achieved simultaneously (gray shading) in an inductively driven scenario by 2024 to inform ITER operation. Color-shaded areas are examples of progress as of the end of FY17.....	2-11
Fig. 2-4.	Primary goals to be achieved simultaneously (gray shading) in a steady-state scenario to inform a next-step burning plasma or DEMO. Color-shaded areas are examples of progress as the end of FY17.....	2-11
Fig. 2-5.	Inductive Scenarios Plan Timeline.....	2-14
Fig. 2-6.	Progress toward RMP-ELM suppression at zero-net NBI torque with $Q=10$ equivalent performance on DIII D, and comparison of the ISS and IBS plasma cross sections.....	2-15
Fig. 2-7.	Progress toward QH-mode at zero-net NBI torque with $Q=10$ equivalent performance on DIII D, and comparison of the plasma cross sections.....	2-16
Fig. 2-8.	Full-orbit Monte Carlo code SPIRAL predicts outer-gap populated by trapped, confined, beam ions orbiting outside the last closed flux surface. Gyro-diameter $\sim 8$ cm, IBS outer gap $\sim 8$ cm.....	2-17
Fig. 2-9.	Zero-torque IBS discharges run without 2/1 tearing modes but still need lower collisionality and ELM control.....	2-18
Fig. 2-10.	Schematic illustration of a radial array of gas injectors near the lower divertor. A similar array on the upper divertor is also planned.....	2-20
Fig. 2-11.	Steady-state Scenario Timeline.....	2-25
Fig. 2-12.	RSAEs are unstable when the radius of $q_{min}$ is aligned with a large fast-ion gradient (top). Moving $q_{min}$ farther off axis and raising $q_0$ with additional external current drive is predicted to eliminate TAEs and reduce RSAE drive (bottom).....	2-27
Fig. 2-13.	DIII D fully non-inductive high $\beta_P$ discharge.....	2-27
Fig. 2-14.	Time history of a steady-state hybrid discharge.....	2-28

Fig. 2-15. Predicted current components of  $q_{min} > 2$ ,  $f_{NI} = 1$  scenario with  $\beta_N = 4.6$  and  $q_{95} = 6$  using 6 MW ECCD and 4 off-axis NBI sources. .... 2-29

Fig. 2-16. Self-consistent  $f_{NI} = 1$  operating parameters vs.  $q_{95}$ . Solid black circles: transport-limited  $\beta_N$ ; red open circles: ideal  $\beta_N$  stability limits with present DIII D vacuum vessel; blue squares: stability limits including inserts. Dashed lines: with 6 MW ECCD; Solid lines: with 9 MW ECCD. .... 2-30

Fig. 2-17. Conceptual design for a conducting insert (red). Present vacuum vessel in black, plasma in blue. .... 2-30

Fig. 2-18. Comparison of FASTRAN and experiment loop voltage profiles. .... 2-32

Fig. 2-19. Comparison of the measured  $T_e$  in high  $\beta_P$  scenario to a prediction using TGLF for turbulent transport and NEO for neoclassical. The new SAT1 saturation model with electromagnetic effects, is a better match to data than the SAT0 model with only electrostatic effects. .... 2-32

Fig. 2-20. Predicted current components in a  $f_{NI} = 1$  discharge with 2 MW helicon.  $\beta_N = 4.97$ ,  $f_{BS} = 70\%$ ,  $f_{GW} = 0.9$ ,  $q_{95} = 6.5$ ,  $B_T = 1.6$  T. .... 2-36

Fig. 2-21. Multi-layered approach to maintaining stable operation and reducing the occurrence of disruptions. .... 2-40

Fig. 2-22. Disruption Mitigation Plan Timeline. .... 2-43

Fig. 2-23. Measurement of  $n = 1$  character of TQ radiated energy during neon MGI [Shiraki 2015]. .... 2-43

Fig. 2-24. TQ radiated energy and corresponding radiation fraction (right axis), as a function of SPI neon quantity showing saturation at  $\sim 10$  Pa-m<sup>3</sup>. Broken pellets (at time of firing) are indicated as red triangles. From [Shiraki 2016]. .... 2-44

Fig. 2-25. Poincare plots of magnetic field lines at three times after core deposition of argon, as modeled by the NIMROD resistive MHD code. Core flux surfaces are stochasticized immediately. Outermost closed flux surfaces are retained until the end of the thermal quench, after which outer field lines become very stochastic. From [Izzo 2017]. .... 2-46

Fig. 2-26. Cartoon of shell pellet injection. (a) Radiating impurity (purple) encased in low-Z shell (green) proceed through plasma without perturbing profiles. (b) Shell ablates in core, releasing radiator and cooling core. .... 2-47

Fig. 2-27. RE seed current at end of TQ estimated using argon pellet ablation for (a) fast pellets and (b) slow pellets as a function of initial RE plateau current. From [Hollmann 2017]. .... 2-50

Fig. 2-28. Core stability research timeline. .... 2-55

Fig. 2-29. Measured current density gradient at both sides of the minimum in ITER baseline discharges, showing that instability is associated with larger gradients. (Shown schematically in the right-hand panel.) [Turco 2016] .... 2-56

Fig. 2-30. A growing island is eliminated without disruption by temporarily reducing the input power, while a rotating  $n = 1$  RMP is applied by the I-coil to prevent wall locking. .... 2-56

Fig. 2-31. Experimentally accessed (a)  $\beta_N$  versus  $I_{li}$  and (b)  $\beta_N$  versus  $q_{min}$  values, with and without RWM feedback control, showing  $\beta$ -collapses due to  $n = 1$  RWM events, and calculated no-wall and ideal-wall ideal MHD stability limits. [Hanson 2017] .... 2-59

Fig. 2-32. Experimental  $n=2$  plasma response amplitude and IPEC prediction at the (a) Low Field Side and (b) High Field Side midplane as upper-lower I-coil phase difference is varied. Cross-section of the computed response at the (c) LFS null and (d) HFS null. [Paz-Soldan 2015a] ..... 2-61

Fig. 2-33. Plasma Control Research Plan Timeline ..... 2-67

Fig. 2-34. Integrated control design process uses validated physics-based models to construct control algorithms, and verifies control system performance against detailed simulations prior to operational use ..... 2-68

Fig. 2-35. Active regulation of impurity or fueling gas puffing at the divertor strike point has been demonstrated to maintain a stable detached plasma using an ITER-relevant control algorithm in DIII D. Although nitrogen and deuterium have been demonstrated in the current DIII D research period, the next period of research will include ITER-relevant Ne injection, along with emulation of ITER-scaled dynamics. .... 2-69

Fig. 2-36. The ITER-relevant Catch and Subdue scheme for repeated suppression of tearing modes has been demonstrated to enable rapid detection and alignment (“Catch”) of ECCD with a growing island, followed by suppression of the island (“Subdue”), using an ITER-relevant control algorithm in DIII D. Additional gyrotrons will enable full suppression of a 2/1 island (the most important mode requiring suppression in ITER as part of an effective disruption prevention system). .... 2-70

Fig. 2-37. Comparison of (a) q-profile resulting from feedforward alone, (b) q-profile resulting from feedforward + feedback using MPC controller. MPC control feedback produces good agreement between target and actual q-profile. .... 2-73

Fig. 2-38. Development of a negative triangularity plasma target through modeling, simulation, and design, opened up a completely new research path for turbulent transport understanding in DIII D. Empirical development of the required plasma target without advanced design methods would have consumed a prohibitive amount of machine time. .... 2-74

Fig. 2-39. Electron temperature fluctuations from a multi-scale simulation..... 2-79

Fig. 2-40. Timeline of Research Challenges in Turbulence and Transport Area, as well as Improvements in Hardware and Diagnostics ..... 2-81

Fig. 2-41. Quantitative comparison of measured density fluctuation spectrum from hybrid H-mode plasma with GYRO simulation with synthetic diagnostic applied. .... 2-82

Fig. 2-42. Ion Temperature profiles with (red) and without (blue) ECH in positive shear (left) and negative shear (right) profiles, corresponding q-profiles, and comparison of relative fluctuation magnitude increase with ECH in PS and NCS. .... 2-85

Fig. 2-44. Frequency spectrum of magnetic fluctuations between ELM crashes as measured by the Cross Polarization Scattering (CPS) diagnostic at  $\rho=0.96$ . .... 2-87

Fig. 2-43. Equilibria in positive (red) and negative (blue) triangularity plasmas produced on DIII-D. .... 2-87

Fig. 2-45.	Simulated kinetic profiles for a DIII-D discharge and comparison with the experimental measurements. The squares in these curves indicate the radii at which TGYRO performed the flux-matching calculations. ....	2-89
Fig. 2-46.	Design of neural network to predict the pedestal height and width using the same input parameters as the EPED1 model. ....	2-90
Fig. 2-47.	Research plan timeline for burning plasma rotation physics.....	2-95
Fig. 2-48.	Measured toroidal rotation profile on DIII-D for an ECH power scan at fixed deposition location [Grierson 2017].....	2-96
Fig. 2-49.	Prediction of the toroidal rotation profile in ITER, where the boundary condition is determined from $\rho^*$ scaling of DIII-D values, and the core profile is determined from TGLF/TGYRO modeling of momentum transport from the NBI torque [Chrystal 2017].....	2-97
Fig. 2-50.	The net power required to access the H-mode as a function of the injected torque for various target densities and heating methods for hydrogen, deuterium and helium. The open symbols denote discharges that failed to transition to H-mode at the applied power. ....	2-98
Fig. 2-51.	The integral NTV torque predicted by GPEC prior to experiment (left) for nonresonant fields for broad braking and edge resonant fields for localized braking contrasted with the experimental torque profiles (right) calculated using the initial time rate of change of the momentum.....	2-101
Fig. 2-52.	EP Plan Timeline.....	2-107
Fig. 2-53.	Conditionally-averaged NPA signal (green) during beam showing distortion from classical predictions (blue) due to AE induced fast-ion transport / flows. TRANSP Kick model prediction which includes AEs (red). From [Heidbrink 2017].....	2-108
Fig. 2-54.	EP phase space trajectories phase space with (left) few unstable AEs and (right) many unstable AEs. MEGA modeling for a DIII D plasma with multiple AEs [Todo 2016].....	2-108
Fig. 2-55.	Comparison of shots using time-variable beam energy to AEs. Early, higher injection energy drives stronger TAEs resulting in enhanced fast-ion transport and lower neutron rates (c). From [Pace 2016].....	2-111
Fig. 2-56.	Fluctuation spectra for two different plasma current ramp rates: (a) $dI/dt=0.6\text{MA/s}$ , $\rho_{qmin}=0.35$ , TAEs and RSAEs are observed; (b) $dI/dt=6.7\text{MA/s}$ , $\rho_{qmin}=0.45$ and NO AEs are observed. ....	2-114
Fig. 2-57.	Heating and current-drive research in FY19-24.....	2-119
Fig. 2-58.	Projected helicon ray paths and current drive efficiency calculated with GENRAY ray tracing code, using equilibrium and profiles from DIII-D discharge 122976.....	2-120
Fig. 2-59.	The low-power prototype comb-line traveling wave antenna as installed in DIII-D during the 2016 campaign. ....	2-120
Fig. 2-60.	HFS LHCD penetrates into plasma core and damps in single pass, whereas, LFS LHCD remains in the plasma periphery until wave upshifts and damps.....	2-121
Fig. 2-61.	(a) LH waves launched from HFS near mid plane penetrate and single pass damp near $\rho\sim 0.6$ for 1.66 T, high $q_{min}$ discharge (147634). (b) Driven current profile – with $\sim 0.4\text{MA/m}^2$ for 1 MW coupled. ....	2-121

Fig. 2-62.	(left) The top-launch EC beam propagates between the 2nd and 3rd harmonic layers. (right) In some cases top launch EC can result in a factor of two higher CD efficiency than LFS launch. ....	2-122
Fig. 3-1.	Divertor closure research plan timeline. ....	3-9
Fig. 3-2.	SAS combines the benefits of horizontal and vertical targets in a slot divertor configuration. Radial profiles of $T_e$ and $q_{\perp}$ , the deposited power flux density across the divertor target surface at a given upstream separatrix density, $n_e \sim 4 \times 10^{19} \text{ m}^{-3}$ , for the different slot divertors, predicted by SOLPS. From [Guo 2017a] .....	3-10
Fig. 3-3.	SAS achieves cold plasma with strong heat flux reduction across the target surface. Profiles of $J_{\text{sat}}$ (top) $T_e$ (middle) and $q_{\perp}$ (bottom) for the open divertor (left column) and SAS (right column) at the same line average density, $n_{e,\text{ave}} \sim 5 \times 10^{19} \text{ m}^{-3}$ , as a function of the normalized magnetic flux function, $\psi_n$ . Private flux region: $\psi_n < 1$ ; separatrix: $\psi_n = 1$ ; SOL: $\psi_n > 1$ . The colors of the symbols indicate different probe locations as shown in [Guo 2017b]. ....	3-10
Fig. 3-4.	D and D2 Recycling Exhibits a Strong Dependence on Plasma Facing Materials (C, W). Ratio of D2/D in recycling neutral fluxes on C and W target between and during ELMs in a H-mode discharge in DIII-D. From [Bykov 2017].....	3-13
Fig. 3-5.	Magnetic configuration research plan timeline .....	3-19
Fig. 3-6.	(a) Pedestal and global parameter sensitivity to changes in magnetic balance; and (b) the recycling radiation ( $D\alpha$ ) at the divertor targets is shown as a function of $dR_{\text{sep}}$ .....	3-21
Fig. 3-7.	Divertor dissipation plan timeline .....	3-32
Fig. 3-8.	Modeled and measured 2D profiles of divertor $T_e$ and $n_e$ in helium plasmas. Modeled and measured pressure profiles from the target to the mid-plane.....	3-33
Fig. 3-9.	Composite of D2 Fulcher band emission taken in six separate plasma discharges [Hollmann 2006]. ....	3-34
Fig. 3-10.	Fraction of parallel heat flux transported by convection as a function of $T_e$ in DIII-D divertor plasma.....	3-35
Fig. 3-11.	Summary of diagnostics improvements proposed for study of dissipative physics in the DIII-D lower divertor. ....	3-37
Fig. 3-12.	SOL and divertor particle transport plan timeline .....	3-42
Fig. 3-13.	Calculated DEGAS neutral flux into the core as a function of poloidal angle for L-mode ( $\circ$ ) and ELMy H-mode plasmas ( $\square$ ). The open (grey) symbols indicate X-point fueling, the closed symbols fueling due to divertor neutral leakage. ....	3-43
Fig. 3-14.	Measured and calculated deuterium velocity at the LFS mid-plane [Boedo 2016].....	3-45
Fig. 3-15.	2D reconstruction of HeII-based flow image in the lower divertor in forward and reversed toroidal field configurations as well as periscope view of CIII flow image in a helium plasma.....	3-47
Fig. 3-16.	SOL and Divertor Radial Transport Plan Timeline.....	3-52

Fig. 3-17.	Multi-machine database of divertor heat flux width as a function of poloidal magnetic field at the outer mid-plane.....	3-53
Fig. 3-18.	Material migration plan timeline .....	3-62
Fig. 3-19.	Tungsten SOL contamination probability (as a function of distance from the separatrix) for two separate LSN discharges from the DIII-D Metal Rings Campaign [Unterberg 2016]. .....	3-63
Fig. 3-20.	Cartoon depiction of the location of isotopically-resolved W tracer rings in the SAS-1 divertor (left, FY20) and the SAS-2 divertor (right, FY22). .....	3-64
Fig. 3-21.	Spectroscopically measured spatially-resolved profiles of the gross erosion of tungsten during ELM events for two different ELM regimes. Calculations from empirical SDTrim.SP sputtering (solid lines) are overlaid [Abrams 2016].....	3-67
Fig. 3-22.	Surface evolution science timeline .....	3-73
Fig. 3-23.	Conceptual design for the Wall Interactions Tile Station (WITS). .....	3-74
Fig. 3-24.	Spectroscopic measurements of the inter-ELM W erosion rate as a function of radial position for the same discharge. ERO+OEDGE predictions are overlaid, displaying better agreement with experiment than less sophisticated SDTrim.SP modeling [Abrams 2017]. .....	3-74
Fig. 3-25.	Measured radial profiles of <sup>13</sup> C deposition on a Mo witness sample after deuterated methane injection. Consistency is observed with ERO modeling after incorporating ExB drifts and assuming a cross-field diffusion coefficient of 0.5 m <sup>2</sup> /s [Ding 2017_1].....	3-77
Fig. 3-26.	Examples of mixed-material next-step reactor walls, using high-Z divertor targets and low-Z main chamber surfaces. ....	3-82
Fig. 3-27.	Innovative material plan timeline .....	3-83
Fig. 3-28.	SEM images of the UFG W showing (a) the top surface, and (b) a cross-section created by focused ion beam profiling. Darker regions of the surface correspond to Ti grains. from [Kolasinski 2016].....	3-85
Fig. 3-29.	SEM images of SiC-coated C foam sample .....	3-86
Fig. 3-30.	(a) temperature dependence of energetic particle sputtering for SiC, C and Si. (b),(c) measured sputtering from DIII-D SiC exposures compared to TRIM.SP sputtering calculations.(b) no enrichment, (c) ~10% Si surface enrichment. ....	3-87
Fig. 3-31.	(a) deuterium retention of W drops substantially and (b) carbon chemical erosion first increases, then decreases, as target temperatures increase.....	3-87
Fig. 4-1.	Research plan overview for ELM control .....	4-9
Fig. 4-2.	Recent progress in obtaining RMP and QH-mode scenarios at low torque .....	4-11
Fig. 4-3.	Wide-pedestal QH mode is obtained over a range of torque and shapes. ....	4-11
Fig. 4-4.	Proposed non-axisymmetric coil configurations for DIII-D with a new mid-plane in-vessel row (left) and comparison to the planned ITER coilset (right). .....	4-12
Fig. 4-5.	Increase in resonant coupling (left), n=2 NTV torque (mid), and n=3 NTV torque (right) capabilities with the addition of an in-vessel midplane (M) coil row. Axis labels describe coilsets used, including existing in-vessel (I, or upper-only IU) and external (C) coils.....	4-13

Fig. 4-6.	Density fluctuations from phase contrast imaging in various plasma regimes. ....	4-14
Fig. 4-7.	Magnetic field variations upon exit from ELM suppression, qualitatively consistent with M3D-C1 modeling. ....	4-15
Fig. 4-8.	Fluctuating fields of flow, temperature, and density in simulations of DIII-D QH modes [King 2017]. ....	4-16
Fig. 4-9.	M3D-C1 results simulating an injected pellet and the associated perturbations to the density and temperature. ....	4-16
Fig. 4-10.	Timeline for Pedestal-DivSOL coupling studies.....	4-22
Fig. 4-11.	$T_{e,sep}$ and $n_{e,sep}$ as functions of $n_{e,ped}$ and power.....	4-23
Fig. 4-12.	During recovery from ELM, electron temperature gradient saturates at same time as saturation in magnetic fluctuations from a Quasi-Coherent Fluctuation (QCF) (A. Diallo et al., PoP 22 (2015) 056111).....	4-25
Fig. 4-13.	More closed divertor (blue) shows broader and less steep $n_e$ profile compared to more open divertor (red). $T_e$ pedestal is higher with more closed divertor. (A.W. Leonard et al., 2016 IAEA-FEC, preprint0581.pdf).....	4-25
Fig. 4-14.	Comparison of QH-mode in EHO phase (Before-blue) and in wide pedestal phase (After-red).....	4-27
Fig. 4-15.	Data points shows that experiment has achieved the predicted Super-H regime.....	4-28
Fig. 4-16.	Research Plan Overview for L-H physics.....	4-34
Fig. 4-17.	Nonlinear energy transfer rate from turbulence ( $k\theta\rho_s \leq 1$ ) to low frequency $E \times B$ flow across the L-H transition; also shown is the ambient turbulence decorrelation rate.....	4-36
Fig. 4-18.	Ion flow acceleration (from CER data, in red) and measured Reynolds stress gradients from BES (in blue), and the sum of the acceleration term and the calculated poloidal flow damping term according to Rozhansky 1992 (green circles), versus radius.....	4-36
Fig. 4-19.	Turbulence wavenumber spectrum (BES) for hydrogen plasmas at (a) low and (b) medium density, showing a clear dual-mode structure at medium density where the L-H threshold power is low.....	4-37
Fig. 4-20.	Research Plan Overview.....	4-49
Fig. 4-21.	Comparison of discharge with metal rings (black lines) and reference discharge (b and c only) without metal rings (dotted red).....	4-50
Fig. 4-22.	Temperature and density profiles for electrons, D+ and C6+.....	4-51
Fig. 4-23.	Pressure gradient and bootstrap current move inward with Li and BCM.....	4-52
Fig. 4-24.	Tungsten erosion rates for (a) 3 MW and (b) 6 MW cases, showing dependence on ELM frequency.....	4-54
Fig. 4-25.	Tungsten density profiles from collector probe, normalized to integrated tungsten source strength, for two different ELM parameters.....	4-54
Fig. 4-26.	Timeline for the Shape and Boundary Configuration studies.....	4-60
Fig. 4-27.	Maximum achieved $\beta_N$ increases with shaping.....	4-61
Fig. 4-28.	Heat (red) and particle (black) flux sharing as magnetic balance is varied.....	4-61
Fig. 4-29.	Experiment (Blue squares) reaches Super-H boundary (red line) predicted by EPED model.....	4-63

Fig. 4-30.	Configurations studied in comparison of divertor geometries for heat flux control.....	4-65
Fig. 4-31.	Integrated Power and Particle Control Timeline .....	4-72
Fig. 4-32.	(a) Near DND configuration for high power with impurity injection. (b) MHD stability analysis shows no ballooning limit at high power and density .....	4-73
Fig. 4-33.	Rapid pumpout of fluorine during RMP ELM suppression .....	4-76
Fig. 4-34.	Schematic (adapted from [Dux 1996]) and physical layout of global particle balanced used to interpret fueling and impurity studies.....	4-79
Fig. 5-1.	Proposed Major Enhancements FY18-FY24. The vertical red lines indicate year 0 – year 5 of the plan. ....	5-1
Fig. 5-2.	DIII-D capabilities allow a wide range of research and technology issues to be addressed. ....	5-3
Fig. 5-3.	Availability by quarter for the period of FY1998 – 2016. Availability is a measure of the fraction of time the DIII-D device and operating systems are available to achieve the goals of the scheduled experiment.....	5-9
Fig. 5-4.	Plan to increase the EC system power to almost 9 MW.....	5-13
Fig. 5-5.	The first 1.5 MW gyrotron was delivered and installed in its socket in mid FY17.....	5-14
Fig. 5-6.	Upgrading EC system towards 10 MW with only 10 gyrotrons. Only one additional power supply, ECPS#5 is required.....	5-15
Fig. 5-7.	ECH top launch system conceptual design, located at the 300 degree upper port sector. The EC power is reflected by a fixed mirror through an existing penetration in the upper divertor.....	5-16
Fig. 5-8.	30 deg. co-/counter-injection beamline (CCNB30) design. ....	5-17
Fig. 5-9.	Modified TF feedpoint at 210 deg. reduced magnetic error field by a factor of 10. ....	5-19
Fig. 5-10.	Upgrade plan for the beamline internal components and ion sources. ....	5-21
Fig. 5-11.	New tile geometries will be incorporated to upper toroidal tile rows to provide a small-angle slot with a pumping aperture. The existing cryopumps (blue) will remain unchanged. ....	5-22
Fig. 5-12.	The lower SAS-II will incorporate a small-angle slot on the current outer floor tile and a new inner floor cooled panel structure.....	5-23
Fig. 5-13.	A midplane coil, the M-coil, (1x12 array of in-vessel coils on the outer midplane) is proposed. ....	5-24
Fig. 5-14.	Photograph of low-power Helicon antenna installed in DIII-D. The 12-module antenna was located above the midplane and was positioned 1 mm behind the surrounding graphite tiles. ....	5-29
Fig. 5-15.	Brazed prototype high-power Helicon antenna module. The darker rods on the top of the module are boron carbide coated TZM Molybdenum Faraday shields. The high power will consist of 30 modules. ....	5-29
Fig. 5-16.	Inside Launcher mounted on the centerpost below vessel midplane. The waveguide is fed from a 0oR-1 port and the “twist” from lower to higher profile of the rectangular waveguide is located on the lower centerpost. ....	5-31
Fig. 5-17.	Construction and installation of a more conformal, conducting surface inside the DIII D vessel on the R+1 and R-1 planes is proposed.....	5-32

Fig. 6-1.	View of the tokamak interior (outer wall) showing some of the internal diagnostics and extensive port access. DIII-D has 24 sectors, with 5 poloidal access ports, plus vertical ports in 10 sectors. ....	6-4
Fig. 6-2.	Planned timeline for the implementation of new or upgraded systems. Within each subsection, the priority runs from high (top) to lower (bottom). Triangles indicate completed (filled) or planned (open) systems, circles indicate an option. ....	6-6
Fig. 6-3.	a) Poloidal magnetic probe. b) Radial field saddle loop c) Compact combined poloidal and radial magnetic probes. ....	6-10
Fig. 6-4.	Conceptual design of the third Fast-Ion Loss Detector, to be located near the midplane for use in reverse BT operation. ....	6-13
Fig. 6-5.	Advanced 2D Divertor Thomson Scattering Imaging System with high triangularity plasma capability (red lines are the selectable laser beam paths, the green line is the path for the upper SAS II slot). ....	6-15
Fig. 6-6.	SAS II upper divertor diagnostic set. Shown through (upper tiles) are the magnetic probes underneath the tiles and the ASDEX gauges. The red lines are the laser beams for the upper divertor Thomson scattering system. ....	6-15
Fig. 6-7.	(Left): Lower divertor bolometer assembly. (Top right): Bolometer detector assembly. (Bottom right): Conceptual assembly of the two bolometer cameras within the lower port. ....	6-18
Fig. 6-8.	Conceptual design of the remote handling system WITS. A second option has also been developed for an equatorial port. ....	6-20
Fig. 6-9.	Schematic of an in-vessel hydrogen sensor. ....	6-20
Fig. 7-1.	The DIII-D control room with real-time displays for the scientific staff. ....	7-5
Fig. 7-2.	DIII-D’s raw data repository (PTDATA) has had year-over-year growth rates between 25% and 50% with an anticipated total size at the end of the proposed five-year plan between 1.2 PB and 2.6 PB. ....	7-7
Fig. 7-3.	In addition to a 20x single process speedup for SURFMN, parallelizing with MPI allows strong scaling over many cores for even more dramatic reduction in time to solution. ....	7-12
Fig. 7-4.	Web applications have been deployed that allow monitoring of the DIII-D shot cycle as well as real-time plasma control data visualization for scientists not physically located in the DIII-D control room. ....	7-14
Fig. 8-1.	National and international collaborations in support of the DIII-D research program. ....	8-2
Fig. 8-2.	DIII-D hosts many students and postdocs, providing a wide range of research experiences. Clockwise from upper left: Oak Ridge Associated Universities postdoc and recent UCLA (DIII-D) graduate Lazlo Bardoczi; UC Irvine postdoc Xiaodi Du; University of Texas graduate student Michael Brookman, and Oak Ridge Associated Universities postdoc Kathreen Thome. ....	8-22
Fig. 8-3.	Flier encouraging participation in the DIII-D research program and the Research Opportunities Forum distributed annually at the APS-DPP meeting. ....	8-29

Fig. 9-1. DIII-D is an important element of the world fusion portfolio, working together to prepare for a successful ITER research program and to establish the basis for operation of future burning plasma devices that will be central to the development of fusion energy. .... 9-2

Fig. 9-2. Experiments were recently carried out remotely on EAST by a team in the GA remote control room. The photo shows the GA team leading experiments during “third shift” (overnight) operation. In this instance, four experiments were carried out over five such shifts in a week. Access to EAST without traveling is valuable to DIII-D staff, but also helps ASIPP increase the utilization of their facility while operating with minimum onsite staff. .... 9-5

## LIST OF TABLES

Table 1-1. Summary of DIII-D Upgrades ..... 1-8

Table 2-1. Inductive Scenarios Challenges, Goals, and Upgrades..... 2-13

Table 2-2. Hardware Improvements for Achieving Q=10 in ITER ..... 2-21

Table 2-3. Diagnostic Improvements for Achieving Q=10 in ITER..... 2-22

Table 2-4. Simulation Codes Used..... 2-22

Table 2-5. Steady-State Scenarios Challenges, Goals, and Upgrades..... 2-24

Table 2-6. Hardware Improvements for Study of the Path to Steady-State ..... 2-36

Table 2-7. Diagnostic Improvements for Study of the Path to Steady-State ..... 2-37

Table 2-8. Simulation Codes Used..... 2-37

Table 2-9. Disruption Mitigation Approaches and Upgrades ..... 2-42

Table 2-10. Hardware Improvements for Disruption Mitigation Research ..... 2-52

Table 2-11. Diagnostic Improvements for Disruption Mitigation Research..... 2-52

Table 2-12. Codes Used for Disruption Mitigation Research ..... 2-52

Table 2-13. Core Stability Control Challenges, Goals, and Enhancements ..... 2-54

Table 2-14. Hardware Improvements for Core Stability Studies ..... 2-63

Table 2-15. Diagnostic Improvements for Core Stability Studies ..... 2-63

Table 2-16. Simulation Code Development Plan..... 2-64

Table 2-17. Plasma Control Research Challenges, Goals, and Capability Improvements ..... 2-66

Table 2-18. Hardware Improvements for Control Studies ..... 2-74

Table 2-19. Diagnostic Improvements for Control Studies ..... 2-75

Table 2-20. Simulation Codes Used for Control Studies ..... 2-75

Table 2-21. High-Level Challenges for the Achievement of Burning Plasma Regimes for Fusion Energy ..... 2-76

Table 2-22. Turbulence and Transport Approaches and Upgrades..... 2-80

Table 2-23.	Comparison of experimental and calculated (GYRO) ion and electron heat flux and density fluctuations. ....	2-82
Table 2-24	Hardware Improvements for Transport Studies.....	2-91
Table 2-25	Diagnostic Improvements for Transport Studies.....	2-91
Table 2-26	Simulation Codes Used.....	2-92
Table 2-27.	High-Level Challenges for the Achievement of Burning Plasma Rotation Physics .....	2-94
Table 2-28.	Hardware Improvements for Rotation Studies .....	2-104
Table 2-29.	Diagnostic Improvements for Rotation Studies.....	2-104
Table 2-30.	Simulation Codes Used.....	2-104
Table 2-31.	EP Challenges, Goals, and Upgrades.....	2-106
Table 2-32.	Control Tools for EP Studies on DIII D .....	2-115
Table 2-33.	Physics Enabled by New Diagnostics for EP Research.....	2-116
Table 2-34.	Codes Used for EP Research .....	2-116
Table 2-35.	Heating and Current Drive, Challenges, Goals and Upgrades.....	2-118
Table 2-36.	Hardware Improvements for Heating and Current-Drive Studies .....	2-127
Table 2-37.	Diagnostic Improvements for Heating and Current-Drive Studies.....	2-127
Table 2-38.	Development and Validation of Simulation/Analysis Codes .....	2-128
Table 3-1.	Divertor Closure Research Challenges, Goals, and Upgrades.....	3-8
Table 3-2.	Facility Enhancements for Divertor Closure Studies on DIII-D .....	3-15
Table 3-3.	Physics Enabled by New Diagnostics for Divertor Closure Research .....	3-16
Table 3-4.	Codes Used for Divertor Optimization.....	3-16
Table 3-5.	Magnetic Configuration Research Challenges, Goals, and Upgrades .....	3-18
Table 3-6.	Hardware Improvements for Magnetic Configuration Studies.....	3-26
Table 3-7.	Diagnostic Enhancements for Magnetic Configuration Studies.....	3-26
Table 3-8.	Simulation Codes Used.....	3-27
Table 3-9.	Divertor Dissipation Challenges, Goals, and Upgrades.....	3-31
Table 3-10.	Facility Enhancements .....	3-38
Table 3-11.	Physics Enabled by New Diagnostics for Divertor Dissipation Research.....	3-38
Table 3-12.	Codes Used for Divertor Dissipation Research .....	3-39
Table 3-13.	SOL and Divertor Particle Transport Challenges, Goals, and Upgrades.....	3-41
Table 3-14.	Facility Enhancements .....	3-49
Table 3-15.	Physics Enabled by New Diagnostics for SOL Particle Transport Research.....	3-49
Table 3-16.	Codes Used for SOL Particle Transport Research.....	3-50
Table 3-17.	SOL and Divertor Radial Transport Challenges, Goals, and Upgrades .....	3-51
Table 3-18.	Facility Enhancements.....	3-56
Table 3-19.	Physics Enabled by New Diagnostics for Divertor Turbulence and Transport .....	3-56
Table 3-20.	Simulation Codes Used for Divertor Turbulence and Transport.....	3-57
Table 3-21.	Material Migration Challenges, Goals, and Capability Enhancements .....	3-61
Table 3-22.	Hardware Enhancements for Material Migration Studies on DIII-D .....	3-70
Table 3-23.	Physics Enabled by New Diagnostics for Material Migration Research.....	3-70
Table 3-24.	Codes Used for Material Migration Research .....	3-70
Table 3-25.	Surface Evolution Science Challenges, Goals, and Enhancements.....	3-72

Table 3-26.	Hardware Enhancements for Surface Evolution Science Studies on DIII-D .....	3-79
Table 3-27.	Physics Enabled by New Diagnostics for Surface Evolution Science Research.....	3-80
Table 3-28.	Codes Used for Surface Evolution Science Research.....	3-80
Table 3-29.	Innovative Materials Challenges, Goals, and Upgrades .....	3-83
Table 3-30.	Facility Enhancements .....	3-88
Table 3-31.	Physics Enabled by New Diagnostics for Innovative Materials Research .....	3-88
Table 3-32.	Codes Used for Innovative Materials Research.....	3-88
Table 4-1.	ELM Control Challenges, Goals and Upgrade Plans.....	4-8
Table 4-2.	Hardware Improvements for ELM Control .....	4-18
Table 4-3.	Diagnostic Improvements for ELM Control.....	4-18
Table 4-4.	Simulation Codes Used for ELM control .....	4-19
Table 4-5.	Pedestal Structure Challenges, Goals and Upgrade Plans .....	4-21
Table 4-6.	Hardware Improvements for DivSOL–Pedestal Coupling Studies .....	4-29
Table 4-7.	Diagnostic Improvements for DivSOL–Pedestal Coupling Studies.....	4-30
Table 4-8.	Simulation Codes Used.....	4-30
Table 4-9.	Challenges, Approach, and Improvements for L-H Transition .....	4-33
Table 4-10.	Hardware Improvements for L-H Transition Studies .....	4-40
Table 4-11.	Diagnostic Improvements for L-H Transition Studies.....	4-41
Table 4-12.	Simulation Codes Used.....	4-41
Table 4-13.	Challenges for Core-Wall Compatibility .....	4-47
Table 4-14.	Hardware Improvements for Transport Studies.....	4-56
Table 4-15.	Diagnostic Improvements for Transport Studies .....	4-56
Table 4-16.	Simulation Codes Used.....	4-57
Table 4-17.	Shape and Boundary Configuration Challenges and Goals.....	4-59
Table 4-18.	Hardware Improvements for Shape and Boundary Configuration Studies .....	4-67
Table 4-19.	Diagnostic Improvements for Shape and Boundary Configuration Studies.....	4-68
Table 4-20.	Simulation Codes Used for Shape and Boundary Configuration Studies .....	4-68
Table 4-21.	Integrated Power and Particle Control Challenges .....	4-70
Table 4-22.	Hardware Improvements for Integrated Power and Particle Control .....	4-78
Table 4-23.	Diagnostic Improvements for Integrated Power and Particle Control.....	4-78
Table 4-24.	Simulation Codes Used.....	4-78
Table 5-1.	Summary of All Major Non-Heating Systems.....	5-2
Table 5-2.	Auxiliary heating system power .....	5-5
Table 5-3.	Major Hardware Upgrades.....	5-12
Table 5-4.	Specifications of Both the Existing and Proposed Supplies .....	5-25
Table 6-1.	Summary of Current DIII-D Diagnostics (Updated 10/12/2017) (Blue text indicates systems that were added or significantly upgraded in the last five years).....	6-2
Table 6-2.	Robust Plasma Scenarios Measurement Needs .....	6-7
Table 6-3.	Transient Measurement Needs.....	6-9
Table 6-4.	Burning Plasma Physics Measurement Needs.....	6-11
Table 6-5.	Boundary Model Validation, Divertor Development and Integration Measurement Needs.....	6-14

Table 6-6.	Advanced Materials Validation Measurement Needs.....	6-19
Table 7-1.	Diagnostics and the Number of Channels Presently Acquired by the DIII-D PCS as Well as Those New Systems to be Added during the Proposed Five-Year Plan .....	7-2
Table 8-1.	Programmatic Responsibilities for Collaborating Institutions with Representation on the DIII-D Executive Committee 2017-18 .....	8-4
Table 8-2.	DIII-D Staff Participating in the ITPA Topical Groups as Members .....	8-8
Table 8-3.	FES Joint Research Targets FY08–FY18 .....	8-17
Table 8-4	Primary Research Interests of University Collaborators in North America (2017) .....	8-20
Table 8-5.	Present (Second Quarter FY17) Graduate Students with Main Focus on DIII-D Data .....	8-23
Table 8-6.	Past Graduate Students at DIII-D .....	8-24
Table 8-7.	Present (FY17) Post-Doctoral Fellows at DIII-D .....	8-26
Table 8-8.	Past Post-Doctoral Fellows at DIII-D .....	8-27
Table 8-9.	Areas of Potential Additional University Collaboration.....	8-30
Table 9-1.	Collaborative Activities Described in this Chapter .....	9-3
Table 9-2.	General and ITPA-Related Experiments Performed on DIII-D in 2017 .....	9-11
Table 9-3.	US Members of the ITPA Topical Groups .....	9-12
Table 9-4.	A Broad Range of Personnel Exchanges Enhance International Collaborations and Joint Experiments (FY2016 and FY2017).....	9-14
Table 9-5.	DIII-D maintains a large number of active international collaborations (2017).....	9-15
Table 10-1	FY18 Research Council Members and Affiliations.....	10-2
Table 11-1.	Major DIII D Contributions to Tokamak Plasma Research.....	11-2
Table 11-2.	Operations Statistics by Fiscal Year .....	11-13

## LIST OF ACRONYMS AND ABBREVIATIONS

Acronym/Abbreviation	Description
AD	Active Directory
AE	Alfvén Eigenmode
AI	Advanced Inductive
ALARA	As Low as Reasonably Achievable
AM	Additive Manufacturing
AMV	Advanced Material Validation
APS	American Physical Society
APS-DPP	American Physical Society-Division of Plasma Physics
ARC reactor	Affordable, Robust Compact Reactor
ARIES-ACT1	ARIES-(Advanced and Conservative Tokamak)1
ASCR	Advanced Scientific Computing Research
ASDEX	Axially Symmetric Divertor Experiment
ASIPP	Institute of Plasma Physics, Chinese Academy of Sciences
AT	Advanced Tokamak
AToM	Advanced Tokamak Modeling
AUG	ASDEX Upgrade
BAAE	Beta-Induced Alfvén-acoustic Eigenmode
BAE	Beta-Induced Alfvén Eigenmode
BES	Beam Emission Spectroscopy
BP	Burning Plasma
BPMIC	Boundary and Plasma Materials Interaction Center
BPO	U.S. Burning Plasma Organization
BPX	Burning Plasma Experiment
CAMAC	Computer Aided Measurement and Control
CAS	Cost Accounting Standards
CCFE	Culham Center for Fusion Energy
CCOANB	Co-counter Off-axis Beam
CECE	Correlation Electron Cyclotron Emission
CEMM	Center for Extended MHD Modeling
CER	Charge Exchange Recombination
CFETR	China Fusion Engineering Test Reactor

## LIST OF ACRONYMS AND ABBREVIATIONS

Acronym/Abbreviation	Description
CG	Critical Gradient
CIS	Coherence Imaging Spectroscopy
CMC	Ceramic Matrix Composite
CPI	Communications Power Industries
CPS	Cross-polarization Scattering
CQ	Current Quench
CSPM	Center for the Study of Plasma Microturbulence
CSWPI	Center for Simulation of Wave-Plasma Interactions
CTP	Cooperation on Tokamak Programs
CTTS	Center for Tokamak Transient Simulations
CVD	Chemical Vapor Deposition
CVS	Core Velocity Shear
CX	Charge Exchange
DBS	Doppler Backscattering System
DEC	DIII-D Executive Committee
DEMO	Demonstration Power Station
DiMES	Divertor Material Evaluation System
DMS	Disruption Mitigation System
DN	Double-null
DND	Double-null Divertor
DOE	U.S. Department of Energy
DPP	Division of Plasma Physics
DR	Disaster Recovery
DTS	Divertor Thomson Scattering
EAST	Experimental Advanced Superconducting Tokamak
EC	Electron Cyclotron
ECC	Edge Coordinating Committee
ECCD	Electron Cyclotron Current Drive
ECE	Electron Cyclotron Emission
ECEI	Electron Cyclotron Emission Imaging
ECH	Electron Cyclotron Heating

## LIST OF ACRONYMS AND ABBREVIATIONS

Acronym/Abbreviation	Description
ECRF	Electron Cyclotron Range of Frequency
EFC	Error Field Compensation
EFDA	European Fusion Development Agreement
EHO	Edge Harmonic Oscillation
ELM	Edge-localized Mode
EM	Electromagnetic
EP	Energetic Particle
EPSI	Edge Physics Simulation
ESCC	ESnet Site Coordinators Committee
ES Division	Experimental Science Division
ESL	Edge Simulation Laboratory
ESnet	Energy Sciences Network
EU	European Union
ETG	Electron Temperature Gradient
EUV	Extreme Ultraviolet
FES	Fusion Energy Sciences
FESAC	Fusion Energy Sciences Advisory Committee
FEC	Fusion Energy Conference
FFCC	Fusion Facilities Coordinating Committee
FIB	Focused Ion Beam
FIDA	Fast-ion D $\alpha$
FILD	Fast-ion Loss Detector
FNSF	Fusion Nuclear Science Facility
FOA	Funding Opportunity Announcement
FPGA	Field-Programmable Gate Array
FRTS	Faster than Real Time Simulation
FY	Fiscal Year
GA	General Atomics
GPI	Gas Puffing Imaging
GPU	Graphics Processor Unit
GRI	Gamma Ray Imager

## LIST OF ACRONYMS AND ABBREVIATIONS

Acronym/Abbreviation	Description
GSEP	Gyro-kinetic Simulation of Energetic Particle Turbulence and Transport
HFS	High-field Side
HPC	High Performance Computing
HPSS	High Performance Storage System
HV	High-voltage
HVPS	High-Voltage Power Supply
IAEA	International Atomic Energy Agency
IBS	ITER Baseline Scenario/Shape
ICE	Ion Cyclotron Emission
ICH	Ion Cyclotron Heating
ICP-MS	Inductively Coupled Plasma Mass Spectrometry
ICRF	Ion Cyclotron Range of Frequencies
IDL	Interactive Data Language
IGBT	Insulated-gate Bipolar Transistor
ILW	ITER-like Wall
IMSE	Imaging Motional Stark Effect
INPA	Imaging Neutral Particle Analysis
IO	ITER Organization
IO-CT	ITER Organization Central Team
IPP	Max Planck Institute for Plasma Physics
IPR	Institute For Plasma Research
IPS	Integrated Plasma Simulator
IPS	Intrusion Prevention System
IR	Infrared
ISS	ITER Similar Shape
ITB	Internal Transport Barrier
ITG	Ion Temperature Gradient
ITPA	International Tokamak Physics Activity
JAEA	Japan Atomic Energy Agency
JAERI	Japan Atomic Energy Research Institute
JET	Joint European Torus

## LIST OF ACRONYMS AND ABBREVIATIONS

Acronym/Abbreviation	Description
JT-60	Japan Torus-60
KBM	Kinetic Ballooning Mode
KSTAR	Korean Superconducting Tokamak Advanced Research
LBO	Laser Blow-off
LCFS	Last Closed Flux Surface
LFS	Low-field Side
LH	Lower Hybrid
LHe	Liquid Helium
LHCD	Lower Hybrid Current Drive
LHRF	Lower Hybrid Range of Frequencies
LLNL	Lawrence Livermore National Laboratory
LM	Locked Mode
LPHP	Long-Pulse, High-Performance
LQG	Linear Quadratic Gaussian
LSN	Lower Single Null
LTO	Long Torus Opening
MARFE	Multifaceted Asymmetric Radiation from the Edge
MAST	Mega-ampere Spherical Tokamak
MAST-U	Mega-ampere Spherical Tokamak Upgrade
MC	Main Chamber
MDS	Multichord Divertor Spectrometer
MFTF	Mirror Fusion Test Facility
MG	Motor Generator
MGI	Massive Gas Injection
MHD	Magnetohydrodynamics
MIMES	Midplane Material Evaluation System
MIR	Microwave Imaging Reflectometry
MIT	Massachusetts Institute of Technology
MPC	Model Predictive Control
MPO	Metadata, Provenance, Ontology
MRC	Metal Rings Campaign

## LIST OF ACRONYMS AND ABBREVIATIONS

Acronym/Abbreviation	Description
MSE	Motional Stark Effect
NAC	Network Access Control
NB	Neutral Beam
NBI	Neutral Beam Injection
NBCD	Neutral Beam Current Drive
NCS	Negative Central Shear
NERSC	National Energy Research Scientific Computing Center
NET	Next European Torus
NIR	Near-infrared
NPA	Neutral Particle Analysis
NRC	National Research Council
NSF	National Science Foundation
NSTX-U	National Spherical Torus Experiment Upgrade
NTM	Neoclassical Tearing Mode
NTV	Neoclassical Toroidal Viscosity
NUV	Near Ultraviolet
O&M	Operation and Maintenance
OANB	Off-axis Neutral Beam
OFHC	Oxygen-free High Thermal Conductivity Copper
OMFIT	One Modeling Framework for Integrated Tasks
ONFR	Off-Normal and Fault Response
ORAU	Oak Ridge Associated Universities
ORISE	Oak Ridge Institute for Science Education
ORNL	Oak Ridge National Laboratory
OS	Operating System
OSP	Outer Strike Point
PAC	Program Advisory Committee
PCI	Phase Contrast Imaging
PCS	Plasma Control System
PDI	Parametric Decay Instability
PF	Poloidal Field

## LIST OF ACRONYMS AND ABBREVIATIONS

Acronym/Abbreviation	Description
PFPO	Pre-fusion Power Operation
PFC	Plasma-facing Component
PFM	Plasma-Facing Materials
PFSM	Plasma-facing Systems Modeling
PMI	Plasma Materials Interaction, Plasma Materials Interface
PPPL	Princeton Plasma Physics Laboratory
PSI	Plasma Surface Interactions
PTDATA	DIII-D’s Raw Data Repository
QA	Quality Assurance
QCF	Quasi-Coherent Fluctuation
QH-mode	Quiescent H-mode
QRE	Quiescent Runaway Electron
QST	National Institutes for Quantum and Radiological Science and Technology
RAMP	Reduced Aperture Masking Plate
RC	Research Council
RE	Runaway Electron
RF	Radio Frequency
RFA	Retarding Field Analyzers
RIP	Radial Interferometer-polarimeter
RMP	Resonant Magnetic Perturbation
RSAE	Reversed Shear Alfvén Eigenmode
RWM	Resistive Wall Mode
SAS	Small Angle Slot
SBIR	Small Business Innovation Research
SciDAC	Scientific Discovery Through Advanced Computing
SCR	Silicon Controlled Rectifier
SCREAM	Simulation Center for Runaway Electron Avoidance and Mitigation
SEM	Scanning Electron Microscope
SES	Surface Evolution Science
SETC	Surface Eroding Thermocouples

## LIST OF ACRONYMS AND ABBREVIATIONS

Acronym/Abbreviation	Description
SFD	Snowflake Divertor
SiC	Silicon Carbide
SLAC	Stanford Linear Accelerator
SMBI	Supersonic Molecular Beam Injector
SND	Single-null Divertor
SNL	Sandia National Laboratory
SNR	Signal-to-noise Ratio
SOL	Scrape-off-layer
SPI	Shattered Pellet Injection
SPRED	Survey, Poor Resolution, Extended Domain
SSL	Secure Sockets Layer
SST-1	Steady-State Superconducting Tokamak - 1
STAC	ITER Council's Science and Technology Advisory Committee
SWIP	Southwestern Institute of Physics
SXR	Soft-X Ray
TAE	Toroidal Alfvén Eigenmodes
TALIF	Two-Photon Absorption Laser Induced Fluorescence
TBM	Test Blanket Module
TCV	Tokamak $\tilde{A}$ Configuration Variable
TEM	Trapped Electron Mode
TGLF	Trapped Gyro-Landau Fluid
TIP	Tangential Interferometer and Polarimeter
TM	Classical Tearing Mode
TQ	Thermal Quench
TTF	U.S. Transport Task Force
TZM	Titanium Zirconium Molybdenum
UCI	University of California, Irvine
UCLA	University of California, Los Angeles
UCSD	University of California, San Diego
UF-CHERS	Ultra-fast Charge Exchange Recombination Spectroscopy
UFG	Ultra-fine Grain

## LIST OF ACRONYMS AND ABBREVIATIONS

Acronym/Abbreviation	Description
UHTC	Ultra-high Temperature Ceramics
USBPO	U.S. Burning Plasma Organization
USN	Upper Single Null
UV	Ultraviolet
VFI	Vertical Field Induction
VIS	Visible
VLT	Virtual Laboratory for Technology
VPN	Virtual Private Network
VUV	Vacuum Ultraviolet
W&M	College of William & Mary
WBS	Work Breakdown Structure
WDM	Whole Device Modeling
WITS	Wall Interaction Tile Station
WFOA	Work for Others Agreement
XCS	X-ray Crystal Spectrometers
XD	X-divertor
XICS	X-ray Imaging Crystal Spectroscopy

## LIST OF COMPUTER CODES AND APPLICATIONS

Code	Purpose
AE3D	Alfvén-eigenmode Instabilities in 3D Toroidal Systems
AORSA RF	rf Wave Propagation and Heating
ASCOT	Guiding-center Particle Orbits
ATLAS	Stochastic Magnetic Field Topology
B2	2D Edge Transport Simulation/Analysis
B2/EIRENE	2D Edge Transport And Neutral Simulation/Analysis Package
BALOO	Ideal MHD Ballooning Stability
BOUT	Edge Turbulence Transport
BOUT++	C++ Edge Turbulence Transport
C2	Transport Simulation
CAMINO	MHD Ballooning Stability
CERAUTO	Automated CER Analysis Code
Condor	An Open Source Queuing System for High Throughput Computing
CORSICA	Transport Simulation
CQL3D	3D Quasi-Linear Evolution Fokker-Planck
CRONOS	Transport Simulation
CURRAY	rf Ray Tracing
D3	Improved JavaScript Library
DCON	Ideal MHD Stability
DEGAS	Neutral Transport
DIVIMP	Edge/Divertor Impurity Transport
DMZ	“Science Data DMZ”
E3D	3D Monte-Carlo Heat Transport Code
EFIT	Equilibrium Reconstruction
EFIT3D	3D Equilibrium Reconstruction
EFITViewer	EFIT Viewing Tool
EGK	Turbulence Simulation
EIRENE	Neutral Transport
ELITE	Edge MHD Stability
EMC3	3D Edge Transport
EMC3-ERIENE	3D Edge Transport With Neutrals
EPED	Pedestal Height And Width Model
EPED1	Pedestal Height And Width Model v1
ERO	3D Monte-Carlo Edge Impurity Transport
FASTRANS	Fast Transport Simulation

## LIST OF COMPUTER CODES AND APPLICATIONS

Code	Purpose
FCQ	Disruption Fast Current Quench Simulation
FIDA	Fast-ion D-alpha Diagnostic
FIDASIM	Fast-ion D-alpha Simulation
GATO	Ideal MHD Stability
GEM	Electromagnetic Gyro-kinetic Turbulent Transport
GENE	Gyro-kinetic Turbulent Transport
GENRAY	rf Ray Tracing
GITR	Global Impurity Transport
GKS	Turbulent Transport
GLF23	Gyro-Landau Fluid Turbulent Transport Model
GPEC	General Perturbed Equilibrium Code
GS2	Gyro-kinetic Turbulent Transport
GTC	Gyro-kinetic Turbulent Transport
GTNEUT	Neutral Transport
GTS	Gyro-kinetic Tokamak Turbulent Simulation
GYRO	Gyro-kinetic Turbulent Transport
HTTP	Hypertext Transfer Protocol
IDL	Scientific Programming Language
IMFIT	Integrated Modeling Analysis Tool
IPEC	Ideal Perturbed Equilibrium
IPEC-NTV	IPEC Neoclassical Toroidal Viscosity
ITMC-DYN	Ion Transport Simulation in Materials and Compounds
JFIT	Current Distribution Reconstruction
JOREK	3D MHD Simulation
KPRAD	Radiation Dynamics
LIGKA	Linear Gyro-kinetic Simulation with Full Orbits
M3D	3D MHD/Two-fluid Dynamics
M3D-C1	3D Non-linear MHD/Two-fluid Simulation
M3D-K	Hybrid 3D Kinetic-MHD Simulation
MAFOT	Invariant Manifold Structure
MARS	Linear Extended MHD Simulation
MARS-F	Linear Extended MHD Simulation
MARS-K	Hybrid Drift-kinetic Linear Extended MHD
MARS-Q	Quasi-linear Extended MHD
MBC	MHD Ballooning Stability

## LIST OF COMPUTER CODES AND APPLICATIONS

Code	Purpose
MDSplus	Data Handling Software System
MISK	Modifications to Ideal Stability by Kinetics
MIST	Impurity Transport
MM	Multi-mode Transport
Nagios®	Computer Monitoring System
NCLASS	Neoclassical Transport
NEO	Drift-kinetic Neoclassical Transport
NFREYA	Neutral Beam Deposition
NIMROD	3D Nonlinear Extended MHD Simulation
NMA	Resistive Wall Modes
NoSQL	Not Only Structured Query Language
NOVA	Linear Energetic-Particle Instabilities
NOVA-K	Linear Kinetic Energetic-Particle Alfvén-eigenmode Instabilities
NUBEAM	Neutral Beam Deposition
OEDGE	Edge/Divertor Interpretive Modeling
OFMC	Monte-Carlo Orbit Following
OMFIT	Integrated Modeling Tool
ONETWO	Transport Simulation/Analysis
ORBIT	Particle Orbits
ORBIT-RF	rf Particle Orbits
PELLET	Pellet Ablation
PEST	Ideal MHD Stability
PEST3	Resistive MHD Stability
Protovis	JavaScript Library
PTRANSP	Transport Simulation/Analysis
Python	Programming Language
REDEP/WBC	Erosion and Redeposition
ReviewPlus	Data Viewing Tool
RTEFIT	Real-time EFIT Equilibrium Reconstruction
Snowflake	Divertor Configuration
SOLPS	Edge Transport Simulation
SOLPS5	Edge Transport Simulation
SOLPS5-EIRENE	Edge Transport Simulation
SPIRAL	Particle Orbits
SQL	Structured Query Language

## LIST OF COMPUTER CODES AND APPLICATIONS

Code	Purpose
STAR	Computer Computational Cluster
Super-X	Divertor Configuration
SURFMN	Fourier Analysis Of Magnetic Topology
TAEFL	Hybrid Reduced-MHD Gyro-Fluid Energetic-Particle Instabilities
TEMPEST	Edge Turbulence
TEQ	Equilibrium Solver
TGLF	Trapped Gyro-Landau Fluid Turbulent Transport Model
TGYRO	Parallel Steady-State Gyro-Kinetic Transport Analysis
TokSys	TOKamak SYStem Control Design/Analysis
TOQ	Equilibrium Solver
TORAY	rf Ray Tracing
TORAY-GA	rf Ray Tracing
TORBEAM	Electron Cyclotron Heating/Current Drive Calculation TORIC rf Wave Modeling
TRANSP	Transport Analysis
3D	3D Magnetic Field Line Topology
TRIP3D	3D Magnetic Field Line Topology
TSC	Tokamak Simulation
UEDGE	Edge Simulation/Analysis
V3FIT	3D Equilibrium Reconstruction
VALEN	3D Conductor with Linearized Plasma MHD Model for RWM Feedback Analysis
Venus	Computational Cluster
VMEC	3D Equilibrium
Wiki	A Web Application that Allows Editing by Users
XGC0	Kinetic Neoclassical Edge Transport
XGC1	Kinetic Turbulent Edge Transport
XHMGC	Extended Hybrid MHD-gyrokinetic Energetic Particle Instabilities
XPTOR	Transport Simulation
ZIPFIT	Between-shot Profile Analysis

## 1. PROGRAM MISSION, STRATEGY, UPGRADES AND IMPACT

### 1.1 OVERVIEW AND BACKGROUND

The goal of fusion research is the realization of a clean and abundant energy source that can satisfy the world’s rapidly growing demand for energy. Achieving a sustained burning plasma for fusion energy production represents a grand scientific and engineering challenge. Remarkable progress has been made on the quest for thermonuclear fusion, establishing the tokamak concept and developing a robust basis to project it to the reactor scale. The recognition of progress is embodied in the world’s decision to proceed with ITER, a partnership between countries representing over half the world’s population. Construction is now over 50% complete on ITER, which will demonstrate for the first time a self-heated burning plasma state sustained for long duration (>500 seconds). The world fusion program eagerly awaits first plasma on ITER within the next decade, which offers an exciting and critical validation of the viability of fusion energy.

The DIII-D National Fusion Program has been instrumental in developing the physics basis for ITER, and many key insights and design requirements have been determined by the research conducted at DIII-D. At the time of this writing, the majority of design issues for ITER have been resolved, and research on DIII-D is turning toward how to take maximum advantage of the ITER facility by addressing its key physics and operational uncertainties, enabled by DIII-D’s diagnostic and operational flexibility and use of predictive integrated modeling, to ensure rapid progress toward high-performance burning plasmas. In parallel, the world program is increasingly focusing on the path to fusion energy through and beyond ITER – to achieve a self-consistent, fully non-inductive plasma that can be sustained continuously.

The DIII-D 2019-24 research plan seeks to provide the scientific basis to project integrated plasma solutions for future burning-plasma devices. Future reactors will operate in different regimes and face greater demands than encountered in the present generation of fusion research devices. To meet this challenge, DIII-D research will investigate plasma phenomena from the core to the edge, combining innovative experimental approaches with leading-edge comprehensive diagnostics and theory/simulation comparisons, to develop the scientific understanding and approaches required to make fusion a practical reality. Facility capabilities will be developed to access reactor-relevant parameters and solutions with reactor-realizable techniques. Transformative enabling advances expected in the 2019-2024 plan are:

- The realization of fully non-inductive high-beta, high-bootstrap fraction modes of operation for steady-state fusion reactors sustained for multiple resistive times;

- Innovative detached divertor solutions that can handle the hot plasma exhaust without erosion for continuous operation;
- Groundbreaking new current-drive techniques that can transform reactor economics and required device size;
- Pioneering high-density pedestal regimes that resolve the conflict between the high-performance core and a dissipative divertor;
- Predictive simulation tools for the burning plasma state to project requirements for reaching high performance in future devices;
- Revolutionary ‘inside-out’ disruption mitigation techniques that deliver particles to the core of the plasma with near 100% efficiency to dissipate energy, current, and runaway electrons;
- Manipulation of 3D fields to selectively control components to suppress ELMs, drive rotation, control ideal magnetohydrodynamics (MHD), and avoid deleterious locked modes;
- Robust disruption-free operation of the tokamak.

A further opportunity lies in exploring the interaction between the various techniques required to develop the physics understanding to project self-consistent integrated ‘core-edge’ solutions for future fusion devices – a key goal of the 2019-2024 five-year plan.

The DIII-D National Fusion Facility is well suited to confront these challenges, thanks to its high level of flexibility, excellent scientific team, outstanding diagnostic set, and strong collaboration with theory and simulation initiatives. The program proposed here, guided by past DIII-D research accomplishments and validated fusion simulation, will establish the facility as a world-leading scientific tool to pioneer solutions for future fusion devices. It will equip U.S. scientists with the knowledge to take a leading role in such facilities, resolving the crucial challenges and techniques required. It will enable the U.S. fusion community to make critical decisions on next-step devices and provide the technical capabilities to proceed with such steps, either in the U.S. or through leading roles in international partnerships. Finally, it will provide a unique user facility to train graduate students, postdoctoral personnel, and early-career scientists to be world leaders in their research and to maintain the U.S. at the cutting edge of magnetic fusion energy and plasma science.

This plan is well-aligned with the high-level priorities outlined by the U.S. Department of Energy Office of Science, Fusion Energy Sciences, described in “A Ten-Year Perspective (2015-2025)” and various community workshop reports in 2015. That document highlighted five areas of critical importance for the U.S. fusion energy sciences enterprise over the next decade:

1. Massively parallel computing with the goal of validated whole-fusion-device modeling will enable a transformation in predictive power, which is required to minimize risk in future fusion energy development steps.
2. Materials science as it relates to plasma and fusion sciences will provide the scientific foundations for greatly improved plasma confinement and heat exhaust.
3. Research in the prediction and control of transient events that can be deleterious to toroidal fusion plasma confinement will provide greater confidence in machine designs and operation with stable plasmas.
4. Continued stewardship of discovery in plasma science that is not expressly driven by the energy goal will address frontier science issues underpinning great mysteries of the visible universe and help attract and retain a new generation of plasma/fusion science leaders.
5. Fusion Energy Sciences (FES) user facilities will be kept world-leading through robust operations support and regular upgrades.

DIII-D research is well aligned with these priorities. The DIII-D team is strongly engaged with theory groups to help deliver validated whole-device modeling tools (#1). The research plan has an emerging and expanding program in materials (#2), and a strong emphasis on transient control (#3). In the past year, DIII-D has expanded its research portfolio to address discovery plasma science research lines (#4), with a 1-week “Frontier Science” experimental campaign conducted in 2017 and another planned in 2018. Finally, the 5-year plan described covering 2019-2024 proposes an aggressive and expansive set of upgrades proposed that will keep the facility at the forefront of fusion research worldwide (#5).

A major strength of the DIII-D program is its international team. Currently the DIII-D team includes carefully fostered partnerships with 106 U.S. and foreign institutions. The tight integration of important contributions from our world-wide team has been an essential ingredient in the success of the DIII-D, as has the closely collaborative research program that has been nurtured and pursued with other fusion facilities across the globe.

## 1.2 MISSION AND STRATEGY

The DIII-D mission is “*To establish the scientific basis for the optimization of the tokamak approach to fusion energy production.*” To this end, DIII-D research is targeted toward innovative solutions aimed at realizing fusion energy and making it more attractive, by pursuing research to achieve a high performance burning plasma, and addressing key challenges to realizing steady-state fusion energy. DIII-D research is performed with a commitment to excellent science and rigorous scientific principles, employing a close coupling between experimental and theoretical

programs to ensure the most efficient and expeditious development of techniques, technologies and predictive understanding for future devices. Hence, while the choice of science pursued on DIII-D is dictated by a focus on energy development, the primary measure of success is the excellence of the science and the degree to which fundamental challenges are resolved. In concert with this mission, DIII-D is maintained as a world-class user facility for the U.S. Department of Energy Office of Science (the only such single-site facility hosted outside a national laboratory) through targeted upgrades to access new physics, an extensive maintenance and refurbishment program, and a highly capable scientific and operations team.

Worldwide, fusion research is shifting emphasis to fusion energy through and beyond ITER, exploring how to enable ITER to deliver successfully on its burning-plasma mission and how to translate burning plasmas to continuously operating steady-state conditions required for a cost-effective fusion power plant. Necessary work remains to prepare for ITER's physics program and to develop the scientific tools required to understand behavior and inform how to improve performance. A number of potential next-step device concepts have emerged (ARIES-Advanced and Conservative Tokamak (-ACT1) and (-ACT2) [Kessel 2015], CFETR [Wan 2014], European-DEMO [Romanelli 2012], Japanese Demonstration Power Station (DEMO) [Tobita 2017], K-DEMO [Kim 2015], affordable, robust compact (ARC) reactor [Sorbom 2015], most with an emphasis on steady-state, based on the aspect ratio  $\sim 3$  tokamak. These devices aim to demonstrate the tokamak's viability as a fusion power plant. However, the technologies and approaches to enable these devices have not yet been fully resolved, motivating research initiatives to develop a viable path. Some of this research is underway, such as research into the high  $\beta$  advanced tokamak scenario and new divertor configurations, novel current drive approaches such as 'helicon' ultra-high harmonic fast wave, or assessment of innovative materials. ITER itself is providing key insights into future reactor design through its own design and fabrication. Other aspects could start soon (such as nuclear irradiation facilities), or might require intermediate-stage devices (for example, a tokamak nuclear science facility), as well as exploitation of existing facilities. One foresees a parallel program to ITER, with results from these steady-state research initiatives combining with critical insights from ITER to provide a robust basis for a commercially attractive fusion power plant.

Understanding plasma behavior and control is thus at the heart of the DIII-D research plan. This plays the key role in setting the scale of the device, its performance, and the interaction with its containment and auxiliary systems. Burning plasma conditions and the large energy fluxes drive processes that define the performance and set limits to what can be achieved in future devices. These processes are complex and happen at a range of scales, from fine-scale instabilities through turbulent eddies to macroscopic structures that can rearrange the configuration entirely. They

depend on the specific mechanisms and channels available to the plasma, and thus their study requires exploration in reactor-relevant conditions and physics regimes, as well as appropriate techniques to probe and measure their behavior. For example:

- Fusion  $\alpha$ 's heat electrons, rather than the ions that are heated in most present devices, which changes the character of turbulent energy transport;
- Steady-state regimes require internal plasma configurations with different magnetic shear and high normalized  $\beta$ , typically with high bootstrap current fraction, altering energetic particle resonances,  $\alpha$  confinement and turbulent transport, as well as accessing new macroscopic instability mechanisms.
- High-performance fusion plasmas require a low collisionality core, but when the plasma exhaust reaches materials, it must be cold enough to avoid erosion – this necessitates innovative divertor solutions in a device that operates continuously.
- Key elements of fusion technology, such as materials or current drive systems, interact with the plasma and require testing in relevant plasma environments with the science of this interaction to be explored.

The DIII-D research program for 2019-2024 emphasizes resolving the essential issues for future burning-plasma fusion facilities ranging from ITER to a Fusion Nuclear Science Facility (FNSF) to an electricity-producing DEMO-class device. The program is oriented across three major areas:

1. *Burning Plasma Core*
2. *Boundary Solutions*
3. *Integration of Core and Boundary*

In the core, research on DIII-D will be targeted toward maximizing the potential of fusion in future devices. This gives a focus to preparing for, and ultimately taking maximum advantage of ITER by resolving critical issues related to baseline operation, and pursuing higher performance solutions that can meet  $Q=10$  on ITER with reduced risk and greater margin. In parallel, research is needed to ensure the viability of steady-state operation on ITER and provide the physics basis to design future steady-state devices and enable them to proceed with confidence. Transient events, either from disruptions or edge-localized modes (ELMs), are a serious concern for future devices due to the possibility of damage to the device, and solutions are urgently needed to deliver robust control of transients in a tokamak, particularly at low edge safety factor ( $q_{95}$ ) and rotation levels where difficulties with these techniques are encountered. Research on DIII-D will address critical issues related to 3D and stability physics, ELM suppression and control techniques, and safe mitigation of disruptions and runaway electrons. Turbulent transport mechanisms are anticipated

to change in burning plasma regimes, and energy confinement is observed to decrease at low rotation and with dominant electron heating. An underlying theme on DIII-D will be to understand the causes for such changes, and to project how to use the available tools in devices like ITER to meet burning-plasma performance requirements or raise performance further. Steady-state fusion poses an even greater challenge, where the plasma must not only self-heat, but ideally also largely sustain its own plasma current, since externally driving current can consume substantial power, potentially driving up device size and the cost to generate fusion power. DIII-D research will explore how to exploit the bootstrap current, while simultaneously developing and evaluating new, efficient off-axis current drive techniques.

In the boundary, DIII-D research will play a major role in developing the scientific basis needed to design a suitable boundary solution for a steady-state reactor, through extensive model validation utilizing state-of-the-art diagnostics. Devices beyond ITER must deal with increasingly higher levels of heat flux and ion fluence. This demands divertors capable of mitigating the plasma exhaust, and materials that can handle the extreme heat and neutron environment. The work will identify the key processes involved in divertor dissipation and resolve the role of drifts and turbulence in divertor dynamics. Advanced divertor development on DIII-D will aim to maximize heat flux dissipation without compromising the required core performance and takes the facility through a series of staged divertor concepts. In parallel, the DIII-D program will have an emphasis on evaluating reactor-relevant materials through research aimed at understanding impurity sourcing, migration and transport, and assessing the compatibility of materials with a high-performance fusion core. Together with research on existing tokamaks and proposed linear facilities, the boundary research described here will form the basis for a national ***Boundary Science Research Program*** to address the key challenges for tokamak power and particle control in a timely and very cost effective manner.

While the core and boundary program are critical areas in their own right, an equally important and significantly expanded emphasis within the DIII-D Program will be the exploration of the physics basis needed for arriving at an ***integrated core-edge solution***. This work explicitly addresses the coupling between the core and boundary through the pedestal, and has at its heart a goal of minimizing the dissipative volume in the boundary to maximize the volume for the fusion core. In many ways, the increase in emphasis on core-edge integration recognizes the progress made to date (and further anticipated in the next five years) in both the core and boundary programs, capitalizes on previous and proposed investments in DIII-D, and represents a critical step in tokamak research directed at realizing fusion energy.

The pedestal plays a vital interface between the core and boundary, and can provide leverage to the overall performance. Research will focus on uncovering the relevant pedestal processes

including turbulent heat transport, rotation physics and impurity transport, and understanding the influence of neutrals. A key aspect of this is developing the basis for optimizing scenarios through manipulation of the pedestal.

With an extensive diagnostic set, operational flexibility and strong connections with other fusion research around the world, DIII-D is an ideal platform for enabling the necessary model validation work to deliver high confidence in an integrated core-edge solution. The coalescing of understanding between the core and boundary research is realized through integrated simulations, including coupled scales and regions of the plasma and utilizing major advances in high-performance computing capability.

The research elements covered within these broad program areas are responsive to the recent FES-sponsored community workshops in 2015. A schematic of the link between the program elements and the pursuit of a predictive understanding for fusion is encapsulated in Fig. 1-1.

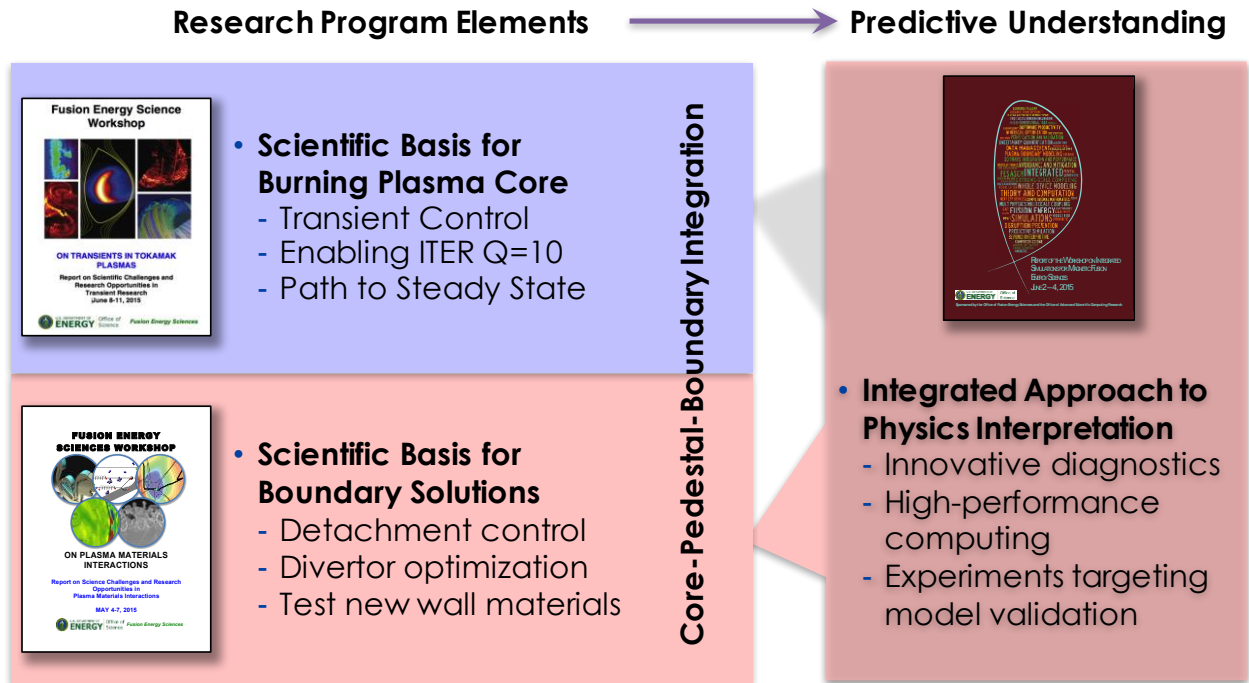


Fig. 1-1. Overview of DIII-D research program elements.

The upgrades described within this plan complement existing capabilities to deliver a highly capable and flexible facility that can address key issues for fusion energy. The proposed upgrades are important to resolving critical issues for fusion. Table 1-1 summarizes the major upgrades proposed for the 2019-2024 five-year plan.

**Table 1-1.**  
**Summary of DIII-D Upgrades**

New Scientific Exploration	Enabled by
Low torque, high beta	2 <sup>nd</sup> co-counter steerable NBI
Electron heated regimes	10 gyrotron system
Reactor current drive schemes	Top-launch EC, Helicon, LHCD
3d spectral flexibility (n=1-4)	New 3d coils and power supplies
Divertor model validation & optimization	Divertor mods and diagnostics
Reactor-relevant materials	New PFCs and tests of materials

### 1.3 ACCOMPLISHMENTS OF THE DIII-D PROGRAM IN THE 2014-2018 PERIOD

DIII-D is at the forefront of work to develop effective and scalable solutions for fusion energy and future reactors. DIII-D research has provided many critical insights (e.g.: shear flow turbulence suppression [Groebner 1990], transport scaling and model validation [Luce 1992, Petty 1995, Candy 2003], Alfvén eigenmodes [Heidbrink 1993], boronization [Jackson 1991]) and pioneered key approaches for ITER (shaping [Osborne 2000], radiative divertor [Leonard 1997], neoclassical tearing mode (NTM) suppression [La Haye 2002], disruption mitigation [Whyte 2002], resonant magnetic perturbation (RMP)-ELM suppression [Evans 2004]). In addition, DIII-D research has been instrumental in establishing the high  $\beta$  potential of the tokamak for steady-state operation (high  $\beta$  with wall stabilization [Strait 1995a], benefits of shaping & profiles [Strait 1995b, Lazarus 1996], kinetic damping [Garofalo 2002, Reimerdes 2011], current drive [Luce 1999, Simonen 1988], bootstrap current [Wade 2004]), and the discovery of exciting new concepts (quiescent H [QH] mode [Burrell 2001], super-H mode [Solomon 2014], neoclassical toroidal viscosity (NTV) rotation [Cole 2011], flux pumping [Petty 2009], and critical gradient phenomena [Hillesheim 2013, Collins 2016]). DIII-D is a highly flexible facility, equipped to access relevant regimes and study many key questions and techniques for fusion energy. Its extensive diagnostic set, strong partnership with national and international collaborators, and deep ties to theory and simulation groups make it an ideal facility to resolve the underlying plasma physics.

The DIII-D research program made significant advances in fusion energy science in the past five years, which motivate the particular research emphases being targeted in the 2019-2024 five-year plan. A few selected highlights from the 2014-2018 period are described below. A more complete history and summary of DIII-D’s accomplishments is given in Section 11.

**ELM control:** DIII-D pioneered ELM suppression using RMPs and provided the main basis for the ELM control coils on ITER. New insights into the physics of RMP ELM suppression have been obtained providing increased confidence in projecting to ITER. Measurements have revealed that ELM suppression is correlated with the magnitude of the plasma response driven on the high-field side (HFS) at low  $q_{95}$  on DIII-D, typical of ITER baseline conditions. The measured edge HFS response is found to be inversely proportional to the pedestal collisionality, but with no dependence on  $\beta_N$ , as would be expected for a current-driven kink mode [Paz Soldan 2016]. This is in contrast to the pressure-driven kink that depends on  $\beta_N$  and is observed on the low-field side (LFS). An emerging scientific picture to describe ELM suppression by RMP fields is that the expansion of the pedestal radially inward is halted by penetration of the field when the electron perpendicular drift velocity is low. This has been supported by measurements in L-mode plasmas showing island formation at the  $q = 2$  surface from an applied field is easiest when the perpendicular electron velocity (as inferred using radial force balance, with ion measurements from charge exchange recombination spectroscopy and Thomson scattering measurements of the electrons) is near zero [Shafer 2017]. ELM-stable operating modes, such as QH-mode have been developed with ITER levels of performance on DIII-D [Garofalo 2015, Solomon 2015]. In QH-mode, the transport usually associated with ELMs is instead driven by an edge harmonic oscillation (EHO) that limits the pedestal to just below the peeling-ballooning stability limit. New modeling of a low- $n$  EHO with the 3D resistive MHD code M3D-C1 finds a linear Eigenmode structure that shows good agreement with the experimental characteristics from magnetics and internal fluctuation diagnostics (Fig. 1-2), and confirms the importance of rotation shear in destabilizing the low- $n$  EHO [Chen 2017].

**Disruptions:** DIII-D has tested both Massive Gas Injection (MGI) and Shattered Pellet Injection (SPI) to safely radiate the plasma's energy, and ITER has selected SPI for its Disruption Mitigation System based on DIII-D's unique experience with both techniques. DIII-D SPI experiments have demonstrated thermal and current quench times that scale to values required for ITER. Relative to massive gas injection (MGI), SPI has shown improved assimilation of the injected impurity species [Commaux 2016]. Experiments using a mixed species SPI technique show how the disruption properties can be tuned to optimize the trade-off in the radiation

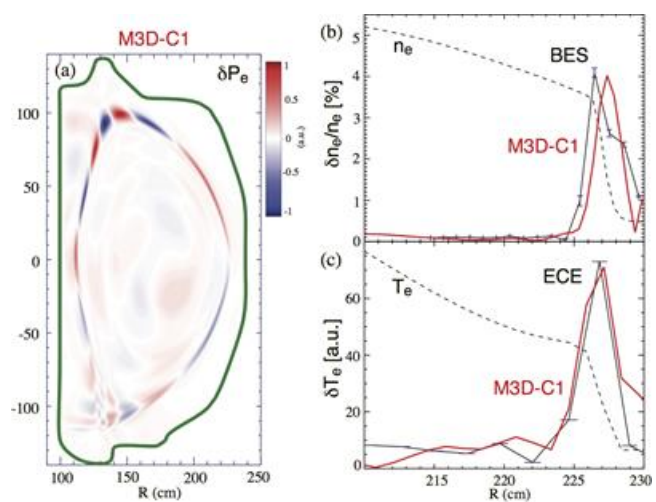


Fig. 1-2. M3D-C1 simulations of an EHO.

fraction and the current quench time [Shiraki 2016]. A novel Gamma Ray Imaging diagnostic was developed by GA, providing energy-resolved measurements during controlled dissipation studies in quiescent runaway experiments. Different growth and dissipation rates were found at different energies, revealing anomalous dissipation occurs at low energies [Paz-Soldan 2014].

**Divertors and detachment:** The Divertor Thomson Scattering (DTS) diagnostic has been used to show that drifts are responsible for in-out asymmetries and shifts in the radial profiles in the divertor leg, a result that is directly illustrated through the reversal of the toroidal field and associated  $E \times B$  drifts. The measured temperature and density asymmetries have been reproduced with the UEDGE code in H-mode discharges and point to the interplay between radial and poloidal  $E \times B$  drifts, where poloidal drifts are responsible for the strong in-out asymmetries in H-mode (Fig. 1-3), while radial drifts shift the density profile [Mclean 2017].

A persistent “radiation shortfall” has been found when performing divertor modeling, in both L- and H-mode deuterium plasmas. This radiation shortfall can be largely eliminated in helium plasma by taking a new approach to modeling the divertor, matching the DTS-measured density near the X-point as a constraint [Canik 2017]. However, in order to produce a well-matched divertor,  $\approx 50\%$  higher upstream density than is measured was needed in the modeling. This suggests that parallel transport may play an important role in the radiation shortfall when upstream data are used to constrain the models, and suggests that the models may be missing contributions to the total scrape-off-layer (SOL) pressure balance. Initial experiments were performed with a modified upper divertor featuring a novel “small angle slot” (SAS) geometry and have confirmed some key trends predicted by the original modeling study using SOLPS [Guo 2017].

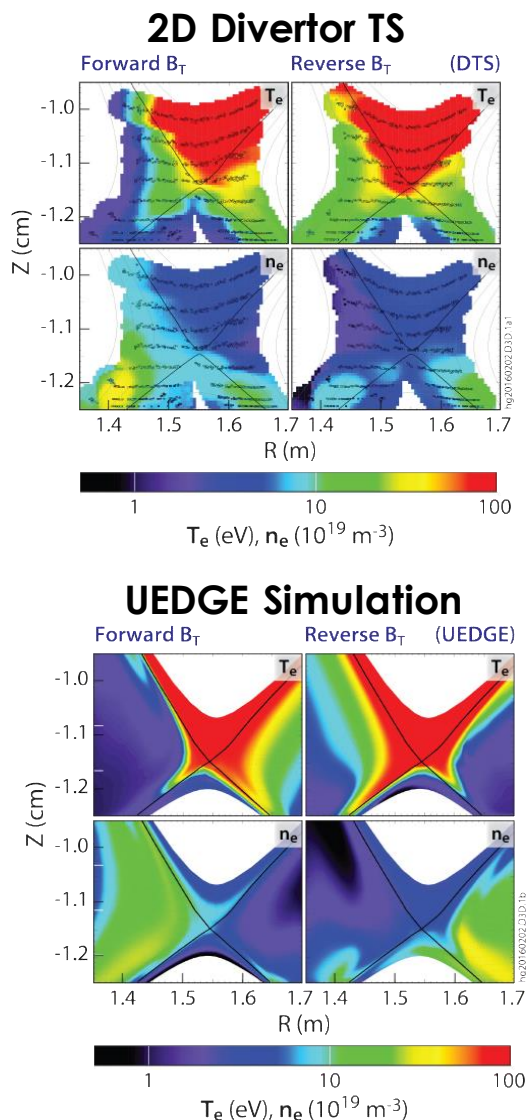


Fig. 1-3. Comparison of measured 2D density and temperature with

**Burning plasma physics:** A key uncertainty for projecting scenarios to future devices is the rotation, which can impact both confinement and stability. Because future large-scale devices are expected to rotate relatively more slowly from beam-injected torque than present-day tokamaks due to the rapid increase in moment-of-inertia with machine size, the intrinsic drive of rotation may play an important role. Dimensionless scaling experiments have suggested a more favorable  $\rho^*$  scaling of the intrinsic torque than expected from theoretical arguments, and joint experiments with Joint European Torus (JET) and Axially Symmetric Divertor Experiment (ASDEX)-Upgrade have confirmed this scaling [Chrystal 2016]. The ITER Baseline Scenario (IBS) on DIII-D is typically challenged by low- $n$  tearing modes, and at low torque, there is a strong tendency for  $m/n = 2/1$  tearing modes to slow and lock, often resulting in disruption. At low torque and low rotation, the pedestal is typically found to be higher than in the standard co-neutral beam injection (NBI) IBS, resulting in a modification to the bootstrap current and change in the overall current density profile shape. As a result, lower-torque plasmas tend to be characterized by a current profile that is more ‘hollow’ in the vicinity of the  $q = 2$  surface. This knowledge has been used to tailor the startup of IBS discharges, resulting in stable discharges with appropriate performance down to zero torque [Turco 2017].

A self-consistent coupling of core and pedestal theoretical models has enabled global predictions of plasma performance to be made, without any free or fit parameters. trapped gyro-Landau fluid (TGLF) is used for the turbulent transport model in the core, NEO is used for neoclassical transport, and EPED provides the pedestal parameters that provide the ‘boundary conditions’ to the core transport models. In a large database of 200 discharges, this coupled modeling predicts the observed  $\beta_N$  to within 15%. Applied to ITER, paths to optimizing fusion gain up to  $Q = 12$  have been found [Meneghini 2017]. A new exciting frontier is now being explored with large multi-scale simulations [Holland 2017] that will lead to further improvements in the transport models and a better treatment of the balance of electron and ion transport.

**Steady-state:** Significant advances have been made in developing steady-state solutions for future fusion reactors. Experiments have established the steady-state hybrid as a potentially attractive scenario, with simultaneous high  $\beta_N \approx 3.7$  and high confinement  $H_{98} \approx 1.6$  achieved with zero loop voltage in a double null shape [Turco 2015]. More recently, complete ELM suppression was achieved in steady-state hybrid plasmas using an ITER similar shape at  $\beta_N \approx 3$  using odd parity  $n = 3$  fields with only modest impact on performance ( $\approx 5\%$  reduction in  $H_{98}$  and  $\approx 10\%$  in pedestal pressure). Unlike at lower  $q_{95}$  for the IBS, ELM suppression is achieved over a wide range in  $q_{95}$  ( $5.9 < q_{95} < 7.0$ ) in the steady-state hybrid (Fig. 1-4). Separately, a high bootstrap fraction, high  $\beta_P \sim 4$  scenario has been developed in partnership with the Experimental Advanced Superconducting Tokamak (EAST) [Garofalo 2015b], with a large radius internal transport barrier (ITB) operating

fully non-inductively at  $q_{95} \approx 12$  and maintaining good confinement and stability even at reduced torque.

In high- $q_{\min}$  plasmas, increased fast ion transport has been observed, which is now understood to be the result of multiple unstable Alfvén Eigenmodes that can lead to ‘stiff’ fast ion transport above a critical gradient [Collins 2016]. The rapid increase in fast ion transport observed with increasing power is well correlated with the degree of stochasticity of the fast ion orbits resulting from the overlapping modes. Poor fast ion confinement is calculated to be a consequence of an undesirable alignment between the fast ion pressure gradient and  $q_{\min}$ , and both simulations and experiments show that moving  $q_{\min}$  to larger radius, where the fast ion pressure gradient is less steep, can effectively mitigate the anomalous fast ion transport.

**Pedestal Physics:** A major success story in understanding the pedestal has been the development of the EPED model [Snyder 2012]. EPED takes scalar inputs of various quantities and calculates the pedestal height as a function of the pedestal width for which kinetic ballooning modes (or KBMs) go unstable, and similarly for peeling ballooning modes. The intersection of these two resulting curves gives the EPED solution. EPED has been validated on multiple devices and is typically found to predict the pedestal height to within about 20%. Various techniques have been utilized to optimize the pedestal performance. Lithium injection is found to result in a pedestal bifurcation with enhanced electron pedestal pressures and twice the pedestal widths. Wide pedestals are also achieved in plasmas with a broadband form of edge turbulence that enables QH-mode at low torque.

A new regime of high performance, dubbed ‘super-H mode’ [Solomon 2014, Snyder 2015] with double the pedestal height at a given density over the usual H-mode pedestal has been discovered (Fig. 1-5). EPED predicts that, with strong shaping, the pedestal solution splits above a critical density, into standard H-mode and higher performance Super H-mode regimes, due to improved pedestal stability between peeling-kink and ballooning branches of stability, amplified by the effects of the kinetic ballooning mode (KBM) constraint on the pressure gradient. More

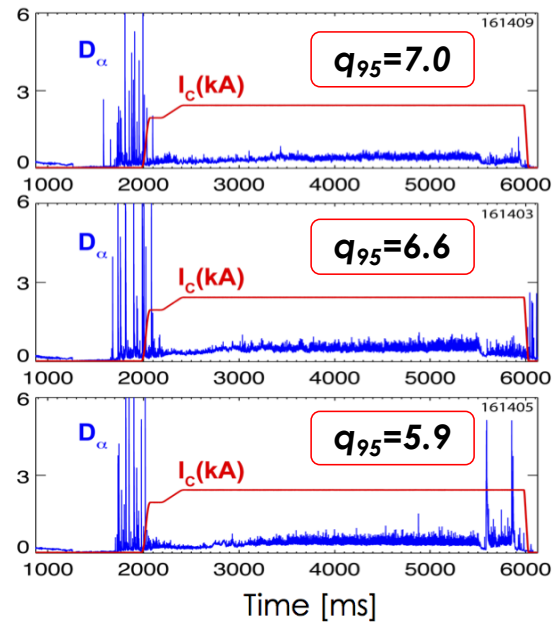


Fig. 1-4. Demonstration of ELM suppression in steady-state hybrid plasma.

recent Super H-mode experiments on DIII-D have achieved comparable or higher levels of absolute fusion performance ( $nT\tau$ ) with less plasma current and smaller volume.

The DIII-D results have had a large impact on the direction of international magnetic fusion research and progress toward fusion energy, and have influenced the designs of several presently operating tokamaks, including the Mega-Ampere Spherical Tokamak (MAST), the National Spherical Torus Experiment Upgrade (NSTX-U), the Korean Superconducting Tokamak Advanced Research (KSTAR), and China’s Experimental Advanced Superconducting Tokamak (EAST), as well as the design of ITER. This success has been driven by the essential contributions from a wide range of collaborative partners from around the world.

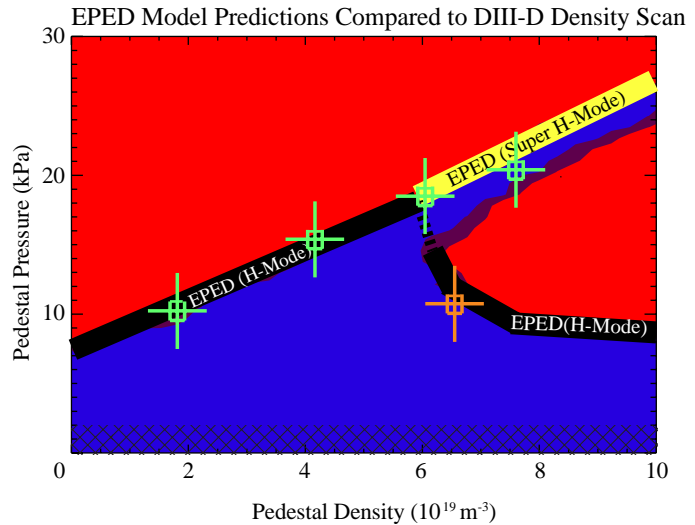


Fig. 1-5. Access to high-pedestal Super H-mode.

#### 1.4 DIII-D RESEARCH PLAN ADDRESSING THE NEEDS OF FUSION ENERGY

A detailed description of the scientific research plan to be conducted in the 2019-2024 five-year period is provided in Sections 2, 3 and 4. Briefly, the research is organized into six areas of emphasis, aimed at resolving critical issues for ITER operation and laying the foundational work for establishing the viability of a steady-state fusion reactor. These areas of emphasis are:

- Resolve the transients challenge
- Understand how to raise burning plasma performance through improved pedestal and core transport
- Establish the viability of steady-state fusion performance
- Discover the principles of an improved divertor solution
- Evaluate material properties for next-step devices
- Develop the physics basis for an integrated core-edge solution

The research draws heavily on the operational flexibility of the DIII-D facility, the proposed upgrades in the 2019-2024 five-year period, and the breadth of experience that constitutes the DIII-D team. A summary of the research is further described below.

***Resolve the transients challenge.*** The potential for damage to internal components in future devices due to transient events, either from disruptions or the repetitive bursts of energy and particles from edge localized modes (ELMs), is well known. As such, transient control is an explicit requirement for operating scenarios in future reactors. In general, DIII-D’s extensive diagnostic capability, coupled with its low risk of component damage from transients, make it ideally suited to developing the physics understanding and relevant techniques needed for transient control.

In disruption research, the DIII-D program has played a critical role in the development of mitigation tools for ITER (e.g., shattered pellet injection [SPI]), and future work will investigate methods for optimizing SPI performance, and extrapolation of the technique will become more robust as a result of collaborations planned with JET. In addition, more effective disruption mitigation techniques will be developed, including so-called “inside-out” mitigation based on shell pellet dust injection. New tools to measure the spatial and energy distribution of the runaway electron (RE) population will be exploited to understand runaway seed formation and dissipation, and future research will examine the role of islands in RE confinement and the impact of 3D perturbations.

In order to prevent disruptions, research is planned in the areas of multi-mode tearing mode control, real-time stability predictions and active resistive wall mode control and 3D fields. An overarching challenge is to maintain stability in burning plasma relevant conditions of low rotation and low collisionality at moderate to low  $q_{95}$ . More details on disruption mitigation and disruption avoidance can be found in sections 2.2.1 and 2.2.2 respectively.

Techniques for eliminating ELMs (e.g., in ELM-stable scenarios such as Quiescent H-mode), suppressing ELMs (e.g., using Resonant Magnetic Perturbations [RMPs]) or controlling ELMs (e.g., through pellet pacing) have been developed on DIII-D. Significant advances in the physics basis for all of these techniques have been realized, particularly in the past five years; nonetheless, key uncertainties remain, and research is directed to delivering high confidence in the extrapolation of these techniques. Future emphasis will be on model validation and stress-testing over a wide operating space, including higher toroidal mode number ( $n \leq 6$ ) and increased harmonic understanding, enabled by new internal coils. The combination of new understanding and capability will be used to extend ELM control solutions to low rotation where application of these techniques has been challenging due to a combination of instabilities and difficulties meeting the required conditions. In addition, multi-scale physics models will be developed that capture the 3D structure of pellet ablation and ELM heat loads and provide predictive understanding of the non-linear evolution of ELM-controlled regimes. The strengthened physics basis obtained through this research will be applied to manipulate the pedestal through shaping, heating, and new 3D

capabilities to expand the operational limits. Further details on ELM control are provided in Section 4.1.1. An overall timeline for transient-related research is shown in Fig. 1-6.

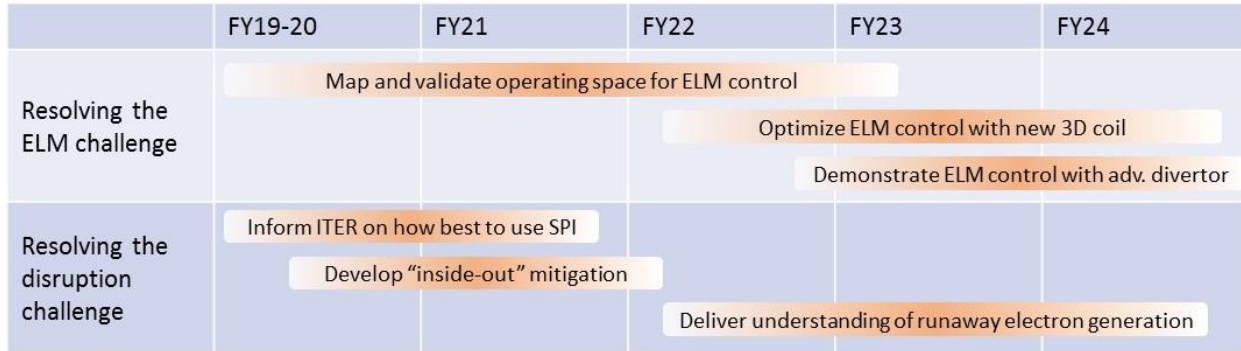


Fig. 1-6. Timeline for transients research

**Understand how to raise burning plasma performance through improved pedestal and core transport.** Burning plasma conditions, where the alpha particles provide the majority of heating to the plasma, will be an exciting new regime and represent the next major milestone in fusion development. The ability to rapidly deliver on ITER’s mission of achieving 500 MW of fusion power with a fusion gain of  $Q=10$  will, in large part, depend on successfully projecting and adapting experience from today’s tokamaks to burning plasma conditions. This, in turn, is a function of the predictive understanding developed on today’s fusion devices.

A key objective for the 2019-2024 five-year plan is to understand how to access high performance in burning plasma conditions. Here critical enhancements to DIII-D will provide access to fusion relevant conditions such as dominant electron heating (with more than a doubling of electron heating power) and low rotation (more than doubling the torque-free heating). Strong emphasis is placed in the 2019-2024 five-year plan on transport model validation and predict-first methods. DIII-D is well positioned to conduct this research, with an extensive fluctuation, energetic particle, and profile diagnostic set, as well as access to state-of-the-art modeling capabilities. While model validation has previously been specialized in terms of the plasmas that provided optimal targets for diagnosis, in recent years, activities have extended toward more reactor-relevant conditions, including lower  $q_{95} \sim 3$  and low rotation, as might be expected in an ITER baseline  $Q=10$  scenario. Even still, significant uncertainty remains in the models, including deficiencies in details of the transport models to reproduce temperature gradients in high-performance plasmas, while a new frontier of understanding is emerging relating to controlling multi-scale turbulence in low-torque plasmas. New possibilities for increasing performance through manipulation of the pedestal are also developing, which can have strong leverage on the fusion power [Kinsey 2011] and might lead to ways to significantly exceed  $Q=10$  performance on ITER [Solomon 2016].

Other transport channels, including momentum, particle, and impurity transport, are significantly less validated, but have equally large consequences on performance, and will have an increasing emphasis in the next 2019-2024 five-year period. For example, accurate rotation prediction including its shear, resulting from intrinsic torques, external momentum input, and 3D fields (neoclassical toroidal viscosity, NTV), is needed for assessing the impact on stability in future devices, and impurity transport is key to determining if and how high-Z material from the divertor contaminates the core. Understanding in all of these transport channels will be utilized to improve performance.

Great strides have also recently been made in energetic particle transport studies, with comprehensive and reduced models accurately reproducing fast ion transport. Research will investigate the interaction of fast ions with 3D fields (anticipated to be needed as part of a comprehensive ELM control strategy) and sensitivity to the current profile to develop a predictive understanding of fast ion transport. It will utilize new capabilities, including variable beam perveance and increased EC heating to reduce susceptibility to energetic particle-driven instabilities and improve discharge performance. Further details on burning plasma research can be found in Section 2.3.

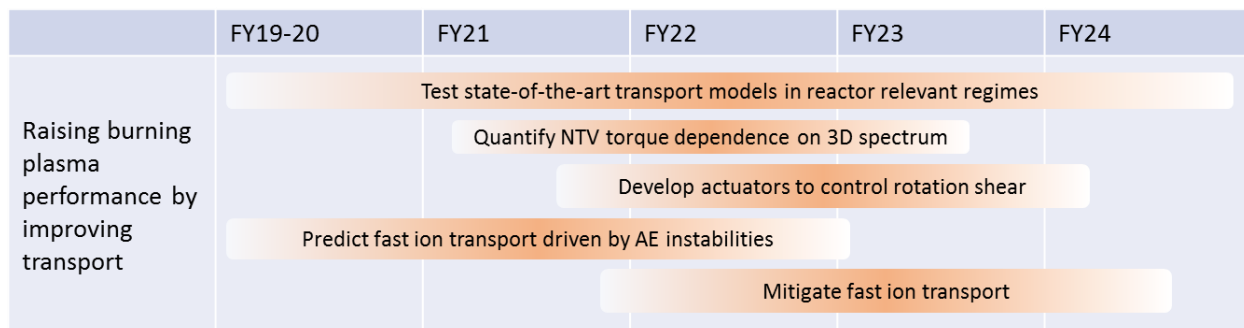


Fig. 1-7. Timeline for burning plasma physics research.

**Establish the viability of steady-state fusion performance.** The mission of the DIII-D program is the optimization of the tokamak for fusion energy, which in practice implies high beta steady-state due to the increased fraction of the current that can be driven by the bootstrap effect.

DIII-D research is aimed toward producing plasmas that are fully non-inductive for longer than a current relaxation time at reactor-relevant levels of beta. In the 2014-2018 period, long stationary steady-state discharges at high beta were demonstrated for the steady-state hybrid regime. New capabilities anticipated at the end of a long machine vent in 2018-2019, specifically a re-orientation of a neutral beam line to deliver eight co-sources, up to four of which will be off-axis, together with progressively increasing ECH power, will allow exploration of  $\beta_N \sim 5$  in the  $q_{min} > 2$  scenario, as envisioned for the ARIES-ACT1 DEMO. A key component of the work is to identify the design and performance advantages of differences in the current profile, shape, collisionality, and beta,

as well as understanding how close one can approach the ideal wall stability limit, and developing techniques and understanding to control other limiting instabilities (e.g., tearing modes and Alfvén Eigenmodes).

An outstanding issue to resolve for a steady-state reactor is how to provide external current drive for q-profile control without adding large amounts of recirculating power. The DIII-D research plan aggressively confronts this issue with a test of three new current-drive techniques: 1) helicon current drive; 2) top-launch electron cyclotron current drive (ECCD); and 3) high-field-side lower hybrid current drive. In addition, the steady-state work extends the challenges of fusion to higher beta and to regimes of high bootstrap fraction, which provides new opportunities for transport understanding and optimization, transient control, and modification to fast ion instabilities. Toward the end of the five-year period, a second steerable co-counter neutral beam line will become available, allowing investigation of high beta steady-state scenarios at very low torque. This is a significant enhancement and builds on the already successful utilization of the first counter beamline in exploring ITER baseline regimes at low torque. More details on current-drive research can be found in Section 2.3.4.

Recognizing the importance of evolving new long-pulse capabilities globally, a key component of the DIII-D research plan involves close partnerships with international research groups, including EAST, KSTAR, and Japan Torus (JT)-60SA (see Section 9). These partnerships have been carefully developed and fostered, particularly over the last several years, to leverage the understanding developed at DIII-D to accelerate fusion energy development on these new superconducting long-pulse facilities as their capabilities and performance begin to develop. A timeline for steady-state related research is shown in Fig. 1-8. Section 2.1.2 contains a more comprehensive description of the DIII-D steady-state research plan.

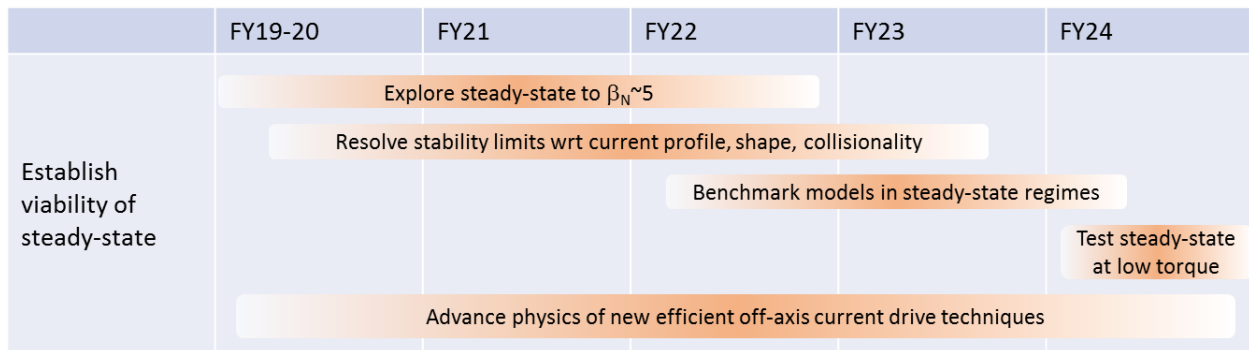


Fig. 1-8. Timeline for steady-state scenario research.

**Discover the principles of an improved divertor solution.** The high-power output from the core of future next-step devices places extremely high demands on the requirement to dissipate the heat flux before reaching the plasma-facing components (PFCs). Validation of models of the

boundary plasma, such as SOLPS and UEDGE, is required to design advanced divertor configurations and qualify plasma-facing materials for reactor conditions that are not directly achievable in today's devices. In some ways, the need for model validation in the boundary is made more critical due to the difficulty in simultaneously achieving the conditions for a high-performance core and a relevant boundary plasma without moving to the reactor scale.

Therefore, research in the 2019-2024 five-year plan focuses on quantifying the physics processes that govern dissipation of the divertor heat flux and parallel momentum, parallel flows, and cross-field drifts in divertor and SOL and turbulent transport mechanisms, described in more detail in Section 3.1. To accomplish this research, key upgrades are planned to DIII-D's already extensive boundary diagnostic set, including new ultraviolet (UV) emission measurements, divertor Thomson improvements, neutral measurements, ion temperature measurements in the SOL, and new bolometry measurements. In addition, planned changes in divertor configurations provide stringent tests for validating boundary simulation codes.

A divertor solution is needed that is compatible with a high-performance fusion core. In particular, it is expected that a divertor will need to maintain the target heat load to an acceptable level (typically  $< 10 \text{ MW/m}^2$ ) with a cold plasma temperature of order a few eV, without forcing an unacceptably high density in the core that compromises performance or any required auxiliary current drive. Although various methods have been developed to reduce the peak heat flux, these have not been adequately demonstrated with high-performance fusion plasmas, and, consequently, considerable uncertainty remains in the extrapolation of these techniques to reactor-class devices. Moreover, while closure has been shown to improve the trapping of neutral particles to the divertor, a robust solution for keeping the temperature low in the entire divertor remains an outstanding challenge. New geometries such as the small-angle-slot (SAS), developed using state-of-the-art boundary codes, appear to offer a promising solution, and the development and evaluation of this geometry is a major emphasis in the 2019-2024 five-year plan. Research also focuses on effectively utilizing the magnetic geometry to make optimal use of the divertor volume through poloidal flux expansion and novel magnetic topologies. Further details on the research plan for divertor development can be found in Section 3.2. A timeline for divertor research activities is shown in Fig. 1-9.

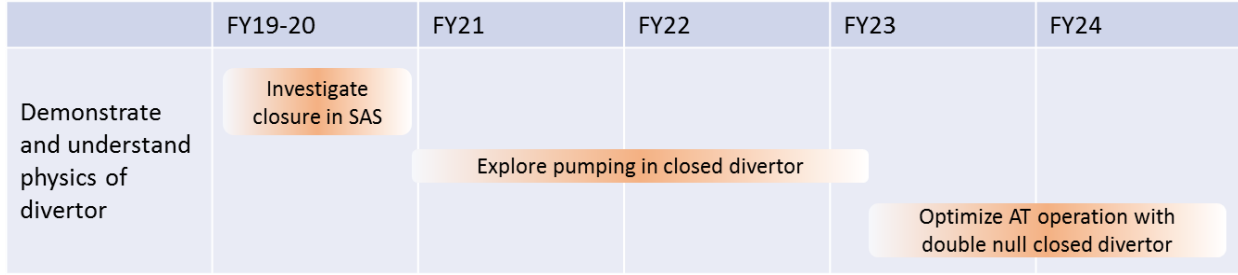


Fig. 1-9. Timeline for divertor research.

**Evaluate material properties for next step devices.** A major outstanding challenge to the realization of fusion energy is a resolution of the interaction between the boundary plasma and the plasma-facing components. Numerous issues exist requiring new plasma materials interaction (PMI) solutions for fusion to take the next step, owing to the huge demands imposed by the power and particle exhaust that push material limits. While low-Z materials are favorable for core performance, tritium retention properties push materials to higher-Z. Hence, innovations in materials are being sought through advanced manufacturing techniques and new exascale computational capability.

In parallel, significant improvements are needed in our understanding of surface evolution, material migration through erosion and redeposition, and the impact of transport of PFC materials to the plasma core. DIII-D will address high-Z migration through studies enabled by isolated installation of metal ring surfaces in the divertor and other key main wall locations. The staged evolution of the divertor will deliver a clear understanding of the impact of high-Z materials in the divertor on detachment dynamics and core performance in a variety of divertor configurations, ranging from open to optimized slots (SAS).

In addition, the program plan looks to develop approaches for mitigating any deleterious impacts, including the use of techniques such as siliconization and applying heating and current drive to modify transport properties. A new Wall Interaction Tile Station (WITS) with extensive diagnostics is being developed to facilitate this research, which will have sufficient linear motion to enable test materials to come close to the limiting plasma surface. Measuring particle and energy flux on the main chamber wall will be key to improving predictive understanding. The output of this research will help validate and advance predictive PMI models and codes. A timeline of PMI research is shown in Fig. 1-10 and further details on the material program is described in Section 3.3.

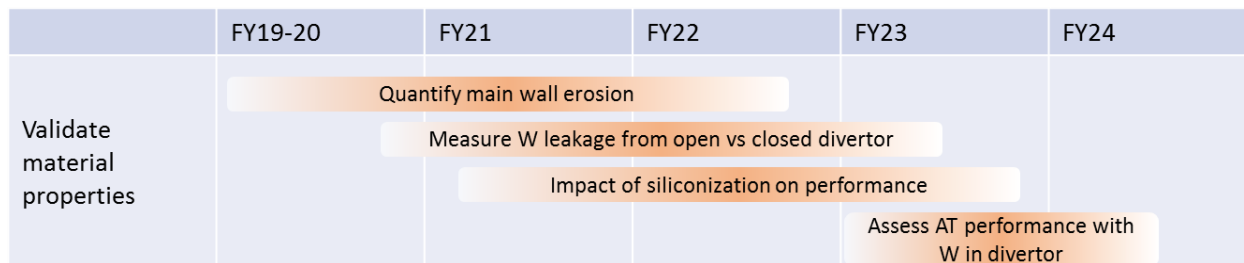


Fig. 1-10. Timeline for PMI research.

**Develop the physics basis for an integrated core-edge solution.** Although the detailed physics of the core and boundary are often best studied in regimes that are optimized for one or the other, an integrated core-edge solution is also critically needed for fusion energy. Indeed, the interaction and constraints between the two regions is what sets the scale of the challenge.

The new capabilities proposed in the 2019-2024 period, coupled with the existing flexibility and capability of DIII-D, make it possible to more vigorously attack core-edge integration in high-performance, steady-state class plasmas, as would be envisioned in a fusion reactor. Fundamental questions to be answered include: the tradeoff between single versus double null; the impact of divertor geometry (baffling and magnetic) on pedestal performance and the impurity “life-cycle” (both from material surfaces and injected for heat flux control); and the ability of both the material surfaces and the core plasma to tolerate ELMs.

Since the pedestal serves as the interfacing layer between the high-performance core and the boundary, research is planned to understand its structure, transport, and stability, as well as knowledge of how to manipulate it to optimize core and boundary performance. The advances in understanding in both the core and the boundary, leveraged against the significant investments in DIII-D in the past and coupled with the upgrades described here, make addressing this long-standing challenge within reach of the fusion community. The core-edge research plan is described in further detail in Section 4.4. A timeline for core-edge related research is summarized in Fig 1-11.

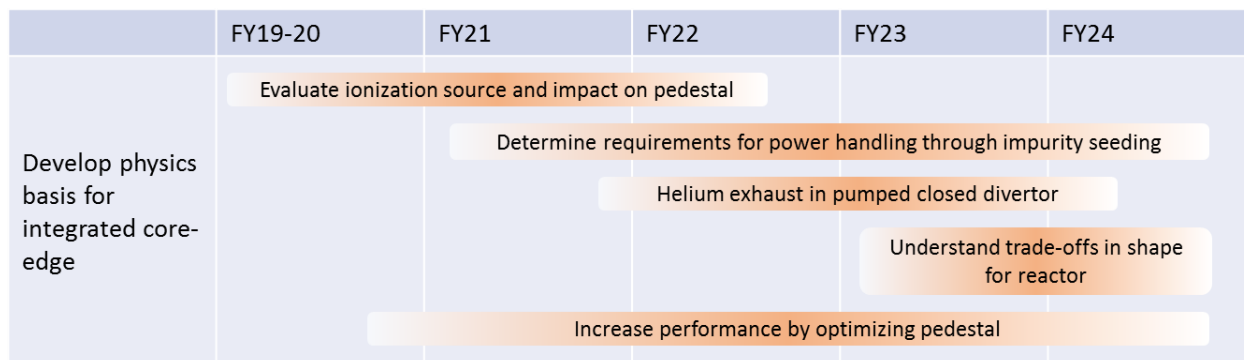


Fig. 1-11. Timeline for core-edge research.

These research elements will place DIII-D and U.S. scientists at the forefront of the world program, enabling U.S. leadership in ITER and developing the technologies to take tokamak-based fusion to steady state. It will lead to a rich diversity of high-impact scientific insights, as well as unique know-how to secure a U.S. stake in future fusion energy development. More specifically, it will enable the U.S. to make decisions on, and have the technical capabilities to proceed with, next-step devices, either in the U.S. or through leading roles in international partnerships.

### 1.5 DIII-D FACILITY CAPABILITIES AND PROPOSED IMPROVEMENTS

From the beginning of the 2019-2024 five-year period, which commences immediately after a major set of enhancements to the facility, DIII-D will be equipped to access new regimes and behaviors, with new research capabilities to explore physics and develop fusion solutions. Key tools available at the start of the plan include enhancements for off-axis current profiles, advanced divertor investigations, and microwave systems. Further enhancements (additional divertor, heating and 3D capabilities) early in the plan will build on these recent enhancements to enable research objectives to be fully investigated. The improvements proposed in the 2019-2024 five-year period will significantly enhance the facility’s capabilities and position DIII-D scientists to develop a physics basis for a fully integrated high-performance solution.

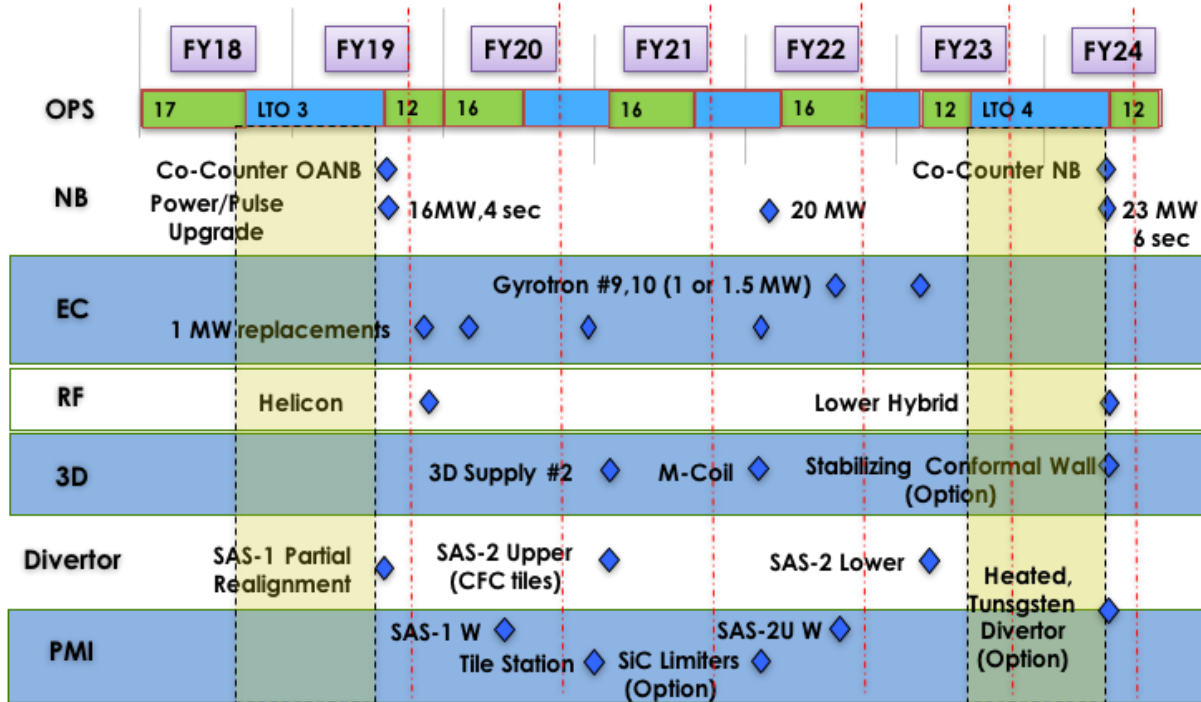


Fig. 1-12. Timeline for major hardware upgrades in DIII-D five-year plan.

Existing capabilities of DIII-D include a highly flexible 2D shaping coil system to produce a wide variety of plasma shapes, flexible heating and current drive systems, three arrays of 3D-field

perturbation coils located both inside and outside the vacuum vessel, multiple disruption quench systems, over 50 state-of-the-art diagnostic systems to examine plasma parameters and fluctuations, and an advanced digital control system for feedback control of the plasma. Recognizing that the long-term success of a research program and its overall productivity is intimately related to new capabilities, major enhancements are proposed in the 2019-2024 five-year period, complementing facility developments made during the past five years, and are described in detail in Section 5.3. The timeline for the upgrades is shown in Fig. 1-12 and includes:

**Electron cyclotron heating (ECH) and current-drive systems.** ECH power on DIII-D will be more than doubled from the present 3.5 MW. A new gyrotron is being commissioned presently that will raise the power to nearly 5 MW and, with two new gyrotrons and a series of replacements, will bring DIII-D to approximately 8.5 MW by the end of the 2019-2024 five-year period. This capitalizes on development of higher power gyrotrons, which reduce the need for high-voltage power supplies, sockets, transmissions lines, and launchers.

The increase in ECH power represents a major advance in DIII-D capabilities, enabling access to torque-free high beta scenarios with significant electron heating, a situation closely mirroring a burning plasma heated primarily by alpha particles. Significant changes in turbulence properties are anticipated in such regimes compared with typical scenarios on present day devices. Moreover, the increased power and number of gyrotrons is important for careful tailoring of the current profile with flexible delivery of current, from on- to off-axis, and for simultaneous control of  $n=1$  and  $n=2$  tearing modes. Recent analysis has shown that the EC current-drive efficiency can be approximately doubled when the power is launched directly above the plasma, and, consequently, so-called “top-launch” ECCD will be tested.

**Neutral beam (NB) heating systems.** Neutral beams have been a workhorse heating system on DIII-D. Coupled with off-axis injection capability and the increased ECH described above, DIII-D is predicted to be able, for the first time, to explore reactor-relevant regimes with high  $\beta_N \sim 5$  and high  $\beta_T$ , sustained for more than a current relaxation time. The 2019-2024 five-year plan will build on the already exceptional flexibility of the DIII-D NB system, which will deliver  $>16$  MW of co-injected power, half of which can be configured off-axis (doubling the present capability for off-axis neutral beam current drive) at the start of the plan. In particular, the program plan calls to increase the total beam power further to 23 MW through a rise in beam voltage and also doubles the net torque-free beam heating with a second steerable co/counter neutral beam line. These improvements to the DIII-D beam system will allow further control of the current profile, optimization of energetic particle confinement, investigation of the impact of rotation on steady-state scenarios, and sustained high  $\beta_N \sim 5$  operation.

**Advanced divertor configurations.** In 2017, a novel new closed-slot divertor geometry utilizing a small target angle dubbed “small angle slot” (SAS) was developed, based on modeling with the SOLPS code. The five-year plan for 2019-2024 continues the development of an advanced divertor through a staged approach that takes an SAS-like configuration and moves it to the main upper divertor, where pumping is incorporated. This will prove an essential step in validating the concept as a viable companion to high-performance operation. This work couples with exploitation of DIII-D magnetic divertor shaping flexibility to establish the basis for a configuration that is better able to detach and isolate the high-density divertor and impurity interactions from the high-performance core. New diagnostics play a central role in this divertor research, with additional pressure gauges, bolometer views, heat flux measurements, Thomson measurements, and multi-species spectroscopy planned.

Based on understanding gained from the upper divertor and further model validation efforts, a second modification is planned for the lower divertor to investigate and optimize the power and particle balance between the upper and lower divertor for Advanced Tokamak (AT) steady-state operation.

**Materials tests** A progressive program of innovative materials testing will be implemented, starting from present divertor material evaluation system (DiMES) and midplane material evaluation system (MiMES) small sample facility, but proceeding with test tiles, rows, and a heated tile facility. A series of dedicated metal ring “mini-campaigns” are planned, following the first successful one performed in 2016, using the new divertor geometries to better understand high-Z sourcing and migration, and evaluate the efficiency of impurity screening provided by the new geometries. As well as determining and optimizing compatibility with traditional high-Z materials, other potentially reactor-relevant materials will be assessed from the perspectives of a more reactor-like boundary for the core, or as new material options for a reactor itself. In addition, a program option is included to evaluate a heated tungsten upper divertor.

**Enhanced 3D field capabilities.** DIII-D has led pioneering research using 3D fields, particularly for control and suppression of ELMs, resistive wall mode (RWM) control, rotation control using neoclassical toroidal viscosity (NTV), and scenario optimization. In the 2019-2024 period, these 3D capabilities will be significantly extended by the addition of a new coil set (M-coil), which will provide 12 additional internal coils along the mid-plane. This will extend DIII-D’s spectral flexibility from  $n \leq 3$  at present to create field configurations spanning  $n=1-6$ , control of the poloidal mode spectrum for  $n=1-3$ , and rigid rotation capability for  $n=1-4$  structures. Sophisticated modeling and analysis that includes the plasma response indicates these new coils will provide the needed capability in terms of accessing the relevant spectra for ELM suppression and NTV optimization. A second “super SPA” power supply, following the successful

implementation and exploitation of the super SPA provided by Institute of Plasma Physics, Chinese Academy of Sciences (ASIPP), will provide much-improved capability to independently control the poloidal spectrum and provide multi-mode error field correction, as well as providing new axisymmetric shaping flexibility.

**New off-axis current-drive technology development.** The DIII-D plan from 2019-2024 features an aggressive program for exploring potentially transformational off-axis current-drive technologies. A key challenge to the ultimate attractiveness of an AT reactor is the amount of recirculating power needed for current profile control, and higher efficiency current drive is needed to alleviate this problem. The proposed research explores three new such technologies: 1) ultra-high frequency helicon current drive [started in the past five years]; 2) top-launch ECCD; and 3) high-field side lower hybrid current drive. The successful demonstration of any or all of these techniques would represent a significant achievement and closing of a gap for a high-performance steady-state reactor, and could represent a potential game changer in device scale and performance.

**Diagnostics.** Building on what is arguably the most comprehensive suite of diagnostics on any fusion device, DIII-D will continue to develop and exploit a wide range of diagnostic techniques in the 2019-2024 five-year plan. Major diagnostic initiatives are planned in the boundary, with a new instrumented tile station (WITS), increased spatial resolution for the Divertor Thomson Scattering system, new divertor  $T_i$  measurements, diagnostics for neutral density and ionization rates, and infrared (IR) camera and thermocouple improvements for heat flux measurements. New 3D magnetics are planned, along with improvements to the tangential Thomson system, a new fast ion loss detector for reverse  $B_T$  (often used for steady-state experiments), motional Stark effect (MSE) upgrades (including an imaging MSE system) and an edge current measurement capability. These new diagnostics were chosen because of their high impact on validating the physics basis for fusion energy. A complete description of the diagnostics being proposed in this plan are described in Section 6, and associated computer systems are detailed in Section 7.

**Enhanced reliability.** In addition to major capability enhancements, the 2019-2024 five-year plan allocates a significant level of resources for major refurbishments and sustaining engineering to ensure safe and reliable operation of the facility and allow optimal exploitation of the facility capabilities. A comprehensive assessment of major system risk and impacts has been conducted for important systems and components. Sustaining engineering activities are proposed in the following systems: gyrotrons (investments are proposed to procure replacements for the four oldest gyrotrons to maintain high availability and successfully deliver the desired increase in power); motor generator power distribution (high-voltage cable replacement is proposed to avoid unanticipated outages or reduction in capability); neutral beam components and power systems;

cryogenic and vacuum systems; power systems; and water systems. These are described in more detail in Section 5.2.

## 1.6 DIII-D FACILITY OPERATIONS

The DIII-D program plan provides, on average, more than 14 weeks of operation annually. The specific number of run weeks in each year are staged to accommodate the proposed upgrades, and vary between 12 and 16 weeks. This level of operation has previously yielded sufficient utilization of the Facility to deliver excellent scientific output and maximize the productivity of the Program while providing sufficient time for maintenance, diagnostic calibration, upgrades, and experimental planning. Toward the end of the 2019-2024 period, another long torus opening is planned to install several major upgrades including the second co-counter steerable neutral beam. This is planned to be similar to the one anticipated in 2018-19 prior to the commencement of the five-year plan covering 2019-2024.

Even with this level of run-time, the DIII-D facility continually operates with a very large research backlog. There is typically a factor of 5-10 reduction in the number of unique experimental ideas proposed at the DIII-D Research Opportunities Forums to the number of experiments that are finally executed in a given year (the experimental planning process is described in more detail in Section 10.2). The proposed schedule is already highly optimized to give the maximum number of run weeks while enabling facility enhancements and refurbishments to proceed as planned. Nonetheless, acknowledging that there is still large additional demand for run time on DIII-D, the program plan contains an option to significantly increase the effective number of run weeks by nearly *doubling the amount of available operations time*.

Doubling the available facility operating time would be achieved by utilizing extended-shift operation of the DIII-D facility. A significant increase in DIII-D staffing would be required to accomplish this; existing scientific and operations staff are insufficient to sustain extended-shift tokamak operation, diagnostic support, and necessary data analysis. In practice, doubling the run-time would require only a 50% increase in the operations and scientific team to deliver on this significant program option. Exercising this option for increased run time could afford the U.S. fusion program many key benefits, including supporting and energizing a significantly expanded user base, further increasing leadership roles for university and lab partners, expanding opportunities for training graduate students and postdocs, new possibilities for diagnostic provision and development, extending fundamental “Frontiers” explorations that could be entirely overseen and managed by the relevant university experts, and acceleration of the schedule for facility enhancements with the additional operations personnel available during maintenance periods.

## 1.7 DIII-D TEAM

The highly capable research and operations personnel that constitute the DIII-D Team provide the foundation for executing the research proposed in the 2019-2024 five-year plan. At its core, the DIII-D Team is a deeply collaborative entity, including experimentalists and theorists from a broad cross section of U.S. national laboratories, universities, and private industry, and attracting strong involvement from the entire world fusion community. Consequently, collaborating institutions and scientific collaborators play significant roles at all levels of the DIII-D program. The DIII-D National Fusion Program presently includes over 600 scientific users from 106 institutions worldwide. The success of the DIII-D research program is closely coupled to the strong engagement of its diverse international team.

The DIII-D Team consists of approximately 90 full-time PhD research scientists on-site, of which more than half are collaborators. The presently active staff of DIII-D includes over 40 Fellows of the American Physical Society (APS) and 17 winners of the APS John Dawson Excellence in Plasma Physics Award (almost all based on research conducted at DIII-D). There were approximately 550 scientific authors on DIII-D papers during the period from 2015-2016. DIII-D researchers come from worldwide locations (see Fig. 1-13).

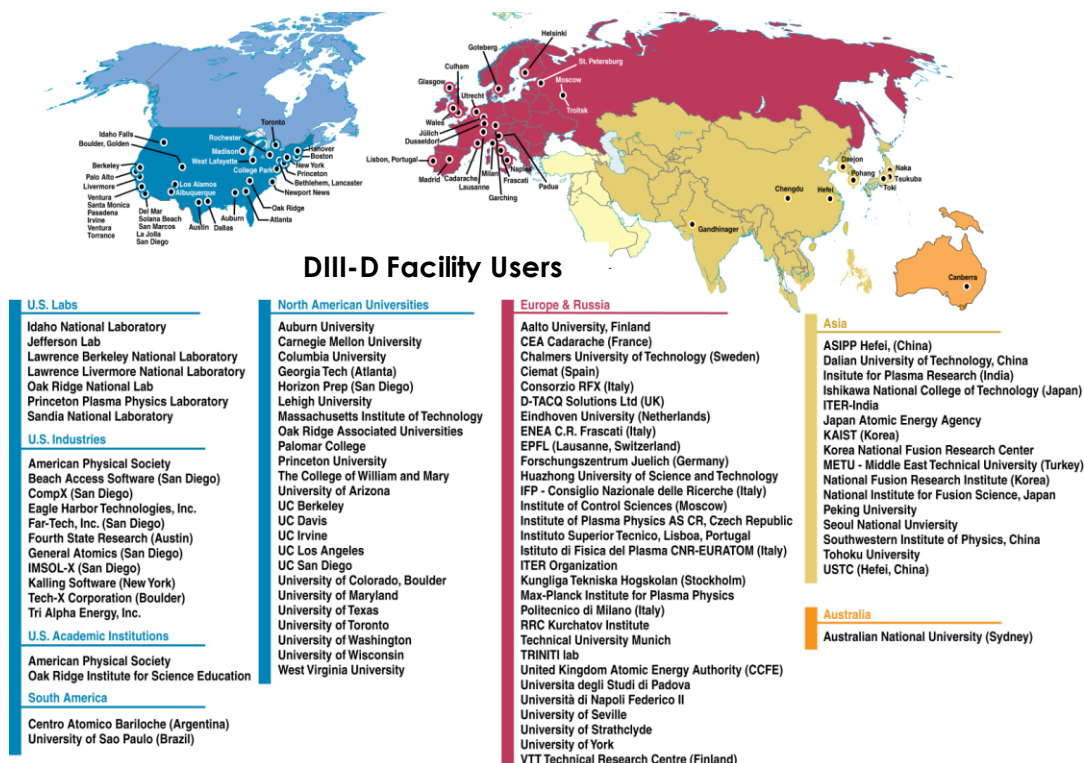


Fig. 1-13. Active collaborations with the DIII-D Program.

Included in the list of DIII-D Facility users are:

- 21 national laboratories [U.S. (7), Europe (8), Korea (3), Japan, India, and Argentina];
- 67 universities (U.S. [28], Europe [18], China [9], Japan [4], Russia [2], Australia, Brazil, Canada, India, Peru, and Turkey); and
- 15 industrial companies (U.S. [13], Europe [2])
- 3 others (ITER Organization, American Physical Society, Oak Ridge Institute for Science Education)

Many scientific users provide direct support to the research program through the development and provision of diagnostics, data analysis and program planning. The DIII-D program benefits from a strong synergy and interaction with both the GA theory group and other theory programs across the U.S. The DIII-D facility user database includes 80 graduate students and 71 postdocs. In the second quarter in FY17, 24 graduate students and 35 postdocs conducted the bulk of their research on site as an integral part of the DIII-D program. A more detailed description of the DIII-D team is presented in Section 8.

While the DIII-D program is hosted and operated by General Atomics for the DOE-FES, the management and program leadership is drawn from the broader DIII-D team through an effective and inclusive system of governance. In addition to GA, there are eleven major collaborating institutions that have broad programmatic responsibilities on multiple topics. Major collaborating institutions join with GA to form the DIII-D Executive Committee (DEC) to guide the program’s strategic and near-term directions. The DEC generally meets quarterly to advise the DIII-D Director on a broad range of programmatic issues including program planning, direction, budgets, and institutional issues. The DIII-D Program Advisory Committee (PAC) is composed of both national and international leaders and experts in fusion who are not directly involved in the DIII-D Program. The PAC provides advice annually on the program plans and other major programmatic issues. The DIII-D Research Council (RC) is a small multi-institutional advisory group with rotating membership selected from the DIII-D team. The RC provides specific advice on the annual experimental plan and relative priority of experimental efforts within that plan. After major research emphases are chosen, experimental proposals are solicited from the entire International DIII-D Team at the Research Opportunities Forum. These proposals are discussed and further developed and prioritized in open meetings. Group leaders present final research plans to the DIII-D RC, and the DIII-D RC provides advice on the program balance for the year. More details are provided in Section 10.

## 1.8 NATIONAL AND INTERNATIONAL LEADERSHIP

In addition to the scientific leadership that the DIII-D Program will provide through execution of this program plan, the DIII-D Program will play a key role of leadership and outreach to other U.S. and international groups including:

- Strong and active participation in coordinating international collaborations that leverage U.S. capabilities through the International Tokamak Physics Activity (ITPA) and International Energy Agency (IEA) Cooperative Tokamak Program implementing agreement.
- Promoting and stimulating theory/model development and validation with the broader theory community through strong alliances with the U.S. Transport Task Force (TTF), Edge Coordinating Committee (ECC), the Scientific Discovery through Advanced Computing (SciDAC) and Simulation Center for Runaway Electron Avoidance and Mitigation (SCREAM) theory efforts, and university theory groups across the U.S.
- Strengthening the role of universities in the U.S. fusion science program by increasing opportunities for graduate students and university research personnel.
- Active participation and leadership of the U.S. Burning Plasma Organization (a separate description of this activity is provided in Volume III).
- Continued active role in evaluating and promoting new initiatives for the U.S. program.
- Participation in developing enabling technologies critical to the success of fusion energy.
- Outreach to the broader science community, communicating the excitement and progress of fusion energy science, making available data from well-diagnosed high-temperature plasmas and making the DIII-D facility available for non-fusion research, as appropriate.

## 1.9 BENEFITS AND IMPACT OF RESEARCH

DIII-D has a demonstrated history of delivering significant impact to the worldwide fusion energy endeavor, with essential contributions to the ITER project and providing fundamental scientific discovery in plasma and atomic physics processes. The research contained in the 2019-2024 proposal will enable FES to continue to reap the significant benefits associated with its major tokamak facility, ensure U.S. leadership in fusion energy research is maintained and extended, and position the U.S. to be ready to capitalize on ITER operation. In particular, there is a close alignment of the DIII-D research activities with the high-priority areas of critical importance to FES strategic goals in realizing fusion energy. The upgrades proposed during the 2019-2024 five-year period will keep DIII-D at the forefront of fusion energy research, delivering a world-class capable facility uniquely equipped with operational flexibility, outstanding diagnostic capabilities, and a world-renowned scientific team. Coupled with expanding international collaboration and outreach to the broader scientific community, the DIII-D Program will provide a compelling

scientific opportunity for U.S. researchers and a vibrant training ground for the next generation of fusion innovators.

**Enabling the success of ITER.** During the 2019-2024 period, DIII-D will contribute critical results to ensure ITER can advance rapidly to achieving its performance missions and allow the U.S. to maximally capitalize on the ITER research program. A well-founded physics basis will be developed to:

- Confidently meet the performance requirements of ITER ( $Q=10$ , 500 MW fusion power and  $Q=5$  steady-state) through demonstration in relevant regimes on DIII-D and the development of validated predictive integrated models;
- Ensure the achievement of optimal, robust and reliable ELM control on ITER without compromising performance requirements;
- Meet the requirements for disruption mitigation to avoid damage to ITER resulting from localized thermal loads or runaway electron generation;
- Reliably avoid disruptions through fundamental advances in stability physics and 3D effects, encapsulated into real-time stability predictions and integrated control;
- Fully exploit ITER capabilities to get the most out of the facility.

**Leveraging international collaborations.** DIII-D is well positioned to ensure the U.S. fusion program can realize benefits associated from fusion programs across the world, including access to unique experimental capabilities overseas, owing to its existing and growing international partnerships. Research in the 2019-2024 five-year plan benefits from:

- Investment by international partners to provide important new capabilities to the DIII-D facility;
- Exchange of scientific and operations personnel, together with exchange of ideas and expertise;
- Opportunities to extend operational scenarios to long-pulse and steady-state conditions in superconducting facilities abroad.

**Strengthening the scientific basis for fusion energy.** The 2019-2024 five-year plan on DIII-D will continue a focus on scientific excellence through the development of fundamental understanding of the underlying processes relevant to fusion and transforming that understanding into validated predictive understanding. Key elements of the plan include:

- Validation of models in reactor-relevant regimes with low torque, electron heating and low collisionality using cutting-edge diagnostics and enhancements in DIII-D's heating and

current-drive capabilities and employing exascale computational capability where appropriate;

- Understanding of rotation generation and damping mechanisms and development of techniques to control the rotation profile to maximize performance and avoid instabilities;
- Enhanced ability to predict energetic particle behavior, allowing development and usage of new control tools to improve fast ion confinement and enable a path to increased performance in steady-state scenarios;
- Development of advanced current-drive technologies for tailoring of the current profile in steady-state plasmas, enabled by scientific evaluation of the interaction of RF waves with the scrape-off-layer and main plasma coupling;
- Identification of the mechanisms that affect temperature and density profiles and understanding of how the pedestal structure is affected by the particle source;
- Improvement of models of the boundary by quantifying uncertainties associated with energy and momentum dissipation and transport;
- Improvement of tokamak performance through experimental investigation and validated predictive simulation, accelerated through the insights gained from theory-experiment comparison.

**Defining fusion systems beyond ITER.** The DIII-D program is well suited to developing and understanding steady-state scenarios appropriate for meeting ITER’s Q=5 steady-state mission, as well as devices conceived to operate beyond ITER, including a fusion nuclear science facility (e.g. CFETR), or a range of potential steady-state reactor devices, including ARIES-ACT1. In the nearer term, DIII-D is well placed, and working closely with collaborators, to achieve scalable steady-state operation in existing devices, including EAST, KSTAR, and JT-60SA. During the 2019-2024 period, DIII-D research will inform decisions on a next-step device for the U.S. and the ultimate potential of fusion energy through:

- Investigating relevant regimes (e.g., low torque resulting from limited NBI use in future devices needing to breed tritium) to inform designs in the choice of parameters for a high nuclear fluence device (e.g., FNSF, CFETR);
- Developing the physics basis for high  $\beta_N$  ( $\sim 5$ ) and high bootstrap fraction steady-state scenarios to help realize the improved economics and reduction in the cost of electricity of a fusion reactor;
- Exploring the compatibility between high performance steady-state core plasmas with reactor-relevant boundary conditions, including expansion of new operating scenarios such as Super H-mode;

- Understanding the expected impurity exhaust for core- and edge-transport processes, determining the choice and location of impurity seeding for power control, and the optimal divertor closure for detachment and pumping efficiency;
- Quantifying the impact of material migration from the divertor and SOL and transport into the core and the impact on overall performance.

## References

- [Burrell 2001] K. H. Burrell, *et al.*, Phys. Plasmas **8**, 2153 (2001)
- [Candy 2003] J. Candy and R. E. Waltz, Phys. Rev. Lett. **91**, 045001 (2003)
- [Canik 2017] J.M. Canik *et al*, Phys. Plasmas **24**, 056116 (2017)
- [Chen 2017] X. Chen *et al* Nucl. Fusion **57** 086008 (2017).
- [Cole 2011] A. J. Cole *et al*, Phys. Rev. Lett. **106**, 225002 (2011)
- [Collins 2016] C.S. Collins *et al* Phys. Rev. Lett. **116** 95001 (2016)
- [Commaux 2016] N. Commaux *et al* Nucl. Fusion **56** 046007 (2016)
- [Evans 2004] T. E. Evans, *et al.*, Phys. Rev. Lett. **92**, 235003 (2004)
- [Garofalo 2002] A. M. Garofalo *et al* Phys. Rev. Lett. **89**, 235001 (2002)
- [Garofalo 2015] A.M. Garofalo *et al* Phys. Plasmas **22** 056116 (2015)
- [Garofalo 2015b] A.M. Garofalo *et al* Nucl. Fusion **55** 123025 (2015)
- [Guo 2017] <http://meetings.aps.org/link/BAPS.2017.DPP.YI2.6>
- [Groebner 1990] R. J. Groebner, K. H. Burrell, and R. P. Seraydarian, Phys. Rev. Lett. **64**, 3015
- [Heidbrink 1993] W. W. Heidbrink *et al*, Phys. Rev. Lett. **71**, 855.
- [Hillesheim 2013] J. C. Hillesheim *et al* Phys. Rev. Lett. **110**, 045003
- [Holland 2017] C. Holland *et al* Nucl. Fusion **57** 066043 (2017)
- [Jackson 1991] G. L. Jackson *et al.*, Phys. Rev. Lett. **67**, 3098
- [Kessel 2015] C.E. Kessel *et al*, Fusion. Sci and Technol., **67**, 1 (2015).
- [Kim 2015] K. Kim *et al*, Nucl. Fusion **55**, 053027 (2015).
- [Kinsey 2011] J.E. Kinsey *et al*, Nucl. Fusion **51** 083001 (2011).
- [La Haye 2002] R. J. La Haye *et al*, Phys. Plasmas **9**, 2051 (2002)
- [Lazarus 1996] E.A. Lazarus *et al.*, Phys. Rev. Lett. **77** 2714 (1996).
- [Leonard 1997] A. W. Leonard *et al*, Phys. Rev. Lett. **78**, 4769 (1997)
- [Luce 1999] T. C. Luce *et al*, Phys. Rev. Lett. **83**, 4550 (1999)
- [Luce 1992] T. C. Luce, C. C. Petty, and J. C. M. de Haas, Phys. Rev. Lett. **68**, 52 (1992)

- [Mclean 2017] A.G. Mclean *et al*, IAEA 2016,  
<https://conferences.iaea.org/indico/event/98/session/9/contribution/369>
- [Meneghini 2017] O. Menghini *et al* Nucl. Fusion **8** 086034 (2017)
- [Osborne 2000] T H Osborne *et al* Plasma Phys. Control. Fusion **42** A175 (2000).
- [Paz-Soldan 2014] C. Paz-Soldan *et al* Phys. Plasmas **21** 022514 (2014)
- [Paz-Soldan 2016] C. Paz Soldan *et al* Nucl. Fusion **56** 056001 (2016).
- [Petty 1995] C. C. Petty *et al*, Phys. Rev. Lett. **74**, 1763 (1995)
- [Petty 2009] C. C. Petty *et al*, Phys. Rev. Lett. **102**, 045005 (2009)
- [Reimerdes 2011] H. Reimerdes *et al*, Phys. Rev. Lett. **106**, 215002 (2011).
- [Romanelli 2012] <https://www.euro-fusion.org/eurofusion/the-road-to-fusion-electricity/>
- [Shafer 2017] Shafer *et al*, IAEA 2016,  
<https://conferences.iaea.org/indico/event/98/session/21/contribution/662>
- [Snyder 2012] P.B. Snyder *et al* Phys. Plasmas **19** 056115 (2012).
- [Simonen 1988] T. C. Simonen *et al.*, Phys. Rev. Lett. **61**, 1720 (1988)
- [Solomon 2014] W.M. Solomon *et al* Phys. Rev. Lett. **113**, 135001 (2014)
- [Solomon 2015] W.M. Solomon *et al* Nucl. Fusion **55** 073031 (2015).
- [Solomon 2016] W.M. Solomon *et al* Phys. Plasma **23** 056105 (2016).
- [Sorbo 2015] B.N. Sorbo *et al*, Fusion Eng. and Design **100**, 378 (2015).
- [Strait 1995a] E. J. Strait *et al*, Phys. Rev. Lett. **74**, 2483 (1995)
- [Strait 1995b] E. J. Strait *et al*, Phys. Rev. Lett. **75**, 4421 (1995).
- [Tobita 2017] K. Tobita *et al*, Fusion Sci and Technol., **72**, 537 (2017).
- [Turco 2015] F. Turco *et al* Phys. Plasmas **22** 056113 (2015)
- [Turco 2017] <http://meetings.aps.org/link/BAPS.2017.DPP.TI3.2>
- [Wade 2004] M. R. Wade *et al*, Phys. Rev. Lett. **92**, 235005 (2004)
- [Wan 2014] B. Wan *et al*, IEEE Trans. Plasma Sci. **42**, 495 (2014).
- [Whyte 2002] D. G. Whyte *et al*, Phys. Rev. Lett. **89**, 055001 (2002)

## 2. SCIENTIFIC BASIS FOR A BURNING PLASMA CORE

*The DIII-D 2019-2024 research plan seeks to provide the scientific basis to project integrated plasma operating scenario solutions for future burning plasma devices and to discover unique new physics insights into plasma behavior.* Research tools and programs are developed to investigate the key challenges and phenomena from plasma core to the edge, combining innovative experimental approaches with leading-edge comprehensive diagnostics and theory/simulation comparisons. Critical enabling advances are expected in each individual research line, such as the development of new regimes, control approaches, plasma science, current drive methods, and divertor configurations. But, perhaps the key opportunity lies in the interaction between the various techniques required to develop the physics basis for self-consistent ‘core-edge’ solutions for future fusion devices – a key goal of this 2019-2024 five-year plan. Thanks to its flexibility and parameter access, DIII-D is uniquely suited to confront this challenge. In this plan, facility developments are implemented which transform capabilities in each area to develop projectable solutions for the reactor scale. These are expected to equip the U.S. with the expertise to undertake a leading role in ITER and other burning plasma devices, as well as provide the plasma physics basis to map the path to steady-state fusion reactors.

### Principle Challenges

*The 2019-2024 five-year plan foresees a transformation in DIII-D capabilities and research focus* in order to access the physics and develop the path for fusion in steady-state burning plasmas. DIII-D will be able to access the range of plasma configurations and regimes necessary to resolve physical mechanisms and techniques for future reactors at the relevant parameters to develop an integrated core-edge physics basis. Critical issues for future reactors have been set out in chapter 1. These organize into two key themes, which serve as the basis for plasma scenario development and drive investigations across the program:

- **Burning plasmas** – to understand how to access high performance in burning plasmas. Here, critical enhancements to DIII-D will access relevant conditions, such as dominant electron heating and low rotation, and establish how to achieve robust and safe control. This will provide a basis to understand how to achieve performance goals in ITER, and extend to even higher performance, as well as to rapidly integrate the new learning from ITER into the scientific framework to project to future power plants.
- **High  $\beta_N$  steady-state operation** – establishing requirements for, and understanding behavior in, steady-state conditions. Key elements include exploring internal magnetic plasma configurations with new current-drive tools and handling the hot plasma exhaust with innovative divertor configurations (Section 3). This will drive research studies across

the entire scientific program to explore the changes, new physical mechanisms, and increased challenge posed by high  $\beta$  steady-state operation.

This program will lead to a rich diversity of high-impact scientific insights, placing U.S. scientists at the forefront of fusion research, as well as developing unique know-how and technologies to secure a U.S. stake in future fusion energy development. More specifically, it will enable the U.S. to take decisions on, and have the technical capabilities to proceed with, next-step devices, either in the U.S. or through leading roles in international partnerships.

### **Research to Prepare for Burning Plasma Devices**

The most important target for burning plasma research is the successful attainment of high fusion performance in a fusion reactor such as ITER. This will be an exciting step, exploring the new regime of the self-heated burning plasma state and operating at a scale never seen before. The need is to equip scientists with the knowledge and tools to ensure rapid progress and reach the highest performance possible to inform the path to fusion energy. However, burning plasma devices operate in particular regimes and conditions, with techniques that have not yet been fully established or optimized for these conditions; they will not have the time to conduct lengthy research programs to explore all issues of plasma physics – focus must be on the new phenomena encountered as a result of the new regimes, parameters, and scales accessed. Understanding must be developed now through vigorous research on present devices that resolves impediments, improves safety, and develops the physics by accessing relevant regimes and developing validated physics models. For example, it is important to grapple with multi-scale multi-species turbulent transport, where present facilities have the flexibility, time, and diagnostics to explore and resolve the complex physics and intensive simulation techniques required.

Key differences relative to most present devices include dominant electron heating, low collisionality and core fueling, low rotation, and, of course, a population of super-Alfvénic particles from fusion  $\alpha$ 's and heating systems. These will have critical impacts on the mechanisms of turbulent and energetic particle transport, as well as MHD stability. A reactor will be equipped with, and need to deploy, more sophisticated tools than present devices to maintain stability and control, such as precisely tuned non-axisymmetric ('3D') fields, precise current-drive deposition, and particle injection systems to safely quench the plasma. Understanding of how to manipulate these actuators is needed to reach optimal performance. Critical issues include:

- **Reaching high performance in reactor-relevant regimes (2.1.1):** through understanding and control of core transport (2.3.1, 2.3.2) and pedestal performance (4.1.2).
- **Maintaining stability** with low rotation and low collisionality plasmas at the ITER q<sub>95</sub>

(2.2.2. and 2.2.3)

- **Edge Localized Modes (ELMs)** must be prevented or reduced to tolerable size, while maintaining good stability, particle and impurity control (see 2.1 for scenario integration and 4.1.1 for underlying physics of techniques used).
- **Termination:** Safely quenching the end of the fusion plasma with acceptable thermal loads, forces, and runaway electron dissipation (2.2.1).
- **Particle and impurity control** to avoid impurity accumulation and exhaust helium through pellet injection and pedestal manipulation (2.1.2, 4.1.2, 4.2).
- **H-mode access**, particularly in the non-activation phase (4.1.3).

It must be stressed that while there is confidence that ITER has the tools to meet these missions, research on the above issues will enable us to rapidly understand and overcome differences encountered in ITER and provide a framework to project results from ITER to future fusion reactors. This will be equally important for other burning plasma devices.

*The 2019-2024 five-year plan for DIII-D provides unique capability to prepare for operation of burning plasma devices.* The approach focuses on providing flexibility and accessing the physics behaviors expected in the future devices, deploying comprehensive diagnostics and leading-edge simulation to interpret behavior and to project how to optimize tokamak operation. Key themes that drive DIII-D facility development and physics investigations for the optimization of performance in future burning plasmas are:

- **Dominant electron heating:** More than doubling microwave electron heating power to access low collisionality,  $T_e \geq T_i$  regimes and conduct perturbative tests of turbulence and pedestal behavior.
- **Low rotation:** More than doubling torque-free injected power to explore stability and transport in regimes with reactor-relevant low rotation and rotational shear.
- **3D field optimization:** doubling the toroidal resolution to  $n=6$  and providing harmonic flexibility at  $n=3$  and 4 to understand ELM, stability, and rotation profile control.

Research will exploit these capabilities to address the critical scientific challenges to achieve stable high-performance burning plasma conditions. Studies will explore both innovation in approach and scientific foundations to enable development and confident projection of required techniques for future reactors. A strong focus will be placed on specific preparation for ITER. An important element will be integrating and showing compatibility of the various techniques required to develop robust solutions. Coupled with strong international collaboration and fusion simulation, this will place the U.S. at the forefront of scientific understanding and thus, a natural and required leader in ITER research, as well as in the physics to project future fusion devices.

## Developing the Path to Steady-State Burning Plasmas

To reach fusion energy, the physics basis and techniques for establishing plasma regimes with continuous operation must be developed. The crucial difference of such regimes compared to present inductive scenarios is that they must be fully non-inductive, and thus have their current driven by a combination of bootstrap current, which requires higher  $\beta$  than the ITER baseline scenario, and auxiliary systems (i.e., without use of solenoid). In a power plant, generating the electricity to power auxiliary current drive systems can drive up the required device size and other parameters, so it is highly desirable to find predominantly self-driven solutions through high bootstrap current fraction regimes. An alternative is to develop regimes and technologies for more efficient auxiliary current drive, which pushes the operating scenario to other extremes.

The challenge, therefore, is to determine if the required performance of both plasma and associated tokamak systems can be achieved. Critical aspects to explore to meet this challenge are:

- The **current profile** will differ from inductive plasmas, altering turbulent transport and energetic particle transport (2.3.1 and 2.3.3).
- **High  $\beta_N$** , necessary for high self-driven current, brings the plasma close to ideal MHD stability limits, which must be understood and controlled (2.2.2), and further modifies turbulence (2.3.1) and 3D interactions used for ELM (4.1.1) and rotation (2.3.2) control.
- A high-density and high-performance edge **pedestal** is highly leveraging to performance, and may also ease the divertor challenge (2.1.2, 4.1.2).
- Efficient methods of **current drive** must be developed that are compatible with the reactor environment and tritium breeding (2.3.4).

Further, a steady-state solution poses new challenges for power and particle handling (addressed in Section 3), and the tradeoffs between this and the core in the overall configuration design must be studied to develop the physics basis to project integrated solutions (Section 4).

The DIII-D program has conducted simulations to explore the key parameters and techniques that leverage the development of a cost-effective, compact, advanced tokamak pilot plant [Buttery 2018]. The studies exploit the FASTRAN suite [Park 2017a] and includes TGLF, EPED, and current-drive models developed and validated in the DIII-D research program [Holcomb 2015, Park 2017b]. The simulations provide self-consistent and fully converged non-inductive steady-state plasmas (Fig. 2-1), predicting performance from physics-based models, which leads to important insights. It is found that a combination of high  $\beta_N$  and high density is desirable to ensure sufficient fusion power and reduce auxiliary current-drive requirements. Efficiency of systems to provide the remaining current drive is also key. Coupled with sufficient toroidal field, a modest scale device can be constructed (4m radius), with tolerable neutron and divertor heat loads. Similar

considerations arise for larger-scale devices that seek to reduce cost and scale, such as ARIES-ACT1 [Kessel 2015].

*The 2019-2024 five-year plan foresees a transformation in DIII-D capabilities and program focus to address this steady-state challenge.*

The facility is being redeveloped to enable access to high-performance steady-state core configurations. This program will benefit from new facility developments already made during the 2014-2018 five-year plan.

Indeed, some of these will become available for first use at the start of the 2019-2024 plan. And this mission will drive the ongoing transformation of the facility through the next five-year period. Key elements discussed in this section include:

- **Off-axis heating and current drive:** More than doubling the off-axis neutral beam and microwave power will provide the means to explore steady-state configurations, assessing the new physics of these regimes and the principles of steady-state configuration design.
- **New current-drive technologies:** The physics of three promising new current-drive technologies will be assessed. Simulations indicate this could lead to greater efficiency in future reactors – a potential game changer in device scale and performance.

The new regimes accessible with these tools define the context and drive the objectives of many further physics areas (such as transport, stability, pedestal, and energetic particle physics) as set out in this and the following two chapters. These elements will combine with the learning, exploration, and application of techniques discussed in the burning plasma preparation theme to develop projectable fusion core solutions. A key focus will be to use DIII-D’s flexibility and comprehensive diagnostic set to understand the underlying processes and physics behind the development of such solutions. In parallel, the program will test innovative new divertor concepts and materials solutions (Section 3), and explore the tradeoffs with the core and overall configuration optimization (Section 4) in order to develop a projectable physics basis to design future steady-state burning plasma devices.

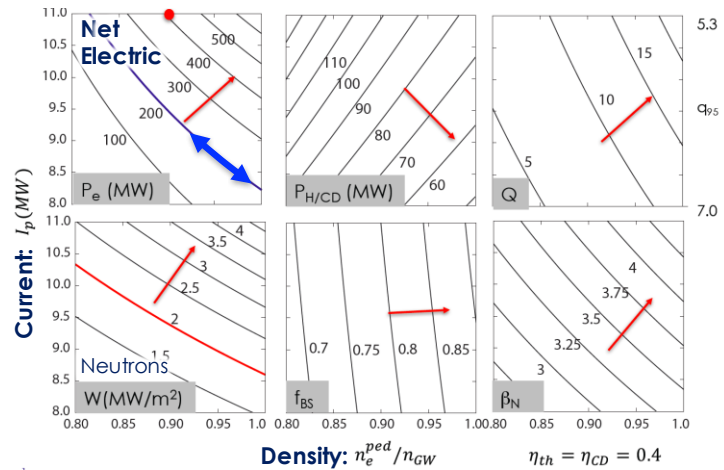


Fig. 2-1. Simulations of fully non-inductive plasmas in a compact net-electric advanced tokamak pilot plant with 4m radius, 7T, and  $\eta_{th} = \eta_{CD} = 0.4$ . Auxiliary heating and current drive is adjusted to ensure each point is fully

## Time Sequence, Priorities, and Organization

The 2019-2024 five-year plan commences directly after a set of major upgrades to DIII-D with enhancements in neutral beam off-axis current drive and power, advanced divertor investigations, new materials, increased microwave systems, and a new helicon current system. Thus, DIII-D will be equipped to access new regimes and behaviors on burning plasma and steady-state missions with new research capabilities to explore the physics and develop fusion solutions from the start of the plan. Further enhancements early in the plan (divertor, heating, and 3D) build on these to enable research objectives to be fully investigated.

The developments in current drive and divertor physics will enable a rapid acceleration of steady-state research from the start of the 2019-2024 research plan. This work is vital to enable a decision on, and preparation for, a follow-on steady-state device, such as a nuclear science facility or a pilot plant in the U.S. or abroad. Nevertheless, ITER will remain the top priority for DIII-D research and, indeed, the burning plasma work set out for ITER is also vitally needed for other burning plasma devices. This work benefits particularly from ECH and 3D improvements. However, it is anticipated that specific demand from ITER for DIII-D investigations will decrease as ITER's operation approaches, physics basis, simulation tools, and modes of operation become developed and team members start to engage more directly with ITER itself.

The parameter space and, thus, challenges for much of this work are defined by two key “scenario” physics initiatives (inductive scenarios and steady-state physics, Section 2.1), which will also explore limits and trade-offs in the various requirements, integrating insights and techniques developed in the wider program to develop integrated scenario solutions. These scenarios drive the focus and particular challenge of many detailed physics investigations throughout DIII-D research areas, described in chapters 2-4. In this chapter, the focus is on core performance and stability activities, explaining first the two scenario strategies for inductive scenarios to meet ITER  $Q=10$  needs and the high  $\beta$  path to develop steady-state fusion scenarios. These are followed by discussions on stability physics and its control, and then performance and current-drive issues. Boundary physics and integration follow in sections 3 and 4.

### 2.1 ROBUST PLASMA SCENARIOS FOR FUTURE REACTORS

Plasma scenario research seeks to identify complete operating schemes for future tokamaks to achieve performance requirements. The hardware design and goals of ITER are now largely defined, so ITER scenario development on DIII-D will continue to evaluate the ability to achieve, or better, exceed the stated goals given the known constraints. The basic question to address is “how can ITER use its many actuators to reach its performance goals?” If necessary, alternate approaches or new requirements (e.g., new actuator capability or modified actuator usage) will be

defined. Beyond ITER, future tokamak reactor concepts are often envisioned to be sustained non-inductively at higher normalized pressure. For these, performance requirements and design are still largely undefined or flexible, opening a wide parameter space to explore; a path must be developed. DIII-D fully non-inductive (i.e., steady-state) scenario research seeks to understand the physics of a largely self-driven plasma state, the interaction between different mechanisms, and the control through advanced heating and current drive approaches in order to obtain sufficient knowledge of potential scenarios to move confidently beyond the conceptual phase to begin building next-step steady-state tokamaks.

Scenario research is necessarily holistic in nature because the size of a useful scenario operating space may be defined by stability boundaries, transport restrictions, and current-drive limitations. Multiple physical mechanisms and their interactions and tradeoffs must be understood. Presently there is relatively high confidence in models of ideal MHD global stability limits, H-mode pedestal height set by peeling-ballooning limits, and current drive (external and bootstrap) under ideal conditions. There is relatively less confidence in models to predict resistive instability boundaries (e.g., neoclassical tearing modes) in transport models to accurately predict density, temperature, and rotation profile details (e.g., gradients of these) and in models for scrape-off layer properties and particle transport that impact the pedestal height. Integrated modeling simulations coupling all of these physics elements will be used to guide DIII-D scenario experiments, but more significantly, experiments will help benchmark the parts of these models that work and provide new data for use in improvement of the parts that do not.

An integrated operating scenario poses a significant challenge. Many different, and often competing elements of the physics and control optimization must be brought together. The physics and limits of each must be understood, along with their interactions; connecting the in-depth physics understanding needed to a practical real-world optimization of how to make fusion better. The scenario itself can be thought of as a set of actuator time histories that results in stable MHD equilibria for the lifetime of the plasma, with sufficient pressure and confinement time during a “flat top” phase to obtain desired performance goals – all without transient MHD instabilities that can damage machine components or excessive heating of divertors. Typical actuators to control the plasma from initiation to extinction include poloidal and toroidal field coil currents, external heating, current drive and torque sources, fueling sources (such as gas valves and pellets), and non-axisymmetric fields for error field control or feedback on MHD modes. The resulting MHD equilibrium in the flat-top phase is largely the defining feature of a scenario – in particular the current density or safety factor profile and normalized pressure beta. Performance goals may include obtaining target  $\beta$ , confinement time, projected fusion gain  $Q$ , pulse length, non-inductive current fraction ( $f_{NI}=I_{NI}/I_P$ ), and bootstrap current fraction  $f_{BS}$ . Transient events to be avoided that

can destroy machine components include disruption-inducing tearing modes and resistive kink modes, and type-I edge localized modes (ELMs).

There are two steps to developing the physics basis for future reactor scenarios:

1. Feasibility: The first step focuses on establishing the feasibility of a particular scenario concept by demonstrating a few key “go or no-go” requirements, even if all of the required parameters to project to a future device cannot be met. An example of this on the steady-state path is to demonstrate current profiles that can be sustained non-inductively and are capable of DEMO-relevant operation at  $\beta_N > 5$ .
2. Projection: Once an existence proof has been established, the next step is to obtain predictive capability to find more optimal solutions, and to project/extrapolate to a future device (for example, in rotation, electron heating, or collisionality). Predictive ability requires validating stability, transport, and current-drive models over a range of relevant parameter spaces that encompass the existence proof demonstrations, as well as resolving underlying physical mechanisms and models. This requires flexible plasma actuators to access a range of conditions, and to perturb plasmas and stretch toward more burning-plasma relevant parameters characterized by low rotation,  $T_e/T_i \sim 1$ , no Type-I ELMs, and a dissipative divertor. This work thus naturally partners with many more topically focused physics efforts described in later sections, with the scenario aspect acting as a driving and parameter-defining focus.

An example of scenario research now in the predictive understanding phase is work on the ITER Baseline Scenario at zero torque. Here, multiple physics interactions, including the dependence on current profile, transport, and rotation of RMP ELM suppression and 2/1 tearing mode avoidance, are being studied at increasingly more ITER-relevant collisionality, rotation, and  $T_e/T_i$ .

During the past five years, the balance of scenario work was tipped toward exploring and validating inductive scenarios for achieving ITER  $Q \geq 10$ , with less time spent on steady-state scenarios. However, with strong progress made on inductive scenarios, and the finalization of hardware decisions, research is turning toward steady-state plasmas in ITER and beyond. Thus, in the 2019-2024 period, this balance will be reversed to put a greater emphasis on steady state, taking advantage of new hardware upgrades that are key to this type of discharge scenario. While ITER will remain the top priority, research requests from ITER, particularly for inductive scenario work, are expected to decrease in number and urgency.

The three basic steady-state scenario concepts are summarized in Fig. 2-2, and described in more detail in later sections.

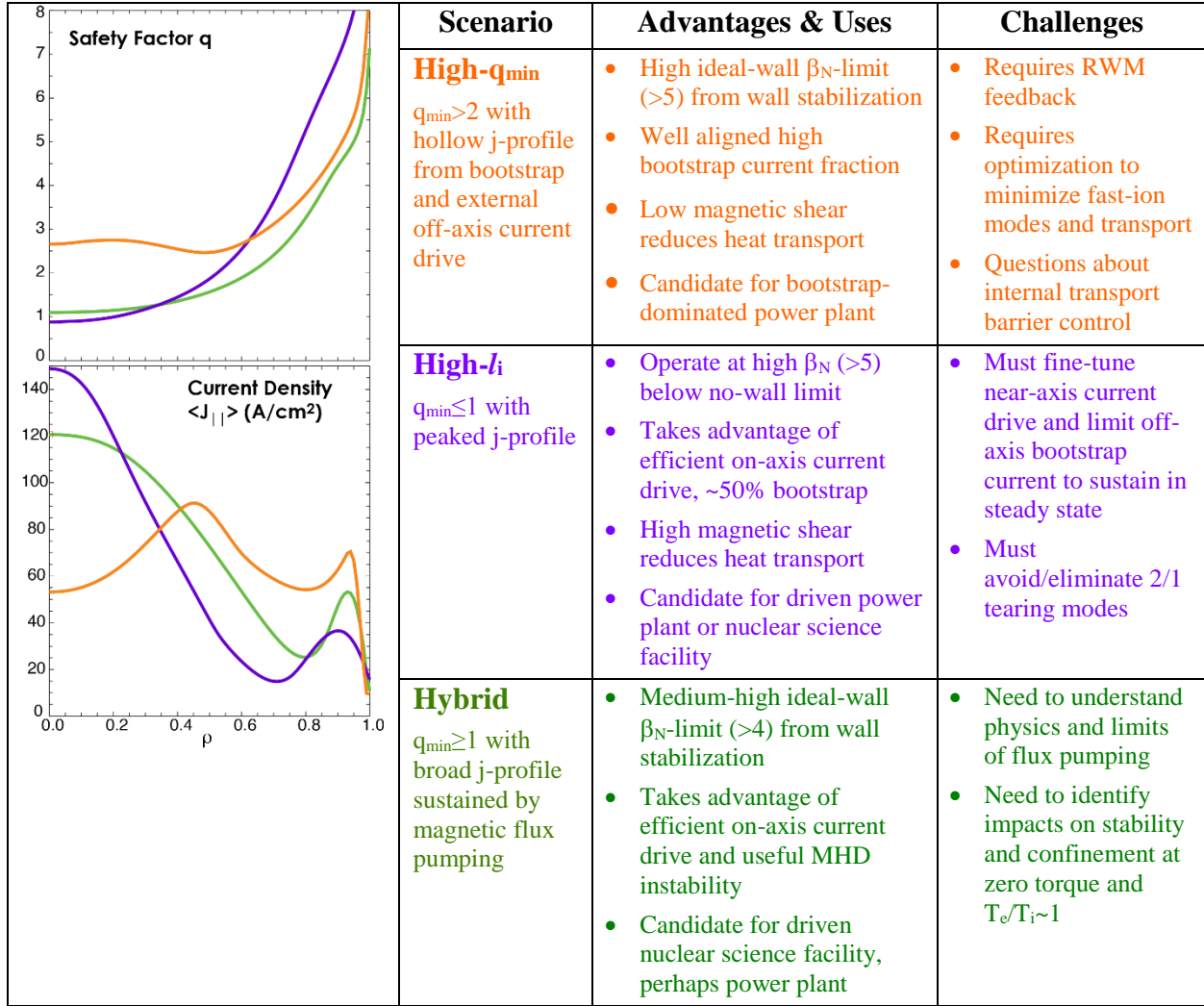


Fig. 2-2. Summary of steady-state scenario concepts being studied on DIII-D.

The five-year plan is structured to address both feasibility and projection aspects of fusion scenarios. The start of the plan comes directly after an upgrade in which off-axis and co-injected neutral beam power will be substantially increased. This will enable tests of the performance limits of the various regimes (as discussed further in sections below) to establish their basic viability and potential. This work also benefits from improvements in electron cyclotron current-drive power. Later in the plan, further upgrades play more strongly to the projection aspect. Notably, a second neutral beam reconfiguration will provide the scope to fully balance injected torque. Continued increases in electron cyclotron power and the potential of additional current drive actuators (top-launch ECH, helicon current drive, and inboard launch lower hybrid) enable increasing capability to project scenarios to low torque and dominant electron heating.

Most steady-state scenarios still require key elements to be demonstrated, although the scientific basis has advanced significantly in some scenarios, such as the high-beta hybrid scenario.

The hybrid is now being tested at lower torque, with RMP ELM control, and coupled to a radiative divertor. In the 2019-2024 plan this scenario will be put on a much firmer predictive basis by extending studies down to zero torque and  $T_e/T_i \sim 1$  with four balanced beamlines and increased gyrotron power, and by obtaining more detailed understanding of the physics of flux pumping that maintains  $q_{\min} > 1$ . Also, the hybrid scenario will be tested for core-edge compatibility by continuing studies of ELM control requirements and divertor heat flux reduction using new 3D coils and advanced divertors, respectively. These studies will help determine if the hybrid scenario can be used as the basis for various steady-state nuclear science facilities, such as an FSNF or CFETR, or perhaps a more driven and larger power plant, such as EU-DEMO.

Other steady-state scenarios will complete initial feasibility tests enabled by hardware upgrades, and then move on to tests in more reactor-relevant conditions that will enable extrapolation (e.g., zero torque, ELM control). Feasibility tests for high- $q_{\min}$  and high- $li$  are to prove access to predicted DEMO-relevant  $\beta_N$  near 5 in steady state using heating and current drive upgrades, with high- $q_{\min}$  relying on strong wall stabilization and RWM feedback, and high- $li$  operating below the no-wall  $\beta_N$  limit. High- $\beta_P$  is a version of the high- $q_{\min}$  scenario that achieves higher bootstrap current fraction ( $>70\%$ ) by operating with a high-radius internal transport barrier (ITB) and at relatively low toroidal  $\beta$  (i.e., low plasma current, high  $q_{95}$ ). The primary feasibility test for high- $\beta_P$  scenario is to sustain an ITB and high bootstrap fraction at higher  $\beta_T$  and plasma current.

Significant work will continue on inductive scenario development for ITER's Q=10 mission. Here efforts will continue to narrow down the best options for ITER, looking at fully integrated scenarios at relevant parameters. Options include the ITER Baseline Scenario (IBS) core scenario with either RMP ELM suppression, QH mode, or pellet-based ELM control. IBS plasmas with  $q_{95} \sim 3$  and  $\beta_N \sim 1.8$  at zero torque have been highly prone to disruptions caused by 2/1 tearing modes. Only recently has progress been made obtaining and understanding 2/1-stable zero-torque IBS plasmas, though at elevated collisionality, but so far attempts to add RMP ELM suppression or QH-mode have been unsuccessful. This will continue to be a focus in the 2019-2024 five-year period. An alternative path is the Advanced Inductive (AI) core scenario with either QH-mode or pellet control. AI operates at higher  $q_{95}$  near 4 for improved core stability, but at the expense of (so far) insufficient energy confinement for ITER Q=10 at zero torque if  $\tau_{98y2}$  confinement scaling is assumed. Integration of AI and QH-mode is expected to raise confinement, so this new approach will be pursued further. The identified best zero torque Q=10 scenario options without type-I ELMs will be used as platforms for further integration studies. These include adapting divertor heat flux mitigation solutions to the scenario and evaluating the effectiveness of real-time control solutions for handling off-normal or fault events (i.e., recovery, safe shutdown, or fire the

disruption mitigation system). Use of improved profile control tools through ECH and stronger and more flexible 3D field capabilities will provide potential to improve stability and performance of these scenarios.

Fig. 2-3 and Fig. 2-4 graphically indicate the integrated performance goals for inductive and steady-state scenarios, respectively. The shaded regions are examples of progress as of the end of FY17. Typically, a few, but not all, performance goals are met simultaneously. The 2019-2024 five-year research plan aims to extend integrated scenario development to simultaneously meet more target objectives than are possible now – i.e., to fill more of the gray area in the following figures.

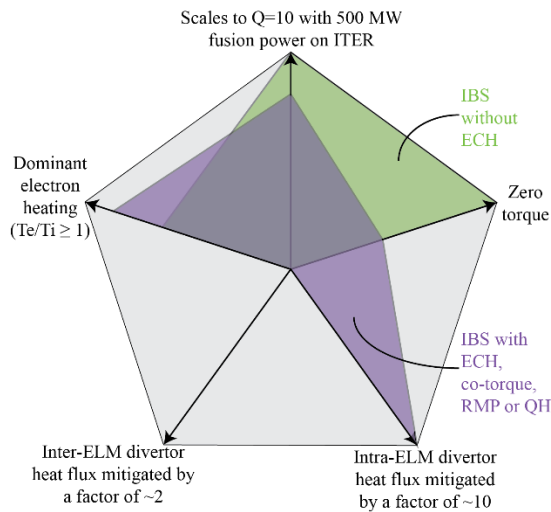


Fig. 2-3. Primary goals to be achieved simultaneously (gray shading) in an inductively driven scenario by 2024 to inform ITER operation. Color-shaded areas are examples of progress as of the end of FY17.

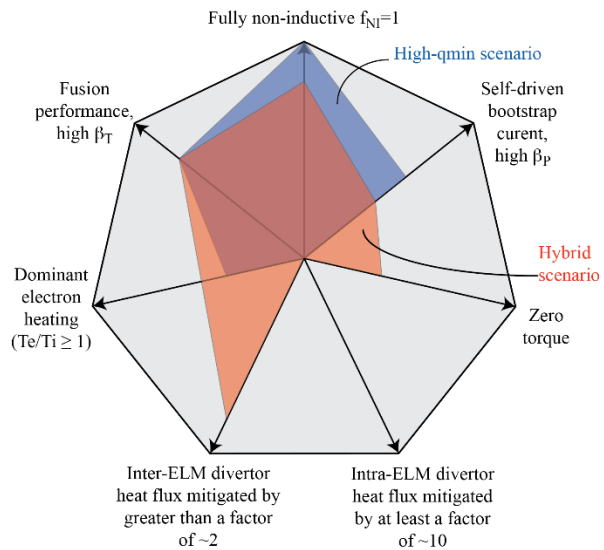


Fig. 2-4. Primary goals to be achieved simultaneously (gray shading) in a steady-state scenario to inform a next-step burning plasma or DEMO. Color-shaded areas are examples of progress as of the end of FY17.

Sections 2.1.1 and 2.1.2 contain detailed descriptions of the physics challenges, research plan approaches, and needed capability improvements for inductive and steady-state scenarios.

### 2.1.1 Inductive Scenarios and Basis for Q=10 in ITER

*Physics Leads:* A. Garofalo (GA), F. Turco (CU), J. Ferron (GA), C. Holcomb (LLNL), R. Nazikian (PPPL), W. Solomon (GA), T. Strait (GA), B. Victor (LLNL), D. Weisberg (GA), T Wilks (MIT)

A primary mission of the DIII-D facility is to develop the understanding and techniques needed to enable high-performance burning plasmas in ITER. ITER’s research mission centers on the understanding of the burning plasma state to establish the physics basis for a follow-on fusion power plant. To this end, ITER has a performance goal to achieve for the first time in any magnetic

fusion device a fusion gain  $Q=10$ , corresponding to a state with 2/3rds of the heating power supplied by fusion alphas. An inductively driven operating scenario that achieves  $Q=10$  must be stable to harmful core MHD modes capable of reducing confinement or causing a disruption, it must not have large Type-1 edge localized modes (ELMs) capable of eroding the divertor, and it must not exceed steady-state heat flux limits for the divertor materials. ITER must avoid the risk and delay of a lengthy research mission to develop possible techniques and solutions to meet these requirements. The world fusion community needs to resolve many of these issues on present-day research facilities before an ITER  $Q=10$  campaign begins.

ITER  $Q=10$  equivalent performance has been demonstrated in a number of existing research devices with strong torque injection and large Type-I ELMs. However, in the past five years DIII-D has shown that plasmas become challenged at ITER-relevant rotation and collisionality, being more readily subject to instabilities and marginal in required energy confinement, while robust ELM control has not yet been integrated at these conditions. Hypotheses have been developed to explain tearing mode and ELM stability dependences on the current profile and rotation. Tearing-stable low-torque IBS plasmas have been achieved, but still with Type-I ELMs and at relatively high collisionality. ELM suppression has been successfully achieved in IBS-like plasmas using either RMP or QH-mode, although not yet at zero torque.

### **2.1.1.1 Challenges and Impact**

The goal of the DIII-D Inductive Scenarios program is to identify the best-integrated solutions for ITER to follow to achieve  $Q=10$  as rapidly as possible without risking device damage. To accomplish this, the program is focused on three key challenges (Table 2-1). The first challenge is to demonstrate integrated low-torque, ELM-stable operation in scenarios that project to  $Q=10$  in ITER. This will be done by using key facility upgrades, notably additional gyrotrons and 3D capabilities, to fine tune profiles in ways predicted to lock-in core stability and ELM mitigation/suppression at low torque and collisionality. The next challenge is to develop power exhaust control for acceptable divertor heat flux in integrated ITER  $Q=10$  scenarios. This will be achieved by taking advantage of a more flexible gas puff system and divertor/scrape-off-layer (SOL) diagnostics to optimize “puff and pump” feedback-controlled radiative divertor techniques. The last challenge is to establish a predictive physics understanding of inductive scenarios for projections to ITER. This will be met by systematic comparison of observed and simulated plasma conditions to identify and improve transport and stability model shortcomings in an ITER-relevant parameter regime. This work also connects to related underlying physics studies discussed in sections 2.2, 2.3, 4.1, and 4.2.

The demonstration of low-torque, ELM-stable operation in scenarios that fulfill ITER’s  $Q=10$  mission will give confidence in ITER’s plan. Further, the research described here will provide a

validated set of tools for predicting discharge behavior in ITER and other nuclear fusion facilities, where each discharge must be modeled ahead of time. It will provide a unique basis to understand how to optimize performance in ITER, and a conceptual and validated simulation framework to project ITER’s learning to future fusion reactors. DIII-D will thus make a unique and vital contribution to ITER’s success in this plan.

**Table 2-1  
Inductive Scenarios Challenges, Goals, and Upgrades**

<b>Challenge</b>	<b>Goals/Deliverables</b>	<b>Upgrades</b>
Demonstrate low-torque, ELM-stable operation in scenarios that project to Q=10 in ITER	<ul style="list-style-type: none"> <li>Evaluate methods and requirements for eliminating Type-I ELMs in low-torque ITER Q=10 scenarios</li> <li>Within the constraints of low torque and ELM control, identify transport and stability tradeoffs in <math>q_{95}</math> and <math>\beta_N</math></li> </ul>	<p><b>Hardware</b></p> <ul style="list-style-type: none"> <li>Additional gyrotrons for ECH/ECCD</li> <li>Additional gas valve locations</li> <li>New 3D coil arrays</li> <li>New individual fully programmable power supplies for 3D coils</li> </ul>
Develop power exhaust control for acceptable divertor heat flux in low-torque, ELM-stable ITER Q=10 scenarios	<ul style="list-style-type: none"> <li>Evaluate compatibility of radiative divertor techniques with different ELM control approaches</li> <li>Optimize puff-and-pump detachment control to achieve greater divertor heat flux reduction with smaller impact on pedestal and core performance</li> </ul>	<p><b>Diagnostic</b></p> <ul style="list-style-type: none"> <li>Better measurements of current density near <math>q=2</math> and the pedestal</li> <li>Neutral deuterium and SOL deuterium ion measurements</li> <li>Advanced imaging of temperature and density fluctuations (ECE-I, MIR)</li> <li>Improved/additional diagnostics for determination of the separatrix location</li> </ul>
Establish predictive understanding of inductive scenarios at high normalized fusion performance, necessary for projections to ITER	<ul style="list-style-type: none"> <li>Ability to predict heat, particle, rotation, and current transport and profiles from core to SOL in ITER Q=10 regimes</li> <li>Ability to predict MHD instability onset, evolution and impacts in ITER Q=10 regimes</li> </ul>	<p><b>Analysis Capabilities</b></p> <ul style="list-style-type: none"> <li>Improved models and codes for time dependent evolution of:                             <ul style="list-style-type: none"> <li>Current profile evolution</li> <li>Pedestal stability</li> <li>Linear MHD</li> <li>Non-linear extended MHD</li> <li>Core transport</li> <li>Scrape-off layer transport</li> </ul> </li> </ul>

**2.1.1.1 Research Plan**

The inductive scenarios research plan is organized by the challenges and goals in Table 2-1. Fig. 2-5 shows the timeline for each challenge, research tasks and milestones, and required capability improvements.

Challenge	FY19-20	FY21	FY22	FY23	FY24
Demonstrate low-torque, ELM-stable operation in scenarios that project to Q=10 in ITER	Understand the rotation requirements for ELM-stable edge in IBS Use 3D fields to optimize plasma rotation for ELM-stable operation at low injected torque Within the constraints of low torque and ELM control, understand confinement and stability trends with $q_{95}$ and $\beta_N$ Compare ELM control at low torque achieved using balanced NBI versus high-power ECH				
Develop power exhaust control for acceptable divertor heat flux in low-torque, ELM-stable ITER Q=10 scenarios	Optimize gas injection for divertor heat flux reduction with smaller impact on core Test compatibility of radiative divertor techniques with different ELM control approaches				
Establish predictive understanding of inductive scenarios at high normalized fusion performance, necessary for projections to ITER	Predict time-dependent equilibria, core plasma profiles, and SOL parameters for a given time dependent set of shape, heating, fueling, and 3D coil current inputs Provide time-dependent synthetic diagnostic signals and compare to experiment Identify conditions where bifurcation in MHD stability is observed and not predicted Devise models that reduce occurrence of missed bifurcation				
Hardware upgrades:	Additional gyrotrons Optimized gas injection for radiative divertor Individual fully programmable power supplies for each of the IC-coil loops Upgraded 3D coil arrays				
Diagnostic Upgrades:	Advanced imaging of temperature and density fluctuations Improved/additional MSE for current density measurements near $q=2$ and the pedestal Neutral deuterium and SOL deuterium ion measurements				
Code development:	Build capability and models for describing time-dependent evolution and bifurcation of behavior Training of neural networks				

Fig. 2-5. Inductive Scenarios Plan Timeline

**Challenge 1: Demonstrate low-torque, ELM-stable operation in scenarios that project to Q=10 in ITER**

**Current Progress.** At the time of the writing of this proposal, ITER’s Q~10 equivalent performance has been achieved in ITER-similar plasmas on DIII-D, either at zero torque with large type I ELMs, or without ELMs but with finite counter- $I_p$  torque. Operation with near-zero-net NBI torque has so far been unobtainable with an ELM-stable edge in the ITER Baseline Scenario (IBS:  $q_{95} \sim 3$   $\beta_N \sim 2$ , ITER-similar shape plasmas). Experimental efforts in the last few years focused on understanding the low-torque limit for both RMP-ELM suppression and QH-mode in the ITER baseline scenario (IBS) on DIII-D. Progress toward zero-net torque has been made with both

approaches to an ELM-stable edge. Note that 0.5-1.5 Nm in the co- $I_p$  direction is an estimate for the range of ITER-equivalent torque on DIII-D, depending on density, so the lower end of this range is usually taken to be the meaning of “low torque.” However, due to the uncertainty of this value, 0 Nm is normally the conservative target in experiments.

The ELM suppression experiments in the IBS were conducted using  $n=3$  RMP fields with the upper row found to be most effective. RMP-ELM suppression in these experiments was accessed with co-NBI injection, corresponding to a torque of  $\sim 4.5$  Nm and pedestal top rotation of about 70 km/s. Addition of even modest amounts of counter- $I_p$  torque (to move towards ITER-relevant  $\sim 0$  Nm) was found to cause type-I ELM activity to return, when the net torque was  $\sim 3.5$  Nm and the rotation still high,  $\sim 50$  km/s [Wade 2015, Moyer 2017]. More recent experiments used a slightly modified shape and  $q_{95}$ . (see Fig. 2-6). These experiments found the pedestal top rotation could be reduced significantly further, to  $\sim 10$  km/s, although this was achieved at comparable NBI torques to the IBS case, indicating substantial differences in momentum confinement or magnetic braking. Further analysis is required to understand why single-row operation is preferred for the IBS scenario while more traditional even parity  $n=3$  fields are less successful. A possible reason for the reduced pedestal rotation is discussed shortly.

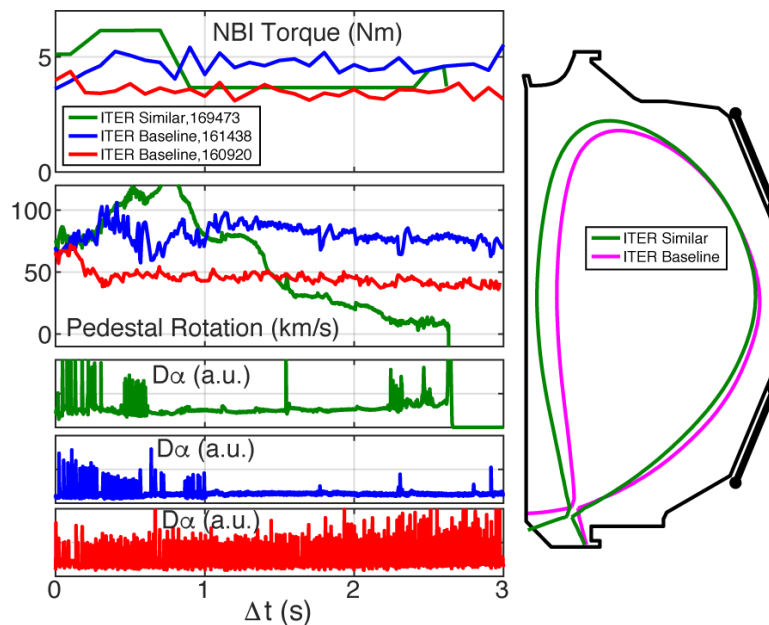


Fig. 2-6. Progress toward RMP-ELM suppression at zero-net NBI torque with  $Q=10$  equivalent performance on DIII-D, and comparison of the ISS and IBS plasma cross sections.

An alternative approach is to use the Quiescent H mode (QH-mode), where ELMs are replaced by benign edge MHD fluctuations, usually in the form of a coherent edge harmonic oscillation (EHO). QH-mode research has made remarkable advances in the understanding of the EHO through comparisons of linear and nonlinear modeling results to DIII-D experiments [Liu 2015,

Garofalo 2015, Chen 2016, King 2017, Liu 2017]. QH-mode experiments in the IBS have made progress toward zero-net NBI torque by operating with RWM feedback (dynamic error-field correction) across the L-H transition to avoid locked modes [Garofalo 2015], and made further progress more recently by operating with a slightly increased outer gap, i.e. the plasma-wall separation at the outer mid-plane (see Fig. 2-7). The lowest net NBI torque without type-I ELM activity is  $\sim 2.2$  Nm (counter- $I_P$  direction), achieved with excellent energy confinement quality  $H_{98y2} \sim 1.4$  at  $\beta_N \sim 2$  and  $q_{95} \sim 3.3$ .

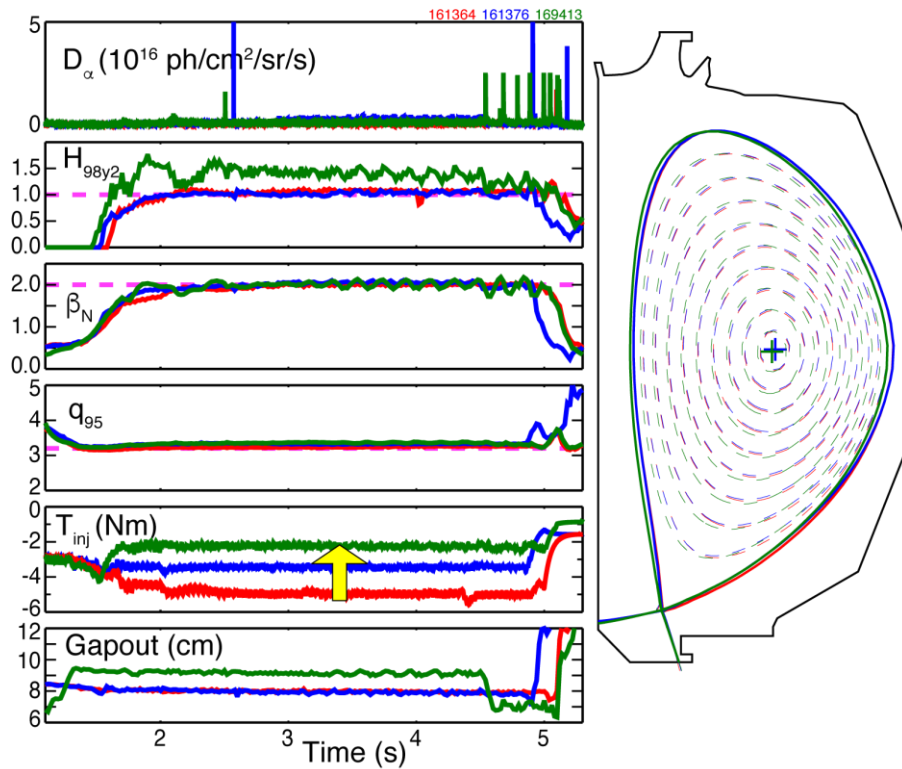


Fig. 2-7. Progress toward QH-mode at zero-net NBI torque with  $Q=10$  equivalent performance on DIII-D, and comparison of the plasma cross sections.

Thus, a common feature of the recent experiments is that lower net NBI torque was achieved with both RMP ELM suppression and QH-mode approaches by using a plasma cross section shape with increased outer gap. In parallel, recent data analysis and modeling have indicated that operation with counter-  $I_P$  NBI on DIII-D creates a thick mantle of fast ions surrounding the low-field side of the plasma [Bortolon 2017]. These are confined fast ions trapped in banana orbits that can travel almost a full gyro-diameter ( $\sim 8$  cm) outside the plasma, as shown in Fig. 2-8. The standard ITER-similar shape on DIII-D has an outer gap of about 8 cm. This mantle of fast ions interacting with the outboard wall surfaces could generate impurity fluxes with important

consequences for both regimes of RMP ELM suppression and QH-mode, which require a low collisionality edge.

Achieving acceptably small ELMs via pellet pacing is another option under development. At zero-net torque, the mantle of fast ions at the edge from counter- $I_P$  NBI presents a challenge for studying ELM pacing, since data shows a large fraction of each pellet is ablated before it reaches the last closed flux surface. This explains why experiments using counter- $I_P$  NBI have found that pellet injection is nearly equivalent to gas injection [Bortolon 2016].

In summary, the presence of an edge mantle of fast ions sourced from the counter- $I_P$  NBI means that DIII-D demonstrations of low-torque ITER scenarios may be complicated by effects not expected to be present in ITER itself. The plan below discusses how such effects will be verified.

Recently, progress has also been made achieving a zero-torque IBS that runs stably without disruption-inducing 2/1 tearing modes. Examples are shown in Fig. 2-8, and the key insights involve improved understanding of the role of the current profile gradient near the  $q=2$  surface that is impacted by changing transport at low rotation. This is explained in Section 2.2.2. As shown in the figure, this scenario presently runs stably over a range of  $I_P$  and internal inductance at ITER target parameters, although the collisionality is still too high and Type-I ELMs remain to be eliminated.

**Goal 1: Evaluate methods and requirements for eliminating Type-I ELMs in zero-torque ITER  $Q=10$  scenarios.**

Work in the next five years aims to understand the requirements for successful ELM-paced (via pellets) and ELM-stable operation (either RMP ELM suppressed or QH-mode) at low torque in the ITER Baseline Scenario, with the help of upgraded hardware, diagnostics, and modeling. New, more ITER-like mid-plane 3D coil arrays and new power supplies will enable much greater flexibility in the 3D field poloidal and toroidal spectra that can be applied to the plasma. Increased 3D field capabilities will be exploited to better control the rotation shear profile to test the hypothesis that this is important for access to both RMP- and QH-mode ELM suppression, especially at low injected torque. The new 3D capabilities will enable research to decouple ELM control, rotation generation, and mode-locking effects. The ability to accurately predict the neoclassical torque from 3D fields is still not at hand. This research will provide the needed

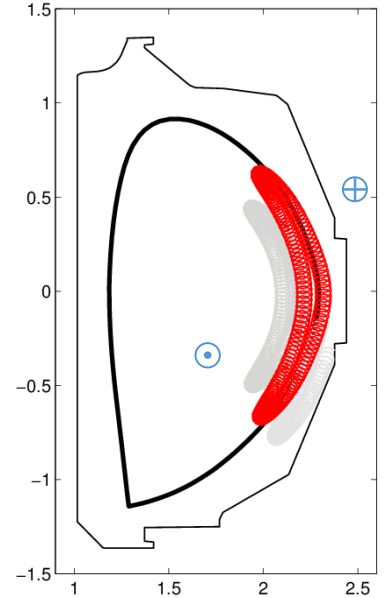


*Fig. 2-8. Full-orbit Monte Carlo code SPIRAL predicts outer-gap populated by trapped, confined, beam ions orbiting outside the last closed flux surface. Gyro-diameter  $\sim 8$  cm, IBS outer gap  $\sim 8$  cm.*

experimental data to validate and improve neoclassical models in the ITER-relevant regime of beta, collisionality, and rotation. In addition to the application of 3D fields, plasma shaping is an actuator that will be varied within relevant limits to alter pedestal gradients and diamagnetic flows. Different paths to zero net torque will be investigated, including ramping down from high torque, and starting from zero torque.

Additional gyrotrons will enable low-torque ITER Q=10 scenario plasmas without using counter- $I_p$  NBI, and this will allow more realistic tests of all three ELM control techniques without the negative impacts of counter- $I_p$  propagating fast ions. Experiments will evaluate if a low-torque plasma achieved using balanced NBI is equivalent to a low-torque plasma achieved using only RF heating. The latter will eliminate large prompt fast-ion losses from the counter- $I_p$  NBI and confined fast ions trapped in banana orbit that extend significantly outside the plasma (also from the counter- $I_p$  NBI). ITER will not have counter- $I_p$  neutral beams, and removing these in DIII-D experiments may have significant impacts on ELM stability, notably through reduced wall interactions and edge collisionality. Experiments will also confirm if the confined fast ions with orbits extending outside the plasma also directly affect pellet ELM pacing techniques by ablating the pellets before they reach the plasma.

**Goal 2: Within the constraints of low torque and ELM control, identify transport and stability tradeoffs in  $q_{95}$  and  $\beta_N$ .**

Work will also focus on whether or not there is a better operating point for ITER's Q=10 mission, away from the standard IBS with  $q_{95} \sim 3$  and  $\beta_N \sim 2$ . Operation at higher  $q_{95}$  (i.e.,  $q_{95} > 3.2$ ) and higher  $\beta_N$  in an Advanced Inductive (AI) scenario regime will be explored. Previous work called into question the adequacy of AI scenario confinement for ITER Q=10 at zero torque [Solomon 2013]. Research will seek to increase energy confinement of the zero torque AI by adding a QH-mode edge to it, enabled by more flexible 3D fields. In more general terms, experiments that scan  $q_{95}$  and  $\beta_N$  will investigate if the prospects for ELM elimination at low torque are improved, if core tearing mode stability is improved, and if projected fusion performance is sufficient for ITER Q=10. This combines pedestal and core optimization, and research will provide opportunities to compare experimental trends with transport and stability models in a broader range of ITER-relevant parameters.

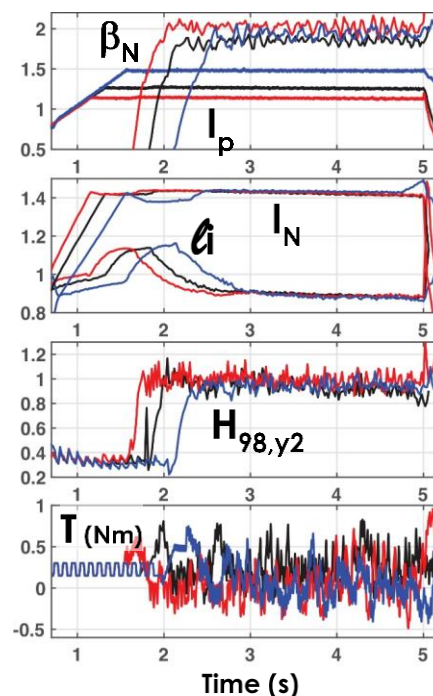


*Fig. 2-9. Zero-torque IBS discharges run without 2/1 tearing modes but still need lower collisionality and ELM control.*

## **Challenge 2: Develop power exhaust control for acceptable divertor heat flux in low torque, ELM-stable ITER Q=10 scenarios**

**Current Progress.** In ITER, where simultaneous high density and low collisionality H-mode pedestals are possible (because of higher toroidal field, energy confinement time, and heating power), strong gas puffing in the divertor area may have little impact on the collisionality of the H-mode pedestal, unlike in DIII-D. Furthermore, core fueling from gas puffing may be less efficient on ITER because neutrals may not be able to penetrate significantly past the separatrix before being ionized. Thus, operation with RMP ELM suppression or QH-mode (requiring a low collisionality pedestal) integrated with a radiative divertor may be easier to achieve in ITER than in DIII-D. So far, power exhaust control on DIII-D has been explored in high-torque, high-power steady-state scenarios without any ELM mitigation, but there has been almost no work to look into the integration of these requirements in a low-torque, ELM-free scenario for ITER's Q=10 mission.

**Goal 1: Evaluate compatibility of radiative divertor techniques with different ELM control approaches.** Research on DIII-D will investigate the possibility of strongly decoupling a radiative divertor from the plasma pedestal and core, focusing on understanding the interconnections and developing the ability to extrapolate. This will provide greater confidence that ELM control and radiative divertor can be integrated in ITER, and could provide essential information for the integration under more challenging requirements, such as in DEMO.

ELM control and radiative divertor have so far been developed separately, but in the next five years, these should be mature enough to begin integration efforts. Initial experiments will identify the limitations for integrating radiative divertor with RMP ELM suppression, QH-mode, and pellet pacing in ITER Q=10 scenarios using the existing divertor and ITER-similar shape. These tests will use puff-and-pump techniques with a variety of impurity gases to increase radiation near the divertor targets while avoiding excessive collisionality increase and loss of ELM control inside the separatrix. Divertor heat flux reductions will be measured and compared to values needed in ITER. Comparison of the three ELM control techniques in similar divertor plasma conditions will help prioritize which techniques may be best for ITER, and DIII-D results will be used to extrapolate to ITER. This work will also evaluate the impacts of a more collisional and radiative edge on core performance, most notably the stability of the q=2 surface that sits not far inside the pedestal, and energy confinement.

**Goal 2: Optimize puff-and-pump technique to achieve greater divertor heat flux reduction with smaller impact on pedestal and core performance.** A key hardware upgrade to address this issue will be a new, flexible gas injection system designed to allow optimization of

the puff-and-pump technique [Petrie 2009] by enabling gas injection from multiple locations, including inside the pumping slot, and close to the strike points on the divertor (see Fig.2-10).

The gas-puff arrays will be toroidally distributed, and injection sites at different poloidal locations (to accommodate for different strike points in different triangularity plasmas) will be independently controlled. The design seeks to increase flexibility of gas flows both in the private flux and the common flux near the divertor to better control the radiation profile near the strike points while limiting core fueling. Similar arrays in both upper and lower divertors will be used to evaluate the effects of drifts and divertor closure on puff-and-pump operation with ELM control in ITER Q=10 scenarios. The best integrated solutions will again be used to inform possible options for ITER.

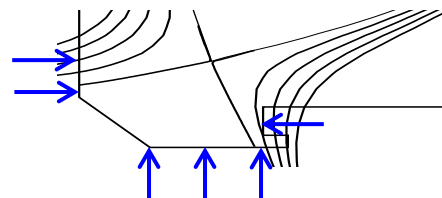


*Fig. 2-10. Schematic illustration of a radial array of gas injectors near the lower divertor. A similar array on the upper divertor is also planned.*

### **Challenge 3: Establish predictive understanding of inductive scenarios at high normalized fusion performance, necessary for projections to ITER.**

**Current Progress.** Every discharge on a future reactor, including ITER, must be validated via simulations ahead of time, and continual predictions during a discharge will provide feedback for how to stay away from stability boundaries that might make the plasma disrupt while maximizing desired fusion performance. In the inductive scenarios on DIII-D, there are a number of processes that interact, including sawteeth, neoclassical tearing modes (NTM), current profile evolution, and kinetic profile evolution (i.e., density, temperature, and rotation). Progress to date on developing predictive capability of core turbulence and transport in ITER Q=10 relevant conditions is described in Section 2.3.1. Chapter 4 contains descriptions of current progress predicting pedestal and SOL parameters. A recent example of integrated modeling is the use of integrated core-pedestal modeling using OMFIT to predict DIII-D plasmas [Meneghini 2015]. The same tools and methods applied to ITER predict Q=10 operation with an optimized pedestal. Lastly, Section 2.2.2 contains a description of the present ability to predict MHD instabilities that occur in ITER Q=10 scenarios. The ITER Inductive Scenarios research program will integrate key physics from many areas of the DIII-D program.

**Goal 1: Predict heat, particle, rotation, and current transport and profiles from core to SOL in ITER Q=10 regimes.** Research will increasingly use state-of-the-art physics-based codes listed in Table 2-4 to predict the evolution of ITER Q=10 scenarios, given preprogrammed actuator waveforms (e.g., plasma shape,  $I_p$ , heating, fueling, 3D coil currents, etc.). This will include predicting time-dependent synthetic diagnostic signals for comparison to real measurements. Any discrepancies between the models and the experiments will be highlighted as issues for improving

model fidelity. Neural networks will be developed and trained for faster, more accurate simulations and for detecting complex nonlinear relationships. New or improved diagnostics, such as turbulence imaging and a laser blow-off system, will be exploited to get a better understanding of transport processes in ITER scenarios.

**Goal 2: Ability to predict MHD instability onset, evolution, and impacts in ITER Q=10 regimes.** Research in this area will include work to better understand the roles of sawtooth, tearing modes, and potentially anomalous resistivity in determining discharge evolution and performance. Experiments and modeling will be performed to determine if the plasma current evolution is consistent with current diffusion based on neoclassical resistivity. Knowing this is a prerequisite for accurate prediction of density, temperature, and impurity profiles, and for predicting sawtooth behavior. This work will rely on improved measurements of the density, temperature, and current profiles. Experiments and modeling will be designed to evaluate to what degree resistivity and, therefore, current profile evolution, is altered by the presence of less harmful 3/2 tearing modes in IBS and AI plasmas. There will be an effort to evaluate models of sawtooth frequency and amplitude, including the impact of neutral beam fast ions, by varying the NBI and ECH mix in ITER scenario plasmas. Models of sawtooth control (destabilization or pacing) by localized ECCD will be tested. A better understanding of sawtooth dynamics will enable evaluation of models of sawtooth control to minimize their impact on ITER’s fusion gain, and models of their role in neoclassical tearing mode triggering. In all cases, the impacts of sawtooth and higher-order (i.e., > 2/1) tearing modes on transport of heat, particles, current, and rotation will be assessed.

**2.1.1.2 Capability Improvements**

The primary improvements enabling research on integrated ITER Q=10 scenarios are described in the following tables. Key hardware upgrades for this include additional ECH power, balanced beams, flexible 3D field systems, and diagnostics and codes to evaluate results.

**Table 2-2.  
Hardware Improvements for Achieving Q=10 in ITER**

<b>Hardware Capability</b>	<b>New Physics</b>
Additional gyrotrons	Explore different paths to low torque plasmas: balanced NBI versus high power ECH
Optimized gas injection for radiative divertor	Achieve divertor heat flux reduction with smaller impact on core plasma density
New power supplies and upgraded 3D coil arrays	Use neoclassical torque from 3D fields to control plasma rotation near the pedestal for ELM-stable operation at low injected torque
Balanced NBI	Explore improved zero-torque scenarios at higher $\beta_N$ and $q_{95}$

**Table 2-3.**  
**Diagnostic Improvements for Achieving Q=10 in ITER**

<b>Scientific Objective</b>	<b>Physics Measurement</b>	<b>Diagnostic Technique</b>
Improved equilibrium reconstructions and stability characterization	Current density measurements near $q=2$ and the pedestal, accurate $T_e$ , $n_e$ profiles	Improved/additional MSE, improved Thomson scattering
Transport model validation	Advanced imaging of temperature and density fluctuations	ECE-I/MIR SNR improvement Imaging MSE, 2 <sup>nd</sup> BES
Improved understanding of the plasma-neutral interaction and its role in PMI and particle, energy, and momentum transport	Poloidally and radially resolved neutral deuterium and SOL deuterium ion measurements	Laser scattering, upper divertor camera, Ly-alpha arrays, pressure gauges, wall Langmuir probes
Understand transport of high-Z impurities in ELM controlled regimes	Spectroscopic/X-ray imaging	Laser blow off/VUV spectroscopy

**Table 2-4.**  
**Simulation Codes Used**

<b>Code</b>	<b>Purpose</b>
OMFIT	Integrated modeling. Predict time-dependent evolution and bifurcation of behavior
Reduced models/Neural networks	Provide faster simulation throughput, and ability to implicitly detect complex nonlinear relationships
ONETWO, TRANSP	Current profile evolution understanding and prediction
GPEC, MARS, DCON, M3D-C1	Linear MHD stability codes, including realistic modeling of 3D perturbations
ELITE, EPED, BOUT++	Understand and predict pedestal stability
NIMROD, M3D-C1, JOREK	Nonlinear extended MHD codes
GS2, TGLF, NEO, CGYRO, XGC	Core turbulent and neoclassical transport
OEDGE, SOLPS	Ionization sources from kinetic neutrals in edge/SOL

### 2.1.2 Fully Non-inductive Scenarios for Steady-State Fusion

*Physics Leads:* J. Ferron (GA), J. Park (ORNL), A. Garofalo (GA), J. Hanson (Columbia), C. Holcomb (LLNL), C. Petty (GA), K. Thome (ORAU), F. Turco (CU), B. Victor (LLNL)

A key mission of the DIII-D program is the development of the physics basis for fully non-inductive steady-state operation at high plasma pressure. This work is strongly motivated by the anticipated improvements in reactor economy and reliability to be gained through operation in steady state and the increase in fusion gain with plasma pressure. DIII-D has a unique capability to advance the steady-state mission as a result of its flexibility. On- and off-axis injected neutral beams (NB) and electron cyclotron (EC) systems enable exploration of plasma current and pressure profiles ranging from peaked to very broad. Cryopumping provides strong density control to achieve advanced current profiles with NBCD, ECCD, and bootstrap current, and to access reactor-relevant low collisionality and low-rotation transport regimes. 18 PF coils enable a wide variety of shapes in single-null and double-null configurations to optimize stability, transport, and divertor pumping. Flexible perturbative 3D coils and steerable EC mirrors provide ELM, resistive kink, and tearing mode control. Finally, a world-class diagnostic set enables a detailed understanding of the outcomes of experiments enabled by this flexibility.

Using these tools, DIII-D has made substantial progress on the steady-state path. Sustained operation above the free boundary ideal MHD limit [Garofalo 2007] is now routine, with resistive wall mode kinetic damping physics largely understood. [Reimerdes 2011]. Transient demonstrations of the advantages of broad current and pressure profiles for achieving power plant-relevant  $\beta_N > 4$  with improved confinement  $H_{98} > 1$  have been made [Ferron 2004, Garofalo 2006, Hanson 2017], as well as similar transient demonstrations of the advantages of very peaked current profiles [Ferron 2015]. Plasma shaping has been optimized for stability, confinement, and density control in steady-state discharges, and the impacts of q-profile on transport assessed [Holcomb 2009, Holcomb 2012]. In the 2014-2018 period, research has identified key energetic particle modes that can harm advanced scenarios, as well as new methods to mitigate these modes [Holcomb 2015, VanZeeland 2017, Kramer 2017, Pace 2017]. Further advances in thermal transport optimization in advanced scenarios have been made [Garofalo 2017, Yoshida 2015] based on q-profile optimization. A steady-state hybrid scenario for ITER and next-step devices has been developed, in some cases with RMP ELM suppression or with a radiative divertor [Turco 2015, Petty 2017]. However, considerable work and facility development is needed to access and develop potential configurations for future fusion reactors, with greater profile range and higher  $\beta_N$  needed. Work to confront this challenge is set out below.

### 2.1.2.1 Challenges and Impact

Experiments will be conducted at DIII-D to address three underlying challenges (see Table 2-5). First, the viability of fully non-inductive, high  $\beta_N$  operation for a power plant must be established. This entails testing a range of advanced current profile scenarios and identifying which are capable of supporting the high  $\beta_N$  required by reactor designs without needing inductive current drive except for the formation phase. Second, a predictive understanding must be developed of the stability, transport, and heating and current drive necessary to achieve the goals of future burning plasmas. This will be achieved by physics studies in scenarios, comparison to advanced simulation and integrated scenario modeling, and pushing to new parameter regimes. Third, compatibility with reactor-relevant boundary conditions must be achieved. This will be explored using a range of hardware upgrades in collaboration with other parts of the DIII-D program.

**Table 2-5.**  
**Steady-State Scenarios Challenges, Goals, and Upgrades**

<b>Challenge</b>	<b>Goals/Deliverables</b>	<b>Upgrades</b>
Develop current profiles consistent with fully non-inductive operation at high $\beta_N$ to establish the viability of future steady-state reactors from ITER to DEMO	<ul style="list-style-type: none"> <li>Identify requirements and optimal scenario paths for plasmas with <math>q_{min}&gt;2</math> and high bootstrap fraction</li> <li>Identify requirements and optimal scenario paths for plasmas with <math>q_{min}\sim 1</math> and efficient central current drive</li> </ul>	<p><i>Hardware</i></p> <ul style="list-style-type: none"> <li>ECCD power increased to 7-9 MW</li> <li>Newly installed 2nd off-axis NBI</li> <li>Raise NBI power to 19 MW co-injection</li> <li>6 s NBI full power pulse length</li> <li>Full-power NBI adjustable between balanced and unidirectional torque</li> <li>Improved RWM feedback</li> <li>New 3D coil set</li> <li>Conformal low-field-side conducting wall</li> <li>Advanced radiative divertor compatible with high-performance core plasmas</li> <li>Helicon and HFS Lower Hybrid</li> </ul>
Develop a predictive understanding of steady-state operation to support ITER and enable the design of future burning plasma tokamaks	<ul style="list-style-type: none"> <li>Validate integrated models that predict self-consistent equilibrium, transport, and stability in non-inductive plasmas</li> <li>Take fully non-inductive, high <math>\beta_N</math> scenarios to reactor-relevant low toroidal rotation and <math>T_e/T_i\sim 1</math>; evaluate and adjust for impacts on stability, transport, and current drive</li> </ul>	<p><i>Diagnostic</i></p> <ul style="list-style-type: none"> <li>Improved <math>T_e</math> and <math>n_e</math> profiles</li> <li>Routine main ion rotation profile</li> <li>Midplane MSE profile with improvements in the outer half of the plasma</li> <li>Routine fast-ion profile diagnostic</li> <li>Laser impurity blow off</li> </ul>
Integrate high-performance steady-state scenario core plasma with power-plant-relevant edge plasma	<ul style="list-style-type: none"> <li>Test compatibility of steady-state scenarios with radiative and advanced geometry divertors; and with ELM mitigation techniques</li> <li>Establish and assess higher density paths to steady-state operation to simplify divertor challenges</li> </ul>	<p><i>Analysis Capabilities</i></p> <ul style="list-style-type: none"> <li>Improved transport models</li> <li>Simultaneous core, edge, scrape-off layer modeling</li> <li>Full-length discharge simulations</li> </ul>

DIII-D advancements in steady-state scenario physics understanding will happen on a schedule that is well timed to aid the newest generation of long-pulse devices, EAST, KSTAR, and JT-60SA. DIII-D will use its flexibility to pioneer scenarios and resolve physics, and then these can be tested in the longer pulse devices, as well as with larger radius in the case of JT-60SA. However, DIII-D will retain the greatest flexibility for further exploration and physics investigation. The predictive understanding gained by DIII-D research will provide a basis to ensure the success of the ITER Q=5 steady-state mission and to design future burning plasma devices, such as fusion nuclear science facilities and DEMO reactors. DIII-D is uniquely suited to identify viable paths for medium-field, conventional aspect ratio, steady-state DEMO tokamaks to achieve the very high  $\beta_N$  near 5 required for high fusion power and bootstrap current fraction.

**2.1.2.2 Research Plan**

The steady-state program research plan is organized by the challenges and goals in Table 2-5, with the timeline for research activities tied to capability improvements in Fig. 2-11.

<b>Challenge</b>	<b>FY19-20</b>	<b>FY21</b>	<b>FY22</b>	<b>FY23</b>	<b>FY24</b>
Develop current profiles to establish steady-state viability	Evaluate improved broad J profiles with $\beta_N = 3-4$ for ITER and FNSF. Extend $f_{NI} = 1$ parameter range in steady-state hybrid to higher $\beta_T$		Explore $f_{NI} = 1$ with $\beta_N = 4-5$ in $q_{min} > 2$ scenario for FNSF and DEMO	Extend $f_{NI} = 1$ duration to $2 \tau_R$	Explore more robust high $\beta_N$ stability with higher ideal-wall limit
Develop a predictive understanding of steady-state operation to support ITER and enable the design of future devices such as FNSF-AT and a DEMO power plant	Evaluate the robustness of each scenario and the control needs				
	Test scenarios with increased Te/Ti, apply to validation of models				
	Study high $f_{NI}$ scenarios w/ reduced toroidal rotation				
	Evaluate the dependence of fully non-inductive operation on $Z_{eff}$ and fast-ion fraction				
	Benchmark fully non-inductive scenarios with various q profiles against improved transport models using time-dependent integrated modeling predictions				
	Validate predictions of AE dependence on q, $\beta_{fast}$				
	Benchmark predicted RWM stability at low toroidal rotation				
Integrate high-performance steady-state scenario core plasma with power-plant-relevant edge plasma	Continue evaluation of radiative divertor with $f_{NI} = 1$ discharges using the steady-state hybrid scenario				
	Evaluate high pedestal $n_e$ Super-H mode compatibility with $f_{NI} = 1$				
	Integrate modified divertor geometries with $f_{NI} = 1$ scenarios				
	Evaluate compatibility of steady-state scenarios with ELM suppression/mitigation techniques				
Capability Improvements	Second off-axis beam 9 MW off-axis beam 19 MW co-beam power 5 MW EC Top-launch EC wall Helicon antenna		7-9 MW EC		Second co-cntr beam 19 MW balanced beam 6 s beam pulse at 22 MW total Stabilizing conformal HFS-launch LHCD system

Fig. 2-11. Steady-state Scenario Timeline

The research timeline is set by the anticipated upgrades schedule. Right from the start of the plan, research will use a newly implemented off-axis co/counter toroidally steerable neutral beam, which more than doubles off-axis neutral beam current drive and increases co- $I_p$  power by a third. Augmented by increases in EC power, sustained, fully non-inductive scenarios with  $\beta_N$  approaching 5 are projected, similar to designs in advanced steady-state DEMO studies. [Najmabadi 2006, Kessel 2015]. Later, a second toroidally steerable beam will enable full-power operation with balanced torque to project regimes to burning plasma relevant conditions. Additional innovative new current-drive tools (see 2.3.4: helicon ultrahigh harmonic fast wave, high-field-side launch lower hybrid current drive) will extend performance at low torque and enable higher density research lines. Near the end of the plan, a new conformal wall will be considered that would widen the range of  $\beta_N$  and  $\beta_T$  that can be accessed at  $f_{NI}=1$ .

**Challenge 1: Develop current profiles consistent with fully non-inductive operation at high  $\beta_N$  to establish the viability of future steady-state reactors from ITER to DEMO**

**Current Progress.** Fully non-inductive tokamak operation at  $\beta_N$  and  $q_{95}$  comparable to that of the ACT1 design for multiple  $\tau_R$  has never been demonstrated. Previous DIII-D experiments [Garofalo 2017] have achieved high  $f_{BS}$  and long-pulse length, but at reduced  $\beta_T$ . Thus, it remains to be proven that a solution at high  $\beta_T$  exists with stationary, self-consistent current and pressure profiles with zero loop voltage everywhere that is stable for duration greater than  $\tau_R$ . This existence proof is a fundamental challenge for the DIII-D program.

A key part of this challenge is to assess the potential of four discharge scenarios with varying  $q$  profile to achieve power-plant-relevant  $\beta_T$  and  $f_{NI} = 1$  operation. These scenarios, in fact, represent points on a continuum of discharge parameters, but it is helpful to understand the distinctions and differences in behavior of these four points. They are grouped here by  $q_{min}$ :

1. Discharges with  $q_{min} > 2$  (“elevated  $q_{min}$ ”)
  - a. “High  $q_{min}$ ”
  - b. “High  $\beta_P$ ”
2. Discharges with  $q_{min} \approx 1$ 
  - a. “Steady-state hybrid”
  - b. “High  $\ell_i$ ”

The high  $q_{min}$  scenario focuses on  $q_{95} \leq 6$  with  $q(0) \approx q_{min}$ . This approach has been studied at DIII-D because, with broad pressure profiles, it scales to high  $\beta_T$ , and thus high  $Q$ , in a power plant. Intervals with  $f_{NI}$  near 1 with duration approaching  $\tau_R$  have been achieved in DIII-D at  $1.5 < q_{min} < 2$  with current density peak value at  $\rho \approx 0.3$  [Holcomb 2009] but, thus far, only limited cases have achieved stationary profiles.

The introduction of off-axis neutral beam injection led to improved capability to operate at  $q_{\min} > 2$ , but thus far at reduced  $\beta_N$  and  $f_{NI}$  [Ferron 2013], largely as a result of increased fast-ion transport caused by unstable Alfvén eigenmodes [Holcomb 2015]. Recent experiments and modeling have shown a variety of options for improving fast-ion confinement in DIII-D high  $q_{\min}$  discharges, including further broadening of the  $q$ -profile with more off-axis NBI, (Fig. 2-12, [Kramer 2017]), AE stabilization using ECH [Van Zeeland 2016], and reduced AE-drive using variable NBI voltage [Pace 2017].

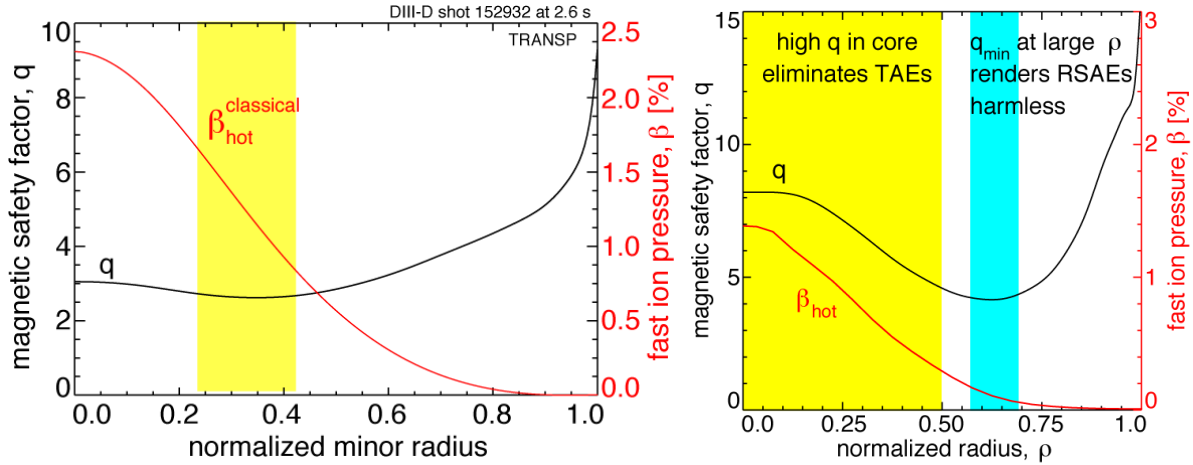


Fig. 2-12. RSAEs are unstable when the radius of  $q_{\min}$  is aligned with a large fast-ion gradient (top). Moving  $q_{\min}$  farther off axis and raising  $q_0$  with additional external current drive is predicted to eliminate TAEs and reduce RSAE drive (bottom).

The high  $\beta_P$  scenario (Fig. 2-13) [Garofalo 2017] provides high  $f_{BS}$  steady-state operation with good confinement. Self-consistent,  $f_{NI} = 1$  operation with stationary profiles has been achieved for duration well above  $\tau_R$  with  $f_{BS} \approx 0.8$  and  $q_{\min} > 2$ . Operation with low values of neutral beam input torque has been achieved. This work has formed a basis for long-pulse operation in the EAST tokamak and is in the parameter regime envisioned for a high  $B_T$  power plant such as ACT2.

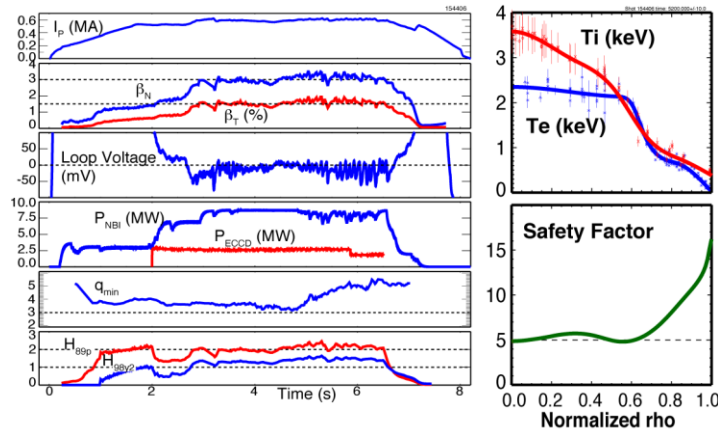


Fig. 2-13. DIII-D fully non-inductive high  $\beta_P$  discharge.

Turning to scenarios with  $q_{\min}$  near 1, the “hybrid” regime of operation [Luce 2014] achieves a stationary, high-performance H-mode scenario with higher confinement and greater stability to disruptive tearing modes than the conventional H-mode regime. It has the attractive characteristic of a self-organized current profile that derives from a “flux pumping” mechanism transferring part of the central current density to an off-axis position, and has been sustained fully non-inductively in DIII-D at the MA level and  $\beta_N$  as high as 3.8 [Turco 2015, Petty 2017]. The scenario has been produced in both the double-null divertor shape and the ITER shape scaled to fit in the DIII-D vacuum vessel. Fully non-inductive operation has been combined with ELM suppression using 3D resonant magnetic perturbations (RMP) in the scaled ITER shape (Fig. 2-14). Projections for operation of the steady-state hybrid scenario in ITER have shown that it can be used to satisfy the ITER goal of demonstrating steady-state operation with  $Q \geq 5$ .

The high  $\ell_i$  regime of operation refers to a scenario in which the internal inductance ( $\ell_i$ ) is increased over what is normally obtained in an H-mode discharge leading to high ideal  $\beta_N$  limits and confinement increase. Discharges with  $\beta_N \approx 5$  and normalized confinement  $H_{98,2} > 1.5$  have been produced in DIII-D with  $\ell_i > 1$  [Ferron 2015].

### Goal 1: Identify requirements and optimal scenario paths for plasmas with $q_{\min} > 2$ and high bootstrap fraction

Fully non-inductive elevated  $q_{\min}$  scenarios will be developed that are capable of meeting expected future burning plasma  $\beta_N$  requirements:  $\beta_N \approx 3$  for ITER or a high-field power plant,  $\beta_N = 3-5$  for possible steady-state nuclear science facilities (e.g., FNSF, CFETR), and  $\beta_N \approx 5$  for medium-field strength DEMO power plants. These tests will rely heavily on the use of new off-axis heating and current-drive sources shown in Table 2-5 and Fig. 2-11 to access broad current and pressure profiles. Exploiting power and pulse length extensions, self-consistent physics models developed in the 2014-2018 five-year period project elevated  $q_{\min}$  discharges will be pushed to reactor-relevant  $\beta_T$ , sustaining the performance for at least  $\sim 2 \tau_R$  to ensure proximity to the ultimate stationary state.

For the high  $q_{\min}$  scenario, FASTRAN integrated modeling [Park 2017] predicts NBI and ECH upgrades available in the 2019-2024 five-year period will enable access to  $f_{NI} = 1$  operation in the

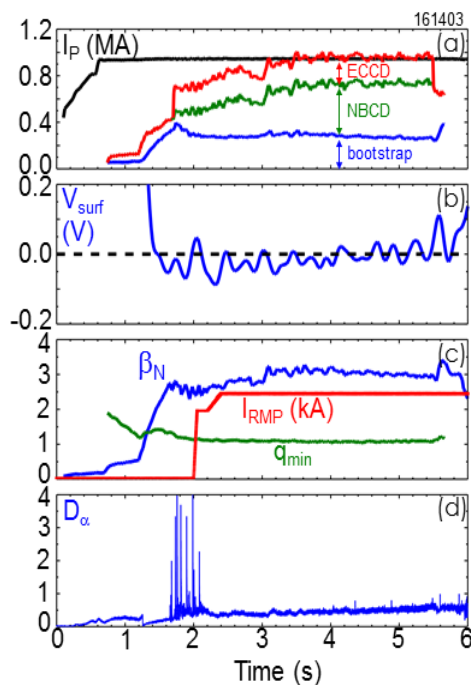


Fig. 2-14. Time history of a steady-state hybrid discharge.

$q_{95}$ ,  $\beta_N$  range relevant to a medium- $B_T$  power plant design, such as ACT1:  $q_{95} \approx 5$ ,  $\beta_N \approx 5$ . Fig. 2-15 shows current density components predicted by FASTRAN with performance approaching these targets. The key upgrades enabling this are increased total neutral beam injection power, an increase in the fraction of the beam power that is injected off axis, and an increase in the available ECCD power for off-axis current drive.

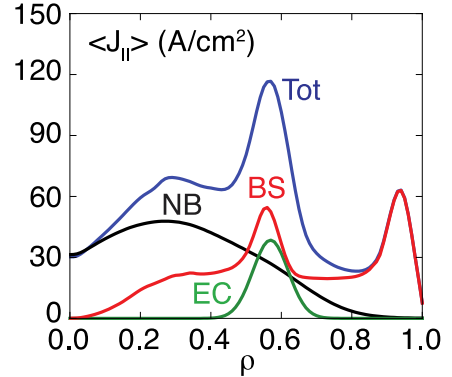


Fig. 2-15. Predicted current components of  $q_{\min} > 2$ ,  $f_{NI} = 1$  scenario with  $\beta_N = 4.6$  and  $q_{95} = 6$  using 6 MW ECCD and 4 off-axis NBI sources.

For the high  $q_{\min}$  scenario, key actions include:

- Broadening the central region of nearly uniform  $q$  using additional off-axis current drive in order to test if stability and confinement are optimized as predicted;
- Maintaining a stationary  $q$  profile with  $q_{\min} > 2$  by combining self-generated bootstrap current with sufficient external current drive for duration at least  $2 \tau_R$ ;
- Exploring fully non-inductive operation over a range of  $q_{95}$  guided by predictive simulations; this will verify the predicted self-consistent values of combinations of  $\beta_N$  and  $q_{95}$  as these are pushed toward the challenging requirements for a DEMO:  $q_{95} \approx 5$  and  $\beta_N \approx 5$ ;
- Evaluating the long-pulse stability limits to  $\beta_N$  as determined by ideal, resistive wall, and tearing modes as a function of the  $q$  profile;
- Mitigating the effects of energetic-particle-driven instabilities such as Alfvén eigenmodes. For more on this see Section 2.3.3.

For the high  $\beta_P$  scenario, key actions include:

- Reducing  $q_{95}$  in order to increase  $\beta_T$  while maintaining a local steep pressure gradient far off axis through operation with negative central magnetic shear as predicted by theory-based modeling. Additional off-axis external current drive should help here also.
- Increasing  $\beta_N$  sufficiently as  $I_p$  is increased in order to maintain  $f_{NI} = 1$ . Document the changes in  $f_{BS}$  and compare with predictive models as  $n_e$  decreases and  $T_e$  increases, thus decreasing collisionality. Understand the effects on  $f_{BS}$  and stability of energetic-particle-driven modes of the corresponding increase in fast-ion stored energy fraction.
- Obtaining control of observed periodic relaxations in the pressure profile using available heating and current drive, 3D fields, and plasma shaping.

The DIII-D research plan also proposes to explore additional methods to implement localized off-axis current drive (Section 2.3.4), which offers the potential to further expand the development of advanced scenarios.

Increasing the available ECCD power enables stable access to  $f_{NI} = 1$  at reduced  $q_{95}$  and increased  $\beta_N$ , pushing toward ACT1-relevant regimes. Fig. 2-16 shows the  $\beta_N$  values for a series of self-consistent  $f_{NI} = 1$  solutions as a function of  $q_{95}$  along with the ideal  $n = 1$  MHD stability limit calculated including the effect of a stabilizing, conducting wall. With the DIII-D vacuum vessel as the conducting wall and 6 MW ECCD power, the region that is stable to ideal modes is at  $q_{95} > 6$  at  $\beta_N \approx 4.5$ , while with 9 MW ECCD power, the stable region expands to  $q_{95} > 5.3$  with  $\beta_N$  close to 5. The range of  $q_{95}$  and  $\beta_N$  where stable operation at  $f_{NI} = 1$  is possible can be expanded through the installation of a conducting wall insert, which is included as an option in the plan. The insert would be of the type illustrated by the conceptual design in Fig. 2-17.

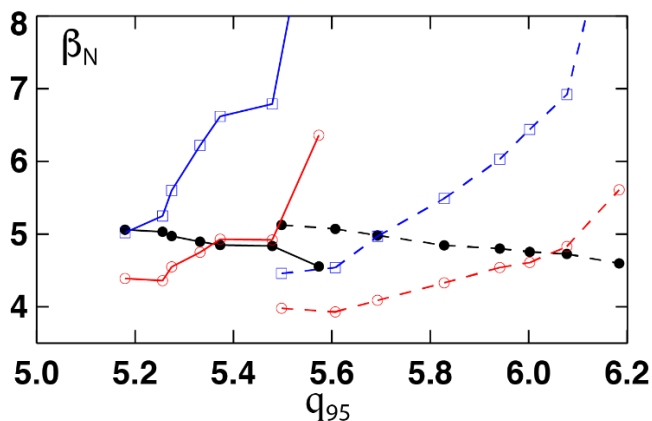


Fig. 2-16. Self-consistent  $f_{NI}=1$  operating parameters vs.  $q_{95}$ . Solid black circles: transport-limited  $\beta_N$ ; red open circles: ideal  $\beta_N$  stability limits with present DIII-D vacuum vessel; blue squares: stability limits including inserts. Dashed lines: with 6 MW ECCD; Solid lines: with 9 MW ECCD.

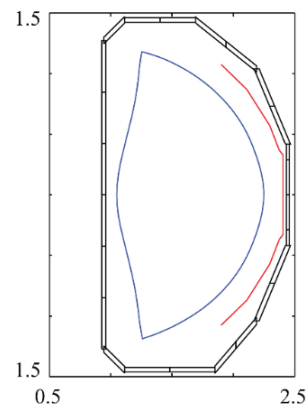


Fig. 2-17. Conceptual design for a conducting insert (red). Present vacuum vessel in black, plasma in blue.

**Goal 2: Identify requirements and optimal scenario paths for plasmas with  $q_{min} \sim 1$  and efficient central current drive.** Fully non-inductive scenarios with  $q_{min} \sim 1$  will also be evaluated for their potential use in future burning plasmas. The planned set of flexible heating and current drive upgrades will be used to push to higher  $\beta_N$ ,  $\beta_T$ , and pulse length. FASTRAN modeling predicts that the upgrades that benefit elevated  $q_{min}$  scenario research also enable the development of a fully non-inductive high  $\ell_i$  scenario with  $\beta_N \approx 4$ , not exceeding the ideal, no-wall MHD stability limit.

The key physics issues in the steady-state hybrid regime that remain for study are primarily directed toward operation closer to parameters that would be characteristic of ITER or a power

plant and the validation at these parameters of models that would be used to project the scenario to those future devices. Planned actions are to:

- Obtain a detailed understanding of the physics of the flux pumping mechanism using improved diagnostics, ECCD to affect tearing modes, 3D coils to affect ELMs, and comparison to models.
- Push fully non-inductive operation to lower  $q_{95} \leq 5$  and higher  $\beta_T$  using additional ECCD.
- Evaluate the limits to stable, long-pulse operation at high  $\beta_N$  and develop techniques to achieve higher values in order to maximize ITER or power plant Q.
- Understand the dependence of the achievable  $\beta_N$  on the pressure profile shape by comparing cases with off-axis and on-axis neutral beam injection.
- Optimize transport in this scenario, including understanding the importance of high-k modes, and methods to suppress them.
- Optimize the high-performance core and H-mode pedestal together. Test if confinement can be improved by raising the pedestal pressure without reaching a global-mode stability limit.

The high  $\ell_i$  scenario has been the least-studied of the four steady-state scenarios. Thus, the most urgent physics issues to be addressed center on a validation that a stationary, fully non-inductive, high  $\ell_i$ , high  $\beta_N$  discharge is possible. Work will:

- Extend high  $\beta_N$ , high  $\ell_i$  discharges to  $q_{95} < 6$  from the presently explored regime of  $q_{95} > 7$  in order to access the regime where self-consistent, stationary operation is predicted.
- Understand how to maintain  $n = 1$  tearing mode, fishbone, and ideal internal mode stability in these discharges where  $q_{\min} \approx 1$ .
- Apply increased ECCD near the axis to maintain a stationary, fully non-inductive discharge.

## **Challenge 2: Develop a predictive understanding of steady-state operation to support ITER and enable the design of future burning plasma tokamaks**

**Current Progress.** The DIII-D steady-state research program is executed in close collaboration with advanced fusion simulations. This is used to guide facility development (not least determining major hardware upgrades set out in this proposal), plasma scenario design and experimental approaches, and to interpret observed behavior. Comparison to experiment enables model validation and identification of required improvements or missing physics. At the heart of this is the FASTRAN suite, which combines TGLF core turbulence models for all transport channels, heating and current drive deposition models, and EPED edge pedestal structure into a

solver that converges stationary equilibrium solutions. TRANSP is another code used worldwide to interpret and simulate time-dependent scenario trajectories. It is used on DIII-D, as described below.

Recent examples of fruitful physics model comparisons to experiment are shown in Figures Fig. 2-18 and Fig. 2-19. Fig. 2-18 shows a comparison of the FASTRAN-predicted stationary loop voltage profile at  $t=\infty$  and the measured loop voltage profile during the high  $\beta$  phase of an elevated  $q_{\min}$  discharge [Holcomb 2014]. The proximity of these two profiles both (i) improves confidence that FASTRAN contains most of the important physics, and (ii) confirms that the experimental discharge was approaching a stationary state. Fig. 2-19 shows how a comparison of simulation and experiment motivated the development of a new TGLF turbulence saturation model that improves agreement between observed and predicted transport in the high  $\beta_P$  regime [Staebler 2017]. This particular regime differs significantly from conditions in which TGLF was originally benchmarked to GYRO, therefore it is the most challenging of all of the steady-state scenarios being studied to account for all transport physics, thus providing an excellent opportunity to expand the range of model validity.

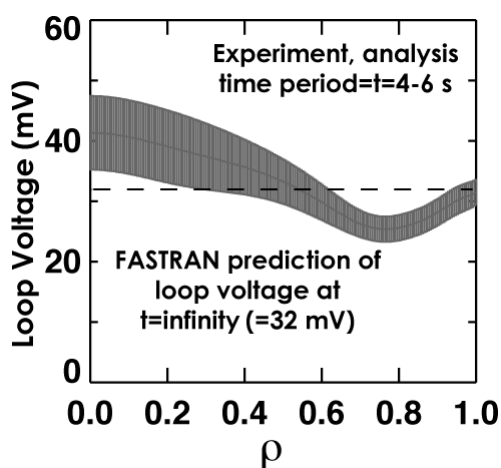


Fig. 2-18 Comparison of FASTRAN and experiment loop voltage profiles.

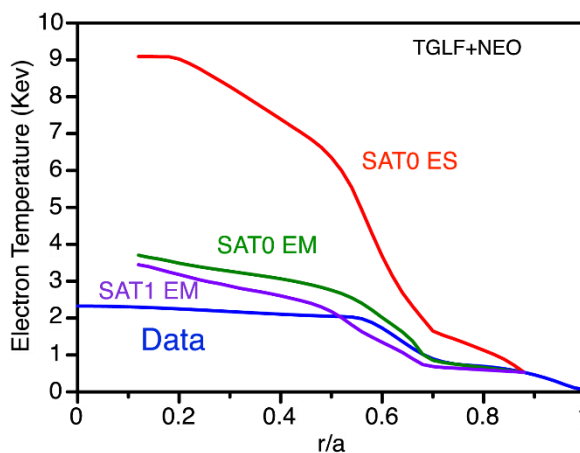


Fig. 2-19. Comparison of the measured  $T_e$  in high  $\beta_P$  scenario to a prediction using TGLF for turbulent transport and NEO for neoclassical. The new SAT1 saturation model with electromagnetic effects, is a better match to data than the SAT0 model with only electrostatic effects.

Obtaining predictive capability for future steady-state reactors will also require pushing present devices to new parameter regimes that have not yet been extensively explored. These are specifically low toroidal rotation and equal electron and ion temperatures. On DIII-D, most steady-state scenario development efforts have so far been done at high torque and  $T_i/T_e > 1$ . In the past few years, some initial forays towards these conditions have begun in the hybrid and high  $\beta_P$

scenarios, but heating and current drive upgrades are planned to expand scenario exploration to reach reactor-relevant parameters.

**Goal 1: Validate integrated models that predict self-consistent equilibrium, transport, and stability in non-inductive plasmas.**

Research will use the FASTRAN suite and TRANSP to interpret behavior in the above-described plasma scenarios in a repeated cycle of scenario design, experimental implementation, and modeling validation. It is particularly important to validate the predictions of current-profile evolution and current-drive self-consistent with transport and stability, which are key to being able to project a steady-state solution for future reactors.

Improvements to FASTRAN are being implemented to increase predictive capability, and these will be tested by comparison to experiment. For the first time, the FASTRAN suite will integrate a self-consistent theory-based model of energetic particle transport associated with Alfvén eigenmodes, to replace the use of approximate and ad-hoc fast-ion diffusion coefficients. Putting this on a predictive footing is an important goal for achievement of simultaneous optimization of thermal and fast-ion confinement. Modeling of tearing mode onset will be also tested using a reduced model (PEST3 / resistive-DCON + critical  $\Delta'$  model) verified against comprehensive non-linear MHD modeling (TAEFL, NIMROD, M3D-C1). Prediction of resistive tearing mode onset as the equilibrium evolves will be essential to optimize access paths into fully non-inductive high  $\beta_N$  conditions.

As the above discussion implies, the validation of models against steady-state scenario data goes deep into the other physics sections in this proposal, where developing and validating advanced simulation capabilities is often at the heart of plans. Rather than repeat those elements here, the reader is referred to the relevant sections, in particular 2.2.2 on stability, 2.3.1 on transport, 2.3.3 on energetic particles, 2.3.4 on heating and current drive, and chapter 4 on core-pedestal-boundary integration.

A key further aspect of the simulation strategy is to utilize TRANSP for time-dependent modeling to project access to steady-state regimes. TRANSP simulation capabilities include free-boundary equilibrium evolution and transport from TGLF to predict the current profile and thermal plasma profiles self-consistently for entire discharge timescales. New physics capabilities being implemented include reduced fast-ion transport models (RBQ-1D), MHD stability with DCON, and pedestal structure with the neutral-network-based EPED model. Additionally, TRANSP interfaces with control algorithms through Simulink to test control methods for the plasma heating, torque, and current drive actuators. This is vital for future reactors, but also quite important to guide discharge development and control on DIII-D. Indeed, as set out in 2.2.3, model-based real-

time profile control is proving highly valuable already for ensuring stability is maintained and target  $q$  profiles are realized.

**Goal 2: Take fully non-inductive, high  $\beta_N$  scenarios to reactor-relevant low toroidal rotation and  $T_e/T_i \sim 1$ ; evaluate and adjust for impacts on stability, transport, and current drive.**

The addition of the capability for full-power neutral beam injection balanced between the co- $I_p$  and counter- $I_p$  directions will allow the study of fully non-inductive conditions with  $\approx 0$  input torque. This neutral beam injection configuration will, however, reduce the amount of beam-driven current so that high-power ECCD is essential to replace this missing current drive. The parameter regime accessible for steady-state DIII-D operation is limited in this case to relatively high  $q_{95}$  and low  $\beta_N$ . Simulations have shown that  $f_{NI} = 1$  operation is possible at  $\beta_N \approx 4$  and  $q_{95} \approx 6$  with 9 MW ECCD.

This will provide a platform to assess more reactor-relevant turbulent transport and stability behavior. In particular, the role of broad current profiles and high  $\beta_N$  electromagnetic effects in turbulence will be assessed at relevant rotational shear and  $T_e/T_i$  values – key parameters influencing turbulent mechanisms (see Section 2.3.1 for more details). Behavior of resistive wall mode stability (and in particular associated dissipative kinetic damping effects), as well as tearing stability, will be assessed at low rotation – a crucial parameter governing these physics mechanisms (see Section 2.2.2). For both aspects, the decreased reliance on neutral beams will reduce fast-ion fractions to enable further assessments of impacts on stability and turbulence, as well as energetic particle-driven resonances (see Section 2.3.4).

Successful implementation of the developmental current-drive tools discussed under Challenge 1 (top launch EC, helicon, and high-field-side LHCD) would further improve the capability to achieve high  $\beta_N$  fully non-inductively at low torque.

**Challenge 3: Integrate high-performance steady-state scenario core plasma with power plant relevant edge plasma**

**Current Progress.** In the past few years, good progress has been made in initial efforts to integrate steady-state scenarios with techniques that lower divertor heat flux and reduce or eliminate ELM heat loads. Experiments using elevated  $q_{min}$  scenarios [Holcomb 2014] and the high  $\beta$  hybrid [Petrie 2017] have explored integrating a puff-and-pump radiative divertor. Discharges with different impurity gases, flow rates, and heating power levels have been compared and impacts on pedestal height, core performance, and heat flux reduction quantified. Similarly, efforts have begun to integrate RMP ELM suppression into high  $\beta$  hybrid operation in the ITER single null shape, as shown in Fig. 2-14. Since the pedestal is the interface between the core plasma and the SOL/divertor plasma, recent advances in pedestal control, such as the ability to access a

high “Super H-mode” pedestal [Solomon 2014], suggest new options for integrated core-edge solutions. This work and other aspects of core-edge integration are described in more detail in Chapter 4. This section has a more narrowly defined scope to assess impacts of integration techniques on steady-state operation, and to pursue the development of a higher density path as a key bridging element to developing compatibility with a dissipative divertor solution.

**Goal 1: Test compatibility of steady-state scenarios with radiative- and advanced-geometry divertors, and with ELM mitigation techniques.**

Radiation of a substantial fraction of the power entering the divertor region is planned through injection of fueling and impurity gases. The gas valve upgrade discussed in Section 2.1.1 will be used to optimize radiative divertor operation in steady-state scenarios. Extra fueling naturally raises the electron density at the separatrix, at the H-mode pedestal top, and in the core, although new divertors will be designed to minimize this increase. Any core density increase will reduce the effectiveness of the principal DIII-D external current-drive sources (neutral beam and electron cyclotron) and push discharges away from  $f_{NI} = 1$  conditions, as would an increase in impurity density in the discharge core. These trade-offs will be explored in terms of impacts on pedestal and core performance, as well as means to overcome them.

The optimum design for the divertor region geometry will be one of the key DIII-D research areas and a substantial modification of the divertor hardware is envisioned for the second half of the proposal period. Continued compatibility of the divertor geometry with plasma shapes that enable high  $\beta_N$ ,  $f_{NI} = 1$  operation will be an important area of research.

Investigations of RMP ELM suppression in steady-state scenarios using expanded 3D coil capability will focus on: (1) achieving suppression in ITER-like single null plasmas at  $q_{95}$  relevant for the Q=5 mission in other scenarios besides the hybrid; (2) achieving suppression in double null steady-state scenarios for the first time; and (3) assessing and adapting to the impacts of RMP fields on core scenario performance.

Research will also extend integrated simulation to the boundary, with the CESOL suite now under development. This code suite combines the FASTRAN/EPED solver with 2D boundary simulation codes such as C2/GTNEUT and SOLPS, in order to project fully integrated solutions from the magnetic axis to the divertor and wall. The development of this suite, and improvement of its composite models, is part of the research plan for this period, with the code development and exploitation led by DIII-D scientists. A critical aspect is to identify reduced transport models at the boundary that can capture 2D transport behavior in the divertor/SOL regions sufficiently well. In the steady-state section of the program, a key issue to explore will be to determine what core parameters are compatible with divertor requirements, and conversely, how boundary techniques

(such as closed divertors) affect core behavior and performance. Iteration between experiment and simulation is vital here.

**Goal 2: Establish and assess higher density paths to steady-state operation to simplify divertor challenges.**

Experiments will begin to look for a high pedestal density scenario with high pedestal pressure, higher bootstrap current fraction and confinement, and increased possibility for reduction of divertor heat flux through detachment. It must be compatible with high ideal stability limits and with fully non-inductive operation given the restrictions on driven current as density and collisionality increase.

This will be focused on the use of Super-H mode coupled to a suitable advanced current profile scenario to substantially increase the pedestal density. The helicon current-drive method (Sec. 2.3.4) has the potential to provide the necessary external current drive at relatively high density, as might high field side lower hybrid current drive, to be tested later in the research plan. Fig. 2-20 shows a FASTRAN fully non-inductive scenario prediction using 2 MW helicon current drive at 90% of the Greenwald density, achieving 70% bootstrap fraction and  $\beta_N$  near 5.

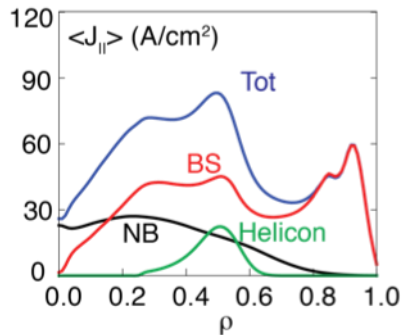


Fig. 2-20. Predicted current components in a  $f_{NI}=1$  discharge with 2 MW helicon.  $\beta_N=4.97$ ,  $f_{BS}=70\%$ ,  $f_{GW}=0.9$ ,  $q_{95}=6.5$ ,  $B_T=1.6$  T.

**2.1.2.3 Improvements in Capabilities**

The DIII-D capability improvements listed in the following tables will enable large steps forward in steady-state scenario research.

**Table 2-6. Hardware Improvements for Study of the Path to Steady-State**

Hardware Capability	New Physics
7-9 MW injected gyrotron power	ECCD, q profile tuning, $T_e=T_i$ , reduced fast-ion stored energy fraction, stabilization of tearing and fast-ion modes
Second off-axis neutral beam line	Broader pressure profile for higher $\beta_N$ limit, reduced on-axis NBCD for higher $q_{min}$ and broader current profile
6 s beam full-power pulse length	$2 \tau_R$ high $\beta_N$ phase duration to approach a stationary state
Increased co-injection and total neutral beam power	Sufficient power to reach $\beta_N=4-5$
Full-power NBI adjustable between balanced and unidirectional torque	Assess the effect of reduced toroidal rotation on access to high $\beta_N$ steady-state discharges

<b>Hardware Capability</b>	<b>New Physics</b>
Stabilizing conformal low-field side wall	Increased ideal-wall $\beta N$ limit for tearing mode and resistive wall mode stable steady-state operation at reactor-relevant toroidal beta
New 3D field coils	Improved 3D field match for ELM suppression at $q_{95} > 5$
New off-axis current drive sources: helicon, LHCD, top-launch ECCD	Improved access to fully non-inductive operation at low $q_{95}$ . Capability to test fully non-inductive scenarios at high density.

**Table 2-7.**  
**Diagnostic Improvements for Study of the Path to Steady-State**

<b>Scientific Objective</b>	<b>Physics Measurement</b>	<b>Diagnostic Technique</b>
Evaluation of bootstrap current density, externally-driven current density, transport, ideal stability analysis	Accurate $T_e$ , $n_e$ profiles are absolutely essential	Improved Thomson scattering at $\rho < 0.9$ , particularly $\rho < 0.5$
Understand the physics of the self-consistent generation of the current density profile and its effects on transport and stability	Midplane profile of the magnetic field pitch angle	MSE diagnostic with improved coverage of the full plasma radius; capability maintained as neutral beam injection geometry is modified
Understand fast-ion loss resulting from energetic particle instabilities and the effect on heating and current drive	Routine fast-ion density profiles and loss spectrum, particularly with the positive toroidal field direction	FIDA (fast-ion $D_\alpha$ ), FILD (fast-ion loss detector) for positive $B_T$
Understand the effects of toroidal rotation on access to fully non-inductive conditions	Routine measurement of the main ion rotation profile	CER (charge exchange recombination)
Understand particle and impurity transport	Transport of injected impurities	Laser blow off

**Table 2-8.**  
**Simulation Codes Used**

<b>Code</b>	<b>Purpose</b>
Integrated suites of codes to evaluate transport, current drive, equilibrium, H-mode pedestal, scrape off layer FASTRAN; TRANSP; ONETWO; IPS (integrated plasma simulator)	Understand, model, and predict the evolution to a stationary state of fully non-inductive discharge scenarios, and in so doing, improve and validate these models to enable future device design
Individual codes: TGLF (turbulent transport); NEO (neoclassical transport); NUBEAM (neutral beam heating and current drive); TORAY (electron cyclotron heating and current drive), EFIT (equilibrium); DCON (ideal and resistive stability); EPED (pedestal); SOLPS; EIRENE (SOL, divertor)	

## 2.2 DISRUPTION CONTROL

Viable operating scenarios for future devices must include methods to control disruptions. Disruptions are caused by MHD instabilities that arise either from an unexpected plant failure (e.g. actuator, device component, programming error), or from undesirable evolution of the plasma to an unstable state. The first case should be rare if actuators are engineered properly, but nonetheless viable recovery or safe-shutdown techniques must be understood and qualified to move forward with devices like ITER. These techniques necessarily involve asynchronous triggering on a detected fault (e.g., heating system failure) to a new real-time control state that must determine the proximity to controllability boundaries and decide on a course of action (recovery or shut down) with the available actuators. The second case can occur even with all actuators working as expected as a result of uncertainties in real-time calculated stability boundaries. Therefore, understanding of stability boundaries and maintaining control is a fundamental requirement. The primary core instabilities that occur in scenarios of interest are classical and neoclassical tearing modes (TM and NTM) that produce non-axisymmetric magnetic islands at low-order rational  $q$ -surfaces, and resistive-wall kink modes (RWM) that globally distort the equilibrium, typically at high  $\beta_N$ . Both TMs and RWMs, at best, only reduce confinement, but in some circumstances the modes can grow to large amplitudes and cause disruption. Plasma-facing components and nearby conducting structures can be damaged by rapid and uncontrolled loss of thermal and magnetic energy, or by the impact of deconfined ‘runaway’ electrons, generated during the plasma current quench.

Compared to larger machines, DIII-D has a much lower risk of actually experiencing component damage from disruptions due to the lower energies involved and its forgiving carbon wall. It is also equipped with a wide range of actuators, to both explore the physics and thresholds, and to provide active control. These include real-time steerable electron cyclotron heating and current drive, three arrays of non-axisymmetric ‘3D’ perturbation coils, fast 3D RWM magnetic feedback systems, massive gas and shattered-pellet injection, and variable voltage beams. Indeed, such tools have already pioneered techniques now adopted in ITER and future reactor designs such as ECCD NTM control, shattered pellet disruption mitigation and high  $\beta$  operation with RWM control (although key questions remain to ensure an effective and rapid implementation). Therefore DIII-D is well suited to develop the physics understanding and control capability to avoid disruptions.

Scenario development research usually includes explicit efforts to build instability control into the scenario in a staged approach. But often more focused, isolated studies on stability and control are needed, and these are carried out in more relaxed plasmas conditions not rigidly constrained by scenario requirements. Therefore, the DIII-D program supports distinct physics topical area work on disruption mitigation solutions (Section 2.2.1), core stability physics (Section 2.2.2), and

plasma control (Section 2.2.3). These are driven by the needs of scenarios, and the results are fed back to improve scenarios (Section 2.1). Core stability physics experiments are designed to test specific physics models when possible, but in other cases experiments are designed to identify correlations to better constrain or build empirical or physics models. Controls research is complimentary to more focused stability studies, both by providing new means to systematically explore relevant parameters to obtain new physics understanding, and by enabling more robust and advanced control solutions that take advantage of the new physics. Together these approaches provide a range of solutions for maintaining passive stability or actively controlling instabilities that can be incorporated into scenarios to effectively avoid or mitigate disruptions.

These solutions will be aided by the development of disruption prediction early warning capabilities using advanced machine-learning approaches as well as physics-based methods, including monitoring proximity to anticipated stability boundaries and the development of an off-normal and fault response (ONFR) system to react in real time to a disruption warning, a detected instability, or a plant failure. Once triggered by such events, ONFR will choose a new action, including switching to a new plasma state, or recovering from an event, or initiating a controlled shutdown, or firing the disruption mitigation system.

Having a reliable and effective disruption mitigation system is critical. Disruption mitigation research on DIII-D is elucidating the detailed physics of how the thermal quench and current quench can be safely managed, and how runaway electrons can be dissipated. This work will evaluate and optimize specific mitigation techniques for ITER and beyond, including finishing work on shattered-pellet injection and moving on to novel shell-pellet injection, which is predicted to be more effective.

The DIII-D vision of a “layered defense” to reduce the occurrence of disruptions is shown in Fig. 2-21. It begins with passively stable discharges achieved through control of the plasma configuration, with active control of certain instabilities when needed. Events such as an uncontrolled instability or a power-supply failure call for a control response that maintains stable operation while either recovering normal discharge operation or terminating the discharge safely. A rapid shutdown with the disruption mitigation system should be a last resort. The Off-Normal and Fault Response system described in Section 2.2.2 will enable the control system to move between the layers in Fig. 2-21, and to engage different elements of each layer, as needed. Techniques of rapid shutdown are discussed in Section 2.2.1 on Disruption Mitigation.

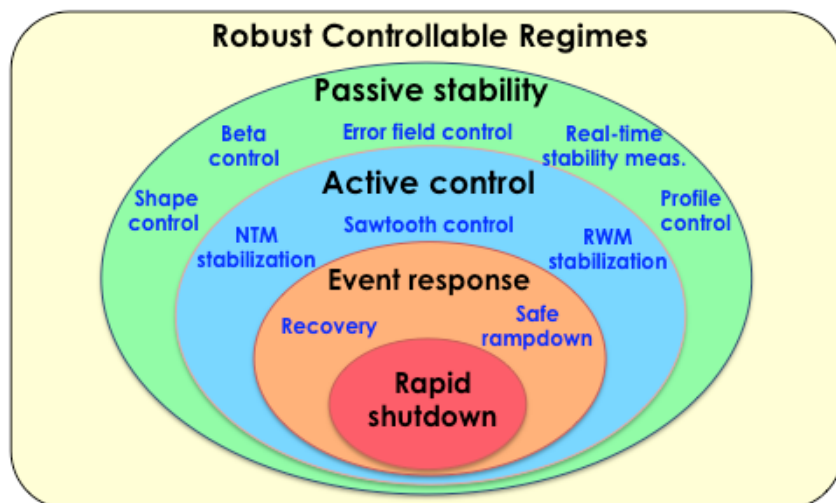


Fig. 2-21. Multi-layered approach to maintaining stable operation and reducing the occurrence of disruptions.

This research will enable the resolution of underlying science and the basis to optimize techniques in DIII-D, understanding how to achieve favorable effects such as maintaining passive stability, and avoiding adverse effects such as rotation braking and locked modes. This will equip scientists with the understanding they need to utilize ITER’s many actuators to establish robust regimes and reach high performance in ITER, as well as resolve requirements and optimal paths for future steady-state fusion reactors. Sections 2.2.1 through 2.2.3 provide more detailed explanations of the challenges, goals, scientific approaches, and key capability improvements related to disruption control.

### 2.2.1 Safely Quenching the Fusion Plasma (Disruption Mitigation)

*Physics Leads: N. Eidietis (GA), D. Shiraki (ORNL), E. Hollmann (UCSD), R. Moyer (UCSD), C. Paz-Soldan (GA), P. Parks (GA).*

The capability to rapidly radiate the thermal and magnetic energy of an unstable discharge to alleviate the consequences of a rapid plasma termination (‘disruption’) is a critical feature of any reactor-scale tokamak. Left unmitigated, disruptions can cause significant damage, leading to delays and cost that can endanger the research goals (ITER) or economic viability (power plant) of the device. The thermal quench (TQ), current quench (CQ), and runaway electron (RE) portions of a disruption each present their own challenges. The ITER disruption mitigation system (DMS) [Lehnen 2015] remains in a state of flux, with unanswered questions regarding its basic capability to meet the necessary mitigation metrics, its construction, and usage. It is unclear if existing plans for shattered-pellet injection will be sufficient, and ITER remains open to additional techniques. This research plan thus aims to underpin the understanding of the ITER baseline DMS design and

physics needs while also pursuing innovative, robust, and reactor-relevant alternate DMS technologies that better meet the mitigation goals of ITER and future fusion reactors.

The DIII-D program has actively addressed many aspects of ITER DMS research in the course of the 2014-2018 five-year plan. The wide variety of impurity injection technologies installed on DIII-D, including the only shattered-pellet injection (SPI) in the world, massive gas injection (MGI), and solid argon pellet injection, enabled flexible exploration of the mitigation problem. MHD activity was identified as a key contributor to radiation asymmetries during TQ mitigation. The limits of SPI for TQ and CQ control were established, with the success of SPI on DIII-D establishing it as the present primary approach for DMS in ITER, and it is now also being tested on JET. Behavior was used to validate non-linear resistive MHD models of the thermal quench and quantify  $n=1$  heat load asymmetries. Key mechanisms for RE plateau dissipation were identified and compared to modern kinetic theories via international theory collaborations, exposing several areas of agreement, as well as inconsistencies between the models and experiment, and the first direct measurements of RE seed generation rates were made.

Moving forward, it is crucial to develop a predictive understanding of the dynamic interaction between mitigation systems and the disrupting plasma in order to develop a robust ITER DMS and ensure safe termination in future reactor concepts. This is the central thrust of this proposal.

### 2.2.1.1 Challenges and Impact

The goal of the DIII-D disruption mitigation research program is to provide the scientific and technical basis to design and operate a robust, effective ITER DMS. To accomplish this, the disruption mitigation program is focused on three key challenges (Table 2-9). The first is to understand the performance scalings and limitations of SPI (the chosen ITER DMS technology) for TQ, CQ, and RE mitigation in order to finalize the SPI implementation and operation plans for ITER, and maximize its effectiveness. For a number of years, DIII-D was the only device possessing SPI, but a proliferation of the technology to numerous devices in 2018 means that this thrust will be a collaborative effort, coordinating and running in parallel with an international effort. The second is to develop a completely new ‘inside-out’ mitigation method and its associated physics, which aims for core deposition of impurities using low-Z shell pellets, to assess if this method can provide the robust, all-in-one mitigation of which early simulations suggest it is capable. Finally, the third challenge is to address the detailed physics driving perhaps the most intractable problem facing the tokamak: RE suppression and dissipation. DIII-D aims to provide unique experiments and capabilities to measure the RE generation and dissipation processes in unprecedented detail. This data will be used, in coordination with multiple theory and modeling collaborations, to test predictions and benchmark codes critical to determining what, if any, path

ITER has to mitigate the RE threat. Indeed, developing validated predictive models will be an underlying theme of all three challenges.

**Table 2-9.**  
**Disruption Mitigation Approaches and Upgrades**

<b>Challenge</b>	<b>Goals/Deliverables</b>	<b>Key Capability Improvements</b>
Develop mitigation metric scalings for ITER SPI system	<ul style="list-style-type: none"> <li>• Determine physics basis to optimize SPI performance for TQ mitigation</li> <li>• Measure impurity transport into RE plateau</li> </ul>	<p><b>Hardware upgrades:</b></p> <ul style="list-style-type: none"> <li>• Cryogenic shell injector</li> <li>• Improved SPI shatter mechanism</li> </ul> <p><b>Diagnostic Upgrades:</b></p> <ul style="list-style-type: none"> <li>• Tangential EUV camera</li> <li>• GRI improvements</li> </ul> <p><b>Code development:</b></p> <ul style="list-style-type: none"> <li>• Collaboration with SCREAM initiative to model highly-coupled multi-scale RE production processes</li> <li>• Continuing SPI modeling and NIMROD modeling</li> <li>• NIMROD 3D-MHD shell modeling</li> <li>• Continuing shell ablation model development</li> </ul>
Achieve “inside-out” disruption mitigation through core dust impurity deposition to robustly meet needs of TQ, CQ, and RE mitigation	<ul style="list-style-type: none"> <li>• Demonstrate inside-out mitigation physics with carbon shells</li> <li>• Develop reactor-relevant magnetically shielded pellet</li> <li>• Increase speed of delivery</li> </ul>	
Develop predictive capability of conditions for effective RE mitigation	<ul style="list-style-type: none"> <li>• Compare measurement and modeling of existence, location, and population of seed RE</li> <li>• Measure spatial/temporal evolution of RE plateau energy distribution</li> </ul>	

The DIII-D disruption mitigation research plan presented above will provide critical knowledge and predictive simulation capability for the development of the ITER DMS. As disruptions represent a significant threat to all large tokamaks, development of such a system is critical to the long-term viability of tokamak fusion reactors.

### 2.2.1.2 Research Plan

The disruption mitigation research plan is organized according to the challenges and goals in Table 2-9. Fig. 2-22 provides the timeline for each challenge, research milestones, and the capability improvements necessary to achieve them.

Challenge	FY19-20	FY21	FY22	FY23	FY24
Developing ITER SPI Scalings	SPI joint comparisons with JET <i>et al.</i> Variations in SPI performance with solid fraction and velocity				
Inside-Out Mitigation	“Inside-out” TQ mitigation evaluation Characterize low-Z dust mitigation Magnetic shielding of cryogenic shell Edge dust injection High-speed injection				
RE Mitigation	Measure 2D RE profiles Test prompt formation of RE seed Measure location / population / timing of RE seed production Compare RE seed generation in edge and core cooled conditions Compare RE seed measurements to models				
New Capabilities:	Diamond shells Modified SPI shatter mechanism Cryogenic shell launcher Dust/D2 SPI hybrid High speed injector Tangential EUV camera GRI detector upgrade				

Fig. 2-22. Disruption Mitigation Plan Timeline

The detailed plan elements are discussed below.

**Challenge 1: Optimize SPI performance for TQ mitigation**

**Current Progress.** The 2014-2018 DIII-D five-year plan period saw significant progress in understanding of the disruption mitigation process, aided by a multi-MGI installation and the world’s only SPI installation. Led by modeling NIMROD resistive 3D MHD modeling predictions [Izzo 2015], TQ MHD was identified as a significant (but tolerable) contributor to toroidal radiation asymmetries during MGI mitigation [Commaux 2014, Shiraki 2015], as shown by the ability to “steer” the n=1 character of the radiation with 3D fields in Fig. 2-23. The effect upon poloidal radiation asymmetries is less pronounced [Eidietis 2017]. SPI provided superior performance, with studies revealing that TQ

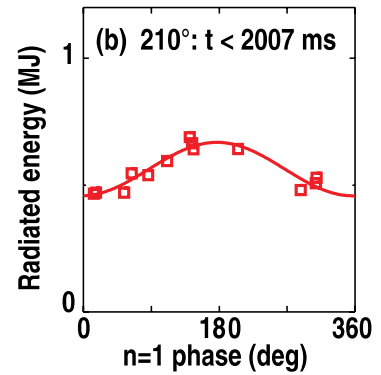


Fig. 2-23. Measurement of n=1 character of TQ radiated energy during neon MGI [Shiraki 2015].

radiation levels using neon SPI saturate near 90% radiation fraction (the ITER goal for radiated mitigated power fraction) at fairly low injected particle quantities (Fig. 2-24) [Shiraki 2016], and a very narrow window where scaled current quench times and the desired radiation fraction meet ITER specifications simultaneously.

Although SPI has now been chosen as the injection technology for the ITER DMS, significant uncertainty remains as to the optimal configuration and quantities of impurities that must be deposited into ITER in order to create the desired TQ radiation, which in turn has ramifications for the final DMS design. Similarly, a wide disparity exists between the ability to dissipate RE beams through impurity injection into the RE plateau on various devices. Mid-size (e.g., DIII-D) and small devices have reported strong dissipation of RE beams by injecting MGI and SPI into the plateau [Hollmann 2013], but with widely varying assimilation efficiency, whereas JET reports almost no effect, even with very large impurity quantities [Reux 2015]. The transport and assimilation of impurities into the RE beam, and the effect of SPI vs MGI on that transport, must be understood in order to project to ITER.

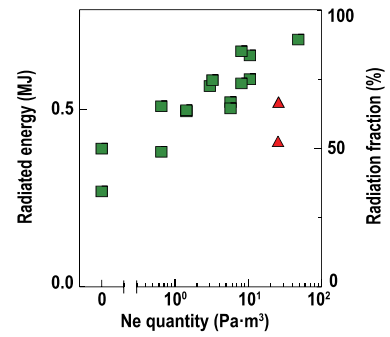


Fig. 2-24. TQ radiated energy and corresponding radiation fraction (right axis), as a function of SPI neon quantity showing saturation at  $\sim 10 \text{ Pa}\cdot\text{m}^3$ . Broken pellets (at time of firing) are indicated as red triangles. From [Shiraki 2016].

Key physics questions remain to be answered:

1. How does the impurity quantity required for  $>90\%$  radiation fraction with SPI scale with plasma volume/energy/pedestal height?
2. How do the SPI characteristics (velocity, solid vs gaseous fraction, fragment size distribution) affect those scalings?
3. What governs the transport of impurities into the RE beam, and what will RE beam assimilation of impurity injection be in ITER?

**Goal 1: Determine physics basis for optimizing SPI performance for TQ mitigation.** The primary component of this research thrust will be jointly planned similarity experiments to develop scalings of SPI TQ mitigation metrics for ITER. These joint experiments will be planned with JET, J-TEXT, and HL-2A, all of which are planned to have SPI systems available in FY18 or soon thereafter. The ITPA MHD Topical Group serves as the forum for organizing these joint experiments, with first discussions having occurred in late 2017.

Numerous questions regarding the operation of SPI remain. SPI is a very complicated process compared to MGI. On the injection level, changes in pellet velocity and shatter angle drastically alter the ratio of the various phases (gas, liquid, solid) of impurities exiting the injector. This may have a significant bearing upon whether SPI acts like a fast version of MGI and MHD mixing dominates the impurity transport into the plasma, or acts like a pellet stream with ballistic transport dominating. The shattering properties will also vary the size distribution of the solid pellet

fragments, potentially leading to vastly different ablation evolution and particle assimilation, which in turn will vary with plasma parameters. Multi-machine comparisons are desirable to explore the many dimensions involved in this problem. The primary studies that will be executed are:

- Measure the quantity of neon at which radiation fraction saturation occurs as a function of thermal energy, plasma volume, and pedestal height;
- Test modifications to the above scalings using pure neon pellets of differing sizes vs equivalent amounts of neon in deuterium/neon SPI mixtures (i.e. test effect of dilution cooling).

In addition, DIII-D will explore the effects upon the SPI mitigation metrics as the SPI injection characteristic are modified. The key injection characteristics are

- SPI solid fraction (fraction of SPI pellet mass that remains in solid form after shattering);
- SPI velocity;
- SPI fragment size.

In the present DIII-D SPI design, the pellet velocity and solid fraction are closely linked. Modifications to the SPI shatter mechanism to allow high solid fraction at high velocities ( $> 200$  m/s) will be pursued.

These experiments will provide benchmarking for, and be guided and interpreted by, modeling through collaboration with the SciDAC Center for Tokamak Transients Simulations (CTTS). CTTS will run the NIMROD and M3DC1 codes, coupled with advanced SPI source models, to simulate SPI mitigation on DIII-D.

**Goal 2: Measure impurity transport into RE plateau.** Research will feature a concentrated effort to quantify and interpret the assimilation dynamics of impurity injection into the RE plateau. This impurity transport will be measured as a function of RE current, thermal core plasma density, and scrape-off plasma density. MGI and SPI assimilation will be compared to determine if SPI avoids the blocking of neutral impurities by warm ( $10^3$  eV), low-density scrape-off plasma as observed in JET [Reux 2015]. Impurity and plasma density profiles will be measured by moving the RE plateau across existing diagnostic lines of sight, while upgrades to the gamma ray imager (GRI) detectors to allow the spatially resolved RE plateau energy spectra to be measured will enable spatially resolved measurement of the effect of the impurity transport upon the RE population. Completion of this research goal will provide the impurity transport dynamics required for existing 0D and 1D RE dissipation models, developed in collaboration with the Simulation Center for Runaway Electron Avoidance and Mitigation (SCREAM) and Max Planck Institute for

Plasma Physics (IPP), to accurately project to the DMS response required to dissipate an ITER RE plateau.

## Challenge 2: Produce “inside-out” disruption mitigation through core dust impurity deposition

**Current Progress.** Recent modeling [Izzo 2017] indicates that core impurity deposition, wherein the injected radiating impurities cool the plasma core without significantly cooling the edge, shows promise to dramatically improve all stages of the disruption-mitigation process over conventional methods that first cool the edge (e.g., MGI or SPI). Core radiation inverts the TQ process, cooling from the inside-out and minimizing heat transport to the scrape-off layer to protect the divertor. 100% impurity assimilation due to deposition in the core enables the use of low-Z impurities (e.g., beryllium dust) to achieve high thermal radiation fraction while still providing a warm CQ with acceptably slow current decay rate to avoid mechanical damage from eddy currents. In addition, inside-out mitigation is predicted to create stochastic regions throughout the entire cross-section of the plasma during the TQ (not just the edge, as in conventional mitigation [Izzo 2011]) that can rapidly deconfine RE seeds and provide high core densities to suppress RE seed formation and avalanche multiplication (Fig. 2-25).

Key physics and technical questions to be addressed are:

- How can impurities be transported to/near core before inducing the TQ?
- How does core impurity deposition alter heat transport and radiation efficiency during TQ?
- What governs transport/confinement of massive dust quantities in cooling plasma?
- Is dust dispersal sufficient to collisionally suppress RE formation throughout plasma?

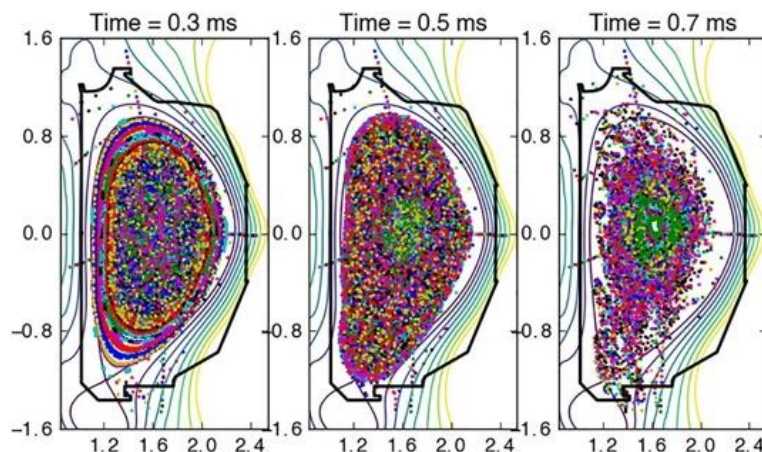


*Fig. 2-25. Poincaré plots of magnetic field lines at three times after core deposition of argon, as modeled by the NIMROD resistive MHD code. Core flux surfaces are stochasticized immediately. Outermost closed flux surfaces are retained until the end of the thermal quench, after which outer field lines become very stochastic. From [Izzo 2017].*

- Can dust payload be tailored with large high-Z grains to increase RE suppression capability without creating excessively fast CQ?
- Is dust quantity required for effective mitigation consistent with ITER deflagration limits?

The most promising candidate for inside-out mitigation is shell-pellet injection, which uses a low-Z shell filled with dust to deliver impurities to the core (Fig. 2-26) [Commaux 2011]. Once the impurity is successfully delivered to the core, the effects of the core deposition upon the TQ radiation efficiency and heat transport need to be verified. In addition, the transport of core-deposited dust in the plasma must be measured to understand where and how much impurity density will be present for RE suppression.

While DIII-D has maintained a low-level effort of shell pellet development over the past several years [e.g. Commaux 2011], technical difficulties have slowed physics progress. Polystyrene shells used in the initial studies that were thick enough to survive to the plasma core proved too perturbative to the plasma (i.e. cooled the plasma significantly before reaching the core), and thinner shells broke up in the injector guide tube at desirable velocities when any curvature was present. Hence, the physics promise described in [Izzo 2017] has yet to be experimentally verified. Moreover, no knowledge exists of the transport of massive dust around and out of the plasma. This knowledge is critical to understanding how much dust is required to provide the desired mitigation, and thus if the required quantity in ITER would be within deflagration safety limits. The shell pellet development plan outlined below is designed to overcome the technical difficulties in a step-wise manner to enable thorough testing of the physics of inside-out mitigation and proceed to a reactor-relevant solution.

**Goal 1: Demonstrate “inside-out” mitigation with carbon shells.** This initial work will focus upon testing and experimentally verifying the physics of inside-out mitigation using core dust injection by the most technologically expedient method. This will utilize room-temperature carbon shells launched by a conventional gas gun injector.

In contrast to previous attempts, the planned studies will use diamond shells to provide greater mechanical strength (allowing higher velocity injection) and ablation energy (reduced perturbation to edge plasma) than the plastic shells used in [Commaux 2011]. These qualities should enable deeper penetration into the plasma core. In addition, the shell injector and guide tube will be

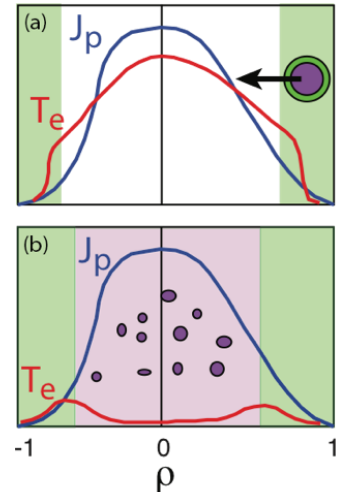


Fig. 2-26. Cartoon of shell pellet injection. (a) Radiating impurity (purple) encased in low-Z shell (green) proceed through plasma without perturbing profiles. (b) Shell ablates in core,

modified to provide a more direct injection path and minimize the chances of shell damage prior to entering the vessel.

The research is comprised of two main steps:

1. Demonstrate “inside-out” TQ mitigation with small, pure C (diamond) shells filled with boron (B) and B+tungsten (W) dust.
2. Explore limits to impurity assimilation and core impurity transport with large B dust filled diamond shells.

Step #1 will allow the basic model of inside-out TQ mitigation to be tested. The key features of the mitigation to verify in Step #1 are:

- Deposition of impurity dust in the plasma core;
- Radiation predominantly from core;
- High radiation fraction with low-Z (B) radiator ;
- Mild CQ  $T_e$  and slow CQ decay rate despite high radiation fraction.

Step #2 will test if sufficiently high densities (some fraction of the “Rosenbluth” density) can be achieved to collisionally suppress RE seed production in the TQ and avalanche multiplication of the RE in the CQ. Key features to measure will be:

- Maximum TQ/CQ density as function of B dust quantity;
- Variation in assimilated quantities with plasma thermal energy;
- Transport of impurity dust from core region of plasma.

Shell-pellet studies will be guided and interpreted by the modeling collaboration with CTTS, which will build upon the initial 3D resistive MHD modeling reported in [Izzo 2017] to ascertain the sensitivity of inside-out mitigation to the deposition radius, predict optimal radiator quantities, and provide interpretation of experimental results.

Should the shell-pellet concept prove technically infeasible, deep dust injection may also be attempted using a B dust + D2 ice hybrid SPI, although the penetration properties of this concept are presently very uncertain.

**Goal 2: Develop reactor-relevant magnetically shielded shell pellet.** Following the basic demonstration of inside-out mitigation outlined above, this research will aim to demonstrate the magnetic shielding of a metallic shell pellet.

A conventional shell pellet would require extraordinary velocities (km/s range) in order to survive to the core of the plasma in ITER or a reactor, due to the high plasma temperature and

large distances the shell must travel. However, a metallic shell (Li in DIII-D, Be in ITER) cryogenically cooled so that it has extremely low resistivity will push the tokamak’s magnetic field around itself, producing “magnetic shielding” that diverts the hot electrons around the shell and dramatically lowers its ablation rate. Magnetic shielding enables core deposition with readily achievable injection velocities (100’s m/s).

The deposition depth of cooled and room-temperature metallic shells will be compared on DIII-D to verify the magnetic shielding concept and validate modeling of the shielding effect. Lithium shells (Beryllium is not compatible with DIII-D operations) and a cryogenic launcher will be developed by GA for these experiments.

**Goal 3: Increase speed of delivery.** Finally, should the shell pellet method show promise, high velocity injection (proposed for DIII-D) will be tested to expand the response time and reduce the need for magnetic shielding in an ITER-relevant shell pellet injector.

### **Challenge 3: Develop predictive capability of conditions for effective RE mitigation**

**Current Progress.** RE mitigation remains the most intractable issue for the ITER DMS. Recent modeling [Konovalov 2016] suggests that dissipation of RE beams, once formed, in ITER may be extremely difficult or impossible due to the additional electric field induced by the almost inevitable vertical instability of the runaway beam. This has had major ramifications for the design of the ITER DMS, forcing a reconfiguration to focus upon RE seed suppression rather than just RE plateau dissipation [Martín-Solís 2017]. Although the primary sources for RE seed formation (Dreicer, hot-tail, Compton scattering, tritium decay) are well studied theoretically, their self-consistent interaction with the TQ MHD and other dissipation and loss mechanisms are not well understood. Understanding the RE seed generation process and verifying the understanding of RE plateau growth and loss mechanisms is critical for defining a robust RE mitigation system.

The primary goal of this research thrust will be to understand the dissipation of RE plateaus and RE seed production to provide guidance as to whether dissipation and/or complete suppression of RE is possible in ITER. Several mechanisms come into play in determining the evolution of an RE plateau, including the driving electric field, scattering, synchrotron losses, line radiation, kinetic instabilities, radial losses, and the evolution of the beam equilibrium. Understanding the relative importance and competition between these various mechanisms will determine whether an existing RE plateau can in fact be mitigated. The exact nature of the RE seed generation mechanisms during the TQ in ITER is also in doubt, as it is unclear if the standard Dreicer and hot-tail mechanisms accurately describe the generation process during massive impurity injection. The only direct measurement of RE seed production to date has been performed on DIII-D using

indirect measurements of pellet ablations (Fig. 2-27) [Hollmann 2017]. Moreover, the interaction of RE seed generation with the dynamic stochastic fields of the TQ remains both unmeasured and poorly modeled.

Key physics questions to be answered for RE seed suppression and plateau dissipation are:

- Does [Konovalov 2016] accurately predict strong RE regeneration due to scrape-off of the flux surfaces in a vertically unstable RE plateau?
- What mechanisms are responsible for inconsistency between measured and modeled RE energy spectra at low energies [Paz-Soldan 2017]?
- What role do kinetic instabilities and radial transport play in RE plateau dissipation, and can they be exploited to enhance RE dissipation?
- At what location(s) do seed RE form after TQ?
- What mechanisms dominate RE seed production (i.e., what is RE seed population)?
- What processes most effectively reduce RE seed population?

**Goal 1: Compare measurement and modeling of existence, location, and population of seed RE.** Work will emphasize detailed measurements of RE seed production and comparison to modeling under various conditions. This will enable the predictive understanding necessary to determine if massive deuterium injection [Martín-Solís 2017] or core dust injection could reliably suppress RE production in ITER, and what quantities are needed. In particular, it will:

- Measure location/population/timing of RE seed production and compare to predictions of close/open flux surfaces from NIMROD;
- Compare RE seed production at vastly different core  $T_e$  to test prediction of prompt conversion of all current to low energy RE [Aleynikov 2015];
- Compare RE seed generation in edge (Ar pellet) and core cooled (shell pellet filled with Ar gas) conditions to test if the core stochastization limits RE seed production.

This research will be enabled by additional diagnostic capability, including an EUV camera to image the location of young, low energy (10's keV) RE seeds, and low-energy GRI detectors to provide imaging of mid-energy (100's keV) RE seeds.

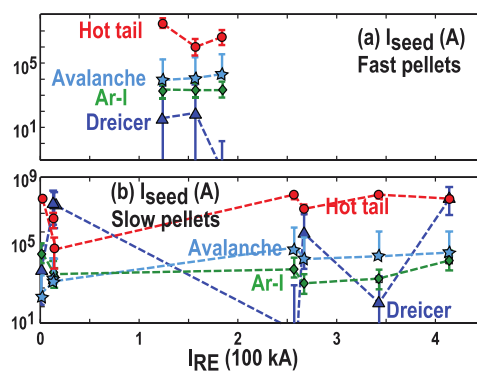


Fig. 2-27. RE seed current at end of TQ estimated using argon pellet ablation for (a) fast pellets and (b) slow pellets as a function of initial RE plateau current. From [Hollmann 2017].

These spatially-resolved measurements will be compared to time-dependent, multi-scale simulation of RE seed interaction in the presence of MHD in collaboration with SCREAM and IPP.

**Goal 2: Measure spatial/temporal evolution of RE plateau energy distribution.** This part of the research plan will pursue detailed measurements of the post-disruption RE plateau energy spectra, expanding upon work done in the flattop quiescent runaway electron (QRE) regime in the past five years. These spatially resolved energy spectra measurements allow the most detailed comparison to theory to identify the primary mechanisms for RE plateau loss and dissipation. This will enable predictive modeling critical to determine if a self-consistent scenario for RE plateau dissipation exists in ITER, and the most effective means for producing that dissipation.

Key parts of this plan will be to:

- Compare the energy deposited to the wall by vertically stable and unstable RE plateau to determine if the energy dissipation rate is much greater in the unstable case [Konovalov 2016], and if it can be significantly modified by collisional damping
- Measure of radial profiles of RE energy distribution to determine role of 1D radial transport in discrepancy between measured and modeled RE energy distribution function [Paz-Soldan 2017]
- Analyze role of kinetic instabilities in limiting the high-energy portion of spectra
- Explore feasibility of induced whistler waves to clamp RE energy distribution to low energies.

This plan will be enabled by planned upgrades to the GRI detectors to avoid saturation of the diagnostic during the high gamma flux of the RE plateau. The resulting data will be used to benchmark models in collaboration with SCREAM, IPP, and Chalmers University.

### 2.2.1.3 Capability Enhancements

The disruption mitigation research program will require numerous enhancements to present impurity injection hardware (Table 2-10). Modification to the SPI shattering mechanism will enable variation of the SPI shard size and distribution to optimize SPI assimilation. Diamond shell pellets will provide an intermediate step for verifying inside-out mitigation at room temperature. This will be progressively followed up by the deployment of cryogenic metallic shells and a cryogenic injector to test reactor-relevant magnetic shielding of the pellets, and subsequently high-speed injection hardware. Runaway studies will be enabled by diagnostic upgrades (

Table 2-11). A tangential extreme ultraviolet (EUV) camera will provide imaging of the location of young, low energy (10's keV) RE seeds, and low-energy GRI detectors to provide tangential imaging of mid-energy (100's keV) RE seeds. In addition, upgrades to the existing

higher-energy (multi-MeV) GRI detectors will allow measurement of spatially-resolved RE energy spectra during post-disruption RE plateau, in addition to the flattop quiescent RE (QRE) that were studied in the past five years.

**Table 2-10.  
Hardware Improvements for Disruption Mitigation Research**

<b>Hardware Capability</b>	<b>New Physics</b>
Improved SPI shatter	Core (deeper) deposition of SPI impurities
Large pure C shells	Core dust mitigation and transport
Cryogenic metal shells and launcher	Magnetic shielding of shell (reactor relevant)
Increased injection speed	Deeper/faster impurity fueling

**Table 2-11.  
Diagnostic Improvements for Disruption Mitigation Research**

<b>Scientific Objective</b>	<b>Physics Measurement</b>	<b>Diagnostic Technique</b>
Visualize location and population of seed RE	EUV bremsstrahlung from low-energy/mid-energy seed RE	EUV imaging (low energy) and modified GRI detectors (mid energy)
Measure 2D RE energy distribution and seeds	RE bremsstrahlung emission	Upgraded GRI detectors

**Table 2-12.  
Codes Used for Disruption Mitigation Research**

<b>Code</b>	<b>Purpose</b>
NIMROD	SPI mitigation modeling. Effect of core impurities upon TQ mitigation and RE generation. Coupling of MHD to other dynamics
SCREAM development	Multi-scale self-consistent RE generation and loss including MHD effects
SOFT	Synthetic synchrotron and bremsstrahlung emission diagnostic code for comparison to camera and GRI images
1D Fokker-Planck RE kinetics code	Predict RE generation mechanisms in impurity dominated plasma

## 2.2.2 Core Stability Control for Disruption-Free Operation

*Physics Leads: E. Strait (GA), J. Hanson (Columbia), N. Logan (PPPL), R. La Haye (GA), W. Choi (Columbia), M. Okabayashi (PPPL), C. Rea (MIT), Z. Taylor (ORAU).*

Reliable operation of tokamak fusion plasmas requires stable operating scenarios, achieved through passive or active means. Stable operation is critical to ITER and to future power plants, in order to minimize the risk of damage to the facility from plasma disruptions, as well as the risk to the scientific mission or interruption of power production that would result. The most dangerous instabilities are long-wavelength tearing modes and kink modes, and these must be avoided by passive means or suppressed by active stability control. ITER and other burning-plasma tokamaks will operate with low plasma rotation (low torque input) and low collisionality, a regime that differs from many existing tokamaks. Solutions to the challenge of stability must be compatible with this regime.

DIII-D research has made significant progress toward the scientific understanding and practical control of tokamak instabilities. ITER-simulation discharges free of tearing or kink instabilities have been demonstrated, techniques have been developed to predict or actively sense an impending instability, and active control methods have removed or limited both ideal and resistive instabilities after they have appeared. Advances in the physics understanding of non-axisymmetric or “3D” fields in tokamaks have enabled new approaches to improving and controlling stability. The work proposed in the 2019-2024 five-year plan is aimed at consolidating these advances and the scientific understanding that underpins them, and incorporating that understanding into an integrated control system that maintains stable operation and handles off-normal events without disruptions.

### 2.2.2.1 Challenges and Impact

The goal of DIII-D stability research is to develop the scientific foundation for integrated, physics-based stability control and disruption avoidance in ITER and other future burning plasmas. This goal entails three significant challenges (Table 2-13).

The first challenge is to improve the stability of conventional inductively driven plasmas, relevant to ITER’s  $Q=10$  mission. This research will be enabled by new tools including additional gyrotrons for multi-mode tearing control with simultaneous control of global profiles for passive stability, new coils for control of 3D magnetic fields and magnetic islands, and new diagnostics for detailed measurements of instabilities and the plasma conditions that cause them.

The second challenge is to establish the scientific basis for stability of high beta, steady-state discharges, which have the added feature of wall stabilization. Here the steerable, variable-voltage

neutral beams and new 3D coils and power supplies will be key tools for investigating both passive stability and feedback stabilization of kink modes at high beta.

**Table 2-13.  
Core Stability Control Challenges, Goals, and Enhancements**

<b>Challenge</b>	<b>Goals/Deliverables</b>	<b>Facility Enhancements</b>
<i>Understand stability and control requirements for disruption-free operation of ITER’s Q=10 mission</i>	Assess tearing mode dependence on current, pressure, and rotation profiles, seeding, and other parameters. Raise stability Validate models of active tearing mode control by ECCD and RMP, and assess requirements for ITER. Develop real-time sensing and prediction of stability limits that can be extrapolated to ITER, and event response strategies.	<b>Hardware:</b> <ul style="list-style-type: none"> <li>• Added EC power, up to 7-9 MW</li> <li>• Co-counter steerable NB</li> <li>• New 3D coils and supplies for expanded n,m spectra</li> <li>• “Conformal wall” for passive stabilization</li> </ul> <b>Diagnostics:</b> <ul style="list-style-type: none"> <li>• 1D profiles (ne, Te, Ti, toroidal rotation, Bz): Improved radial and time resolution for axisymmetric control</li> <li>• 2D and 3D: Toroidally resolved MSE, ECE or ECE-Imaging for MHD mode analysis</li> </ul> <b>Analysis Capabilities:</b> <ul style="list-style-type: none"> <li>• Stability models to predict linear/nonlinear tearing stability limits</li> <li>• Real-time codes for ideal and resistive stability</li> <li>• Integrated analysis of extended 3D magnetics and other diagnostics</li> </ul>
<i>Understand stability and control requirements for high-performance steady-state operation</i>	Validate kinetic stabilization physics at low rotation, and optimize for high-β stability. Establish active stabilization of RWMs (kink modes) beyond passive stability limits, using ITER-relevant coils. Assess stability of high-li and other high-β scenarios that do not require wall stabilization.	
<i>Understand and apply 3D physics to improve the stability of tokamak plasmas</i>	Optimize active control of intrinsic 3D fields (error fields) at multiple n. Establish control of resonant drive for higher n tearing and kink instabilities in ITER-relevant scenarios. Assess the impact on stability of flow and flow shear generated by 3D fields.	

The third challenge is to advance the scientific understanding of small non-axisymmetric “3D” fields and their use to control instabilities, compensate intrinsic “error” fields that may cause magnetic islands or other deleterious effects, and control plasma rotation. In the near term, additional power supplies will enable full utilization of the existing 3D coils for control of locked tearing modes, resistive wall kink modes (RWMs) and error fields. Later, new 3D coils will enable optimization of the applied toroidal and poloidal spectra, opening a wide range of control and 3D physics studies. It is noted that ITER is well equipped with internal and external 3D coil sets; this work on DIII-D will be key in understanding how to apply these tools in ITER.

Successful completion of the planned research will establish the basis for the disruption free tokamak, and in particular robust operation of ITER and future fusion devices. This will:

- Advance the fundamental stability physics of tokamak plasmas;
- Advance the scientific understanding of 3D field effects in toroidal plasmas;
- Develop reliable real-time prediction and detection of tokamak stability limits;

- Develop the physics basis for robustly stable operation through integrated control.

Measurable, physics-based progress toward a solution to the problem of disruptions in tokamaks will enhance confidence in tokamak-based fusion within the scientific community, funding agencies, and the energy industry. The techniques to be developed through the research proposed in the present section will form the building blocks of an integrated control system to maintain stable operation and handle off-normal events without disruptions, which will be supervised by the Off-Normal and Fault Response system described in Section 2.2.3. A rapid shutdown with the disruption mitigation system, discussed in Section 2.2.2, acts as a last resort.

**2.2.2.2 Research Plan**

The core stability research plan is organized according to the challenges and goals in Table 2-13. The timeline for each challenge is given in Fig. 2-28, with the research elements and key facility improvements necessary to achieve it.

Challenge	FY19-20	FY21	FY22	FY23	FY24				
Disruption-free operation for ITER’s Q=10 mission	Multi-mode active tearing control with ECCD and RMP Passive stability through equilibrium control Real-time stability prediction for Q=10 Off-normal and fault responses for robust stability								
Robustly stable scenarios for high-β steady-state plasmas	Active RWM control: reactor-relevant coils, advanced controllers Physics of kinetic stabilization at low torque Real-time stability prediction for steady state Improved wall stabilization								
3D physics for stability of tokamak plasmas	Active control of n=1, 2 error fields Flow and flow shear generation by 3D fields Active control of 1≤n≤3 error fields Optimize resonant vs. non-res. fields								
Facility Improvements	2 <sup>nd</sup> off-axis NB Co/ctr NB 5 → 7 → 9 MW EC power 3D supply #2 2D imaging, toroidally resolved profiles					NB power/pulse upgrade 3D coils 3D magnetics (phase II)		2 <sup>nd</sup> Co/ctr NB Conformal wall (option)	

*Fig. 2-28. Core stability research timeline*

**Challenge 1: Establish the basis for disruption-free operation in ITER’s Q=10 mission**

**Current progress.** In the past five years, there has been significant progress toward development of passively stable scenarios without m/n=2/1 tearing modes. Critical features of the current density profile have been identified [Turco 2016] (Fig. 2-29) but there is as yet no quantitative predictive capability. Nevertheless, this has helped guide experiments that have

achieved reliably stable discharges with the  $\beta_N$  and  $q_{95}$  values of ITER’s baseline scenario, and net neutral beam torque of zero [Turco 2017], at elevated collisionality. Growth of the 2/1 tearing mode is often preceded by internal phase-locking of rotating rational surfaces [Tobias 2016], which may help to explain previous observations that tearing instabilities are correlated with reduced rotational shear [LaHaye 2010, Jackson 2013].

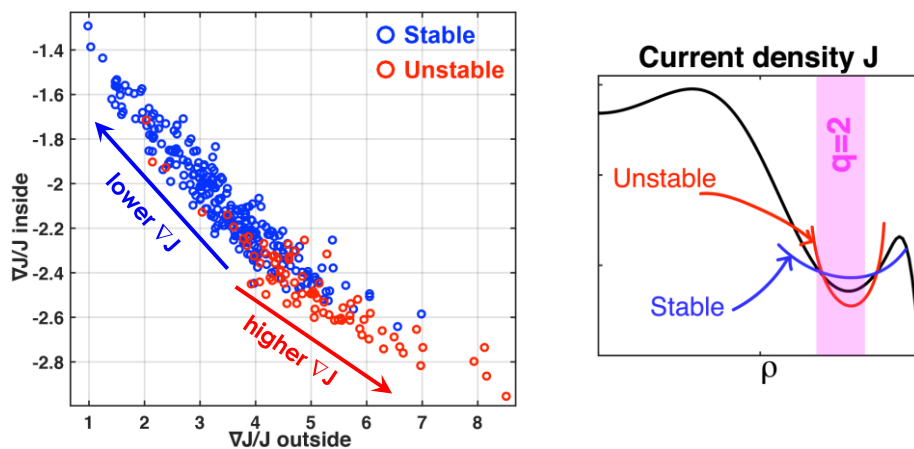


Fig. 2-29. Measured current density gradient at both sides of the minimum in ITER baseline discharges, showing that instability is associated with larger gradients. (Shown schematically in the right-hand panel.) [Turco 2016]

DIII-D experiments have demonstrated integrated control of 2/1 tearing modes, in which electron cyclotron current drive (ECCD) is automatically enabled and steered to the island location when an unstable mode is detected [Welander 2013, Kolemén 2014]. Preemptive stabilization has been demonstrated in low-torque, low-rotation ITER baseline scenario discharges [LaHaye 2017]. Recent research has also explored feedback-controlled rotation of large islands using resonant magnetic perturbations (RMP) to avoid wall-locking and disruption. Rotation shear and/or wall stabilization effects alone may postpone disruption [Okabayashi 2017], allowing time for other actions to recover stable operation (Fig. 2-30). Alternatively, ECCD can be applied synchronously with the driven island rotation for stabilization [Choi 2017, Volpe 2015]. While this progress demonstrates many of the ingredients of a tearing mode control system, implementation in the highly

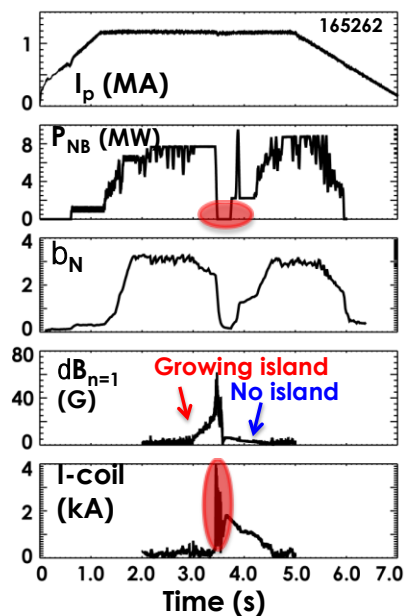


Fig. 2-30. A growing island is eliminated without disruption by temporarily reducing the input power, while a rotating  $n=1$  RMP is applied by the I-coil to prevent wall locking.

disruptive ITER baseline regime remains challenging, particularly at the ITER collisionality and ITER-relevant torque, with further needs to integrate sensing and control techniques.

DIII-D is pursuing multiple approaches to the prediction of stability limits and disruptions. Active MHD spectroscopy appears to show a resonant response before the onset of tearing modes, both at kink mode frequencies [Turco 2016] and at tearing mode frequencies [LaHaye 2016], raising the exciting possibility of predicting the approach to instability while the plasma remains stable, as well as a method to probe the underlying physics. Efficient methods of simultaneously determining the stability of multiple plasma modes also show promising results [Wang 2016]. Real-time kinetic equilibrium reconstruction [Kolemen 2016], a prerequisite to real-time stability calculations, is under development. Several approaches [Rea 2017, Kleijwegt 2017, Parsons 2016] are being developed to apply sophisticated “machine learning” techniques to the prediction of disruptions, based on correlation of key plasma parameters in the existing DIII-D database, and offline analysis has yielded disruption predictions with better than 90% accuracy [Rea 2017, Kleijwegt 2017].

**Goal 1: Assess and improve tearing mode stability.** A key goal here is to gain an actual predictive capability for tearing instability, as well as to understand and develop the techniques to improve stability to enable robust ITER baseline scenario operation. Research will thus explore control of the current density profile near the  $q=2$  surface and other parameters. The emphasis will be on indirect methods, including modification of the H-mode pedestal temperature and bootstrap current by variation of the pedestal density and plasma shape. Linear and nonlinear resistive MHD modeling and improved 1D and 2D profile diagnostics will be crucial to this effort, in order to interpret experimental results and to develop the capability to predict (for DIII-D and for ITER) discharge configurations with robust stability to tearing modes. The influence of rotational shear in tearing mode stability will also be investigated, including its possible role in screening of electromagnetic coupling from other rational surfaces. Magnetic probing and control techniques (below) also play a role in developing this understanding.

**Goal 2: Validate active tearing mode control.** Work will focus on extending and integrating techniques to develop robust tearing mode response systems to recover performance or allow safe termination. Experiments will quantify the requirements on ECCD power, pulse length, and alignment for detection and suppression of the 2/1 tearing mode before the island locks, and the possible effects of current drive broadening by edge turbulence. Event response sequences will be tested, including the deployment of 3D fields to control or rotate modes while ECCD is applied. Research will also investigate the nonlinear physics of neoclassical tearing mode onset and saturation, including the possibility of indirect stabilization by control of “seeding” events that may trigger the tearing mode. The stability physics of a saturated island with forced rotation by

electromagnetic torque will be investigated using experiments and nonlinear 3D codes such as NIMROD or M3D-C1. Understanding the recovery of H-mode operation during controlled island reduction will require integrated modeling, including transport and H-mode pedestal physics. A practical goal is to bring tearing mode control, with techniques using both ECCD and 3D fields, into routine use as part of DIII-D’s Off-Normal and Fault Response system.

**Goal 3: Develop real-time sensing and prediction of stability limits.** The physics basis for active MHD spectroscopy of tearing modes will be established through detailed experiments and comparison to stability modeling. This work will also be used to probe and improve underlying physics understanding of the modes. Disruption predictions based on machine learning will be implemented in real-time calculations. Fast, accurate equilibrium and stability calculations will also be developed and tested in real time. Successful techniques will be incorporated into DIII-D’s Off-Normal and Fault Response system, and used to trigger and guide appropriate actions to prevent or mitigate a disruption. Modeling and cross-machine testing will evaluate the portability of these techniques to ITER.

### **Challenge 2: Establish the scientific basis for stability of high $\beta_N$ , steady-state operation**

**Current progress.** As shown in Fig. 2-31, DIII-D discharges routinely exceed the ideal MHD, no-wall stability limit in configurations having high normalized beta,  $\beta_N$ , and high minimum safety factor,  $q_{\min}$ , compatible with steady-state operation [Hanson 2017]. The stability of the resistive wall mode (RWM) with  $\beta_N$  above this limit has been understood in terms of kinetic stabilization by resonant interactions of the mode with the bounce and precession frequencies of trapped ions [Wang 2015]. Modeling indicates that resonant interactions with fast ions from neutral beam injection may also be important for RWM stability [Turco 2015]. When the minimum safety factor  $q_{\min}$  is greater than 2, these high- $\beta$  discharges do not have  $\beta$  collapses or disruptions caused by locked tearing modes.

Simple “proportional gain” feedback stabilization of the RWM with internal control coils (I-coils) has enabled discharges compatible with steady-state operation to reach beta values significantly above the passive stability limit [Hanson 2017], as shown by the magenta points in Fig. 2-31. More recently, an initial test of a model-based Linear Quadratic Gaussian (LQG) controller for the external control coils (C-coils) has shown stabilization comparable to that with the internal coils and the simpler control algorithm [Clement 2017], an important development for future fusion reactors.

Earlier experiments have shown that both the ideal MHD stability limits and the confinement increase with high internal inductance  $l_i$ . Discharges with  $\beta_N \sim 5$  and very good confinement have been achieved with  $l_i$  greater than unity [Ferron 2015], although such configurations have not been

sustained for long pulses. They are calculated to be stable without a wall up to  $\beta_N \sim 4$ , and the most common instability is a 2/1 tearing mode.

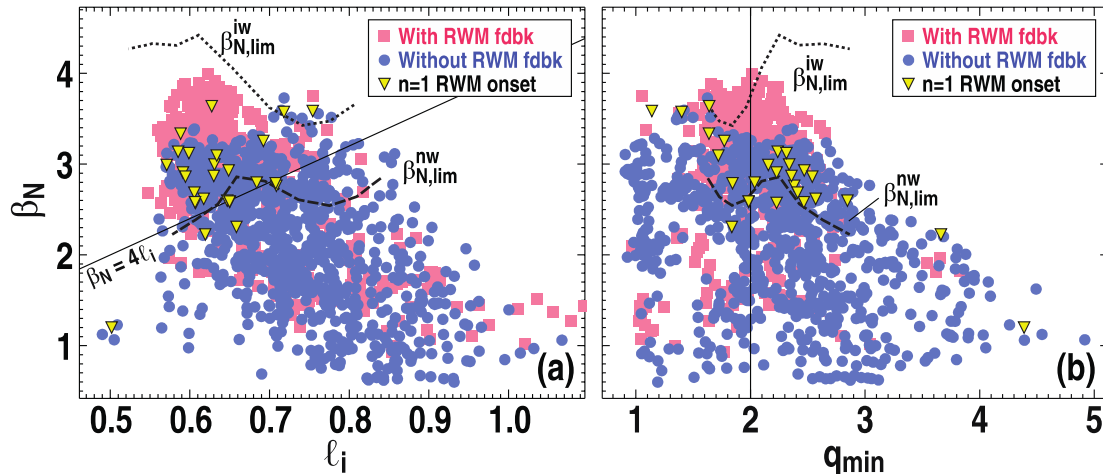


Fig. 2-31. Experimentally accessed (a)  $\beta_N$  versus  $l_i$  and (b)  $\beta_N$  versus  $q_{min}$  values, with and without RWM feedback control, showing  $\beta$ -collapses due to  $n = 1$  RWM events, and calculated no-wall and ideal-wall ideal MHD stability limits. [Hanson 2017]

**Goal 1: Validate and optimize kinetic stabilization of kink modes at high beta.** The key challenge here is to test and validate damping models in more advanced regimes with higher  $\beta_N$  and  $q_{min}$ , and lower fast-ion fraction, to determine if the potential of the advanced tokamak concept can be fulfilled. In particular, studies will test behavior and limits very close to ideal MHD, with-wall  $\beta_N$  driven kink thresholds. Research will validate models of kinetic stabilization in these regimes and also as the plasma rotation is reduced to reactor-relevant values. The role of fast ions in kinetic stabilization will be tested using steerable and variable voltage neutral beams, also deploying greater electron cyclotron heating power to vary fast-ion content. The strength of the kinetic damping will also be validated, since weak damping can leave the discharge vulnerable to destabilization by transients and error fields. Modeling predicts kinetic stabilization almost to the ideal wall limit [Hanson 2017]. Future experiments will investigate the hypothesis that limits in reaching the ideal limit in Fig. 2.3 are due to imperfect error field correction, using improved multi-mode error field correction enabled by new power supplies and, later, by an additional set of 3D coils. The critical role of tearing stability in these limits will also be explored, noting that a pole in the classical tearing instability index is predicted at the ideal limit. As discussed in Section 2.1.2, the proposed option of close-fitting “conformal” wall inserts will significantly increase the ideal-wall stability limit, and will further test the hypothesis that the tearing mode limit follows the ideal kink mode limit.

**Goal 2: Establish active stabilization of kink modes beyond passive stability limits.** The initial promise of advanced state-space (LQG) controllers and reactor-relevant external control coils will be rigorously explored, assessing behavior and limits in higher  $\beta_N$  plasmas close to with-wall ideal MHD limits that will be accessed in the 2019-2024 five-year plan. New power supplies and, later, new active coils (M-coils) will improve the simultaneous control of RWMs and error fields. Research will exploit the greater poloidal spectral flexibility gained by using the M-coils in combination with existing coils to develop RWM control that avoids undesired rotation braking or destabilization of other modes, and greater toroidal mode number range to extend capabilities to investigate control of the full range of RWMs expected to pose a concern ( $n=1, 2, 3$ ), noting that studies have already shown differences in underlying stability between  $n=1$  and  $n=2$  modes (see Challenge #3). An upgraded set of magnetic diagnostics to accompany the M-coils will be critical to exploiting these new capabilities. Ultimately this advanced control will be implemented for routine use in experiments on high-beta, steady-state scenarios.

**Goal 3: Assess stability of high- $l_i$  and other high- $\beta$  scenarios that do not require wall stabilization.** Although the stability limits of high- $l_i$  discharges are less well characterized than those of ITER-like inductive discharges or high- $q_{\min}$  steady-state discharges, existing data shows that the limiting instability is often a 2/1 tearing mode. Research will focus on tearing mode control in this configuration, using techniques outlined under Challenge #1. The sensitivity of stability to the current density profile will be assessed. Direct stabilization by local ECCD may be readily achievable with the more central location of the low-order rational surfaces. If needed, the advanced RWM control described above will be adapted for stabilization at high  $l_i$  and high  $\beta$ .

### **Challenge 3: Use 3D physics to improve the stability of tokamak plasmas**

**Current progress.** DIII-D research has shown that the plasma's magnetic response to external  $n=1$  perturbations is in good agreement with linear, ideal MHD models [King 2015]. At moderate beta, the plasma  $n=1$  response is well described by a single stable mode [Paz-Soldan 2014, Lancot 2017a], and therefore  $n=1$  error field compensation (EFC) simply requires a control coil set that couples to that mode. Real-time optimization of single-mode  $n=1$  EFC by minimizing rotation braking has been demonstrated [Lancot 2016], and may be useful for ITER. In contrast, recent research shows a multi-modal response to  $n=2$  fields, depending on the spatial structure of the external field [Paz-Soldan 2015a] (Fig. 2-32). The dependence of  $n=2$  error field penetration (driven reconnection) on plasma parameters is similar to previous  $n=1$  results [Lancot 2017b]. However, unlike  $n=1$ , single-mode  $n=2$  EFC does not fully recover the plasma performance of the case without error field [Paz-Soldan 2015b], confirming that additional modes are important. A

new paradigm of “reluctance eigenmodes” explains the complexities of the plasma response in terms of a strong response by very stable modes as well as by weakly stable ones [Logan 2016].

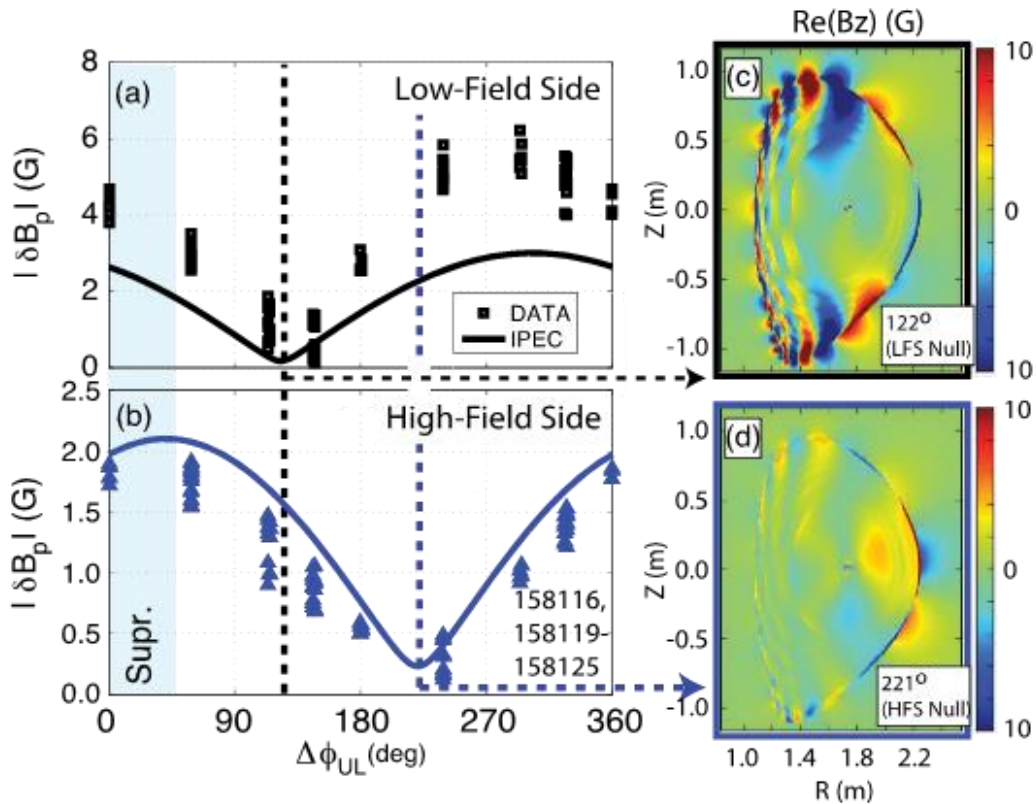


Fig. 2-32. Experimental  $n=2$  plasma response amplitude and IPEC prediction at the (a) Low Field Side and (b) High Field Side midplane as upper-lower I-coil phase difference is varied. Cross-section of the computed response at the (c) LFS null and (d) HFS null. [Paz-Soldan 2015a]

DIII-D experiments have also confirmed that in plasmas with low neutral beam torque, neoclassical toroidal viscosity (NTV) can accelerate the plasma to a rotation rate of the order of the ion diamagnetic drift frequency [Garofalo 2008]. This effect has been exploited to enable high-performance QH-mode plasmas with near-zero neutral beam torque [Burrell 2012]. Taking account of the stable plasma response, it has been estimated that the offset rotation driven by  $n=3$  fields in ITER could be as large as the neutral beam-driven rotation [Garofalo 2009, Burrell 2013]. Similarly, a recent empirical scaling study [Chrystal 2017] suggests that “intrinsic torque” in ITER, including NTV as well as other effects, could be comparable to ITER’s expected neutral beam torque.

Having laid these foundations, the challenge remains to resolve the multi-modal resonance and non-resonance responses in order to understand how to simultaneously avoid braking, optimize

(or avoid problems with) NTV torques, while enabling additional 3D functions such as ELM or RWM control.

**Goal 1: Optimize active control of error fields with multiple mode numbers.** Research will develop multi-mode error field compensation. Planned additional power supplies for the existing 3D coils will enable simultaneous  $n=1$  and  $n=2$  EFC in routine operation. The multi- $n$  EFC should improve the stability of both the low-torque ITER baseline scenario, where  $n=2$  penetration and locking often leads to  $n=1$  mode growth and disruption, and of high-beta steady-state scenarios, where a strong response to  $n=2$  error fields may alter the rotation and kinetic damping of  $n=1$  RWMs. At present, ITER has no plan for  $n=2$  EFC, so it is crucial to establish the implications of its absence and advise ITER on required strategies.

**Goal 2: Establish control of resonant drive for higher  $n$  tearing and kink instabilities.** Later in the five-year period, a proposed additional set of internal coils at the midplane will extend studies of 3D physics to higher toroidal mode numbers (up to 6) and finer control of the poloidal mode spectrum (notably providing harmonic control at  $n=3$  and 4 for the first time). The enhanced spectral flexibility will be used to test control of multiple 3D effects – for example, compensation of resonant error fields while minimizing non-resonant braking of rotation.

**Goal 3: Assess the impact of flow and flow shear generated by 3D fields.** DIII-D research will investigate the possible use of rotation modification by 3D fields to improve stability of discharges with little or no neutral beam torque. In plasmas with zero neutral beam torque, NTV rotation driven by non-resonant fields could reduce the susceptibility to penetration of resonant error fields, and could play a role in kinetic stabilization of resistive wall modes. In plasmas with small, ITER-equivalent neutral beam torque, selective braking by NTV could enhance local rotational shear for tearing mode stability. The proposed M-coils will enable much greater flexibility in the poloidal spectra of applied  $n=2$  and  $n=3$  fields, allowing more control of the NTV torque amplitude and radial location. *The physics of the NTV effect will also be explored in Section 2.3.2 as part of studies in rotation profile control and projection.*

### 2.2.2.3 Improvements in Capabilities

In the 2019-2024 five-year period, a broad range of physics inquiries will be enabled by enhancements of the DIII-D facility (Table 2-14) and its diagnostic instrumentation (Table 2-15) and of the modeling tools for prediction and interpretation of experiments (Table 2-16). Key enablers of this program include the 3D upgrades and increased ECCD power.

**Table 2-14.**  
**Hardware Improvements for Core Stability Studies**

<b>Hardware Capability</b>	<b>New Physics</b>
Increased EC power, 7-9 MW	<ul style="list-style-type: none"> <li>• Validation of passive stability limits with controlled variation of current density profile and fast-ion beta fraction</li> <li>• Active stabilization of multiple MHD modes</li> <li>• Optimization of stability by simultaneous control of background current profile and active stabilization</li> </ul>
Two co-counter steerable NB injectors	<ul style="list-style-type: none"> <li>• Validation of stability limits vs. current density profile</li> <li>• Validation of stability limits vs. plasma rotation</li> </ul>
New 3D coils and power supplies	<ul style="list-style-type: none"> <li>• Optimization of stable plasma response to 3D fields with <math>n &gt; 2</math>, and with varying poloidal spectrum</li> <li>• Understanding of stability limits in tokamaks with external 3D fields</li> <li>• Active probing of plasma stability while coils simultaneously provide error-field control, ELM suppression, etc.</li> <li>• Active stabilization of resistive wall modes, with multi-mode control and/or improved spatial spectrum selection</li> </ul>
Close-fitting “conformal wall” inserts	<ul style="list-style-type: none"> <li>• Validate the link between global kink stability and tearing stability in high-performance scenarios</li> <li>• Enable stable, high-<math>\beta</math>, steady-state scenarios by raising the wall-stabilized limit</li> </ul>

**Table 2-15.**  
**Diagnostic Improvements for Core Stability Studies**

<b>Scientific Objectives</b>	<b>Physics Measurement</b>	<b>Diagnostic Technique</b>
Understanding and prediction of stability limits in tokamaks	1D profiles ( $n_e$ , $T_e$ , $T_i$ , $\Omega$ , $J$ ) with improved precision, time resolution, radial resolution	Upgrade existing profile diagnostics (Thomson scattering, ECE, CER, MSE, polarimetry)
Profile control and real-time stability assessment	Continuous real-time profile measurements ( $n_e$ , $T_e$ , $T_i$ , $\Omega$ , $J$ )	PCS enhancements
Real-time prediction of stability limits, robustly stable operation	Real-time kinetic equilibrium and stability analysis	PCS enhancements
Validation of predicted internal structure of MHD modes, early warning of growing instabilities	2D and 3D measurements of macroscopic non-axisymmetries: stable and unstable modes	Toroidally resolved 1D profiles (ECE) or 2D imaging (Thomson, MSE, ECE); upgrade high-frequency magnetics array
Measurement of plasma response to the fields applied by new non-axisymmetric coils (“M-coils”)	Toroidally and poloidally resolved $\delta B$ for toroidal modes $n$ up to 6	Upgrade existing arrays of external magnetic diagnostics (i.e. 3D magnetics, Phase II)

**Table 2-16.**  
**Simulation Code Development Plan**

<b>Code</b>	<b>Purpose</b>
Linear and nonlinear, nonideal MHD stability codes (MARS, DCON, NIMROD, M3D-C1)	Realistic modeling of linear/nonlinear tearing mode stability, enabling reliable prediction of experimental stability limits
	Realistic modeling of non-ideal effects in the stable response and stability limits of wall-stabilized kink modes at high beta
deal and resistive stability codes (e.g., DCON) adapted for real-time operation	Real-time assessment of stability limits, enabling plasma control for robustly stable operation
Ideal and resistive MHD stability codes (e.g. MARS-F, VMEC/V3FIT, M3D-C1) adapted for fitting 2D and 3D experimental data from multiple diagnostics	Physics understanding of observed unstable modes and the stable plasma response to 3D fields

### 2.2.3 Plasma Control

*D. Humphreys (GA), M. Walker (GA), N. Eidietis (GA), J. Ferron (GA), E. Kolemen (Princeton U.), A. Hyatt (GA), E. Schuster (Lehigh U.)*

Plasma Control research at DIII-D seeks to develop the knowledge and solutions needed for ITER and power reactors to satisfy their control requirements and *operate disruption-free* with specified levels of robust high performance. Control science research provides the principal methods for managing uncertainty inherent in physics understanding, and provides the essential knowledge through which plasma physics understanding is transformed into operational reality. Advanced tokamak regimes, characterized by operation beyond various open loop stability limits (i.e. points beyond which some plasma mode is unstable in the absence of feedback control), are particularly demanding of control advancements, and continue to drive DIII-D to maintain its leadership role in plasma control science. DIII-D has had a unique emphasis on control physics and mathematics since its inception, and is the most highly-controlled and controllable tokamak in the world [Humphreys 2007, Humphreys 2009]. Both ITER and next-generation reactors will demand control performance and reliability far beyond that required by presently operating devices, yet with significantly more constraints on control actuators and diagnostics. Future reactors including FNSF, CFETR, and DEMO, will require still more reliability than ITER, likely operating in AT regimes with even stronger cost and resource constraints.

Significant progress was made in control science in the 2014-2018 DIII-D research period, including reduction to practice of q-profile control using a variety of algorithmic approaches [Schuster 2016], development of off-normal and fault response algorithms and ITER-relevant methods for integrated design and generation of real-time code for operational algorithms [Eidietis 2017], development of ITER-relevant methods for shot validation with control-level simulations [Walker 2017], and deployment of many algorithms to support DIII-D experimental physics goals (e.g. [Eldon 2017]).

### **2.2.3.1 Challenges and Impact**

While many control advances have been made along the path to ITER and fusion power plants, substantial work remains in order to establish the control solutions needed to make tokamak fusion power viable. To accomplish this, the DIII-D Plasma Control research program focuses on four principal challenges (Table 2-17). The first challenge addressed is to develop and demonstrate the fundamental individual and integrated control solutions needed by ITER. Research addressing this challenge will develop controllers for continuous regulation of ITER scenarios, including multivariable shape and vertical stability control, current profile regulation, and divertor operation control. Asynchronous control related to this challenge includes algorithms and scenarios for handling exceptions (off-normal events requiring real-time modification to control policies). The second challenge is to develop the specific understanding and solutions needed to ensure minimal disruptivity in ITER, and true disruption-free sustained operation required for a power plant [Humphreys 2015]. Addressing this challenge will entail developing mathematical robustness metrics for low disruptivity and research in quantifiably robust control algorithms. The third challenge is to identify and/or develop appropriate model-based design approaches to address plasma control problems. Although plasma control research at DIII-D and elsewhere has demonstrated the quantified performance possible with model-based design, the solutions needed for ITER and beyond have not yet been fully developed. Research to address this challenge will include development of specific control-level models for design, including MHD stability and machine learning-derived profile response models. The fourth priority challenge is to determine the advanced control solutions needed to support the DIII-D experimental program. The research in this area will be driven by the developing needs of DIII-D, but will develop and make use of advanced algorithms to enable experimental operation and elucidate relevant physics in specific experiments.

The understanding and solutions developed in this research program will contribute to enabling ITER to operate robustly with minimal disruptivity, help establish the viability of a disruption-free tokamak reactor, qualify the model-based design approach to control needed for all burning plasmas, and continue to provide the essential control solutions that enable much of the DIII-D

physics research program. As such, DIII-D Plasma Control research will play a key role in enabling ITER to be licensed, to achieve its physics goals, and to operate with sufficient machine protection effectiveness throughout its lifetime.

**Table 2-17.**  
**Plasma Control Research Challenges, Goals, and Capability Improvements**

<b>Challenge</b>	<b>Goals</b>	<b>Key Capability Improvements</b>
Develop understanding, methods, and solutions needed for integrated, <b>robust control of ITER</b>	<ul style="list-style-type: none"> <li>• Develop and assess individual ITER control algorithms: equilibrium, n=0 stability, current profile, divertor regulation, exception handling</li> <li>• Emulate ITER with DIII-D to assess and validate integrated ITER PF control solutions</li> </ul>	<p>Hardware upgrades:</p> <ul style="list-style-type: none"> <li>• Continual PCS hardware upgrades</li> <li>• New power supplies to enable increasing-fidelity emulation of ITER PF control</li> </ul> <p>Diagnostic Upgrades:</p>
Develop understanding and control methods to <b>prevent disruptions in ITER and AT reactors</b>	<ul style="list-style-type: none"> <li>• Develop/quantify robust disruption-prevention control: profile regulation robustness to transport variation, n=0 stability robustness to MHD disturbances and impurity influx</li> <li>• Develop/assess off-normal/ fault response (ONFR) finite state machine algorithms for preventing disruption in ITER</li> </ul>	<ul style="list-style-type: none"> <li>• Continual advancement of diagnostics to real-time capability in support of operations and experimental control goals</li> <li>• Increasing integration of 3D diagnostics in control applications</li> </ul> <p>Code development:</p>
Identify high-performance <b>model-based control approaches</b> capable of effective control without empirical tuning	<ul style="list-style-type: none"> <li>• Develop/assess linear MHD equilibrium and stability models, machine learning-derived profile response models</li> <li>• Quantify and compare performance of model-based design approaches including Model Predictive Control, convolutional neural networks, and adaptive methods</li> </ul>	<ul style="list-style-type: none"> <li>• Continual development of PCS software, algorithms</li> <li>• Continual development of finite state machine (ONFR) algorithms</li> <li>• Continual TokSys upgrades</li> <li>• Real-time stability and controllability calculation</li> <li>• Real-time calculation of relevant models and control algorithms</li> </ul>
Determine advanced control solutions to best enable, support, and accelerate <b>the DIII-D program</b>	<ul style="list-style-type: none"> <li>• Design/apply advanced control algorithms for DIII-D VFI-less equilibria, SAS2, profile regulation for steady-state targets</li> <li>• Regulate MHD stability to enable transformational elucidation of physics in DIII-D</li> </ul>	<ul style="list-style-type: none"> <li>• Faster than Real-Time Simulation of plasma state</li> <li>• Control testing and shot validation simulations, both offline and connected to PCS</li> </ul>

**2.2.3.2 Research Plan**

The DIII-D Plasma Control research program in FY 2019-2024 will be organized around the challenges articulated in Table 2-17. Fig. 2-33 provides timelines for each challenge area, key research activities and milestones, and capability improvements enabling these activities.

Challenge	FY19-20	FY21	FY22	FY23	FY24
<b>Robust ITER Control</b>	← ITER actuator sharing, EH → ← Integrated ITER control emulation → ← Demo end-to-end ITER control →				
<b>Disruption prevention</b>	← Balanced plasma state/stability ctrl → ← ONFR for disruption prevention → ← Demo/quantify disruption-free in ITER and AT →				
<b>Model-based Control</b>	← Online model/algorithm calculation → ← Faster than Real-Time Simulation in PCS → ← Performance quantification →				
<b>DIII-D Control</b>	← Expanded shape space →      ← Full VFI-less equilibria w/ new SSPAs → ← Routine profile/TM/ONFR control → ← Increased profile control robustness with new ECH → ← Simserver: transition from limited to routine →				
<b>New Capabilities</b>	SSPAs:    ← Use in shape control →      ← Full VFI-less → ECH:      ← Improved TM suppression →   ← ITER-like actuator sharing → 3D diags: ← RT stab bound detection →   ← RT stab bound control → Codes:    ← Increasing simserver use →   ← ITER-like shot validation → ← Continuous advancement of TokSys environment → PCS:      ← Continuous advancement of PCS hardware/software →				

(Key: VFI=Vertical Field Inductor, TM=tearing modes, ONFR=off-normal/fault response, EH=exception handling, AT=advanced tokamak, SSPAs=Super-SPAs, RT=real-time, PCS=Plasma Control System, TokSys=GA Tokamak System Toolbox, FRTS=Faster-than-Real-Time-Simulation)

*Fig. 2-33. Plasma Control Research Plan Timeline*

**Challenge #1: Develop understanding, methods, and solutions needed for integrated, robust control of ITER**

**Current Progress.** The unique demands of the ITER physics research and operations plans have led to specification of a particular set of requirements for ITER control. For example, ITER will follow a rigorous integrated control model-design-simulate-validate-apply design philosophy (see Fig. 2-34 and [Humphreys 2015]), with quantified model accuracy and controller performance specifications, and will include mandated whole-shot validation prior to execution of a discharge. This approach will be applied to all controlled quantities in ITER: plasma equilibrium boundary and vertical stability, divertor radiation and detachment, tearing mode stability, kinetic characteristics, burn state, etc. Significant progress has been made in the current and previous

DIII-D research periods toward developing and studying many individual ITER-relevant control algorithms [Humphreys 2007], including ITER axisymmetric stability control [Humphreys 2009], ITER-type shot validation [Walker 2017], and divertor detachment control [Eldon 2017] (Fig. 2-35). However, many aspects of this control design and qualification process require further research and development, and the end-to-end process has yet to be fully demonstrated on operating devices. The flexibility of DIII-D, control expertise of the DIII-D team, and strong connection with both the ITER project and other superconducting devices (e.g., EAST and KSTAR), make the DIII-D control research program ideal for addressing this challenge. This area of research will include demonstration and study of individual ITER control algorithms, as well as emulation of key ITER characteristics in executing such algorithms with DIII-D (as well as EAST and KSTAR, to the degree enabled by collaborations with those devices). Common use of the DIII-D PCS by EAST and KSTAR greatly facilitates such cross-machine testing of control algorithms.

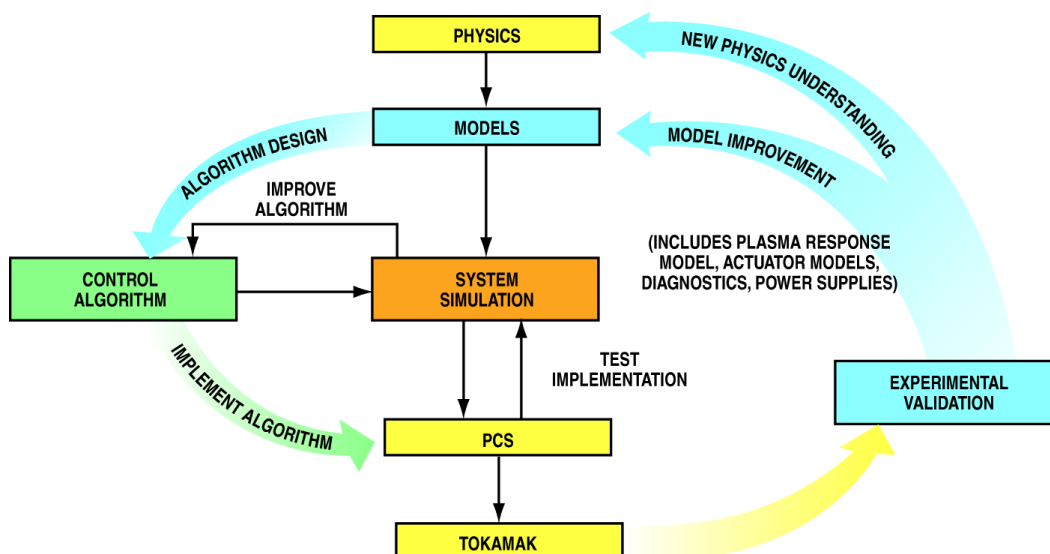
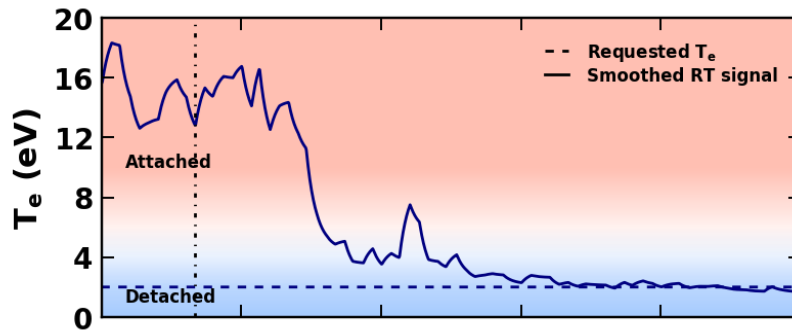


Fig. 2-34. Integrated control design process uses validated physics-based models to construct control algorithms, and verifies control system performance against detailed simulations prior to operational use

**Goal 1: Develop and assess individual ITER control algorithms.** This research program will see continued focus on studying and developing plasma control science to enable the success of ITER. This focus will include research in integrated control for robustly achieving and maintaining the ITER target scenarios, including advanced equilibrium and  $n=0$  stability control, gap-basis shape control, fully-populated gain matrices designed from magnetic plasma response models for boundary and divertor configuration control, ITER-relevant divertor detachment and radiation control, burn control using DIII-D neutral beam proxies for alpha heating, ITER Catch-and-Subdue (continuously active) tearing mode suppression,

**Goal 2: Emulate ITER with DIII-D to assess and validate integrated ITER control solutions.** Prior to commissioning of ITER control algorithms, it is important to demonstrate their operation and performance in present devices. The ability to control all F-coils individually in DIII-D, made possible by several advancements including new Super-SPA power supplies, will enable emulation of the type of equilibrium regulation required in superconducting devices such as ITER, KSTAR, and EAST. DIII-D will emulate many aspects of ITER integrated control in experimental use, including ITER-relevant profile control actuators and algorithms, actuator sharing using priority assignment and real-time QP optimization, and exception handling for key responses including loss of VS3 availability and proxy disruption prediction time intervals leading to rapid shutdown requests. Demonstration of the full ITER model-design-simulate-validate-apply design approach will be a key deliverable in this effort (Fig. 2-34).



*Fig. 2-35. Active regulation of impurity or fueling gas puffing at the divertor strike point has been demonstrated to maintain a stable detached plasma using an ITER-relevant control algorithm in DIII-D. Although nitrogen and deuterium have been demonstrated in the current DIII-D research period, the next period of research will include ITER-relevant Ne injection, along with emulation of ITER-scaled dynamics.*

## **Challenge #2: Develop understanding, methods, and solutions to prevent disruptions in ITER and AT reactors**

**Current Progress.** Both ITER and future advanced tokamak reactors are characterized by a high level of active control to sustain a desired plasma configuration and stabilize certain instabilities in order to meet performance targets (e.g., fusion power and gain). Achieving the required level of control at  $Q=10$  in ITER places significant demands on control capability in an environment with limited measurement and actuator access. Although ITER is designed to tolerate  $\sim 10\%$  disruptivity in principle, the operational intent is to target a disruption rate that is as low as reasonably achievable without adversely impacting the experimental physics mission. The DIII-D control program strives to provide understanding and solutions toward this goal. Significant progress has been made in disruption prevention research in the 2014–2018 five-year period, including demonstration of the Catch and Subdue continuous tearing mode control scenario and

associated algorithms [Welander 2013] (Fig. 2-36), and development of the DIII-D Off-Normal and Fault Response (ONFR) framework and related algorithms [Eidietis 2017]. Advances have also been made in rapid shutdown scenarios and algorithm development [Barr 2018]. The ongoing research to address these challenges will require many of the approaches and solutions developed in other areas, coupled with a unique focus on quantifiably disruption-free operation, high efficiency in use of limited sensors and heating/current-drive systems, and consistency of control resources with long-pulse operation (e.g., use of non-magnetic boundary control).

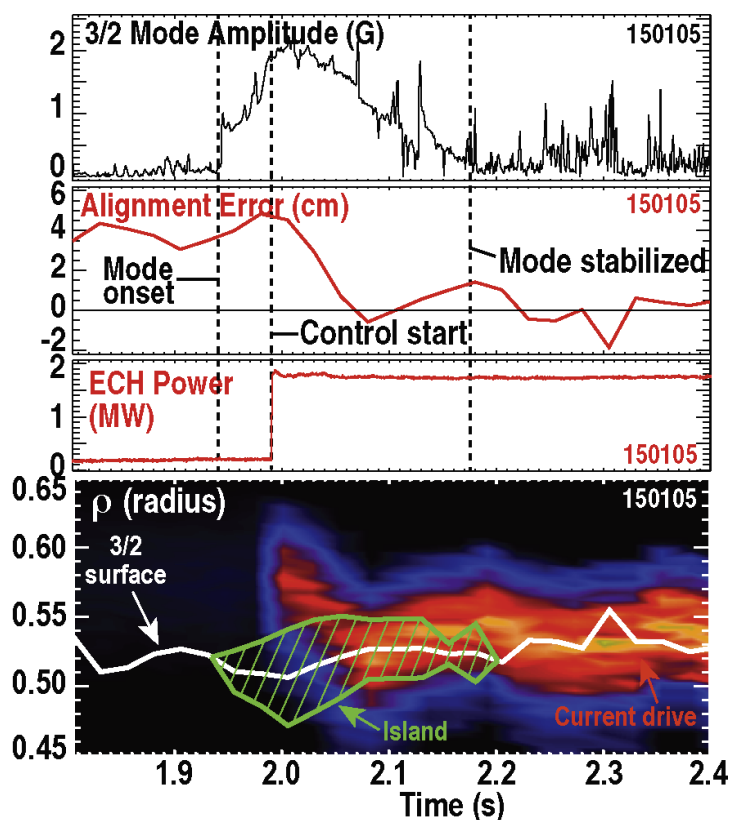


Fig. 2-36. The ITER-relevant Catch and Subdue scheme for repeated suppression of tearing modes has been demonstrated to enable rapid detection and alignment (“Catch”) of ECCD with a growing island, followed by suppression of the island (“Subdue”), using an ITER-relevant control algorithm in DIII-D. Additional gyrotrons will enable full suppression of a 2/1 island (the most important mode requiring suppression in ITER as part of an effective disruption prevention system).

**Goal 1: Develop and quantify robust disruption-prevention control.** Research toward this goal will focus on approaches and solutions to enable quantifiably robust control capable of preventing disruptions in ITER and steady-state burning plasma devices. This research will focus on developing methods for quantifying and guaranteeing high-performance control to a specified

level of reliability (ultimately that required by power reactors) using new DIII-D heating and current systems, including additional gyrotrons and high-power helicon for enhanced current profile control. Disruption prevention control approaches to be studied include integrated boundary and profile control based on online model calculation for sustainment of ITER and steady-state targets maintaining distance from tearing and vertical stability controllability boundaries, and mathematical metrics for profile parameters and relative MHD stability to enable active regulation of controllability itself. Application of new Super-SPA power supplies will enable expansion of the robust operating space and study of disruption prevention through algorithmic management of approaching operational limits.

**Goal 2: Develop and assess off-normal/fault response (ONFR) finite state machine algorithms for preventing disruption in ITER.** In addition to developing quantified high reliability control under *nominal* plasma scenario operating conditions, a disruption-free tokamak must have effective control responses that will *prevent* disruptions even under off-normal and fault conditions. Research toward this goal will develop off-normal and fault response algorithms for asynchronous response to predicted tearing and other key MHD mode onset, as well as to operational variances resulting from system faults and failures. Several mathematical approaches to real-time assessment of disruptivity risk and determination of control action will be studied including machine-learning derivations and first principles synthesis of controllers for asynchronous response. Machine-learning research will focus primarily on producing continuous assessments and demonstrably effective signals, rather than simple unqualified “alarm” signals. ONFR solutions are key to enabling *avoidance* of disruptions that would occur under fault conditions without proper control action.

**Challenge #3: Identify high-performance model-based control approaches to enable effective control without empirical tuning in operating and future tokamaks**

**Current Progress.** Limitations on DIII-D experimental time available for control tuning, coupled with the increasing need of high-performance control to elucidate detailed physics have driven increased demand for model-based control. Controllers designed from sufficiently accurate models can provide high confidence in quantified performance with minimal need for design iteration or tuning. ITER and other next-generation reactors will have even more limited discharge time available for control optimization, and higher demand for quantified control performance and robustness. Prior to operational application of a given algorithm, only control designs based on quantifiably validated models can provide such high confidence performance. ITER – and an eventual commercial reactor – will not be licensable without sufficient qualification of both the fundamental design approach, and specific model-based designs. Because this research area underpins tokamak control for all devices including DIII-D and ITER, significant effort has been

applied to the field and significant advances have been made. These include strides in physics model-based current and q-profile control [Schuster 2016] and model-based advanced divertor configuration control [Kolemen 2015]. Research and development in this field, with corresponding advances in both control physics and control mathematics, constitute the third key focus of the Control research program. In the 2019-2024 period, this area of research will include development and validation of models appropriate to each type of control, quantification of performance tradeoffs in different design approaches, and demonstration of high-performance control without empirical tuning.

**Goal 1: Develop and assess real-time linear MHD stability models and profile response models for control design.** Research toward this goal seeks to advance understanding and solutions in the field of model-based control design, applied to the key challenges in tokamak plasma control. A key goal of this understanding is to identify effective methods of real-time model generation capable of supporting regulation of proximity to controllability boundaries, and enabling various real-time algorithm adaptation. Relevant research toward this goal will also include implementation of real-time plasma evolution models such as RAPTOR, the TokSys gsevolve model, and the Lehigh COTSIM model, along with advancement of real-time DCON for linear MHD assessment and machine learning-based models of tokamak stability space.

**Goal 2: Quantify and compare performance of model-based control approaches.** Research in this area will focus on developing controllers, and quantifying and comparing performance of key model-based design approaches, including online model and controller calculation for multivariable model-based shape control (based on fully-populated state space gain matrices for isoflux measurements mapped to coil commands), advancement of model-based profile control, including online Model Predictive Control (MPC; see Fig. 2-37), online implementation of Faster than Real-Time Simulation for plasma state prediction, and development of methods for performance quantification from model-based approaches used in plasma scenario and stability control. These advances are expected to play key roles in developing AT scenarios, maintaining stability through current profile evolution, and reaching desired target profiles. Performance quantification includes quantified robustness to specified noise and disturbance levels, as well as to uncertainty and errors in modeled plasma responses. Quantification of performance in such metrics is required for licensing of ITER and fusion reactors.

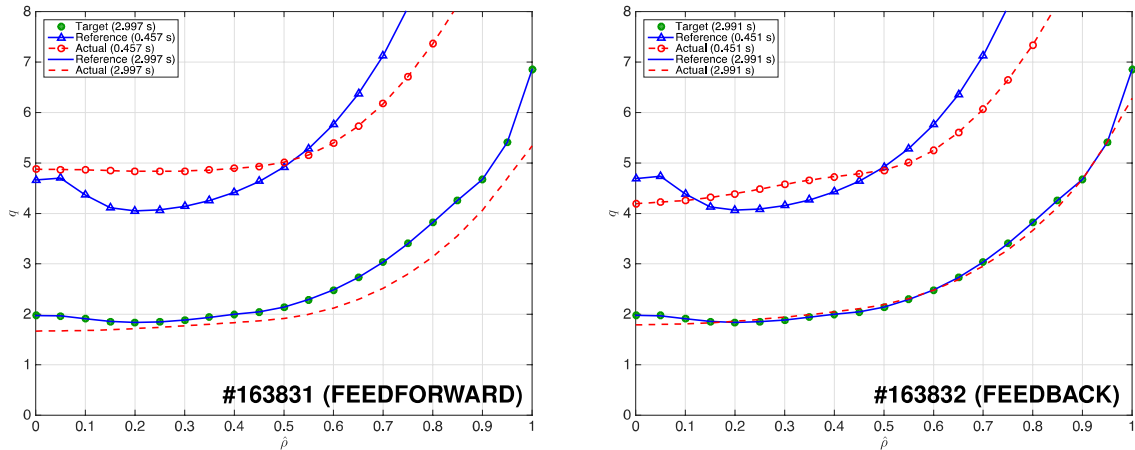


Fig. 2-37. Comparison of (a)  $q$ -profile resulting from feedforward alone, (b)  $q$ -profile resulting from feedforward + feedback using MPC controller. MPC control feedback produces good agreement between target and actual  $q$ -profile.

#### Challenge #4: Determine advanced control solutions to best enable, support, and accelerate the DIII-D program

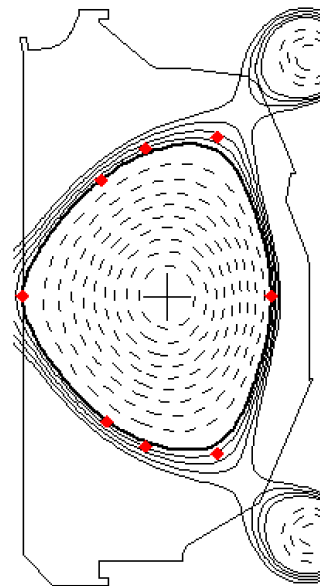
**Background and Current Progress.** Increasing complexity of DIII-D physics experiments and increasing premium on machine time have demanded steadily more advanced approaches to control through the years, now routinely requiring highly integrated, multivariable, high-performance controllers with minimal need for operational tuning. For example, Small Angle Slot divertor studies are enabled by millimeter-scale strikepoint control made possible by DIII-D’s high order multivariable isoflux boundary control, high-accuracy real-time equilibrium reconstruction, and gain optimization through simulation iteration. Model-based profile control research has enabled unprecedented reproducibility in  $q$ -profile trajectory and target for steady-state scenarios, divertor detachment control has enabled groundbreaking elucidation of the  $T_e$  “cliff” phenomenon [Eldon 2017], and negative triangularity plasma transport studies were proposed and made possible within one campaign by advanced control design and optimization (Fig. 2-38). These ongoing research challenges for DIII-D experiments will be met with a robust program in control physics and mathematics, developing appropriate control-level models guided by physics phenomena requiring understanding, and applying appropriate mathematical design and analysis theorems to achieve the needed level of regulation. Tokamak experimental physics productivity is maximized by investing sufficient effort in both control understanding and algorithms that enable the level of resolution needed to regulate and observe the phenomena of interest.

**Goal 1: Design and apply advanced control algorithms for DIII-D based on physics models derived from scenario, core stability, and boundary research.**

Research in this area will include use of Super-SPA power supplies to expand the shape operating space of DIII-D and enable independent regulation of all F-coils, emulation of shape control in superconducting devices, model-based profile control to access and sustain current profiles in desired plasma regimes, and deployment of tearing mode stabilization algorithms as a general tool for experiments in which growth of such modes is undesirable.

**Goal 2: Optimize control designs for experimental needs and elucidation of physics in DIII-D.**

Research toward this goal will include development and application of control solutions and tools for optimizing control effectiveness in experimental application. Advances in profile control developed through research for ITER and disruption-free reactor operation will be adapted and optimized for DIII-D experiments. New plasma equilibrium and divertor configuration algorithms will continue to be advanced and studied. The simserver capability of connecting simulations to the DIII-D Plasma Control System for testing of new algorithms and discharge scenarios will be developed from limited use by experts to routine use by physics operators. Deliverables in this area will continue to be determined by the needs of evolving experimental campaigns.



165779, run = EFITRT1, time = 1005.25

*Fig. 2-38. Development of a negative triangularity plasma target through modeling, simulation, and design, opened up a completely new research path for turbulent transport understanding in DIII-D. Empirical development of the required plasma target without advanced design methods would have consumed a prohibitive amount of machine time.*

**2.2.3.3 Improvements in Capabilities**

**Table 2-18.  
Hardware Improvements for Control Studies**

<b>Hardware Advancements</b>	<b>New Capabilities</b>
Plasma Control System advancement	
Hardware: added cpus/gpus	Faster execution of algorithms
Software: algorithm development	Increasingly complex algorithms including FRTS
SSPAs	Ability to operate DIII-D without VFI constraint
	Ability to emulate superconducting, independent PF coils
Expanded/integrated 3D diagnostics	RT stability calculations, regulation of proximity to boundaries

**Table 2-19.  
Diagnostic Improvements for Control Studies**

<b>Scientific Objective</b>	<b>Physics Measurement</b>	<b>Diagnostic Techniques</b>
RT stability calculations, regulation of proximity to boundaries	Expanded and data-fused 3D diagnostics	Magnetics, ECE, TS, CER
RT calculation of models and control algorithms	Expanded availability of profile measurements in real-time PCS	ECE, TS, CER, SXR

**Table 2-20.  
Simulation Codes Used for Control Studies**

<b>Code</b>	<b>Purpose</b>
GA TokSys	Control-level modeling and simulation, design of algorithms, engineering analysis
GA Simserver	Hardware/software-in-loop simulation of real-time control, shot validation

### 2.3 BURNING PLASMA PHYSICS

An essential feature of fusion power production is the establishment of a “burning plasma” in which sufficient alpha particle heating is generated to sustain the fusion process with minimal external heating. The burning plasma regime will involve highly non-linear processes that suggest a sophisticated predictive understanding is needed to project designs, parameters, and performance in future devices, as well as to raise performance and improve fusion prospects by manipulation of the configuration or choice of parameters and techniques. Consequently, Burning Plasma Physics research in DIII-D has two primary goals: 1) to advance the predictive capability for critical physics phenomena through understanding the underlying physical mechanisms that produce the observed phenomena; and 2) to explore complex behavior in the highly nonlinear burning plasma environment. The high-level challenges, principle approaches, and key capability improvements are set out in Table 2-21. Addressing these challenges will provide new insights into complicated processes of matter in the high-temperature state, and contribute to the design and successful operation of future fusion devices. DIII-D is well positioned to contribute to this physics knowledge with a flexible set of control tools, an extensive operating space, and a comprehensive diagnostic set capable of providing both spatial and temporal information during plasma experiments. DIII-D’s strong connections to the theoretical and experimental communities both in the U.S. and internationally will enable the program to adapt quickly to the latest developments in fusion research worldwide and investigate pertinent issues for ITER.

**Table 2-21.  
High-Level Challenges for the Achievement of Burning Plasma Regimes for Fusion Energy**

<b>Challenge</b>	<b>Approach</b>	<b>Key Capability Improvements</b>
Validate turbulent transport models on multi-scales, multi-levels and with multi-channels to project and optimize future reactors (Section 2.3.1)	Test state-of-the-art transport models using simultaneous measurements of turbulent fluctuations and heat/particle fluxes at both long and short wavelengths	Hardware upgrades: <ul style="list-style-type: none"> <li>• High power ECH</li> <li>• Fully articulated beamline; variable permeance beams</li> <li>• Upgraded 3D coil set</li> <li>• SAS divertor (open/closed)</li> <li>• Helicon antenna, klystron</li> <li>• High field side LHCD</li> </ul>
Predict the rotation profile in ITER, especially the role of intrinsic rotation and the application of 3D fields to improve flow shear (Section 2.3.2)	Characterize main ion and impurity rotation profiles, vary NTV using upgraded 3D coil set, and use perturbative methods to measure momentum sources and transport	Diagnostic Upgrades: <ul style="list-style-type: none"> <li>• Laser blow-off system</li> <li>• Full radius BES</li> <li>• High-k backscattering/PCI</li> <li>• XICS</li> <li>• 2<sup>nd</sup> DBS/CPS</li> <li>• Int.-k CECE</li> <li>• UF-CHERS</li> <li>• Tangential TS</li> <li>• FIDA imaging</li> <li>• Reverse B<sub>T</sub> FILD</li> </ul>
Validate an integrated suite of models to predict and control fast-ion transport by instabilities (Section 2.3.3)	Compare phase-space resolved measurements of fast-ion transport to simulations; explore real-time detection and control of EP mode properties	Code development: <ul style="list-style-type: none"> <li>• TGLF/GYRO/CGYRO</li> <li>• GPEC into TRANSP</li> <li>• 3D gyrokinetic codes</li> <li>• Reduced and first-principles EP models</li> <li>• Physical optics codes for RF</li> </ul>
Establish new methods for efficient, off-axis current drive that are reactor relevant (Section 2.3.4)	Install new current-drive technologies and use multi-channel MSE to measure current-drive profiles for top-launch ECCD, helicon waves at high electron beta, and HFS-launch LHCD; compare with ray tracing models	

A new frontier in fusion science is emerging that is exemplified by the use of detailed experimental measurements in the validation of predictions from simulation codes. These codes employ state-of-the-art theoretical descriptions of fundamental plasma behavior. Particular emphasis will be placed on important research topics for which DIII-D has unique capabilities. Once validated, these simulation codes will serve as a key resource in utilizing the knowledge gained from the physics research program to design future burning plasma experiments and operational scenarios. The research themes in Table 2-21 will adapt to the new experimental discoveries and theoretical developments that are advanced as the full research program unfolds.

Burning plasma research topics are closely connected to each other and also to other DIII-D research areas. Micro-turbulence in plasmas not only can lead to anomalous cross-field diffusion of particles, energy and momentum, but it can also trigger the L-H transition and affect RF ray trajectories through refraction in the plasma edge. Alfvén eigenmodes not only can result in fast-ion transport but also electron thermal transport. Transport issues are also important to develop

high-confinement inductive (Section 2.1.1) and non-inductive (Section 2.1.2) scenarios, and edge transport appears to contribute to the physics of edge localized mode (ELM)-suppressed regimes (Section 4.1.1.). Transport issues also permeate the core-pedestal-boundary integration research activities described in Section 4. Additionally, the physics of heating and current drive, and the confinement of energetic particles, are important to the creation and optimization of fully non-inductive regimes (Section 2.1.2) and stability (Section 2.2.2).

The ability to control and diagnose plasma properties with high spatial and temporal resolution is a key enabling feature of DIII-D research in these areas. This benefits from key developments on the facility:

- The electron cyclotron heating (ECH) power upgrade is an essential component of the Burning Plasma Physics plan, as it allows greater control of plasma instabilities [both turbulent and magnetohydrodynamic (MHD)], better matching of reactor-relevant conditions, and enables transient transport measurements. For example, the absorbed ECH power needs to be increased to ~6.5 MW to obtain equal electron and ion heat fluxes in high-performance plasmas using 8 beam sources. For transport stiffness experiments, ECH power needs to exceed the NBI power by ~50% [DeBoo 2012], requiring around ~7.5 MW of ECH in the ITER baseline scenario, which typically uses 5 MW of NBI.
- The upgraded 3D coil set and changes to the neutral beam injection (NBI) system will allow DIII-D to enhance its program to control instabilities and transport (both thermal and fast ion). In particular, the fully articulated beamline and variable perveance beams will give DIII-D great flexibility in varying the injected torque at full heating power, and can substantially alter the drive for energetic particle instabilities.
- Diagnostic innovation (Section 6) will continue to be a high priority for the DIII-D program as new measurements naturally lead to new physics ideas, some of which will become transformational breakthroughs. State-of-the-art measurements of plasma profiles, turbulence, and imaging are needed and planned to advance fundamental science understanding, mainly by testing the best-available theoretical model.
- The plasma control system (PCS) on DIII-D is able to dynamically control global parameters such as the plasma shape, density, and  $\beta$ , as well as dynamically control local values of the current density, toroidal rotation, and temperatures. Additional power supplies will enable fully independent poloidal field coil control for the first time on DIII-D. These control capabilities allow scientists to isolate plasma parameters, thereby enabling the elucidation of the important physical processes.

With these hardware developments (and, not least, the improvements installed at the end of the presently operating plan) and diagnostic systems, DIII-D will be equipped to investigate the critical questions and simulation basis to enable interpretation and optimization in ITER, and to project configurations for future fusion reactors.

### 2.3.1 Turbulence and Transport

*Physics Leads: C. Petty (GA), G. McKee (UWM), T. Rhodes (UCLA), M. Austin (UTA), K. Burrell (GA), D. Ernst (MIT), C. Holland (UCSD), N. Howard (MIT), A. Marinoni (MIT), O. Meneghini (GA), S. Mordijck (CWM), C. Rost (MIT), S. Smith (GA), Z. Yan (UWM).*

A comprehensive and detailed understanding of the underlying dynamics of turbulence and the resulting cross-field turbulent transport remains a key challenge to plasma physics and to the development of fusion energy. Radial transport of particles, energy, and momentum determines the global energy confinement time of magnetically confined fusion plasmas, and thus the size, and ultimately cost, of fusion energy systems. It also plays a critical role in determining a self-consistent equilibria and profiles for advanced tokamak plasmas, where steady-state kinetic profiles are determined by a balance of heat and particle sources, transport properties and sinks, which in turn impact MHD stability, self-driven currents and fusion performance. To address the complex relation between turbulence, transport, and profiles, research in this area has a strong emphasis on developing and testing state-of-the-art nonlinear simulations of turbulent transport. The understanding gained will allow the optimization of transport (or at least mitigate the deleterious consequences of turbulence) in different operational scenarios, particularly those approaching burning plasma conditions (low rotation, low collisionality, strong electron heating) and steady-state conditions (high beta, broad current and pressure profiles), to improve global performance, reliability and robustness.

During the past five years, the DIII-D team has made strong progress in understanding the behavior and dynamics of turbulence and transport properties in fusion-grade tokamak plasmas. The DIII-D program has invested significantly to build arguably the most sophisticated and comprehensive sets of turbulence diagnostics at any fusion research facility in the world, measuring multiple fluctuating fields across a range of spatial locations and wavenumbers, along with one of the most complete, reliable, accurate, and well-maintained sets of kinetic profiles and equilibrium diagnostics. A great example of recent progress made is the explanation of local density flattening during strong ECH in QH-mode plasmas [Ernst 2016]. Here, trapped electron modes (TEMs) are directly observed by Doppler backscattering (DBS) as a band of discrete mode numbers, whilst GYRO simulation results simultaneously match flux and density fluctuation spectra, both with and without ECH. The results indicate that density-gradient-driven TEM

turbulence increases particle transport as  $T_e/T_i$  increases. Another recent key result from DIII-D fluctuation diagnostics is the first observation of localized modulation of density turbulence by neoclassical tearing modes (NTM), showing that magnetic islands exhibit a reduction in turbulence that leads to faster NTM growth [Bardoczi 2016, Bardoczi 2017]. Close interaction between the DIII-D community and domestic and international transport programs, as well as between theorists, experimentalists, and computationalists has provided a source of innovative and novel ideas for new experiments, measurements, analysis, and simulation. Overall, this program has validated, and in some areas led to revision of, linear and nonlinear models of turbulent transport, explaining key trends in behavior with flow,  $T_e/T_i$ , current profile and other parameters. However, experiments have also revealed a complex multi-scale and coupled multi-species nature to turbulence in which behavior in one species is found to influence transport in another [Howard 2016, Fig. 2-39]. This is a central focus of the forward research program.

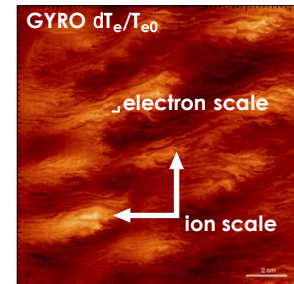


*Fig. 2-39. Electron temperature fluctuations from a multi-scale simulation.*

### 2.3.1.1 Challenges and Impact

The goal of this research is to develop a confident understanding of turbulent transport so that models can be used to optimize the path to fusion energy. This can be addressed by asking whether the models agree, using appropriate metrics [Holland 2016], with measurements from fundamental to global parameters (i.e., turbulence spectra, correlation lengths, gradients, fluxes, profiles), across multiple scales (i.e., ion gyroradius, electron gyroradius) and multiple transport channels (i.e., particle, energy, momentum). This key question is reflected in the first challenge of Table 2-22, which will enable a reliable prediction of burning plasma performance and determine how ITER can use its tools to optimize performance. This research needs to anticipate the multi-scale/field/species behavior at burning plasma relevant parameters, such as  $T_e/T_i \sim 1$ , low torque and low collisionality. The second challenge of Table 2-22 addresses the goal of high confinement in steady-state conditions, which requires high beta operation with self-consistent pressure and current profiles. There are a number of key issues to address: (1) what is the impact of high beta and electromagnetic effects on turbulence, (2) what is the role of q-profile and magnetic shear on turbulence drive and suppression, (3) can particle, high-Z impurity, thermal and momentum transport be differentially controlled, and (4) do EP-driven modes impact plasma power balance significantly beyond just redistributing beam ions? This research will have a high impact if it leads to situations in AT regimes where local transport changes modify the plasma profiles such that the result is improved global confinement.

Since a fundamental understanding of plasma turbulence underpins the above transport work, Table 2-22 includes a third challenge that focuses on the exploration of turbulence across multiple spatial scales and multiple fluctuation fields. A distinguishing difference between this challenge and the two prior ones is that here the regime is chosen to optimize the testing of critical turbulent characteristics, as opposed to optimizing reactor-relevance. Detailed questions about turbulence can be asked here, such as how do gradient-driven linear instabilities drive turbulence, how does turbulence saturate via zonal flows or other mechanisms, and how do 3D radial fields impact turbulence and transport properties? Finally, the fourth challenge of Table 2-22 seeks to develop a well-established and widely-employed modeling capability for designing and optimizing plasma experiments. The key issue is whether a widely used and accepted transport modeling capability, based upon first-principles simulations and backed by substantial experimental testing, can be used to design and optimize fusion plasma experiments. If successful, this will allow scientists to model discharges prior to running them, either on current devices or ITER, allowing scenarios to be developed more quickly and reducing major disruptive events.

**Table 2-22.**  
**Turbulence and Transport Approaches and Upgrades**

<b>Challenge</b>	<b>Goals/Deliverables</b>	<b>Upgrades</b>
<b>1. To predict burning plasma regime – performance, profiles and behavior</b>	<ul style="list-style-type: none"> <li>Assess multi-channel (heat, particle, momentum) transport in both ion and electron scales, test transport stiffness properties</li> <li>Test and validate transport models and optimize transport for conditions of low torque, strong electron heating, low <math>v^*</math></li> <li>Resolve discrepancies in traditionally problematic regimes</li> </ul>	<p><b>Hardware upgrades:</b></p> <ul style="list-style-type: none"> <li>Higher power ECH</li> <li>Fully articulated beamline</li> <li>Upgraded 3D coil set</li> </ul> <p><b>Diagnostic Upgrades:</b></p> <ul style="list-style-type: none"> <li>Laser blow off system</li> <li>Full radius BES with improved sensitivity</li> <li>High-k backscattering and upgraded PCI for <math>\tilde{n}(k_\theta)</math></li> <li>Tangential Thomson scattering</li> <li>2D and 3D turbulence diagnostics via toroidally/poloidally spaced DBS/CPS</li> <li>CECE upgrade for int.-k <math>T_e</math></li> <li>UF-CHERS for <math>T_i</math></li> <li>ECEI/MIR upgrades</li> </ul> <p><b>Code development:</b></p> <ul style="list-style-type: none"> <li>GYRO</li> <li>TGYRO</li> <li>CGYRO</li> <li>TGLF</li> <li>BOUT++</li> </ul>
<b>2. Project advanced H-mode scenarios to regimes with high pressure and modified shear</b>	<ul style="list-style-type: none"> <li>Understand transport at high beta to assess electromagnetic effects, including from EP instabilities, on turbulence</li> <li>Assess the role of safety factor and magnetic shear in altering turbulence drive and suppression</li> </ul>	
<b>3. Expand fundamental knowledge of nonlinear interactions, self-driven flows and saturation mechanisms of turbulence</b>	<ul style="list-style-type: none"> <li>Identify correct and incorrect saturation processes in simulations, poloidal transport asymmetries, differences between positive and negative triangularity.</li> </ul>	
<b>4. Develop a well-established and widely employed modeling capability for designing and optimizing plasma experiments</b>	<ul style="list-style-type: none"> <li>Broadly use integrated reduced models (based on “predict first” framework) to plan experiments and interpret experimental results</li> <li>Streamline ability to run integrated models</li> </ul>	

### 2.3.1.1 Research Plan

The central objectives of turbulence and transport research during the 2019-2024 five-year plan will be to achieve a predictive knowledge of the turbulent instabilities and processes at play in burning plasma scenarios, identifying missing physics in transport simulations, developing new measurement capabilities and performing focused experiments that increase understanding and optimize performance. The program for turbulence and transport research is organized according to the challenges and goals in Table 2-22. The timeline for each challenge and research milestones is shown in Fig. 2-40. Key enablers of this research are improvements in ECH power and diagnostics.

Challenge	FY19-20	FY21	FY22	FY23	FY24
<b>Burning Plasma Regimes</b>	<i>Test and validate models in ITER-baseline regimes</i> <i>Resolve L-mode Shortfall</i> <i>Understand transport in pedestal and no-man's land</i> <i>Isotope scaling experiments</i> <i>Impurity transport</i>				
<b>Advanced H-modes</b>	<i>Testing methods to control and improve transport</i> <i>Negative triangularity in new operational regimes</i>				
<b>Fundamentals of Turbulence</b>	<i>Measure and quantify turbulent transport</i> <i>Identify saturation mechanisms/characterize zonal flows</i>				
<b>Predict-First Modeling</b>	<i>Test and improve TGLF reduced transport model across multiple operational regimes</i> <i>(hybrid      ITER baseline      steady-state advanced scenario)</i>				
<b>Hardware and Diagnostic Improvements</b>	<ul style="list-style-type: none"> <li>• Expanded/upgraded BES</li> <li>• 2<sup>nd</sup> DBS system (240°) <ul style="list-style-type: none"> <li>• Tangential TS upgrade <ul style="list-style-type: none"> <li>• XICS/x-ray spectroscopy</li> <li>• Upgraded CECE</li> </ul> </li> <li>• ECEI/MIR upgrades</li> <li>• 2<sup>nd</sup> ECE radiometer</li> <li>• High-k scattering (R-2)</li> </ul> </li> <li>• 2<sup>nd</sup> off-axis beamline, NBI perveance</li> <li>• 5 MW ECH <ul style="list-style-type: none"> <li>• Advanced 3D coils</li> <li>• 7-9 MW ECH</li> </ul> </li> <li>• 2<sup>nd</sup> co-ctr beamline</li> </ul>				

Fig. 2-40. Timeline of Research Challenges in Turbulence and Transport Area, as well as Improvements in Hardware and Diagnostics

**Challenge 1: Predict burning plasma regime – performance, profiles, and behavior**

**Current Progress.** One of the great advances in recent years has been the development of first-principles nonlinear gyrokinetic simulation codes and reduced models that predict turbulence and transport for given kinetic profiles, gradients therein, and magnetic geometry. As an example of reasonably good agreement, Fig. 2-41 shows a quantitative comparison of the normalized ( $\tilde{n}/n$ ) long-wavelength density fluctuation spectrum, measured with Beam Emission Spectroscopy [McKee 2010], to that calculated from a GYRO simulation [Candy 2003] for a high-performance hybrid plasma on DIII-D. The GYRO calculation used experimental profiles and equilibrium and was run nonlinearly with flux-tube geometry, including electromagnetic effects and low-wavenumber (ion scale) modes, but not high-k modes. For the calculated frequency spectrum from GYRO (light blue dashed line in Fig. 2-41), synthetic diagnostic predictions for BES signals (solid blue), are made to compare with the measured BES spectrum (red). It should be emphasized that the spectra are absolute values, not arbitrary units; indicating that both the normalized density fluctuation amplitudes and frequencies agree well. The calculated thermal heat fluxes from GYRO are also compared to the experimentally interpreted values from ONETWO transport analysis in Table 2-23; this comparison demonstrates reasonably good agreement for the ion heat fluxes and density fluctuation amplitudes, but poorer agreement between the simulated and experimental electron heat fluxes, possibly due to the contribution from higher-k modes that are not included in this simulation to electron transport. Thus further work is needed to develop required predictive capabilities.

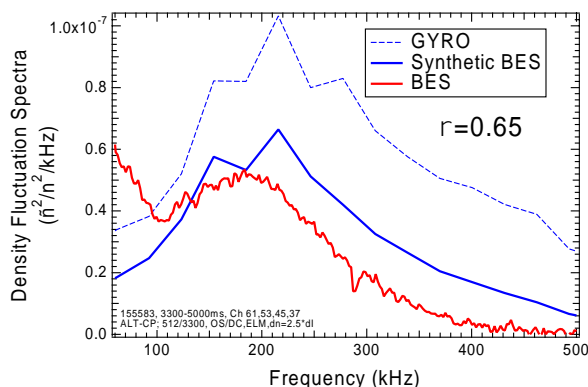


*Fig. 2-41. Quantitative comparison of measured density fluctuation spectrum from hybrid H-mode plasma with GYRO simulation with synthetic diagnostic applied.*

**Table 2-23.**  
**Comparison of experimental and calculated (GYRO) ion and electron heat flux and density fluctuations.**

	$Q_i$ (W/cm <sup>2</sup> )	$Q_e$ (W/cm <sup>2</sup> )	$\tilde{n}/n(\%)$
<b>Exp</b>	<b>4.8</b>	<b>7.6</b>	<b>0.33</b>
<b>GYRO</b>	<b>5.9</b>	<b>5.5</b>	<b>0.37</b>

**Goal 1: Access multi-channel transport in both ion and electron scales, test transport stiffness properties.** Since the simulation in Table 2-23 was performed for low-k modes only, the under prediction of the electron heat flux by GYRO indirectly suggests that higher-k modes may be active and contributing significantly to the experimental heat flux. This potential contribution

of higher- $k$  modes points to a new proposed direction in transport physics research, which is understanding the role of both low- and high- $k$  modes, and, importantly, their interactions.

The nature of the multi-scale interactions will be investigated experimentally by (1) using the upgraded external systems (NBI, ECH, 3D fields) to generate ion and electron heat fluxes in burning plasma-relevant regimes, and (2) employing a range of fluctuation diagnostics (DBS [Hillesheim 2009], PCI [Dorris 2009], BES [McKee 2010]) to monitor the resulting turbulence over a range of low-to-high wavenumbers simultaneously. Development of short wavelength fluctuation diagnostics will be a major focus. The “predict first” modeling discussed in Challenge 4 is important for this work in order to identify the most relevant conditions for observing the mixture of high- and low- $k$  modes. For example, parameter scans that are expected to affect the mixture of high- and low- $k$  modes are (1) the  $T_e/T_i$  ratio and (2) the  $E \times B$  shear (which affects low- $k$  modes more than high- $k$  modes).

Transport stiffness studies will, for the first time, be extended to test behavior in high-performance H-mode plasmas, including IBS and advanced hybrid scenarios. These studies utilize modulated ECH [DeBoo 2010], requiring considerable power to assess reactor-relevant dominantly electron-heated regimes; enabled by the increased heating power planned ( $\sim 6$  MW). Measurements of localized electron temperature in response to ECH pulses will allow for identification of the convective and diffusive components of thermal heat flux; corresponding measurements of fluctuations will provide more direct and quantitative comparisons and correlations of electron temperature gradient variation with turbulence parameters. This research will be conducted in concert with requests from ITER, as well as the goals and objectives of the broader fusion energy sciences program, including collaborating national laboratory and university research programs. This is an opportunity for U.S. scientific leadership in ITER.

**Goal 2: Test and validate transport models and optimize transport for conditions of low torque, strong electron heating, low  $v^*$ .** Burning plasma conditions of equilibrated temperatures and low injected torque present several challenges to the current understanding. The  $T_e/T_i$  ratio has been shown experimentally to strongly impact turbulence and transport. Sound scientific practice motivates us to make experiment/theory comparisons across the “primacy hierarchy” [Terry 2008] by including basic turbulence quantities (spectra, correlation lengths, decorrelation times, phase relationships in multiple fields), profiles and profile gradients, and global parameters [Holland 2009]. The metrics by which this validation procedure is assessed have been identified [Holland 2016].

A major goal of the proposed transport research program is to expand the operational regimes and parameter space over which transport models have been qualified. Crucial to this effort will be availability of increased ECH power and larger balanced NBI to equilibrate temperatures in

low-torque H-mode plasmas. Increasing the ECH power to  $\geq 5$  MW will allow DIII-D to achieve or exceed  $T_e/T_i=1$  in moderate beta ( $\beta_N \sim 2$ ), low  $q_{95}$  ITER-similar plasmas. The increased transport with increased ECH may result not only from increased fluctuation amplitude, but also from changes in the phases between fluctuating quantities. To ascertain this, plasmas will be designed that can achieve good access and measurement capability for temperature fluctuation measurements, including as CECE ( $\tilde{T}_e$ ) and UF-CHERS ( $\tilde{T}_i$ ), along with the suite of density fluctuation diagnostics. By combining DBS and CECE diagnostics and, separately, the BES and UF-CHERS diagnostics, it should be possible to measure and relate any changes in the  $\langle \tilde{n} \tilde{T} \rangle$  cross-phase relationship to related turbulent transport changes and compare with transport models [White 2010]. Besides equilibrated temperatures and low rotation/shear, another dimensionless parameter that is associated with burning plasma conditions is low collisionality. Collisionality strongly impacts which instabilities are most strongly driven. While DIII-D has previously investigated the  $v^*$  dependence of transport in L-mode and H-mode plasmas [Petty 1999], new collisionality experiments will study the complex interdependence between particle and thermal transport on operational regime,  $T_e/T_i$ , and q-profile, as well as the peaking of the electron density profile and high-Z impurity accumulation.

**Goal 3: Identify mechanisms behind isotope effect.** The isotope mass and/or isotopic mixture of the working (fuel) ions strongly and beneficially impacts transport and global energy confinement. The dependence of  $\tau_E$  on isotope mass has been extensively documented on multiple experiments, and yet the basic turbulence mechanisms behind this have yet to be identified, validated and quantified. Furthermore, the experimental evidence from TFTR, JET, DIII-D and JT-60U has been somewhat inconsistent.

We therefore propose to perform a set of experiments in different plasma scenarios that vary the content of hydrogen and deuterium, obtain comprehensive measurements of kinetic profiles and fluctuations, and perform nonlinear simulations with GYRO or other codes. Linear gyrokinetic theory would suggest that transport should increase with ion mass (from increased gyroradius), but this is not observed. Recent nonlinear simulations have suggested that electromagnetic effects, zonal flow damping and other nonlinear processes may contribute to and cause the typically observed isotope effect [Garcia 2017]. Measuring the effect in multiple plasma regimes (L-mode, H-mode, ELM-suppressed H-mode, QH-mode, hybrid or advanced inductive) will allow for a more complete understanding of core and pedestal transport dependencies on isotope mass. This set of experiments would also address key aspects of Challenge #3 that seeks to understand fundamental physics of turbulent transport and turbulence saturation.

**Goal 4: Resolve discrepancies in traditionally problematic regimes.** Certain plasma regimes and conditions have continued to pose challenges to accurate transport simulation,

especially near the plasma edge. The region between core and pedestal ( $0.75 < \rho < 0.9$ ) is of particular interest. In H-mode this region is impacted by ELMs and is identified as “No Man’s Land” since most research has focused on the mid-radius transport zones ( $\rho < 0.75$ ) or the pedestal region ( $\rho > 0.9$ ). Another problem area is the outer region, sometimes extending between  $\rho = 0.5$  and  $\rho = 1.0$ , of L-mode plasmas. Here, high transport levels are observed but transport models like GYRO and TGLF often predict low transport levels. This is referred to as the “edge transport shortfall”.

Future work to resolve these discrepancies will look at two aspects of the problem. First, it will be examined whether the transport models are partially or fully to blame by comparing transport codes of differing provenance. For example, there is evidence that the GENE code has less of an edge transport shortfall problem than does GYRO. The important differences in the codes will be compared to see if there is a relationship between a superior physics model and better experiment/theory agreement. Second, experiments will be designed to fully diagnose and probe the “No Man’s Land” and “edge transport shortfall” regions with the suite of available fluctuation diagnostics and tools, including modulated-ECH, gas puffing and perturbative neutral beam torque modulation at constant power. The dependences (e.g., safety factor) of the discrepancies will also be investigated. This will provide the database necessary to identify just where the transport models go wrong.

**Challenge 2: Project advanced H-mode scenarios to regimes with high pressure and modified shear**

**Current Progress.** The safety factor profile and magnetic shear have long been known to impact transport, with core negative magnetic shear observed to reduce ion transport to near neoclassical levels [Lazarus 1996]. However, these plasmas were typically transient or MHD unstable due to the uncontrollability of the q-profile and peaking of the core pressure profile. More recent experiments have demonstrated that negative shear can reduce or eliminate the increase in transport that typically occurs approaching equilibrated temperatures [Yoshida 2017]. An example is shown in Fig. 2-42. , where the ion temperature is observed to increase with increasing  $T_e/T_i$  in negative central magnetic shear plasmas, while it decreases in positive magnetic shear plasmas. Likewise, the relative increase in

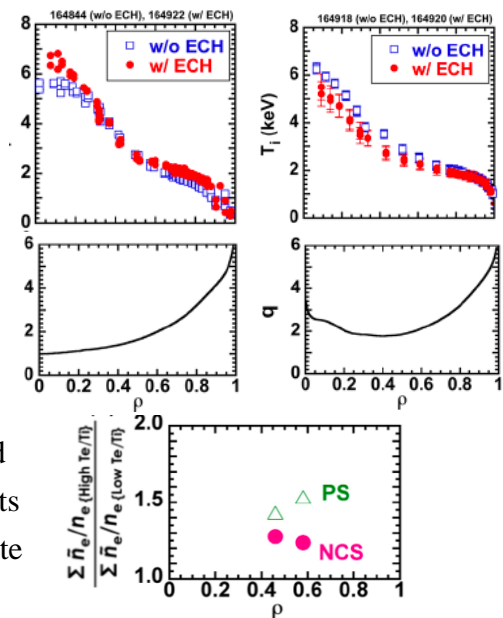


Fig. 2-42. Ion Temperature profiles with (red) and without (blue) ECH in positive shear (left) and negative shear (right) profiles, corresponding q-profiles, and comparison of relative fluctuation magnitude increase with ECH in PS and NCS.

turbulence with  $T_e/T_i$  is reduced in negative central shear. This suggests that the deleterious effects of increasing  $T_e/T_i$  on transport are at least partially mitigated with NCS. These results are also consistent with observations on JT-60U.

**Goal 1: Understand transport at high beta to assess EM effects, including from EP instabilities, on turbulence.** Advanced H-mode scenarios seek to achieve a high bootstrap current fraction without sacrificing fusion power density or fusion gain. Models of drift-wave turbulence generally predict a strong increase in transport from EM effects when beta exceeds some fraction (typically 50%) of the ideal ballooning stability limit. Additionally, there has been considerable recent interest in the possibility that EP instabilities can drive electron thermal transport.

A focus of transport experiments in DIII-D will be determining if EM effects, such as from magnetic flutter transport or micro-tearing modes, are limiting the confinement in high-beta regimes. This will exploit the considerable expansion in performance and  $\beta$  of advanced tokamak regimes in this five-year plan. A key advance will be the fluctuation diagnostics on DIII-D (*i.e.*, CPS and RIP) that are capable of measuring magnetic turbulence. If it is determined that EM modes limit confinement in advanced H-mode scenarios, then the predicted dependences of these modes can be used to reduce their strength and improve confinement. For example, the safety factor and plasma shape can be optimized to increase the ideal ballooning stability limit, and the collisionality and density gradient can be reduced to weaken micro-tearing modes. This work will be performed jointly with the steady-state scenario group.

**Goal 2: Assess the role of safety factor and magnetic shear in altering turbulence drive and suppression.** New actuators, including increased ECH/ECCD power and off-axis neutral beam injection, will allow increased control and tailoring of the q-profile in future experiments. It is proposed to explore how the safety factor and magnetic shear interact with rotation and ExB shear to affect transport over the expanded region of operational space enabled by new gyrotrons and OANB capability. Emphasis will be placed on modeling this behavior using TGLF and GYRO, since some analyses indicate that NCS reduces growth rates. This process will ultimately allow for increased confidence in determination of global energy confinement times, fusion output and energy gain,  $Q=P_{\text{FUS}}/P_{\text{INPUT}}$ , in advanced tokamak H-mode scenarios, and inform overall configuration performance optimization.

### **Challenge 3: Expand fundamental knowledge of nonlinear interactions, self-driven flows and saturation mechanisms of turbulence**

**Current Progress.** Plasma turbulence is a multiscale, multi-field phenomenon with fluctuations in density, temperature, flows, as well as electrostatic and magnetic fields, and extending from low wavenumber ion gyroscale modes (such as ITG, KBM, or even lower-k

trapped-ion modes) up to electron gyroscale modes. Over the past five years, experiments on DIII-D have made substantial progress in characterizing the wavenumber spectrum for different fluctuation quantities, which has important implications for revealing the nature of the driving instabilities and understanding the energy cascade process that saturates turbulent transport. New turbulence diagnostics on DIII-D have measured fluctuations in the magnetic fields (CPS, RIP), the carbon ion temperature and carbon toroidal rotation (UF-CHERS), and imaging density fluctuations (MIR). Fig. 2-44 shows a measurement of magnetic fluctuations between ELM crashes using the Cross Polarization Scattering (CPS) diagnostic, which can be compared to predictions from ELM models.

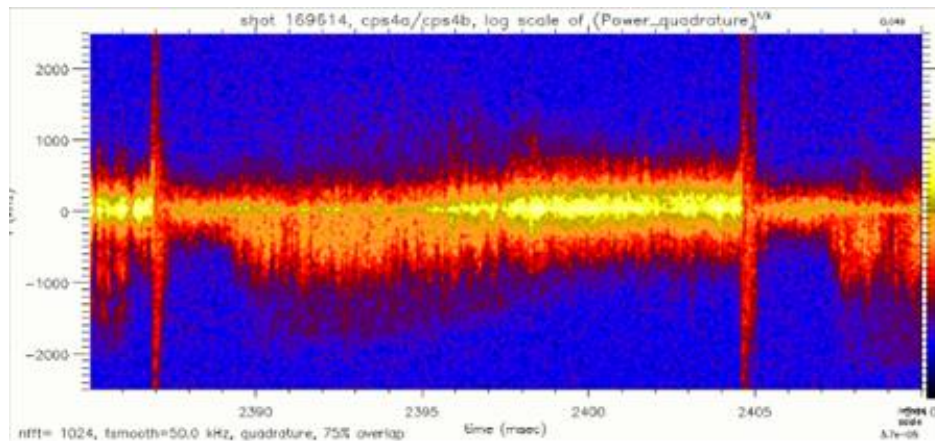


Fig. 2-44. Frequency spectrum of magnetic fluctuations between ELM crashes as measured by the Cross Polarization Scattering (CPS) diagnostic at  $\rho=0.96$ .

An interesting example of a basic turbulence dependence on plasma shape comes from recent experiments in DIII-D that studied changes in transport between positive and negative triangularity. Negative triangularity is an extreme example of shape variation, and ECH L-mode experiments on TCV [Camenen 2007, Marinoni 2009] discovered that negative triangularity plasmas have improved transport relative to similar positive triangularity plasmas, with the difference increasing at lower collisionality, but the underlying mechanisms were not identified. Fig. 2-43 shows a set of positive and negative triangularity equilibria from studies at DIII-D that found reduced transport with negative triangularity, achieving H-mode like performance with an L-mode edge plasma condition [Austin 2017]. Measurements with PCI and BES suggest that fluctuations are lower at negative triangularity, consistent with reduced thermal transport.

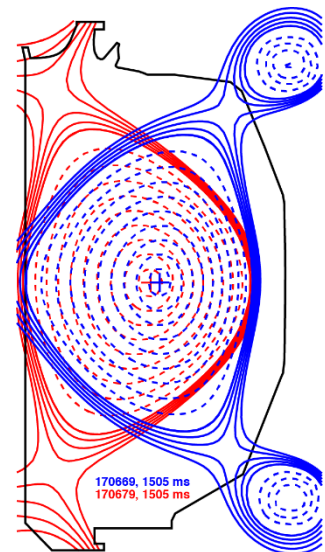


Fig. 2-43. Equilibria in positive (red) and negative (blue) triangularity plasmas produced on DIII-D.

**Goal 1: Identify correct and incorrect saturation processes in simulations and poloidal transport asymmetries.** While linear transport codes are fast and convenient, turbulent transport is inherently a nonlinear phenomenon. Toward the goal of validating nonlinear modeling, new experiments in DIII-D will investigate how the growth of turbulence amplitudes saturate via zonal flows or other mechanisms. The strength of zonal flows can be altered by varying the damping mechanisms (collisions, 3D fields) and fluctuation diagnostics like BES and DBS can quantify the flows. New insights into the nonlinear nature of plasma turbulence will also be gained by measuring the poloidal asymmetries of fluctuations using two diagnostics that view different vertical locations in the plasma. One proposal to do this is via toroidally/poloidally spaced DBS and CPS. Key aspects of these studies are expanding the range of parameters and scenarios for which nonlinear simulations are qualified, improving model accuracy, and identifying missing physics elements.

Identifying the role and contribution of low- and high-k modes, and, importantly, their interactions to electron and ion transport, is key to understanding the nonlinear and multiscale nature of transport. Nonlinear simulation results have demonstrated that not only are higher-k modes relevant to electron heat transport, but that they can interact strongly with lower-k modes and the nonlinearly driven zonal flows and thus impact ion transport as well. We propose to investigate the nature of the multiscale interactions experimentally by employing a range of fluctuation diagnostics (DBS [Hillesheim 2009], PCI [Dorris 2009], BES [McKee 2010]) that observe a range of wave numbers simultaneously. Predictions for DIII-D indicate that the mixture of high and low-k modes is subject to the electron to ion temperature ratio and ExB shear, and will thus change significantly as burning plasma conditions of equilibrated temperatures and low rotation/shear are approached.

Transport is inherently a multifield process, and turbulence is manifest as fluctuations in multiple parameters: density, electron and ion temperature, rotation, electrostatic potential, and magnetic field. DIII-D has now implemented diagnostics to measure fluctuations in nearly all of these fields and is poised to fully characterize turbulence and to directly measure turbulent transport in the core and edge regions of various scenarios. This will require increased coordination and spatiotemporal synchronization of diagnostic measurements and development of new analysis techniques to directly calculate turbulent fluxes of particles, heat and momentum that result from correlated fluctuations in these fields. This approach will enable far more fundamental and quantitative measurements of turbulent transport and saturation processes and provide more direct comparisons with simulation for validation studies.

#### Challenge 4: Develop a well-established and widely employed modeling capability for designing and optimizing plasma experiments

**Current Progress.** Significant progress has been made in developing accurate predictions of the plasma profiles without using experimental boundary conditions by taking into account the strong interplay between core transport, pedestal structure, current profile and plasma equilibrium. An integrated model capable of calculating the steady-state self-consistent solution to this strongly coupled problem has been created that leverages state-of-the-art components for collisional and turbulent core transport, equilibrium, and pedestal stability [Meneghini 2016].

As shown in Fig. 2-45, testing against a DIII-D discharge shows that the model is capable of robustly predicting the kinetic profiles (electron and ion temperature and electron density) from the axis to the separatrix in good agreement with the experiments. This self-consistent model has been used to show that the fusion power in ITER will be a strong function of the pedestal electron density and pedestal impurity content, both of which will likely need to be actively controlled during ITER operations to optimize the fusion performance and satisfy the requirements imposed by the density limit.

**Goal 1: Broadly use integrated reduced models to plan experiments and interpret experimental results.** The goal is to develop a widely used and accepted reduced-transport modeling capability based upon first principles simulations and backed by substantial experimental testing. The plan is to use the developed “predict first” capability to better design future experiments on DIII-D, both for determining if a certain experiment is feasible (e.g., is there enough current drive, momentum injection, heating power, etc.) and identifying the most promising type of scan (e.g., does varying the density or collisionality yield a more definitive test of the hypothesis). The predict-first capability is also useful for interpreting the physics results since it can be used to compare a synthetic “idealized” experiment to the actual experiment. For example, in an investigation of ion transport stiffness, the predict-first simulation can take into account the (expected) change in the pedestal height as the ion heat flux is scanned, a constraint that is difficult to achieve in an actual experiment.

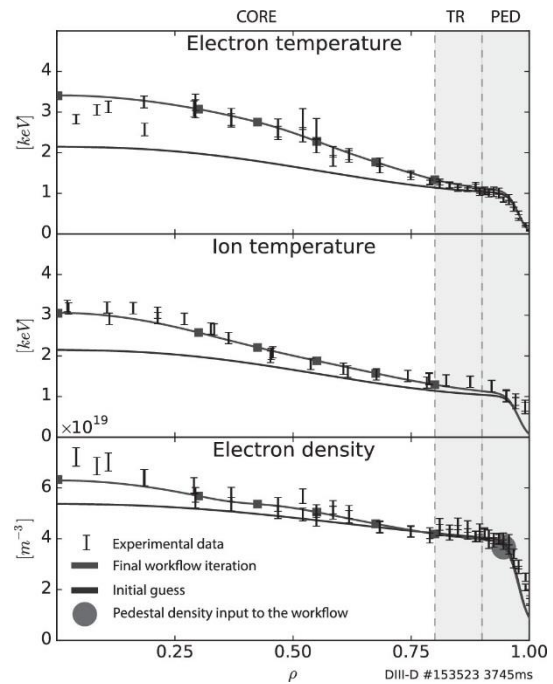


Fig. 2-45. Simulated kinetic profiles for a DIII-D discharge and comparison with the experimental measurements. The squares in these curves indicate the radii at which TGYRO performed the flux-matching calculations.

**Goal 2: Streamline ability to run integrated models.** The need to allow integrated models to be accessible to a large number of DIII-D scientists and fast enough to handle a large number of cases means that workflow management needs to be streamlined. DIII-D scientists are engaged in a long-term process to develop an iterative workflow that connects various physics modules together in a self-consistent manner via coupling of the One Modeling Framework for Integrated Tasks (OMFIT) and Integrated Plasma Simulator (IPS) frameworks [Meneghini 2016]. Currently the user controls the integrated simulation with OMFIT (i.e., TGYRO, ONETWO, EFIT, etc.) while relying on the IPS to provide the High-Performance Computing (HPC) enabled IPS-EPED1 workflow. Future plans to improve the physics in these routines and include new physics models/modules, may result in an increased computational complexity of the modules and more difficult management of the information passed between modules. One area of investigation will be the use of machine learning to accelerate the computations, especially in cases where calculations from certain physics modules have become too lengthy to be used in an iterative procedure.

An example of this is given in Fig. 2-46, which shows the design of a neural network regression of EPED1 simulations that calculate the pedestal height and width. Such a neural network is fast enough to enable “whole device” modeling and plasma control applications. These tools will act as a key element in developing robust and advanced whole-device modeling and advancing sophistication and validation of models for fusion energy.

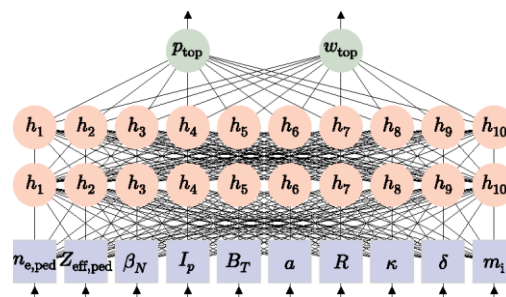


Fig. 2-46. Design of neural network to predict the pedestal height and width using the same input parameters as the EPED1 model.

### 2.3.1.2 Capability Enhancements

Advancing the scientific knowledge base for transport physics will rely on implementing several new technologies, actuators, and diagnostics. The motivation, rationale, and importance of these systems are briefly outlined. Anticipated new hardware capabilities are summarized in Table 2-24, new diagnostics in Table 2-25 and new or updated modeling and simulation capabilities in Table 2-26. These capability enhancements will expand and advance DIII-D’s world-leading turbulent transport research program, taking it forward to address the critical questions for future fusion devices, while maintaining and strengthening this field as an area of U.S. leadership.

**Table 2-24  
Hardware Improvements for Transport Studies**

<b>Hardware Capability</b>	<b>New Physics</b>
Increased electron heating capability with additional gyrotrons	Understanding transport for $T_e/T_i \geq 1$ , control of $T_e$ scale length, heating without particle or torque injection, control of q profile using current drive, providing modulated localized heat deposition to determine transport response. Modeling shows ~5 MW is needed in IBS for $T_e/T_i=1$ . Twice this ECH power is needed to do modulation studies of the $T_e$ gradient response.
Flexible Neutral Beam Injection (co/counter, off-axis, variable perveance)	Transport with negative magnetic shear, interaction with current density profile, stability; dependence on more controllable deposition and source profiles
Helicon wave system	Central electron heating at high density
LFS launch LHCD	Optimize turbulent transport and plasma stability by control of q profile
3D radial magnetic field coils	Turbulence and transport variation with non-axisymmetric magnetic fields; density pump-out, NTV torque, changes in edge shear, ELM suppression

**Table 2-25  
Diagnostic Improvements for Transport Studies**

<b>Scientific Objective</b>	<b>Physics Measurement</b>	<b>Diagnostic Technique</b>
Understanding role of electron thermal turbulence in transport	Electron temperature fluctuations	ECE-I/MIR upgrades, int-k CECE, high-k scattering
Medium to High-Z impurity particle transport	Controlled impurity injection quantity and timing	Laser Blow Off
Multiscale interactions of turbulence with MHD, Alfvénic instabilities, 3D perturbations	Wide-field high-frequency density fluctuation measurements	Full-radius BES, expanded DBS
Multifield interactions and measured turbulent transport	Ion temperature, toroidal rotation, density and magnetic fluctuations	CECE, UF-CHERS, XICS, RIP
Non-axisymmetric perturbations	Zonal Flow, n-number	Toroidally displaced DBS/CPS, CECE
Role of intermediate wavenumber instabilities.	2D High resolution pedestal and core density fluctuations	BES-HD
Understand role of ELM crash structure in transport	Electron temperature and density perturbations	ECE-I/MIR upgrades
Core electron thermal transport	Core electron temperature and density for all $B_T$ values	Tangential TS upgrade

**Table 2-26**  
**Simulation Codes Used**

<b>Code</b>	<b>Purpose</b>
GYRO	Linear and nonlinear simulations, electrostatic, electromagnetic, ion to electron modes
CGYRO	Modified GYRO with pseudospectral algorithm for collision operator to handle higher collisionality regimes, multi-impurity species
TGYRO	Transport solver; flux matching implementation for GYRO
TGLF	Reduced model calibrated against set of GYRO simulations, applicable to wider operational regimes, very fast computation [Staebler-PoP-2007]
BOUT++	Boundary turbulence from outer core to SOL, full 2D geometry, modified fluid equations, modular design [Dudson-CPC-2009]
FDTD2D	Full-wave simulations of X-Mode and O-Mode based microwave diagnostics including DBS, CECE, CPS for synthetic diagnostics applied to gyrokinetic simulations
EC2D	Reconstruct ELM image with synthetic imaging code
FWR2D/3D	Understanding pedestal pressure 2D structure with synthetic imaging

### 2.3.2 Rotation Generation and Momentum Transport

*Physics Leads: J. deGrassie (GA), C. Chrystal (GA), B. Grierson (PPPL), J. Boedo (UCSD), N. Logan (PPPL), G. McKee (UWM), C. Holland (UCSD), C. Petty (GA), W. Solomon (GA).*

Large, high-temperature tokamaks have for the most part benefitted from high levels of toroidal rotation driven by the significant neutral beam injection needed to attain reactor-relevant levels of  $\beta$ . Toroidal rotation can be beneficial for plasma MHD stability and for energy confinement [deGrassie 2009], and it also affects the L-H transition power threshold [Gohil 2008]. However, ITER and future burning plasma devices are projected to have insufficient NBI torque to achieve rotation levels necessary to obtain benefits that are routine on current high temperature tokamaks. The decrease in the relative amount of NBI torque in ITER and future burning plasma devices is caused by the moment of inertia scaling as  $R^5$  and the requirement for an order of magnitude higher neutral beam energy (necessary for penetrating a larger, denser plasma), which leads to less torque per MW.

Fortunately, experiments have shown that tokamaks manifest a toroidal torque apart from NBI [Solomon 2007], which appears in the plasma edge region [Solomon 2010] and drives rotation and rotation shear in the co- $I_P$  direction across the plasma [deGrassie 2016, Chrystal 2017]. Rotation shear throughout the core of the plasma is also manifest even in the absence of a core source of momentum. It is important to understand and predict the level of this “intrinsic” rotation (all rotation not driven by NBI torque) in ITER and other burning plasma devices in order to determine the associated benefits to stability and confinement. Furthermore, it is envisioned that this

understanding will lead to actuators that can be used to further enhance the rotation profile in regard to stability and confinement. While theory and modeling are sufficiently mature to predict temperature and density profiles in ITER with some confidence, this is not yet the case for a detailed rotation profile.

Essential to this area of research is the ability to decouple the power and torque input to the plasma. The ability to study plasmas with low amounts of auxiliary momentum input is one theme that permeates this five-year plan. Ten years ago, the NBI system in DIII-D was modified to allow some torque balance of NBI, giving DIII-D the ability to study more burning plasma-relevant heating conditions. Enhancing this capability is an important part of the 2019-2024 five-year plan. Two key actuators; 3D fields that impart torque without power, and ECH that provides power without torque are both directly beneficial for this purpose. Also, the addition of neutral density measurements in the edge and pedestal is a diagnostic improvement that is key to understanding the edge intrinsic rotation.

### 2.3.2.1 Challenges and Impact

The DIII-D research activities in plasma rotation for the 2019-2024 five-year period, identified in Table 2-27, have the common goal of understanding the sources and transport of momentum to allow an accurate prediction of toroidal rotation and core velocity shear (CVS) in a tokamak reactor.

The first challenge emerges from the need to determine the source of intrinsic torque and test models of turbulence-induced momentum flux in the plasma core. A key issue is whether non-NBI heating can create an intrinsic rotation profile that provides enough ExB shear to improve energy confinement. Theoretically, several turbulence-driven mechanisms have been identified as possible causes of intrinsic rotation [Dominguez 1993, Waltz 2007, Peeters 2007, Camenen 2009, Waltz 2011]. The details of tokamak turbulence, *e.g.*, dominant modes, intensity, intensity profiles, spectrum and so on, depend upon the density and temperature profiles and the rotation profile. Experiments will be designed to discover ways to modify the nature of the turbulence advantageously for rotation, and hence for plasma performance. The impact of this work will be to determine if the intrinsic torque is sufficient to obtain the desired stability and confinement in ITER (and to what extent external momentum sources are needed), to identify the best actuator to drive core velocity shear in burning plasma devices, and to better design future 3D coil systems to minimize unwanted effects (like locked modes) and tailor the desirable effects (like edge torque) to improve quantities like the L-H threshold power.

The second challenge focuses on the predictive understanding of mechanisms that control the intrinsic rotation near the H-mode pedestal. The pedestal region affects the entire rotation profile

because the momentum “source” must pass through the edge, as can be shown by general theoretical arguments [Pustovitov 2011]. Furthermore, edge rotation control can make the L-H transition easier and optimize the height and width of the pedestal. This challenge seeks to identify dominant turbulence mechanisms or actuators that can bring in co- $I_p$  momentum or expel counter- $I_p$  momentum, which can be important for RMP ELM suppression (see Section 4.1.2).

The third challenge is to tackle the effects of the 3D fields on the resultant rotation profile, because many sources of 3D fields will exist in ITER, such as the toroidal field ripple, the ferritic Test Blanket Modules, magnetic islands and RMPs. The plan is to achieve quantitative validation of models of the torques and drags produced by 3D fields in order to increase confidence in the projection of ITER’s toroidal rotation and structure of ExB flow, which is critical for tearing stability and RMP ELM suppression. If ITER appears to be in locked mode danger, then the goal becomes to increase the core toroidal rotation by manipulating the 3D magnetic spectrum.

**Table 2-27.**  
**High-Level Challenges for the Achievement of Burning Plasma Rotation Physics**

<b>Challenge</b>	<b>Goals/Deliverables</b>	<b>Capability Enhancements</b>
<i>Test models of turbulence-induced momentum flux and potential for improving core plasma performance</i>	<ul style="list-style-type: none"> <li>• Characterize turbulent fluctuations at low and high wavenumber associated with co-<math>I_p</math> and ctr-<math>I_p</math> intrinsic torques for a range of collisionality and electron-to-ion heat flux</li> <li>• Excite particular turbulent modes that achieve maximum ExB shear by using core ECH/ECCD that produce direct (<math>T_e</math>, <math>T_i</math>) and indirect (q-shear) effects</li> </ul>	<p><b>Hardware upgrades:</b></p> <ul style="list-style-type: none"> <li>• Development of variable perveance neutral beams with energy range 45-80 kV</li> <li>• Fully articulated co/ctr NBI injection including steerable 30 deg beamline</li> <li>• Increased RF power for torque-free heating and current profile tailoring</li> <li>• ‘3D’ power supply and coil upgrades</li> </ul> <p><b>Diagnostic Upgrades:</b></p> <ul style="list-style-type: none"> <li>• Neutral density diagnostic for measuring poloidal distribution of neutrals causing momentum transport near the plasma boundary</li> </ul> <p><b>Code development:</b></p> <ul style="list-style-type: none"> <li>• Incorporate 3D field induced momentum sources from NTV theory and ripple losses from GPEC in transport code TRANSP</li> <li>• Improve the use of general geometry including up/down asymmetries in quasi-linear turbulent transport model TGLF</li> <li>• Develop numerical methods for robustly solving the coupled energy/particle/momentum equations in TGYRO for strongly nonlinear regime</li> <li>• Incorporate reduced models of edge rotation for integrated simulations</li> </ul>
<i>Acquire predictive understanding of the mechanisms that control the intrinsic rotation near the H-mode pedestal</i>	<ul style="list-style-type: none"> <li>• Produce detailed characterization of the main-ion and impurity rotation profiles and dependence on magnetic geometry and plasma boundary (SOL) conditions</li> <li>• Use perturbations and ultra-fast CER measurements to assess the role of neoclassical and turbulent momentum transport mechanisms in the pedestal</li> </ul>	
<i>Develop predictive capability to optimize the effect intrinsic and applied 3D fields have on the magnitude and structure of the rotation profile</i>	<ul style="list-style-type: none"> <li>• Validate multimodal NTV models combining non-resonant and resonant nonambipolar transport to optimize the torque for rotation shear control in low torque plasmas</li> <li>• Assess the role of 3D field induced torque and transport in establishing and/or expanding the operational regimes of low NBI torque scenarios</li> <li>• Determine the MHD-induced drag due to tearing instabilities, including the impact of their nonresonant components, for inclusion in momentum transport modeling</li> </ul>	

### 2.3.2.2 Research Plan

The plasma rotation research plan is organized according to the challenges and goals in Table 2-27. The timelines for each challenge, research milestone, as well as the capability improvements necessary to achieve them, are shown in Fig. 2-47.

Challenge	FY19-20	FY21	FY22	FY23	FY24
Test models of turbulence-induced momentum flux and potential for improving core plasma performance	<ul style="list-style-type: none"> <li>■ Establish an actuator for Core Velocity Shear                             <ul style="list-style-type: none"> <li>■ Demonstrate ITER baseline parameters with 5 MW EC (minimal NBI)                                     <ul style="list-style-type: none"> <li>■ Shear (CVS) control</li> </ul> </li> </ul> </li> <li>■ Validate reduced gyrokinetic models for dependence of core energy confinement on CVS</li> </ul>				
Acquire predictive understanding of the mechanisms that control the intrinsic rotation near the H-mode pedestal	<ul style="list-style-type: none"> <li>■ Establish how edge rotation affects L to H power threshold                             <ul style="list-style-type: none"> <li>■ Demonstrate ExB shear pedestal modification                                     <ul style="list-style-type: none"> <li>■ Untangle cause and effect in the L to H transition by making ultra-fast main-ion and carbon 2D velocity measurements</li> </ul> </li> </ul> </li> </ul>				
Develop predictive capability to optimize the effect intrinsic and applied 3D fields have on the magnitude and structure of the rotation profile	<ul style="list-style-type: none"> <li>■ LM limits on ITER’s 3D fields for intrinsic rotation only                             <ul style="list-style-type: none"> <li>■ Quantify NTV torque as a function of magnetic spectrum                                     <ul style="list-style-type: none"> <li>■ Mitigate LM boundaries with 3D coils   <ul style="list-style-type: none"> <li>■ Understand the effect of core NTMs on CVS, and the effect with ECCD NTM suppression</li> </ul> </li> </ul> </li> </ul> </li> </ul>				
New capabilities	<ul style="list-style-type: none"> <li>■ Fully integrated NBI dynamic voltage and perveance control</li> <li>■ Co-Counter OANB 210 beamline</li> <li>■ 5 MW EC power beamline                             <ul style="list-style-type: none"> <li>■ XICS</li> <li>■ Advanced 3D coils</li> <li>■ 2<sup>nd</sup> Super-SPA power supply</li> </ul> </li> <li>■ Co-Counter 30</li> </ul>				

Fig. 2-47. Research plan timeline for burning plasma rotation physics

#### Challenge 1: Test Models of Turbulence-Induced Momentum Flux and Potential for Improving Core Plasma Performance

**Current Progress.** Over the past five years, research emphasis on intrinsic rotation has moved from the examination of scalar quantities to investigations of profile effects. One important study in ECH-only plasmas (i.e., no external torque) found that the rotation profile can be peaked or hollow, even reversed and passing through zero with added electron heating, as shown in Fig. 2-48 [Grierson 2017]. Nonlinear gyrokinetic simulations showed that the residual stress associated with electrostatic ion temperature gradient turbulence possesses the correct radial location and stress structure to cause the observed hollow rotation profile.

Previous studies on DIII-D have also sought to understand the poloidal rotation, which is an important topic because at low toroidal rotation the poloidal rotation contribution to the radial electric field and its shear is significant. Studies found that the deuterium poloidal rotation found by invoking the radial force balance relation exceeds the neoclassical prediction, being more ion diamagnetic, in low collisionality ( $\nu_{*i} < 0.1$ ) plasmas [Grierson 2013], similar to earlier studies in carbon [Solomon PoP 2006].

Additionally, novel measurements of the poloidal rotation from high-field-side and low-field-side CER data found poloidal rotation spin up during ITB formation that made a large contribution to the ExB shearing rate [Chrystal 2014]. While the present five-year plan has established some key principles and validations of the underlying physics, development of a fully predictive physics model requires tests across a wider range of regimes.

**Goal 1: Characterize turbulent fluctuations at low and high wavenumber associated with co-Ip and ctr-Ip intrinsic torques for a range of collisionality and electron-to-ion heat flux.**

This goal emerges from the need to determine the source of intrinsic torque and test models of turbulence-induced momentum flux in the plasma core. Experiments will be designed to improve and validate reduced gyrokinetic models, e.g., TGLF, for core turbulent energy and momentum transport. Dimensionless parameter (e.g.,  $\nu^*$ ,  $T_e/T_i$ , etc.) scans will be an important part of these studies as this is the most natural way to extrapolate to future devices. Additionally, it is important to discern the toroidal rotation profile driven by intrinsic torque alone in an IBS discharge, free from any significant external torque. Such work needs, in particular, to make the connection between empirical trends and underlying turbulent transport mechanisms. This will serve as the baseline for transport model validation and for the 3D field studies in challenge 3 below. This work will be carried out in close collaboration with ITER scenario development discussed in Sec. 2.1.1.

These low-torque experiments will require auxiliary heating upgrades as planned, namely, additional ECH power, an additional reversible off axis NBI source and full implementation of dynamic control of NBI source voltage and perveance. This latter capability will potentially allow detailed nulling of the injected net torque density profile for toroidally opposing NBI sources. Further capability enhancements of note include an option for a form of x-ray spectroscopy, such

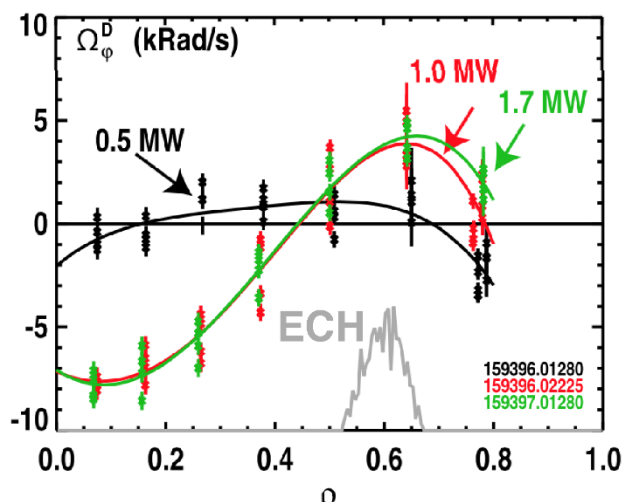


Fig. 2-48. Measured toroidal rotation profile on DIII-D for an ECH power scan at fixed deposition location [Grierson 2017].

as XICS, to measure the rotation rate of impurity ions, and an expansion of the suite of fluctuation diagnostics to allow greater spatial coverage at both high and low wavenumbers.

**Goal 2: Excite particular turbulent modes that achieve maximum ExB shear by using core ECH/ECCD that produce direct ( $T_e$ ,  $T_i$ ) and indirect (q-shear) effects.** A key issue is whether non-NBI heating can create an intrinsic rotation profile that provides enough ExB shear to improve energy confinement. Theoretically, several turbulence-driven mechanisms have been identified as possible causes of intrinsic rotation [Dominguez 1993, Waltz 2007, Peeters 2007, Camenen 2009, Waltz 2011]. The details of tokamak turbulence (i.e., dominant modes, mode intensity, mode spectrum, etc.) depend upon the density, temperature, and equilibrium profiles, as well as the magnetic shear and rotation profile. Experiments using directed heating and current drive will be used to investigate ways to modify the nature of the turbulence advantageously for rotation and, hence, plasma performance. This can be viewed as developing an actuator to affect the core intrinsic rotation profile to give maximum core velocity shear (CVS).

The judicious application of ECH and/or ECCD, possibly with shaping as another knob, is anticipated to provide some control over CVS. Other RF waves, such as lower hybrid or helicon, might be needed to gain maximum CVS, but the goal is to understand what is needed. This goal will also verify the predicted effect of enhanced CVS increasing the core plasma pressure.

### Challenge 2: Acquire Predictive Understanding of the Mechanisms That Control the Intrinsic Rotation Near the H-mode pedestal

**Current Progress.** The pedestal region affects the entire rotation profile as the momentum “source” must pass through the edge. Recent experiments have measured the  $\rho^*$  scaling of the edge intrinsic torque, resulting in a predicted rotation profile for ITER with a strong experimental basis, as seen in Fig. 2-49 [Chrystal 2017]. While there is a small level of NBI torque in ITER that needs to be taken into account [Chrystal 2017], this figure shows that the intrinsic rotation near the H-mode pedestal is the dominant factor in determining ITER’s rotation rate.

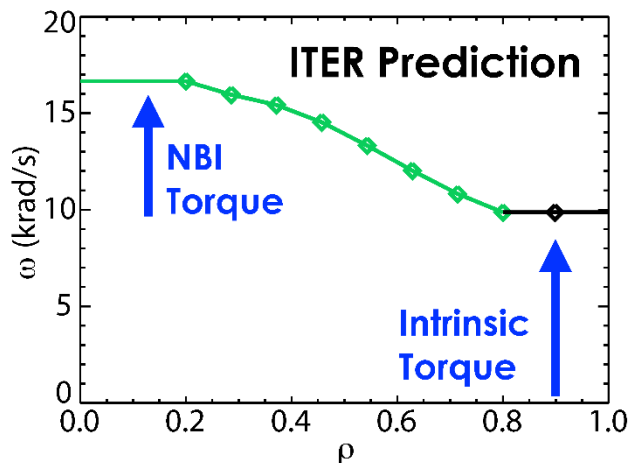


Fig. 2-49. Prediction of the toroidal rotation profile in ITER, where the boundary condition is determined from  $\rho^*$  scaling of DIII-D values, and the core profile is determined from TGLF/TGYRO modeling of momentum transport from the NBI torque [Chrystal 2017].

Another recent advance in momentum transport studies has been the separate measurement of the main-ion and impurity-ion rotation profiles. DIII-D has recently made significant

enhancements to the Charge Exchange Spectroscopy (CER) measurement and analysis systems that allows the measurement of the main-ion ( $D^+$ ) temperature and velocity [Grierson 2012], no longer limited to the trace impurity measurements of fully ionized carbon. Notably, it has been found that the velocity of  $D^+$  and  $C^{6+}$  differ greatly in the important pedestal region, whereas in the interior (the inside 80% in minor radius), they are very similar. Present indications are that the edge difference can be understood by neoclassical theory. It is crucial to make measurements of the main ion in order to be able to untangle the physics of the pedestal.

**Goal 1: Produce detailed characterization of the main-ion and impurity rotation profiles and dependence on magnetic geometry and plasma boundary (SOL) conditions.**

Measurements of main-ion rotation through the pedestal region and up to the last closed flux surface have recently been made available with main-ion CER. These measurements will become increasingly routine throughout the 2019-2024 five-year period. This capability allows important questions about the intrinsic momentum and intrinsic momentum transport to be assessed. As with the particle and energy channels, there are many factors that affect the momentum channel near the edge of the plasma, but of particular concern are the magnetic geometry and SOL conditions, which can affect preferential loss of momentum. This is the typical explanation for the near-SOL intrinsic rotation being in the same direction as the plasma current, but precise model validation is not complete. This is a key issue because this rotation serves as a boundary condition for the rest of the intrinsic rotation profile. In addition, past experiments in DIII-D have established that NBI torque affects the L-H confinement transition threshold,  $P_{TH}$ , as shown in Fig. 2-50, but the physics parameter that matters is likely related to toroidal rotation near the SOL. In this way, the efforts in this goal couple to L-H transition physics (Section 4.1.3).

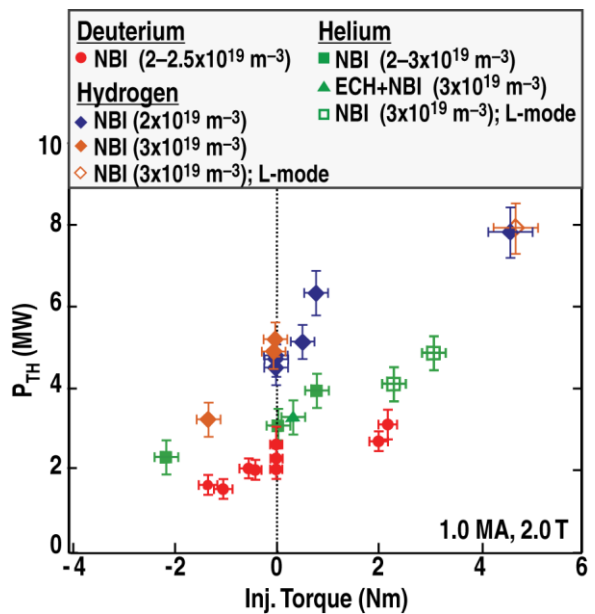


Fig. 2-50. The net power required to access the H-mode as a function of the injected torque for various target densities and heating methods for hydrogen, deuterium and helium. The open symbols denote discharges that failed to transition to H-mode at the applied power.

Experiments will measure the intrinsic rotation profiles for both the main-ion and impurity species as the plasma shape, SOL temperatures, and densities are varied. A key diagnostic improvement that will aid these investigations is a neutral density measurement, which is necessary for characterizing particle transport (which affects momentum transport through

convection) as well as potential direct effects of the neutrals on the intrinsic momentum generation mechanism. Multiple models that attempt to predict the main-ion intrinsic flow near the last closed flux surface (using calculations of asymmetries in orbit loss, turbulent transport, etc.) will be tested against this data to determine which underlying mechanisms are most important. These results will be used to create a composite model that can capture the dynamics of the intrinsic rotation in this region as accurately as possible. This model will be used to predict effects on the L-H power threshold in ITER as well as the potential for access to regimes that depend on particular profiles of  $E_r$  in the pedestal, e.g., RMP ELM suppression and QH-mode.

**Goal 2: Use perturbations and ultra-fast CER measurements to assess the role of neoclassical and turbulent momentum transport mechanisms in the pedestal.** The toroidal and poloidal plasma flow velocities in the pedestal region are self-consistently related to the electric field. Predicting the electric field requires accurate modeling of momentum transport in the pedestal with both the toroidal momentum transport and poloidal momentum damping and drive being key results of the underlying turbulence and neoclassical effects. Both impurity and main-ion CER measurements are important for this work as the impurity measurements are needed to determine  $E_r$  and are also used to infer the main-ion poloidal rotation. Neoclassical theory is typically used to determine poloidal rotation despite known discrepancies with measurements. While neoclassical theory of poloidal rotation itself may be incomplete, a more likely issue is a breaking down of the low inverse gradient scale length ordering in the theory and the absence of residual stress and orbit loss effects. Main-ion toroidal rotation is most important for total momentum accounting, and key for determining the radial flux of toroidal momentum that, in contrast to poloidal momentum, is not strongly damped.

To increase our understanding and ability to model momentum transport in the pedestal, experiments will focus on measuring  $E_r$  and inferring main-ion poloidal rotation so that comparisons can be made to neoclassical theory. Changes in the gradient scale length will be used to determine if this is a key factor in the accuracy of neoclassical models. These results could lead to focused efforts on improving neoclassical calculations for the difficult to model pedestal region. In addition, turbulence measurements will allow relative changes in residual stress drive to be estimated to determine if this is a possible cause of measured discrepancies, and fast measurements of the poloidal rotation will be used in an effort to measure poloidal rotation damping due to brief application of a 3D field or the prompt torque from NBI. Similar perturbations to the toroidal rotation will also be measured with high time resolution in order to determine how this momentum propagates in the pedestal. This investigation is key to verifying how the momentum generated near the boundary with the SOL is transported into the core of the plasma. These results will be

combined with models for stationary intrinsic toroidal rotation (Goal 1) to determine how changes to the pedestal structure will affect momentum transport and the intrinsic rotation pedestal.

Crucial to these experiments is the high time resolution of the CER system ( $< 0.5$  ms integration time) and the turbulence diagnostic suite on DIII-D. Several planned upgrades to the DIII-D fluctuation diagnostics will enhance the investigation of the rapid connections between turbulence, profiles, and the radial electron field in the pedestal region. The “high definition” BES and expansions of DBS and MIR will allow wide-field, high-frequency measurements of density fluctuations. Fluctuations and perturbations in the carbon rotation profile will be measured by UF-CHERS.

### **Challenge 3: Assess the role of intrinsic and applied 3D fields in determining the rotation profile**

**Current Progress.** Investigations over the past five years have improved understanding of the torques generated by resonant and nonresonant 3D perturbations in the magnetic fields through the mechanism of neoclassical toroidal viscosity (NTV). DIII-D has led the validation of many key NTV theory components such as the offset rotation and collisionality regimes. However, work has hitherto concentrated on comparisons of the scalar, integral torque. The 2019-2024 five-year plan expands the measurement, model validation, and utilization of NTV across the full profile. This necessarily encompasses multiple regimes, resonant as well as nonresonant fields, and a more detailed integration of the 3D effects in the equilibrium force balance as well as the momentum evolution equations. Motivation for this work is shown in Fig. 2-51, which presents an initial comparison between predicted and measured NTV torque profiles for resonant and nonresonant fields. The nonresonant prediction shows quantitative agreement between the prediction and experiment, but the resonant fields that lead to density pump out have a much broader effective impact on the rotation profile than predicted by the GPEC model without any ambipolar transport [Park 2017]. This motivates the integration of NTV nonambipolar transport models, such as GPEC with standard particle and momentum transport models, such as TRANSP.

**Goal 1: Validate multimodal NTV models, combining non-resonant and resonant nonambipolar transport to optimize the torque for rotation shear control for low torque plasmas.** The physics of 3D field rotation generation and drag resulting from NTV will be investigated to understand and optimize its uses in ITER. As mentioned above, DIII-D has begun pushing NTV models towards validated torque profiles. This necessarily involves fast, detailed CER measurements of the rotation evolution across the profile, and especially in the edge where kinetic resonances are expected to concentrate much of the NTV torque (in synergy with Challenge 2). This is a much more difficult challenge to the NTV theory community, and careful validation

is required. The models must accurately include both resonant and nonresonant applied fields, as well as the multi-modal plasma response to these spectra. New capabilities of the advanced 3D coils and power supplies to access a wider variety of, and more finely tuned, poloidal spectra will enable tests for these components of the NTV and their nonlinear combinations. The additional extension to toroidal modes  $n=3$  and  $n=4$  will further test the critical  $n$  dependencies that are used to link the more easily measured RMP physics to toroidal field ripple effects (and tolerances for future devices).

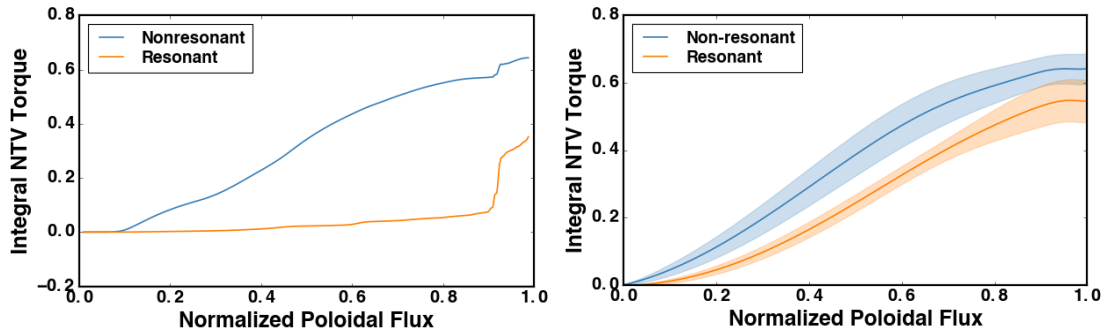


*Fig. 2-51. The integral NTV torque predicted by GPEC prior to experiment (left) for nonresonant fields for broad braking and edge resonant fields for localized braking contrasted with the experimental torque profiles (right) calculated using the initial time rate of change of the momentum.*

As the currently validated NTV theory is being more rigorously applied to detailed profiles, the theory itself will continue to be improved to extend its validity to new important regimes. The role of finite orbit width effects as well as the possibility of NTV torque due to interaction of the applied field and energetic particles will be investigated for model validation in new regimes that have larger variation in orbit width and energetic particle distribution functions. The resulting model insight and/or improvements may be critical in explaining the sharp kinetic resonances seen in NTV modeling (see the orange profile in Fig 2-51) but yet to be shown in experiment near the edge of DIII-D.

In addition, a key open question in this area is how the NTV and resonant particle transport interact nonlinearly with the changes they create in the kinetic profiles in order to determine the final stationary state. Momentum sources and transport will be measured during repeated 3D field perturbations as well as during long duration pulses to determine the net effect on absolute rotation levels and rotation shear. This is critical for assessing the capabilities of NTV torque as a rotation profile control actuator. Modeling efforts here will concentrate on integrating the nonambipolar transport NTV models such as GPEC with particle and momentum transport models included, for example, in TRANSP. The goal will be to develop a predictive model of the rotation profile resulting from a change in the applied 3D field spectrum (for RMP ELM suppression, for example).

Finally, these techniques will be applied to key regimes that can benefit from improved performance arising from NTV induced rotation shear, such as QH-mode. Discovered abilities to change rotation and rotation shear in the core and edge will also be explored as possible candidates for reducing the L-H power threshold and increasing performance in other scenarios.

**Goal 2: Assess the role of 3D field induced torque and transport in establishing and/or expanding the operational regimes of low NBI torque scenarios.** While intrinsic rotation arises in axisymmetric conditions, the ultimate rotation profile will also be affected by the toroidal asymmetries of the magnetic field. The known 3D fields in ITER will come from the ripple generated by the toroidal field coils, the ferritic blanket modules, and the resonant magnetic perturbation (RMP) coils added for ELM suppression [see Section 4.1.1]. A broad investigation in this area is possible through the 3D coil upgrades and new coil power supplies. These tools will provide a basis to develop reactor relevant demonstration scenarios incorporating 3D fields, as well as extensive perturbative capabilities to explore the underlying interaction between scenario specific intrinsic rotation and the 3D fields. For a given 3D field and scenario, the absolute rotation level as well as the rotation shear that is needed to avoid the onset of a locked mode (LM) is an open question. Important aspects of this question are the torque from seed islands as well as the effect of islands on momentum, particle, and energetic particle transport.

After finding a reliable ITER target scenario with low torque injection using ECH that establishes a baseline condition, the next step will be to experimentally determine the minimum rotation/torque needed in ITER to avoid locked modes given the expected ITER 3D fields. These fields will be duplicated in DIII-D using a similar spectrum from our advanced 3D coil set. Measurements of torque and momentum transport due to 3D fields and any stable islands will be used to create a scaled scenario of ITER operation that determines the available operating space that is expected to be free of LMs. The important dependences of this LM-free space, e.g., collisionality and ion temperature (which affects non-ambipolar transport), will be determined. This work will be conducted in close collaboration with the stability program discussed in 2.2.2.

If the ITER operating window is determined to be too narrow, then it is a necessity to learn how to mitigate the undesirable 3D field effect, using other applied 3D fields, in order to expand the operating window. A goal is to develop a complete model that will compute the 3D torque drag given a particular 3D field spectrum and the specific plasma equilibrium, including nonlinear interactions between the rotation and the 3D field effect. This will provide a general understanding of how to make 3D field “corrections” so that unforeseen 3D effects in ITER can be operationally addressed when necessary.

**Goal 3: Determine the MHD-induced drag due to tearing instabilities, including the impact of their nonresonant components, for inclusion in momentum transport modeling.**

With the validated ITER target scenario, DIII-D has the capabilities experimentally to look at the effect of NTMs on the core velocity shear, especially for cases where the rotation profile is primarily generated by intrinsic torque. This also encompasses the benefits to plasma rotation that comes from ECCD suppression of NTMs, as planned for ITER. With an understanding of core CVS control (challenge 1), an optimum scenario will be sought that quenches NTMs, while maintaining a confinement-enhancing CVS.

In addition to investigating the quenching of NTMs as part of rotation limited scenarios, the drag of islands will be found by varying the amount of suppression supplied (and hence the size of the NTM) and measuring the rotation response. This will be most clearly shown with control of suppression that varies between primarily heating to primarily current drive at a similar location in the plasma. The observed changes in the rotation profile will inform models of momentum transport due to NTMs, while observed changes in contained angular momentum will inform models of the NTM drag. Although reduced models exist for the torque between the resonant NTM and 3D field sources external to the plasma (eddy currents, error fields, etc.), the full drag profile is of interest in the low torque DIII-D scenarios. New measurements of this torque will again benefit from improved CER. Additional physics, including more realistic geometries, will be added to existing models and those will be integrated with momentum transport equations. The NTM itself is also more than just a single resonant harmonic perturbation. It induces nonresonant perturbations throughout the plasma profile and, thus, is theorized to affect the rotation profile through NTV torque. Investigation of the NTV in and around islands will be initiated to more accurately predict the rotation evolution and final rotation profile in the presence of NTMs. Improved understanding of these drags and their impacts on the total profile will provide insight into how best to mitigate their deleterious effects when they arise in low torque scenarios.

### **2.3.2.3 Capability Enhancements**

Advances in understanding of plasma rotation, especially under low torque conditions, will require several new technologies, actuators, and diagnostics. The motivation, rationale, and importance of these systems are briefly outlined. Planned new hardware capabilities are summarized in Table 2-28, new diagnostics in Table 2-29 and new or updated modeling and simulation capabilities in Table 2-30. The plasma rotation program that results from these enhancements will be physics rich, utilizing perturbative tools and DIII-D's leading diagnostic set to resolve physics models of underlying behavior, as well as a practical understanding of how to project and optimize performance. This will provide a definitive basis to project rotation and its control in ITER and future fusion reactors.

**Table 2-28.  
Hardware Improvements for Rotation Studies**

<b>Hardware Capability</b>	<b>New Physics</b>
Complete development of Variable Perveance NBI at 45-80 kV	Modify torque-to-power ratio continuously without the need for pulsing beams.
Fully articulated beamline, starting with 30 degree line	Flexible balanced or unbalanced torque in both directions.
Increased RF power for torque-free heating.	Critical need to project to ITER scenarios with same heating, low torque, mix.
New M coils and 3D power supplies	Understand generation and optimization of NTV effects

**Table 2-29.  
Diagnostic Improvements for Rotation Studies**

<b>Scientific Objective</b>	<b>Physics Measurement</b>	<b>Diagnostic Technique</b>
Measure ion poloidal/toroidal rotation and radial electric field for high-power/low-torque conditions	Ion velocity, density and $T_i$	Rearrange CER channels among 30 and 330 beamlines to accommodate co/counter switchable 30 beamline
Measure intrinsic rotation profile in RF-heated discharges (no beams)	Impurity ion velocity	XICS/X-ray spectroscopy
Multi-field turbulence interactions	Ion temperature, toroidal rotation	UF-CHERS
Role of intermediate wavenumber instabilities	2D high-resolution pedestal and core density fluctuations	BES-HD, MIR upgrades
Multi-scale interactions of turbulence with MHD, 3D fields	Wide-field high-frequency density fluctuation measurements	Full-radius BES, expanded DBS

**Table 2-30.  
Simulation Codes Used**

<b>Code</b>	<b>Purpose</b>
OMFIT, TRANSP	Integrated modeling
TGLF, GYRO, NEO	Neoclassical and gyrokinetic modeling of turbulence-driven momentum transport, intrinsic rotation profile
EPED, ELITE, M3D-C1	Pedestal modeling
GPEC, MARS	Modeling of non-axisymmetric fields and NTV torque

### 2.3.3 Energetic Particles

*Physics Leads: W. Heidbrink (UCI), M. Van Zeeland (GA), C. Collins (GA), G. Kramer (PPPL), D. Pace (GA), M. Podesta (PPPL), D. Spong (ORNL).*

Future burning plasma experiments like ITER will have a variety of fast-ion populations, including 3.5 MeV alphas, 1 MeV beam ions, and tail ions generated by ion cyclotron heating. These energetic particles (EPs) play critical roles in heating, current drive, momentum input, and sometimes plasma stability, making their successful confinement essential in a fusion reactor. Achieving adequate confinement, however, requires facing several issues. These particles can excite a variety of Alfvén eigenmodes (AE) and other instabilities, which in turn can lead to a range of transport mechanisms and other effects. The resultant fast-ion transport and loss can reduce fusion performance, redistribute currents or cause localized heating, and damage of first-wall components. Consequently, developing validated models that describe these interactions, along with control techniques to suppress or exploit these effects, is critical for extrapolating to ITER and beyond.

The DIII-D team has made strong progress in addressing these issues in recent years, in collaboration with the international community. Key instabilities have been identified and their linear thresholds assessed. EP transport mechanisms and thresholds have been identified. The effect of externally applied 3D fields on EP confinement is consistent with measurements. The key element in moving to a predictive and useful capability for future reactor optimization is to develop a non-linear understanding of EP behavior, its coupling to AEs and other modes, and how this leads to fast-ion transport. This is the central thrust of this proposal.

#### 2.3.3.1 Challenges and Impact

The goal of the DIII-D EP research program is to provide the scientific basis for projecting configurations and techniques that avoid adverse effects of EP losses or other deleterious impacts on plasma behavior in future burning plasma devices. To accomplish this, the EP program is focused on three key challenges (Table 2-31). First, it must gain the capability to reliably predict fast-ion transport by instabilities. To this end, the team is using DIII-D’s ability to inject and control various sources of fast ions in reactor-relevant plasma operating regimes, and is employing its extensive diagnostics to observe modes and fast-ion populations, transport, and losses. These observations will be used to test and refine a range of models for EP transport. Second, the program needs to mitigate and control EP-driven instabilities through the use of actuators which manipulate properties such as electron heating, EP energy distribution, and 3-D fields. Third, the program needs to achieve good fast-ion confinement in DIII-D AT demonstration discharges by using its flexible heating and current-drive systems, combined with mitigation methods, to find plasma

configurations that adequately confine EPs and help chart the path to high performance in future reactors.

The tools developed through these experiments and validation efforts will thus help develop scenarios for DIII-D, ITER, and future burning plasma experiments that minimize the negative consequences of EP transport, maximize performance, and avoid potential scenarios that can damage device integrity through mechanisms triggered by excessive loss of fast particles.

### 2.3.3.2 Research Plan

The EP program research plan is organized according to the challenges and goals in Table 2-31. Fig. 2-52 gives the timeline for each challenge, research milestones, and the capability improvements necessary to achieve them.

**Table 2-31.  
EP Challenges, Goals, and Upgrades**

<b>Challenge</b>	<b>Goals/Deliverables</b>	<b>Upgrades</b>
Predict fast-ion transport by instabilities	<ul style="list-style-type: none"> <li>• Use phase-space-resolved measurements of fast-ion transport to test details of wave-particle interaction</li> <li>• Compare first-principles EP models to data over the entire primacy hierarchy: Mode properties, linear stability, nonlinear dynamics, and transport</li> <li>• Test and refine critical gradient and kick models that allow rapid prediction of EP transport</li> </ul>	<p><b>Hardware</b></p> <ul style="list-style-type: none"> <li>• Variable beam perveance</li> <li>• More off-axis NBI (210 beam modification)</li> </ul> <p><b>Diagnostic</b></p> <ul style="list-style-type: none"> <li>• Fast-ion phase space diagnostics: Imaging NPA, FIDA imaging, reversed <math>B_T</math> fast-ion loss detector</li> <li>• High-n AE mode numbers</li> </ul>
Mitigate and control EP-driven instabilities	<ul style="list-style-type: none"> <li>• Develop real-time sensors that detect mode activity as well as regimes with unfavorable fast-ion transport</li> <li>• Control AEs by feedback on actuators (beam voltage, ECH, 3D fields)</li> </ul>	<p><b>Analysis Capabilities</b></p> <ul style="list-style-type: none"> <li>• Orbit-based inference of the distribution function</li> <li>• TRANSP “kick” model</li> <li>• Reduced and first-principles models developed by EP SciDAC</li> </ul>
Achieve good fast-ion confinement in DIII-D AT demonstration discharges	<ul style="list-style-type: none"> <li>• Use validated fast-ion transport models to predict AT regimes with improved EP confinement</li> <li>• Demonstrate acceptable EP confinement, using control tools as necessary</li> </ul>	

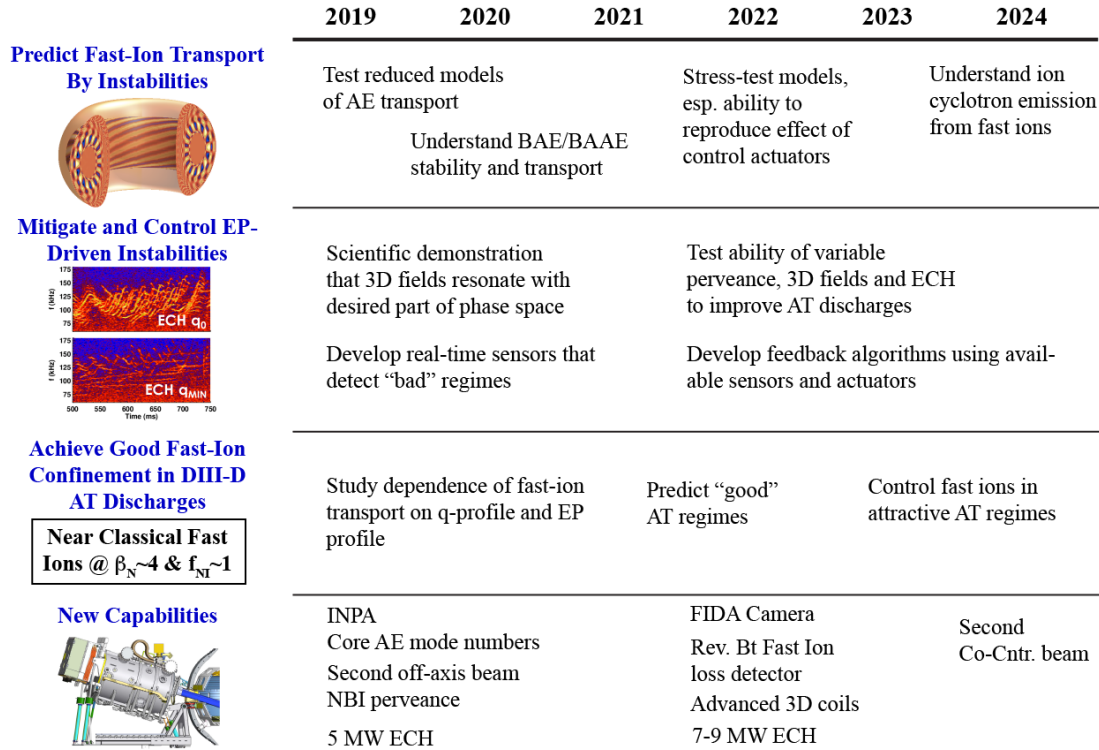


Fig. 2-52. EP Plan Timeline

### Challenge 1: Predict Fast-Ion Transport by Instabilities

**Current Progress.** The 2014-2018 five-year period saw rapid progress in understanding of AEs and their consequences as well as the ability of simulations to accurately resolve many key features of fast-ion transport phenomena. Experimentally, new techniques to probe transport in selected regions of phase space were developed. One technique, dubbed the “light-ion beam probe” [Chen 2014], measures the displacement caused by AEs, 3D fields, or other modes in a single transit through the wave fields. Another technique uses the combination of beam modulation of a selected source and diagnostics with different phase-space sensitivities to probe fast-ion transport in different parts of phase space [Heidbrink 2016]. These phase-space sensitivities are known as the “weight function.” DIII-D has six different angles of beam injection available, each of which populates different portions of phase space. When the weight function, modulated source, and wave-particle resonances all overlap in the same part of phase space, the measured signals deviate from classical predictions. Fig. 2-53 shows an example of deviations in an NPA signal produced by toroidal and reversed-shear AEs (TAEs and RSAEs). Theoretical modeling has also progressed rapidly. As shown in Fig. 2-53, with the mode amplitudes provided by experiment, the phase-space “kick” model implemented in TRANSP successfully reproduces features of the experimental signals [Podesta 2013, Heidbrink 2017].

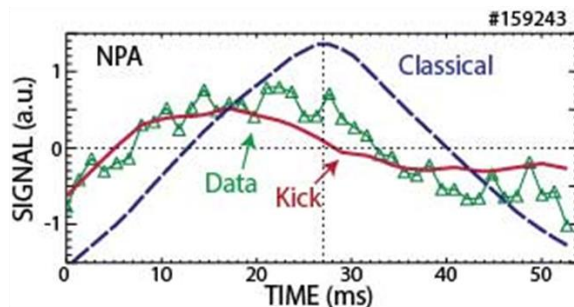


Fig. 2-53. Conditionally-averaged NPA signal (green) during beam showing distortion from classical predictions (blue) due to AE induced fast-ion transport / flows. TRANSP Kick model prediction which includes AEs (red). From [Heidbrink 2017].

Progress has also been made toward self-consistent predictions of the modes and the consequent transport. The most impressive results to date are from the MEGA code [Todo 2016], which treats the fast ions kinetically and models the background plasma with resistive MHD. As Fig. 2-54 shows, this code successfully reproduces the DIII-D experimentally observed trend that at low levels of AE activity the fast-ion orbits remain regular in phase space, but at high levels of AE activity the orbits become chaotic and the transport becomes large. Observed mode structures at experimental amplitudes are also predicted [Todo 2014].

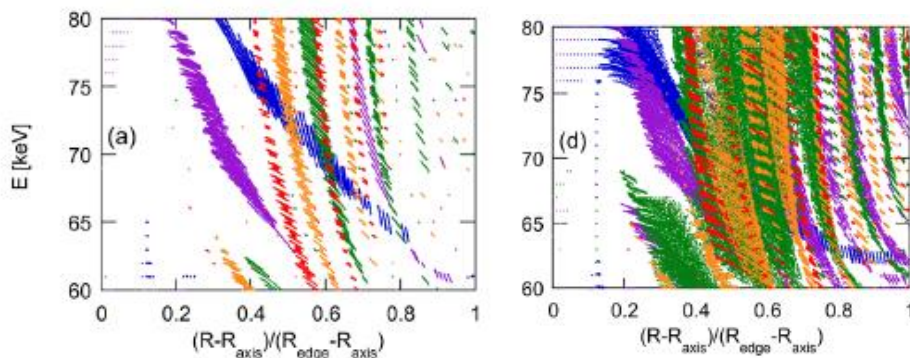


Fig. 2-54. EP phase space trajectories phase space with (left) few unstable AEs and (right) many unstable AEs. MEGA modeling for a DIII-D plasma with multiple AEs [Todo 2016].

**Goal 1: Use Phase-Space Resolved Measurements of Fast-Ion Transport to Test Details of Wave Particle Interaction.** Work in the next five years will emphasize detailed measurements of phase-space flows, which will yield direct evidence as to whether the picture of fast-ion transport from interactions with single and/or multiple instabilities is correct or not.

The new imaging NPA diagnostic will vastly improve the spatial and energy resolution of DIII-D NPA measurements from essentially three single points in fast-ion phase space to  $10^4$  points, giving energy-resolved radial profiles of the confined fast-ion distribution function across

the entire midplane. This, combined with the addition of a FIDA imaging camera for a similar increase in FIDA spatial resolution (from individual channels to imaging), will allow unprecedented resolution of the fast-ion distribution function and its evolution in the presence of instabilities. Local phase space flows of confined fast ions in the presence of AEs, fishbones, and other instabilities will be directly measured for the first time and compared to first principles simulations like the MEGA code. By measuring EP flows for a range of injected beam geometry and powers the phase space dependent point at which EP transport due to AEs becomes stochastic, as opposed to relatively benign, will be directly measured and compared to modeling. Exactly what modes cause EP transport in high- $q_{\min}$  steady-state plasmas and what part of phase space interacts most intensely will be measured and used to predict a path to “Challenge 3: Achieve good fast-ion confinement in DIII-D AT discharges.”

While much of 4D fast-ion phase space ( $R$ ,  $z$ ,  $E$ , pitch) will now be covered by new diagnostics, the practical impact on beam torque or NBCD by instability induced fast-ion transport can depend on unmeasured portions of the distribution function and/or portions which are sampled with a complicated diagnostic weight function. Inversion techniques to infer the velocity-space distribution function from a set of EP measurements [Salewski 2012, Stagner 2017], will be extended from 2D to allow reconstructions of the full fast-ion phase space. Powerful orbit-based tomographic approaches, like those which will be implemented, leverage measurements in one location to actually probe the details of transport in a separate location.

**Goal 2: Compare First-Principles Models to Data over the Entire Primacy Hierarchy.** Research in the next five years will feature a concentrated effort to validate first principles predictions across the “primacy hierarchy,” beginning with basic mode properties (polarization and frequency), linear stability, nonlinear dynamics, and finally the actual fast-ion transport. Work will continue on RSAE and TAEs, however, focus will shift to lower frequency modes such as the beta-induced AE (BAE) [Heidbrink 1995] and beta-induced Alfvén-acoustic eigenmode (BAAE) [Gorelenkov 2009], which often cause substantial fast-ion transport, yet are not well understood, even to the basic level of mode frequency. This validation effort will enable accurate predictions of fast-ion transport from multiple RSAEs, TAEs, BAEs, and BAAEs to be routinely performed without first needing information about the modes from experiment.

**Goal 3: Test and Refine Critical Gradient (CG) and Kick Models That Allow Rapid Prediction of EP Transport.**

Work in this area will take both “critical gradient” and “kick” models for EP transport from one-off type analysis to streamlined and validated for the prediction and interpretation of EP transport in DIII-D and other devices. Initial work will focus on improving the process by which these models are run through either the OMFIT workflow and/or TRANSP, then validating key

assumptions of each model. Experimentally, it has been found that the self-organized criticality paradigm and CG models can describe the measured interaction of fast ions with many small-amplitude AEs [Collins 2016, Heidbrink 2017, Collins 2017, Waltz 2014, Ghantous 2012]. Through phase space resolved measurements of EP transport and careful documentation of phase space gradients as well as fluctuations (both coherent and incoherent) in a range of conditions, this work will determine what sets the most important parameter for CG models – the threshold for rapid transport. Assumptions from various CG models will be compared to measurement, including: when AEs are linearly unstable, when AE growth rates are above turbulent growth rates, and when resonance overlap occurs. The same datasets will be used to validate TRANSP kick modeling of AE transport through comparison of phase space dependent quantities (that will not likely be captured by CG models) such as NBCD and NBI torque in the presence of AEs. As the TRANSP kick model is improved from interpretative (requiring experimentally measured modes) to predictive, with some estimate for the unstable mode spectrum, details of the unstable modes such as frequency, toroidal mode number, and structure will be compared directly to measurements.

Progress on this goal will enable rapid, inexpensive analysis of fast-ion transport in existing discharges as well as believable, predictive parameter scans for the development of scenarios with improved EP confinement.

## **Challenge 2: Mitigate and Control EP-Driven Instabilities**

**Current Progress.** The purpose of this research is to gain the capability to control and potentially exploit fast-ion instabilities and EP transport on DIII-D. EP control research will use the physics understanding gained in the instability validation studies to form the basis for EP control tools.

DIII-D has made significant progress in developing EP actuators and techniques. One of the most significant is the ability to control the NBI voltage, power, and current during the discharge through variation in the neutral-beam perveance. Fig. 2-55 shows how this new capability can alter the virulence of AE activity and the consequent degradation in fast-ion confinement in L-mode discharges. Subsequent experiments during the 2017 campaign have begun to extend these studies to high-performance plasmas. Another related area of progress has been the understanding of ECH as an actuator to control AEs. DIII-D was the first device to show that ECH can alter RSAE stability [Van Zeeland, 2008], spurring a strong international effort to understand the phenomenon. Additional experiments and analysis have shown that the RSAE suppression is associated with the pressure and pressure gradient produced by the ECH [Van Zeeland 2016]. In addition to ECH, progress has also been made in exploring the effect of applied 3D fields on fast-ion confinement.

The modeled fast-ion losses and density of confined fast ions during application of I-coil fields are consistent with experimental data [Van Zeeland 2014, Van Zeeland 2015] when plasma response is included.

Going beyond physics tests of various actuators, actual EP instability control will require the development and integration of real-time sensors, actuators, and a control algorithm in the DIII-D plasma control system (PCS). Recently, the PCS algorithm that uses ECE data to monitor NTMs was successfully modified to provide a real-time sensor of AE amplitude, and this signal enabled the first attempt to actively control AE levels in a DIII-D discharge. The goals below describe the basic elements planned to expand on this work.

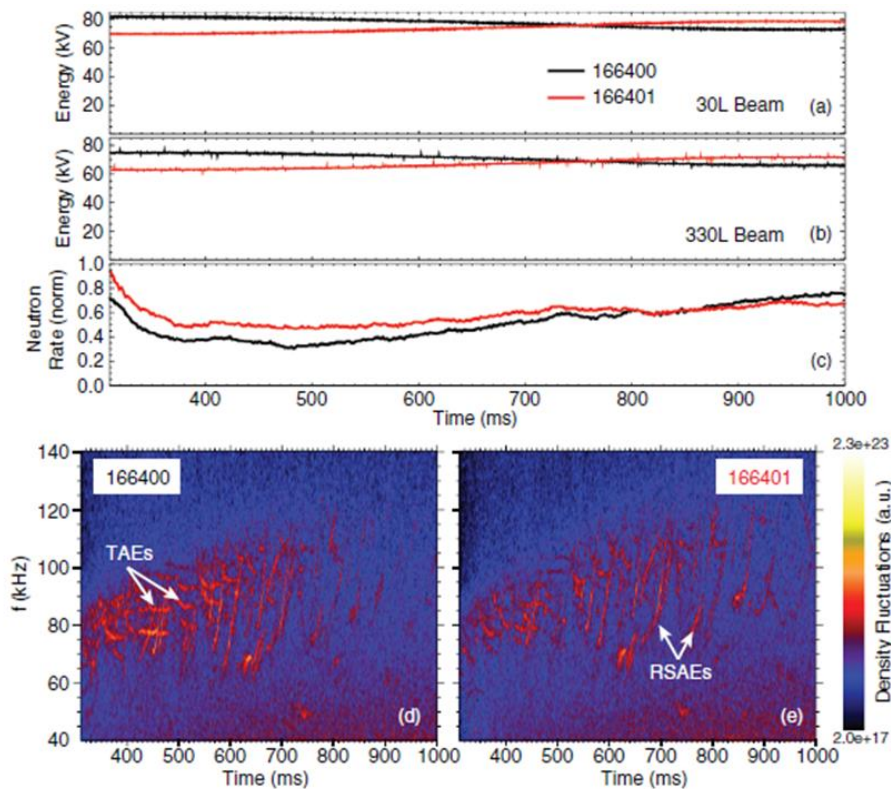


Fig. 2-55. Comparison of shots using time-variable beam energy to AEs. Early, higher injection energy drives stronger TAEs resulting in enhanced fast-ion transport and lower neutron rates (c). From [Pace 2016]

**Goal 1: Develop Real-Time Sensors That Detect Mode Activity as Well as Regimes with Unfavorable Fast-Ion Transport.** Moving forward, the EP program will develop the ratio of the measured neutron rate to the classically-predicted rate as a real-time sensor. This ratio is an excellent measure of instability induced fast-ion transport. An important aspect of this work will be the development of tools for the real-time predictions of classical EP confinement. For

additional instability information, the ECE mode monitor will be upgraded to provide mode localization and the CO<sub>2</sub> interferometer system will provide additional real-time AE amplitude information. Ultimately, this work will enable control algorithms that combine measurements of the AE amplitude with measurements of fast-ion degradation which is expected to be the most effective approach for real-time AE control with the goal of improved performance.

**Goal 2: Control AEs by Feedback on Actuators.** Research in this area will include two aspects, the development and testing of actuators to control AEs and the testing of algorithms which translate real-time sensors of the mode activity or impact (discussed above) into a response. Previously mentioned ECH results, as well as the variable beam perveance results shown in Fig. 2-55, will be extended to high-performance AT regimes and ECCD will be tested as an AE actuator. So far, little work has focused on the impact of ECCD on AEs and other EP driven instabilities. Theoretically, however, ECCD can cause local changes to the magnetic shear which could actually have a dramatic impact on mode stability by changing the continuum interaction or by moving the mode location to a region with reduced EP gradient drive. Additionally, the modeling that successfully reproduced measurements during previous 3D field experiments indicates that it is possible to use 3D fields to selectively alter the fast-ion transport in localized regions of phase space. After a scientific demonstration of this capability, its effect on mode stability under a variety of conditions will be investigated. Working with the control group, measurements of the impact of these actuators will be used to develop and tune algorithms to respond to AEs in the target high  $q_{\min}$  AT conditions with the goal of improved EP confinement and, consequently, performance.

### **Challenge 3: Achieve Good Fast-Ion Confinement in DIII-D AT Demonstration Discharges**

**Current Progress.** Due to AE activity, many DIII-D AT discharges with  $q_{\min} \sim 2$  suffer unacceptably large fast-ion transport [Heidbrink 2014, Holcomb 2015]. In contrast, some high  $\beta_p$  discharges have fast-ion profiles that are close to classical predictions [Heidbrink 2014, Holcomb 2015]. Analysis of these cases suggests ways to improve the  $q_{\min} \sim 2$  scenario [Kramer 2017] that the EP program has begun to explore experimentally. For example, if the negative magnetic shear region can be expanded so that the  $q_{\min}$  radius is moved outwards where there are fewer fast ions, then the drive of RSAEs (and perhaps other EP modes) should be greatly reduced. A proof-of-principle demonstration of this behavior is shown in Fig. 2-56, which compares spectrograms of density fluctuations for two L-mode discharges with varying current ramp rates and  $q_{\min}$  radii. AEs were successfully suppressed in the fast  $I_p$  ramp discharge with the larger value of  $\rho_{q_{\min}}$ . The increase in off-axis NBCD and ECCD power displayed in **Goal 2: Demonstrate Acceptable EP Confinement, Using Control Tools as Necessary**. This goal represents the culmination of work

performed in all other sections. Wherever possible, modeling will guide scenario development leading to the experimental demonstration of AT scenarios with improved EP confinement. Experimentally, increased ECH and off-axis NBI will be leveraged to create discharges with reduced drive for AEs through overall reduced EP gradients and larger  $\rho_{qmin}$ . Capabilities will progressively increase as more ECH power becomes available, and with the possible use of helicon and high-field-side launch lower hybrid current drive, which offer the prospect of even broader current profiles. The addition of a new fast-ion loss detector for reversed  $B_t$  discharges, typical of AT scenarios, will allow direct measurement of fast-ion losses and scenario optimization to reduce those losses.

The program will also utilize active control of AEs and other EP instabilities developed in pursuit of challenge 2. An attractive steady-state plasma may require continuous application of control actuators, or it may be that the actuators are required to navigate the transient formation period. Application of variable NBI perveance, ECH, and 3D fields are all possibilities, but substantial exploration will be required. The data from these experiments will provide additional “stress testing” and refinement of the theoretical models developed by the EP SciDAC center.

Ultimately, AT scenarios are extremely promising yet often the most susceptible to EP-driven instabilities. The prediction of AT operating regimes with minimal fast-ion transport and the experimental demonstration of these regimes would be a success similar to that of the Super H-mode prediction with the EPED and its experimental demonstration discussed in Section 1.

### 2.3.3.3 Capability Enhancements

A new second off-axis neutral beam will provide broad current profiles with high power, beta, and EP content. This is augmented with progressive rises in electron-cyclotron heating and current drive, which also provides the opportunity to reduce EP fractions. The recent development of variable voltage neutral beams can isolate EP resonances and help develop control. Later advances in power supplies and perturbative 3D coils will help understand the interaction with 3D non-axisymmetric fields and avoid losses when such fields are used for other control purposes. Central to understanding these physics are advances in diagnostics (Table 2-33). A new imaging NPA will provide an enormous increase in EP phase space coverage to isolate interactions (three NPA channels become essentially  $10^4$ ). A new loss detector will measure fast-ion losses in the highest performance AT plasmas. In combination with existing ECE and BES diagnostics, detection of the toroidal mode numbers of core modes will thoroughly diagnose unstable AEs. Table 2-34 lists the primary codes to be utilized in this effort.

Table 2-32 will enable AT discharges with larger values of  $\rho_{qmin}$  to be created and maintained.

Work in this area in the next five years will heavily leverage progress in the two other research strands as well as facility upgrades.

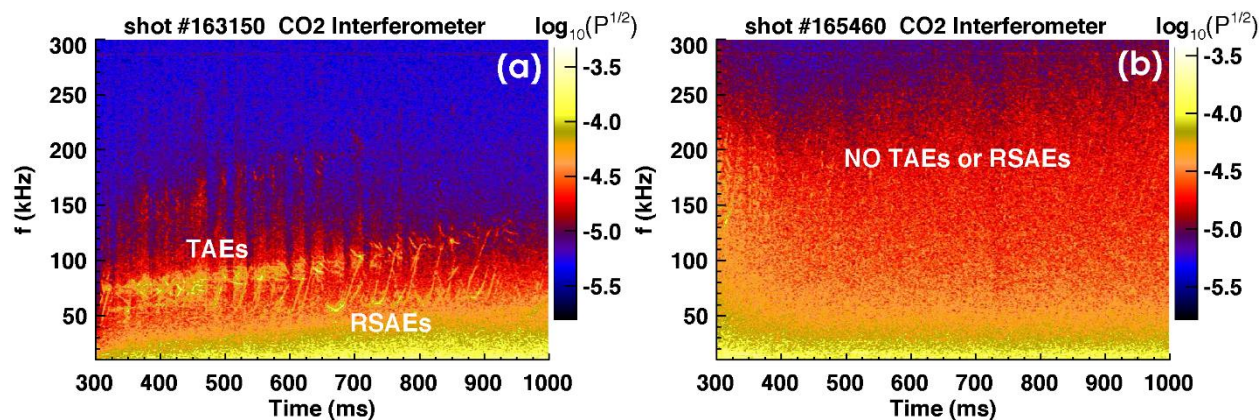


Fig. 2-56. Fluctuation spectra for two different plasma current ramp rates: (a)  $dI/dt=0.6\text{MA/s}$ ,  $\rho_{q\text{min}}=0.35$ , TAEs and RSAEs are observed; (b)  $dI/dt=6.7\text{MA/s}$ ,  $\rho_{q\text{min}}=0.45$  and NO AEs are observed.

**Goal 1: Use Validated Fast-Ion Transport Models to Predict AT Regimes with Improved EP Confinement.** Development of reduced models that accurately describe EP transport in a range of DIII-D conditions is a major goal of the validation efforts in Challenge 1. Once developed, these codes will be used to predict fast-ion behavior in AT regimes incorporating the expanded parameter space made available through upgrades. Experiments will follow and the results will guide improvements to modelling as well as assess whether or not full first principles simulations are required to reproduce the measured fast-ion transport or reduced models are suitable.

**Goal 2: Demonstrate Acceptable EP Confinement, Using Control Tools as Necessary.** This goal represents the culmination of work performed in all other sections. Wherever possible, modeling will guide scenario development leading to the experimental demonstration of AT scenarios with improved EP confinement. Experimentally, increased ECH and off-axis NBI will be leveraged to create discharges with reduced drive for AEs through overall reduced EP gradients and larger  $\rho_{q\text{min}}$ . Capabilities will progressively increase as more ECH power becomes available, and with the possible use of helicon and high-field-side launch lower hybrid current drive, which offer the prospect of even broader current profiles. The addition of a new fast-ion loss detector for reversed  $B_t$  discharges, typical of AT scenarios, will allow direct measurement of fast-ion losses and scenario optimization to reduce those losses.

The program will also utilize active control of AEs and other EP instabilities developed in pursuit of challenge 2. An attractive steady-state plasma may require continuous application of control actuators, or it may be that the actuators are required to navigate the transient formation period. Application of variable NBI perveance, ECH, and 3D fields are all possibilities, but

substantial exploration will be required. The data from these experiments will provide additional “stress testing” and refinement of the theoretical models developed by the EP SciDAC center.

Ultimately, AT scenarios are extremely promising yet often the most susceptible to EP-driven instabilities. The prediction of AT operating regimes with minimal fast-ion transport and the experimental demonstration of these regimes would be a success similar to that of the Super H-mode prediction with the EPED and its experimental demonstration discussed in Section 1.

#### 2.3.3.4 Capability Enhancements

A new second off-axis neutral beam will provide broad current profiles with high power, beta, and EP content. This is augmented with progressive rises in electron-cyclotron heating and current drive, which also provides the opportunity to reduce EP fractions. The recent development of variable voltage neutral beams can isolate EP resonances and help develop control. Later advances in power supplies and perturbative 3D coils will help understand the interaction with 3D non-axisymmetric fields and avoid losses when such fields are used for other control purposes. Central to understanding these physics are advances in diagnostics (Table 2-33). A new imaging NPA will provide an enormous increase in EP phase space coverage to isolate interactions (three NPA channels become essentially  $10^4$ ). A new loss detector will measure fast-ion losses in the highest performance AT plasmas. In combination with existing ECE and BES diagnostics, detection of the toroidal mode numbers of core modes will thoroughly diagnose unstable AEs. Table 2-34 lists the primary codes to be utilized in this effort.

**Table 2-32.**  
**Control Tools for EP Studies on DIII-D**

<b>Control Tool</b>	<b>Parameter Being Controlled</b>	<b>Purpose</b>
Neutral beam perveance	In-shot variation of NBI voltage and current	Alter AE drive
Advanced 3D-Coils	Helical magnetic field perturbations	Induce orbit stochasticity for EPs, rotate perturbations with toroidal mode numbers up to $n=4$
2 <sup>nd</sup> off-axis neutral beam, higher injection energy	Fast-ion density profile	Alter AE drive
ECH	Pressure profile	Alter AE stability

**Table 2-33.  
Physics Enabled by New Diagnostics for EP Research**

<b>Desired Measurement Capability</b>	<b>New Physics Enabled</b>	<b>Proposed Diagnostic</b>
AE toroidal mode number	Better mode identification in model validation	Toroidally displaced CO2 chord
Internal magnetic fluctuations	Distinguish electrostatic instabilities from electromagnetic modes	B fluctuations from polarimetry
Structure of density fluctuations	Better mode identification, search for wave-wave interactions, zonal flows associated with wave couplings	More BES channels for routine radial array
Fast-ion radial profile, ion distribution function	Improved radial resolution of confined ion redistribution, wave-particle couplings, phase space engineering	Imaging NPA and FIDA
Fast-ion losses with reversed toroidal field	Diagnose losses in highest performance AT plasmas	Third fast-ion loss detector

**Table 2-34.  
Codes Used for EP Research**

<b>Code</b>	<b>EP Related Purpose</b>
GTC, GYRO, GEM, LIGKA	Gyrokinetic - EP instability drive/damping/structure, thermal and EP fluxes, interaction with turbulence
TAEFL	Gyrofluid - AE instabilities
MEGA, M3D-K, XHMGC	Kinetic/MHD hybrid – EP studies including AEs, Fishbones, EGAM
M3D-C1	Two fluid MHD – 3D fields
GA and PPPL Critical Gradient models	Reduced model predictions of fast-ion profiles
NOVA/NOVA-K, AE3D	Ideal MHD + kinetic extension – AE instabilities
SPIRAL, ORBIT	Full orbit or guiding center following in axisymmetric and non-axisymmetric fields
TRANSP	Calculations of the fast-ion distribution function that include Coulomb collisions, atomic physics, and (when using the kick model) transport by instabilities
FIDASIM	FIDA and NPA synthetic diagnostic
Orbit-based distribution function inversion	Tool to invert fast-ion measurements to obtain confined distribution function

### 2.3.4 Heating and Current-Drive Physics

*Physics Leads: R.I. Pinsky (GA), X. Chen (GA), J.S. deGrassie (GA), J.M. Lohr (GA), A. Nagy (PPPL), C.C. Petty (GA), M. Porkolab (MIT), R. Perkins (PPPL), J.T. Scoville (GA), S.J. Wukitch (MIT)*

The development of powerful plasma heating systems to supplement Ohmic heating in the 1970s and 1980s was the most important driver of the rapid advances in tokamak performance from the T-3 tokamak via the intermediate-sized devices PLT, PDX/PBX, ASDEX, and Doublet III/DIII-D to TFTR, JET, and JT-60. Current drive with these techniques was demonstrated in the 1980-2000 period and, along with the experimental validation of the long-predicted neoclassical bootstrap current, this led to a new vision for a steady-state Advanced Tokamak (AT) in the 1990s, in which most of the plasma current arises from the bootstrap effect and the remainder is provided by various forms of non-inductive current drive.

DIII-D has demonstrated many of the key principles of the AT concept, as discussed in Section 2.1.2, with fully non-inductive scenarios routinely explored and underlying transport and stability physics established. This work has validated predictive models that show that the path to efficient reactor scenarios requires high  $\beta_N$  with more off-axis current drive [Park 2017]. To achieve this, a major upgrade is planned in 2018 to reconfigure half the neutral beams for off-axis current drive, together with increases in electron cyclotron current-drive power. However, future reactors require more efficient current-drive technologies than these that are compatible with reactor conditions. DIII-D also needs further current-drive flexibility to extend its AT studies to reactor-relevant low rotation levels (achieved by balancing neutral beam torques, which also eliminates beam-driven current) and high density for core-edge integration studies (where electron cyclotron current drive becomes cut off). Therefore, the DIII-D program has been developing new current-drive concepts to meet these needs, as set out below. This has included successful low-power testing of one technique (“helicon” [Pinsky 2016]), installation in 2018 for high-power tests for this and a second technique, and design and tests for a third. The principal requirements for the 2019-2024 period are to carry these forward to provide:

- Substantial and flexible current-drive methods to allow the exploration and optimization of AT scenarios with different safety factor profiles over a range of parameters;
- Development of efficient current-drive techniques that are relevant for future fusion reactors, to reduce recycled power, required device scale, and the cost of electricity.

#### 2.3.4.1 Challenges and Impact

The 2019-2024 five-year plan foresees a major initiative to explore improved current-drive actuators for future fusion reactors. This work could be transformational for fusion energy prospects, by enabling more cost-effective fusion reactors, as discussed above. The approach is

focused on development of comprehensive predictive models for neutral-beam heating and current drive, for electron-cyclotron heating and current drive and for other forms of heating and current drive such as 'helicon' waves (fast waves in the LHRF) and LHCD (which uses slow waves in the LHRF). In particular, Challenge 1 in Table 2-1 sets out three key approaches to high current drive efficiency with high power (MW level) tests of helicon ultra-high harmonic fast wave, top-launch ECCD and high-field-side LHCD. Further work will test and improve techniques for X-mode ECCD for high-density access (Challenge 2) and explore RF-SOL interactions (Challenge 3). The challenges, proposed goals/deliverables which will address those challenges and related enhancements to the DIII-D facility are summarized in Table 2-35.

**Table 2-35.**  
**Heating and Current Drive, Challenges, Goals and Upgrades**

<b>Challenge</b>	<b>Goals/Deliverables</b>	<b>Upgrades</b>
<b>1. Establish new methods of efficient, off-axis current drive that are reactor relevant</b>	<ul style="list-style-type: none"> <li>• Measure efficiency of high-power helicon (fast wave) current drive and evaluate limiting effects</li> <li>• Explore HFS-launch lower hybrid (slow wave) current drive and assess advantages over conventional outside-launch LHCD</li> <li>• Test top-launch ECCD to demonstrate the large predicted increase in efficiency</li> <li>• Evaluate impact of instabilities on NBCD with increased off-axis beam power</li> </ul>	<ul style="list-style-type: none"> <li>• Comb-line antenna, SLAC klystron and power supply</li> <li>• Transfer 2 MW system from MIT, develop new launcher for centerpost</li> <li>• New launcher; for initial test use existing gyrotrons with waveguide switch</li> <li>• 2 off-axis beamlines, one co-counter steerable beamline</li> </ul>
<b>2. Centrally heat electrons at high density, above existing limit for 110 GHz EC system (<math>\sim 5 \times 10^{19} \text{ m}^{-3}</math>)</b>	<ul style="list-style-type: none"> <li>• Develop and validate model beyond ray-tracing to characterize X-mode EC wave, especially near cutoff</li> </ul>	<ul style="list-style-type: none"> <li>• EC diagnostics, such as sniffers and transmission measurements</li> <li>• Physical optics code development</li> </ul>
<b>3. Actively control SOL to optimize RF coupling</b>	<ul style="list-style-type: none"> <li>• Introduce controllable, localized sources of neutrals in the far SOL and localized power to ionize those neutrals</li> </ul>	<ul style="list-style-type: none"> <li>• Gas injectors</li> <li>• Ionization sources (low frequency EC system of <math>\sim 10\text{-}100 \text{ kW}</math>, etc.)</li> <li>• SOL diagnostics near midplane, i.e. low-frequency reflect., probes, etc.</li> </ul>

This work will make critical impacts to the path to fusion energy, primarily through the development of a more efficient means of off-axis current drive. As control of the safety factor profile is one key to optimizing the AT regime, this could be transformational to enabling an efficient and more modest-scale fusion reactor by reducing the amount of electricity needed to be generated to power auxiliary systems. Critical elements of this research will resolve:

- Evaluation and possible demonstration of helicon ultrahigh harmonic fast wave as well as high-field-side lower hybrid slow waves as highly efficient current-drive techniques;
- Access to high-density AT research lines at high  $\beta_N$  in DIII-D;
- Extension of DIII-D fully non-inductive plasmas to higher  $\beta_N$  at low rotation;

- Development of top-launch ECCD as more efficient method for EC current drive;
- Assessment and possible demonstration of high-density EC heating techniques;
- Understanding of the interaction between RF techniques and scrape-off layer properties, and development of techniques to optimize coupling.

Taken together, this represents a comprehensive and world-leading program to develop the current-drive physics basis for future reactors. This is apt, given DIII-D’s unique flexibility to also access and study the advanced tokamak regimes to which these techniques must couple. This work will therefore enable validation of integrated solutions for future steady-state facilities with required performance scenarios and compatible actuators.

Challenge	FY19-20	FY21	FY22	FY23	FY24
Establish new methods of efficient, off-axis current drive that are reactor relevant	1 MW helicon experiments Coupling at high power 1 MW top-launch ECCD experiments	Validate current drive	Apply helicon CD in AT		Test HFS launch LH at 1 MW coupled (2 MW source)
Centrally heat electrons at high density, above existing limit for 110 GHz EC	Develop more complete model of EC at high density		Validate model, establish realistic limits on EC operation at high density		
Actively Control SOL to Optimize RF Coupling		Apply active control of SOL for optimization of helicon coupling			Use active control of SOL for LH
Enhancements Required	Co/ctr NB at 210 Deg. Helicon antenna Top-launch EC antenna	Increase EC power Diagnostics for EC, rf in edge Active control of far SOL parameters			2nd co/ctr NB at 30 deg HFS-LHCD

Fig. 2-57. Heating and current-drive research in FY19-24

### 2.3.4.2 Research Plan for Heating and Current Drive

The heating and current-drive program research plan is organized according to the challenges and goals in Table 2-35. Fig. 2-57 gives the timeline for each challenge, research milestones, and the capability improvements necessary to achieve them. Heating and current-drive research in the period 2019-2024 benefits from a considerable range of facility developments, as set out in Table 2-36. At the start, work will begin to test the newly installed 1-MW helicon comb-line antenna, with a progressive program to assess its physics. In parallel top launch ECCD will be assessed,

and further developed if proof-of-principle tests prove fruitful. Later, high-field-side (HFS) LHCD will be similarly assessed.

### Challenge 1: Establish New Methods of Efficient, Off-axis Current Drive that are Reactor Relevant

**Current Progress:** An essential feature of the advanced tokamak approach to fusion energy is that most of the toroidal plasma current in steady state must be self-driven from the bootstrap effect. Other non-inductive current sources will also be required, primarily off-axis for reasons of stability and performance; however, all methods investigated thus far are characterized by an efficiency for reactor-scale plasmas that is too low for an economically attractive steady-state fully driven fusion reactor. Fortunately, several techniques investigated in the past five years, through initial scoping studies and small scale tests, show promise for higher efficiency off-axis current drive solutions. These solutions include helicon current drive, HFS-launch lower hybrid current drive and top-launch electron-cyclotron current drive.

Recent studies suggested that helicon waves with high first-pass absorption and potential for current drive could be launched in high-beta DIII-D plasmas [Vdovin 2013]. Through additional calculations, it was later verified that in a suitable high-performance discharge, approximately 60 kA/MW of current could be driven at  $\rho \sim 0.55$  at a high density (see Fig. 2-58) [Prater 2014]. It is noted that this level of predicted current-drive efficiency is a *factor of 2-4 times larger than present DIII-D off-axis non-inductive current sources*. As a first step to test this prediction, a 12-module low power prototype comb-line antenna operated at 476 MHz (shown in Fig. 2-59) was constructed and antenna-plasma coupling measurements were made. The results [Pinsker 2016] were encouraging and consistent with being able to couple  $> 75\%$  of the applied power to the plasma for a projected 30-element high-power antenna (to be experimentally demonstrated as part of this plan).

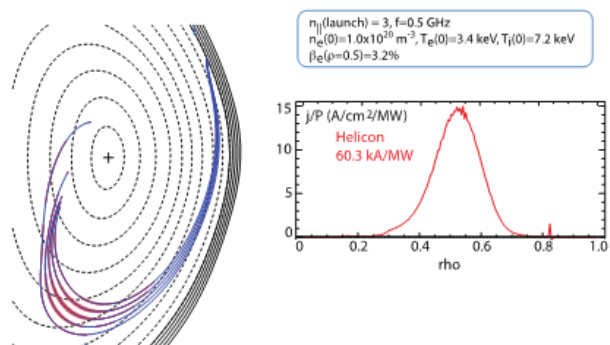


Fig. 2-58. Projected helicon ray paths and current drive efficiency calculated with GENRAY ray tracing code, using equilibrium and profiles from DIII-D discharge 122976.



Fig. 2-59. The low-power prototype comb-line traveling wave antenna as installed in DIII-D during the 2016 campaign.

In FY2016, initial studies of lower hybrid current drive (LHCD) for application on DIII-D also began. LHCD is among the most promising techniques for high efficiency off-axis current drive and is included in many future reactor designs. The harsh reactor environment, however, poses challenges for LHCD launching structures, which must be placed near the plasma. Additionally, the strong electron damping characteristic of the slow wave makes penetration to mid-radius difficult at fusion-relevant densities and temperatures.

A promising solution to this complex problem has recently been suggested: launch the LH waves from the high-field-side (HFS) instead of the low-field-side (LFS) [Wallace 2015]. Relocating the LHCD launcher to the HFS of the tokamak is predicted to dramatically improve wave penetration (see Fig. 2-60), CD efficiency, reduce PMI issues, and increase launcher robustness in a reactor environment. On the HFS, the toroidal field is higher and allows launch of lower  $n_{\parallel}$  waves that penetrate farther into the plasma core before damping. Furthermore, the lower  $n_{\parallel}$  waves are absorbed at higher  $T_e$ , yielding a higher current-drive efficiency that scales as  $\sim 1/n_{\parallel}^2$  [Fisch 1978]. The reduction in the PMI issues is due to several effects which, among other things, act to reduce the overall heat and particle fluxes (thermals, impurities, fast ions, runaway electrons, and neutrons) significantly [Petrie 2003, Smick 2013, Boswell 2004, Labombard 2017, Wukitch 2004].

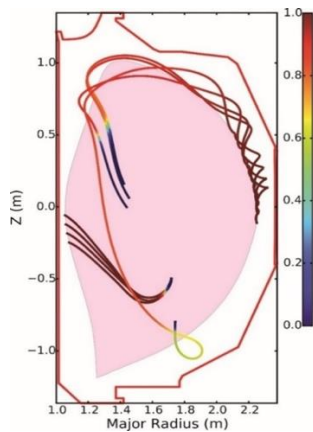


Fig. 2-60. HFS LHCD penetrates into plasma core and damps in single pass, whereas, LFS LHCD remains in the plasma periphery until wave upshifts and damps.

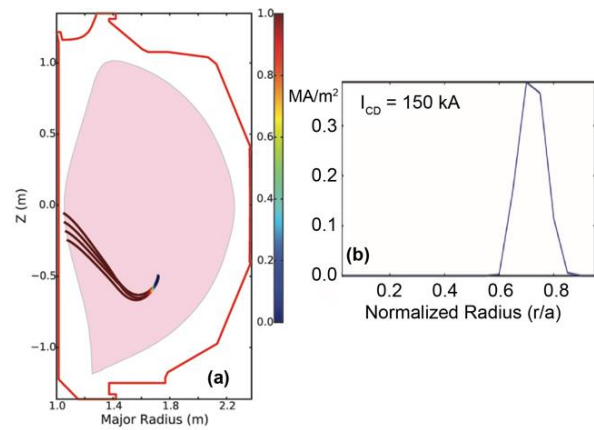


Fig. 2-61. (a) LH waves launched from HFS near mid plane penetrate and single pass damp near  $\rho \sim 0.6$  for 1.66 T, high  $q_{min}$  discharge (147634). (b) Driven current profile – with  $\sim 0.4 \text{ MA/m}^2$  for 1 MW coupled.

HFS LHCD simulations indicate existing and target AT discharges are characterized by single-pass absorption, efficient off-axis current drive for  $B_T \geq 1.6 \text{ T}$ ,  $n_e < 9 \times 10^{19} \text{ m}^{-3}$  and deposition peaked between  $\rho = 0.6-0.8$ . In Fig. 2-61 (a), the rays from a coupler positioned at poloidal positions 3-24 cm below the mid plane with a launch spectrum peaked at  $n_{\parallel} = 2.7 \pm 0.2$  are shown. The rays penetrate, damp on a single pass and drive  $\sim 150 \text{ kA/MW}$  peaked near  $\rho \sim 0.7$  with a corresponding

efficiency  $0.12 \times 10^{20}$  A/W/m<sup>2</sup>. As shown in Fig. 2-61 (b), the simulation suggests 1 MW of coupled power can drive the required off-axis current in the range of  $\rho \sim 0.6-0.8$  with current density approaching  $0.4 \text{ MA/m}^2$  for AT discharges.

Relative to the other wave-based current-drive approaches listed above, Electron Cyclotron Current Drive (ECCD) has a number of important advantages, including vacuum propagation, localized absorption at cyclotron harmonics, small diameter evacuated waveguides, and small required penetrations in the vacuum vessel. The most significant weakness of EC schemes for current drive, however, is a relatively low efficiency. Recently, it has been proposed [Poli 2013] that the ECCD efficiency can be improved by moving the launch point to the top (or bottom) of the torus, at a slightly larger major radius than that of the cyclotron harmonic resonance layer, with a large toroidal steering angle. For DIII-D, as well as for some reactor studies, an increase in the current-drive efficiency of 35-100% by comparison to “conventional” ECCD (outside launch) has been predicted. An example calculation for DIII-D is shown in Fig. 2-62 where the path of the EC beam in the poloidal plane and the kind of current drive efficiency enhancement that can be achieved relative to LFS launch in DIII-D are shown.

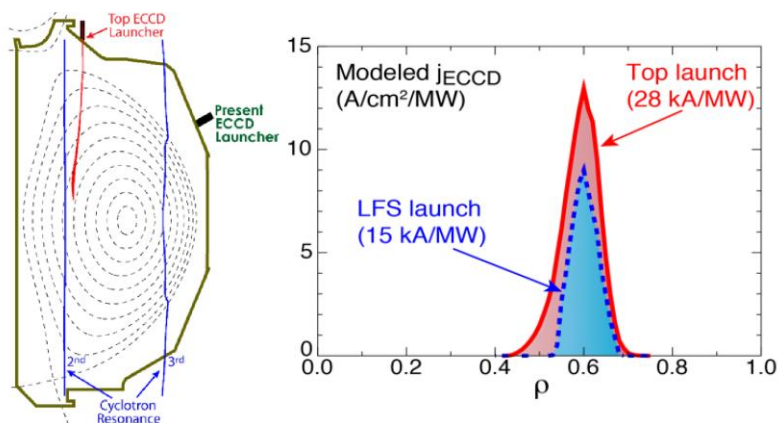


Fig. 2-62. (left) The top-launch EC beam propagates between the 2nd and 3rd harmonic layers. (right) In some cases top launch EC can result in a factor of two higher CD efficiency than LFS launch.

Work covered in the 2019-2024 period will experimentally test many of the predictions mentioned above and evaluate the viability of helicon CD, HFS LHCD, top launch ECCD, and, through work carried out in the energetic particle group (see Section 2.3.3), will also investigate important limiting factors of the more established neutral beam current drive.

**Goal 1: Measure efficiency of high-power helicon (fast wave) current drive and evaluate limiting effects.** The helicon wave research plan takes advantage of a new 1.2 MW 476 MHz Klystron that will be installed in FY18-19 (described in Section 5.3.9) and focuses on measuring the current-drive profile and assessing possible differences between low power (linear regime) and

high power (non-linear regime) antenna coupling. The same motional-Stark effect (MSE)-based techniques employed in the past to measure ECCD and beam-driven current profiles to a resolution of ~10-15 kA out of 1 MA total current will be used for these studies [Petty 2003]. Additionally, when available, the new 2D imaging MSE system will further improve the obtainable resolution.

The main physics result of these current-drive studies will be a comparison between the theoretically predicted current-drive profile for helicon waves and experiment. In particular, the following attributes will be verified:

- Dependence of the deposition location on the electron beta. For moderate values, the helicon waves should be absorbed near the plasma center, but at high values the absorption should move off axis.
- A well-defined, relatively narrow current-drive profile for off-axis absorption. This will indicate that the helicon waves have a well-defined  $n_{||}$  value and are not being scattered during their propagation through the plasma.
- High current-drive efficiency.

Besides the current-drive measurements, these high-power helicon studies will examine non-linear wave phenomena which can lead to:

- A reduction of the antenna loading beyond that obtained in the linear regime during low power tests;
- Parametric decay instability (PDI), which can reduce the power available to drive current in the plasma core and lead to edge power deposition. The measured level of current drive and the known efficiency (Amperes per core-absorbed Watt) will be used to determine the fraction of power lost via these nonlinear processes.

If successful, a higher power helicon system will be considered to provide additional current-drive capabilities for the AT program.

**Goal 2: Explore HFS-launch lower hybrid (slow wave) current drive and assess advantages over conventional outside-launch LHCD.** The HFS-launch LHCD research plan will use a new centerpost-mounted launcher (described in 5.3.10) and will focus on measuring the driven current profile dependence on plasma parameters and launch spectrum. Simulations predict the technique will be very sensitive to toroidal field, density, and temperature. For example, by increasing the toroidal field from 1.6 T for the case shown in Fig. 2-61, the driven current is predicted to increase from 150 kA/MW to 190 kA/MW. Testing these dependencies by measuring the driven current for a range of conditions and scenarios will allow validation of the RF

simulations and the technique to build confidence in predictions for future experiments and reactors.

In addition to the dependences discussed above, characterizing the HFS SOL and coupling characteristics, demonstrating density control via magnetic equilibrium, impurity screening effectiveness, impact of edge fast electron accelerated by RF near fields, and assessment of plasma material interaction are key physics/technological issues that will be investigated. If successful, HFS LHCD experiments could demonstrate that challenges for LHCD (coupling and launcher survivability) are largely mitigated by locating the LHCD coupler on the HFS.

**Goal 3: Test top-launch ECCD to demonstrate the large predicted increase in efficiency.**

Testing the predicted increase in ECCD efficiency for top launch relative to typical outside launch will be accomplished by taking advantage of existing gyrotron systems and transmission lines with only a simple new top launcher and a waveguide switch being required. Initially, fixed launcher angles will be used so this will be a proof-of-principle test, as high ECCD efficiency can be obtained only over a limited range of toroidal fields. Initial tests with one or two gyrotrons at a coupled power of ~1 MW will be carried out early in the 2019-2024 five-year plan. If the driven currents are consistent with expectations, a more flexible 2nd generation top launcher will be designed and installed later in the five-year period. The methodology for measuring the top launch ECCD profile is the same as described previously for helicon studies, where the fiducial case can be established using outside-launch ECH with radial injection. Given the very strong arguments for EC as a highly reactor-relevant heating and current-drive technology, it is imperative that any potentially significant enhancement of the current-drive efficiency be explored and proven out experimentally.

**Challenge 2: Centrally Heat Electrons at High Density, Above Existing Limit for 110 GHz EC System ( $\sim 5 \times 10^{19} \text{ m}^{-3}$ )**

**Current Progress.** High-performance operating scenarios often push toward increasing density targets, however, the EC system on DIII-D, based on 2nd harmonic X-mode absorption, has an upper density limit due to the X-mode cutoff. Above an electron density in the neighborhood of  $5 \times 10^{19} \text{ m}^{-3}$  (for 110 GHz), the exact value depending on details of the equilibrium, the shape of the density profile, and other factors, the rf beam is strongly refracted away from the high-density region and is not absorbed in the plasma. In the most extreme cases, the beam can propagate back out of the plasma and interact with an area of the outer wall or with plasma-facing hardware and cause damage. To prevent this scenario, EC operations is presently restricted at high density by a combination of PCS-based and administrative controls developed over the past five years. The real-time protection level setting the maximum allowed density is determined using ray-tracing

analysis of previous discharges. This procedure has some limitations: the subsequent discharge may end up evolving differently than the one on which the density limit was set, and more fundamentally, the ray-tracing approximation, embodied in the TORAY code, in principle breaks down exactly under the circumstances of interest, i.e., when refraction becomes strong in the neighborhood of the cut-off.

Given the growing interest in operation with EC at densities challenging the density limit, essentially as a result of divertor studies and also for discharge regimes with improved stability with heavy gas puffing, improvement of the tools for electron heating at high density has become an important issue and will be focused on during the 2019-2024 period

**Goal 1: Develop and validate model beyond ray-tracing to characterize X-mode EC wave, especially near cutoff.** Investigation of new diagnostics to observe unabsorbed power, such as rf 'sniffers' (receivers sensitive to EC radiation) and transmission measurements, along with validation and benchmarking of more realistic computational approaches than ray-tracing, will lead to improvement in this area. Ray-tracing is the computationally least intensive (the DIII-D PCS can run a ray-tracing model in real time to correct the EC aiming for refraction when ECCD is used for NTM stabilization) and least realistic model, while a full-wave approach is the most realistic and computationally least practical approach. It is possible that an intermediate approach, such as beam tracing, can be employed and perhaps benchmarked with specific cases of full-wave analysis (at significant computational cost). Dedicated experiments after installation of the new diagnostics will test the more refined model results in DIII-D to enable safe operation of the EC system up to the maximum density that refraction permits, possibly by incorporating some of the diagnostics (sniffers) into the DIII-D real-time control system.

### **Challenge 3: Actively Control SOL to Optimize RF Coupling**

**Current Progress.** Waves used for tokamak heating and current drive at frequencies below the ECRF, such as the helicon and the lower hybrid slow wave, cannot propagate in vacuum and must tunnel through an evanescent layer in front of the wave-launching structure up to the density at which they begin to propagate. The wave parameters must be chosen so that the density at which the waves begin to propagate is low enough that the evanescent layer is not too thick to achieve a practical level of wave coupling. Hence, that value of the density must appear in the scrape-off layer (SOL). Since the coupling is exponentially sensitive to the thickness of that evanescent zone, and the SOL density is not usually a parameter that is feedback controlled, the rf coupling can vary over a wide range. Conversely, application of high-power rf in these frequency ranges always causes a significant effect on the SOL, in some cases limiting the range of plasmas in which the rf can be utilized, or leading to an operational requirement involving wall conditioning (boronization,

lithiumization, etc.) Were it to prove possible to actively control the SOL density other than by controlling the separatrix/wall gap distance, the range of application of rf heating and current drive techniques could significantly increase.

A possible scheme for such a control involves local gas puffing coupled with a local power source to ionize the gas in the far SOL. JET showed in the 1990s that a small fraction of the power applied to a LHCD wave launcher (grill) provided the necessary ionization power to make this scheme successful in that case [Pericoli 2004]; however, similar experiments in the ICRF on DIII-D and elsewhere [Pinsker 2010, Jacquet 2016] have generally indicated that the ICRF power itself does not provide much local ionization. Instead, in cases where local gas puffing was successful in increasing the ICRF antenna coupling, it seemed that the power exhaust from the plasma caused ionization of the gas in the entire SOL, rather than being a localized effect. Detailed edge modeling in a few cases has shown that 3D details of the hardware determine the effectiveness of these techniques in the ICRF [Zhang 2017].

Experiments will focus on improving the controllability of the SOL density and obtaining a quantitative understanding of the underlying effects.

**Goal 1: Introduce controllable, localized sources of neutrals in the far SOL and localized power to ionize those neutrals.**

Experiments will compare ‘local’ to ‘global’ sources of neutrals by installing new gas injectors near the helicon and LHCD antennas. The gas injectors should have the ability to feedback control the flow rate depending upon the antenna loading, which means that the feed tubes should not be too long or narrow. It is likely that the helicon and LHCD antennas will not fully ionize the gas around them since they are not optimized for that purpose; therefore, the plan includes a provision for ionization sources, likely a low-frequency EC system with power between 10-100 kW, to ensure that the gas puffed locally near the antenna is ionized into plasma. The improvement in coupling would be applied to helicon antennas in DIII-D at first, and could be used for the HFS-launch lower-hybrid system when that wave launcher is installed. Efficient coupling is obviously a critical element of any wave-based current drive scheme and progress in this area via improved controllability of the SOL density will directly impact the viability of these approaches for future devices. To obtain a quantitative understanding of the underlying effects, new SOL diagnostics near midplane, such as a low-frequency density reflectometer and Langmuir probes, are planned.

### **2.3.4.3 Capability Development**

The tables in this section provide an overview of planned hardware and diagnostic developments, and use of simulation codes.

**Table 2-36.  
Hardware Improvements for Heating and Current-Drive Studies**

<b>Hardware Capability</b>	<b>New Physics</b>
Complete development of Variable Perveance NBI at 45-80 kV	Modify torque-to-power ratio continuously without the need for pulsing beams.
1 MW helicon system	Enable study of helicon current drive at level at which driven current can be measured, and in regime where non-linear effects on the wave coupling are expected (parametric decay instabilities, ponderomotive effects, etc.)
2 MW HFS-launch lower hybrid current-drive system	Evaluate reactor-relevance of high-field-side-launch lower hybrid current drive; application of off-axis current drive to AT studies
Top-launch ECCD system (first tests require only a new launcher and a waveguide switch and will use existing gyrotrons and transmission lines)	Demonstrate projected factor of two improvement in ECCD efficiency in some parameter ranges
Additional gas puffing capabilities and localized plasma sources in far SOL	Enable study of control of far SOL to facilitate wave coupling and possibly reduce deleterious effects of rf on SOL in lower-hybrid range of frequencies (lower hybrid waves, helicon waves)

**Table 2-37.  
Diagnostic Improvements for Heating and Current-Drive Studies**

<b>Scientific Objective</b>	<b>Physics Measurement</b>	<b>Diagnostic Techniques</b>
Accurate measurement of the current-drive profile	Spatiotemporal evolution of the poloidal magnetic flux	MSE upgrades, including IMSE
Compare antenna coupling with modeling for wave launchers in the lower-hybrid range of frequencies	Measure far-SOL density profiles on both high- and low-field sides	Swing and fixed Langmuir probes on HFS and LFS Profile reflectometer for SOL
Compare characteristics of waves in the lower-hybrid range of frequencies within the plasma with expectations from modeling	Measure wavelengths and amplitudes of rf waves in the plasma	Extend phase-contrast imaging to rf frequency for density fluct. (MIT) Extend bandwidth of microwave reflect. to rf freq.(UCLA, UCD) RF Stark-effect diagnostic (ORNL) Miniature rf probe arrays to charac. $n_{  }$ spectrum in the SOL (MIT)
Compare EC waves in the SOL with modeling in ranges near cut-off	Measure EC wave amplitudes in SOL	RF Sniffer probes EC transmission measurements (detectors at high-field side)
Characterize effects of high-power rf in LHRF on SOL	Study power deposition at divertor, rf-specific impurity influx, electron temp. and floating potential changes in SOL with high-power rf	Infrared cameras Langmuir probes, gridded energy analyzers Spatially localized spectroscopy

**Table 2-38.**  
**Development and Validation of Simulation/Analysis Codes**

<b>Code</b>	<b>Simulation/Analysis Purpose/Key Facets</b>
COMSOL	(Commercial) EM modeling of wave launchers, possibly with plasma model
QuickWave	(Commercial) EM modeling of wave launchers, no plasma model
VSimEM/VSimPD	(Tech-X: Commercial) EM modeling of wave launchers, detailed plasma model
GENRAY	Ray-tracing of waves in LHRF with absorption model
TORAY	Ray-tracing of waves in ECRF (O-mode, X-mode) with absorption model
TORBEAM	Paraxial approximation to do beam tracing for ECRF with diffraction
CQL3D	Fokker-Planck solver, typically coupled with ray-tracing model
AORSA	Full-wave solver for LHRF or lower, detailed ion absorption model
TORIC-LH	Full-wave solver for LHRF
MFEM-TORIC	(MIT) integrated coupler-SOL-core solver for LHRF
MPPDI	Model for parametric decay instabilities
NVLOOP	Current drive analysis tool based on time-dependent equilibrium series
DAMSED	Direct Analysis of <i>MSE</i> Data for current drive analysis

## References

- [Aleynikov 2017] P. Aleynikov et al., *Nucl. Fusion* 57 (2017) 046009
- [Austin 2017] M. Austin et al., *Bull. Am. Phys. Society* 62 (12), 25 (2017)
- [Bardoczi 2016] L. Bardoczi et al., *Phys. Rev. Lett.* 116, 215001 (2016).
- [Bardoczi 2017] L. Bardoczi et al., *Phys. Plasmas* 24, 056106 (2017).
- [Barr2018] Barr, J, N. Eidietis, D. Humphreys, T. Luce, B. Sammuli, “Fast ITER-Relevant low-disruptivity rampdowns in DIII-D and EAST,” to be submitted to 27<sup>th</sup> IAEA FEC 2018
- [Bortolon 2016]: A. Bortolon et al, *Nucl. Fusion* 56 056008 (2016)
- [Bortolon 2017]: A. Bortolon et al, “Fast-ion induced ablation of Li granules in DIII-D”, presented at the ITPA-PEP meeting, Naka, Japan, October 2016
- [Boswell 2004] C.J. Boswell, et.al., *Plasma Phys. Control. Fusion* 46 (2004) 1247
- [Burrell 2013] K.H. Burrell, et al., *Nucl. Fusion* 53, 073038 (2013)
- [Burrell 2012] K.H. Burrell, et al., *Phys. Plasmas* 19, 056117 (2012)
- [Buttery 2018] R. J. Buttery et al., ‘Physics Principles and Research Requirements for a Compact Advanced Tokamak Fusion Pilot Plant’ submitted to *Nuclear Fusion* journal
- [Camenen 2007] Y. Camenen et al., *Nucl. Fusion* 47, 510 (2007)
- [Camenen 2009] Y. Camenen et al., *Phys. Plasmas* 16, 062501 (2009)
- [Candy 2003] J. Candy, *J. Comp. Phys.* 186, 545 (2003)

- [Chen 2014] X. Chen, et.al., RSI 85, 11E701 (2014)
- [Chen 2016]: X. Chen, et al, Nucl. Fusion 56 076011 (2016)
- [Choi 2017] W. Choi, et al., “Feedforward and feedback control of locked mode phase and rotation in DIII-D with application to modulated ECCD experiments,” submitted to Nuclear Fusion (2017)
- [Chrystal 2014] C. Chrystal *et al.*, Phys. Plasmas 21, 072504 (2014)
- [Chrystal 2017] C. Chrystal *et al.*, Phys. Plasmas, 24, 042501 (2017)
- [Chrystal 2017] C. Chrystal *et al.*, Phys. Plasmas 24, 056113 (2017)
- [Chrystal 2017] C. Chrystal, et al., Phys. Plasmas 24, 042501 (2017)
- [Clement 2017] M. Clement, et al., Control Engineering Practice 68, 15 (2017)
- [Collins 2016] C.S. Collins, et.al., Phys. Rev. Lett. 116, 095001
- [Collins 2017] C.S. Collins et al 2017 Nucl. Fusion 57 086005
- [Commaux 2011] N. Commaux *et al.*, *Nucl. Fusion* 51 (2011) 103001
- [Commaux 2014] N. Commaux *et al.*, *Nucl. Fusion* 56 (2016) 046007
- [DeBoo 2010] J.C. DeBoo *et al.*, Phys. Plasmas 17, 056105 (2010)
- [DeBoo 2012] J.C. DeBoo *et al.*, *Phys. Plasmas* 19, 082518 (2012)
- [deGrassie 2009] J.S. deGrassie, Plasma Phys. Control. Fusion, 51, 124047 (2009)
- [deGrassie 2016] J.S. deGrassie *et al.*, Phys. Plasmas, 23, 082501 (2016)
- [Dominguez 1993] R.R. Dominguez and G.M. Staebler, Phys. Fluids B5, 3876 (1993)
- [Dorris 2009] J.R. Dorris, J.C. Rost, M. Porkolab, Rev. Sci. Instrum. 80, 023503 (2009)
- [Eidietis 2017] N. Eidietis *et al.*, *Phys. Plasmas* 24 (2017) 102504.
- [Eidietis2017] Eidietis, N.W., Hahn, S.H., Humphreys, D.A., Sammuli, B.S., Walker, M.L., “Implementing a Finite State Off-Normal and Fault Response System for Disruption Avoidance in Tokamaks,” Submitted for publication to Pl. Phys. Control. Fusion, Feb. 2017
- [Eldon2017] D. Eldon, E. Kolemen, A. W. Hyatt, J. L. Barton, A. R. Briesemeister, N. Eidietis, D. A. Humphreys, A. E. Järvinen, A. W. Leonard, A. G. McLean, A. L. Moser, T. W. Petrie, B. Sammuli, and M. L. Walker, “Divertor Control Development at DIII-D and Implications for ITER,” 11<sup>th</sup> IAEA Tech. Mtg. on Control, Data Acquisition, and Remote Participation for Fusion Research, Greifswald, Germany (2017); submitted for publication to Fus. Eng. And Design, May 2017
- [Ernst 2016] D.R. Ernst *et al.*, Phys. Plasmas 23, 056112 (2016).
- [Ferron 2013] Ferron J.R. et al. Physics Plasmas 20 092504
- [Ferron 2013] J.R. Ferron, et al., Phys. Plasmas 20, 092504 (2013)

- [Ferron 2015] Ferron J.R. et al. 2015 Nuclear Fusion 55 073030
- [Ferron 2015] J.R. Ferron, et al., Nucl. Fusion 55, 073030 (2015)
- [Ferron 2015a] Ferron J.R. et al. “High internal inductance for high  $\beta_N$  steady-state tokamak operation”, Bulletin of the American Physical Society, 60 2015 pg. 210
- [Fisch 1978] N. J. Fisch, Phys. Rev. Lett. 41, 873 (1978)
- [Garcia 2017] J. Garcia *et al.*, Nucl. Fusion 57, 014007 (2017).
- [Garofalo 2007] Garofalo A.M. *et al.* 2007 Nuclear Fusion 47 1121
- [Garofalo 2008] A.M. Garofalo, et al., Phys. Rev. Lett. 101, 195005 (2008)
- [Garofalo 2009] A.M. Garofalo, et al., Phys. Plasmas 16, 056119 (2009)
- [Garofalo 2015]: A.M. Garofalo et al, Phys. Plasmas 22 056116 (2015)
- [Garofalo 2017] Garofalo A.M. et al., “Joint DIII-D/EAST research on the development of a high poloidal beta scenario for the steady state missions of ITER and CFETR”, accepted for publication in Plasma Physics Controlled Fusion, 2017
- [Ghantous 2012] K. Ghantous, et.al., Phys. Plasmas, 19, 092511 (2012)
- [Gohil 2008] P. Gohil *et al*, Journal of Physics; Conference Series 123, 012017 (2008)
- [Gorelenkov 2009] N.N. Gorelenkov, et.al.Phys. Plasmas, 16, 056107 !2009"
- [Grierson 2012] B.A. Grierson *et al*, Phys. Plasmas 19, 056107 (2012)
- [Grierson 2013] B.A. Grierson *et al.*, Nucl. Fusion 53, 063010 (2013)
- [Grierson 2017] B.A. Grierson *et al.*, Phys. Rev. Lett. 118, 015002 (2017)
- [Hanson 2017] Hanson J.W. *et al.* 2017 Nuclear Fusion 57 056009
- [Hanson 2017] J.M. Hanson, et al., Nucl. Fusion 57, 056009 (2017)
- [Heidbrink 1995] W.W. Heidbrink et al 1995 Nucl. Fusion 35 1481
- [Heidbrink 2014] W W Heidbrink et al 2014 PPCF 56 095030
- [Heidbrink 2016] W.W. Heidbrink et al 2016 Nucl. Fusion 56 112011
- [Heidbrink 2017] W.W. Heidbrink,et.al, Phys. Plasmas, 24, 056109 (2017)
- [Hillesheim 2009] J.C. Hillesheim *et al.*, Rev. Sci. Instrum. 80, 083507 (2009)
- [Holcomb 2009] Holcomb C.T. et al. 2009 Physics Plasmas 16 056116
- [Holcomb 2012] Holcomb, C.T. *et al.* 2012 Physics of Plasmas 19, 032501
- [Holcomb 2014] C.T. Holcomb et al., Nucl. Fusion 54 093009 (2014)
- [Holcomb 2014] Holcomb C.T. et al., 2014 Nuclear Fusion 54 093009
- [Holcomb 2015] C.T. Holcomb, et.al., Phys. Plasmas, 22, 055904 (2015)
- [Holcomb 2015] Holcomb, C.T. *et al.* 2015 Physics of Plasmas 22, 055904
- [Holland 2009] C. Holland *et al.*, Phys. Plasmas 16, 052301 (2009)

- [Holland 2016] C. Holland, *Phys. Plasmas* 23, 060901 (2016)
- [Hollmann 2015] E.M. Hollmann et al., *Phys. Plasmas* 22 (2015) 056108
- [Hollmann 2017] E.M. Hollmann et al., *Nucl. Fusion* 57 (2017) 016008
- [Howard 2016] N.T. Howard et al., *Nucl. Fusion* 56, 014004 (2016)
- [Humphreys2007] Humphreys, D.A., Ferron, J.R., Bakhtiari, M., Blair, J., In, Y., Jackson, G.L., Jhang, H., Johnson, R.D., Kim, J.S., La Haye, R.J., Leuer, J.A., Penaflor, B.G., Schuster, E., Walker, M.L., Wang, H., Welander, A.S., D.G. Whyte, “Development of ITER-Relevant Plasma Control Solutions at DIII-D,” *Nucl. Fusion* 47 (2007) 943
- [Humphreys2009] Humphreys, D.A., Casper, T.A., Eidietis, N., Ferrara, M., Gates, D.A., Hutchinson, I.H., Jackson, G.L., Kolemen, E., Leuer, J.A., Lister, J., Lodestro, L.L., Meyer, W.H., Pearlstein, L.D., Sartori, F., Walker, M.L., Welander, A.S., Wolfe, S.M., “Experimental Vertical Stability Studies for ITER Performance and Design Guidance,” *Nucl. Fusion* 49 (2009) 115003
- [Humphreys2015] D. Humphreys, G. Ambrosino, P. de Vries, F. Felici, S.H. Kim, G. Jackson, A. Kallenbach, E. Kolemen, J. Lister, D. Moreau, A. Pironti, G. Raupp, O. Sauter, E. Schuster, J. Snipes, W. Treutterer, M. Walker, A. Welander, A. Winter, L. Zabeo, “Novel Aspects of Plasma Control in ITER,” *Phys. Plasmas* 22 (2015) 021806
- [Izzo 2011] V.A. Izzo et al., *Nucl. Fusion* 51 (2011) 063032
- [Izzo 2015] V.A. Izzo et al., *Nucl. Fusion* 55 (2015) 073032
- [Izzo 2017] V. A. Izzo and P. B. Parks, *Phys. Plasmas* 24 (2017) 060705
- [Jackson 2015] G.L. Jackson, et al., *Nucl. Fusion* 55, 023004 (2015)
- [Jacquet 2016] P. Jacquet et al 2016 *Nucl. Fusion* 56 046001
- [Kessel 2015] C. E. Kessel Et Al., *Fusion Science and Technology* Vol. 67 JAN. 2015, <http://dx.doi.org/10.13182/FST14-794>
- [Kessel 2015] Kessel C.E. et al. 2015 *Fusion Science and Technology* 67, 1
- [King 2015] J.D. King, et al., *Phys. Plasmas* 22, 072501 (2015)
- [King 2017]: J.R. King, et al, *Phys. Plasmas* 24, 055902 (2017); J.R. King, et al., *Nucl. Fusion* 57, 022002 (2017)
- [Kleijwegt 2017] K. Kleijwegt, et al., “Disruption prediction using machine learning algorithms for DIII-D,” to be submitted to *Nuclear Fusion* (2017)
- [Kolemen 2014] E. Kolemen, et al., *Nucl. Fusion* 54, 073020 (2014)
- [Kolemen 2016] E. Kolemen, et al., “Transient-Free Operations With Physics-Based Real-time Analysis and Control,” 58th Annual Meeting of the APS Division of Plasma Physics (San Jose, Oct. 31-Nov. 4, 2016), abstract BAPS.2016.DPP.TO4.8
- [Kolemen2015] E. Kolemen, S.L. Allen, B.D. Bray, M.E. Fenstermacher, D.A. Humphreys, A.W. Hyatt, C.J. Lasnier, A.W. Leonard, M.A. Makowski, A.G. McLean, R. Maingi,

- R. Nazikian, T.W. Petrie, V.A. Soukhanovskii, and E.A. Unterberg, “Heat flux management via advanced magnetic divertor configurations and divertor detachment,” *J. Nucl. Materials* 463 (2015) 1186
- [Konovalov 2016] S. Konovalov *et al.*, 2016 Assessment of the Runaway Electron Energy Dissipation in ITER Preprint: 2016 IAEA Fusion Energy Conf. (Kyoto, Japan, 17–22 October 2016) IAEA CN-234-0321.
- [Kramer 2017] G.J. Kramer *et al.* 2017 *Nucl. Fusion* 57 056024
- [Kramer 2017] Kramer, G.J. *et al.*, 2017 *Nuclear Fusion* 57 056024
- [Labombard 2017] B. Labombard, *et al.*, *Nuclear Fusion* 57, 076021 (2017)
- [LaHaye 2010] R.J. La Haye, *et al.*, *Phys. Plasmas* 17, 056110 (2010)
- [LaHaye 2016] R.J. La Haye, *et al.*, Proc. 43<sup>rd</sup> EPS Conf. on Plasma Physics, (Leuven, Belgium, July 4-8, 2016), *Europhysics Conference Abstracts* 40A, P5.026 (2016)
- [LaHaye 2017] R.J. La Haye, “Forecasting electron cyclotron current-drive stabilization of neoclassical tearing modes in ITER,” *Proceedings of the 22nd Topical Conference on RF Power in Plasmas* (Aix en Provence, France, May 30-June 2, 2017)
- [Lanctot 2016] M.J. Lanctot, *et al.*, *Nucl. Fusion* 56, 076003 (2016)
- [Lanctot 2017a] M.J. Lanctot, *et al.*, *Nucl. Fusion* 57, 036004 (2017)
- [Lanctot 2017b] M.J. Lanctot, *et al.*, *Phys. Plasmas* 24, 056117 (2017)
- [Lazarus 1996] E.A. Lazarus *et al.*, *Phys. Rev. Lett.* 77, 2714 (1996)
- [Lehnen 2015] M. Lehnen *et al.*, *J. Nucl. Mater.* 463 (2015) 39–48
- [Liu 2015]: F. Liu, *et al.*, *Nucl. Fusion* 55 083026 (2015)
- [Liu 2017]: F. Liu, *et al.*, “Non-linear MHD simulations of QH-mode DIII-D plasmas and implications for ITER high Q scenarios”, accepted for publication in *Plasma Physics Controlled Fusion*, 2017
- [Logan 2016] N.C. Logan, *et al.*, *Phys. Plasmas* 23, 056110 (2016)
- [Luce 2014] Luce T.C. *et al.* 2014 *Nuclear Fusion* 54 013015
- [Marinoni 2009] A. Marinoni *et al.*, *Plasma Phys. Control. Fusion* 51, 055016 (2009)
- [Martín-Solís 2017] J.R. Martín-Solís *et al.*, *Nucl. Fusion* 57 (2017) 066025
- [McKee 2010] G. McKee *et al.*, *Rev. Sci. Instrum.* 81, 10D741 (2010)
- [Meneghini 2015]: O. Meneghini *et al.*, *Nuclear Fusion* 55 083008 (2015)
- [Meneghini 2016] O. Meneghini *et al.*, *Phys. Plasmas* 23, 042507 (2016)
- [Moyer 2017]: R. Moyer *et al.*, *Phys. Plasmas* 24 102501 (2017)
- [Najmabadi 2006] Najmabadi F. *et al.* 2006 *Fusion Engineering and Design* 80, 3-23
- [Okabayashi 2017] M. Okabayashi, *et al.*, *Nucl. Fusion* 57, 016035 (2017)
- [Pace 2016] D.C. Pace, *et al.*, 2017 *Nucl. Fusion* 57 014001

- [Pace 2017] Pace, D.C. *et al.*, 2017 *Nuclear Fusion* 57 014001
- [Park 2017] J.-K. Park and N. C. Logan, *Physics of Plasmas* 24, 032505 (2017).
- [Park 2017] Park J.M. et al. 2017 “Integrated modeling of high  $\beta_N$  steady-state scenarios on DIII-D”, in preparation
- [Park 2017a] J.M. Park et al, *Comput. Phys. Commun.* 214, 1 (2017)
- [Park 2017b] J. M. Park et al., submitted to *Phys. Plasmas* (2017)
- [Park 2017b] J. M. Park et al., submitted to *Phys. Plasmas* (2017)
- [Parsons 2016] M. Parsons, et al., “Application of the Disruption Predictor Feature Developer to developing a machine-portable disruption predictor,” 58th Annual Meeting of the APS Division of Plasma Physics (San Jose, Oct. 31-Nov. 4, 2016), abstract BAPS.2016.DPP.YP10.91
- [Paz-Soldan 2014] C. Paz-Soldan, et al., *Phys. Plasmas* 21, 072503 (2014)
- [Paz-Soldan 2015a] C. Paz-Soldan, et al., *Phys. Rev. Lett.* 114, 105001 (2015)
- [Paz-Soldan 2015b] C. Paz-Soldan, et al., *Nucl. Fusion* 55, 083012 (2015)
- [Paz-Soldan 2014] C. Paz-Soldan *et al.*, *Phys. Plasmas* 21 (2014) 022514
- [Paz-Soldan 2017] C. Paz-Soldan *et al.*, *Phys. Rev. Lett.* 118 (2017) 255002
- [Peeters 2007] A.G. Peeters *et al*, *Phys. Rev. Lett.*, 98, 265003 (2007)
- [Pericoli 2004] V. Pericoli Ridolfini, et al 2004 *Plasma Phys. Control. Fusion* 46 349
- [Petrie 2003] T.W. Petrie, et.al., *Nucl. Fusion* 43, 910 (2003)
- [Petrie 2009]: T. Petrie et al, *Nucl. Fusion* 49 065013 (2009)
- [Petrie 2017] Petrie, T.W. et al, 2017 *Nuclear Fusion* 57 086004
- [Petty 1999] C.C. Petty, T.C. Luce, *Phys. Plasmas* 6, 909 (1999)
- [Petty 2003] C.C. Petty, R. Prater, T.C. Luce, et al 2003 *Nucl. Fusion* 43 700
- [Petty 2016] C.C. Petty, et al., *Nucl. Fusion* 56, 016016 (2016)
- [Petty 2017] Petty C.C. et al. “Advances in the steady-state hybrid regime in DIII-D – A Fully non-inductive, ELM-suppressed scenario for ITER”, accepted for publication in *Nuclear Fusion* 2017
- [Pinsker 2010] R.I. Pinsker, et al., “Experiments on gas puffing to enhance ICRF antenna coupling”, EPS 2010, <http://ocs.ciemat.es/EPS2010PAP/pdf/O4.124.pdf>
- [Pinsker 2016] R.I. Pinsker, et al. submitted to *Nuclear Fusion* (2018), also paper EX/P3-22, IAEA FEC Kyoto 2016, preprint GA-A28396 (2016).
- [Piovesan] P. Piovesan, “Impact of ideal mhd stability limits on high-beta hybrid operation,” *Plasma Phys. Control. Fusion* 59 (2017)
- [Podesta 2014] M. Podesta, M. Gorelenkova, R. White, *PPCF* 56 (2014) 055003
- [Poli 2013] E. Poli et al 2013 *Nucl. Fusion* 53 013011

- [Prater 2014] R. Prater, C.P. Moeller, R.I. Pinsky, et al 2014 Nucl. Fusion 54 083024
- [Pustovitov 2011] V.D. Pustovitov, Nucl. Fusion 51, 013006 (2011)
- [Rea 2017] C. Rea and R. Granetz, “Exploratory Machine Learning studies for disruption prediction using large databases on DIII-D,” submitted to Fus. Sci. Technology (2017)
- [Reimerdes 2011] Reimerdes H. *et al.* 2011 Physical Review Letters 106, 215002
- [Reux 2015] C. Reux *et al.*, *Nucl. Fusion* 55 (2015) 093013
- [Salewski 2016] M. Salewski et al 2012 Nucl. Fusion 52 103008
- [Schuster2016] E. Schuster, et al, “Improved Reproducibility of Plasma Discharges via Model-Based q-profile Feedback Control in DIII-D,” Proc. 26<sup>th</sup> IAEA Fusion Energy Conference, Kyoto, Japan (2016) EX/P3-23
- [Shiraki 2015] D. Shiraki et al., *Nucl. Fusion* 55 (2015) 073029
- [Shiraki 2016] D. Shiraki *et al.*, *Phys. Plasmas* 23 (2016) 062516
- [Smick 2013] N. Smick, et.al., *Nucl. Fusion* 53, 023001 (2013)
- [Solomon 2007] W.M. Solomon *et al.*, *Plasma Phys. Controlled Fusion* 49, B313 (2007)
- [Solomon 2010] W.M. Solomon *et al.*, *Nucl Fusion* 51, 073010 (2011)
- [Solomon 2013]: W.M. Solomon et al, *Nucl. Fusion* 53, 093033 (2013)
- [Solomon 2014] Solomon W.M. *et al.* 2014 *Phys. Rev. Lett.* 113 135001
- [Staebler 2017] Staebler, G.M. *et al.* to be submitted to *Physics of Plasmas*
- [Stagner 2017] L. Stagner and W.W. Heidbrink, *Phys. Plasmas* 24, 092505 (2017)
- [Taylor 2018] N.Z. Taylor et al submitted to *Nuclear Fusion* (2018)
- [Terry 2008] P. Terry *et al.*, *Phys. Plasmas* 15, 062503 (2008)
- [Tobias 2016] B. Tobias, et al., *Phys. Plasmas* 23, 056107 (2016)
- [Todo 2014] Y. Todo et al 2014 *Nucl. Fusion* 54 104012
- [Todo 2016] Y. Todo et al 2016 *Nucl. Fusion* 56 112008
- [Turco 2012] F. Turco, et al., *Phys. Plasmas* 19, 122506 (2012)
- [Turco 2012] Turco F. *et al.* *Physics Plasmas* 19 122506
- [Turco 2015] F. Turco, et al., *Phys. Plasmas* 22, 022503 (2015)
- [Turco 2015] Turco F. *et al.* 2015 *Physics Plasmas* 22 056113
- [Turco 2016] F. Turco, et al., 2016 IAEA Fusion Energy Conf. (Kyoto, Japan, 17–22 October 2016), paper EX/P3-14.
- [Turco 2017] F. Turco, “Understanding the stability of the low torque ITER Baseline Scenario in DIII-D,” 59th Annual Meeting of the APS Division of Plasma Physics (Milwaukee, Oct. 23-27, 2017), abstract BAPS.2017.DPP.TI3.2

- [Van Zeeland 2014] M.A. Van Zeeland et al 2014 PPCF 56 015009
- [Van Zeeland 2015] M.A. Van Zeeland et al 2015 Nucl. Fusion 55 073028
- [Van Zeeland 2016] M.A. Van Zeeland et al 2016 Nucl. Fusion 56 112007
- [Van Zeeland 2016] Van Zeeland, M.A. *et al.* 2016 Nuclear Fusion 56 112007
- [Van Zeeland, 2008] M.A. Van Zeeland et al 2008 PPCF 50 035009
- [Vdovin 2013] V.L. Vdovin 2013 Plasma Phys. Rep. 39 95
- [Volpe 2015] F.A. Volpe, et al., Phys. Rev. Lett. 115, 175002 (2015)
- [Wade 2015]: M.R. Wade et al, Nucl. Fusion 55 023002 (2015)
- [Walker2017] Walker, M.L., “Enabling Co-Simulation of Tokamak Plant Models and Plasma Control Systems,” 11<sup>th</sup> IAEA Tech. Mtg. on Control, Data Acquisition, and Remote Participation for Fusion Research, Greifswald, Germany (2017); submitted for publication to Fus. Eng. and Design, May 2017
- [Wallace 2015] G.M. Wallace et al., “High field side launch of RF waves: a new approach to reactor actuators”, in Radio Frequency Power in Plasmas, AIP Conf. Proc. 1689, 030017, doi: 10.1063/1.4936482 (2015)
- [Waltz 2007] R.E. Waltz *et al*, Phys. Plasmas, 14, 122507 (2007)
- [Waltz 2011] R.E. Waltz *et al*, Phys. Plasmas 18, 042504 (2011)
- [Waltz 2014] R.E. Waltz and E.M. Bass, Nucl. Fusion 54, (2014) 104006
- [Wang 2015] Z.R. Wang, et al., Phys. Rev. Lett. 114, 145005 (2015)
- [Wang 2016] Z.R. Wang, et al., 2016 IAEA Fusion Energy Conf. (Kyoto, Japan, 17–22 October 2016), paper TH/P1-21.
- [Welander 2013] A.S. Welander, et al., Plasma Phys. Control. Fusion 55, 124033 (2013)
- [Welander2013] A S Welander, E Kolemen, R J La Haye, N W Eidietis, D A Humphreys, J Lohr, S Noraky, B G Penaflo, R Prater and F Turco, “Advanced control of neoclassical tearing modes in DIII-D with real-time steering of the electron cyclotron current drive,” Plasma Phys. Control. Fusion 55 (2013) 124033
- [White 2010] A.E. White *et al.*, Phys. Plasmas 17, 056103 (2010)
- [Wukitch 2004] S.J. Wukitch et al., Plasma Phys. Control. Fusion 46, 1479 (2004)
- [Yoshida 2017] M. Yoshida *et al.*, Nucl. Fusion 57, 056027 (2017)
- [Zhang 2017] W. Zhang et al 2017 Nucl. Fusion 57 056042



### 3. SCIENTIFIC BASIS FOR A FUSION BOUNDARY SOLUTION

A major challenge facing the design and operation of future high-power steady-state fusion devices is developing boundary solutions for expected order-of-magnitude increases in power handling capability relative to present experiments, while having acceptable PFC surface erosion to ensure adequate reactor lifetime. Specifically, these solutions require: 1) divertor target surface heat load:  $q_t \leq 10 \text{ MW/m}^2$ ; and 2) divertor target plasma electron temperature:  $T_t \leq 5 \text{ eV}$  across the entire target, to suppress erosion [e.g., Stangeby 2011], and 3) compatibility with high-performance core plasmas. The ITER divertor is expected to meet the surface heat load requirement, with divertor plasma  $T_e \leq 5 \text{ eV}$  near the strike point, though  $T_e$  will remain high elsewhere on the target. These requirements may pose additional challenges for long-pulse AT scenarios, e.g., for the FNSF [Garofalo 2014] and CFETR [Chan 2015], which also seek efficient current drive, pushing to normalized Greenwald density fraction  $n_e/n_{GW} \sim 0.5$ , in contrast to  $n_e/n_{GW} \sim 1$  for ITER.

In response to this challenge, DIII-D has placed increased emphasis on the plasma-material interface, or plasma-material interactions, also known as PMI, to evaluate boundary/PMI solutions applicable to next step fusion experiments beyond ITER.

#### Develop Key Divertor Design Concepts and Validate Models

The goal of advanced divertor development is to maximize the volume available inside the TF coils to produce fusion power while minimizing the volume and complexity of the systems needed to handle the power and particle exhaust. Radiative dissipation maximally spreads the heat load, while detached divertor operation minimizes surface erosion by elimination of the plasma sheath at material surfaces. The configurational flexibility of DIII-D, coupled with a comprehensive set of divertor diagnostics, provides a unique opportunity to identify key physics and design parameters that maximize radiative dissipation and detachment, while testing simulation codes. During the next five years, the DIII-D Boundary Program plans to carry out

- Staged modifications to the divertor structure to optimize closure for the control of neutrals,
- Systematic variation of the divertor magnetic configuration to control the detachment front,
- Diagnostic enhancements to better resolve the physical processes governing detachment, impact on material erosion, and the mediating role of the SOL and edge pedestal, and
- Rigorous application of numerical simulation for designing experiments, diagnostic interpretation, and data analysis.

DIII-D will first leverage the present SAS prototype divertor experiments to inform the design and operation of a new upper divertor (SAS-2U) for power and particle control (pumping) in high-performance core/pedestal plasma scenarios. Then the advanced divertor concepts will be integrated with advanced tokamak operation by upgrading the lower divertor (SAS-2L) toward the end of the 2019-2024 five-year period. In addition, DIII-D will further explore advanced magnetic configurations, including the Snowflake divertor (SFD) and X-Divertor (XD), with enhanced capability to independently control two X-points in the divertor region, as well as the coupling between divertor closure and advanced magnetic configurations. These approaches are necessarily coupled to some degree, but the proposed staged approach and use of two separate divertors in a single tokamak will provide a clean and well-diagnosed comparison with simulation unobtainable by other means. The proposed research will also couple advanced divertor development with reactor-relevant plasma-facing material (PFM), in particular, to address power exhaust in a W slot divertor while minimizing impact on core. Coupling of SAS with W target will enable DIII-D to make unique contributions toward core-edge integration in a reactor-relevant divertor environment.

### **Evaluate Reactor-Relevant PMI Solutions**

PMI remains a major challenge for successful operation of fusion reactors. Reliable, long-lived PFCs must be developed for next step devices and are a universal challenge to fusion energy, regardless of confinement concept. DIII-D plans to study the impact of the tokamak boundary plasma on advanced materials and to evaluate the impact of materials on the confined plasma. Close collaboration with linear materials testing facilities provides integrated systems testing of candidate materials and components from inception to utilization, including exposure to off-normal plasma events and a broad spectrum of plasma energy and particle-fluxes.

DIII-D is preparing to address the PMI challenge by providing a flexible, well-diagnosed environment for materials evaluation and integrated testing. DIII-D has been focusing on local PMI studies on erosion, redeposition and plasma-surface evolution of different PFMs, including both Mo and W, using the unique experimental capability of DiMES and MiMES in DIII-D. This is greatly facilitated by DIII-D's carbon PFCs since high-Z materials are truly trace elements. In the 2019-2024 five-year period, DIII-D is proposing increased emphasis on the following:

- Understanding the mitigation of high-Z PFMs and their impacts on high performance tokamak operation,
- Understanding surface evolution under plasma loading, focusing on PFM erosion, redeposition and surface morphology evolution,

- Evaluating reactor-relevant PFMs by characterizing their intrinsic properties such as conductivity, erosion/redeposition, and fuel retention/permeation in realistic fusion environments.

DIII-D will continue local PMI studies to understand surface evolution and evaluate new PFMs leveraging the unique DiMES facility in the divertor, and a new WITS in the main chamber, complementing DiMES in the divertor. In addition, DIII-D will evaluate the impact of high-Z target PFMs in advanced divertors by incorporating two or more W rings inside SAS 1 and SAS 2U divertors to determine W sourcing and leakage from different divertor locations, and assess compatibility with high performance AT operational regimes. Finally, converting SAS 2U into a full, heated W divertor toward the end of the five-year plan period would provide an opportunity to develop integrated divertor/PMI solutions for advanced tokamaks in a W-equivalent divertor environment.

### **Advance Scientific Understanding and Predictive Capability**

Achieving this goal requires a coordinated effort between experiment and modeling to validate predictive physics models and design codes, since the complexity and reach of integrating design choices into a capable divertor and PFCs for fusion lies well beyond the capability of simplified models or empirical scaling relationships. Progress requires efficient platforms for conducting simulation, and state-of-the-art tools for comparing data and simulation. DIII-D provides a capable platform for conducting research, because of its comprehensive diagnostic set, flexible divertor geometry, and wide range of boundary plasma parameter space [Buttery 2015]. Advancing scientific understanding and validating complex simulation codes for use in divertor and PFC design activities requires a systematic approach encompassing both targeted diagnostic development and plasma parameter scans, as well as systematic tokamak modifications. The latter is essential in the design of clean experiments to calibrate simulations and quantify the key physical processes governing radiative dissipation and plasma detachment (e.g., differentiate the effect of neutral reflection/trapping from magnetic flux expansion).

The boundary model validation program emphasizes the following three critical facets:

- Dissipation of energy and parallel momentum (pressure) from the mid-plane to the divertor target, through atomic, molecular and neutral-ion physics,
- Particle transport through parallel flow and cross field drifts in the divertor/SOL, and radial transport of energy and particles throughout the boundary plasma,
- PMI setting boundary conditions for the SOL and divertor plasma.

DIII-D plans to advance scientific understanding and validate complex simulation codes for use in divertor and PFC design activities by taking a systematic approach encompassing both targeted diagnostic development and plasma parameter scans, as well as systematic tokamak modifications in the next five years, as described above. The latter is essential in the design of clean experiments to calibrate simulations and quantify the key physical processes governing radiative dissipation and plasma detachment (e.g., differentiate the effect of neutral reflection/trapping from magnetic flux expansion). Experiments in DIII-D utilize two divertors and a flexible control system allowing independent operation of each, consistent with different divertor configurations. This provides direct divertor comparisons in a single device, in a configuration compatible with AT operation. DIII-D expects that these efforts will lead to experimental and model evaluation of advanced divertor/PMI solutions for developing a scientific basis for next-step steady-state fusion devices.

In concert with research on existing tokamaks and proposed linear facilities, the activities described in Sections 3 and 4 can form the basis for a national ***Boundary Science Research Program*** for the US that can address the key challenges for tokamak power and particle control in a timely and very cost effective manner. The operational and configurational flexibility, highly capable operations staff, highly collaborative research environment, comprehensive data analysis infrastructure, and relatively easy diagnostic access available to US scientists make this an attractive option for the US Fusion Program. Existing tokamaks, enhanced by proposed capability improvements, can access the relevant geometry, parameters, and physics governing the tokamak edge, scrape-off layer (near and far), and divertor regions needed for model development and validation. The report from the *2015 Fusion Energy Sciences Workshop on Plasma Materials Interactions Report* identified four high-level scientific questions which can be addressed in existing facilities:

1. What are the physics mechanisms of divertor dissipation, detachment, stability and control?
2. What are the effects of divertor magnetic topology, geometry and materials, including solid and liquid?
3. What are the physics mechanisms underlying Near SOL heat flux width and its scaling?
4. How can we extrapolate to reactor regimes?

Towards these ends, the report advocated a strong US program developing fully predictive models for near-SOL physics and divertor dissipation/detachment. Developing and testing these models must address topics common to all divertor concepts, such as near/far SOL transport (neutrals, impurities, and fuel ions), collisional-radiative processes, sheath physics, neutral recycling, and surface sputtering, which can be accomplished most rapidly by fully exploiting and upgrading existing divertor experiments and leveraging participation in overseas experiments. In this way, a

strong national *Boundary Science Research Program* within the US would be ready to take full advantage of the large extension in divertor operating space provided by ITER or possible future divertor test tokamaks.

### 3.1 DIVERTOR DEVELOPMENT AND INTEGRATION

Development of a viable divertor solution for the control of the heat loading and erosion of the plasma-facing components is presently recognized as a major open issue for the development of fusion reactors. The need for advanced divertor solutions to efficiently dissipate heat from fusion reactors is critical because the maximum steady-state power load for PFCs is limited to  $q_t \leq 10$  MW/m<sup>2</sup> on PFC surfaces, while the undissipated power loads will be an order of magnitude higher. This will pose a challenge for long-pulse AT scenarios, such as an FNSF, which will have lower plasma density than ITER with a normalized Greenwald density fraction  $n_e/n_{GW} \sim 0.5$ , in contrast to  $n_e/n_{GW} = 1$  for ITER.

The configuration flexibility of DIII-D, coupled with a comprehensive set of divertor diagnostics, provides a unique opportunity to explore and quantify key divertor design parameters controlling divertor detachment and energy dissipation in a single device, and to validate models for extrapolation to reactor conditions. The research is divided into the following two thrusts:

**Optimization of divertor closure.** Development of advanced divertors requires effective use of neutral and impurity dissipation processes. Divertor targets and baffling need to be designed to promote reionization of recycled neutrals and sputtered impurities in the divertor, so the divertor power dissipation is maximized for a given volume, and particle fueling of the core is controlled. A new small-angle slot (SAS) divertor concept has been developed, using SOLPS 5.0/B2-EIRENE edge code, and early results are promising. SAS leverages strong synergy between a gas tight slot and a critical small angle target to enhance buildup of neutrals in the slot to achieve detachment at low plasma density, as required for non-inductive current drive in future steady-state tokamaks. The major focus in the 2019-2024 period is to test and further optimize the newly developed SAS concept on DIII-D. Development of SAS is staged: the present SAS-1 divertor is a research divertor to study the effectiveness of plasma “plugging” in the closed slot structure, while SAS-2 applies those concepts to power and particle control for high performance core/pedestal plasma scenarios, including double null (DN) ATs with SAS-2U (upper) and SAS-2L (lower) divertors. Specifically, the divertor closure research will address the following key issues:

- Optimize SAS to achieve detachment at low density: The proposed research will use model-based divertor modifications to optimize the shape of the target and baffle of SAS, and assess the interplay between divertor closure and magnetic configurations for the control of neutrals to facilitate divertor detachment.

- Improve particle control in SAS: Investigate the impact of in-slot pumping on divertor detachment to further optimize SAS for simultaneous control of divertor heat and particle fluxes. The research needs to optimize pumping efficiency in SAS and explore particle control techniques, compatible with high core performance, including both ITER-like single null (SN) and DN AT scenarios.
- Develop power and particle exhaust solutions for ATs with W divertor: The proposed research aims to address power exhaust in a W slot divertor while minimizing impact on core, which poses a serious issue with W operation facing in the modern fusion devices. Coupling of SAS with W target will enable DIII-D to make unique contributions toward core-edge integration in a reactor-relevant divertor environment.

**Optimization of magnetic configuration.** DIII-D features two divertors with a flexible poloidal field control system, enabling the exploration of various magnetic configurations. While both the single-null divertor shape and the double-null divertor shape have been proposed as candidates for advanced tokamaks, our focus will be on the opportunities (and drawbacks) arising from the double-null divertor (DND) approach. This proposal includes not only the possibilities offered by conventional DN shapes, but also opportunities presented with non-conventional DN shapes, particularly with regard to reducing divertor heat flux, controlling density, and maintaining high performance plasma metrics, leveraging the new SAS concept. Efforts will also be made to further examine non-conventional magnetic topologies, specifically the XD and SFD. The initial focus will be on adapting the XD and SFD shapes to conform to the DIII-D pumping and divertor baffling configuration, and then evaluating how well the plasmas perform under high performance radiative and non-radiative regimes. This will be primarily carried out with the lower divertor, while the SAS 2 in the upper divertor will play a major role in high performance DND plasma operation. The main goals for the magnetic configuration research program are as follows:

- Determine how the interplay between divertor closure, magnetic balance, and particle drift behavior affect high performance DN plasma metrics, particularly with respect to heat flux reduction, particle control, impurity entrainment, and achieving and maintaining acceptably high confinement.
- Assess the influence of each of the four divertor targets, including the SAS-2, and their synergistic effects on *overall* divertor performance (e.g., deuterium and impurity control) and, based on the findings, determine whether additional baffling at the three non-slot divertor locations is beneficial.
- Assess the prospects for the SFD and XD configurations to successfully operate under high power, fully-pumped radiating divertor conditions and determine their viability as alternatives to the conventional DN divertor-based approach in future tokamak designs.

### 3.1.1 Divertor Closure

*Physics Leads: H. Guo (GA), B. Covele (GA), T. Petrie (GA), A. Moser (GA), M. Shafer (ORNL), H. Wang (ORAU).*

Addressing power exhaust in tokamaks is presently recognized as a major open issue for the development of fusion reactors. The need for advanced divertor solutions to efficiently dissipate heat from fusion reactors is critical because the maximum steady-state power load for plasma-facing components (PFC) is limited to  $q_t \leq 10 \text{ MW/m}^2$  on PFC surfaces, while the undissipated power loads will be an order of magnitude higher. Such an advanced divertor design should feature (1) highly dissipative operation to mitigate surface heat load and erosion; and (2) controlled density, neutral fueling, and impurity influx compatible with high performance core plasma operation. These requirements will pose a special challenge for long-pulse AT scenarios, such as for an FNSF, which will have lower plasma density than ITER with a normalized Greenwald density fraction  $n_e/n_{GW} \sim 0.5$ , in contrast to  $n_e/n_{GW} = 1$  for ITER.

Development of advanced divertors requires effective use of neutral and impurity dissipation processes. Increasing divertor closure tends to access detachment at reduced density. DIII-D has demonstrated that the relatively more closed, upper divertor detaches at  $\sim 20\%$  lower main plasma density than the lower, open divertor in high confinement (H-mode) plasmas. Recently, a new small-angle slot (SAS) divertor concept was developed, using the SOLPS 5.0/B2-EIRENE edge code, predicted to achieve detachment at even lower plasma density, as required for non-inductive current drive in future steady-state tokamaks. A prototype SAS divertor is now being evaluated in DIII-D, and initial results are promising. DIII-D plans to further optimize the SAS divertor concept for the control of neutrals to achieve as efficient and complete energy dissipation as possible, consistent with the requirements of efficient current drive and robust high performance operation.

#### 3.1.1.1 Challenges and Impact

The goal of the DIII-D divertor closure research program is to provide experimental evaluations of the SAS divertor concept as a potential power handling solution for steady-state fusion reactors, as well as to provide data for validation of the models that are used to design the divertor configurations. The research program is focused on the following key challenges, which are further detailed in Table 3-1.

- ***Optimize SAS to achieve detachment at low density:*** The proposed research will use model-based divertor modifications to optimize the shape of the target and baffle of the SAS divertor, and assess the interplay between divertor closure and magnetic configurations for the control of neutrals to facilitate divertor detachment.

- **Improve particle control in SAS:** Investigate the impact of in-slot pumping on divertor detachment to further optimize the SAS for simultaneous control of divertor heat and particle fluxes. The research will aim to optimize pumping efficiency in the SAS and explore particle control techniques, compatible with high core performance, including both ITER-like single null and double null AT scenarios.
- **Develop power and particle exhaust solutions for ATs with W divertor:** The proposed research aims to address power exhaust in a tungsten slot divertor, while minimizing impact on the core. An option under consideration is the addition of heated tungsten targets to remove carbon deposits to aid in investigating the impact of changes in atomic physics.

The proposed research will take a staged approach to improve divertor configurations and validate codes in the next five years: (1) converting the upper main divertor into a pumped-SAS in 2020, based on model optimization and SAS tests with pressure gauges in the slot; (2) upgrading the lower divertor for core-edge integration studies with a double null SAS in 2022; (3) evaluating the impact of a high-Z target in the SAS, with the option of a heated divertor under consideration toward the end of the next five-year period. It is expected that these efforts will provide experimental and model evaluation of the SAS divertor toward developing a scientific basis for advanced divertor solutions in next-step devices.

**Table 3-1.  
Divertor Closure Research Challenges, Goals, and Upgrades**

<b>Challenge</b>	<b>Goals/Deliverables</b>	<b>Upgrades</b>
Optimize SAS to achieve detachment at low density	<ul style="list-style-type: none"> <li>• Optimize divertor closure and target shape to control neutral dynamics in SAS</li> <li>• Assess interplay between divertor closure and magnetic geometries</li> </ul>	<p><b>Hardware</b></p> <ul style="list-style-type: none"> <li>• SAS-1 W rings</li> <li>• SAS-2 upper (U) target/baffling</li> <li>• SAS-2U W rings</li> <li>• SAS-2 lower (L) target/baffling</li> <li>• SAS-2U heated W target (Option)</li> </ul> <p><b>Diagnostic</b></p> <ul style="list-style-type: none"> <li>• ASDEX (Hass) gauges</li> <li>• Fast thermocouples</li> <li>• Langmuir probes</li> <li>• Divertor bolometer chords</li> <li>• Filterscopes</li> </ul> <p><b>Modeling</b></p> <ul style="list-style-type: none"> <li>• SOLPS-ITER with drifts</li> <li>• OEDGE/DIVIMP</li> </ul>
Improve particle control in SAS	<ul style="list-style-type: none"> <li>• Optimize pumping efficiency in SAS</li> <li>• Achieve both heat and particle control for ATs</li> </ul>	
Develop power and particle exhaust solutions for ATs with W divertor	<ul style="list-style-type: none"> <li>• Demonstrate adequate power handling in a W divertor for high-performance core scenarios</li> <li>• Assess the impact of change in atomic physics associated with W on detachment in SAS with heated W targets (Option)</li> </ul>	

### 3.1.1.2 Research Plan

The research plan for divertor closure is organized according to the challenges and goals in Table 3-1. Fig. 3-1 provides a timeline for each challenge, research milestone, and hardware and diagnostic enhancement, which are needed to achieve these research goals.

Challenge	2019-20	2021	2022	2023	2024
<b>Optimize SAS to achieve detachment at low density</b>	Characterize SAS-1 detachment, power balance Design and optimize SAS-2U target w/ SOLPS	Explore SAS-2U detachment and coupling with magnetic configuration	Design and optimize SAS-2L w/ SOLPS	Explore SAS-2L w/ DN	
<b>Improve particle control in SAS</b>	Optimize SAS-2U pumping with SOLPS	Explore SAS-2U pumping w/ AT		Particle control w/ DN SAS	
<b>Develop power and particle exhaust solutions for ATs with W divertor</b>	Study W leakage in SAS-1 w/ W rings	Develop radiative divertor w/ impurity seeding in SAS-2U	Mitigate W leakage in SAS-2U w/ W rings	Impact of W surface properties on detachment in SAS-2U w/ heated W target (Option)	
<b>Hardware Improvements</b>	SAS-1 w/ W rings SAS-2U		SAS-2U w/ W rings SAS-2L	SAS-2U w/ heated W target (Option)	
<b>Diagnostic Enhancements</b>	Enhanced bolometer for SAS-1 and SAS-1 W rings	New diagnostics for SAS-2U: LPs, bolometer, filterscopes, ASDEX gauges	Extended diagnostics for SAS-2L (same as in SAS-2U)		

Fig. 3-1. Divertor closure research plan timeline.

#### Challenge 1: Optimize SAS to Achieve Detachment at Low Density

**Current progress.** The SAS divertor concept [Guo 2017a] has been developed using SOLPS 5.0/B2-EIRENE [Schneider 2006] to achieve detachment at relatively low plasma density with cold plasma extended over the target surface (Fig. 3-2), as required for non-inductive current drive in future steady-state tokamaks.

A prototype SAS divertor is now being evaluated in DIII-D. Previous DIII-D data show that the relatively more closed, non-SAS upper divertor detaches at ~20% lower main plasma density than the lower, open divertor target on the bottom shelf in high confinement (H-mode) plasmas [Moser 2016]. Initial tests of the prototype SAS have achieved divertor detachment at nearly 40% further density reduction compared to the non-SAS closed divertor, with cold plasma,  $T_e < 5$  eV,

extending over the entire target surface, as measured by the Langmuir probes under a high confinement plasma condition (Fig. 3-3).

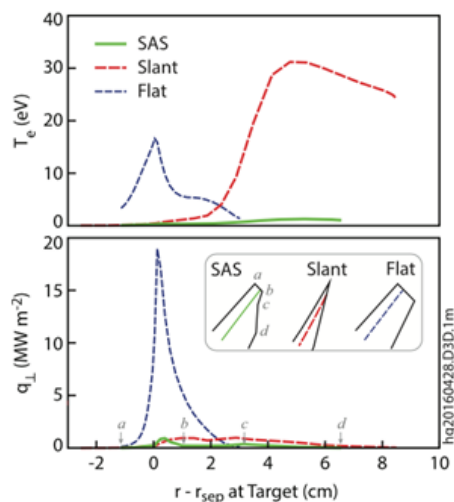


Fig. 3-2. SAS combines the benefits of horizontal and vertical targets in a slot divertor configuration. Radial profiles of  $T_e$  and  $q_{\perp}$ , the deposited power flux density across the divertor target surface at a given upstream separatrix density,  $n_e \sim 4 \times 10^{19} \text{ m}^{-3}$ , for the different slot divertors, predicted by SOLPS. From [Guo 2017a]

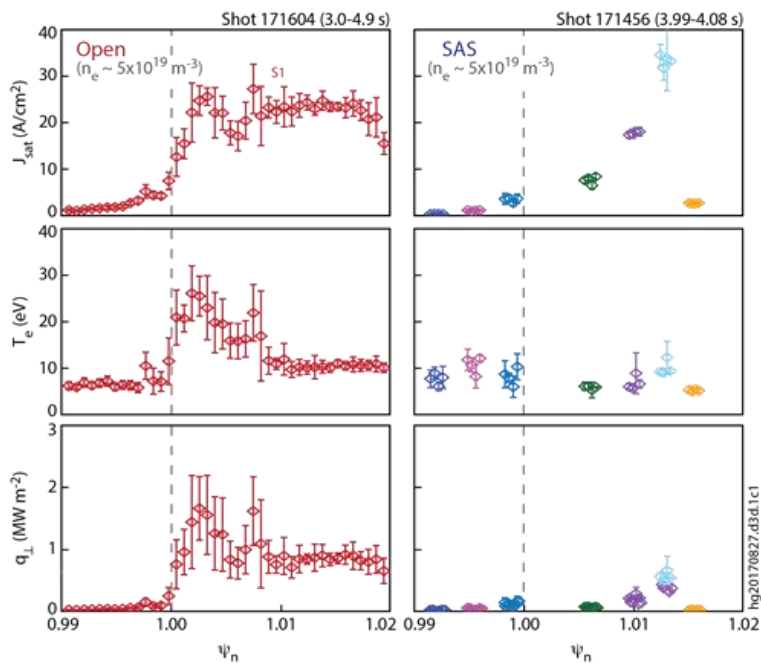


Fig. 3-3. SAS achieves cold plasma with strong heat flux reduction across the target surface. Profiles of  $J_{sat}$  (top)  $T_e$  (middle) and  $q_{\perp}$  (bottom) for the open divertor (left column) and SAS (right column) at the same line average density,  $n_{e,ave} \sim 5 \times 10^{19} \text{ m}^{-3}$ , as a function of the normalized magnetic flux function,  $\psi_n$ . Private flux region:  $\psi_n < 1$ ; separatrix:  $\psi_n = 1$ ; SOL:  $\psi_n > 1$ . The colors of the symbols indicate different probe locations as shown in [Guo 2017b].

Recent results from DIII-D have demonstrated reduced particle and heat fluxes to the target, facilitating detachment onset at 10-20% lower upstream density than an open divertor [Covele 2017]. SOLPS modeling suggests that this effect arises from the poloidal field flaring near the target, not merely due to the increase in total connection length. It was found that poloidal flaring must work synergistically with divertor closure to most effectively reduce the detachment density threshold. These promising results show that the coupling of the new SAS concept with advanced magnetic geometry may provide an effective means to address the challenge of divertor heat dispersal for steady-state fusion.

### Goal 1: Optimize divertor closure and target shape to control neutral dynamics in SAS.

Research will focus on optimization of the target shape in a closed slot divertor structure to improve neutral and impurity energy dissipation processes.

Optimization of the SAS divertor will require understanding dynamics of recycling neutrals. Modeling with SOLPS [Schneider 2006] will be the engine that drives this understanding, followed by experiments for model validation. It is apparent that greater neutral particle trapping near the divertor target due to closure can expand the operating window for detachment. The new SAS concept [Guo 2017a], in which the target is designed to build recycled neutral densities preferentially near the strike point, represents the beginning of such an effort. The prototypical SAS-1, already installed on DIII-D, will provide important experimental feedback for the more optimized, future SAS-2 divertor. The proposed research will optimize the following critical divertor parameters and validate models:

- ***Small field line-to-target angle***, directing recycling neutrals toward the separatrix, enhancing plasma cooling near the strike point, as in the conventional vertical target configuration, *e.g.*, in ITER.
- ***Progressive target flaring outboard of the strike point***, spreading neutrals into the far SOL, extending plasma cooling across the divertor target plate, in contrast to the vertical target where plasma remains hot in the far SOL, thus combining the benefits of both horizontal and vertical target configurations.
- ***Closed slot structure***, further enhancing neutral retention in the divertor. With the SAS configuration, the slot width would only need to accommodate the flux surfaces outside the separatrix within a *few*  $\lambda_q$  to reduce the leakage of neutrals from both SOL and private flux regions.  $\lambda_q$  scales as  $\sim 1/I_p$  independent of machine size [Eich 2013], which is  $\sim 2$  mm (at the outside mid-plane ) for an H-mode plasma in DIII-D with  $I_p \sim 1$  MA.

Changes to target recycling conditions, impurity species, and drifts can be expected to affect power dissipation, and will also be studied for target optimization.

**Goal 2: Assess interplay between divertor closure and magnetic geometries.** The purpose of this work is to explore the coupling between a slot structure and variations in magnetic geometry.

The proposed research will examine and optimize the coupling of SAS with different magnetic geometries for high core performance scenarios. In addition, research will explore the interplay between a closed slot structure and local magnetic flux expansion, in particular, near the divertor target, as in an XD configuration [Kotschenreuther 2004]. Efforts will be made to reduce the detachment density threshold with the addition of target flux expansion from an XD like configuration and SAS-like closure. In addition, research will examine potentially improved detachment stability with magnetic flaring near the target, and actively control the detachment

front to achieve maximize power dissipation in the divertor without affecting the pedestal and core performance.

## **Challenge 2: Improve Particle Control in SAS**

**Current progress.** The purpose of this research is to gain the capability to optimize pumping in SAS for simultaneous control of heat and particle exhaust in ATs.

SOLPS models found that SAS can achieve high levels of divertor performance by building up recycling neutrals, leading to unusually high neutral pressures in the slot, and revealed a remarkably strong and simple correlation between the D<sub>2</sub> molecular deuterium density,  $n_{D_2}$ , and the reduction in plasma temperature,  $T_e$ , at the target [Guo 2017a, Stangeby 2017]. This correlation is an entirely new discovery and is clearly central to the efficacy of the SAS divertor concept.

However, as SAS-2U will need to accommodate high-power, steady-state (AT) scenarios, suitable pumping capability will also be necessary for particle control, and this needs to be achieved without compromising the benefit of SAS for detachment. Therefore, new modeling in support of detachment facilitation will be accompanied by modeling in support of efficient neutral pumping, while minimizing impact on detachment. The Eirene kinetic neutral code will be used in combination with analytic calculations of conductance to design pumping concepts for SAS-2U appropriate for AT operation.

**Goal 1: Optimize pumping efficiency in SAS.** The purpose of this work is to provide adequate pumping for particle exhaust, while maintaining the benefit of SAS for detachment.

Localized neutral concentrations in the SAS slot may improve pumping efficiency, and thus greater global particle control. In order to optimize the SAS target shaping specifically for pumping, and identify the appropriate pumping location, kinetic modeling of the neutral dynamics will be critical, for which SOLPS's Eirene code [Reiter 2005] is suitable. Furthermore, understanding how pumping efficiency in the SAS divertor scales with power will be necessary for predictive modeling of particle control for high-power scenarios. The extent to which SAS divertor optimization for detachment and optimization for particle control are coincident will be ascertained; it is likely that many iterations of the SAS model and the divertor geometry will be necessary to balance the needs of heat flux control and particle control.

**Goal 2: Achieve both heat and particle control for ATs.** The primary objective of DIII-D divertor research is to develop a viable divertor solution for ATs, in particular for ATs with a double-null (DN) magnetic configuration with two outer divertors.

Research will be focused on the effect of top/bottom power balance in closed divertor systems. In addition, efforts will be made to explore the possibility of separately controlling power and

particle exhaust with DN. The use of DN, in particular, an unbalanced DN magnetic configuration may allow for strategically decoupling the particle and heat exhaust channels: an unbalanced DN can be used where one of the outer divertors is designed to take more of the power load than the other, while the gas pumping load and He ash removal would be divided oppositely. Thus, the divertor that required the stronger SAS effect would not have to be pumped as strongly.

Modeling will primarily employ SOLPS to carry out the design and optimization of SAS-2L. The present SAS design was done with SOLPS5.0, which employs a version of the EIRENE Monte Carlo neutral code that does not include neutral-neutral (n-n) collisions. The n-n collisions exhibit little influence on the divertor plasma conditions [Kotov 2008], although they can have a significant impact on divertor pumping, i.e., in the regions outside the plasma [Kukushkin 2011]. Further code analysis will be performed with SOLPS-ITER, including full classical drifts, n-n collisions, pumping, as well as extrinsic impurity seeding, to identify the sensitivity of the dissipative/detached divertor conditions to various input parameters such as the degree of magnetic balance for DN ATs.

### Challenge 3: Develop Power and Particle Exhaust Solutions for ATs with W Divertor

**Current progress.** Development of heat flux and particle control solutions in a W divertor environment appropriate for a high performance core is critical, and solutions are urgently needed.

Due to concerns over high erosion and tritium retention with graphite, there has been renewed interest in tungsten as a technologically mature, low-erosion, low-retention, highly conductive target material for a future fusion reactor [Pitts 2011]. From a plasma operations perspective, however, tungsten carries its own challenges for the divertor and the core. Main ion recycling by tungsten has recently been shown to result in a lower molecular fraction of the neutral population than graphite, Fig. 3-4 [Bykov 2017]; the reduction of the colder deuterium molecule source in the

divertor is likely to inhibit heat dissipation. Furthermore, unlike graphite, high-Z tungsten's eroded impurities do not radiate strongly in the divertor, further reducing divertor heat dissipation via radiation. Tungsten impurities which escape the divertor and enter the core, however, will radiate

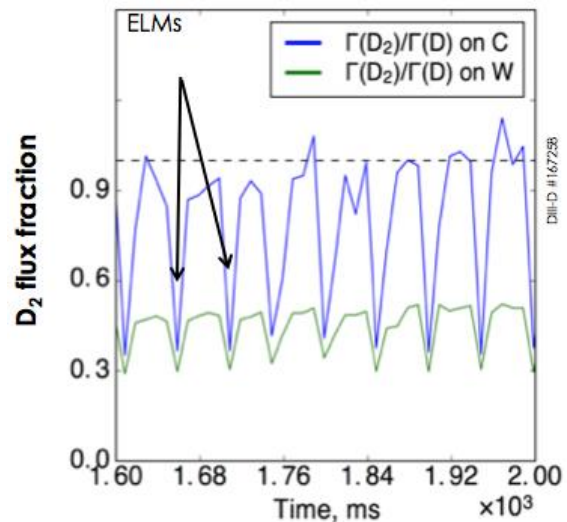


Fig. 3-4. *D and D<sub>2</sub> Recycling Exhibits a Strong Dependence on Plasma Facing Materials (C, W). Ratio of D<sub>2</sub>/D in recycling neutral fluxes on C and W target between and during ELMs in a H-mode discharge in DIII-D. From [Bykov 2017]*

strongly, which can result in lower H-mode energy confinement above a certain concentration [Romanelli 2013], thereby restricting access to high confinement scenarios.

DIII-D plans to develop integrated divertor/PMI solutions compatible with high performance core plasma scenarios with an emphasis on divertor optimization to mitigate impact of high-Z impurities. In particular, coupling of SAS with W target will enable DIII-D to make unique contributions toward core-edge integration in a reactor-relevant divertor environment.

**Goal 1: Demonstrate adequate power handling in a W slot divertor for high-performance core scenarios.** Research aims to address power exhaust issues with a W divertor for steady-state AT operation.

The SAS divertor's unique approach to closure can potentially address many of the challenges of tungsten targets, while retaining the benefits, thus offering a solution to accommodate tungsten plasma-facing materials compatible with core performance. In DIII-D to date, the intrinsic source of low-Z impurity radiation in the divertor has been the graphite target. For divertor operation with tungsten targets, (1) the divertor radiation fraction, *i.e.*, because of a lack of a carbon radiator, must be recovered by means of other extrinsic, low-Z impurities, and (2) high-Z intrinsic impurities must be sufficiently screened from the core. As SAS is specifically designed to encourage reionization and prompt redeposition of impurities, the SAS slot may also effectively provide the desired screening of tungsten impurities. Hence, the SAS configuration may enable new divertor operational scenarios in which tungsten becomes an attractive divertor material. Research will assess the effectiveness of divertor closure to screen high-Z impurities in SAS-1 and further optimize SAS-2U by incorporating toroidally continuous tungsten rings during the next five years, and determine the degree of detachment (*i.e.*, energy dissipation) needed to adequately reduce tungsten influx into high performance plasmas. This will require a detailed study of divertor/SOL screening for tungsten in highly dissipative divertor conditions with and without impurity seeding with nitrogen, neon, or argon.

**Goal 2: Assess the impact of changing atomic physics associated with tungsten on detachment in the SAS divertor with a heated tungsten target (Option).** The purpose of this work is to understand and optimize energy dissipation for divertor detachment in a metal-equivalent slot divertor. Research will emphasize understanding the impact of D/D<sub>2</sub> recycling on the carbon-free tungsten target compared to graphite for a common SAS divertor configuration. The full tungsten slot would uniquely enable study of the changes in the complex recycling conditions in the tungsten-equivalent closed slot. Achieving this goal will require heating the tungsten target in SAS-2U to remove carbon deposits from the main chamber walls, and preserve the integrity of clean surface conditions.

The results from the recent DIII-D metal rings campaign have demonstrated near-complete coverage of tungsten rings by carbon deposition except in close vicinity to the strike point. Carbon deposition on tungsten may be more severe in the high- $n_e$ /low- $T_e$  conditions typical within the SAS slot. Therefore, it is critical to heat the tungsten target to remove carbon deposits and preserve the high-Z surface characteristics. An ambitious divertor/materials collaboration with a SAS tungsten target is proposed as an optional research line for 2024 and beyond. Toward this end, research work will first quantify the temperature dependence of carbon coverage on a tungsten surface in high performance plasmas using the heated DiMES system on DIII-D. Efforts will also be made to assess the role of neutrals on detachment in the graphite SAS-1 and SAS-2U, and develop detachment control techniques in the presence of tungsten targets with dedicated campaigns in the next five years. This research work, coupled with modeling, would provide a physics basis for the design and operation of a full, heated tungsten divertor toward the end of the 2019-2024 proposal period.

### 3.1.1.3 Capability Enhancements

The DIII-D divertor closure research program requires staged divertor enhancements (Table 3-2). A new, optimized SAS in the upper divertor, SAS-2U, will have pumping capability to provide both power and particle exhaust for use with ATs. Both SAS-1 and SAS-2U will be integrated with toroidally continuous tungsten rings to evaluate tungsten sourcing and leakage with a closed divertor, and for development of detachment control with the tungsten target. The lower divertor will be upgraded, i.e., SAS-2L, to improve power and particle control in DN configurations, which will play a major role in high performance AT operation. Finally, a full, heated tungsten SAS-2U would enable DIII-D to advance divertor physics study in a W-equivalent wall environment and is an option under consideration. Diagnostics enhancements, as listed in Table 3-3, will provide critical information to identify the underlying physics mechanisms of divertor closure effects, and to validate models (Table 3-4) for extrapolation to fusion reactors.

**Table 3-2.**  
**Facility Enhancements for Divertor Closure Studies on DIII-D**

<b>Hardware Capability</b>	<b>New Physics</b>
SAS-1 w/ W rings	Impurity sourcing and screening with divertor closure
SAS-2U	SAS neutral trapping, divertor particle control with AT operations
SAS-2U w/ W rings	Detachment and control with W target
SAS-2L	Symmetric SAS neutral trapping/fueling, symmetric particle control with AT DN operations
SAS-2U heated W target (Option)	Molecular recycling and extrinsic impurity seeding on detachment dynamics in a W-equivalent closed divertor

**Table 3-3.**  
**Physics Enabled by New Diagnostics for Divertor Closure Research**

<b>Desired Measurement Capability</b>	<b>New Physics Enabled</b>	<b>Proposed Diagnostic</b>
Divertor total radiated power	Determine radiation in the SAS slot during detachment processes	Bolometer
Ion saturation current, $T_e$	Track plasma conditions at the SAS target with degree of detachment	Langmuir probe
Incident heat flux	Quantify power exhaust capability	Fast thermocouple
$D_\alpha$ , $D_\beta$ , $D_\gamma$ emissions, some carbon lines	Understand role of neutrals and impurities on detachment onset	Filterscope
Neutral pressure distribution	Understand neutral dynamics during the detachment process, determine optimal pumping location for SAS-2	ASDEX gauge
Atomic/molecular spectra	Create 2D maps of divertor radiating spectra, identify dominant power dissipators	2D imaging
2D $n_e$ , $T_e$	Create 2D maps of divertor plasma background, i.e. electron density and temperature	Thomson scattering
Surface temperature	Build target heat flux profiles for detachment assessment	IR camera

**Table 3-4.**  
**Codes Used for Divertor Optimization**

<b>Code</b>	<b>EP Related Purpose</b>
EFIT/CORSICA	Magnetic equilibrium generation/reconstruction for SAS experiment and modeling
SOLPS	Divertor detachment and neutral dynamics
SOLPS-ITER	Effect of drifts on detachment and particle transport
OEDGE/DIVIMP	W sourcing and transport

### 3.1.2 Magnetic Configuration

*Physics Leads: T. Petrie (GA), B. Grierson (PPPL), B. Covele (GA), H. Guo (GA), T. Osborne (GA), C. Petty (GA), F. Turco (Columbia U)*

Successful power-producing tokamaks of the future must be able to (1) access and maintain sufficiently high energy confinement, (2) have adequate fueling and impurity control, and (3) limit power loading at their divertor targets to acceptable levels. Simultaneously satisfying all three criteria for high power, high performance DN (and near-DN) plasmas in the present DIII-D vessel configuration has proved elusive. Analysis of the data over several experimental campaigns has indicated that the key impediments to achieving this “trifecta” are the relative openness of the

present DIII-D divertors, the degree to which the plasma is magnetically balanced (particularly near DN), and the problematic impact of particle drifts on particle control. Unless these impediments can be successfully negotiated, confidence in the DN concept and other non-conventional shaping concepts, such as the SFD [Ryutov 2007] and XD [Kotschenreuther 2007], as a basis for a future power producing reactor is diminished. By re-configuring the divertor baffling inside the DIII-D vessel for better particle control, by improving divertor and core diagnostics, and by validating the modeling needed to further improve the understanding of the key physical processes involved, DIII-D will explore the viability of these conventional and non-conventional approaches to future power-producing tokamaks.

The DIII-D team in cooperation with international collaborators has previously evaluated the contributions of particle drifts, plasma shaping, and divertor closure to energy confinement, fueling, impurity control, and heat flux reduction in DN and near-DN geometries, although these studies were done at lower power. At very high power input, the DIII-D team and collaborators have recently uncovered operating regimes that are very favorable to improved energy and particle confinement, although operating in these regimes can complicate successful heat flux reduction via a radiating divertor [Petrie 2017]. Such results have highlighted the difficulty in attempting to study plasma behaviors in the core, pedestal, and divertor in isolation and in the 2019-2024 five-year plan, all three regions will be considered more holistically (see Section 4). The overall objective of the plan is to extend present understanding to a level needed to successfully achieve the “trifecta” for high power, high performance DN plasmas.

### 3.1.2.1 Challenges and Impact

The goal of the DIII-D Magnetic Configuration plan is to provide a solid foundation for projecting promising plasma configurations and techniques to future high power, high performance plasma devices. In order to do this, the program focuses on three principal challenges (Table 3-5). First, it is essential to understand the complicated interplay of magnetic balance, divertor closure, and particle drifts on core and divertor plasma performance in DN and near-DN topologies. Second, as the program progresses, improved understanding of how fuel ions and impurity ions can be more effectively controlled would allow the team to identify (and perhaps install, if warranted) a more optimal reconfiguration of the in-vessel baffling. Third, it may be prudent not to lock the fusion program into a DN-based configuration before fairly testing out other promising alternatives that can also achieve high performance metrics.

The insight obtained from these studies, coupled with the confidence gained in validation of the codes used in the analysis, will be a major step in which approaches are plausible and which are likely dead-end for DIII-D and future high power plasma tokamaks.

**Table 3-5.  
Magnetic Configuration Research Challenges, Goals, and Upgrades**

Challenges	Goals/Deliverables	Key Capability Improvements
<p>1. Assess the interplay of magnetic balance, divertor closure, and particle drifts on core and divertor plasma performance in near-DN topologies.</p>	<ul style="list-style-type: none"> <li>• Use DIII-D shaping and diagnostic capabilities to quantitatively determine how <math>dR_{sep}</math> variation in upper-biased (“closed”) cases and separately in lower-biased (“open”) cases affects                             <ul style="list-style-type: none"> <li>(a) density and impurity control,</li> <li>(b) heat flux reduction,</li> <li>(c) sensitivity to detachment</li> <li>(d) preserving a favorable pedestal</li> </ul> </li> <li>• Validate SOLPS divertor modeling with data to establish/confirm the key physics involved in each case ---extrapolate to power tokamaks</li> </ul>	<p><b>Hardware Upgrades:</b></p> <ul style="list-style-type: none"> <li>• Significantly upgraded gas injection capability                             <ul style="list-style-type: none"> <li>- Various depths inside slot</li> <li>- Fast time response</li> <li>- Toroidal symmetry</li> </ul> </li> <li>• Centerpost baffling for the inner divertors, if needed</li> <li>• Additional baffling for the outer divertors, if needed</li> </ul> <p><b>Diagnostic Upgrades:</b></p>
<p>2. Explore the interplay between Slot (SAS-2U) target and non-slot divertor targets on overall divertor performance and the need for additional divertor baffling</p>	<ul style="list-style-type: none"> <li>• Assess the relative importance of each divertor target by controlling local plasma and impurity behavior</li> <li>• Determine the need for improved baffling at the non-divertor slot targets</li> <li>• Determine the impact of changing outer divertor strike point location within the slot on divertor effectiveness</li> </ul>	<ul style="list-style-type: none"> <li>• IR camera monitoring inner and outer targets of the upper divertor</li> <li>• Fast thermocouples to record power loading at each of the four divertor targets</li> <li>• Divertor bolometer arrays for both divertors</li> <li>• VUV SPRED for both divertors</li> <li>• Upper and lower divertor Thomson scattering</li> </ul>
<p>3. Assess the potential of the XD or SFD as an alternative to the conventional DN under high performance conditions</p>	<ul style="list-style-type: none"> <li>• Reconfigure the XD and SFD shaping for optimum particle and heat flux control using the available DIII-D divertor and pumping configuration</li> <li>• Make a systematic comparison of XD and SFD plasma performance with comparable DN plasma performance under both attached and detached conditions and evaluate the relative advantages and disadvantages of each</li> </ul>	<ul style="list-style-type: none"> <li>• Main ion temperature in the pedestal, SOL, and divertor</li> <li>• Penning gauges located in all three pumping plenums</li> </ul> <p><b>Code Development:</b> SOLPS with DN or near-DN grids with drifts</p>

No credible argument for a future power producing tokamak based on a DN configuration can be made unless the effects of changing divertor closure, magnetic balance, and particle drift behavior are taken into consideration and well understood. This is because reaching the “trifecta” of optimal high performance operation depends on how the divertor, pedestal, and core plasma behaviors respond to the changes in the three parameters. Thus, while the overall focus is primarily on the performance of the SAS-2 slot divertor, plasma and neutrals behaviors at the three other divertor targets in the DN will also be considered. The XD and SFD, both of which have previously shown promise in safely dissipating high levels of divertor heat loads while maintaining good plasma performance, are investigated from the standpoint of being credible alternatives to the DN.

Overall, successful completion of the 2019-2024 five-year plan will provide data not only useful in understanding the key divertor physics involved with high power AT-class plasmas on DIII-D, but also will provide a firmer basis for projecting to future divertor designs based on the DN concept, such as in a DEMO.

**3.1.2.2 Research Plan**

The proposed timeline is shown in Fig. 3-5.

Challenge	FY19-20	FY21	FY22	FY23	FY24
<b>1. Assess the physical processes that lead to an optimum combination of magnetic balance and divertor closure</b>	Assess the combinations of magnetic balance and closure that lead to favorable density and heat flux control	Explore detached high power DN H-modes	Application to high performance plasmas		
<b>2. Assess the coupling between slot (SAS_2U) and non-slot divertor targets on overall divertor performance and the need for additional baffling</b>	Evaluate density and impurity behavior at each divertor target Determine an optimal slot width	Explore high power AT with DN slot/non-slot divertors SOLPS analysis	Design additional baffling, incl oiwert divertor	Install baffling →	Assess AT DN in new configuration
<b>3. Evaluate the prospects for non-conventional topologies to operate successfully under pumped radiating divertor conditions</b>	Investigate the limitations of XD and SFD operation with DIII-D pumping/baffling		Design changes to baffling and pumping in the lower divertor to optimize XD and SFD performance	Install -->	Compare AT XD and SFD w/AT DN
<b>Hardware improvements</b>		SAS_2U Upgraded gas injection capability			
<b>Diagnostic enhancements</b>		High resolution divertor bolometry	Upgraded Spectroscopy		
		Increased IR camera	Fast thermocouple coverage		
		Upper and lower divertor Thomson scattering			
		Divertor ion temperature			
		Penning gauges			

Fig. 3-5. Magnetic configuration research plan timeline

Much of Challenge 1 dealing with tradeoffs between divertor closure, magnetic balance, and ion  $\mathbf{B} \times \nabla B$  direction is anticipated during the first two-three years. The results from this early phase will influence any subsequent changes in DIII-D divertor design in later phases. For this reason, experiments focusing on the effect of non-slot divertor targets on overall divertor performance and on the need for additional divertor baffling, are front-loaded. Much of Challenge 1 and 2 can be done in parallel with each other. Evaluating the prospects for the XD and SFD configurations as alternatives to the standard DN divertor shape has (relatively) less urgency, and so Challenge 3 is more evenly distributed across the research time line.

An upgraded gas injection capability is needed for properly executing Challenges 1 and 2 and thus is frontloaded in the program timeline. This is also the case for the other listed diagnostic upgrades, which will be discussed in subsequent sections.

### **Challenge 1: Assess the Interplay of Magnetic Balance, Divertor Closure, Particle Drifts on Core and Divertor Plasma Performance**

**Current progress.** For the conventional DN and near-DN topologies, previous studies have shown the degree to which divertor magnetic balance is a major consideration in determining how heat flux is distributed to the four active divertor targets [Petrie 2001], how effectively the main plasma is fueled [Petrie 2005], and how effectively an impurity species can be kept from contaminating the main plasma [Petrie 2008, Petrie 2009]. Separately, other studies have addressed the importance of divertor closure in moderating heat flux at and near the divertor targets, particularly by detachment [Moser 2016, Sang 2017]. The focus for this part of the program is to improve the team’s insight into how small changes in magnetic balance, divertor closure, and  $\mathbf{B} \times \nabla B$  direction can be leveraged into large changes in heat flux reduction and particle control and how the particle and heat flux scrape-off widths in the SOL are increased and decreased, respectively, as magnetic balance is approached. The desired outcome of Challenge 1 is an improved understanding of how slot divertors can be optimized to serve important multiple tasks: divertor heat flux reduction, particle inventory control, and impurity entrainment. Such understanding would impact not only future divertor designs on DIII-D but also provide a solid platform in the divertor design of future power-producing tokamaks, such as a DEMO.

The plasma shaping capability of DIII-D played an integral role in previous experiments that demonstrated how small changes in magnetic balance could simultaneously affect plasma behavior in the divertor, pedestal, and core regions in near-DND [Petrie 2003]. Fig. 3-6 (a), for example, shows that changing the magnetic balance parameter  $dR_{sep}$  from 0 (i.e., DND) to +1.5 cm (DND biased slightly upward) had measureable effects on both pedestal density (electron pressure) and

total stored energy, while Fig. 3-6 (b) also showed strong variation in  $D_\alpha$ -recycling over the same  $dR_{sep}$  interval.

Thus, the present DIII-D plasma control system will be satisfactory in fine tuning the shaping and magnetic balance that is needed to successfully execute this study. For comparing the open versus closed aspects of this study, DIII-D employs the relative openness of the lower outer divertor versus the closed nature of the upper outer (SAS 2U) divertor. Further modifications to the divertor closure are anticipated to take place during the course of the five-year plan, which would extend the closure study.

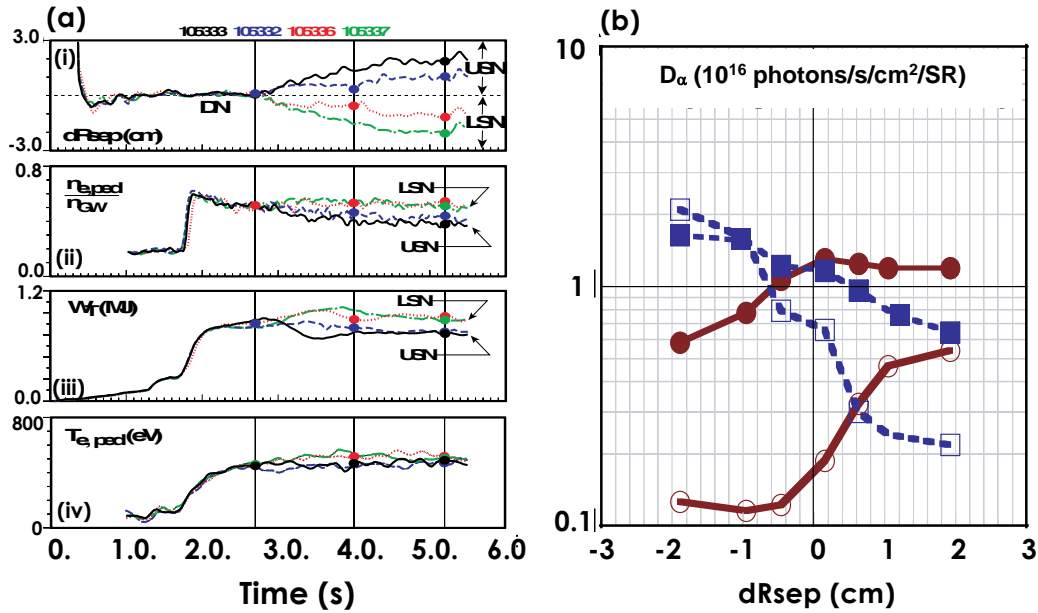


Fig. 3-6. (a) Pedestal and global parameter sensitivity to changes in magnetic balance; and (b) the recycling radiation ( $D_\alpha$ ) at the divertor targets is shown as a function of  $dR_{sep}$

**Goal 1: Determine how variation in divertor closure, magnetic balance and ion  $B \times \nabla B$  direction affect divertor and core performance.**

Preliminary experiments are proposed to document how changes in magnetic balance, divertor closure, and particle drift behavior affect plasma density control, impurity control, and divertor heat flux reduction, and secondarily how they affect particle and energy confinement in the core. The approach will use the existing DIII-D capability to actively pump particles in both the open and closed divertor configurations, as well as a significantly improved neutral gas injection capability, which allows deuterium and impurity injection from several poloidal and toroidal locations *within* the slot. The combination of having particle pumping at the divertor target and deuterium gas injected upstream (but still within the slot) is expected to generate a strong local plasma flow toward the divertor target, and would be beneficial to impeding impurity ions from

escaping into the main chamber, e.g., in a “puff-and-pump” scenario [Wade 1998]. The program will exploit the capabilities of new diagnostics, such as IR camera and fast thermocouples for determining divertor heat flux, divertor bolometer arrays, Penning gauges, and VUV SPRED for determining radiated power and impurity behavior inside the slot, along with divertor Thomson scattering and Langmuir probes for electron density and temperature inside the slot. Localized deuterium injection from *within* the slot is expected to not only lead to more effective entrainment of injected impurities but also better density control of the main plasma, as opposed to deuterium injection into the *main* chamber which is presently used in “puff-and-pump” experiments.

The diagnostics that will be available in DIII-D for this project, together with the methodologies developed over the past 15 years, will provide the wherewithal to also address a related issue, specifically dealing with how well impurities injected into the slot can be “entrained” in the slot as the outer leg begins to show signs of detachment. In this regard, particle flows in and around the slot that are generated by the presence **E** and/or **B** and the response of these flows to changes in slot width and variation in magnetic balance ( $dR_{sep}$ ) will be mapped out in detail.

Because the plasmas in this study are “high performance,” e.g.,  $\beta_N > 3$  and  $H_{98} > 1.3$ , maintaining favorable pedestal characteristics is also an important facet in this study. Recent experiments have shown that pedestal and core behavior may depend very sensitively on pedestal density and pressure at high power input [Petrie 2017]. Since the scans highlighted in the previous paragraph involve highly-powered DN plasmas in high temperature regimes which have not been fully explored, mapping out the response of plasma behavior in the pedestal and core during these scans is also an important part of goal 1. As Fig. 3-5 shows, much of this work in Challenge 1 (above) can be completed in the first two years of this plan.

## **Goal 2: Validation of SOLPS divertor modeling.**

Divertor modelling with sophisticated SOL transport codes, such as SOLPS or UEDGE, is absolutely essential for providing the theoretical framework needed in clarifying the physics mechanisms involved in the Goal 1 studies. Validating the modeling needed to help the team to identify the important physical processes involved in these high power, high performance plasma regimes will be a very challenging task due to the complex geometry and physics involved. Even state-of-the-art divertor codes like SOLPS and UEDGE have rarely attempted analysis of a magnetically-unbalanced DN configuration with particle drifts. The only attempt at modeling unbalanced DNs with drifts was done several years ago using the UEDGE code (Petrie, 2010) and this analysis was successful only in interpreting the available data in a more qualitative sense. Hence, whether one use SOLPS or UEDGE as the platform for modeling these data, a dedicated

effort by the team to improve the divertor analysis of unbalanced DN configurations with drifts must be undertaken immediately.

### **Challenge 2: Explore the Interplay Between Slot (SAS-2U) Target and Non-Slot Divertor Targets on the Need for Additional Baffling**

**Current progress:** The success of the present “closed” divertor and a future SAS-2 (2021) “slot” divertor in DN and near-DN also depends on how well the other divertor targets deal with particle influx and power loading. The SAS-2 encloses the upper outer divertor leg of a DIII-D DN; the upper inner-, lower outer- and lower inner divertors comprise the other three targets. The electric and magnetic fields that are present in the divertor and SOL plasmas play a major role in how particles (and the energy they carry with them) are distributed at the four divertor targets. While Challenge 1 is largely focused on issues related to SAS-2, DIII-D will also investigate how plasma behavior at the *other* three divertor targets may influence slot divertor performance, as overall divertor particle control. We expect that the results of Challenge 2 will also inform us as to whether additional baffling would be efficacious in particle control.

#### **Goal 1: Assess the relative importance of each divertor target in controlling fuel particles and impurities.**

While the slot structure in the primary divertor will be a crucial part in the future DIII-D program starting in 2021, successful *overall* divertor performance with the DN, particularly with regard to density control and heat flux reduction, will also depend on how particle and heat exhaust are dealt with at the other three divertor targets. Hence, it is important to determine plasma behavior at each of the three (non-slot) targets and how this behavior, in turn, can individually contribute to overall divertor performance.

An approach for determining the relative importance of each divertor target in overall deuterium and impurity control is to assess the degree to which deuterium and impurities accumulate at a given divertor target and the possibility of pumping these particles. For each selection of  $dR_{sep}$  and slot closure, the presence of deuterium recycling and impurity accumulation at each of the three non-slot divertor locations will be evaluated by spectrometer ( $D_{\alpha}$ , VUV-SPRED) and bolometer measurements. The effectiveness of each of the four divertor targets in pumping deuterium and impurities will be determined by exhaust measurements via ASDEX and Penning gauge techniques. Power loading at each target will be determined by IR cameras and fast thermocouple measurements. With this information, the relative importance of each divertor target to particle and heat flux control can be gauged. Since the ion  $\mathbf{B} \times \nabla B$  drift direction has been shown to be very important in distributing particles around the SOL and divertor, both ion  $\mathbf{B} \times \nabla B$  drift directions will be investigated [Petrie 2008, Petrie 2009].

**Goal 2: Determine the need for improved baffling at the non-slot divertor targets.**

With these data, the second stage of Challenge 2 focuses on identifying and understanding the key physics at each of the four divertor targets of the DN. This goal, however, is complicated by the fact that all four divertor targets are magnetically connected directly or indirectly via the SOL, so that individual divertor targets cannot be viewed in isolation. Sophisticated SOL transport code analysis (SOLPS) will be used to help interpret the data. Once the data from the above studies have been processed and the supporting modeling analysis completed, the team will exploit these results by proposing an improved divertor baffling/pumping configuration for the DIII-D divertor, if justified, that may include up to all four targets.

**Goal 3: Determine the impact of changing outer divertor strike point location within the slot on divertor effectiveness.**

While much of this plan is focused on magnetic balance, degree of divertor closure and particle drift behavior and their effects on density control, impurity control, and divertor heat flux reduction, the plan also exploits the DIII-D plasma shaping, pumping, and fueling capabilities to investigate how placement of the outer strike point *within* the slot affects particle control (both deuterium and impurity) and heat flux reduction, and how changes in target density, temperature, and radiated power in the divertor slot affect these results.

In addition, because of the closure in the SAS-2 divertor, it will be an excellent testing bed for providing insight into what an “optimum” closed divertor might require, specifically with regard to slot width. At pre-selected values of  $dR_{sep}$ , the plan is to effectively “change” the width of the slot by repositioning the outer strike point within the slot. The key metrics are: heat and particle flux behavior *outside* the slot and carbon sputtering behavior at and near the slot entrance (and its effect on the main plasma). From previous experiments, placing the outer strike point nearer to the pumping plenum lip on the low-field side resulted in significant carbon erosion at the slot lip, particularly for the high power considered in Challenge 2. The results here will determine the “minimum” slot width requirement to avoid significant erosion outside the slot.

Note that parts of the methodology used in Challenge 2 overlap parts of Challenge 1, so that some of the work in Challenge 2 can be done in parallel with Challenge 1. However, the focus in Challenge 2 is clearly different.

**Challenge 3: Assess the Potential of the XD and SFD as an Alternative to the DN Divertor Under High-Performance Conditions**

**Current progress:** SFD and XD topologies have shown considerable promise as an effective way of reducing divertor heat flux by changing the characteristic way that power is dissipated in

the divertor. Based largely on their greater poloidal flux expansion at their divertor targets and the longer parallel connection lengths of their field lines in their divertors in comparison with the DN, power flow into the XD [Kotschenreuther 2013] and SFD [Soukhanovskii 2012] is spread over a wider area in their respective divertors than in DNs, resulting in lower localized heating at their respective targets; the DN must use other means to avoid such damaging localized heating, e.g., radiating divertor. One major drawback to these two approaches has been in the difficulty in achieving adequate particle control, particularly under radiating divertor conditions.

**Goal 1: Reconfigure the XD and the SFD shaping for optimum particle and heat flux control.**

Focus is initially on adapting the XD and SFD shapes to the existing DIII-D divertor vessel configuration. The XD or SFD flux expansion is activated in the lower (primary) divertor, while the upper (secondary) divertor resembles a conventional “standard” divertor shape with pumping. The team plans to exploit this arrangement as a means for controlling heat flux and particle inventory in the XD and SFD: primary divertor dissipates a high fraction of the incoming power flow, while the secondary divertor provides the density control. Note that parts of the lower divertor may have to be re-configured to optimize XD or SFD high performance shapes, since plasma shaping requirements may result in the baffling around the lower divertor pumping plenum intersecting unacceptably high levels of heat flux in the SOL.

The potential for *further* divertor heat flux reduction by operating in a radiating divertor environment is the next step, which would be to identify the optimal location for impurity seed injection. Injection locations to be investigated include from the private flux region, from the divertor targets, and from the main chamber. Divertor conditions, e.g., electron temperature, would dictate the appropriate seed impurity that would be used.

**Goal 2: Systematic comparison of the XD and SFD plasma performance with DN performance under both attached and detached conditions.**

During the course of this study, the data may indicate that reconfiguring the lower divertor baffling and pumping may be beneficial in significantly improving particle control. If that is the case, any reconfiguring would occur in the latter half of the Five-Year Plan so as not to interfere with Challenges 1 and 2. The issue for successful SFD or XD operation to be studied will be particle control, specifically control over the injected seed impurities needed during radiating divertor operation. The main “knobs” for particle control will be the degree of magnetic balance and the direction chosen for the ion  $\mathbf{B} \times \nabla B$  drift; addition baffling (closure) may also be helpful, depending on the results from Goal 1. At this point, comparisons of the SFD and XD plasmas with comparable DN plasmas under high power fully-pumped radiating divertor conditions can be

carried out. If Challenge 3 is successfully completed, one or both of these alternative divertor configurations may provide additional options for consideration in future generation tokamaks.

### 3.1.2.3 Capability Enhancements

The hardware improvements recommended for these studies are described in Table 3-6. To achieve the scientific objectives discussed above will require some diagnostic upgrades, as described in Table 3-7. The SOLPS code (Table 3-8) will be one of the primary tools in interpreting the data from these studies; as discussed previously, one would expect a considerable effort is necessary for applying this analysis code to unbalanced DN, XD, and SFD plasmas when particle drifts are activated.

**Table 3-6.  
Hardware Improvements for Magnetic Configuration Studies**

<b>Hardware Capability</b>	<b>New Physics</b>
Upgraded gas injection capability	Improved understanding of impurity trapping inside a slot divertor
Additional baffling for centerpost and lower divertor baffling, if needed	Improved trapping of fuel and impurity particles at inner divertor and secondary divertor locations

**Table 3-7.  
Diagnostic Enhancements for Magnetic Configuration Studies**

<b>Scientific objective</b>	<b>Physics measurement</b>	<b>Diagnostic technique</b>
Understanding divertor heat flux behavior	Surface temperatures of divertor tiles	Infrared camera measurements
Understanding heat flux behavior inside a slot divertor	Spatially-resolved temperature variation along surfaces inside the slot	Fast thermocouple array
Understanding the role of radiated power inside the slot	Radiated power inside the slot	New divertor bolometer arrays for both divertors
Assessing the presence of impurities inside the slot and near the slot	Intensity of radiation from selected impurity wavelengths	VUV SPRED for both divertors
Characterizing plasma inside the slot divertor	Electron density and temperature	Upper divertor Thomson scattering
Assess changes in the ion temperature in the divertor and SOL under various scenarios	Ion temperature in divertor and SOL	Doppler spectroscopy
Assess the effectiveness of impurity pumping by the three divertor cryo-pumps	Impurity pumping rate at each divertor pumping location	Penning gauges

**Table 3-8.**  
**Simulation Codes Used**

<b>Code</b>	<b>Purpose</b>
SOLPS with DN grid with drifts	Understanding the plasma/neutrals dynamics in and around the slot divertor
SOLPS with XD grid with drifts	Understanding the plasma/neutrals dynamics dealing with particle exhaust
SOLPS with SFD grid with drifts	Understanding the plasma/neutrals dynamics dealing with particle exhaust

### 3.2 MODEL VALIDATION FOR BOUNDARY PLASMA SOLUTIONS

Validated models of the tokamak boundary plasma will be needed for the design of divertor configurations, plasma-facing components (PFCs), and operational regimes for next step burning plasma tokamaks. This is primarily due to the inability of existing tokamak facilities to simultaneously produce the plasma conditions and configurations that will be employed in these future tokamaks. In particular, the DIII-D boundary model validation effort is aimed at identifying and quantifying the important physical processes and plasma control parameters that control dissipation of divertor target heat flux while maintaining compatibility with core plasma operational scenarios. Validating models of the boundary plasma is a challenging task with multiple physics processes that are tightly coupled. To address this challenge, the boundary model validation program will utilize DIII-D's extensive diagnostic set and operational flexibility to isolate and individually test the relevant physics processes as implemented in the existing suite of boundary modeling codes. These models range from 2D fluid codes such as SOLPS, UEDGE and OEDGE, to codes such as BOUT++ and XGC that implement the more complex physics of neoclassical ion transport and turbulent driven transport. The boundary model validation program is organized along three critical aspects of the boundary plasma, 1) Dissipation of energy and parallel momentum (pressure) from the mid-plane to the divertor target, 2) Particle transport through parallel flow and cross field drifts in the SOL and divertor, and 3) Radial transport of energy and particles through turbulent processes in the boundary plasma.

Dissipation of plasma energy and momentum (pressure) is the primary requirement of a boundary plasma solution in future devices in order to ensure the integrity and lifetime of PFCs, particularly the divertor target. Models used in the design of future devices must quantitatively capture this dissipation for the appropriate upstream separatrix conditions to ensure compatibility with the core plasma operational scenario. Dissipation in the boundary plasma is accomplished by the atomic and molecular processes of radiative emission from hydrogenic fuel and intrinsic or seeded impurities and plasma interaction with recycling neutrals. Validating the rates of these

dissipative processes requires measuring the important radiative transmissions and the plasma density and temperature at which they take place. This will be accomplished by increased spectral coverage of emission lines in both the Vacuum Ultraviolet (VUV) and Near-Infrared (NIR) wavelengths while the local plasma conditions of  $n_e$  and  $T_e$  will be measured by Thomson scattering. Validating energy and momentum transport and dissipation from the mid-plane to the target requires measuring the additional parameters of ion temperature and plasma flow. Parallel energy transport through electron conduction can be inferred from Thomson scattering  $T_e$  measurements, while the convective contribution will be determined with plasma flow measurements from insertable probes and Coherence Imaging Spectroscopy (CIS) and new ion temperature ( $T_i$ ) measurements from probes and spectroscopy. Momentum dissipation, or pressure balance, also requires measuring  $T_i$  and plasma flow from the mid-plane to the divertor. Finally, these dissipative processes must be accurately scaled to reactor-relevant conditions of higher power. This will require improving the spatial coverage of power balance (bolometry and IR), spectroscopy and divertor Thomson measurements to higher triangularity configurations where high-power discharges can be run more stably.

Particle transport and the resulting plasma flow is another critical aspect of the boundary plasma. Plasma flow is important in energy and momentum transport as previously described. Plasma flow is also critical for understanding and predicting the transport of both intrinsic and seeded impurities. The viscous force from plasma flow into the divertor is a key factor in confining seeded impurities in the divertor and keeping them out of the core plasma to aid radiative dissipation. Plasma flow is also responsible for carrying material eroded from PFCs to other parts of the device. Plasma flow parallel to the magnetic field is driven by gradients in plasma pressure due to plasma sources and sinks and other factors. Validating models of parallel plasma flow requires measurements of plasma ionization sources and their sinks at the target plate and through recombination. Additional measurements of neutral pressure, ionization and recombination spectroscopy, and ion flux to PFCs with probes will be made to benchmark the models of plasma sources and sinks.  $T_i$  measurements to address pressure-driven flows will also be made. Plasma flow can also be driven perpendicular to the magnetic field by electric fields set up by several processes, including gradients in  $T_e$ , ion orbit loss and perpendicular viscosity. Testing models of these processes will include measuring the mechanisms responsible for the electric fields and the resulting gradients in plasma potential themselves. This will require increased coverage plasma  $T_e$  and  $n_e$  measurements from Thomson scattering and plasma potential measured by insertable probes. Improved measurements of plasma flow, including main ion CER and CIS will be used to determine how momentum is transported radially.

Radial transport of energy and particles is another key aspect of boundary plasmas for which improved models are needed. Fluid models of the boundary, such as SOLPS and UEDGE, typically use ad hoc radial transport coefficients that are chosen to achieve the desired plasma density and temperature gradients and the associated radial fluxes. This can be appropriate for interpreting existing experimental data and testing the code's models of dissipation and transport as described previously. However, without a physics basis for scaling, such ad hoc choices for radial transport will not provide predictive capability for future devices operating in different parameter regimes. A key consequence of SOL radial transport is the actual magnitude of the heat-flux width and power density flowing into the divertor. A boundary solution for a future device cannot be designed with confidence without an accurate description of the radial transport. The DIII-D program will develop key measurements of radial transport to guide and test development of codes that model the underlying physics mechanisms leading to radial transport. Radial transport in the SOL and divertor is thought to be primarily a consequence of turbulence driven by gradients and neoclassical transport from ion orbit loss. Models of turbulent transport predict a number of characteristics, including the turbulence-frequency spectrum, the radial scale length of turbulent structures, and the poloidal variation of the turbulence amplitude and turbulent driven fluxes. Measurements of these turbulence parameters will be obtained through diagnostic development of gas puff imaging, improved instrumentation for insertable probes, and turbulence measurements based on other diagnostic techniques, such as microwave scattering and beam-emission spectroscopy (BES).

Boundary plasma codes encompassing the physics described above have been developed and are maintained and upgraded by the larger international fusion community. The DIII-D program will coordinate its experimental efforts in this area with the community and institutions that are responsible for these codes, in order to provide the most relevant data to test and improve these codes. Properly designed diagnostics and experimental parameter scans can guide additions and improvements to models for more accurate prediction of boundary plasmas in future devices.

### 3.2.1 Divertor Dissipation

*Physics Leads: A. McLean (LLNL), M. Groth (Aalto U.), A. Jaervinen (LLNL), C. Lasnier (LLNL), C. Samuell (LLNL), J. Lore (ORNL), J. Canik (ORNL), A. Leonard (GA)*

A primary role of the divertor plasma is to dissipate the majority of the power exhausted from the core plasma before it can damage the divertor target plates. An accurate model for describing this dissipation is necessary for designing divertor configurations and operational regimes for future burning plasma tokamaks. The most critical aspect of such a model is accurate prediction of the upstream mid-plane main ion and impurity densities that are required for detached divertor plasmas that can dissipate most all of the exhaust power. The upstream densities are the most important parameters for compatibility with the core plasma scenario. Since multiple processes are involved in dissipation of power and momentum (plasma pressure) it is important to separately examine each of these processes in order to test and guide development of models that will be used for the design of divertors in future tokamaks.

DIII-D has played an important role in the international community in developing the concept of detached divertor operation for divertor target heat-flux control. DIII-D's contributions to this effort have included demonstration of detached divertor compatibility with high confinement in H-mode plasmas, direct measurements of low  $T_e \leq 5$  eV, required for significant recombination of plasma flux, the role of impurities for inducing divertor radiation and detachment, and the importance of parallel convective transport in the divertor. The proposed work is now aimed at verifying that these processes are accurately represented in the important boundary modeling codes.

#### 3.2.1.1 Challenges and Impact

The goal of this research program is to verify that the physics processes leading to divertor dissipation are accurately represented in boundary models, particularly for the 2D fluid codes (SOLPS, UEDGE, and EDGE2D) that are the workhorses for divertor experiment interpretation and future divertor design. Previous modeling efforts with these fluid codes have typically under-predicted the level of observed radiative dissipation by  $\sim 50\%$  when the model constrains the upstream mid-plane density profile to the experimental measurements [Groth 2011]. Alternatively the models can reasonably reproduce the observed radiation levels only if the upstream density is increased to 30% - 50% above the experiment. This research effort aims to identify the cause(s) of this discrepancy by isolating and separately verifying that each of the various dissipation processes are accurately represented in the models. The important physics processes for divertor dissipation are grouped in the three challenges, 1) Quantify any discrepancy in the modeling of energy and momentum dissipation due to atomic, molecular and neutral interaction, 2) Quantify any

discrepancy in models of parallel energy transport that can affect achievable levels of dissipation, and 3) Validate the model scaling of these processes toward more reactor-relevant conditions, particularly higher power densities.

Any discrepancies or inaccuracies in models that are uncovered in this research will be presented to the creators and maintainers of boundary plasma models so that they can be addressed. This should ultimately result in improved models and greater confidence in using these models for the design of future burning plasma tokamaks. Table 3-9 provides the divertor dissipation challenges, goals, and upgrades.

**Table 3-9.  
Divertor Dissipation Challenges, Goals, and Upgrades**

<b>Challenge</b>	<b>Goals/Deliverables</b>	<b>Upgrades</b>
Quantify discrepancies in physics models of energy and momentum dissipation due to atomic, molecular and neutral interactions	<ul style="list-style-type: none"> <li>• Measure discrepancies between experimental radiative emissivity from hydrogenic and impurity species, and 2D fluid models constrained by diagnostic measurements</li> <li>• Measure total parallel pressure loss from mid-plane to target and compare with fluid and kinetic models</li> </ul>	<p><b>Hardware</b></p> <ul style="list-style-type: none"> <li>• Improved auxiliary heating systems</li> <li>• Increased upper divertor closure with SAS-2</li> </ul> <p><b>Diagnostics</b></p> <ul style="list-style-type: none"> <li>• 2D divertor Thomson scattering</li> <li>• Extended divertor Thomson scattering for closed geometry</li> <li>• Increased spatial coverage of divertor EUV/VUV spectroscopy</li> <li>• Ly-<math>\alpha</math> imaging</li> </ul>
Quantify discrepancies in physics models of parallel energy transport	<ul style="list-style-type: none"> <li>• Compare 2D fluid models of conductive and convective contributions to divertor parallel energy transport with that inferred from experimental measurements of power balance, <math>n_e</math>, <math>T_e</math>, <math>T_i</math> and plasma flow</li> </ul>	<ul style="list-style-type: none"> <li>• Main ion temperature at the mid-plane and divertor</li> <li>• Additional filterscope line emission coverage</li> <li>• Coherence imaging spectroscopy for flow in closed geometries</li> <li>• IR camera upgrades in spatial resolution and calibration</li> <li>• Increased bolometry spatial coverage and resolution in upper and lower divertors</li> <li>• Additional fast neutral pressure gauges</li> </ul>
Test model scaling to reactor-relevant divertor conditions of high power density and neutral opacity	<ul style="list-style-type: none"> <li>• Evaluate scaling of detachment characteristics to highest available power and configurations with highest neutral opacity</li> </ul>	<p><b>Modeling</b></p> <p>Synthetic diagnostic capability for 2D models</p> <ul style="list-style-type: none"> <li>• SOLPS-ITER</li> <li>• UEDGE</li> <li>• OEDGE</li> <li>• XGCa</li> </ul>

### 3.2.1.2 Research Plan

The Divertor Dissipation research plan is organized according to the challenges and goals in Table 3-9. Fig. 3-7 gives the timeline for each challenge, research milestone, and the capability improvements necessary to achieve them.

Challenge	FY19-20	FY21	FY22	FY23	FY24
Energy and momentum dissipation	Measure hydrogenic atomic and molecular emission rates  Test models for hydrogenic emission against experiment  Measure total parallel pressure balance From mid-plane to target for model tests				
Parallel divertor energy transport	Measure conductive and convective contribution to parallel energy transport in dissipative divertor plasmas  Test fluid codes against experiment for achieving parallel Convective transport in divertor				
Scaling to reactor conditions	Measure detachment characteristics including onset requirements at high power.  Compare detachment characteristics in SAS-2 against open divertor detachment				
Hardware Improvements	Increased NBI and ECH power  SAS-2 upper divertor with improved diagnostics				
Diagnostic Enhancements	Extended spatial and spectral coverage Of UV emission  Main ion $T_i$ at mid-plane and divertor  Extended $n_e$ and $T_e$ coverage from Thomson scattering				

Fig. 3-7. Divertor dissipation plan timeline

### Challenge 1: Quantify Discrepancies in Atomic and Molecular Radiative Emission Rates

**Current progress.** Previous measurements in DIII-D have documented the important role of both impurities and the main fuel hydrogenic species in radiative dissipation in detached divertor plasmas [Fenstermacher 1997]. However, these radiative contributions have not yet been quantitatively and systematically compared to that predicted by 2D fluid modeling codes. It is therefore unknown to what extent any inaccuracies in the radiation rates employed in the models contribute to their under-prediction of radiative dissipation observed in experiment. For intrinsic and seeded impurities, comparison between experiment and modeling has relied on impurity emission in the visible wavelengths. The relationship between these measured rates of the upper-level transitions and the lower-level transitions in the UV spectral range where most of the radiative dissipation occurs becomes increasingly uncertain for the low values of  $T_e$  characteristic of detached plasmas. The rates of hydrogenic species emission is equally uncertain with numerous atomic and molecular processes that have not been systematically tested for their relative

contributions in experiment or modeling. To test the radiative emission processes and rates employed by the models it is therefore necessary to measure both the important radiating lines in the UV and the local  $T_e$  and  $n_e$  in the radiating region. DIII-D is uniquely equipped to carry out this task with its Divertor Thomson Scattering (DTS) diagnostic for local  $n_e$  and  $T_e$  measurements and the proposed upgrades for UV spectroscopic measurements.

Another potential mechanism for models to under-predict divertor dissipation for measured upstream plasma conditions is improperly describing parallel pressure balance.

In helium plasmas with simpler atomic physics, 2D modeling was able to reproduce the divertor radiative emission and plasma parameters, but only by raising the upstream mid-plane densities (and pressure)  $\sim 50\%$  above the experimental values as shown in Fig. 3-8 [Canik 2017]. As stated earlier, the upstream density is a critical parameter for constraining boundary plasma prediction of compatibility with the core plasma. An upstream separatrix value of  $T_i$  higher than  $T_e$  could account for this difference, and though main ion  $T_i$  has been measured a factor of 2-3 higher than  $T_e$  in L-mode plasmas, it has rarely been measured in H-mode. Additionally plasma simulations of DIII-D with the XGCa code have found that parallel pressure balance can be significantly affected by the off-diagonal elements of the pressure tensor [Churchill 2017]. DIII-D is well suited to address this issue with its high spatial resolution mid-plane Thomson scattering diagnostic, main ion CER measurements, mid-plane insertable probe, and extensive suite of divertor diagnostics.

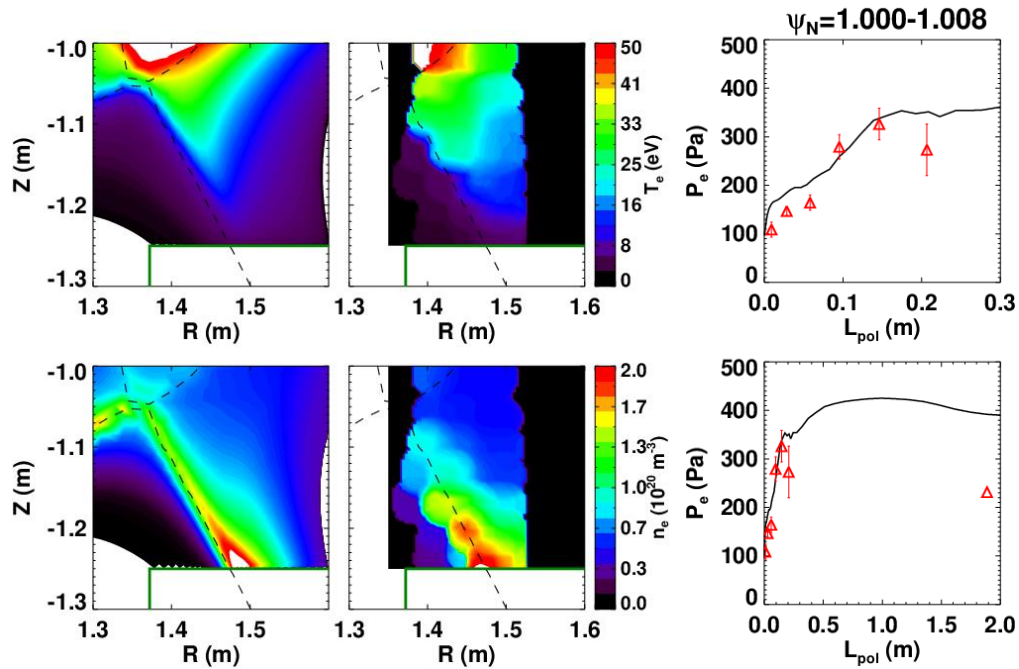


Fig. 3-8. Modeled and measured 2D profiles of divertor  $T_e$  and  $n_e$  in helium plasmas. Modeled and measured pressure profiles from the target to the mid-plane.

**Goal 1: Test atomic and molecular emission rates employed by 2D fluid modeling codes.**

Of primary concern are the emission rates of the hydrogenic atomic and molecular transitions. Descriptions of the multiple ionization, disassociation, and excitation processes are provided by the ADAS database through the EIRENE Monte Carlo code [Reiter 2005] coupled to the SOLPS fluid code and as a neutral fluid for the UEDGE code. A number of these rates are uncertain at the densities and low temperatures of detached plasmas. Quantitative measurements of these processes will be made by spectroscopic measurements in the appropriate wavelengths along with local measurements of  $n_e$  and  $T_e$  by DTS in the region of the emission source. These multiple processes lead to a complex emission spectrum with an example shown for the D2 Fulcher band in Fig. 3-9. While the spectrum of Fig. 3-9 required six repeat discharges for the Multichord Divertor Spectrometer (MDS), spectroscopic upgrades will allow this spectral region to be covered routinely. Additional measurements for constraining and testing the models will come from imaging the significant contribution of radiated power from Ly- $\alpha$  emission and the neutral density from additional fast pressure gauges.

To adequately constrain the SOLPS and UEDGE modeling for these tests, the radiative contributions from intrinsic and seeded impurities will be measured using the recently reinstalled divertor SPRED (divSPRED), which provides that capability with measurements in the extreme UV (EUV) wavelengths. Local measurements of local  $n_e$  and  $T_e$  provide interpretation of impurity density for further constraint of the modeling. With these measurement constraints SOLPS and UEDGE modeling will be probed with synthetic diagnostics in regions with the same  $n_e$  and  $T_e$  as measured by DTS for a direct comparison of emission rates between modeling and experiment.

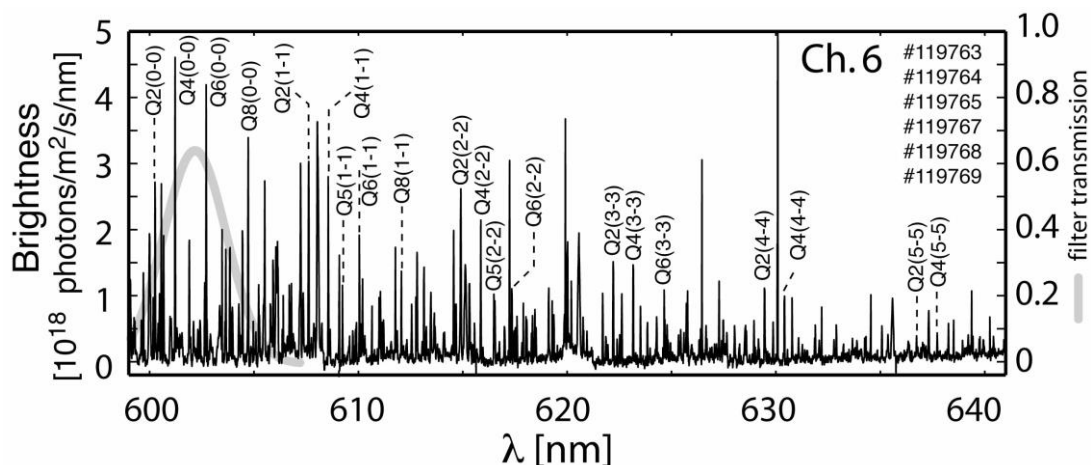


Fig. 3-9. Composite of D<sub>2</sub> Fulcher band emission taken in six separate plasma discharges [Hollmann 2006].

**Goal 2: Measure total pressure balance from mid-plane to target.** Pressure (momentum) dissipation from the mid-plane to the target is a critical factor in setting the mid-plane density required for highly dissipative divertor operation. The models will be tested for this process by measuring the main ion  $T_i$  at the mid-plane and divertor by a number of techniques. In the divertor, where the main and impurity ions are likely to be in thermal equilibrium,  $T_i$  will be assessed by extensions to Coherence Imaging Spectroscopy (CIS) of intrinsic carbon ions and potentially Retarding Field Analyzers (RFA) probes mounted at the target. For mid-plane measurements of  $T_i$ , main ion CER, as described in Section 4, will extend toward the separatrix. Additional measurements of  $T_i$  could also include an RFA probe installed on the mid-plane insertable probe diagnostic. These measurements will be used to test and constrain the 2D fluid models, and will also provide tests for the XGCa code which includes important kinetic and neoclassical physics.

### Challenge 2: Quantify Discrepancies in Physics Models of Parallel Energy Transport

**Current progress.** Parallel transport of heat flux through convection has previously been shown in DIII-D to play an important role in determining what fraction of the exhaust power can be effectively dissipated [Leonard 2012]. Parallel transport in the SOL and divertor is often assumed to be dominated by electron thermal conduction, thereby limiting the volume of plasma

with  $T_e \leq 5$  eV, the  $T_e$  range most efficient for radiative dissipation. Increasing levels of plasma convection relaxes  $T_e$  gradients in this critical temperature region, thereby increasing the total fraction of divertor heat-flux dissipation. In DIII-D, parallel convective transport inferred from power balance and DTS measurements was found to carry the bulk of the exhaust power in the region of low temperature as shown in Fig. 3-10. Additional, more direct measurements of plasma flow from Mach probes [Boedo 1998] and spectroscopy [Isler 1999] also indicated significant convective transport. While direct comparisons of this important transport

mechanism with divertor models have not yet been made, most modeling to date finds convection becomes dominant only for lower  $T_e$  below 10 eV. This research area will focus on quantifying this discrepancy in DIII-D highly dissipative divertor plasmas. Identifying the causes of this discrepancy and improving the models will be the focus of research on particle transport described in Section 3.2.2

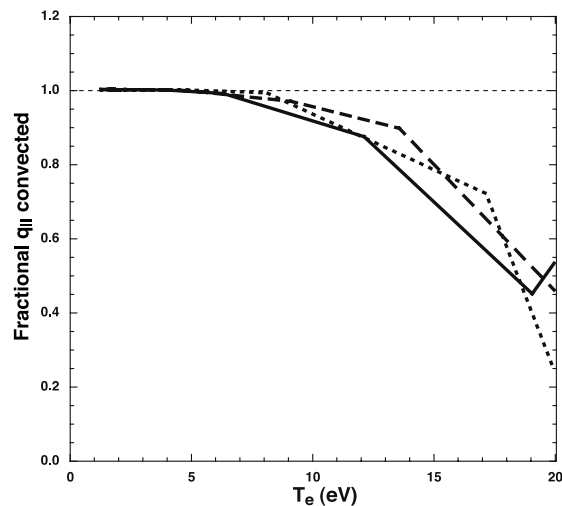


Fig. 3-10. Fraction of parallel heat flux transported by convection as a function of  $T_e$  in DIII-D divertor plasma.

DIII-D is well equipped to address issues with power balance measurements from bolometry and IR cameras and 2D profiles of divertor plasma parameters from DTS. Improved measurements of 2D flow from CIS and insertable probes will provide more direct assessment of convective transport.

**Goal 1: Quantify discrepancies in mechanisms of parallel energy transport.** Discrepancies between experiment and modeling of divertor parallel energy transport will be more routinely measured in order to determine to what extent they contribute to under-prediction of divertor radiation by models. Total heat flux flowing through the divertor will be measured by target plate heat flux measurements from IR cameras radiated power profiles from bolometry. The convected fraction of this power will be determined by subtracting the power carried by electron thermal conduction inferred from the  $T_e$  profiles measured by DTS. Confirmation of the convected energy flux will be made with direct measurement of plasma flow from the insertable divertor Mach probe and CIS measurements of the 2D profile carbon impurity flow velocity and  $T_i$ . Synthetic diagnostics for these same measurements will be developed for the SOLPS and UEDGE codes for careful comparison across a range of divertor conditions. The extent to which models fail to reproduce the experimental levels of convective transport will be evaluated for its contribution to the modeling codes' under-prediction of divertor radiation. Differences between experimental and model values of plasma flow will also serve to test the more general issue of particle transport throughout the SOL and divertor, as described in Section 3.2.2.

### **Challenge 3: Scaling Divertor Dissipation to More Reactor-relevant Conditions**

**Current progress.** Most previous DIII-D studies of dissipative divertor plasmas have been carried out in the lower open divertor at low-to-modest heating power levels. This has been due to the constraints imposed by the lower divertor configuration for optimal access to DIII-D's extensive diagnostic set. While the open divertor allows for flexible divertor configurations and excellent diagnostic access for 2D profiles, the open configuration also allows neutral recycling escape to the main chamber. In addition, the lower divertor configuration with good divertor diagnostic access can only tolerate moderate heating power due to the lower core plasma MHD stability limit of this configuration. Divertor density typically scales nearly linearly with power, since optimal divertor dissipation occurs at fixed  $T_e$ . However, dissipation processes scale nonlinearly with density, with radiation scaling as  $n^2$  for fixed impurity fraction and plasma recombination scaling as  $n^3$ . Higher power and plasma density also results in higher neutral density, such that the neutrals have a much shorter ionization distance compared to the spatial scale of the divertor. The higher collisionality at these densities also results in the neutrals behaving more like a fluid than ballistic particles. Finally, higher density can trap plasma radiation,

particularly Ly- $\alpha$ , making it harder to fully dissipate exhaust power. To ensure accuracy under these more reactor-like conditions, models should be tested at higher power and neutral densities, approaching that of burning plasmas. While higher power density dissipative divertor plasmas have been previously produced at ASDEX-Upgrade [Kallenbach 2015] and Alcator C-mod [Goetz 1999] they have not yet been studied with the extensive diagnostic coverage required to examine divertor transport and dissipation processes described earlier in this section.

DIII-D will examine divertor dissipation at high power and neutral densities by extension of diagnostic coverage to higher triangularity configurations in the lower divertor and the more closed SAS-2 divertor installation in the upper divertor.

**Goal 1: Extend divertor detachment studies to higher power and neutral densities.** Higher power and neutral density dissipative divertor plasmas will be examined by expanding divertor diagnostic coverage to new configurations. Operating tokamak discharges with high levels of auxiliary heating,  $\geq 10$  MW, requires core plasma configurations with high MHD stability limits. High triangularity configurations are typically employed to achieve stable discharges at high power and  $\beta$  without deleterious MHD instabilities. To diagnose divertor dissipation in the higher triangularity lower divertor configuration, a number of diagnostic extensions will be made. These include 2D Thomson scattering with new measurement locations as shown in Fig. 3-11, new bolometer chords to provide increased coverage and spatial resolution, and improved IR camera viewing optics. Making use of improved heating systems and the expanded diagnostics, the experimental scaling from low to high power will be compared with the 2D models. Important metrics for comparison are the mid-plane density at divertor detachment onset and total fraction of exhaust power that can be radiatively dissipated before formation of an X-point MARFE. Evidence for trapping of Ly- $\alpha$  radiation at high power and plasma density which can limit total power dissipation will also be looked for in experiment and modeling.

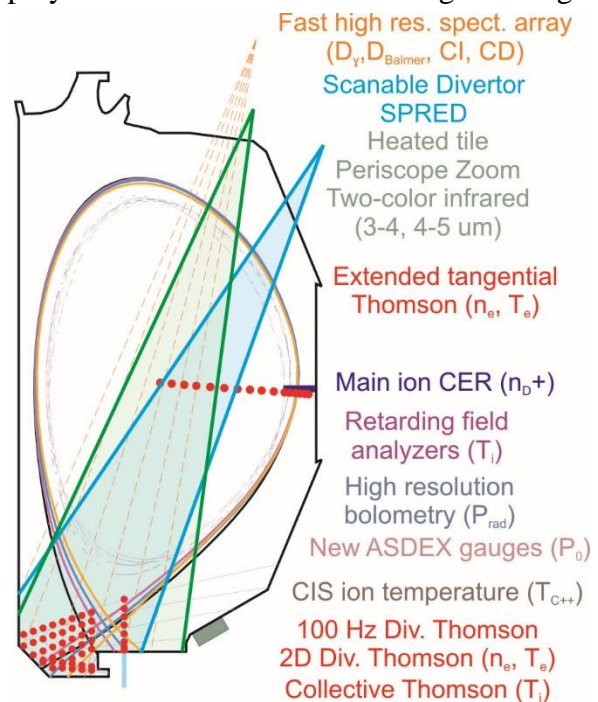


Fig. 3-11. Summary of diagnostics improvements proposed for study of dissipative physics in the DIII-D lower divertor.

Divertor transport and dissipation studies will also be extended to new upper divertor installation, SAS-2, as described in Section 3.1. Expanded diagnostic coverage in SAS-2 with 2D

Thomson scattering, bolometer, and IR camera coverage will allow for studies beyond divertor configuration optimization described in Section 3.1, to include basic physics of divertor dissipation in new regimes of higher neutral density. An important aspect will be to compare levels of convective transport and resulting power dissipation to determine how divertor closure affects particle recycling paths and plasma flow in the important radiating region of  $T_e \leq 5$  eV.

### 3.2.1.3 Capability Enhancements

The primary enhancements for divertor dissipation research will be through new diagnostic measurements and expanded spatial coverage and resolution for existing diagnostic techniques. The new measurements include that for quantifying the important contribution to radiation power with UV spectroscopy, Ly- $\alpha$  imaging. The ion temperature, a parameter poorly characterized in all SOL and divertor plasmas, will be measured with a variety of techniques including spectroscopy and probes. Expanded diagnostic coverage includes divertor Thomson scattering and additional pressure gauges. Facility enhancements will also provide capability to examine divertor plasmas in new parameter regimes. Improvements to the heating systems described in Section 2 will provide for higher power density divertor plasmas. The SAS-2 facility will provide a more closed divertor configuration for higher neutral densities.

**Table 3-10.  
Facility Enhancements**

<b>Hardware Capability</b>	<b>New Physics</b>
Increased heating power	Scaling divertor dissipation to more reactor like conditions
SAS-2 (pumped)	Test roles of neutral density for energy and momentum dissipation, and models of neutral opacity
	Full-power AT scenarios with optimized divertor for detachment and pumping for particle control

**Table 3-11.  
Physics Enabled by New Diagnostics for Divertor Dissipation Research**

<b>Scientific Objective</b>	<b>Physics Measurement</b>	<b>Diagnostic Technique</b>
Validate model radiation rates	Spectroscopic radiating constituents in the EUV and UV	Divertor SPRED
Plasma neutral interactions for momentum dissipation	Deuterium neutral density	Ly- $\alpha$ imaging, ASDEX gauges
Divertor convective transport	2D divertor flow profile	Coherence Imaging Spectroscopy
Scaling to reactor conditions	Plasma characterization in high power configuration	Expanded DTS measurements
Main ion contribution to pressure balance	$T_i$ in SOL and divertor	Impurity coherence imaging Main ion CER Collective Thomson scattering Reciprocating probe $T_i$
Sources and sinks for divertor	Neutral density	Divertor SPRED, Ly- $\alpha$ divertor imaging, pressure gauges

**Table 3-12.**  
**Codes Used for Divertor Dissipation Research**

<b>Code</b>	<b>Purpose</b>
SOLPS-ITER	Divertor/SOL fluid transport, ionization source Primary boundary modeling code for ITER simulation
UEDGE	Divertor/SOL fluid transport, ionization source Test models of energy and momentum dissipation Cross-compare results between multiple fluid codes
XGCa	Kinetic Monte Carlo codes for kinetic and neoclassical effects in full 2D geometry with separatrix
OEDGE	Interpretive divertor/SOL modeling, ionization source Test radiation and neutral transport models used in 2D fluid codes
OMFIT	Integrated modeling and experimental data analysis

### 3.2.2 SOL and Divertor Particle Transport

*Physics Leads: A. Jaervinen (LLNL), C. Samuel (LLNL), J. Boedo (UCSD), S. Allen (LLNL), A. Leonard (GA)*

Particle transport plays a key role in a number of aspects and overall performance of SOL and divertor plasmas. The divertor plasma characteristics affected by particle transport include in-out divertor asymmetries of particle density, temperature and radiation, and parallel energy transport in dissipative divertors, as previously described in Section 3.2.1. Particle transport, and particularly parallel plasma flow, can be responsible for long-range migration of intrinsic and seeded impurities as discussed in the following Section 3.3. Particle flux can also significantly affect the core plasma with divertor recycling representing the primary fueling source for the H-mode pedestal in existing devices and plasma flow at the separatrix providing a boundary condition for core plasma rotation. Therefore, it is critical to measure particle transport, both ions and neutrals, throughout the tokamak for interpretation of existing experiments and simulation capability for accurate prediction of particle transport in future devices.

Particle transport and plasma flow has historically been an important topic for the international fusion community. DIII-D has made significant contributions toward addressing this issue [Boedo 2011, Groth 2009, Roglien 1999, Groth 2005, Boedo 2016], including measurements of plasma flow profiles including impurity entrainment, and the importance of parallel plasma flow for increasing the fraction of exhaust power that can be dissipated in the divertor. Finally, DIII-D research on SOL and divertor particle transport is contributing to DIII-D pedestal transport research as described in Section 4.1.2. In the 2019-2024 five-year plan proposal, research on

particle transport is advancing to focus on the mechanisms that drive particle transport and develop predictive capability for particle transport and circulation throughout the plasma boundary.

### 3.2.2.1 Challenges and Impact

Plasma flows in the SOL and divertor have been measured and characterized across a range of conditions and configurations [Asakura 2007, Smick 2013, Boedo 2011]. However, boundary models have struggled to quantitatively reproduce many of the features of the plasma flow. In particular, 2D fluid models typically under-predict the strong SOL plasma flow toward the inboard divertor in H-mode in the favorable toroidal field direction,  $\mathbf{B} \times \nabla B$  toward the divertor [Groth 2009]. To uncover the source of such discrepancies and to test and improve models of the boundary plasma, the underlying mechanisms driving main ion and impurity particle transport must be examined and verified. The first challenge for this effort is to measure the 2D profile of plasma sources and sinks, i.e. from ionization source to recombination sink, and then verify the processes that drive transport from origin to destination. These include processes that drive plasma along field lines as well as perpendicular transport. Transport of impurity ions will be examined in a similar manner, but in this case the research on impurity transport will focus on verifying that the primary forces of the main plasma ions acting on impurities are properly represented in the models. The interaction of plasma flow between the core and SOL plasmas will also be examined as a mutual boundary condition affecting both regions. Finally, scaling particle transport and plasma flow with high power and more closed divertor configurations will be carried out to further test models toward more reactor-relevant conditions.

Measurement and understanding of particle transport in the boundary plasma has long been an impediment to interpretation of both core and boundary plasma experiments, as well as prediction of plasma behavior in future tokamaks. The increased understanding provided by this work will help address several critical issues for future burning plasma tokamaks including control of seeded impurities for power dissipation, long-range migration of material eroded from plasma-facing components and interaction between the SOL and core pedestal plasma.

### 3.2.2.2 Research plan

The SOL and Divertor Particle Transport research plan is organized according to the challenges and goals set out in Table 3-13. Fig. 3-12 gives the timeline for each challenge, research milestone, and the capability improvements necessary to achieve them.

**Table 3-13.**  
**SOL and Divertor Particle Transport Challenges, Goals, and Upgrades**

<b>Challenge</b>	<b>Goals/Deliverables</b>	<b>Upgrades</b>
Predict parallel and radial particle flux throughout the SOL and divertor	<ul style="list-style-type: none"> <li>• Test models of particle sources, sinks and pressure balance as drivers of parallel plasma flow</li> <li>• Measure <math>\mathbf{E} \times \mathbf{B}</math> driven radial particle fluxes for tests of boundary models</li> </ul>	<p><i>Hardware</i></p> <ul style="list-style-type: none"> <li>• Improved heating systems</li> <li>• Increased upper divertor closure with SAS-2</li> </ul> <p><i>Diagnostics</i></p> <ul style="list-style-type: none"> <li>• Coherence Imaging Spectroscopy (CIS) for improved coverage of plasma flow measurements</li> <li>• CIS for <math>T_i</math> with CIII</li> <li>• Ly-<math>\alpha</math> imaging</li> <li>• Mid-plane reciprocating probe for <math>T_i</math> measurements</li> <li>• Inner wall swing probes</li> <li>• Additional filterscope line emission coverage</li> <li>• Additional fast neutral pressure gauges</li> </ul> <p><i>Modeling</i></p> <p>Synthetic diagnostic capability for 2D models</p> <ul style="list-style-type: none"> <li>• SOLPS-ITER</li> <li>• UEDGE</li> <li>• OEDGE</li> </ul>
Quantify separatrix boundary conditions for SOL flow	<ul style="list-style-type: none"> <li>• Utilize <math>E_r</math> and toroidal rotation measurements to quantify separatrix boundary conditions for SOL flow</li> </ul>	
Validate impurity parallel transport models in the SOL	<ul style="list-style-type: none"> <li>• Measure main and impurity ion flows along with <math>T_i</math> profiles to test models of parallel impurity transport</li> </ul>	
Extrapolate understanding of SOL flow to more reactor-relevant conditions of high density and neutral opacity	<ul style="list-style-type: none"> <li>• Measure plasma flows with increased heating power and divertor closure for tests of model scaling toward reactor-like conditions</li> </ul>	

**Challenge 1: Predict Main-Ion Parallel and Perpendicular Particle Flux Throughout the SOL and Divertor**

**Current progress.** Insertable Mach probes on a number of devices have provided a consistent picture of SOL plasma flow in tokamaks, where in single-null configurations with the  $\mathbf{B} \times \nabla B$ -drift toward the active X-point, the SOL flow stagnates near the low field side (LFS) mid-plane, but then increases significantly from there toward both targets reaching Mach numbers of the order of 0.2 – 1 [Asakura 2007, Smick 2013, Boedo 2011]. Reversing the toroidal field has been observed to move the stagnation point toward the crown of the SOL, toward the inboard divertor, consistent with reversal of drift-driven redistribution of plasma flux in the SOL. 2D fluid models such as SOLPS [Schneider 2006], UEDGE [Rognlien 1999], and EDGE2D-EIRENE [Simonini 1994, Reiter 1992] have typically struggled to produce the same level of SOL plasma flow as observed in experiment, even with cross-field drifts included [Chankin 2009]. In a more analytic approach, the poloidal variation of SOL flow was found to be consistent with Pfirsch-Schlüter flows resulting from radial gradients in pressure and electric potential combined with particle balance in a toroidal

geometry [Asakura 2000, Chankin 2007]. However the overall level of plasma superimposed on this poloidal variation is typically under-predicted by the 2D fluid models [Groth 2009].

Challenge	FY19-20	FY21	FY22	FY23	FY24
Predict parallel and radial particle flux throughout the divertor	Determine 2D profile of particle sources and sinks Through interpretive modeling  Measure $T_i$ for determining pressure driven parallel flow  Measure 2D profile of $\mathbf{E} \times \mathbf{B}$ driven radial particle fluxes to determine contribution to particle balance				
Quantify separatrix boundary conditions for SOL flow	Measure flow shear between core and SOL plasma For testing models of perpendicular momentum transport				
Validate impurity parallel transport models in the SOL	Measure impurity parallel flow and its drivers, $T_i$ gradients and viscosity with main ion flow.  Test model prediction of impurity flow constrained by the experimental measurements				
Extrapolate understanding of SOL flow to more reactor-relevant conditions of high density and neutral opacity	Measure plasma flow profiles in plasmas with increased heating power  Measure plasma and impurity flow in closed SAS-2 divertor				
Hardware Improvements	Increased NBI and ECH power  SAS-2 upper divertor with improved diagnostics				
Diagnostic Enhancements	Additional pressure gauges, Ly- $\alpha$ imaging, inner wall swing probes  Main ion $T_i$ at mid-plane and divertor  CIS flow in closed divertor Extended $n_e$ and $T_e$ coverage from Thomson scattering				

Fig. 3-12. SOL and divertor particle transport plan timeline

To more fully test and isolate discrepancies between models and experiment, measurements of the complete profile of particle ionization sources and recombination sinks are needed. From there the models can be probed to test mechanisms that drive plasma from source to sinks. While particle recombination sinks can be reasonably assessed through ion flux measurements to PFCs with Langmuir probes and some contribution from recombination in the divertor plasma measured by spectroscopy, the 2D ionization profile has proved more difficult. An assessment of poloidal fueling through interpretive modeling using profiles measured in DIII-D (Fig. 3-13) found reasonable agreement with divertor diagnostics [Groth 2005]. However, such interpretive

modeling of ionization sources has only rarely been carried out due to the extensive diagnostic and modeling effort required.

Parallel plasma flow resulting from ionization and recombination is driven by total pressure balance where bulk flow ram pressure,  $n_i m_i v_i^2$  makes up for gradients in thermal pressure,  $n_i T_i$ . However, lack of main ion  $T_i$  measurements has prevented a comparison of such pressure-driven parallel flows between modeling and experiment. With the diagnostic improvements outlined in this proposal, such comparisons can be made.

The circulation of particles from source to sink can also be closed by radial transport. Radial and poloidal plasma flux due to  $\mathbf{E} \times \mathbf{B}$  drifts measured to carry as much as 50% of the outboard ion flux to the inboard divertor [Boedo 2000] has also been modeled with similar levels of plasma flux [Jaervinen 2016]. This level of flow can have significant impact in the overall circulation of particles within the boundary and core plasma. DIII-D has the diagnostic tools to constrain models and verify the processes that give rise to these  $\mathbf{E}$ -fields, including plasma temperature gradients and sheath potential.

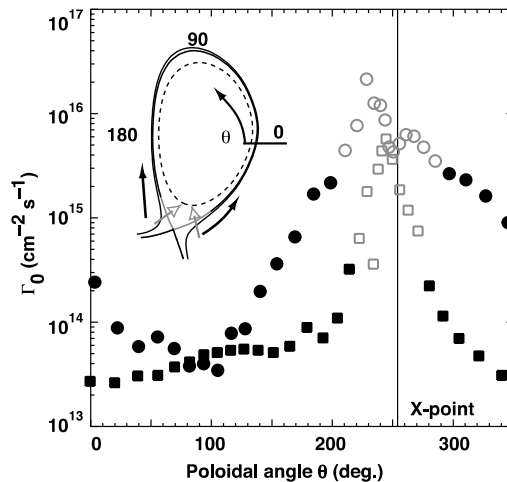


Fig. 3-13. Calculated DEGAS neutral flux into the core as a function of poloidal angle for L-mode ( $\circ$ ) and ELMy H-mode plasmas ( $\bullet$ ). The open (grey) symbols indicate X-point fueling, the closed symbols fueling due to divertor neutral leakage.

**Goal 1: Test models of particle sources, sinks, and pressure balance as drivers of parallel plasma flow.** Global plasma particle balance, its ionization sources, and recombination sinks must first be measured to properly assess particle transport. Ion sinks in the form of ion flux to PFCs are routinely monitored with surface-mounted Langmuir probes. Some additional loss of ions from plasma recombination can occur in detached divertor conditions, and can be estimated through spectroscopy, though it is not routinely done so. Additional coverage of hydrogenic spectroscopy from visible line ratios and Ly- $\alpha$  imaging will be added to make this estimate more routine. The

plasma ionization profile presents a more challenging estimate, with the interpretation of spectroscopy being very density- and temperature-dependent. Interpretive analysis will be carried out with a Monte Carlo code, such as EIRENE or DEGAS, to follow neutrals launched into a reconstructed background plasma. The neutral source profile for the EIRENE calculation is taken to be the same as the ion sink distribution described above. This interpretive analysis requires extensive diagnostic analysis to adequately constrain the background plasma and to cross-check the resulting ionization profile with hydrogenic spectroscopy. The plasma reconstruction is carried out by fluid codes such as SOLPS, UEDGE and OEDGE constrained by diagnostics including Thomson scattering for divertor, SOL and core plasma, divertor Langmuir probes and visible imaging of impurity and hydrogenic radiation. To test the EIRENE calculation for accuracy and sensitivity additional neutral pressure gauges and Ly- $\alpha$  imaging will be installed. Finally, the analysis infrastructure will be developed to carry out the interpretive analysis more efficiently. This same analysis, and expanded diagnostic set will be employed for pedestal density transport analysis described in Section 4.1.2.

With global particle circulation determined from the interpretive analysis described above, differences in parallel plasma flow between experiment and modeling will be examined. With parallel pressure balance being a primary driver of plasma flow along field lines, this research will be tightly coupled to that in Section 3.2.1 on pressure dissipation. Profiles of parallel plasma flow will be examined in the context of total pressure, thermal (nT) plus kinetic (nmv<sup>2</sup>), and pressure loss mechanisms such as ion-neutral collisions and other momentum dissipation mechanisms studied in Section 3.2.1. Testing these processes giving rise to plasma flow in the models requires pressure balance measurements between the mid-plane and divertor. Along with improvements to the Thomson scattering system, new measurements of  $T_i$  in the mid-plane SOL as well as the divertor will be made. Increased coverage of plasma flow measurements with inner-wall swing Langmuir probes and CIS imaging of impurity flow will be made for assessing response to the driving parameters.

**Goal 2: Measure  $E \times B$ -driven radial particle fluxes for tests of boundary models.** Particle transport perpendicular to magnetic fields can arise from radial diffusion and turbulence, or  $E \times B$  plasma drifts. Research on particle transport due to plasma drifts is described in this section while perpendicular transport due to turbulence is more generally described in the next section, 3.2.3. To test models of particle transport due to plasma drifts, the underlying mechanisms driving the drifts will be examined. Poloidal cross-field drifts arise primarily from radial gradients in  $T_e$  and sheath potential, while radial drifts arise from poloidal gradients in  $T_e$ . The 2D profile of  $T_e$  will be measured with the DTS while the  $E$ -field will be determined by plasma potential measurements from the lower divertor insertable probe. The fluid models, SOLPS, UEDGE, etc., will be tested

by constraining the simulations to match the measured temperature and density profiles and then compare modeled and measured plasma potential. Potential mechanisms for any discrepancies that are uncovered will be studied and could include models of the sheath potential and modifications to the parallel Ohm's law due to non-thermal electron energy distribution.

## Challenge 2: Quantify Separatrix Boundary Conditions for SOL Flow

**Current progress.** Coupling of pedestal rotation and SOL flows is an area of physics that is poorly included in the predictive tools developed for divertor and SOL plasmas. The interaction at the separatrix with the pedestal plasma provides both a direct momentum source/sink for the SOL plasma as well as impacts the radial electric field profile at the separatrix driving the cross-field flows in the SOL [Boedo 2011, Chankin 2009, LaBombard 2005]. Recent studies at DIII-D have shown that the momentum coupling between the pedestal and SOL, as well as ion orbit loss physics in the vicinity of the separatrix can have a significant impact on the near SOL flow profiles at the outer mid-plane as shown in Fig. 3-14 [Boedo 2016]. However, these mechanisms are not yet understood well enough to have been included in 2D SOL fluid. These mechanisms could potentially account for at least part of observed discrepancies in SOL fluid models, such as the model's inability to predict the large SOL flow toward the inboard divertor, thus, close observed particle flux loops. Lack of validated models of this interaction also impedes pedestal research issues, such as intrinsic momentum and the H-mode transition described in Section 4.1.

Future work proposed in this area will seek to make use of improved diagnostics and detailed kinetic and turbulence codes to develop reduced models for inclusion in the 2D SOL fluid codes.

**Goal 1: Utilize  $E_r$  and toroidal rotation measurements to quantify separatrix boundary conditions for SOL flow.** This research will use the SOL reciprocating probes, divertor Thomson scattering, and pedestal main ion and impurity charge exchange recombination (CER) spectroscopy to characterize the flow shear between the SOL and pedestal plasma and the radial electric field in the vicinity of the separatrix in various SOL conditions and collisionalities. Analysis of this data will be used to interpret 2D SOL fluid models and estimate the magnitude of the effect that coupling of momentum and electric potential across the separatrix can have on fluid

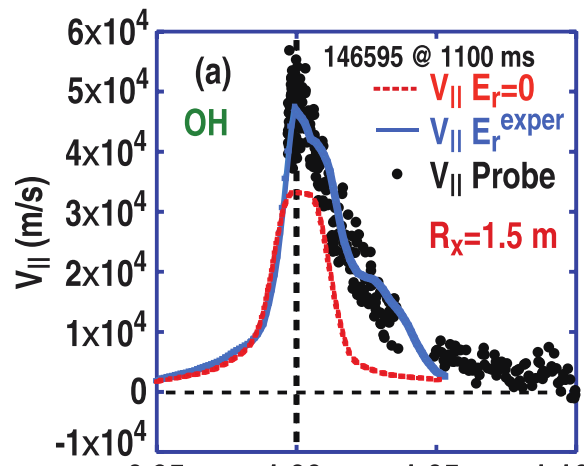


Fig. 3-14. Measured and calculated deuterium velocity at the LFS mid-plane [Boedo 2016].

model simulations. In addition the data will help to guide and test development of models that include these physics effects in realistic 2D geometry, including the SOL turbulence code BOUT++ and the ion orbit-following kinetic code XGC. The aim is to use these more sophisticated codes to produce reduced models that can be incorporated into the 2D SOL fluid models of SOLPS and/or UEDGE. Research in this proposal will focus on the acquisition of the experimental data and its analysis. The code development will be carried out through joint work with US and international collaborations with DIII-D.

### **Challenge 3: Validate Impurity Parallel Transport Models in the SOL**

**Current progress.** International research on impurity transport in the divertor and SOL has been focused on intrinsic and seeded impurities sourced in the divertor and their upstream migration where turbulent transport processes can carry them into the core plasma. For low-Z seeded impurities such as neon, nitrogen, or intrinsic carbon in DIII-D, this upstream transport represents a limiting factor on how much divertor impurity density and resulting radiative dissipation can be tolerated before excessively polluting the core of future burning plasma tokamaks. For high-Z divertor targets parallel transport may dictate the divertor conditions required to limit core impurity accumulation. Impurity transport in the SOL has been understood as the relative balance between the ion temperature gradient force pulling impurities toward the main plasma, and the friction force between the impurity and the main ion flow toward the divertor target [Neuhauser 1984]. This understanding has been exploited to better confine radiating impurities in the divertor with varying success on DIII-D [Wade 1998], ASDEX-Upgrade [Bosch1996] and JT-60U [Asakura 2001] by puffing fuel into the main chamber SOL and strong pumping of recycling neutrals in the divertor to increase SOL flow. While some measurements of impurity entrainment with plasma flow in the SOL have been made in DIII-D [Groth 2009], direct measurement of impurity and main ion flows, as well as the ion temperature gradients, have not been simultaneously made to fully test this model.

Recent installation of the CIS impurity flow imaging diagnostic can now provide 2D flow profile information such as that shown in Fig. 3-15. This proposed research will exploit this diagnostic along with new measurements of  $T_i$  to more fully test models of impurity parallel transport.

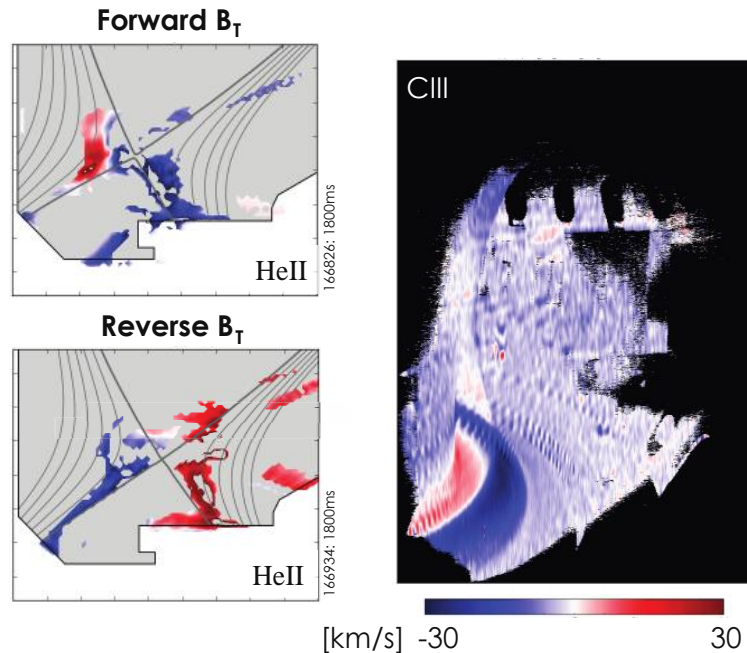


Fig. 3-15. 2D reconstruction of HeII-based flow image in the lower divertor in forward and reversed toroidal field configurations as well as periscope view of CIII flow image in a helium plasma.

**Goal 1: Validate impurity parallel transport models in the SOL.** This proposed research aims to validate impurity entrainment models in the SOL by contrasting model predictions against measurements of main and impurity ion flow and ion temperature gradients under a variety of conditions. The unique CIS diagnostic with laser calibration provides direct measurements of 2D impurity parallel flow profiles as shown in Fig. 3-15. The background main ion flow will be measured by a lower divertor insertable Mach probe and inner wall swing probe for the HFS SOL plasma flow. As models of main ion impurity flow are to be tested in the research described in Challenge 1 of this section, the key measurements of this research will be the difference in parallel flow velocity between the impurity and main ions in response to the parallel ion temperature gradient. This velocity difference will be measured as the competing forces of viscosity with the main ions and the ion temperature gradient being varied by parameter scans in density/collisionality, heating power, and magnetic configuration. The models of impurity entrainment will then be tested by comparing this velocity difference to that from simulations with the SOLPS and/or UEDGE codes where the main ion characteristics are constrained to match the measurements. Finally, the ability of the main ion flow to confine seeded impurities in the divertor will be exploited in the new SAS-2 divertor. Strong pumping in the SAS-2 divertor, along with gas injection in the main chamber, is expected to increase the plasma flowing into the divertor. By comparing the flow of impurities seeded into SAS-2 with CIS, the response of divertor impurity compression to the additional SOL flow will be compared between pumping and no-pumping operation.

## **Challenge 4: Extrapolate Understanding of SOL Flow to More Reactor-Relevant Conditions of High Density and Neutral Opacity**

**Current progress.** Previous studies of impurity transport and entrainment on DIII-D were carried out in mostly moderate power H-mode plasmas in the more open lower divertor configuration. The divertors of future burning plasma tokamaks are expected to be at higher power density and in a more closed configuration. Higher power density could lead to higher  $T_i$  gradients in the divertor and SOL. Also, divertor closure combined with shorter ionization lengths for recycling neutrals could result in very different plasma flow patterns than currently observed. It is therefore important to test scaling of these parameters as they approach those expected in the future. The challenges of producing and diagnosing high power, closed divertor configurations were previously discussed in Challenge 3 of Section 3.2.1 on divertor dissipation. The research proposed here will follow along similar lines with higher power and expanded diagnostic coverage.

**Goal 1: Measure plasma flows with increased heating power and divertor closure for tests of model scaling toward reactor-like conditions.** Higher power and more closed divertor configurations expected in future burning plasma tokamaks could significantly alter main ion and impurity transport behavior from that in existing tokamaks. The combination of shorter ionization length at high power and density, and the increased neutral confinement from increased divertor closure could significantly affect recycling neutrals and the resulting plasma flow patterns. In addition, the high power may increase  $T_i$  gradients, affecting the parallel transport of impurities. Carrying out main ion and impurity transport studies described in Challenge 1 and 3 of this section, at higher power and in the proposed upper SAS-2 closed divertor will test the scaling of the models results toward more reactor-relevant conditions. These experiments will exploit the planned higher auxiliary heating power and the SAS-2 closed divertor. The diagnostic upgrades for this work primarily involves expanded spatial coverage for high triangularity configurations in the lower divertor and the proposed upper SAS-2 divertor. The diagnostics upgrades include new Thomson scattering measurement locations, additional bolometer chords, Ly- $\alpha$  imaging, and improved IR camera optics.

### **3.2.2.3 Capability Enhancements**

The new measurements include Ly- $\alpha$  imaging, additional pressure gauges and measurements of  $T_i$  in the SOL and divertor. The diagnostic upgrades also include expanded coverage and capability for divertor Thomson scattering, bolometer chords, inner-wall swing probes and IR camera viewing optics.

Improvements to the heating systems described in Section 2 will provide for higher power density divertor plasmas. The SAS-2 facility will provide a more-closed divertor configuration for higher neutral densities.

**Table 3-14.  
Facility Enhancements**

<b>Hardware Capability</b>	<b>New Physics</b>
Increased heating power	Scaling particle and impurity transport to more reactor like conditions
SAS-2 (pumped)	Test scaling of main ion and impurity transport toward closed divertor configurations

**Table 3-15.  
Physics Enabled by New Diagnostics for SOL Particle Transport Research**

<b>Scientific Objective</b>	<b>Physics Measurement</b>	<b>Diagnostic Technique</b>
Validate the breakdown of total pressure to static and dynamic components	Flow velocities of deuterium and impurity ions, ion temperature measurements	Coherence imaging spectroscopy. Swing and Mach probes for deuterium. Tunnel probe and RFE. Spectroscopic methods (MDS, CER).
Plasma neutral interaction for driving SOL flows	Neutral density and ionization	Ly- $\alpha$ imaging. Deuterium spectroscopy. ASDEX gauges.
Validate impurity ion entrainment to main ion flow	Impurity and main ion flow velocities in the SOL	Coherence imaging. Swing and Mach probes.
Coupling of pedestal and SOL $E_r$ profiles	$E_r$ measurements in pedestal and SOL.	CER. Reciprocating probes. DTS.
Coupling of pedestal and SOL toroidal flows	Flow measurements in pedestal and SOL	CER. Coherence imaging. Mach and swing probes.
Extrapolate SOL flow studies to high power conditions	Flow measurements that are capable for high power operation	CER. Coherence imaging.

**Table 3-16.**  
**Codes Used for SOL Particle Transport Research**

<b>Code</b>	<b>Purpose</b>
SOLPS (5.0, 5.1, and ITER) and UEDGE	Interpretation of experimental measurements. Validation of the code predictions for SOL flows. Cross-field drifts are essential for this task. However, they are not anticipated to be sufficient for quantitative match with experiments, and further theoretical and numerical code development is foreseen necessary to obtain quantitative predictive capability. Work toward numerical stability with cross-field drifts is required to be able to run simulations routinely with drifts.
OEDGE	Interpretive analysis of neutral ionization source profiles
BOUT++	Simulations of turbulent fluxes in the SOL and their relation to the SOL flows and momentum transport.

### 3.2.3 SOL and Divertor Radial Transport

*Physics Leads: J. Boedo (UCSD), D. Rudakov (UCSD), C. Lasnier (LLNL), A. Leonard (GA)*

Radial transport in the SOL and divertor remains a key issue for the prediction of boundary plasma behavior in future tokamaks. In the near SOL, radial transport sets the width of the heat flux channel into the divertor and, thus, the level of divertor dissipation that will be required to not exceed target plate material limits. Evidence for enhanced turbulence within the divertor plasma suggests a spreading of heat flux that could potentially reduce the dissipation requirement. Radial particle transport throughout the SOL leads to plasma-wall interaction throughout the main chamber affecting particle circulation patterns throughout the discharge and can result in adverse erosion from the PFCs throughout the device. A predictive model of these processes will be required to design boundary plasma and PFC solutions for future burning plasma tokamaks.

DIII-D has played an important role in the international community in developing empirical scalings of radial transport in the SOL. In the past five years DIII-D has provided key data in the international development of a divertor heat flux scaling law. DIII-D has also contributed measurements of the radial fluxes in the far SOL that have become part of international studies. In this proposed work, fundamental turbulence analysis of SOL plasmas, similar to what has been done for core plasmas, will be made to provide a physics basis for predicting radial transport as a complement to the existing empirical scalings.

#### 3.2.3.1 Challenges and Impact

The goal of this proposed research is to provide a more fundamental physics basis for prediction of radial transport in the plasma boundary. DIII-D results can be used to develop

reduced models of transport for inclusion in 2D fluid simulations used for design and prediction of future burning plasma tokamaks. This work will focus on three major challenges for understanding boundary plasma transport. For the first challenge, turbulent radial transport will be examined in the near and far SOL. The first goal of this challenge is to measure the scaling of the near-SOL turbulence properties, including scale lengths, frequency distribution, and poloidal asymmetry for testing and developing of computational models incorporating the fundamental physics of transport. The far SOL will also be examined for scaling of radial particle transport that can affect global circulation particles and main chamber plasma-material interaction. The second challenge will be to characterize and understand turbulence arising within the divertor itself that may contribute to additional heat flux dissipation, but that also may affect upstream plasma transport. Finally, the third challenge will be to determine what role kinetic effects play in the divertor and SOL plasmas in order to include any important features in boundary models. These challenges and goals are outlined in Table 3-17.

**Table 3-17.**  
**SOL and Divertor Radial Transport Challenges, Goals, and Upgrades**

<b>Challenge</b>	<b>Goals/Deliverables</b>	<b>Upgrades</b>
Develop predictive capability for SOL radial transport	<ul style="list-style-type: none"> <li>• Measure scaling of SOL turbulence characteristics for tests and development of fundamental SOL transport models</li> <li>• Measure scaling of SOL radial particle flux for guiding and testing models under development.</li> </ul>	<p><b>Hardware</b></p> <ul style="list-style-type: none"> <li>• Increased upper divertor closure with SAS-2</li> </ul> <p><b>Diagnostic</b></p> <ul style="list-style-type: none"> <li>• Gas puff imaging of SOL turbulence</li> <li>• Fast <math>T_e</math> with X-point reciprocating probe</li> <li>• Main ion <math>T_i</math> in the SOL and divertor</li> <li>• Inner wall swing probes</li> <li>• 2D expansion of divertor Thomson scattering</li> </ul>
Include role of divertor turbulence in models of heat flux dissipation	<ul style="list-style-type: none"> <li>• Measure turbulence characteristics and dependencies in dissipative divertor plasmas</li> </ul>	
Include important kinetic effects in models of SOL and divertor plasmas	<ul style="list-style-type: none"> <li>• Determine the role kinetic effects play in the SOL and divertor transport</li> </ul>	<p><b>Model Development</b></p> <ul style="list-style-type: none"> <li>• XGC0</li> <li>• XGC1</li> <li>• BOUT++</li> <li>• SOLT</li> <li>• PW1</li> <li>• SOLPS</li> <li>• UEDGE</li> </ul>

Progress in understanding and scaling of fundamental radial transport processes in the divertor and SOL provided by this research will directly contribute to confidence in the design of boundary

plasma solutions for future tokamaks. It is critical that a physics basis be developed to underlie the empirical models based on existing experiments as they are extrapolated to the parameters of burning plasmas.

### 3.2.3.2 Research Plan

The SOL and Divertor Radial Transport research plan is organized according to the challenges and goals in Table 3-17. Fig. 3-16 gives the timeline for each challenge, research milestone, and the capability improvements necessary to achieve them.

Challenge	FY19-20	FY21	FY22	FY23	FY24
Develop predictive model of SOL radial transport	Measure scale lengths, poloidal asymmetry and turbulent fluxes in near SOL  Measure scaling of radial fluxes and other characteristics of far SOL turbulent transport				
Include role of divertor turbulence in models of heat flux dissipation	Measure parametric dependencies of divertor turbulence in detached conditions				
Include important kinetic effects in models of SOL and divertor plasmas	Measure non-thermal contributions to target sheath formation, parallel heat transport and radiative emission				
Hardware Improvements	SAS-2 upper divertor with improved diagnostics				
Diagnostic Enhancements	Gas puff imaging  Fast $T_e$ for X-point probe  Main ion $T_i$ at mid-plane and divertor  Extended $n_e$ and $T_e$ coverage from Thomson scattering				

Fig. 3-16. SOL and Divertor Radial Transport Plan Timeline

#### Challenge 1: Develop Predictive Model of SOL Radial Transport

**Current progress.** For 2D fluid plasma models, such as SOLPS and UEDGE, that are the workhorse of divertor design for future tokamaks, radial transport is modeled by ad hoc diffusive transport coefficients. The recent development of a multi-machine empirical scaling for divertor heat flux in H-mode plasmas, Fig. 3-17 [Eich 2014], has provided a means for estimating those transport coefficients over the parameter regime of existing tokamaks. However, a physics basis for the observed empirical scaling is needed if the radial transport is to be extrapolated with confidence to the parameters of future burning tokamaks. A heuristic model based on  $\nabla\mathbf{B}$  drifts of

the plasma fluid has reproduced the observed heat flux width database in both absolute magnitude and scaling [Goldston 2012]. The XGC1 gyrokinetic code also reproduced the scaling of this dataset with the width similarly set by the ion-magnetic drift [Chang 2017]. However both the XGC1 and more analytic models [Myra 2016a] suggest that turbulence may dominate the spatial scale of radial transport once tokamaks increase in size to ITER and beyond. The models suggest that while the drift width scales with the poloidal ion gyroradius, the radial scale length of curvature-driven turbulence has an additional dependence increasing with machine size. The expectation is that the turbulence width may become larger than the drift width for future larger tokamaks and thereby increase the heat flux width beyond the empirical scaling.

Radial transport in the far SOL has for some time been observed to be convective and intermittent in nature [Rudakov 2002, Boedo 2003]. At the high densities required for divertor dissipation and detachment, the far SOL density radial scale length increases with significant interaction with the main chamber wall [Carralero 2017]. The increase in radial transport may be due to a collisionality criteria at the field line intersection with material surfaces that leads to increased filamentation [Myra 2006b]. An accurate model of this process is needed for prediction of recycling patterns and resulting plasma flow in the far SOL and plasma interaction with the main chamber.

**Goal 1: Measure scaling of SOL turbulence characteristics in the near SOL.** The goal of this work is to measure a number of characteristics of turbulence active in the SOL for testing and development of turbulence models. The important characteristics to measure include the turbulence radial scale lengths, poloidal asymmetry and frequency spectrum, along with the actual turbulent

radial fluxes. The scaling of these parameters with collisionality and poloidal magnetic field are also important. The most complete turbulence characteristics are now provided by the existing insertable mid-plane Langmuir probe. This diagnostic can measure in one location the plasma fluctuating parameters for calculating turbulent fluxes,  $q_{\perp} \approx \langle \tilde{v} \times \tilde{p} \rangle$ . To provide better measurements of the spatial scales of the turbulence a gas-puff imaging (GPI) diagnostic will be installed in DIII-D. Additional GPI systems will later be installed at different locations to measure the poloidal asymmetry of turbulence, a critical feature of ballooning-driven transport. Existing

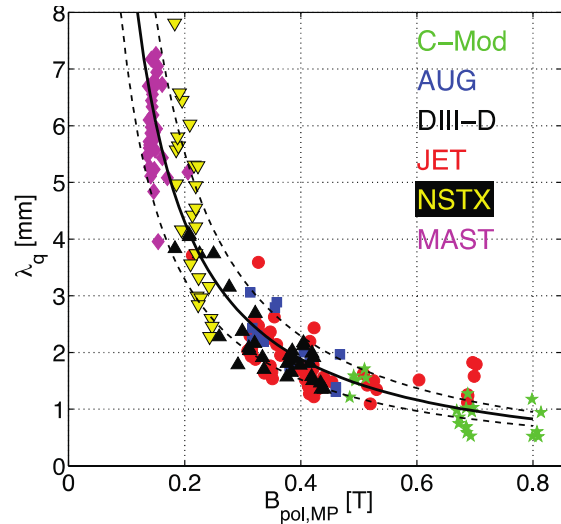


Fig. 3-17. Multi-machine database of divertor heat flux width as a function of poloidal magnetic field at the outer mid-plane.

complementary edge turbulence diagnostics to provide additional details include BES, reflectometry and ECE.

The comparison of models will be carried out in collaboration with institutions responsible for development of the computational models. The computational models include XGC1, BOUT++, SOLT, and PW1. As the models are validated, the collaborating institutions will couple these turbulence properties with 2D fluid codes, such as SOLPS and UEDGE, to provide specified radial fluxes instead of ad hoc transport coefficients. Reduced models of radial transport from the codes will also be developed to provide direct specification of transport coefficients with more predictive capability. The boundary profile diagnostics described in the previous sections 3.2.1 and 3.2.2 and the turbulence diagnostics described here will be used to guide and test this model development.

**Goal 2: Test model predictions of SOL radial particle flux.** Radial transport in the far SOL will be examined for correlation with divertor target conditions. Previous work [Carralero 2017] that found far SOL density scale lengths to be dependent upon divertor collisionality will be expanded with profile dependence. Mid-plane convective filamentary transport will be measured by the insertable mid-plane Langmuir probe and the proposed GPI system will be correlated with the corresponding conditions along the same magnetic field line at the target by divertor Thomson and fixed-target Langmuir probes. Of particular importance is the radial location of the origin of the filamentary structures. Theoretical models [Myra 2006] have suggested that a critical collisionality at the target suppresses the closing of electrical current within a flux tube allowing filament formation. Though, for flux lines near the separatrix the X-point may serve to close this circuit. Therefore, measuring the relationship between distance from the separatrix, target collisionality, and filament formation will be critical for testing models that aim to predict SOL radial transport for main chamber wall fluxes and global particle circulation patterns.

## **Challenge 2: Include Role of Divertor Turbulence in Models of Heat Flux Dissipation**

**Current progress.** Turbulence may well affect the level of dissipation within the divertor plasma, but it is not currently taken into account in the 2D fluid models used for divertor design. Experimentally, high levels of turbulence have been measured in detached dissipative divertors [McLean 2015, Poetzl 2013, Pigarov 2006]. However, these measurements have been made with limited frequency response and correlation with other parameters. Theory and modeling also suggests turbulence plays a significant role in dissipative divertors. Modeling of detached plasmas in ASDEX-Upgrade with SOLPS found better agreement with experiment when the radial transport coefficient in the divertor region was increased by a factor of 10 above that in the SOL [Reimold 2015]. Theory has found that instabilities can arise due to nonlinear interactions between ion and neutral particle content, radiation instabilities, and interactions between detachment of the

inboard and outboard divertors [Krashenninikov 2017]. These fluctuations could affect the divertor plasma by increasing radial diffusion, thereby relaxing the requirement for radiative dissipation. Fluctuations could also potentially increase divertor radiation by relaxing sharp parallel  $T_e$  gradients and thereby increase the plasma volume for efficient radiation,  $T_e \leq 5$  eV. The turbulence of detached divertor plasmas is in fact poorly characterized with few publications documenting behavior and overall parameter dependencies. This proposal aims to provide more comprehensive fluctuation measurements with systematic parameter scans to guide theory and model development as well as assess the overall implications of divertor turbulence.

**Goal 1: Measure turbulence characteristics and dependencies in dissipative divertor plasmas.** This research will make use of DIII-D’s extensive divertor diagnostic set to better characterize turbulence in detached divertor plasmas and to assess its implications for divertor dissipation. The insertable X-point Langmuir probe will be instrumented for fast  $T_e$  measurements of local fluctuations. These measurements can be correlated with other fast measurements from spectroscopy and DTS. Scans of a number of divertor parameters, including density, power, and divertor configuration, will be made to determine the fluctuation characteristics’ parametric dependencies. With diagnostic coverage expanded to the proposed SAS-2 divertor, the role of closure and neutral particle control on divertor turbulence will also be explored. Finally, the effect of divertor turbulence on upstream profiles will also be examined. Fluctuations that increase radial transport of density in the divertor affect upstream mid-plane profiles, as well due to fast parallel transport. Observations and trends will be used to guide the development of theory that is still in its early stages, for later inclusion in more global SOL and divertor models.

### **Challenge 3: Determine the Role Kinetic Effects Play in the SOL and Divertor Transport**

**Current progress.** Kinetic effects have been posited to have significant effects in SOL and divertor plasmas [Batishchev 1997]. Deviation of hot particles from thermal distribution functions can affect modeled heat flux as half the power is carried by particles with energies greater than  $7T_e$ . While fluid models make allowance for kinetic effects at low collisionality with heat flux limits consistent with PiC (Particle-in-Cell) simulations, non-thermal distributions might seriously affect these estimates [Stangeby 2010]. Additionally, an energetic electron tail can affect the sheath potential and, thus, plasma  $\mathbf{E} \times \mathbf{B}$  cross-field drifts as described in Section 3.2.2. Evidence for a population of energetic particles has been indirectly observed through floating Langmuir probe, floating potential measurements, and heat flux sheath transmission coefficient analysis at the divertor target. However, these observations are mostly anecdotal and no comprehensive model for non-thermal effects exist. Research on this topic will aim for establishing the role that kinetic and non-thermal distribution functions plays in overall divertor performance.

**Goal 1: Determine the role kinetic effects play in the SOL and divertor transport.** Evidence for non-thermal particles will be sought after, relying on several diagnostics including Langmuir probe measurements, Retarding Field Analysers (RFAs) installed on insertable probes, and spectroscopy. Interpretive modeling will be applied to reconcile disparate measurements such as Thomson scattering and rates of upper-level atomic transitions. Important dependencies will be explored including collisionality through density and power scans, and divertor closure for neutral density. Measurements will also be reconciled with kinetic simulations, such as PW1. Finally, implications of observed non-thermal particles will be assessed with the standard fluid codes SOLPS and UEDGE.

### 3.2.3.3 Capability Enhancements

The primary enhancements for radial transport research are additional diagnostics of turbulence characteristics. This includes Gas-Puff Imaging (GPI) for turbulence imaging at the outer mid-plane and later extension to other poloidal locations. Instrumentation upgrades for insertable probes will also be installed. SOL and divertor turbulence and transport studies will also benefit from the other diagnostics upgrades described in Sections 3.2.1 and 3.2.2 by further constraining modeling interpretation. Finally, the SAS-2 facility will provide a more closed divertor configuration examining turbulent transport at higher neutral densities.

**Table 3-18.  
Facility Enhancements**

<b>Hardware Capability</b>	<b>New Physics</b>
Increased heating power	Scaling turbulence characteristics to more reactor like conditions
SAS-2 (pumped)	Test roles of neutral density on turbulence characteristics

**Table 3-19.  
Physics Enabled by New Diagnostics for Divertor Turbulence and Transport**

<b>Scientific Objective</b>	<b>Physics Measurement</b>	<b>Diagnostic Technique</b>
Characterize near SOL turbulence including radial spatial scales	SOL turbulence imaging	Gas-Puff Imaging (GPI)
Poloidal asymmetry of SOL turbulence	Turbulence imaging in additional locations	Additional GPI installations
Measure turbulence driven fluxes	$T_e$ and $n_e$ divertor turbulence	Fast $T_e$ and $n_e$ from divertor reciprocating probe
Measure non-thermal electron and ion distribution functions	Distribution function of $T_e$ and $T_i$	Retarding Field Analyzer (RFA), spectroscopy and Langmuir probes

**Table 3-20.**  
**Simulation Codes Used for Divertor Turbulence and Transport**

<b>Code</b>	<b>Purpose</b>
XGC0 XGC1 PW1	Kinetic modeling, test for non-thermal populations, particle losses
BOUT++ SOLT	Turbulence codes to predict transport levels and asymmetries
SOLPS UEDGE	Fluid codes to test transport models and couple to turbulence models

### 3.3 ADVANCED MATERIALS EVALUATION

#### Introduction

Plasma-material interactions (PMI) continue to be a primary challenge for advancing the science and reality of fusion energy. Recent strategic planning reports have highlighted the need for more PMI research within the US fusion energy development program as well as better integration of existing efforts [US DOE, OFES 2015-1]. Furthermore, the current state of research on fusion development was reviewed in a series of community workshops. Each workshop produced a comprehensive overview report, and the plan laid out here references heavily from the workshops on both PMI and transients (e.g. ELMs and disruptions) [US DOE, OFES 2015-2, US DOE, OFES 2015-1]. The research path presented here for the DIII-D Advanced Material Validation (AMV) group is based in great measure on the recommendations of these reports.

The AMV research mission is to assess the physics governing the interaction of any reactor-relevant candidate materials with plasma to: a) determine the implications for core plasma operations and control; b) develop mitigation techniques for deleterious effects; and c) help to develop predictive PMI models. This mission is addressed in three facets: global PMI physics to develop a predictive capability for *material migration and mitigation*; local PMI physics to understand the synergies of *surface evolution science*; and the evaluation of *innovative materials* solutions as a means to facilitate the success in any next-step devices.

Developing a predictive capability for how material is sourced from the tokamak divertor, its leakage and transport through the scrape-off-layer, as well as the corresponding impact on SOL/pedestal physics and core impurity accumulation is a crucial goal for fusion science. Significant knowledge gaps remain in understanding the mechanisms which govern impurity erosion, transport into the core plasma, long-range migration, and how these processes can be

actuated or controlled. DIII-D will address the key physics issues of how high-Z leakage from the divertor region can be mitigated through innovative divertor design, how different levels and types of coexisting low-Z materials influence high-Z source and leakage, the impact of transients on divertor-sourced impurity leakage and transport, and material migration properties in the main chamber. Detailed studies of high-Z sourcing and transport will be performed, taking advantage of the low-Z background on DIII-D, using isotopic tracer techniques to localize the high-Z source and estimate the long-range migration efficiency. The mitigation of high-Z impurity leakage from the divertor region will be studied by taking advantage of divertor optimization research using the Small Angle Slot (SAS) divertor in concert with tungsten inserts. The way in which W leakage from the SAS divertor is modified as a function of the low-Z seeded impurity will be tested. In addition, an option for heated W inserts will allow studies of high-Z sourcing and transport with a W target surface free of low-Z deposits (as in a fusion reactor), which no other fusion devices are ready to do in the next decade. ELM control tools will be used, including pellet pacing and increased divertor screening via gas puffing, to examine how to mitigate the ELM-induced sources. Further, installing toroidally symmetric limiters would allow for symmetrization of the main chamber, greatly simplifying the diagnosis and comparison to modeling of main chamber material migration.

Underlying the problem of material migration is the basic science that determines the local surface evolution. The plasma-material interface in a fusion energy device will be a dynamic region of material that is constantly eroded and re-deposited. Extrapolating forward to a reactor, with erosion rates at PFMs being many orders of magnitude larger than current devices (particularly for the main chamber wall) leads to a mixed-material environment that goes well beyond the current understanding of PFC, with new questions of slag management, tritium retention via co-deposition, and material lifetime limits. DIII-D will address two key physics issues of surface evolution. First, DIII-D's local PMI study on erosion and redeposition in the divertor will be expanded to the main chamber, by coupling the successful ensemble of divertor surface diagnostics, DiMES manipulator and a new Wall Interaction Test Station (WITS) with improved modeling capability in the 2019-2024 timeframe. WITS will provide the environment to expose tile-sized components to controlled main chamber plasmas mounted on a moveable limiter, in close proximity to a comprehensive diagnostics cluster. The test samples will be heated (to study surface evolution at reactor-relevant temperatures) as well as biased (to investigate main chamber sheath physics). WITS will provide detailed information about the main chamber neutral and background plasma flux and energy spectrum, and the advanced sample exposure capability will provide valuable information for benchmarking models of main chamber material erosion and re-deposition. Secondly, techniques for study of the active re-deposition of material onto main chamber and divertor PFCs will be developed in order to enhance material lifetime limits and as a

tool for mitigating tritium retention in co-deposits. These studies will use DIII-D's diagnostic ability to characterize intra- vs. inter-ELM erosion/re-deposition in the divertor and thereby account for ELM-induced PMI on the main chamber walls. Another aspect will be to address the impact of real material surface morphology on the dynamics of these eroded and re-deposited layers, which will be benchmarked against state-of-the-art PMI modeling code suites, incorporating realistic surface roughness effects.

Finally, the development of suitable plasma-facing materials is a key issue for fusion energy production. A successful PFM must withstand the energy and particle fluxes at the plasma periphery without unduly contaminating the core plasma and without significantly retaining the deuterium/tritium fuel. The materials must perform at high temperature and retain their performance in the presence of intense neutron irradiation. Any erosion or wear will need to be mitigated in some fashion for adequate long-term operation. Currently, there is no viable material satisfying all of these interrelated requirements for fusion reactors. The materials science community is now developing novel materials such as advanced ceramics and ceramic/metal composites, and new manufacturing techniques including additive manufacturing, which may play a role in future fusion applications if properly tested and optimized. DIII-D will address several key physics issues associated with testing of innovative materials in a relevant PMI environment, including more accurate characterization of the gross and net erosion of various tungsten alloy and composites using the DiMES flexibility with high time- and spatially-resolved measurements, tests of basic PMI properties of novel ceramic materials which have some attractive features but unknown real-world performance, extension of these measurements to the main chamber environment using WITS, and extension of DIII-D's extensive PMI erosion/ redeposition measurement capability at reactor-relevant temperatures using both heated DiMES and WITS, as well as an optional program element for heated W inserts in the SAS divertors mentioned previously.

These three AMV areas – material migration, surface evolution, and innovative materials evaluation – represent issues that can be addressed aggressively in next few years in the DIII-D program. The proposed research is covered in detail in the following sections, highlighting the near-term challenges in each, as well as the approach to address the challenges and hardware/diagnostic upgrades needed for the approach. In the end, the efforts presented here should be integrated into a larger US program to evaluate and develop fusion materials and plasma wall interactions.

### 3.3.1 Understanding Material Migration and Mitigation

*Physics Leads: T. Abrams (GA), E.A. Unterberg (ORNL), D.L. Rudakov (UCSD), D.M. Thomas (GA), D. Donovan (UTK), J.D. Elder (U. Toronto), D. Ennis (Auburn U.).*

Developing a predictive capability for how material is sourced from the tokamak divertor, its leakage and transport through the scrape-off-layer, as well as the corresponding impact on SOL/pedestal physics and core impurity accumulation is a crucial goal for fusion science. Advancing this understanding has been identified as Priority Research Directions (PRDs) C (*First-Wall Solutions and Actuators*) and E (*Core-Edge Plasma Compatibility*) in the 2015 PMI report [US DOE OFES 2015\_2]. Significant knowledge gaps remain in understanding the mechanisms which govern impurity erosion, transport into the core plasma, long-range migration, and how these processes can be actuated or controlled. In the next five-year plan, DIII-D aims to fill in crucial gaps in this knowledge outlined in the Challenges and Impact Section below.

DIII-D has several key features that have enabled, and will continue to enable, significant progress in these areas. The low-Z background of DIII-D allows detailed studies of high-Z sourcing and transport, which can be further enhanced by using isotopic tracer techniques. Such capability has already begun to be leveraged with the FY16 Metal Rings Campaign (MRC). This mini-campaign utilized a novel isotopic W tracer technique in the outer divertor to gain unique insights into W sourcing and SOL transport in the presence of a predominantly low-Z (i.e., C) material background. Notably, it was observed that the W atomic escape probability from the divertor region depends crucially on both the W source location and the edge-localized mode (ELM) behavior. In addition, asymmetries observed in the W collection pattern along two sides of a mid-plane collector probe were consistent with the formation of a 'potential well' driven primarily by the ion temperature gradient (ITG) force, with additional physics insight into these results gained via ERO and DIVIMP modeling. Validation of state-of-the-art PMI and SOL impurity transport models will continue to be a key component of DIII-D plasma-materials interaction (PMI) research efforts in the next five years.

#### 3.3.1.1 Challenges and Impact

The mission of the DIII-D Advanced Materials Validation group is to evaluate plasma-facing component (PFC) solutions relevant to next-step devices. Such PFCs in the divertor must have high thermal conductivity to satisfy stringent power exhaust requirements, as well as low sputtering yield to conform to severe limitations on tritium retention via co-deposition and overall material lifetime. High-Z materials (i.e., tungsten) remain the leading solution for such a divertor PFC. Therefore, studying the outstanding physics issues for tungsten divertor material sourcing and transport form the main focus of the Advanced Materials Validation research.

Studies of W plasma PMI will be carried out synergistically with the Divertor Optimization research goals outlined in Section 3.1. To complement these studies, it is extremely important to *test whether the SAS divertor solution provides effective mitigation of high-Z impurity leakage from the divertor region*, both on DIII-D and in extrapolations to future devices. It thus follows that developing a predictive capability for how material from the SAS divertor, its leakage and transport through the scrape-off-layer, as well as the corresponding impact on SOL/pedestal physics and core impurity accumulation is a crucial goal for DIII-D and fusion science. Understanding both the steady-state and transient-induced W leakage from the SAS divertor are the key intended impacts of in this research plan, as described in Table 3-21.

The final challenge in this area focuses on developing an understanding of material migration properties in the main chamber (MC). The research conducted in this challenge will provide progress on the path to a predictive capability for material erosion and re-deposition rates in the main chamber, enhancing confidence in extrapolations to the tritium-retention rates and overall MC material lifetime limits in high-fluence, reactor-level devices.

**Table 3-21.**  
**Material Migration Challenges, Goals, and Capability Enhancements**

<b>Challenge</b>	<b>Goals/Deliverables</b>	<b>Enhancements</b>
Understand high-Z impurity leakage from the SAS divertor	<ul style="list-style-type: none"> <li>Evaluate how degree of divertor closure impacts W leakage from different poloidal locations</li> <li>Test and predict how W leakage from the SAS divertor is modified as a function of the dominant low-Z seeded impurity</li> </ul>	<p><b>Hardware</b></p> <ul style="list-style-type: none"> <li>SAS-1 w/ W rings</li> <li>SAS-2 w/ W rings</li> <li>Heated Full-W SAS-2 (option)</li> <li>Toroidal belt limiters (option)</li> <li>Siliconization</li> </ul>
Achieve maximum tolerable transient sizes in open and closed high-Z divertors	<ul style="list-style-type: none"> <li>Characterize balance of inter-ELM and ELM-induced W leakage from LFS &amp; HFS vs. level of ELM mitigation</li> <li>Develop control techniques to mitigate W leakage from the SAS divertor during transient events</li> </ul>	<p><b>Diagnostic</b></p> <ul style="list-style-type: none"> <li>UV/VUV spectroscopy</li> <li>Core VUV/X-ray spec.</li> <li>Additional collector probe locations</li> </ul> <p><b>Analysis Capabilities</b></p> <ul style="list-style-type: none"> <li>ELM-resolved W leakage</li> <li>Spectroscopic re-deposition</li> </ul>
Identify main pathways for main chamber material migration	<ul style="list-style-type: none"> <li>Unravel the primary migration pathways for low-Z main chamber material in a 2D symmetrized system</li> </ul>	

### 3.3.1.2 Research Plan

The Material Migration program research plan is organized according to the challenges, goals, and capability enhancements outlined in Fig. 3-18. The key approach in this area will be to systematically add isotopic high-Z tracer sources to different poloidal locations in the SAS divertors, as well as in the upper inner divertor.

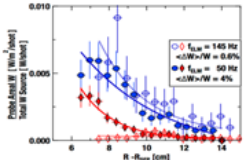
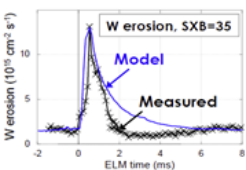
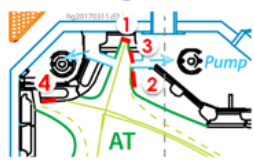
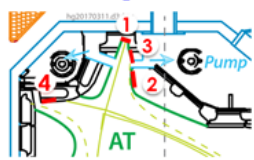
	2019	2020	2021	2022	2023	2024
<p><b>Understand W Impurity Leakage from SAS Divertors</b></p> 	Characterize SAS W leakage via impurity gas puffing			Scale SAS W leakage studies to high power (AT)		Test low W leakage scales with dominant low-Z impurity
<p><b>Determine Tolerable ELM Sizes on W Divertors</b></p> 	Understand ELM-resolved W erosion and re-deposition to predict local W source	Compare W leakage during ELMs from HFS and LFS		Develop and deploy effective active control techniques for mitigating W leakage during transients		
<p><b>Identify Key Pathways for Main Chamber Material Migration</b></p> 	Quantify low-Z impurity leakage from SAS 1	Understand low-Z MC material pathways in a 2D symmetrized system	Understand low-Z MC material pathways in a 2D symmetrized system	Evaluate impact of low-Z innovative materials on pedestal performance		
<p><b>New Capabilities</b></p> 	Fast MDS cam. Spectroscopic W re-deposition	SAS 1 W rings UV/VUV spectroscopy Multiple collector probes	Toroidal limiters (optional)	SAS 2 W rings ELM-resolved collector probes Core VUV/X-ray spec.	SAS 2 full-W w/ heating (optional)	

Fig. 3-18. Material migration plan timeline

#### Challenge 1: Understand High-Z Impurity Leakage from the SAS Divertor

**Current progress.** Suppression of high-Z impurity leakage is crucial for maintaining a robust, high-performance plasma scenario, as even small W core concentrations ( $>10^{-4}$ ) result in substantial core radiation and no access to the Lawson criterion for any core temperature [Putterich 2010].

DIII-D’s strengths to study high-Z leakage in open divertors were leveraged in the later years of the 2014-2018 Five-Year Plan with the FY16 Metal Rings Campaign (MRC). During this campaign, two toroidally continuous rings of isotopically-enriched tungsten-coated tiles were installed at two different locations, i.e., at outer strike point (OSP) and divertor entrance. A novel isotopic detection technique, inductively coupled plasma mass spectrometry (ICP-MS) was

utilized to distinguish W isotopes on an upstream collector probe situated in the far-SOL near the outboard mid-plane. One notable finding from the MRC was that for large ELMs at moderate frequency, SOL W leakage was equally efficient from strike point and far-target regions. In contrast, at high power and high ELM frequency, the divertor W source at the strike point becomes the dominant SOL contamination location (Fig. 3-19). Asymmetries were also observed in the tungsten collection pattern along the two sides of the mid-plane collector probe, which were consistent with the theoretical expectation of the formation of a potential well via the ion temperature gradient (ITG) force along SOL flux tubes near the separatrix, concentrating impurities near the plasma “crown.” The principal features of this W collection profile were reproduced by interpretive DIVIMP SOL impurity transport modeling [Unterberg 2016].

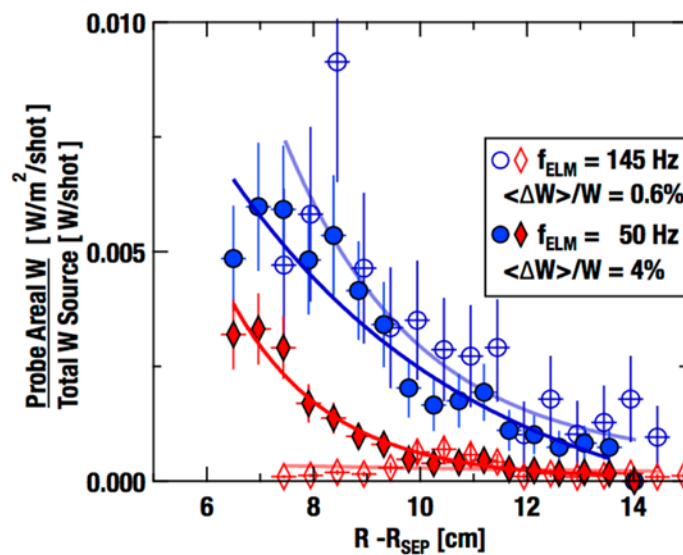


Fig. 3-19. Tungsten SOL contamination probability (as a function of distance from the separatrix) for two separate LSN discharges from the DIII-D Metal Rings Campaign [Unterberg 2016].

In addition to a high-Z divertor, some level of low-Z material, passively supplied by an eroding wall and/or actively via impurity seeding, is also essential in a reactor solution to provide adequate levels of volumetric divertor dissipation. Moving from typical single-element walls in current devices to mixed-material systems introduces substantial additional challenges in predictive capability. In the 2019-2024 five-year period, DIII-D will provide crucial insight into how different low-Z impurities actuate the level of W leakage from the SAS divertor in reactor-relevant high-performance scenarios. In addition, DIII-D considers evaluating W sourcing and transport with a clear W target surface, free of low-Z deposits, via the installation of a heated full-W SAS-2 divertor near the end of the five-year plan. This will enable DIII-D to make unique contributions toward developing viable plasma-interface solutions for full-W wall reactors.

**Goal 1: Evaluate how degree of divertor closure impacts W leakage from different poloidal locations.**

Work will focus on extending the knowledge gained in high-Z sourcing, leakage, and SOL transport in open divertors, as described above, to the closed SAS divertor configuration. These studies will identify the dominant physics mechanisms which drive W leakage in the SAS divertor. For example, it is expected that the net erosion of W will decrease in the SAS divertor, and that the divertor screening for W will be improved, because low target electron temperatures lead to low physical sputtering yields of W, and high electron densities lead to high re-deposition fractions of W. However, the lower upstream densities implied by the SAS configuration may lead to strongly enhanced parallel ITG forces, potentially leading to more efficient W impurity transport from the divertor into the main SOL and the core plasma. Edge impurity transport models such as DIVIMP, ER2.0, and GTR have difficulties making predictions of the W leakage due to the uncertainties in a number of parameters to which the models are sensitive (e.g., perpendicular diffusion coefficients, prompt re-deposition physics, drift effects, and ion temperature profiles) so more empirical studies are necessary to enhance the understanding and constrain these models.

Experiments will be conducted to study the relative leakage of high-Z impurities into the SOL and core from the SAS-1 and SAS-2U divertors. Proposed locations of isotopically-coated W rings within these two iterations of the SAS divertor are depicted in Fig. 3-20. Visible/UV/VUV divertor spectroscopic analysis of neutral and the low-impurity ionization states will be essential to correlate local screening processes such as ionization and re-deposition with the overall impurity migration pattern. Edge spectroscopy will also be utilized to determine the speed and magnitude of the impurity transport from the divertor into the main SOL, and core VUV and x-ray spectroscopy will be used to diagnose core W accumulation. Core high-Z impurity transport studies are synergistic with the core-edge integration goals in Chapter 4.

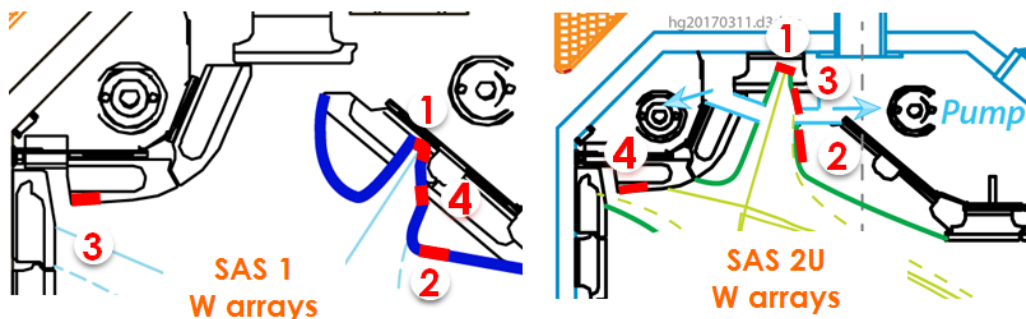


Fig. 3-20. Cartoon depiction of the location of isotopically-resolved W tracer rings in the SAS-1 divertor (left, FY20) and the SAS-2 divertor (right, FY22).

These studies will involve the use of isotopically separated tracers to compare the impurity sourcing and screening simultaneously from different poloidal locations. This will be enabled by collector probes at various poloidal locations, including near the plasma crown (DiMES), at mid-plane, and near the upper divertor itself. Collector probes will continue to serve as the primary diagnostics for determining overall high-Z divertor leakage. The main focus will be to continue interpretive and predictive model benchmarking (Table 3-24) while further incorporating collector probe information. Coupling these efforts through modeling will provide a comprehensive understanding of high-Z divertor leakage from the SAS divertor, leading to strongly enhanced confidence in predictions of W leakage for next-step devices.

**Goal 2: Test and predict how W leakage from the SAS divertor is modified as a function of the dominant low-Z seeded impurity.**

To first order, W sourcing scales with the atomic mass of the dominant divertor impurity because physical sputtering yields of W increase with the target ion atomic mass. Such trends are consistent with the effects of changing from a dominant C to Be impurity on JET [van Rooij 2013], changing from a C to W wall on ASDEX-U [Dux 2009], or when performing active nitrogen seeding experiments with a high-Z divertor [van Rooij 2013]. However, the impact of impurity Z on overall W divertor leakage is not well understood, particularly in the closed SAS divertors, where the dynamic balance between W sputtering, electron temperature, impurity radiation, and neutral trapping is fundamentally different from previous open divertor studies.

Progress in this area will focus on documenting and understanding the relationship between Z-effective of the low-Z seeded impurity and the W source and leakage from the SAS divertor. The primary tool to carry out this study will be the SAS-2U divertor, fully clad in W armor tiles. An option to install active heating elements in SAS-2U to heat the W surface up to  $\sim 600$  °C, a temperature at which C deposits are very efficiently removed from W surfaces [Ueda 2009], is included in the plan. To further suppress the influence of the C impurity, impurity deposition techniques such as gas puffing, power dropping, and glow-based vapor deposition will be utilized to actively actuate Z-effective within the SAS divertor slot. In conjunction, enhanced plasma spectroscopy and radiated power diagnostics will be added to SAS-2U, as detailed in Table 3-23. This research line ties in closely with high-priority detachment physics studies planned by the Divertor Optimization research area discussed in Section 3.1.

**Challenge 2: Achieve Maximum Tolerable Transient Sizes in Open and Closed High-Z Divertors.**

**Current progress.** It is widely accepted that transients such as ELMs have the potential to be severely detrimental to high-Z divertors and the optimal metric for maximum tolerable ELM size

for W PFCs is still being evaluated. Often, constraints are developed based on macroscopic damage thresholds (cracking, melting, etc.). This is how the maximum tolerable ELM size for mitigated ELMs in the ITER divertor is being determined [Loewenhoff 2011, Gunn 2017]. Developing a predictive capability for natural and mitigated ELM sizes on ITER also remains a high-priority research goal for ITER [Pitts 2013, Eich 2017].

This challenge focuses on the development of a supplementary metric for transient sizes on next step devices, namely their impact on high-Z sourcing and divertor leakage, in the context of the strict limits on core W contamination discussed in Challenge 1. Progress on this challenge has so far been led by studies on JET-ILW, which discovered that the overall W source and W core contamination scale strongly non-linearly with ELM size and ELM frequency [Den Harder 2016]. It has also been observed that ELM 'burn-through' results in substantial W sourcing in detached, open W divertors [Brezinsek 2015]. DIII-D progress on this topic has focused on understanding inter- and intra-ELM tungsten-sourcing profiles using perturbative W samples in DiMES experiments. In Fig. 3-20, the intra-ELM W source profile is shown as a function of distance from the outer strike point (OSP) for two very different ELM scenarios. It is evident that ELM size and magnetic field direction strongly impact the intra-ELM W source profile. In both cases, the results are consistent with SDTrim.SP sputtering modeling using measured ion saturation currents and impact energies during ELMs as input and an *ad-hoc* 2% C<sup>2+</sup> impurity flux fraction and 80% C mixed-material fraction deposited on the W surface. Recent studies have also begun examining the impact of ELMs on neutral recycling; initial results suggest that both D and D<sub>2</sub> recycling on high-Z surfaces decreases during ELMs, i.e., there is a higher fraction of promptly reflected atoms and molecules [Bykov 2017].

In the next five years, particular emphasis will be placed on how to mitigate ELM-induced W leakage via innovative control techniques, such as pellet pacing or increased divertor screening via gas puffing [Ding 2017\_1, Ding 2017\_2] in collaboration with the divertor physics research and pedestal/ELM teams. This class of open issues was highly prioritized in the 2015 FES Transients in Tokamaks Plasmas Report [US DOE OFES 2015\_3]. This report acknowledged that a crucial goal for fusion science is predicting the impact of transients on plasma-wall interactions, material erosion and migration, and the "back reaction" of the eroded material on pedestal and core impurity contamination. DIII-D's extensive ELM and disruption control tools will be leveraged to make substantial progress on this goal.

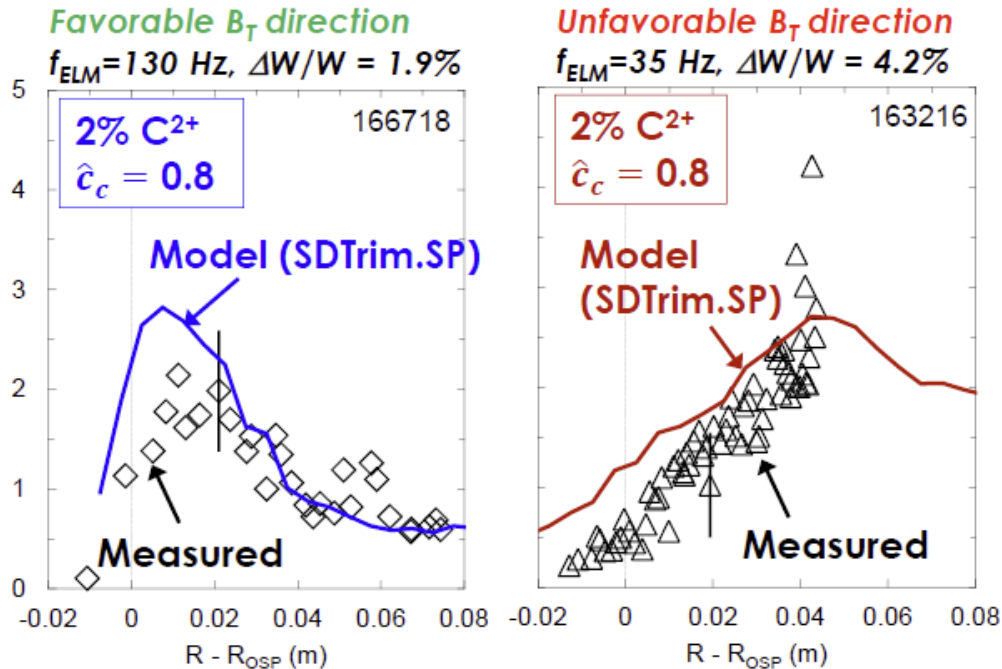


Fig. 3-21. Spectroscopically measured spatially-resolved profiles of the gross erosion of tungsten during ELM events for two different ELM regimes. Calculations from empirical SDTrim.SP sputtering (solid lines) are overlaid [Abrams 2016].

**Goal 1: Characterize balance of inter-ELM and ELM-induced W leakage from LFS and HFS vs. level of ELM mitigation.** In devices with open W divertors, the total W source tends to be dominated by the outer target between ELMs, but the W source from the inner target and outer target regions are roughly comparable during ELMs [Brezinsek 2015, Dux 2009]. Very sparse information exists, however, on the overall contribution of the inner and outer W sources separately to core W contamination. Similarly, the impact of a high-Z SAS divertor on SOL flows, impurity entrainment, and ITG forces is unclear. Finally, the physics of ELM 'burn-through,' where the plasma tends to re-attach during ELM events and initiate substantial W sourcing, is not well studied or understood. The goal of this research area is to make progress unraveling the complex interactions between the ELM dynamics, divertor closure, and W leakage from the inner and outer divertor regions, validated against state-of-the-art impurity transport models.

During the isotopic W tracer studies in the SAS-1 and SAS-2U divertors discussed in Challenge 1 above, an additional W ring will be placed on the inner target (Fig. 3-20). While the ISP often tends to be naturally detached between ELMs in the DIII-D lower divertor, it is expected that the cryo-pumping capability on the HFS ISP will provide sufficient divertor density control to maintain relatively high electron temperature at that location even in the inter-ELM phase. This may result in substantial W erosion via physical sputtering even between ELMs. Studies will be performed to quantify the balance of intra-ELM and inter-ELM W leakage from an ISP and OSP

W sources. Carefully designed experiments, utilizing the enhanced collector probe and spectroscopy diagnostics, will examine how the W source and W leakage scale with pedestal height (related to ITG forces), SOL density (related to collisional entrainment forces), and ELM size. Such efforts will enhance the understanding of LFS vs. HFS W divertor leakage to constrain physics models, enabling the control techniques discussed in Goal 2 below.

**Goal 2: Develop control techniques to mitigate W leakage from the SAS divertor during transient events.** Research in this area will flow naturally from the theme discussed above. Once the constraints surrounding ELM-resolved W leakage are understood, the challenge becomes sufficiently mitigating these high-Z sources to acceptable levels of core contamination. DIII-D possesses many state-of-the-art techniques for transient mitigation and ELM-free operation, including pellet pacing, RMP fields, ECH actuation, and QH-mode operation. Experiments will be performed to develop and understand scenarios in which high-Z leakage from the SAS divertor is substantially mitigated, as measured by "upstream" diagnostics including the suite of SOL W collector probes and VUV/X-ray spectroscopy. The efficiency of each control technique will be systematically evaluated and physics extrapolations will be performed using SOL impurity transport models to gauge the effectiveness of such methods under reactor-level heat and particle fluxes in an SAS-like divertor.

### **Challenge 3: Identify Main Pathways for Main Chamber Material Migration.**

**Current progress.** Substantial progress in understanding main chamber C impurity migration on DIII-D was accomplished approximately ten years ago. A series of studies were carried out in which isotopically-enriched C impurity gas was injected in the DIII-D main chamber in L-mode plasmas. Post-mortem measurements of the poloidal distribution of deposited  $^{13}\text{C}$  on the main chamber and divertor tiles were performed [Wampler 2005]. Appreciable  $^{13}\text{C}$  deposition occurred primarily on the tile rows near the inner strike point. Interpretive modeling, closely coupled to spectroscopic measurements, determined that approximately 2/3 of the injected methane impurity was efficiently ionized within and transported along the SOL to the inner divertor, driven primarily by SOL flow [McLean 2005, Elder 2005].

In general, limited systematic tests of mixed-material environments in high-performance tokamak operation have been performed; JET's very recent ITER-like wall (ILW) [Brezinsek 2015] and a brief period for ASDEX-U [Krieger 1999] are the only notable exceptions.

**Goal 1: Unravel the primary migration pathways for low-Z main chamber material in a 2D symmetrized system.** Research in this area will focus on understanding main chamber material migration from both intrinsic low-Z impurity sources, as well as externally injected impurities with a wide variety of atomic numbers. Material erosion and migration properties in the main chamber

differ from divertor erosion and migration due to long ionization lengths of eroded impurity atoms. Furthermore, such studies are usually complicated by 3D structures in the main chamber, but within DIII-D there is a possibility of symmetrizing the MC, i.e., making it 2D as is the divertor in most tokamaks. The main benefit of this approach is that it allows for better diagnosis (by assuming symmetry) and therefore easier coupling with modeling. As an option, two toroidally symmetric “belt” limiters will be placed above and below the mid-plane ports, becoming the first (and only) plasma contact in the main chamber and can then be changed to different material, e.g., a low-Z material identified as a promising candidate for next-step devices by the Innovative Materials Evaluation research line in Section 3.3.3. With this setup, it is also possible to change the main chamber wall to a material distinct from the toroidal limiters, e.g., high-Z at the wall and low-Z on the limiters. Some reactor device schemes have such a first-wall arrangement, and this would be the first assessment of such an arrangement in a diverted tokamak.

### 3.3.1.3 Capability Enhancements

The primary hardware enhancements in this research area are outlined in Table 3-22. As discussed above, these primarily involve the progressive addition of isotopically enriched high-Z rings in DIII-D's innovative Small Angle Slot (SAS) divertors. This culminates in the addition of a full-W SAS-2U divertor near the end of the proposed five-year plan. This divertor may be actively heated to remove C deposits, allowing for actuation of the dominant low-Z seeded divertor impurity. Toroidal bumper limiters are also proposed as an option for 2D symmetrized studies of main chamber material migration. The primary diagnostics needed to achieve the desired physics insights are displayed in Table 3-23. Notably, the fast MDS camera and UV/VUV spectroscopy in SAS-1 and SAS-2 will provide detailed measurements of ELM-resolved W sourcing. SOL collector probes in multiple poloidal locations and multichordal core VUV spectroscopy will provide detailed information on high-Z SOL impurity fluxes and core W accumulation, respectively. Finally, the modeling codes that will be utilized to gain physics understanding into high-Z leakage from the SAS divertor and main chamber material transport are provided in Table 3-24.

**Table 3-22.**  
**Hardware Enhancements for Material Migration Studies on DIII-D**

<b>Hardware</b>	<b>Primary Physics to be Studied</b>	<b>Research Goal</b>
SAS-1 W rings, SAS-2U W rings	High-Z leakage rate from different poloidal locations	Evaluate how SAS divertor closure impacts W leakage from different poloidal locations
(Option) SAS-2U-HW	Cumulative W leakage from SAS divertor	Understand W leakage in high-power AT-coupled SAS divertor
Low-Z impurity gas puffing and powder dropping	Dominant low-Z seeded divertor impurity	Test how W leakage from SAS is modified as a function of the dominant low-Z seeded impurity
Toroidal bumper limiters (Option)	Main chamber material migration	Identify main pathways for main chamber material migration in a 2D symmetrized system

**Table 3-23.**  
**Physics Enabled by New Diagnostics for Material Migration Research**

<b>Desired Measurement Capability</b>	<b>New Physics Enabled</b>	<b>Proposed Diagnostic</b>
SOL impurity fluxes	Diagnose impact of ITG forces, SOL flows and drifts on high-Z impurities	Collector probes
ELM-resolved neutral W and W <sup>+</sup> source rates	ELM-resolved high-Z sputtering, prompt re-deposition	Fast MDS camera
Spatial profile of neutral W and W <sup>+</sup> impurity content	Evaluation of high-Z divertor leakage in a closed divertor geometry	UV/VUV spectroscopy in SAS-1 and SAS-2
Ion saturation current during ELMs	Effect of intra-ELM ion fluxes and ion impact energies on W sourcing	Higher I,V limits for Langmuir probes
High-Z core contamination	Impact of divertor closure on W leakage from SAS-1 and SAS-2	Multichordal core VUV/X-ray spectroscopy

**Table 3-24.**  
**Codes Used for Material Migration Research**

<b>Code</b>	<b>Material Migration Related Purpose</b>
ERO1.0, SDTrim.SP	ELM-resolved local PMI source physics – sputtering, implantation, ionization, reflection, re-deposition
ERO2.0, OEDGE/DIVIMP	Interpretive SOL impurity transport – ITG forces, perp. diffusion, drifts, entrainment, flows
WALLDYN, GITR+SOLPS	Predictive SOL impurity transport including mixed-material effects
ADAS Atomic Physics codes	Relate in-situ spectroscopy measurements to gross/net material erosion and edge impurity densities

### 3.3.2 Surface Evolution Science

*Physics Leads: D.L. Rudakov (UCSD), T. Abrams (GA), D.M. Thomas (GA), W.R. Wampler (SNL), R. Ding (ASIPP), A. Lasa (ORNL)*

The plasma-material interface in a fusion energy device is a dynamic, evolving region of material that is constantly eroded and re-deposited many times over. Extrapolating forward to a reactor, with main chamber wall and divertor erosion rates many orders of magnitude larger than current devices, leads to a mixed-material environment that goes well beyond the current understanding of PFC slag management, tritium retention via co-deposition, and material lifetime limits. Within this context, the work at DIII-D will continue to address the science needed to advance the understanding and prediction of the above situation. This research area will address the PMI workshop report's Priority Research Directions (PRD) D (*Understand the science of evolving materials at reactor-relevant plasma conditions and how novel materials and manufacturing methods enable improved plasma performance*) [US DOE OFES 2015\_2].

Historically, this research has relied on the well-established Divertor Material Evaluation System (DiMES) program, a linear manipulator allowing for exposure of material samples in the lower divertor of DIII-D under well-diagnosed ITER-relevant plasma conditions [Wong 2007, Rudakov 2017]. Plasma parameters during the exposures are characterized by an extensive diagnostic suite including a number of spectroscopic diagnostics, Langmuir probes, IR imaging, and Divertor Thomson Scattering. Post-mortem measurements of net erosion/deposition on the samples are done by Ion Beam Analysis. In the past five years, experimental results modelled by the ERO and REDEP/WBC codes, coupled to plasma background information produced by OEDGE, have provided substantial insight into the local physics of high-Z sputtering, re-deposition, and material mixing in the DIII-D divertor [Brooks 2015, Ding 2016, Guterl 2016, Abrams 2017]. Expanding these model-validation efforts to the main chamber wall, and eventually to more global material deposition phenomena, becomes the focus of the 2019-2024 five-year plan in this topical area.

#### 3.3.2.1 Challenges and Impact

The first high-priority challenge identified for the Surface Evolution Science (SES) group is the quantification of main chamber (MC) erosion, particularly due to charge exchange (CX) neutrals and energetic particles, with an emphasis on plasmas and divertor conditions near detachment where main chamber walls become more prevalent [Kotov 2009, Verbeek 1998]. The primary tool for facilitating advancements in this topical area is the proposed Wall Interaction Tile Station (WITS), described in Challenge 1 below. WITS will provide detailed information about the main chamber neutral and background plasma flux and energy spectrum, and the advanced

sample exposure capability will provide valuable information for benchmarking models of main chamber material erosion and re-deposition. If successful, this research will enable extrapolations of MC material erosion models forward to future devices to gain predictive capability in a reactor-like mixed-material environment.

In parallel, a second major challenge for the SES area involves developing techniques for the active re-deposition of material onto main chamber and divertor plasma-facing components (PFCs). An important facet of this challenge will be characterization of intra-ELM vs inter-ELM erosion/re-deposition in the divertor and accounting for ELM-induced PMI on the main chamber walls. Another crucial knowledge gap to address is the impact of real material surface morphology on the dynamics of these eroded and re-deposited layers, which will be benchmarked against state-of-the-art PMI modeling code suites incorporating realistic surface roughness effects. Should these techniques prove effective, this research will provide solutions to enhance MC wall material lifetime limits, and to the development of strategies to mitigate tritium retention via co-deposition, in reactor-level devices.

**Table 3-25.**  
**Surface Evolution Science Challenges, Goals, and Enhancements**

<b>Challenge</b>	<b>Goals/Deliverables</b>	<b>Enhancements</b>
Test predictive models of main chamber material erosion	<ul style="list-style-type: none"> <li>• Characterize and test models of background MC CX neutrals, main ions, and impurities</li> <li>• Understand impact of MC PMI on main chamber plasma-facing components</li> </ul>	<p><b>Hardware</b></p> <ul style="list-style-type: none"> <li>• WITS</li> <li>• Addl. DiMES heating</li> </ul> <p><b>Diagnostic</b></p> <ul style="list-style-type: none"> <li>• CX hydrogen sensors</li> <li>• WITS TCs, LPs</li> <li>• WITS spectroscopy</li> <li>• DiMES microscopy</li> </ul>
Develop active methods of renewable PFM surface conditioning	<ul style="list-style-type: none"> <li>• Validate models of local low-Z and high-Z prompt material re-deposition</li> <li>• Determine effects of surface morphology on local material transport and benchmark against PMI modeling codes</li> <li>• Evaluate impact of novel wall conditioning techniques on edge plasma</li> </ul>	<p><b>Analysis Capabilities</b></p> <ul style="list-style-type: none"> <li>• MC synthetic diagnostics</li> <li>• Extended modeling grids</li> </ul>

### 3.3.2.2 Research Plan

The Surface Evolution Science program research plan is organized according to the challenges and goals in Fig. 3-22, which provides the timeline for each challenge, research milestones, and the capability improvements necessary to achieve them.

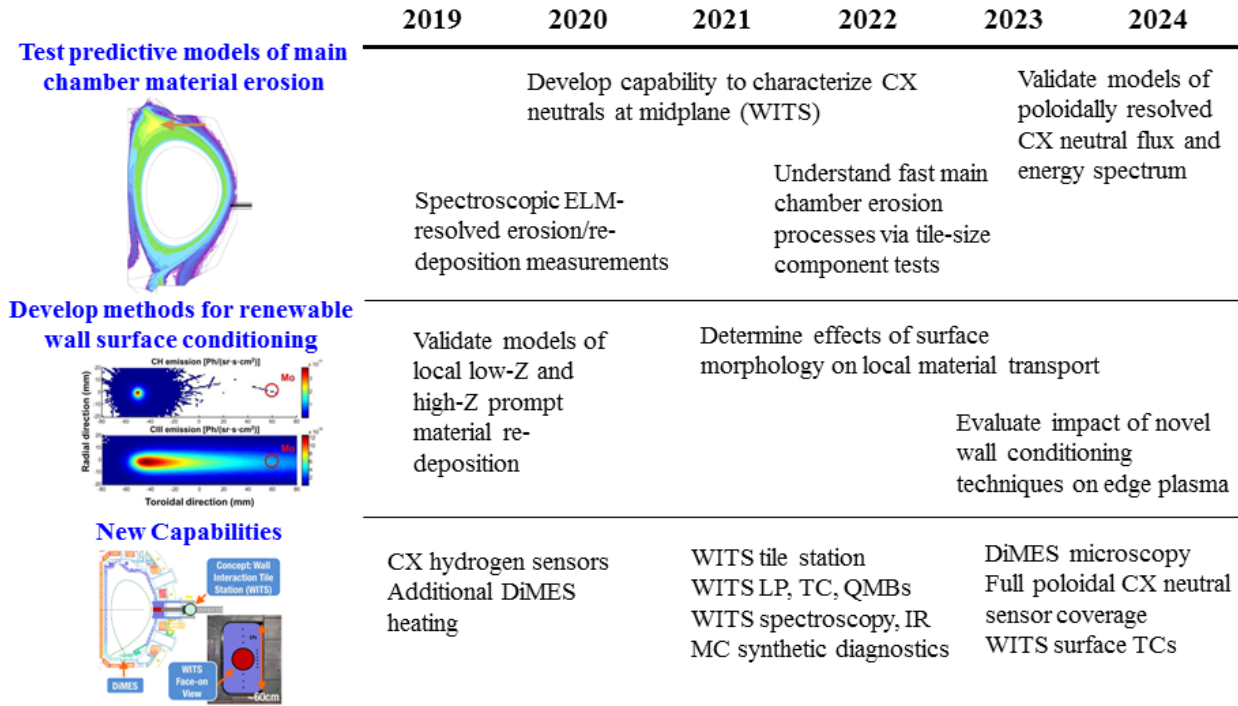


Fig. 3-22. Surface evolution science timeline

### Challenge 1: Test Predictive Models of Main Chamber Material Erosion

**Current progress.** The past five years saw rapid progress in DIII-D’s understanding of high-Z erosion and re-deposition physics in the DIII-D divertor region. Using the world leading DiMES capability, coupled primarily to OEDGE+ERO model validation, many local PMI physics elements were successfully benchmarked against experiments. It was observed that the gross erosion rates of Mo and W high-Z material can be well explained by physical sputtering due to main ion and C impurity impacts, including the effect of C/W material mixing, in L-mode plasma conditions [Brooks 2015, Ding 2016]. In these studies, the prompt re-deposition fractions measured via a novel experimental technique, involving high-Z thin coatings of different diameter, were also consistent with ERO and WBC-REDEP predictive PMI modeling calculations. The development of high-Z ELM resolved spectroscopy techniques also provided confirmation that the gross erosion of W PFCs in inter-ELM H-mode plasmas, shown in Fig. 3-22, are dominated by C ion impact sputtering and C/W material mixing [Abrams 2017]. Many predictions exist for the sputtering and re-deposition rates due to energetic CX neutrals as a function of poloidal angle in the main chamber [Verbeek 1998], but few systematic benchmarking studies have been performed against actual experimental measurements of main chamber erosion rates.

The primary tool for facilitating advancements in this topical area is the proposed Wall Interaction Tile Station (WITS). A conceptual design for this station is displayed in Fig. 3-23. This tool will consist of a large-scale (~60 cm) high-density PMI diagnostics cluster mounted on a

movable limiter. WITS will also add the capability of exposing tile-size (~10 cm) components to controlled main chamber plasma conditions. An option is included for active surface heating of these sample components up to ~600 °C (in addition to plasma heating) and actuation of the PMI sheath physics via sample biasing. This manipulator will be coupled to a DiMES-like sample exchange chamber allowing between-shot sample interchange and *in-vacuo* analysis.

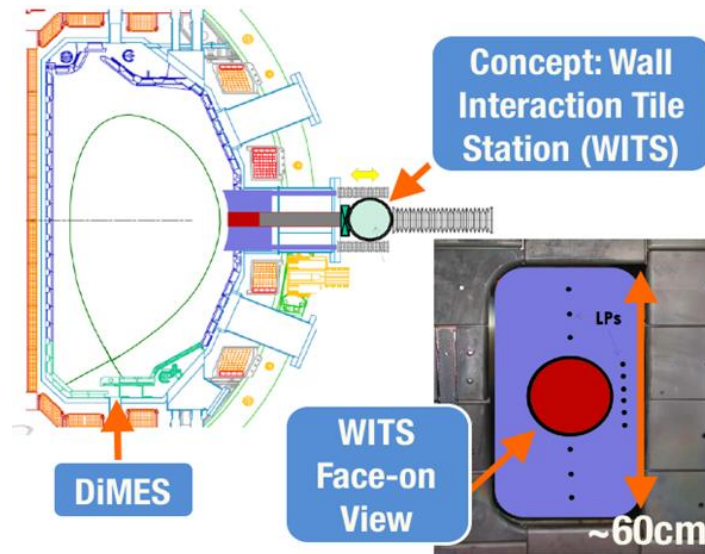


Fig. 3-23. Conceptual design for the Wall Interactions Tile Station (WITS).

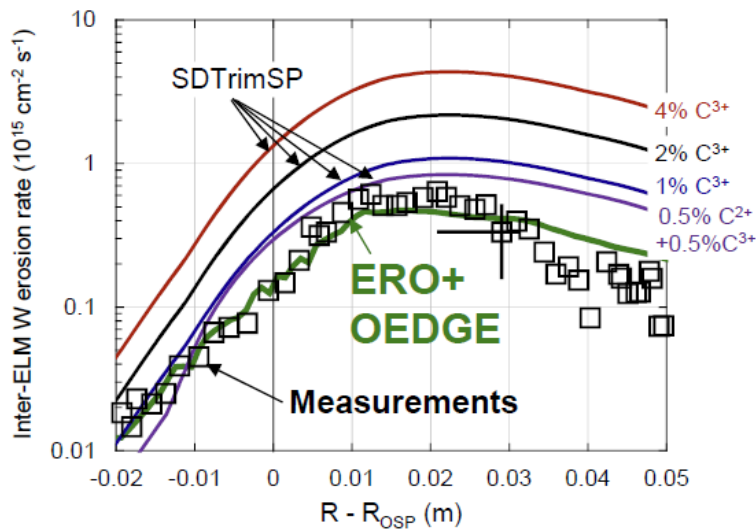


Fig. 3-24. Spectroscopic measurements of the inter-ELM W erosion rate as a function of radial position for the same discharge. ERO+OEDGE predictions are overlaid, displaying better agreement with experiment than less sophisticated SDTrimSP modeling [Abrams 2017].

**Goal 1: Characterize and test models of background main chamber CX neutrals, main ions, and impurities.**

This work will emphasize detailed measurements of MC erosion processes, both in steady state and due to transients such as ELMs and fast ions. Particular effort will focus on incorporating the impact of charge exchange neutrals and fast ions into the modeling. This will require measuring charge exchange neutral fluxes and energies at multiple poloidal locations. The main diagnostic enhancement to support this effort will be incorporating hydrogen sensors first on WITS, then at multiple poloidal locations on the main chamber wall. The removable sample exposure probe portion of WITS will enable dynamic tests of different iterations of CX neutral sensors to rapidly optimize the deployment of this crucial diagnostic. Measurements of the poloidal charge exchange flux and energy spectrum will be benchmarked against EIRENE modeling within OEDGE and SOLPS. Work has already begun to extend the EIRENE and DIVIMP grids within OEDGE all the way to the outer wall [Elder 2017], essential to understand main chamber erosion and re-deposition, which occurs deep in the far scrape-off-layer. Routine operation of main chamber PMI modeling codes with these extended grid codes will be developed to robustly test these enhanced models against experiments.

**Goal 2: Understand impact of MC PMI on main chamber plasma-facing components.**

The second facet of this challenge involves developing an understanding, via carefully designed experiments coupled to interpretive modeling, of the "back reaction" of the main chamber neutral and plasma species on the main chamber PFCs. Using the new WITS capability described above, large sample components will be exposed to main chamber plasma fluxes, varying the position of the WITS sample exposure limiter with respect to the separatrix, the temperature of the sample surface, and the depth of the plasma sheath via negative sample biasing. These studies will provide a wealth of information for understanding main chamber PMI physics coupled to modeling. New codes like GITR and ERO2.0 will be deployed, which provide Monte Carlo based calculations of main chamber PMI on the substantially larger scales (tens of cm) of sputtered material ionization lengths in the main chamber. In addition, new synthetic diagnostics will be developed within these codes, building upon the existing ERO2.0 framework developed to model the inner wall limiters on the JET-ILW [Romazanov 2017], to facilitate the quantitative benchmarking of model calculations with experimental data. The extensive WITS diagnostic suite will provide detailed measurements of background plasma parameters, such as main chamber ion and electron temperature, to provide better constraints on ERO2.0 and GITR modeling than has been possible in previous studies. Finally, studies of PMI phenomena caused by fast transients will require fast diagnostics. They will rely on imaging of DiMES and WITS using the existing fast visible and IR cameras.

## Challenge 2: Develop Active Methods of Renewable PFM Surface Conditioning

**Current progress.** Simple extrapolations using the well-known physical sputtering yields of candidate main chamber wall material reveals that in reactor-level devices tons/year of material will be eroded from the main chamber wall, likely flowing primarily to the divertor region [Stangeby 2011]. This dramatic "slag management" issue has potentially dire implications for material lifetimes and tritium retention limits via co-deposition in the divertor. The goal of this second challenge is to develop techniques to extend material lifetimes via active replenishment of the material surface in the main chamber and mitigate hydrogen co-deposition, primarily in the divertor via techniques such as surface heating and mechanical removal of low-Z co-deposits. In the past five years, extensive progress has been made in understanding the formation rate and dynamic mixed-material nature of these co-deposits in the divertor region. During experiments in which deuterated methane ( $\text{CD}_4$ ) was injected into the divertor, it was determined that the radial C impurity deposition profile on high-Z surfaces is strongly influenced by ExB drifts and cross-field diffusion, and the cross-field diffusion coefficient was determined to be  $\sim 0.5 \text{ m}^2/\text{s}$  using experimental data as constraints on ERO modeling, as depicted in Fig. 3-25 [Ding 2017\_1]. It was also observed that these deposited C layers on high-Z surfaces could be actively removed during transient events [Guterl 2016]. Similar experiments using  $\text{D}_2$  gas puffing were also executed to mitigate high-Z erosion via reduction of the divertor electron temperature, and erosion rates predicted by ERO were consistent with experiment [Ding 2017\_2].

Global studies of high-Z surface migration via successive prompt re-deposition steps revealed the importance of C/W material mixing in determining the overall W surface migration rate [Wampler 2017]. The simple mixed-material model integrated into ERO was not capable of quantitatively or qualitatively reproducing the measured magnitude of W re-deposition, motivating further refinements to modeling studies. The physics of prompt re-deposition via ionization and gyro-motion has been demonstrated to be strongly non-linear with the initial surface mixed material fraction [Guterl 2017], indicating the importance of precise experimental measurements of the surface conditions, as described in Table 3-27.

Finally, preliminary investigations of the impact of surface roughness on material re-deposition in the DIII-D divertor indicate that ion impact angles become, on average, substantially shallower near the surface plane, leading to strongly asymmetric angular sputtering distributions and substantial fractions of surface area shadowed from ion impact [Chrobak 2018]. Studies in this area over the next five years will focus on directly incorporating surface roughness effects into the ERO1.0/2.0 and GITR models, and then testing these models against existing and newly enhanced experimental measurements.

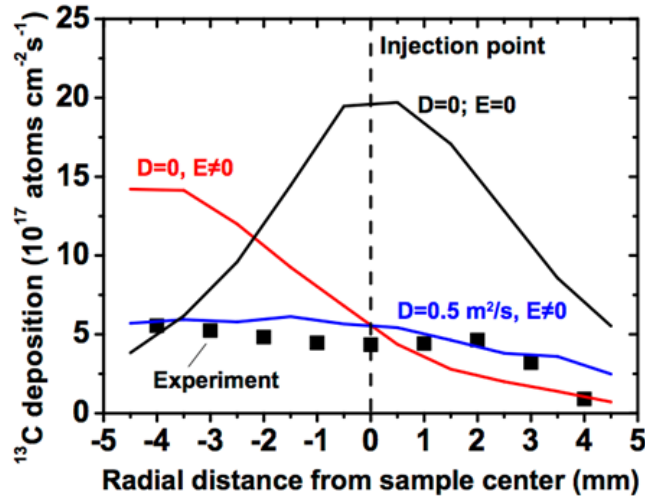


Fig. 3-25. Measured radial profiles of  $^{13}\text{C}$  deposition on a Mo witness sample after deuterated methane injection. Consistency is observed with ERO modeling after incorporating ExB drifts and assuming a cross-field diffusion coefficient of  $0.5 \text{ m}^2/\text{s}$  [Ding 2017\_1].

### Goal 1: Validate Models of Local Low-Z and High-Z Material Deposition

As discussed above, a primary goal within this challenge involves understanding the gradual migration of low-Z and high-Z material across the divertor and main chamber surfaces via successive prompt re-deposition steps. Note that this is a fundamentally different impurity transport mechanism from direct SOL impurity transport discussed in Section 3.3.1, as it involves the direct migration of material across the surface without ever escaping the divertor region. Such effects have minimal impacts in current short-pulse devices; in fact, even measuring their effect requires many repeated plasma discharges [Wampler 2017]. Extrapolations to long pulse or steady state reactors are essential to understand the impact on the reactor PFCs.

Initial steps toward this goal will involve continued analysis and careful model benchmarking of existing data sets from the Metal Rings Campaign. Notably, a more sophisticated mixed-material model will be incorporated into ERO2.0 and GITR by DIII-D collaborators, and the sensitivity of calculations to cross-field drifts and long-range material transport will be evaluated. These models will leverage existing data sets detailing the differences in surface material properties of re-constituted layers on plasma-material surfaces [Doerner 2012], which will guide the design of additional experiments to fill in gaps in this database as they are discovered. Model "stress testing" against experimental impurity spectroscopy profiles will be performed to evaluate the level of agreement with existing atomics physics models of electron-impact ionization and photon emissivity. This will involve carefully designed experiments utilizing passive re-deposition methods by bombarding material samples on DiMES and WITS, as well as active material re-

deposition via impurity gas puffing. Studies will also be further enabled by the addition of quartz microbalances (QMBs) on DiMES or WITS to measure real-time material deposition rates *in-situ*.

**Goal 2: Determine effects of surface morphology on local material transport.**

Nearly all current PMI physics models assume a perfectly smooth plasma-facing surface. In reality, even pristine ITER-grade W surfaces can have roughness on the order of microns, and PMI effects such as micro-fracturing, dust deposition, and unipolar arcing can induce tens of micron scale defects in the material. Therefore, detailed studies must be performed of how surface roughness impacts the erosion and re-deposition rates of low-Z and high-Z material. DiMES and WITS samples will be developed utilizing innovative surface patterning methods, such as additive manufacturing and focused ion beam (FIB) milling, to understand how surface morphology patterns impact material erosion and deposition. In parallel, the GITR and ERO Monte Carlo PMI codes will be enhanced to directly incorporate the impact of surface roughness on sheath physics, sputtering, and prompt re-deposition. An innovative *in-situ* optical microscopy system installed on DiMES or WITS will provide direct characterization of the shot-by-shot evolution of the surface morphology of these samples, providing accurate input into the modeling codes. These studies are synergistic with goals in the Innovative Materials research area (Section 3.3.3) to develop novel material patterning techniques to reduce net erosion rates via increased self-shadowing of the sputtered material. Such effects have previously been observed during exposures of W nano-tendrill surfaces in the DIII-D divertor [Rudakov 2015].

**Goal 3: Evaluate impact of novel wall conditioning techniques on edge plasma.**

The capstone goal of this research direction builds upon the foundation established through the first two goals – namely, a validated physics understanding and predictive capability for how actively and passively injected impurity material re-deposits locally on the plasma-facing surface. This final initiative extends these studies globally to the entire material wall, with the target of developing reactor-relevant scenarios in which the first-wall material can be replenished in steady state during plasma discharges. In conjunction, active techniques will be evaluated to mitigate hydrogenic retention in co-deposited material layers. For example, the materials can be heated to very high temperatures via active heating on WITS and as an option being considered in SAS-2U-HW (Section 3.3.1), as well as directly via plasma contact heating. In addition, techniques such as direct mechanical removal of material co-deposits [Stangeby 2017] will be developed and tested. These studies will incorporate material deposition data from DiMES, WITS, and additional collector probes discussed in more detail in Section 3.3.1. In conjunction, the impact of new global wall conditioning techniques, such as extending inter-day glow-based boron wall conditioning to silicon or other low-Z materials will be investigated. In conjunction with the core-edge integration

thrusters in Chapter 4, studies will be performed to evaluate how the radiating mantle in the SOL plasma varies as a function of the impurity utilized for wall conditioning and main chamber material replenishment.

### 3.3.2.3 Capability Enhancements

The flagship capability enhancement proposed in this research area is the Wall Interactions Tile Station (WITS), which will provide a platform for detailed measurements of the CX neutral and ion fluxed in the main chamber, and will facilitate the exposure of large-scale sample components to main chamber plasma conditions. In conjunction, additional impurity injection capabilities will be added to assist in the development of active methods for renewable wall surface conditioning. This will mandate understanding the impact of surface morphology on erosion and re-deposition patterns in the divertor and main chamber, motivating the installation of *in-situ* optical microscopy diagnostics and high-resolution WITS visible and UV imaging.

Excellent diagnostics are mandatory for the validation elements of this challenge. Table 3-27 summarizes the planned diagnostic upgrades and the rationale for these improvements, while Table 3-28 lists many of the codes employed in this research.

**Table 3-26.**  
**Hardware Enhancements for Surface Evolution Science Studies on DIII-D**

<b>Hardware</b>	<b>Primary Physics to be Studied</b>	<b>Research Goal</b>
Wall Interactions Tile Station (WITS)	CX neutral and main ion flux and energy spectrum, sputtering and ionization of MC materials	Quantify main chamber CX neutrals and background plasma, validate models of main chamber PMI
Low-Z and High-Z impurity puffing and powder dropping	Re-constitution of material surfaces via re-deposition	Understand prompt re-deposition physics of actively injected wall material
DiMES and WITS heating capability	Impact of surface temperature on sputtering and sticking coefficients	Actively remove low-Z co-deposits from high-Z surfaces
Heated W divertor (optional)	Impact of surface temperature on D retention in the divertor	Control C/D codeposition and D recycling on W target

**Table 3-27.**  
**Physics Enabled by New Diagnostics for Surface Evolution Science Research**

<b>Desired Measurement Capability</b>	<b>New Physics Enabled</b>	<b>Proposed Diagnostic</b>
Poloidal charge exchange flux and energy spectrum	Quantify and understand main chamber erosion via energetic neutrals	Neutral CX hydrogen sensors
Main chamber plasma heat and particle fluxes	Validate models of main chamber PMI with accurate plasma background information	WITS Langmuir probes, surface thermocouples, IR camera
Surface morphology	Impact of surface patterning on erosion and re-deposition profiles	In-situ optical microscopy
Variations of surface layer areal densities	Time-resolved material erosion and re-deposition rates in the main chamber	WITS UV/visible spectroscopy, In-situ quartz microbalances (QMBs)

**Table 3-28.**  
**Codes Used for Surface Evolution Science Research**

<b>Code</b>	<b>Material Migration Related Purpose</b>
ERO1.0, SDTrim.SP	ELM-resolved local PMI source physics – sputtering, implantation, ionization, reflection, re-deposition
ERO2.0, OEDGE/DIVIMP	Interpretive SOL impurity transport – ITG forces, perp. diffusion, drifts, entrainment, flows
WALLDYN, GITR+SOLPS	Predictive SOL impurity transport including mixed-material effects
ADAS Atomic Physics codes	Relate in-situ spectroscopy measurements to gross/net material erosion and edge impurity densities

### 3.3.3 Evaluation of Reactor-Relevant Materials

*Physics Leads: D. Thomas (GA), T. Abrams (GA), S. Bringuier (GA), J. Barton (SNL), Y. Katoh (ORNL), D. Rudakov (UCSD), Z. Unterberg (ORNL)*

The development of suitable plasma-facing materials (PFM) is a key issue for future fusion energy production. A successful PFM must withstand the energy and particle fluxes at the plasma periphery without unduly contaminating the core plasma and without significantly retaining the deuterium/tritium fuel. The materials must perform at high temperature and retain their performance in the presence of intense neutron irradiation. Any erosion or wear will need to be mitigated in some fashion for adequate long-term operation. Currently there is no viable material satisfying all of these interrelated requirements for fusion reactors. The most used elements to date have consisted of single-element, mono-block designs primarily made of carbon, tungsten, or

beryllium. Not only do each of these materials choices have sub-optimal properties when exposed to a fusion plasma environment (e.g., large hydrogen retention/permeation, low melting temperatures, poor neutron compatibility, and/or detrimental to the core fusion performance), there has been little effort to demonstrate the integration of these materials into overall components that would be useful in reactor conditions.

Developing new materials that may be optimized to solve one or more of these requirements will help in an eventual integrated solution of the PFM problem. The materials science community is now developing novel materials (such as advanced ceramics and ceramic/metal composites) and new manufacturing techniques (including additive manufacturing) that may play a role in future fusion applications, if properly tested and optimized. A key element of this involves testing of the materials in plasma environments, characterizing their performance and extrapolating their performance to reactor conditions. This information would feed back into further manufacturing and materials improvements.

DIII-D has played an important role in characterizing plasma-materials interactions through the use of its Divertor Materials Evaluation System (DiMES) in combination with its well-diagnosed divertor plasma environment. [Wong, 2007, Rudakov, 2015]. This combination is a unique strength of the DIII-D boundary program. This capability will be employed to characterize and model the behavior of reactor-relevant materials in the divertor, and be extended to address the issue of PFM in the main chamber (this has historically received less attention, but is equally important to an integrated solution). The goal is to study materials for which we can test specific hypotheses about the role of such parameters as morphology, sputtering yield, erosion, mitigation, and temperature dependence on PFM behavior in the DIII-D boundary plasma environment. These studies will have the additional benefit of identifying potential upgrades to the existing DIII-D wall which might extrapolate to improved performance of the core plasma, due to changes in the underlying plasma material interaction. This would allow the option to pursue an integrated (Core + Boundary) development path that would enhance future DIII-D operation.

### 3.3.3.1 Challenges and Impact

The goal of this research program is to study the PMI of new materials in the DIII-D environment in order to develop the physics basis for reactor plasma-facing wall solutions. The challenge is to optimize the mix of high-Z divertor targets (chosen to minimize sputtering) and low-Z main chamber (chosen to minimize core contamination effects) resulting in a mixed-material environment (Fig. 3-26). This environment arises for several physics reasons. Transients aside, high-Z (e.g., tungsten) targets can handle power with little or no erosion or core contamination under detached divertor conditions. Under these same conditions, the main chamber may dominate the core contamination, making low-Z materials attractive for these surfaces. When

considering transients such as ELMs, a determination needs to be made of the maximum tolerable size for W-targets.

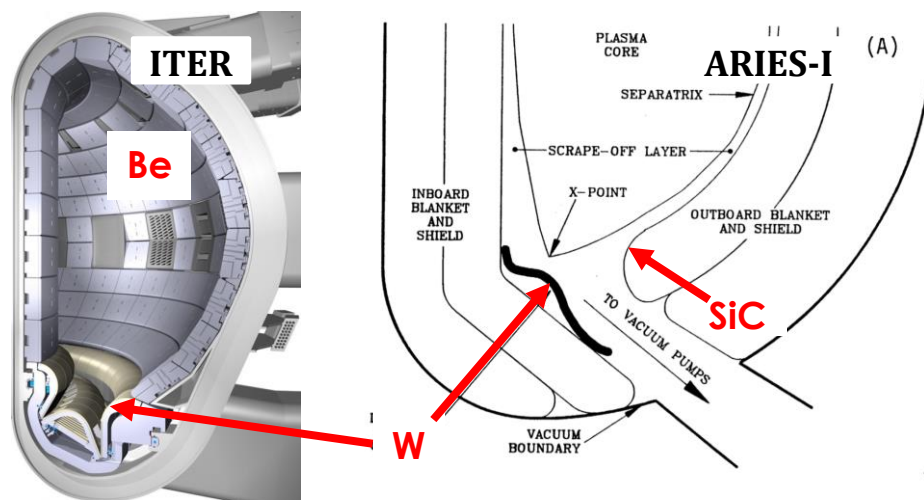


Fig. 3-26. Examples of mixed-material next-step reactor walls, using high-Z divertor targets and low-Z main chamber surfaces.

In the case of tungsten, successful future use must address many specific challenges. Some of these are due to thermo-mechanical limitations; in particular its loss of strength and ductility under neutron irradiation, oxidation limitations, and its loss of fracture toughness below the ductile brittle transformation temperature. In addition, its transmutation and activation can lead to substantial nuclear decay heat and severe remote handling/radwaste issues. Finally, the lack of complete ionization for high-Z atoms even in reactor-grade plasmas will lead to unsustainable radiative losses from the core, precluding breakeven for any but the smallest core concentrations ( $n_Z/n_e < \sim 10^{-5}$ ). In the case of low-Z materials, a complementary set of challenges exist. Foremost among these is the significantly higher erosion and redeposition of first-wall material due to higher sputtering rates, and the typically (significantly) higher chemical reaction rates with hydrogen isotopes in carbon and carbon-based PFMs. The combination of these effects can lead to unacceptable fuel retention in the co-deposited layers, and unacceptable amounts of gross material redeposition and migration.

The impact of solving these challenges would be to improve the performance and safety margin of future reactor designs. Nearer term, the solutions may be applicable in DIII-D future options to increase the power handling capability and energy confinement, leading to enhanced near-term performance.

Table 3-29 presents the associated goals and upgrades needed to make scientific progress on these high-level challenges.

**Table 3-29.**  
**Innovative Materials Challenges, Goals, and Upgrades**

<b>Challenge</b>	<b>Goals/Deliverables</b>	<b>Upgrades</b>
<p>What solid materials beyond bulk C, Be, &amp; W are appropriate to scale to next-step devices? And can additive manufacturing (AM) be used to extend PFC performance &amp; lifetime?</p>	<ul style="list-style-type: none"> <li>• Measure candidate materials with favorable properties using DiMES and/or WITS exposures for erosion and heat handling capabilities</li> <li>• Other W-alloys, such as W-fiber/Wand ultra fine grain W</li> <li>• CMC-SiC (SiCf/SiC) exposures at coupon-level and tile-level</li> <li>• Other Composite SiC, e.g. Cf/SiC, W/SiC</li> <li>• investigate other AM methods such as foaming for reducing sputtering and/or high heat removal</li> </ul>	<p><b>Hardware</b></p> <ul style="list-style-type: none"> <li>• WITS (with heating)</li> </ul> <p><b>Diagnostics</b></p> <ul style="list-style-type: none"> <li>• Deep blue spectroscopy</li> <li>• Deep blue imaging</li> <li>• DiMES diagnostics (e.g., LIBS)</li> <li>• emission coverage</li> </ul> <p><b>Modeling / Code Development</b></p> <ul style="list-style-type: none"> <li>• ERO</li> <li>• WallDYN</li> </ul>

**3.3.3.2 Research Plan**

The Innovative Materials research plan is organized according to the challenges and goals in Table 3-29. Fig. 3-27 gives the timeline for each challenge, research milestones, and the capability improvements necessary to achieve them.

<b>Challenge</b>	<b>FY19-20</b>	<b>FY21</b>	<b>FY22</b>	<b>FY23</b>	<b>FY24</b>
Investigation of novel solid PFC candidates, in divertor and main chamber, including additively manufactured (AM)	DiMES evaluation of high-Z (e.g., W-alloys, W/SiC, Wf/SiC, etc.) and low-Z (e.g. CMC-SiC, UHTC, Max-phase ceramics, etc.) as divertor PFMs WITS evaluation of main chamber PFM candidates SAS divertor evaluation of W-alloys and composites				
Hardware Improvements	Increased NBI and ECH power			SAS-U heated W divertor (optional)	
Diagnostic Enhancements	Extended spatial and spectral coverage of deep-blue spectroscopy Hydrogen sensors to characterize CX fluxes Main chamber SOL characterization using WITS deployed diagnostics				
	WITS SIC Limiters (optional)				

*Fig. 3-27. Innovative material plan timeline*

## **Challenge 1: What Solid Materials Beyond Bulk C, Be, & W Are Appropriate to Scale to Next-Step Devices and Can Additive Manufacturing (AM) Be Used to Extend PFC Performance and Lifetime?**

**Current progress.** DIII-D, in contrast to many other operating tokamaks, has chosen to stay with a low Z graphite wall in order to enable successful advanced tokamak research by avoiding the problem of high-Z buildup and performance degradation. In this environment, a successful research program on high-Z materials using the DiMES probe has enabled studies of the physics of tungsten fuzz erosion, leading edge enhancement suppression of erosion, the effect of ion impact energy using biased probe heads, and other parametric variations in the well-diagnosed lower divertor. In addition, a successful metal rings campaign using tungsten coated divertor tiles has been carried out (see Section 3.3.1). Within this testing process, the DIII-D facility, as a toroidal device, provides access to the physics of surface morphology with realistic flux angles and energy profiles – both are key to understanding how surfaces erode and reconstitute. This is a complimentary step to validate any understanding of material properties that is learned from, for example, single physics linear devices. Recent improvements to 400.9 nm WI spectroscopy [Abrams 2017] and target design have allowed DIII-D to determine with good accuracy (20%) the local gross and net erosion rates with high time resolution. Additional work on deep blue spectroscopy to assess other WI lines is in progress.

At a low level of effort, explorations have begun into the possibility and limitations of using silicon carbide (SiC) as a first-wall material. Many reactor studies have SiC, along with W, as the plasma-facing material (PFM) of choice. As plasma impurities, Si and C radiate minimally in the core. As a fusion material SiC has the promise of neutron damage resilience, low activation, effective barrier to T permeation, and high temperature operation. However, this promise needs to be validated by systematically investigating the many open questions posed by SiC use. These include the issue of tritium retention in the co-deposited layers, permeation in SiC/SiC composites, preferential sputtering leading to preferential surface enrichment, and thermal/electrical conductivity changes during irradiation. Without solutions to these questions SiC cannot be considered as a viable PFC. To date there has been very limited characterization in toroidal devices. DIII-D has begun by conducting first SiC exposure tests in DiMES to measure sputtering yields, as well as installing two SiC-coated graphite tiles to obtain initial data on long term behavior in a main chamber environment.

**Goal 1: Investigate the PMI performance of novel tungsten alloys.** Using the DiMES apparatus, DIII-D will expose samples which have been prepared, either through conventional or additive manufacturing techniques, to address specific shortcomings of bulk tungsten. Some representative examples are listed below.

Fig. 3-28 shows the top surface of an ultra-fine-grain (UFG) tungsten sample, which was prepared using powder metallurgy with a dispersion of  $\text{TiO}_2$  particles to act as grain growth inhibitors [Kolasinski,2016]. These materials have been shown to have good ductility at room temperature, are resistant to recrystallization/grain growth, and have demonstrated resistance to damage from transient heat loading. Additionally, retention experiments in linear devices have demonstrated minimal formation of surface bubbles/blisters under high deuterium fluence ( $10^{25} \text{ D/m}^2$ ), compared to, say, ITER-grade tungsten.

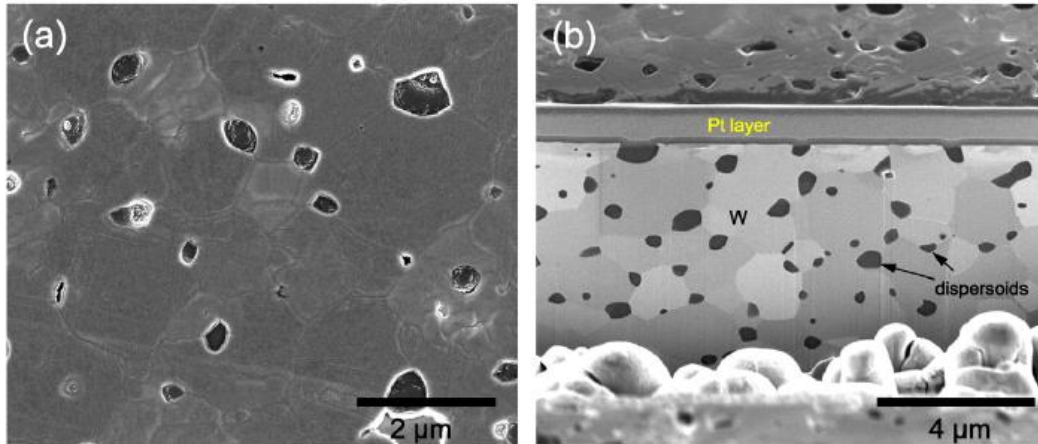


Fig. 3-28. SEM images of the UFG W showing (a) the top surface, and (b) a cross-section created by focused ion beam profiling. Darker regions of the surface correspond to Ti grains. from [Kolasinski 2016]

Also under consideration are composite materials such as tungsten fiber/tungsten matrix composites, or SiC fiber/tungsten composites, which are intended to extend the mechanical strength of bulk W [Linsmeier 2017, Zinkle 2013].

For these materials, exposure to a range of power levels and temperatures, and in-situ and post-exposure analysis, will provide basic data on their erosion properties, their behavior under ELM transients, morphological changes, and hydrogenic uptake (through subsequent thermal desorption spectroscopy). These data will be compared to existing tungsten DiMES data and will be used for more comprehensive modeling using erosion codes such as ERO. Improvements in the 200-400 nm or “deep blue” spectroscopy will allow observation of several other WI lines and improve the calculations by improving the S/XB ratios used to relate line brightness to sputtering rates.

**Goal 2: Test the basic PMI performance of novel ceramic materials** like MAX-phase ceramics and ultra-high temperature ceramics (UHTCs), as well as CVD SiC. MAX phase refers to a family of layered compounds with the chemical formula  $\text{M}_{n+1}\text{AX}_n$  where M is an early transition metal (e.g., Ti), A is an A-group element (e.g., Si, Al, ...) and X is either carbon or nitrogen. These materials demonstrate a mix of metal and ceramic properties, including: high toughness, thermal conductivity, fatigue resistance, temperature tolerance, and thermal shock

resistance. Recent works [Tallman 2015, Clark 2016] analyzing irradiation properties have identified  $Ti_3SiC_2$  and  $Ti_2AlC$  as two promising candidates. It is expected that exposure of these materials in DIII-D will identify their basic behavior since there are presently no published plasma exposure experiments. This will include their stability to decomposition under a range of heat flux loads, and their response to thermal shock from ELMs.

In addition, data on the performance of SiC composites manufactured using various techniques will be obtained, comparing them with CVD SiC. The measurements and modeling necessary to determine gross sputtering rates for both Si and C will be developed, similar to techniques successfully applied to the existing tungsten erosion studies. Detailed data on the evolution of the SiC surfaces, their erosion and redeposition, and characterization of hydrogen retention under varying plasma conditions will be obtained and again used to broaden the modeling base using the erosion codes. One example of an engineered material for testing is SiC coated graphitic foam, shown in Fig. 3-29, which enables studies of SiC surface evolution at varying surface roughness. The underlying foam exhibits enhanced thermal conductivity compared to bulk graphite.

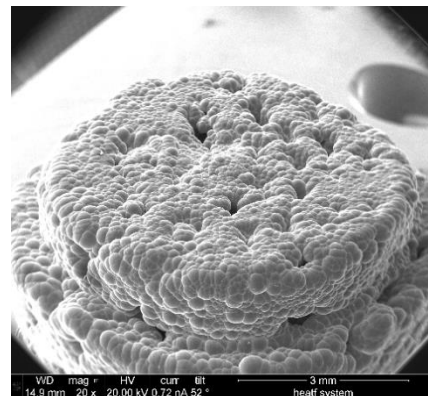


*Fig. 3-29. SEM images of SiC-coated C foam sample*

**Goal 3: Characterize the PMI of candidate materials under main chamber plasma conditions using the new WITS capability.** As mentioned in the previous section, the development and installation of the WITS will allow DIII-D to study the properties of these materials in the main chamber of DIII-D, with up to tile-scale samples being deployed. Using this tool and associated main-chamber diagnostics, we will be able to quantify the effects of fast ions and charge exchange neutrals on material parameters such as sputtering and hydrogen retention, for the various candidate materials. Fig. 3-30 shows the energy dependence of erosion for SiC compared to pure Si and C. The preferential sputtering of C implies that surface enhancement of Si may be expected, particularly for elevated temperatures. This behavior is consistent with initial DIII-D measurements on SiC using estimated rates from TRIM.SP calculations [Abrams 2017]. Such unique measurements are important for assessing the future utility of this material.

In conjunction with this goal, Section 3.3.1 discussed an option for possible installation of main chamber belt limiters to simplify the SOL modeling situation by symmetrizing the 3-S SOL environment to approximately 2-D. If installed, this offers the possibility to retrofit non-graphitic (e.g., SiC) surfaces on these limiters. This would provide additional main-chamber data which would be particularly attractive from a modeling standpoint.

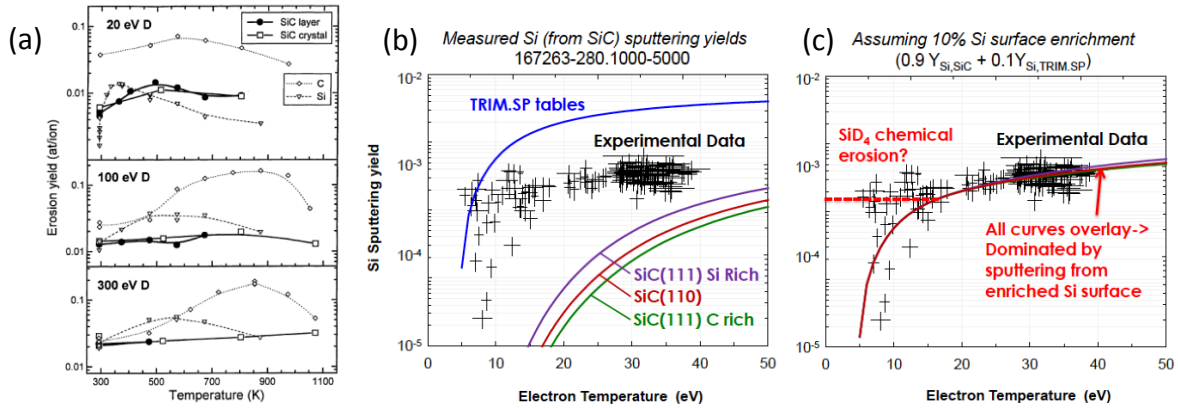


Fig. 3-30. (a) temperature dependence of energetic particle sputtering for SiC, C and Si. (b),(c) measured sputtering from DIII-D SiC exposures compared to TRIM.SP sputtering calculations.(b) no enrichment, (c) ~10% Si surface enrichment.

**Goal 4: Characterize the PMI of both high-Z and low-Z samples at elevated temperatures.** Prior to the beginning of the 2019-2024 five-year plan, the high-temperature range for DiMES sample exposures will be extended (by heater modifications) to the 500°C-600°C range. A similar extended temperature range is anticipated in the WITS sample holder as well. This will give us a unique capability to study sputtering yields and deuterium retention at reactor-relevant temperatures, in both the divertor and main chamber, for various materials.

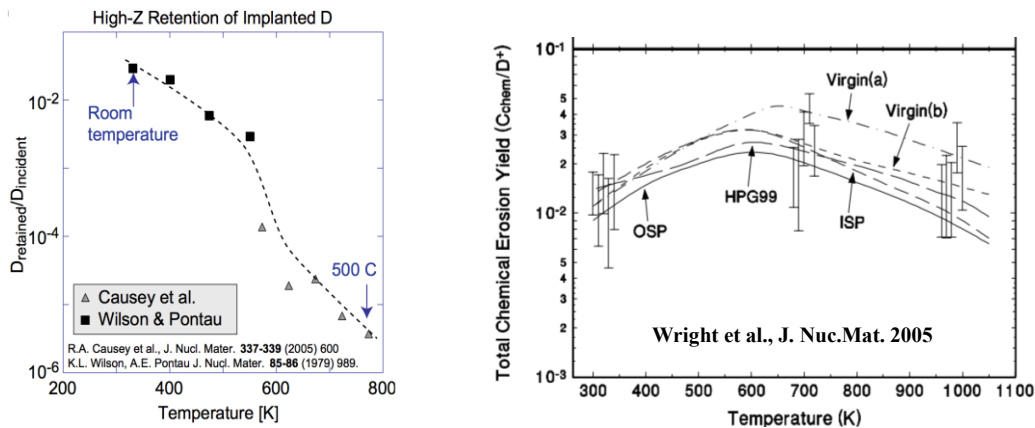


Fig. 3-31. (a) deuterium retention of W drops substantially and (b) carbon chemical erosion first increases, then decreases, as target temperatures increase.

An optional heated W target in SAS-2 is proposed for near the end of the five-year period. This research is intended to remove C deposits from the tungsten surface and obtain a clean W divertor environment, which should lead to reduced D recycling and consequently different slot divertor performance as a result. This will provide valuable information on large-scale PMI in a reactor-like divertor environment.

### 3.3.3.3 Capability Enhancements

The primary facility enhancement for reactor-relevant PFM evaluation research in the five-year plan timescale will be the design and deployment of the Wall Interaction Test Stand (WITS), described in Section 3.3.2 and its associated diagnostics to provide a well-characterized main chamber boundary plasma environment for material exposure. Facility enhancements will also provide capability to expose DiMES samples in divertor plasmas in new parameter regimes. Improvements to the heating systems described in Section 2 will allow for higher power density divertor plasmas. The SAS-2 facility will provide a more closed divertor configuration for higher neutral divertor densities and decoupling from the main chamber neutral density.

**Table 3-30.  
Facility Enhancements**

Hardware Capability	New Physics
WITS	Improved understanding of main chamber PMI

**Table 3-31.  
Physics Enabled by New Diagnostics for Innovative Materials Research**

Scientific objective	Physics measurement	Diagnostic Technique
Determine sputtering yields from wall, both inter- and intra-ELM	Low charge state carbon, tungsten and silicon spectroscopy	Deep blue spectrometers and/or filterscopes; high time resolution
Characterize charge exchange (CX) neutral particle flux	Neutral charge-exchange spectroscopy	in-situ neutral particle detectors
In-situ thermo-mechanical evaluation of test materials	Tile/Wall temperature in main chamber and on WITS	Thermocouples and/or main chamber IR

**Table 3-32.  
Codes Used for Innovative Materials Research**

Code	Purpose
SOLPS	Divertor/SOL fluid transport, ionization source Primary boundary modeling code to provide plasma background for erosion calculations.
ERO	Local erosion rates, including sputtering calculations Primary code for comparing to experimental erosion tests of materials
WALLDYN	Global impurity migration code

## References

- [Abrams 2016] T. Abrams et al., "Impact of ELMs on the tungsten source distribution near the DIII-D outer strike point," PSI-22 2016 O29.
- [Abrams 2017] T. Abrams et al., *Nuc. Fusion* **57** (2017) 056034
- [Abrams 2017] T. Abrams et al., *Nucl. Fusion* **57** (2017) 056034.
- [Asakura 2000] N. Asakura et al 2000 *Phys. Rev. Lett.* **84** 3093
- [Asakura 2001] N. Asakura et al 2001 *Jour. Nucl. Mater.* 290-293 825
- [Asakura 2007] N. Asakura et al 2007 *Jour. Nucl. Mater.* 363-365 41
- [Baklen 2001] M. Baklen et al., *J. Nuc. Mat.* 209-233 (2001) 47
- [Batishchev 1997] O.V. Batishchev et al 1997 *Phys. Plasmas* **4** 1672
- [Boedo 1998] J.A. Boedo et al 1998 *Phys. Plasmas* **5** 4305
- [Boedo 2000] J.A. Boedo et al 2000 *Phys Plasmas* **7** 1075
- [Boedo 2003] J.A. Boedo et al 2003 *Phys. Plasmas* **10** 1670
- [Boedo 2011] J.A. Boedo et al 2011 *Phys. Plasmas* **18** 032510
- [Boedo 2016] J.A. Boedo et al 2016 *Phys. Plasmas* **23** 092506
- [Bosch 1996] H.-S. Bosch et al 1996 *Phys. Rev. Lett.* **76** 2499
- [Braams 1987] B. J. Braams, "A multi-fluid code for simulation of the edge plasma in tokamaks", Next European Torus (NET) report, EUR-FU/XII-80/87/68, January 1987.
- [Brezinsek 2015] S. Brezinsek, *J. Nucl. Mat.* **463** (2015) 11.
- [Brezinsek 2015] S. Brezinsek, *J. Nucl. Mater.* **463** (2015) 11.
- [Buttery 2015] R. J. Buttery and the DIII-D Team, *Nucl. Fusion* **55** (2015) 104017.
- [Bykov 2017] I. Bykov et al 2017 "Impact of target material on D and D2 recycling in DIII-D ELMy H-mode discharges", BO4 13 *Bull. Am. Phys.* 2017 (<http://meetings.aps.org/Meeting/DPP17/Session/BO4.13>)
- [Bykov 2017] I. Bykov et al., "Impact of target material on D and D2 recycling in DIII-D ELMy H-mode discharges," APS-DPP 2017 BO4.
- [Canik 2015] J. M. Canik et al., *J. Nucl. Mater.* **463** (2015) 569.
- [Canik 2017] J. M. Canik et al 2017 *Phys. Plasmas* **24** 056116
- [Canik 2017] J. M. Canik et al., *Phys. Plasmas* **24** (2017) 056116.
- [Carralero 2017] D. Carralero et al 2017 *Nucl. Fusion* **57** 056044
- [Chan 2015] V. S. Chan et al., *Nucl. Fusion* **55** (2015) 023017.
- [Chang 2017] C.S. Chang et al 2017 *Nucl. Fusion* **57** 116023
- [Chankin 2007] A. V. Chankin et al 2007 *Nucl. Fusion* **47** 762

- [Chankin 2009] A.V. et al Jour. Nucl. Fusion 390–391 319
- [Chrobak 2018] C.P. Chrobak et al., "Measurement and Modeling of Aluminum Sputtering and Ionization in the DIII-D Divertor Including Magnetic Pre-Sheath Effects," Nucl. Fusion (2018) submitted.
- [Churchill 2017] R.M. Churchill et al 2017 Nucl. Fusion 57 046029
- [Clark 2016] D.W. Clark et al. Acta Mater. 105 (2016) 130
- [Covele 2017] B. Covele et al 2017 Nucl. Fusion 57 086017
- [Den Harder 2016] N. Den Harder et al., Nucl. Fusion 56 (2016) 026014.
- [Ding 2016] R. Ding et al., Nucl. Fusion **56** (2016) 016021.
- [Ding 2017] R. Ding et al. Nucl. Fusion **57** (2017) 056016.
- [Ding 2017\_1] R. Ding et al., "High-Z material erosion and its control in DIII-D carbon divertor", Nucl. Mat. Energy (2017) <https://doi.org/10.1016/j.nme.2017.03.012>
- [Ding 2017\_1] R. Ding et al., "High-Z material erosion and its control in DIII-D carbon divertor", Nucl. Mat. Energy (2017) <https://doi.org/10.1016/j.nme.2017.03.012>
- [Ding 2017\_1] R. Ding et al., Nucl. Fusion **57** (2017) 056016.
- [Ding 2017\_2] R. Ding et al., (2017) Nucl. Fusion 57, 056016 <https://doi.org/10.1088/1741-4326/aa6451>
- [Ding 2017\_2] R. Ding et al., (2017) Nucl. Fusion 57, 056016 <https://doi.org/10.1088/1741-4326/aa6451>
- [Ding 2017\_2] R. Ding et al., Nucl. Mater. Energy **12** (2017) 247–252.
- [Doerner 2012] R.P. Doerner et al., Nucl. Fusion **52** (2012) 103003.
- [Dux 2009] R. Dux et al., J. Nucl. Mater 390–391 (2009) 858–863.
- [Eich 2013] T. Eich et al 2013 Nucl. Fusion 53 093031
- [Eich 2013] T. Eich et al 2013 Nucl. Fusion 53 093031
- [Eich 2017] T. Eich et al., Nucl. Mater. Energy 12 (2017) 84–90.
- [Elder 2005] J.D. Elder et al., J. Nucl. Mater. 337–339 (2005) 79–83
- [Elder 2017] J.D. Elder et al., "OEDGE Modeling of Collector Probe measurements in L-mode from the DIII-D Metal Rings Campaign," APS-DPP (2017) NP11.
- [Fenstermacher 1997] M. E. Fenstermacher et al 1997 Phys. Plasmas 4 1761
- [FESAC\_1] Fusion Energy Sciences Advisory Committee (FESAC) Transformative Enabling Capabilities (TEC) subpanel (report to come). Information Retrieved from: <https://www.burningplasma.org/activities/?article=FESAC%20TEC%20Panel%20Public%20Info%20Home%20Page>
- [Garofalo 2014] AA. M. Garofalo et al., Fusion Eng. Des. **89** (2014) 876–881.

- [Goetz 1999] J. A. Goetz et al 1999 Phys. Plasmas 6 1899
- [Goldston 2012] R.J. Goldston 2012 Nucl. Fusion 52 013009
- [Groth 2005] M. Groth et al 2005 Jour. Nucl. Mater. 337-339 425
- [Groth 2009] M. Groth et al 2009 Nucl. Fusion 49 115002
- [Groth 2011] M. Groth et al 2011 Jour. Nucl. Mater. 415 S530
- [Gunn 2017] J.P. Gunn et al., Nucl. Mater. Energy 12 (2017) 75–83.
- [Guo 2017] H. Y. Guo et al., Nucl. Fusion **57** (2017) 044001.
- [Guo 2017a] H.Y. Guo et al 2017 Nucl. Fusion 57 044001
- [Guo 2017b] H.Y. Guo et al 2017 “An innovative small angle slot divertor concept for long pulse advanced tokamaks”, YI2 6 Bull. Am. Phys. 2017  
(<http://meetings.aps.org/Meeting/DPP17/Session/YI2.6>)
- [Guterl 2017\_1] J. Guterl et al., Nucl. Mater. Energy **12** (2017) 392–398.
- [Guterl 2017\_2] J. Guterl et al., "Modeling and analysis of tungsten sourcing in the outer divertor during the DIII-D metal ring campaign," PET-16 (2017).
- [Hollmann 2006] E.M. Hollmann et al 2005 Plasma Phys. Control. Fusion 48 1165
- [Isler 1999] R. C. Isler et al 1999 Phys. Plasmas 6 541
- [Jaervinen 2016] A. E. Jaervinen et al 2016 Proc. 36th EPS Conference
- [Jaervinen 2016] A.E. Jaervinen et al., “Investigations of detachment bifurcations in DIII-D with UEDGE”, Bull. American Physical Society 61 (Proc. 58th Annual Meeting of APS Division of Plasma Physics), CO4.00004 (2016).
- [Kallenbach 2015] A. Kallenbach et al 2015 Nucl. Fusion 55 053026
- [Kessel 2015] C. Kessel et al., Fusion Sci. Tech. 67 (2015) 1.
- [Kolasinski 2016] R. Kolasinski et al., Int. J. Ref. Metals and Hard Mat. (2016).
- [Kotov 2008] V. Kotov et al 2008 Plasma Phys. Control. Fusion 50 105012
- [Kotov 2009] V. Kotov et al, Phys. Scr. T138 (2009) 014020.
- [Kotov 2009] V. Kotov et al, Phys. Scr. T138 (2009) 014020.
- [Kotschenreuther 2004] M. Kotschenreuther et al, in Proceedings of the 20th International Conference on Fusion Energy, Vilamoura, Portugal (International Atomic Energy Agency, Vienna, 2004), IC/P6-43
- [Kotschenreuther 2004] M. Kotschenreuther, P. Valanju, J. Wiley, T. Rognlein, S. Mahajan, and M. Pekker, in Proceedings of the 20th International Conference on Fusion Energy, Vilamoura, Portugal (International Atomic Energy Agency, Vienna, 2004), IC/P6-43.
- [Kotschenreuther 2007] M. Kotschenreuther, P. M. Valanju, S.M. Mahajan, and J.C. Wiley, Phys. Plasmas 14 (2007) 072502. n

- [Kotschenreuther 2013] M. Kotschenreuther, P.M. Valanju, B. Covele, and S.M. Mahajan, *Phys. Plasmas* 20 (2013) 102507.
- [Krashennikov 2017] S.I. Krashennikov et al 2016 *J. Plasma Phys.* 23 055602
- [Krieger 1999] K. Krieger et al., *J. Nucl. Mat.* 266-269 (1999) 207.
- [Krieger 1999] K. Krieger et al., *J. Nucl. Mater.* 266-269 (1999) 207.
- [Kukushkin 2011] A. S. Kukushkin et al 2011 *Fusion Engineering and Design* 86 2865
- [LaBombard 2005] B. LaBombard et al 2005 *Phys. Plasmas* 12 056111
- [LaBombard 2015] B. LaBombard et al., *Nucl Fusion* **55** (2015) 053020.
- [Leonard 2012] A.W. Leonard et al 2012 *Nucl. Fusion* 52 063015
- [Linsmeier 2017] Ch. Linsmeier et al., *Nucl. Fusion* 57 (2017) 092007.
- [Loewenhoff 2011] Th. Loewenhoff et al., *Phys. Scr.* T145 (2011) 014057.
- [McLean 2005] A.G. McLean et al., *J. Nucl. Mater* 337–339 (2005) 124–128.
- [McLean 2015] A. G. McLean et al., *J. Nucl. Mater.* **463**, 533 (2015)
- [McLean 2015] A.G. McLean et al 2015 *Jour. Nucl. Mater.* 463 533
- [Moser 2016] A.L. Moser, A.W. Leonard, S.L. Allen, et al, "Effect of divertor closure on pedestal fueling and divertor detachment onset in DIII-D", 22nd International Conference on Plasma Surface Interactions in Controlled Fusion Devices, 2016.
- [Moser 2016] A. M. Moser et al "Effect of divertor closure on pedestal fueling and divertor detachment onset in DIII-D", presented at the 22nd International Conference on Plasma Surface Interactions in Controlled Fusion Devices, Rome, Italy, May 30-June 3, 2016
- [Myra 2006] J. Myra et al 2006 *Phys. Plasmas* 13 112502
- [Myra 2016] J. Myra et al 2016 *Phys. Plasmas* 23 112502
- [Neuhauser 1984] J. Neuhauser et al 1984 *Nucl. Fusion* 24 1
- [Petrie 2001] T.W. Petrie, C.M. Greenfield, R.J. Groebner, et al., *J. Nucl. Mater.* 290-293 (2001) 935.
- [Petrie 2003] T.W. Petrie, J.G. Watkins, L.R. Baylor, et al., *J. Nucl. Mater.* 313-316 (2003) 834.
- [Petrie 2005] T.W. Petrie, N.H. Brooks, M.E. Fenstermacher, et al., *J. Nucl. Mater.* 337-339 (2005) 216.
- [Petrie 2008] T.W. Petrie, N.H. Brooks, M.E. Fenstermacher, et al., *Nucl. Fusion* 48 (2008) 045010.
- [Petrie 2009] T.W. Petrie, G.D. Porter, N.H. Brooks, et al., *Nucl. Fusion* 49 (2009) 065013.
- [Petrie 2017] T.W. Petrie, T. Osborne, M.E. Fenstermacher, et al., *Nucl. Fusion* 57 (2017) 086004.
- [Pigarov 2006] A.Yu. Pigarov et al *Contrib. Plasma Phys.* 46 604

- [Pitts 2011] R. A. Pitts et al 2011 J. Nucl. Mat. 415 S957
- [Pitts 2013] R.A. Pitts et al., J. Nucl. Mater. 438 (2013) S48–S56.
- [Potzel 2013] S. Potzel et al 2013 Jour. Nucl. Mater 438 S285
- [Putterich 2010] T. Putterich et al., Nucl. Fusion 50 (2010) 025012.
- [Reimold 2015] R. Reimold et al 2015 Jour. Nucl. Mater. 463 128
- [Reiter 1992] D. Reiter et al 1992 Jour. Nucl. Mater. 196-198 80
- [Reiter 2005] D. Reiter et al 2005 Fusion Science and Technology 47 172
- [Reiter 2005] D. Reiter et al 2006 Plasma Phys. Control. Fusion 44 1723
- [Rognlien 1999] T.D. Rognlien 1999 Phys. Plasmas 6 1851
- [Rognlien 2016] T.D. Rognlien et al., “Comparison of 2D simulations of detached divertor plasmas with divertor Thomson measurements in the DIII-D tokamak”, Nuclear Materials and Energy (in press). DOI: <https://doi.org/10.1016/j.nme.2016.12.002>.
- [Rohm & Haas 2008] Rohm & Haas CVD SiC Data Sheet, 2008
- [Romanelli 2013] F. Romanelli et al 2013 Nuclear Fusion 53 104002
- [Romazanov 2017] J. Romazanov et al., Phys. Scr. **T170** (2017) 014018.
- [Rudakov 2002] D. Rudakov et al 2002 Plasma Phys. Control. Fusion 44 717
- [Rudakov 2015] D.L. Rudakov et al., Phys. Scr. **T167** (2016) 014055.
- [Rudakov 2017] D.L. Rudakov et al., “DiMES PMI research at DIII-D in support of ITER and beyond”, Fusion Eng. Des. (2017) <http://dx.doi.org/10.1016/j.fusengdes.2017.03.007>
- [Rudakov 2017] D.L. Rudakov et al., Fusion Eng. Des. **124** (2017) 196-201
- [Ryutov 2007] D.D. Ryutov, Phys. Plasmas **14** (2007) 064502.
- [Ryutov 2007] D.D. Ryutov, Phys. Plasmas 14 (2007) 064502.
- [Sang 2017] C.F. Sang, P.C. Stangeby, H.Y. Guo, et al., Plasma Phys. Control. Fusion 59 (2017) 025009.
- [Schneider 2006] R. Schneider et al 2006 Contrib. Plasma Phys. 46 3
- [Schneider 2006] R. Schneider et al 2006 Contributions to Plasma Phys. 46 3.
- [Simonini 1994] R. Simonini et al Contrib. Plasma Phys. 34 368
- [Smick 2013] N. Smick et al 2013 Nucl. Fusion 53 023001
- [Soukhanovskii 2012] V.A. Soukhanovskii, et al., Phys. Plasmas 19 (2012) 082504.
- [Stangeby 2010] P.C. Stangeby et al 2010 Nucl. Fusion 50 125003
- [Stangeby 2011] P. C. Stangeby and A. W. Leonard, Nucl. Fusion **51**, 063001 (2011).
- [Stangeby 2011] P.C. Stangeby et al., Nucl. Fusion **51** (2011) 063001.
- [Stangeby 2017] P.C. Stangeby and Chaofeng Sang 2017 Nucl. Fusion 57 056007

- [Stangeby 2017] P.C. Stangeby et al., "Developing refractory low-Z ceramic-clad plasma facing components for robust burning plasma device operation," NAS Madison Workshop (2017). Retrieved from: <https://drive.google.com/open?id=0B-OTJcxoAAQFaTFuMmhqOHplUW8>
- [Tallman 2015] D.J. Tallman et al. *Acta Mater.* 85 (2015) 132
- [Tillack 2015] M. Tillack et al., *Fusion Sci. Tech.* 67 (2015) 49.
- [Tobita 2009] K Tobita et al., *Nucl. Fusion* **49** (2009) 075029.
- [Ueda 2009] Y. Ueda et al., *J. Nucl. Mater.* 390–391 (2009) 44–48.
- [Unterberg 2016] EA Unterberg et al., "Characterization of Different Divertor Tungsten Sources, Migration and Impact on the Core in DIII-D ELM-y H-mode Conditions", IAEA-FEC 2016 PDP-6.
- [Unterberg 2016] EA Unterberg et al., "Characterization of Different Divertor Tungsten Sources, Migration and Impact on the Core in DIII-D ELM-y H-mode Conditions", IAEA-FEC 2016 PDP-6.
- [US DOE OFES 2015\_1] US Department of Energy, Office of Science Fusion Energy Sciences (2015). *Fusion Energy Sciences: A Ten-Year Perspective (2015-2025)*. Retrieved from: [https://science.energy.gov/~media/fes/pdf/program-documents/FES\\_A\\_Ten-Year\\_Perspective\\_2015-2025.pdf](https://science.energy.gov/~media/fes/pdf/program-documents/FES_A_Ten-Year_Perspective_2015-2025.pdf)
- [US DOE OFES 2015\_1] US Department of Energy, Office of Science Fusion Energy Sciences (2015). *Fusion Energy Sciences: A Ten-Year Perspective (2015-2025)*. Retrieved from: [https://science.energy.gov/~media/fes/pdf/program-documents/FES\\_A\\_Ten-Year\\_Perspective\\_2015-2025.pdf](https://science.energy.gov/~media/fes/pdf/program-documents/FES_A_Ten-Year_Perspective_2015-2025.pdf)
- [US DOE OFES 2015\_2] US Department of Energy, Office of Science Fusion Energy Sciences (2015). *Report on Science Challenges and Research Opportunities for Plasma Materials Interactions*. Retrieved from: [https://science.energy.gov/~media/fes/pdf/workshop-reports/2016/PMI\\_fullreport\\_21Aug2015.pdf](https://science.energy.gov/~media/fes/pdf/workshop-reports/2016/PMI_fullreport_21Aug2015.pdf)
- [US DOE OFES 2015\_2] US Department of Energy, Office of Science Fusion Energy Sciences (2015). *Report on Science Challenges and Research Opportunities for Plasma Materials Interactions*. Retrieved from: [https://science.energy.gov/~media/fes/pdf/workshop-reports/2016/PMI\\_fullreport\\_21Aug2015.pdf](https://science.energy.gov/~media/fes/pdf/workshop-reports/2016/PMI_fullreport_21Aug2015.pdf)
- [US DOE OFES 2015\_2] US Department of Energy, Office of Science Fusion Energy Sciences (2015). *Report on Science Challenges and Research Opportunities for Plasma Materials Interactions*. Retrieved from: [https://science.energy.gov/~media/fes/pdf/workshop-reports/2016/PMI\\_fullreport\\_21Aug2015.pdf](https://science.energy.gov/~media/fes/pdf/workshop-reports/2016/PMI_fullreport_21Aug2015.pdf)
- [US DOE OFES 2015\_3] US Department of Energy, Office of Science Fusion Energy Sciences (2015). *Report on Science Challenges and Research Opportunities for Transient Events in*

- Tokamak Plasmas. Retrieved from: [https://science.energy.gov/~media/fes/pdf/program-news/Transients\\_Report.pdf](https://science.energy.gov/~media/fes/pdf/program-news/Transients_Report.pdf)
- [US DOE OFES 2015\_3] US Department of Energy, Office of Science Fusion Energy Sciences (2015). *Report on Science Challenges and Research Opportunities for Transient Events in Tokamak Plasmas*. Retrieved from: [https://science.energy.gov/~media/fes/pdf/program-news/Transients\\_Report.pdf](https://science.energy.gov/~media/fes/pdf/program-news/Transients_Report.pdf)
- [US DOE OFES 2015\_3] US Department of Energy, Office of Science Fusion Energy Sciences (2015). Report on Science Challenges and Research Opportunities for Transient Events in Tokamak Plasmas. Retrieved from: [https://science.energy.gov/~media/fes/pdf/program-news/Transients\\_Report.pdf](https://science.energy.gov/~media/fes/pdf/program-news/Transients_Report.pdf)
- [US DOE, OFES 2015-1] US Department of Energy, Office of Science Fusion Energy Sciences (2015). Fusion Energy Sciences: A Ten-Year Perspective (2015-2025). Retrieved from: [https://science.energy.gov/~media/fes/pdf/program-documents/FES\\_A\\_Ten-Year\\_Perspective\\_2015-2025.pdf](https://science.energy.gov/~media/fes/pdf/program-documents/FES_A_Ten-Year_Perspective_2015-2025.pdf)
- [US DOE, OFES 2015-2] US Department of Energy, Office of Science Fusion Energy Sciences (2015). Report on Science Challenges and Research Opportunities for Plasma Materials Interactions. Retrieved from: [https://science.energy.gov/~media/fes/pdf/workshop-reports/2016/PMI\\_fullreport\\_21Aug2015.pdf](https://science.energy.gov/~media/fes/pdf/workshop-reports/2016/PMI_fullreport_21Aug2015.pdf)
- [US DOE, OFES 2015-3] US Department of Energy, Office of Science Fusion Energy Sciences (2015). Report on Science Challenges and Research Opportunities for Transient Events in Tokamak Plasmas. Retrieved from: [https://science.energy.gov/~media/fes/pdf/program-news/Transients\\_Report.pdf](https://science.energy.gov/~media/fes/pdf/program-news/Transients_Report.pdf)
- [Valanju 2009] P. M. Valanju, M. Kotschenreuther,<sup>1</sup> S. M. Mahajan,<sup>1</sup> and J. Canik, *Phys. Plasmas* **16** (2009) 056110.
- [van Rooij 2013] G.J. van Rooij et al., *J. Nucl. Mater.* 438 (2013) S42–S47.
- [Verbeek 1998] H. Verbeek et al, *Nucl. Fusion* 38 (1998) 1789.
- [Verbeek 1998] H. Verbeek et al, *Nucl. Fusion* 38 (1998) 1789.
- [Wade 1998] M.R. Wade et al 1998 *Nucl. Fusion* 38 12
- [Wade 1998] M.R. Wade, J.T. Hogan, S.L. Allen, et al., *Nucl. Fusion* 38 (1998) 1839.
- [Wampler 2005] W.R. Wampler et al., *J. Nucl. Mater.* 337–339 (2005) 134–138.
- [Wampler 2017] W.R. Wampler et al., *Phys. Scr.* **T170** (2017) 014041.
- [Winter 1996] J. Winter, *Plasma Phys. Control. Fusion* 38 (1996) 1503.
- [Wong 2007] C.P.C. Wong, et al., *J. Nucl. Mater.* **363–365** (2007) 276-281.
- [Wong 2007] C.P.C. Wong, et al., *J. Nucl. Mater.* 363–365 (2007) 276-281.
- [Zinkle 2013] S.J. Zinkle, *Fus. Sci. Tech.* 64 (2013) 65.



#### 4. PHYSICS OF INTEGRATION OF CORE AND BOUNDARY SOLUTIONS

Future fusion reactors require the simultaneous achievement of a high performance core plasma and a highly dissipative boundary plasma. The previous two sections have discussed the physics of the core and the boundary separately, to understand the physical mechanisms involved and the basis for developing effective solutions in each to provide access to required performance and stability. However, these two regions are strongly coupled, with parameters and techniques in one region placing significant constraints on the other; a tension between them exists. A dissipative divertor is more readily achieved at high density, but the resulting influx of gas can reduce pedestal and fusion performance. Particles from the core can erode plasma facing materials, which may in turn propagate back into the plasma and accumulate, leading to radiative collapse. Transient heat bursts due to Edge Localized Modes (ELMs) must be eliminated to avoid erosion. Innovative approaches must be developed to overcome this tension and establish the physics basis to project a compatible core-and-edge solution.

The critical region of interaction is the H-mode pedestal, which mediates this tension between core and edge and plays a defining role in the performance of both. Pedestal height acts as a strong lever on core performance. Heat load to the divertor can be mitigated by radiative techniques (raising density, adding more radiative impurities), but such approaches are limited by the requirement for sufficient power throughput to access and maintain H-mode access, as well as sustain good pedestal performance. The pedestal must also be regulated to avoid exceeding edge stability limits that result in ELMs. DIII-D provides a unique opportunity to study these issues thanks to its world leading comprehensive diagnostics and strong flexibility in shaping, 3-D fields, heating and particle control. Research in this proposal seeks to learn how to manipulate this region in order to enhance performance and divertor compatibility (Section 4.1).

Beyond the pedestal, the broader interaction between core and edge must be understood, developing the basis for compatible overall solutions. Compatibility with a reactor relevant wall material is a critical issue. Here the present carbon walled DIII-D provides a benign background to study impurity dynamics and sourcing. Reactor relevant materials can thus be studied perturbatively, with progressive programs of testing tiles, arrays and regions, exploring compatibility and dynamics with core scenarios and new divertor techniques (Section 4.2.1). Proposed siliconization and SiC tile arrays will be deployed to reduce carbon induced sputtering and radiation, enabling more comprehensive model tests and development.

Finally, the overall optimization of the configuration must be developed. The first question goes to basic shape of the plasma, which has a defining influence on divertor and core behavior. The impacts and trade-offs must be assessed including the integration of advanced divertor

configurations developed in Section 3. Work here exploits DIII-D’s extreme shape flexibility with 18 PF coils and double pumped divertors, benefiting from improved power supplies and projected access to higher density AT scenarios with new current drive actuators (see 2.1.2 and 2.3.4), to provide precise, full control to explore the integration and physics of the trade-offs involved, as set out in Section 4.2.2. The resulting configurations must then be integrated with required radiative mantle techniques, understanding both the particle dynamics and the interaction with pedestal performance and ELM control (Section 4.2.3). A critical aspect of this is to understand the limits on radiation and density, including the role of Greenwald density limit, and indeed determining which density metric sets and projects limits for future devices.

There has been remarkable progress on these issues during the current research program. A major accomplishment is the validation of the EPED model [Snyder 2011] of pedestal height and width, developed and initially validated on DIII-D, and now on six tokamaks [Snyder 2015, Komm 2017] over two orders of magnitude in pedestal pressure, including close to the predicted ITER pedestal height [Hughes 2018]. Importantly, this is now being used to project how to raise performance, with innovative new regimes such as super-H mode predicted [Snyder 2015] and discovered [Solomon 2014] on DIII-D. Similar progress has been made in the understanding and extension of ELM suppression techniques, with plasma response-based understanding of RMP-ELM suppression developed and validated [PazSoldan 2015, Nazikian 2015], and used to extend operational windows [Sun 2017], while non-linear MHD and turbulence calculations are capturing the physics of pellet pacing [Futatani 2014] and QH mode [Liu 2017], and how transport enhances pedestal performance in this regime at low torque [King 2017]. Furthermore, an innovative new small angle slot divertor configuration has been discovered [Guo 2017], demonstrating how increased closure can facilitate detachment across the scrape off layer and permit lower upstream density.

The challenge now is to understand how to extend and project these techniques to reactor relevant regimes. Critical questions that need to be addressed include:

- Should a future reactor have 1 or 2 divertors? What is the optimal balance between space for the core and space for the divertor? How can modified divertor geometries improve particle handling to enable high performance cores?
- What are the physical mechanisms governing pedestal structure and how can they be manipulated to raise performance and divertor compatibility?
- How do radiative impurities transport about the plasma, and how can they be used to dissipate heat while ensuring compatibility with a high-performance core and pedestal?
- How to exhaust Helium from the plasma?

- How and from where do interactions of relevant core plasmas with relevant wall materials lead to impurity influxes?
- To what degree are ELMs tolerable? How to achieve sufficient mitigation?

To meet this challenge, research focuses in part on the physics of behavior and improvements within each region – for instance, a higher density pedestal with good core performance (as observed in super H-mode regimes) could lead to enhanced radiative heat dissipation in the divertor. A particle and turbulence based understanding of pedestal structure is sought to project pedestal density and interactions with the divertor (Section 4.1.2). The interaction and optimization of RMP fields for ELM suppression and pedestal manipulation will be explored by developing new flexibility in  $n=3$  and  $n=4$  field structure (4.1.1). Techniques will also be tested to explore improved access to H-mode (4.1.3). However, it is clear that achievement of the most effective integrated solution (and possibly any viable solution whatsoever) requires an understanding of the interactions and trade-offs between these two regions – both to learn how to optimize compatibility with one another, and to determine where best to make the compromises. The interaction with reactor relevant material will be assessed to understand influxes and transport in relevant configurations (4.2.1). More advanced divertor configurations, through closure or magnetic geometry, can confine particles better, promoting detachment to reduce erosion, while also reducing flows of neutrals into the pedestal which may otherwise affect performance. The compatibility of such innovative new divertor configurations and radiative techniques will be assessed with the new core plasma scenarios accessible through planned heating and current drive upgrades (4.2.2 and 4.2.3).

Developing validated predictive understanding will be at the heart of this effort, both in simulating individual phenomena with leading edge codes such as MARS, M3D-C1, NIMROD, JOEK, SOLPS, BOUT and UEDGE, but also through the development and validation of integrated core-edge “Whole Device Modeling” (WDM) solvers, such as the CESOL simulation suite under the DIII-D program. It is important to note that because of its size and parameters (significantly different than a fusion reactor), DIII-D as presently configured cannot simultaneously achieve reactor-relevant core and edge demonstration integrated solutions, because different parts of the problem scale with different parameters, that cannot simultaneously be set to reactor-like values within DIII-D capabilities. However, by testing techniques together and exploring interactions between them, the physics governing how behaviors in different regions trade-off against each other can be understood. This will then be used to constrain models, stress testing them at crucial parameters, to develop a validated simulation basis to project integrated core-edge solutions.

Thus, the research plan afforded by this proposed core-boundary research program on DIII-D provides a unique opportunity to develop the physics for core-edge integration and project the requirements for future fusion reactors.

#### **4.1 PEDESTAL AND ELMS**

The key region of interaction between the core and boundary is the pedestal – a narrow layer of low transport that occurs just within the separatrix leading to the so-called “H-mode” (high) confinement regime. Future burning plasma experiments, including ITER, are designed to operate in the H-mode state to achieve their objectives and therefore these devices will have an H-mode pedestal. This insulating layer plays a crucial role in defining the performance and conditions (not least, density) in the core. It is also key in governing particle dynamics of the plasma, as it exhausts helium ash in a reactor and responds to influxes of neutrals and impurities from the divertor. This mode of operation places important constraints on the design of the machine and the characteristics of the pedestal. First, the machine must have enough heating power to enable a transition into H-mode confinement. Second, the H-mode pedestal must have a sufficiently high pedestal pressure to enable the global confinement to achieve its design values. Third, the H-mode pedestal must not expel large pulses of heat and particles, such as from ELMs, in order to protect plasma components from rapid erosion and damage.

DIII-D has been at the forefront of international fusion research to identify and understand the important physics processes in the pedestal. This has resulted in a first principles physics model, EPED, without free parameters, that predicts pedestal height and width, given pedestal density. However, this model assumes pedestal gradients are limited by kinetic ballooning instabilities and cannot predict individual kinetic profiles, particle dynamics, or situations where different turbulent instabilities govern gradients (as is sometimes observed). These additional considerations can be important in governing pedestal performance, ELM control, H mode access and indeed interaction with the divertor. Work in the 2019-2024 five-year period is planned to better understand these issues and develop improved capability to resolve and improve the power threshold for the L-H transition, to develop understanding of the processes controlling pedestal structure and improved models for prediction of pedestal height and density, and to establish the scientific basis for ELM control to extend it to reactor relevant regimes and provide confident prediction. These three research areas are briefly discussed here.

The most critical pedestal issue is the elimination of ELM transients, which can damage plasma facing surfaces in future large reactors. The central aim of ELM control research on DIII-D is to develop techniques to mitigate or eliminate the ELM instability as well as to develop a predictive understanding of these techniques in order to confidently extrapolate their performance to future tokamaks such as ITER. DIII-D research advances three candidate

techniques to control ELMs – RMPs, pellets, and ELM-stable operating modes such as QH-mode. Although each technique relies on different physical mechanisms to achieve ELM control, the research plan will be structured to address these important themes that are common to all techniques: 1) Understand the physics mechanisms that enable each technique to work and expand the operating space for ELM suppression to the parameters required in a reactor; 2) Determine if the impurity transport is adequate to maintain the required purity of the plasma; 3) Develop understanding of the non-linear evolution of ELM controlled states so that quantitative predictions can be made for future devices. Some of the important enhancements that will enable this work include the addition of coils and power supplies that for the first time will allow manipulation of harmonic content of 3D fields with toroidal periodicity of  $n=3$  and 4 in order to determine what spectrum is best for ELM suppression. Increased EC heating power, upgrades to divertors, diagnostics to measure edge current density and diagnostics to measure deuterium neutral density in the pedestal will further elucidate the physics. The proposed research plan is discussed in Section 4.1.1.

The central aim of the DIII-D pedestal program is to provide the scientific basis for predicting and optimizing pedestal structure in machines. The five-year plan described here aims to gain a particle based understanding of pedestal performance through fueling and turbulence, to resolve its relationship to divertor conditions and its optimization for core performance and good particle/impurity control. The over-riding philosophy of the proposed research is to obtain a qualitative and quantitative understanding of how the pedestal couples the SOL to the core plasmas and the research plan is divided into three themes:

1. Identify and understand the physics processes that couple the pedestal to the SOL/divertor plasma with a significant focus placed on understanding how separatrix density and temperature are set.
2. Understand how the pedestal profiles are determined by sources and transport. Significant research will be done to quantify the pedestal heat and particle sources, particularly the ionization source, and to better understand how fluctuations affect pedestal gradients.
3. Develop techniques and understanding to manipulate the pedestal and SOL in order to raise core performance.

A significant focus in this research will be to understand how the interaction between the core, pedestal and SOL sets the pedestal top parameters. Key hardware enhancements that will enable this work include upgrades to divertors to improve baffling and upgrades to gas injectors to reduce recycling. Enhancements to neutrals-related diagnostics will enable much improved measurements of the ionization source, which will be central to much of the planned research. Other key diagnostic upgrades include a measurement of the pedestal current density and an

upgrade to the tangential Thomson system that will enable improved alignment of electron and ion profiles at the separatrix. The proposed research plan is discussed in Section 4.1.2.

The final challenge is related to access and maintenance of H-mode. This challenge is a critical issue, because divertor exhaust mitigation requires a radiative mantle inside the separatrix; if such radiation is too high, this will prevent or collapse the H-mode pedestal. The goal of the DIII-D L-H physics research program is to develop a physics-based model for the power thresholds for the L-H and H-L transitions so that these transitions can be predicted and safely achieved in future machines, including ITER, and to understand the techniques to optimize H-mode access, or avoid H-mode loss (as can arise when 3D fields are applied). This research area will focus on the following three themes:

1. Develop a predictive quantitative capability for the L-H power threshold. Part of the required research will be to identify the physics processes in the L-H transition.
2. Develop a possible scenario in ITER and other future devices where RMP fields are applied before the L-H transition in order to completely eliminate ELMs. It is anticipated that RMP fields will increase the threshold and therefore research will be performed to study this scenario and to find techniques to reduce the H-mode power threshold.
3. find ways to control the ramp-down from H- to L-mode in order to avoid a large uncontrolled energy release at the H-L transition. This research is also focused on operational needs of ITER, which has limited control capability to handle a large energy release at the transition.

Important hardware enhancements that will help enable this work include divertor upgrades to increase baffling, increased EC power and upgrades to the 3D coil set. Important diagnostic upgrades will provide measurement capability for parallel turbulence correlations, localized magnetic fluctuations and fluctuations in  $T_e$  and  $T_i$ . The proposed research plan is discussed in Section 4.1.3.

All three of the research areas are strongly focused on developing predictive capability. Thus, the research will use state-of-the-art linear and non-linear models to identify and understand relevant physics and develop a predictive capability. These codes are discussed in each section. There will also be some overlap between these various physics areas, particularly between 4.1.1 on ELM control and 4.1.2 on pedestal structure, and significant beneficial collaboration will occur as the work is performed. In addition, the pedestal and ELM control research here will strongly feed into the core-edge integration work, discussed in Section 4.2. The research discussed here aims to get a detailed understanding of pedestal physics. The integration research

in Section 4.2 will use and build on the results obtained here (Section 4.1) to perform its research to couple high performance core plasmas to highly dissipative divertor plasmas.

#### 4.1.1 ELM Control

*Physics Leads: C. Paz-Soldan (GA), X. Chen (GA), L. Baylor (ORNL), A. Bortolon (PPPL), K. Burrell (GA), T. Evans (GA), A. Garofalo (GA), R. Moyer (UCSD), R. Nazikian (PPPL), R. Wilcox (ORNL)*

Control of the edge localized mode (ELM) is an essential aspect of robust and reliable tokamak operation. While ELMs are tolerable on existing devices, predicted ELM size increases in reactor-scale plasmas such as ITER indicate that divertor lifetime will be severely affected by the ELM if it is un-mitigated [Loarte 2014]. To avoid this, the ELM-induced peak heat flux must be mitigated by a significant fraction ( $\sim 50x$  in ITER). DIII-D research pursues several techniques to achieve this goal: the application of resonant magnetic perturbations (RMPs) from non-axisymmetric coils, the use of externally injected pellets to trigger ELMs, and the development of naturally ELM-free stationary regimes such as Quiescent H-mode (QH-mode) and I-mode. This research is essential to demonstrate that reliable high performance tokamak operation can be achieved without suffering deleterious effects from ELMs.

The DIII-D team has made many important advances on this topic in the past 5 years. A quantitative plasma response based understanding of RMP interactions has been developed and validated experimentally. Critical processes and parameters governing RMP ELM suppression and QH-mode access have been determined, with non-linear MHD simulations capturing key elements of behavior. High speed deuterium pellets and impurity granules have been employed and evaluated for ELM mitigation. All three techniques have been pushed towards more ITER relevant regimes with an emphasis on low torque operation. Nevertheless, there remains a considerable challenge to understand how to tailor the techniques to achieve required performance at required parameters in future devices, a vital mission.

##### 4.1.1.1 Challenges and Impact

The central aim of ELM control research on DIII-D is to develop techniques to mitigate or eliminate the ELM instability as well as to develop a predictive understanding of these techniques in order to confidently extrapolate their performance to future tokamaks such as ITER. DIII-D research advances three candidate techniques to control ELMs – RMPs, pellets, and natural ELM-free operating modes. While each technique relies on different physical mechanisms to achieve ELM control, their challenges and approaches can be placed on a similar framework, as shown in Table 4-1. The key research challenges are (i) expand the operational space for effective ELM control in future reactors, (ii) resolve the optimization of fuel and

impurity particle transport, and (iii) develop a predictive understanding of non-linear evolution and sustainment of ELM controlled regimes through validating simulation.

**Table 4-1.  
ELM Control Challenges, Goals and Upgrade Plans**

<b>Challenge</b>	<b>Goals</b>	<b>Key Capability Improvements</b>
Understand and expand operating space of ELM suppressed regimes towards relevant plasma parameters	<ul style="list-style-type: none"> <li>• Expand operating space of ELM controlled regimes by pedestal manipulation</li> <li>• Expand operating space of ELM controlled regimes with NTV torque, optimization of 3D plasma response</li> <li>• Tailor pellet properties to control ELM heat flux mitigation</li> </ul>	<p><i>Hardware Upgrades</i></p> <ul style="list-style-type: none"> <li>• Increased ECH power</li> <li>• Additional 3D coil power supplies</li> <li>• Additional 3D field control coils</li> <li>• Advanced divertor configurations</li> <li>• Tangential pellet injector w/ size selection ability</li> <li>• Impurity Granule Injector w/ regularized frequency, radiative materials</li> </ul> <p><i>Diagnostics Upgrades</i></p> <ul style="list-style-type: none"> <li>• Edge current measurements (imaging MSE)</li> <li>• Spectroscopic/X-ray imaging diagnostics for high-z impurity transport</li> <li>• Edge neutral measurement</li> <li>• Tangential Thomson Scattering upgrade (co-located w/ CER)</li> <li>• 3D magnetics phase 2</li> <li>• Profile diagnostics distributed toroidally for 3D reconstructions (2<sup>nd</sup> BES, 2<sup>nd</sup> ECE)</li> <li>• Advanced imaging of temperature and density fluctuations (ECE-I, MIR)</li> <li>• 3D pellet ablation cloud imaging</li> <li>• 3D wall particle/heat flux imaging</li> </ul> <p><i>Codes:</i></p> <ul style="list-style-type: none"> <li>• Pedestal stability codes (ELITE, EPED, BOUT++)</li> <li>• Linear MHD stability codes (GPEC, MARS, DCON, M3D-C1)</li> <li>• Non-linear extended MHD codes (NIMROD, M3D-C1, JOREK)</li> <li>• Transport codes (GS2, TGLF, CGYRO, XGC)</li> <li>• Integration tools (OMFIT)</li> </ul>
Understand enhancement of main ion, impurity, and ash transport in ELM controlled regimes	<ul style="list-style-type: none"> <li>• Determine role of 3D fields and fluctuations in driving pedestal particle transport</li> <li>• Compare high-Z and He ash transport properties for all ELM suppressed regimes</li> </ul>	
Develop predictive understanding of non-linear evolution and sustainment of ELM controlled regimes.	<p>Through detailed measurements of physical processes in comparison to linear and non-linear simulations:</p> <ul style="list-style-type: none"> <li>• Develop prediction of RMP-ELM suppression</li> <li>• Understand QH-edge transport enhancements</li> <li>• Simulate ELM mitigation with pellet pacing</li> </ul>	

This research is essential to the achievement of robust ELM control with good performance in future tokamaks such as ITER, and will advance our predictive understanding of these techniques to enable confident extrapolation of how to achieve this using ITER’s highly flexible 3D coil set. Specifically, the research will: (i) expand the operating space of ELM controlled regimes towards reactor-relevant conditions; (ii) develop the physical basis for the optimization of applied 3D magnetic perturbations and validate the 3D fields spectra needed for optimal ELM control in RMP and QH mode regimes; (iii) demonstrate quantitative understanding of the effectiveness of ELM controlled regimes in regulating pedestal impurity and ash populations; (iv) establish how to optimize pellet properties to specific operating scenarios, validating models

to predict the optimal pellet type; and (v) develop predictive non-linear simulations to project the evolution and sustainment of ELM controlled regimes to future fusion devices.

**4.1.1.2 Research Plan**

The research plan for ELM control is summarized in Fig. 4-1. A critical element is the increase in 3D field capabilities with new power supplies and coils to manipulate the resonant field spectrum and non-resonant NTV rotation generation enabling first-time spectral optimization at n=3, access to higher-n perturbations, and improved opportunities for spectral optimization with n=1, 2. The plan further builds on the considerable device flexibility of DIII-D through axisymmetric shaping, heating/fueling mix, and divertor geometry. This flexibility allows the operational boundaries of ELM controlled regimes to be modified in order to influence the pedestal structure and identify how to access ELM suppression. These capabilities are augmented significantly with increased ECH and balanced torque beams to extend the range of low torque regimes, and new divertor geometries (which will further impact pedestal structure) to assess compatibility with dissipative divertors. Increased flexibility in the size, composition, and frequency of injected pellets, coupled with stereoscopic imaging, will enable exploration and tailoring of the pellet properties for ELM pacing.

Challenge	FY19-20	FY21	FY22	FY23	FY24	
Understand and expand operating space of ELM suppressed regimes towards relevant plasma parameters, incl. demonstration of optimized 3D plasma response	Map regime operating space for model validation Manipulate pedestal with shaping/heating to confront operational limits Improve spectral control of existing coils Optimize coupling with new coil set Tailor pellet properties to optimize mitigation Assess synergistic effects of pellets Show ELM control with adv. divertor					
Understand enhancement of main ion, impurity, and ash transport in ELM controlled regimes	Evaluate neutral source Evaluate source impact on ELM stability Comparison of high-Z/ash transport in ELM controlled plasmas					
Develop extrapolation through predictive simulation of non-linear evolution and sustainment of ELM controlled regimes	Develop multi-scale physics models (for RMP, QH, pellet pacing) Characterize 3D structures for non-linear validation Resolve the 3D structure of pellet ablation and ELM heat load Validate heat flux mitigation models with pellets					
Improvements	Additional EC power 3D supply #2 2D imaging & profiles Neutral diagnostics Tangential D2 pellet Advanced divertor (SAS-2U)					balanced NBI 3D coils upgrade 3D magnetics (phase II) Mid-Z impurity pellet Advanced div. (SAS-2L)

Fig. 4-1. Research plan overview for ELM control

Recent diagnostic upgrades (main ion CER, divertor Thomson scattering, IR periscope, 3D magnetics, dual SXR imaging, etc.) have positioned the DIII-D program to make rapid advances in the validation of models. Further diagnostics will address key gap issues. Notably, edge current profile measurements are vital to quantitatively validating simulations, while edge neutral measurements, high-Z impurity profiles, and a planned new array of gas injection valves will be important to study particle dynamics and pedestal structure. Toroidally-resolved ion/electron profiles and 3D magnetics upgrades will be key to understanding interaction of higher  $n$  fields for ELM and rotation optimization. Improved pedestal turbulence and profile diagnostics (see Section 4.1.2) will also be important in characterizing and understanding pedestal transport, the ELM cycle and QH mode regulation.

### **Challenge 1: Understand and expand operating space of ELM suppressed regimes towards relevant plasma parameters**

**Current progress.** During the past five years, major advances were made in expanding the operational range of ELM controlled regimes and in obtaining physics understanding of these regimes. Most fundamentally, physics understanding has moved from a vacuum model interpretation of 3D field interactions to account for the plasma response, with validation of key physics models [King 2015], identification of the multi-modal response [PazSoldan 2015], and development of quantitative predictive tools for RMP effects and optimization (illustrated below). Experiments and theoretical simulation show that plasma response and rotation are crucial aspects of RMP ELM suppression [Moyer 2017] and rotation shear is a critical aspect of obtaining QH-mode operation [Chen 2016]. DIII-D experiments demonstrated the critical role of plasma shape (triangularity) in RMP response, informing collaborative studies that achieved complete RMP ELM suppression for the first time on ASDEX-Upgrade. RMP ELM suppression was also demonstrated in helium discharges in support of the ITER non-nuclear phase of operation [Evans 2017] and in fully non-inductive hybrid discharges [Petty 2017]. Experiments with frozen deuterium pellets and impurity granules show that the deposition location in the plasma is crucial for good ELM mitigation by pacing.

A major focus of research was obtaining ELM control at low torque, motivated by concerns that future tokamaks will operate at low rotation. Fig. 4-2 demonstrates recent progress in reducing the input torque while maintaining ELM controlled scenarios in near-ITER baseline parameters for both RMP ELM suppressed and standard QH-mode discharges. ELM control has also been achieved at ITER relevant torque in some DIII-D scenarios. To illustrate this point, the newly discovered wide-pedestal QH mode regime [Chen 2017] can operate in a wide range of NBI torques and shaping parameters as shown in Fig. 4.3 (without 3D fields). Pellet pacing also does not exhibit direct torque dependencies. An operational issue specific to pellet pacing is that

results can have unexpectedly large variability – differences in the pellet parameters can lead to very different degrees of peak heat flux mitigation [Bortolon 2016].

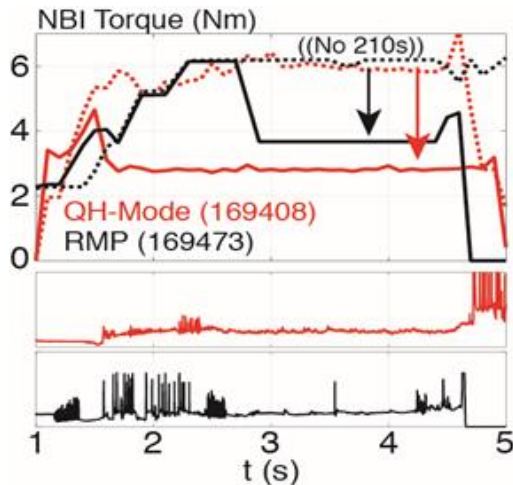


Fig. 4-2. Recent progress in obtaining RMP and QH-mode scenarios at low torque

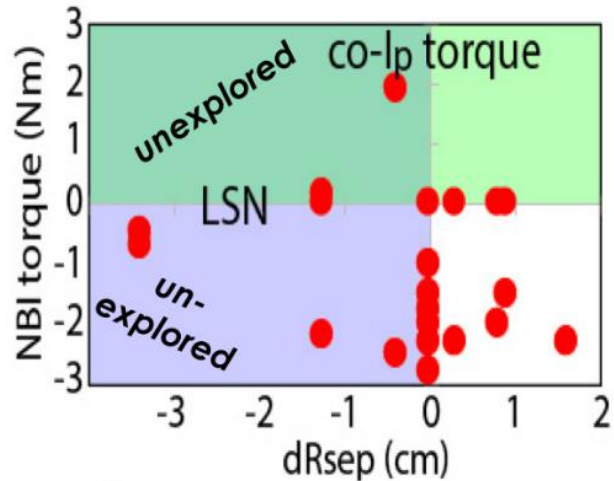


Fig. 4-3. Wide-pedestal QH mode is obtained over a range of torque and shapes.

### Goal 1: Expand operating space of ELM controlled regimes by pedestal manipulation.

In the 2019-2024 period, pedestal profile optimization will be used to reduce the toroidal rotation needed in ELM controlled regimes. For example, through diamagnetic flows pedestal gradients can modify electron rotation zero-crossings for RMP and critical ExB shear for QH-mode. The degree to which optimizing these flows can extend operating space will be assessed, with optimization achieved by varying 2-D and 3D shaping, electron heating and neutral beam mix. Research will move beyond input torque demonstrations towards understanding which rotation profiles are important and how they extrapolate to future devices. This will help elucidate why torque limits are not fundamental to all ELM control techniques. For regimes that have only recently been discovered on DIII-D, such as the I-mode, stationary high performance will be targeted [Marinoni 2015]. Pedestal manipulation via actuator changes (such as axisymmetric shaping, heating mix, fueling mix) will be pursued to understand and extend the operational boundaries of these regimes in rotation, pressure, collisionality, etc. Studies will be guided by predictive simulation, as was used to guide the discovery of the super-H mode [Solomon2014], with integration of RMP response and ELM suppression criteria planned.

The introduction of advanced divertor geometries with cryopumping in DIII-D (see Section 3.2.1) also affords a key opportunity to assess ELM suppressed regimes in dissipative divertor regimes. Present research on existing tokamaks has to choose between dissipative divertor (which requires high collisionality) and ELM suppressed operation (which requires low collisionality). The proposed more closed SAS divertor is predicted to access detachment at low

upstream densities, potentially resolving this conflict. Experiments will assess compatibility of the two requirements to determine integrated core-edge solutions that include ELM control. Studies will contrast different ELM control techniques in terms of their core-edge integration compatibility. The role of neutrals will be assessed in terms of their influence on pedestal profile and ELM control access. This work will also enable assessment of detached divertor plasmas without ELMs.

**Goal 2: Expand operating space of ELM controlled regimes with NTV torque and optimization of 3D plasma response**

Improved 3D field spectral optimization will be deployed to improve the performance and robustness of DIII-D ELM controlled regimes, utilizing new 3D coil and power supply actuators to increase the spectral flexibility available on DIII-D.

Using validated simulation capabilities developed in the past few years, the proposed addition of a midplane row of in-vessel coils (as pictured in Fig. 4-4) has been found in IPEC and MARS-F calculations to significantly increase the amount of edge resonant coupling and available NTV torque drive (Fig. 4-5). These two metrics relate to enhanced robustness and access to RMP-ELM control and QH-mode, respectively. The proposed midplane (M) coil row would comprise 12 coils to be commensurate with the periodicity of the vacuum vessel and also to enable the application of toroidal mode number  $n=1$  to  $n=6$  perturbations, and rotate up to  $n=4$  perturbations. M-coil  $n=3$  rotation together with the fixed  $n=3$  spectrum of the existing in-vessel coils will enable first-time poloidal harmonic spectral response and optimization with  $n=3$ . Additionally, rotation of  $n=1$  and  $n=2$  on all new and existing coils will deliver superb spectral control at low  $n$ , to help reduce incidence of locked modes while achieving ELM suppression. Spectral flexibility up to  $n=3$  enables optimization of the applied spectrum for resonant coupling for RMP-ELM control and NTV torque for QH-mode, as predicted by quantitative calculations using the MARS-F [Liu 2012] and GPEC [Park 2017] codes. Both calculations predict that a two- to three-fold increase in coupling and NTV torque can be achieved.

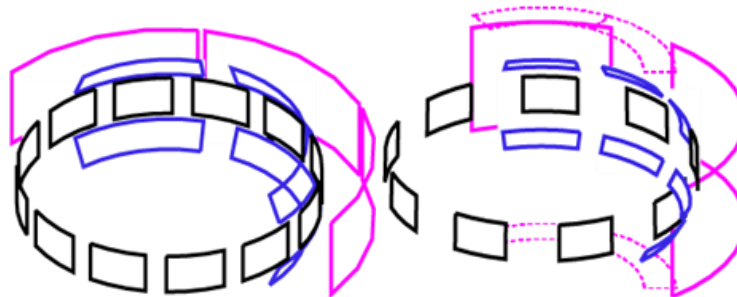


*Fig. 4-4. Proposed non-axisymmetric coil configurations for DIII-D with a new mid-plane in-vessel row (left) and comparison to the planned ITER coilset (right).*

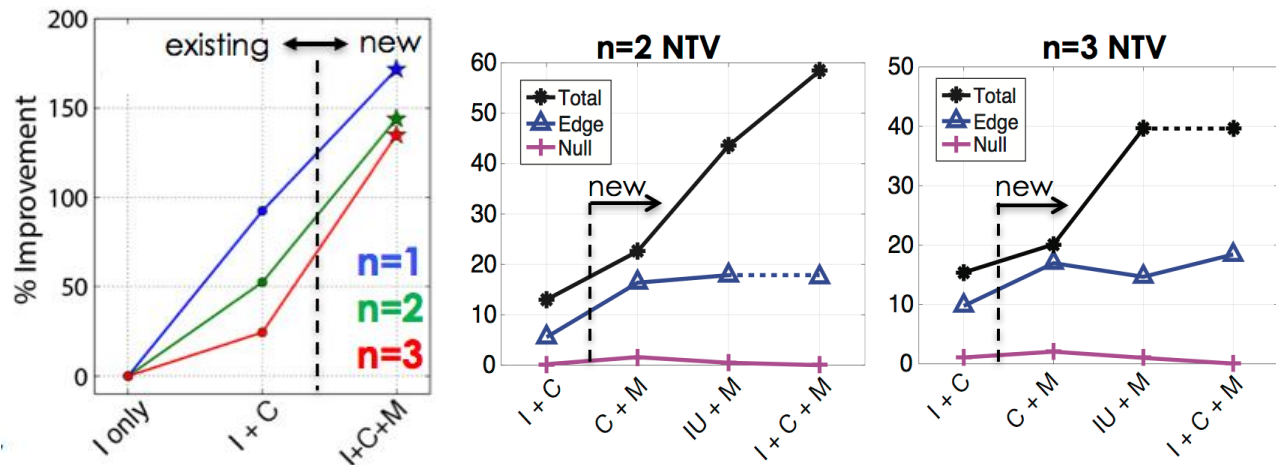


Fig. 4-5. Increase in resonant coupling (left),  $n=2$  NTV torque (mid), and  $n=3$  NTV torque (right) capabilities with the addition of an in-vessel midplane (M) coil row. Axis labels describe coilsets used, including existing in-vessel (I, or upper-only IU) and external (C) coils.

Experiments will be conducted to empirically determine optimized spectra for the regime of interest, and these measurements will be compared to predictive modeling. This research will allow determination of optimal metrics for 3D control, and deliver insights into the underlying physics setting the optimization, providing deep insight into how ITER can optimally use its coil set to meet the ELM control mission. Beyond optimization at low  $n$ ,  $n=4, 5, 6$  perturbations will be newly accessible and may offer improved performance for ELM suppression or NTV rotation shear generation. Studies will be conducted collaboratively with other devices such as AUG, EAST and MAST-U, which aim to understand and extend RMP ELM suppression for distinctive regimes those devices operate (long pulse, metal wall, low aspect ratio), and to explore QH-mode operation

### Goal 3: Tailor pellet properties to control ELM heat flux mitigation

Research in the 2019-2024 five-year period will aim to tailor the pellet properties to match specific DIII-D operating scenarios, and in so doing improve the underlying physical basis for the choice of pellet parameters. The central focus of this work will be on validation and improvement of pellet interaction models so that applicability to future devices can be predicted with confidence. This work is essential since previous DIII-D experience demonstrates that pellet effects are not always reproducible – differences in the pellet parameters can lead to very different degrees of peak heat flux mitigation [Bortolon 2016]. The effect of the pellet frequency, the pellet size, the injection geometry (radial vs. tangential), and the pellet composition (low Z, high Z) will be assessed in different regimes of interest. The impact of variations in target plasma parameters, such as collisionality, on the optimal pellet configuration will be investigated. Compatibility with core pellet fueling will also be addressed in this time period.

## Challenge 2: Understand Enhancement of Main Ion, Impurity, and Ash Transport in ELM Controlled Regimes

ELM controlled regimes offer special challenges and opportunities in the transport of the main ions, impurities, and ash. Additionally, studies of these regimes simplify measurement and simulation by allowing the neglect of the ELM-induced transport, and typically offer more quiescent conditions. Generally, the particle transport is increased – with beneficial effects for impurity and ash transport. Fluctuations are candidates for driving enhanced particle transport with the application of ELM control techniques. A rich fluctuation phenomenology is observed across the various ELM controlled regimes [Marinoni 2015]. For example, Fig. 4-6 shows spectra of density fluctuations from several regimes, as obtained from the DIII-D phase contrast imaging diagnostic.

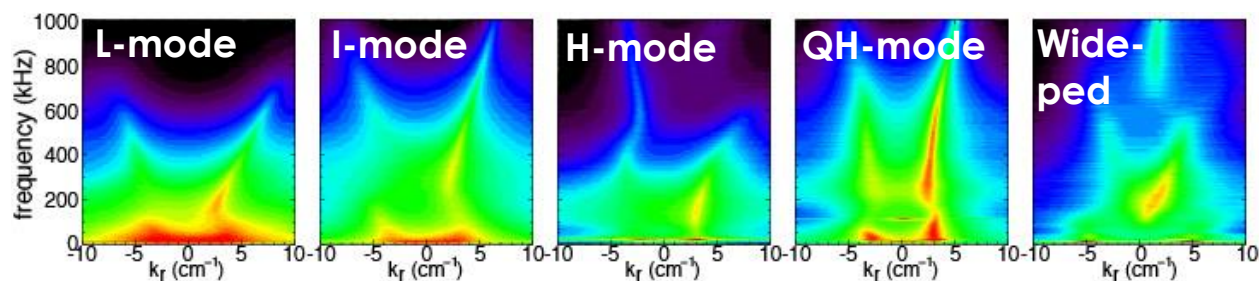


Fig. 4-6. Density fluctuations from phase contrast imaging in various plasma regimes.

### Goal 1: Determine role of 3D fields and fluctuations in driving pedestal particle transport.

Research will continue to resolve the origin and extrapolation of particle transport effects, both experimentally and in simulation. Increases in electron heating will extend studies to more reactor-relevant core conditions, and the development of more closed divertor geometries will extend research to more reactor-relevant divertor regimes. The extensive DIII-D turbulence diagnostic set plus diagnostic enhancements will be deployed to understand and contrast the fluctuation behavior of each ELM controlled regime. Experimental efforts will focus on varying the gradient drives in the density, temperature, and rotation shear profiles to identify the turbulent modes present and what destabilizes them [McKee 2013, Sung 2017, Ernst 2016]. A particular focus lies in understanding how changes to fluctuations may play a role in influencing transport in ELM suppressed regimes to arrest the ELM cycle or otherwise modify ELM behavior. This understanding will be used to guide simulation efforts by ensuring accurate mode spectra are predicted (CGYRO) and to validate predicted transport fluxes against experiments.

### Goal 2: Compare high-Z and He ash transport properties for all ELM suppressed regimes.

The increased particle transport present in ELM controlled regimes yields an opportunity to optimize the transport to preferentially expel unwanted species such as high-Z impurities,

medium-Z radiators, and low-Z ash [Grierson 2015]. Research will utilize gas puffing and the new laser blow-off system to measure the transport of these species across the various ELM controlled regimes. Furthermore, actuators such as 3D fields and electron heating will be applied in each regime to test the ability of the actuators to expel unwanted species. Comparison of different regimes will enable empirical identification of regimes that are superior for transporting each impurity class, and improve the physical basis to understand these effects. These measurements will be compared to model predictions (CGYRO, GENE, GTC, etc.) to gain quantitative understanding of the observed effects and their extrapolation.

### Challenge 3: Develop Predictive Understanding of Non-Linear Evolution and Sustainment of ELM-Controlled Regimes

The pedestals of ELM-free regimes such as RMP and wide pedestal QH-mode often operate away from the predicted peeling-ballooning stability boundary, consistent with the lack of ELMs. Thus standard tools such as the EPED model are often found to be insufficient, with some regimes operating below the EPED predicted limit (RMP-ELM) and others operating above the limit (wide pedestal QH). To address this, continued development of non-linear modeling tools is planned in order to gain a predictive understanding of the access and sustainment of the ELM-controlled edge. While this work is largely conducted by offsite collaborators, DIII-D plays a crucial role in providing guidance to theoretical groups as well as providing experimental data for model validation.

#### Goal 1: Develop prediction of RMP-ELM suppression.

Performance and predictions of access to RMP-ELM suppressed regimes requires coupling MHD and transport processes. Measurements have indicated that the entry to the RMP-ELM suppressed state is accompanied by changes in the magnetic response on the wall consistent with field penetration as predicted by MHD modeling (Fig. 4-7), [Nazikian 2015, Lyons 2017]).

Several open questions remain. The prediction of the field penetration requires coupling of the tearing-layer properties with global prediction of magnetic braking effects from the 3D field [Callen 2016]. Such work has begun with the extended MHD codes NIMROD and M3D-C1 [Biedler 2017] and will be supported with high-resolution experimental data for validation. Predicting field penetration impacts on neoclassical

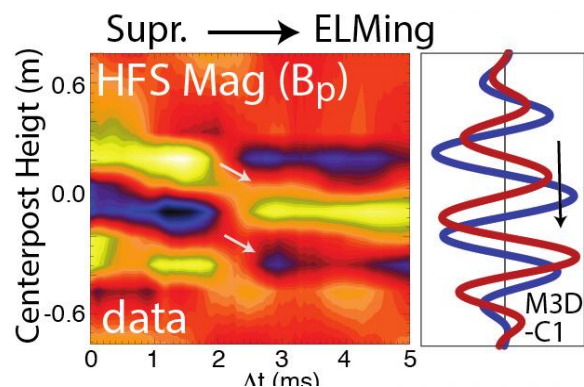


Fig. 4-7. Magnetic field variations upon exit from ELM suppression, qualitatively consistent with M3D-C1 modeling.

and turbulent transport levels is still a frontier topic, requiring coupling MHD and transport processes. Experimental data will continue to be provided to theoretical groups that have begun to bridge this gap (e.g., GTC [Holod 2017]). Trends developed from simulation will be tested against experimental data, with a focus on known limits in toroidal rotation or collisionality.

## Goal 2: Understand QH-edge transport enhancements.

3D structures are also found to increase the transport in QH mode, either through the EHO or the so-called broadband MHD. As with RMPs, prediction of the associated transport also requires coupling of the macroscopic phenomena such as the EHO or broadband MHD to the underlying transport. Critical issues include prediction of the nature and transport impacts of these modes and understanding the non-linear saturation of modes that provides the observed smooth regulation of pedestal profiles. Extended MHD simulations with JOEK quantify the relative role of pedestal pressure and current in the excitation and saturation of the EHO [Liu 2017]. Further work simulating QH-like fluctuations with the extended MHD code NIMROD has highlighted the importance of the in-phase density and flow fluctuations in driving preferential density transport, illustrated in Fig. 4-8 [King 2017]. Experiments will validate these specific predictions by measuring the phase difference between fluctuating fields in plasmas with EHOs, using for example the UF-CHERS diagnostic. Simulations will continue to be supported by providing experimental data and maintaining a close dialog with simulation. These include, for example, gyrokinetic calculations to better understand the enhanced pedestal transport in the wide pedestal QH edge. These models will also be improved by better quantifying the transport fluxes found in simulation runs and further developing synthetic diagnostics to compare modeled fluctuations with experimental measurements.

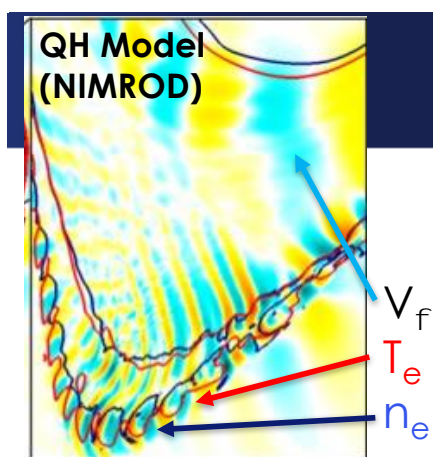


Fig. 4-8. Fluctuating fields of flow, temperature, and density in simulations of DIII-D QH modes [King 2017].

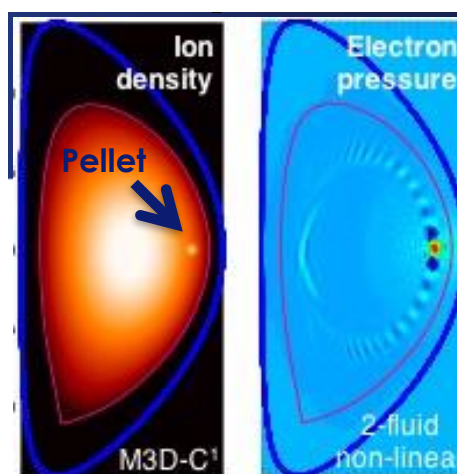


Fig. 4-9. M3D-C1 results simulating an injected pellet and the associated perturbations to the density and temperature.

### **Goal 3: Simulate ELM mitigation with pellet pacing.**

Extended MHD modeling of pellet pacing phenomena will be expanded in the 2019-2024 five-year period to validate the key empirical observations made in the experimental program. For example, the critical pellet size for ELM triggering, previously identified with JOREK modeling [Futatani 2014], will be simulated in M3D-C1 (Fig. 4-9) for the wide variety of pellet compositions achievable in experiment, supporting the variable size injectors planned for DIII-D. Predictions of the MHD mode structures (peeling, ballooning, or otherwise) excited by the edge pellets will be validated against stereoscopic measurements of the pellet ablation cloud and improved resolution of the particle and heat flux on the divertor. These steps support the long-term goal of predicting the degree of peak heat flux mitigation arising from pellet-triggered ELMs.

#### **4.1.1.3 Capability Enhancements**

The research described above benefits directly from several proposed improvements in hardware and diagnostic capability (Table 4-2 and Table 4-3). Addition of ECH heating power will provide torque-free heating to improve access to high pressure, low rotation scenarios and improve their ability to reach the low collisionalities needed for ELM control. The improved 3D control coils and power supplies proposed in this plan provide needed increases in the coupling to the edge rational surfaces for RMP-ELM control and increase the maximum edge NTV torque to improve access to QH mode. Improvements in pellet injection systems will include injectors with the ability to vary the size of the injected pellets as well as injection geometry (radial vs tangential). Impurity injectors will be upgraded to vary the impurity composition (going to higher  $Z$ ) and regularize the injection frequency.

Implementation of an edge current density diagnostic will provide a key parameter for the stability calculation of the pedestal and the ELM itself. An upgrade to the tangential Thomson scattering viewing geometry will allow for co-located electron and ion measurements, providing improved alignment of profiles and computed 2D and 3D magnetic equilibria. Planned second views for ECE and BES measurements will also yield direct data to resolve 3D structures and locate the 3D edge. The 3D coil upgrade will be accompanied by improvements to magnetic diagnostics to resolve the structures induced by the coil. Transport of high- $Z$  impurities will be studied with the aid of a new laser blow-off system to inject impurities and improvements in VUV spectroscopy. Upgrades to the imaging MSE system and the ECE-I/MIR systems will provide important 2D edge measurements for studying transport in ELM controlled regimes. Additional cameras covering the pellet injection region will enable stereoscopic images of the pellet ablation cloud to improve modeling. Additional tile current monitors will provide better

spatially resolved measurements of the ELM wetted area. The primary diagnostic improvements for ELM control discussed here are summarized in Table 4-3.

Simultaneous modeling improvements, while mostly outside of the scope of the DIII-D cooperative agreement, are crucial to the research plan of the ELM control group, as described above. The codes described in Table 4-4 will be deployed to understand various aspects of ELM control physics. The OMFIT framework will be used to control much of the integrated modeling for this research; the framework simplifies coupling of data to codes and coupling of multiple codes, when appropriate, to obtain a more holistic understanding of ELM control physics.

**Table 4-2.**  
**Hardware Improvements for ELM Control**

<b>Hardware Capability</b>	<b>New Physics</b>
Additional 3D control coils and power supplies	Optimize the 3D plasma response for resonant coupling or non-resonant rotation profile control and expand operational boundaries of ELM controlled regimes
Increased EC power	Explore operational limits of ELM suppressed regimes with torque-free heating in low collisionality regimes
Advanced divertor configurations	Explore compatibility of ELM controlled regimes with dissipative divertor operation with reduced wall heat flux
Tangential pellet injector w/ size selection ability	Manipulate pellet size, injection geometry, and composition to optimize pellet pacing for specific plasma conditions and mitigation requirements
Impurity Granule Injector w/ regularized frequency, radiative materials	

**Table 4-3.**  
**Diagnostic Improvements for ELM Control**

<b>Scientific Objective</b>	<b>Physics Measurement</b>	<b>Diagnostic Technique</b>
Determine impact of edge current density in ELM and pedestal stability	Edge current measurements	Imaging MSE
Understand transport of high-Z impurities in ELM controlled regimes	Spectroscopic/X-ray imaging diagnostics for high-z impurity transport	Divertor SPRED VUV spectroscopy
Understand the particle source in the pedestal	Edge neutral measurement	Upper divertor camera, Ly-alpha arrays, pressure gauges, wall probes
Improve diagnosis of the 3D equilibrium state as input to stability and transport modeling	Electron and ion profile measurements at the same location Duplicate profile measurement at different toroidal location Higher temporal and spatial	Co-located TS & CER Additional TS or CER view 3D magnetics phase 2 2 <sup>nd</sup> ECE view, 2 <sup>nd</sup> BES view

Scientific Objective	Physics Measurement	Diagnostic Technique
	resolution 3D magnetic field measurements	
Determine role of local effects in transport enhancement in ELM controlled regimes	Advanced imaging of temperature and density fluctuations	ECE-I/MIR SNR improvement Imaging MSE 2 <sup>nd</sup> BES
Measure 3D dynamics of pellet ELM triggering and induced heat flux on the wall	3D pellet ablation cloud imaging 3D wall particle/heat flux imaging	Stereoscopic pellet imaging Tile current / Langmuir probes

**Table 4-4.**  
**Simulation Codes Used for ELM control**

Code	Purpose
Pedestal stability codes (ELITE, EPED, BOUT++)	Predict achievable pedestal profiles without encountering ELMs and optimize for best performance
Linear MHD stability codes (GPEC, MARS, DCON, M3D-C1)	Realistically model the 3D plasma state as perturbed by 3D effects (RMP, EHO, etc.)
Non-linear extended MHD codes (NIMROD, M3D-C1, JOEK)	Understand impact of 3D effects on the plasma state and model 3D dynamics (RMP, EHO, pellets, ELMs)
Transport codes (GS2, TGLF, CGYRO, GENE, GTC, XGC)	Model turbulent fluctuations, their drives, and impact on profile gradients and thus pedestal stability
Integration tools (OMFIT)	Facilitate interaction between codes to understand integrated dependencies

#### 4.1.2 Pedestal Structure, Fueling, and Transport

*Physics Leads: R. Groebner (GA), T. Osborne (GA), A. Moser (GA), M. Shafer (ORNL), A. Leonard (GA), A. Diallo (PPPL), J. Hughes (MIT), S. Mordjick (W&M), P. Snyder (GA)*

The H-mode pedestal plays a crucial role as the interface between the core and boundary plasmas. Future burning plasma experiments place strong requirements on this interface because they need a pedestal with a height that is compatible with desired core performance while also having a separatrix density that is consistent with desired divertor detachment solutions. Moreover, the pedestal must not send large fluxes of particles and heat to the divertor via ELM events (the control of which is discussed in Section 4.1.2). These simultaneous requirements lead to the need for better understanding of pedestal structure via improved knowledge of its transport and response to sources. This knowledge will enable the development of validated models for self-consistent solutions of core and divertor plasmas for future machines.

The DIII-D team has made numerous advancements in understanding pedestal structure through its experiments and interaction with the global community. A key accomplishment is the

development and validation of the EPED model [Snyder 2011], a first principles no-free-parameters predictor of pedestal pressure height and width, which has become the standard tool to project and interpret tokamak behavior as well as access to improved regimes such as super H-mode [Solomon 2014] and wide pedestal QH mode [Burrell 2016]. Much of this work has thus focused on the role of pressure in the pedestal; more recent research is focusing on the physics of individual density and temperature profiles. Data from DIII-D and other machines shows evidence of pedestal fluctuations limiting the  $T_e$  gradient. Divertor closure experiments in DIII-D have provided evidence that the neutral source controls the density pedestal height. Specific regimes have been found in which increases in pedestal turbulence decrease pedestal gradients and enable a higher pedestal height. Turning to the 2019-2024 five-year period, the need is to go beyond the EPED pedestal pressure model, to develop a particle and transport based understanding, in terms of its interaction with the divertor, underlying turbulence, the prediction of pedestal density and individual kinetic profiles, and the development of improved performance regimes. DIII-D represents a key facility to make such advances due to world leading profile and fluctuation diagnostics, and its strong flexibility in parameter access, shape and divertor to probe physics and explore improved modes of operation.

#### **4.1.2.1 Challenges and Impact**

The goal of the DIII-D pedestal program is to provide the scientific basis for predicting and optimizing pedestal structure. For this purpose, research will focus on three key challenges, set out in Table 4-5. The first challenge is motivated by the need to understand how the separatrix density is set and will focus on identifying the physics processes that couple the pedestal to the scrape-off layer (SOL). Key approaches to achieve this are to develop a very much improved measurement of the neutral particle source and to modify this source through such techniques as divertor closure in order to determine the effect of neutrals on pedestal structure and separatrix conditions. A second challenge is to develop an understanding of the physics processes that control the pedestal structure. Experiments will be performed to identify which physics parameters and mechanisms are associated with the saturation of density and temperature gradients in the pedestal. Theoretical modeling, coupled with cutting edge diagnosis will be crucial for interpretation to identify the physics processes that set the gradients. A third challenge is to develop an understanding of how to manipulate the pedestal and SOL in order to improve the pedestal height. This research will test how to apply actuators to control discharge trajectory and pedestal performance, also using theoretical guidance from the EPED and transport models.

The scientific results obtained through this work will identify the physics processes that control transport in the pedestal and provide benchmarking of theoretical modeling codes for pedestal structure. The results will provide an improved understanding of the role of fueling and

other sources in pedestal structure. This research will provide crucial input into the design of operating scenarios for ITER and the hardware design of future burning plasma machines in order to develop higher fusion performance operating regimes that are compatible with divertor and materials requirements. An in-depth understanding of pedestal physics is key to developing controlled and suitably performing fusion scenarios, and to the controlling ELMs. Success in enabling a high-performance core compatible with a dissipative divertor solution could be transformational to the prospects for fusion energy.

**Table 4-5.  
Pedestal Structure Challenges, Goals and Upgrade Plans**

<b>Challenge</b>	<b>Goals/Deliverables</b>	<b>Key Capability Improvements</b>
Identify and understand processes that couple pedestal and SOL/DIV	<ul style="list-style-type: none"> <li>• Develop model for separatrix density</li> <li>• Determine how divertor detachment affects pedestal to identify techniques to improve performance compatible with divertor needs.</li> </ul>	<p><b>Hardware Upgrades</b></p> <ul style="list-style-type: none"> <li>• SAS-I and SAS-II divertors</li> <li>• Gas injector upgrades to reduce recycling</li> </ul> <p><b>Diagnostic Upgrades for Pedestal/SOL Structure:</b></p> <ul style="list-style-type: none"> <li>• Pedestal ionization source</li> <li>• Pedestal current density</li> <li>• Tangential midplane Thomson</li> <li>• Pedestal/SOL DBS</li> <li>• 2<sup>nd</sup> ECE radiometer toroidally displaced</li> </ul>
Understand how individual pedestal profiles are determined by transport and sources	<ul style="list-style-type: none"> <li>• Validate models of turbulent fluctuations and other physics processes that control transport of individual pedestal profiles</li> </ul>	<p><b>Diagnostic Upgrades for ELM Studies</b></p> <ul style="list-style-type: none"> <li>• Fast IR coverage for ELMs, 3D heat loads</li> <li>• Upgrades to fast camera system</li> <li>• Upgrades to tile probes to measure ELMs</li> </ul> <p><b>Diagnostic Upgrades for Divertor Studies</b></p> <ul style="list-style-type: none"> <li>• Upper DTS</li> <li>• Upper bolometers</li> <li>• Divertor SPRED</li> </ul>
Manipulate pedestal/SOL/DIV coupling to raise core performance	<ul style="list-style-type: none"> <li>• Develop understanding and techniques to achieve high, wide pedestals through a range of actuators and device flexibility.</li> </ul>	<ul style="list-style-type: none"> <li>• Fast thermocouples</li> <li>• Divertor Ti, 2D DTS</li> <li>• IR and visible imaging in upper divertor</li> <li>• High resolution VUV/VIS spectroscopy</li> </ul> <p><b>Code Development</b></p> <ul style="list-style-type: none"> <li>• Routine capability to evaluate neutral source</li> <li>• Codes to simulate pedestal transport, TGLF benchmarked to CGYRO, BOUT++, ...</li> <li>• Coupled 2D Edge code to pedestal transport code</li> <li>• CESOL, OMFIT, ERO, OEDGE, SOLPS, UEDGE, EPED, STRAHL</li> </ul>

**4.1.2.2 Research Plan**

The research plan for pedestal structure and coupling to the SOL will focus on the challenges and goals shown in Table 4-5. A timeline for addressing these challenges and providing needed facility upgrades is shown in Fig. 4-10. The plan benefits from significant diagnostic upgrades to better characterize profiles, neutrals and turbulence in the early stages. Use of SAS divertor and improved 3D capabilities will provide greater control of density and assess interactions with

closure. In parallel with this plan, engagement with and development of state of the art simulation will form a strong part of this research (see Table 4-8).

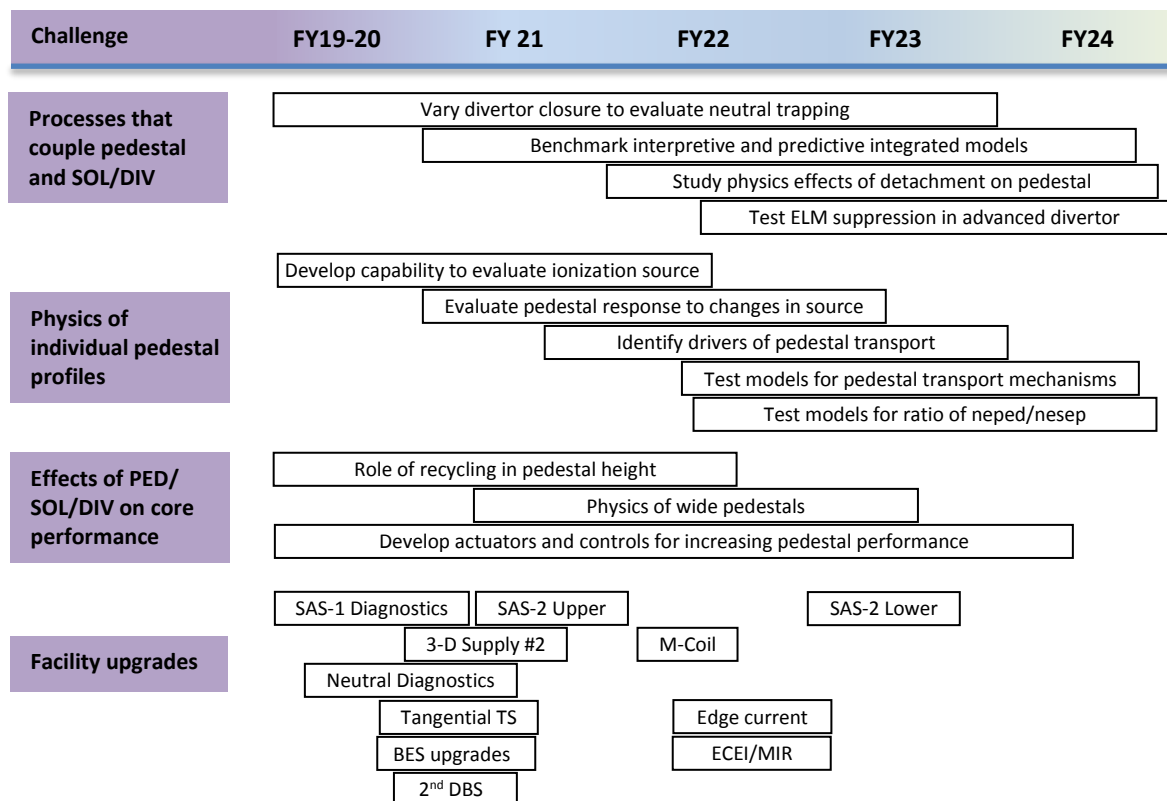


Fig. 4-10. Timeline for Pedestal-DivSOL coupling studies

### Challenge 1: Identify and Understand Processes That Couple Pedestal and SOL/DIV

**Current progress.** The issue of coupling of the pedestal to the SOL/divertor gained importance in the DIII-D program in the past five years with some key results on identifying the physics that controls the separatrix electron density,  $n_{e,sep}$  [Leonard 2017]. As shown in Fig. 4-11,  $n_{e,sep}$  shows a relatively weak dependence on heating power, which is comparable to expectations from the 2-point divertor model, whereas  $n_{e,ped}$  shows a fairly strong dependence on  $n_{e,ped}$ . This latter behavior is not well understood, and will be a focus of research in the 2019-2024 five-year plan.  $T_{e,sep}$  shows a weak dependence on heating power, as expected from the 2 point divertor model. Experiments and analysis were performed to study the dependence of pedestal height with divertor detachment [Leonard 2015]. The pedestal height decreased as the divertor was pushed towards detachment due to a reduction of the bootstrap current, and therefore pedestal MHD stability, as the pedestal density and collisionality were increased to achieve detachment.

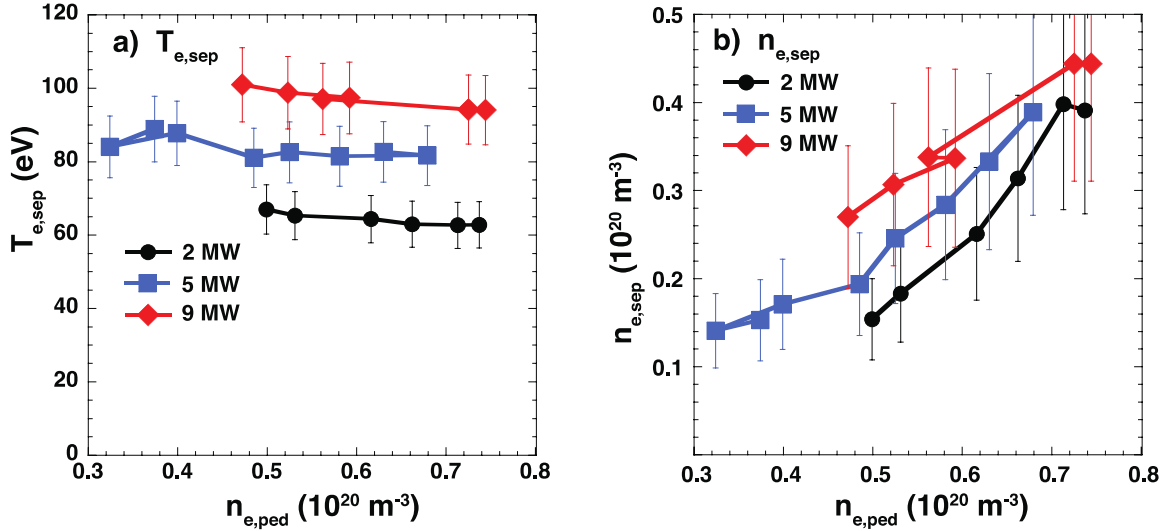


Fig. 4-11.  $T_{e,sep}$  and  $n_{e,sep}$  as functions of  $n_{e,ped}$  and power

### Goal 1: Develop model for separatrix density.

In the 2019-2024 five-year plan, a key goal of the DIII-D pedestal physics research will be to develop a predictive model for the separatrix density. For this goal, a major effort will be made to understand the role of neutral fueling in setting the separatrix density (and the pedestal density). Diagnostics that provide measurements for the determination of neutral density will be substantially upgraded and will include more complete spatial coverage than is now available. In parallel, the process by which edge 2D codes model the edge plasma and compute the ionization source, based on constraints from experimental measurements, will be streamlined, primarily through the OMFIT framework. The upgraded tangential Thomson system will also provide important capability for this work since it will improve the measurement of separatrix electron density at the midplane, where many of the important diagnostics make measurements.

In addition, hardware developments will be implemented to improve control of recycling neutrals; these improvements will provide important flexibility for studying the role of particle sources in pedestal and boundary physics. The improvements include divertor modifications, particularly to the SAS, to increase divertor closure with reduction of pedestal neutrals. SAS upgrades will be done in 3 steps and include the following: 1) improved diagnosis of SAS 1, 2) installation of SAS 2 upper divertor to be compatible with Advanced Tokamak plasmas and to have pumping, 3) installation of SAS 2 for lower divertor with capability to handle high power and to be pumped as SAS 2 upper. Improvements to gas valves to raise fuelling efficiency are additional options that will be considered for control of recycling. Experiments will be performed to modify the neutral source in the pedestal, via changes in closure and other techniques, and the response of separatrix electron density will be measured. For analysis of the

results and the development of a predictive model, a significant emphasis will be placed on the use of integrated codes, such as CESOL (see Section 2.1.2, Challenge 3), which self-consistently model the interaction of the core, pedestal and boundary plasmas, in order to understand important physics processes setting separatrix parameters.

**Goal 2: Determine how divertor detachment affects pedestal and identify techniques to improve performance compatible with divertor needs.**

As noted above, there is evidence that divertor detachment can degrade the pedestal height through increases in the pedestal collisionality and therefore the reduction of pedestal MHD stability. To test this hypothesis further, and explore the interplay with closure, experiments will be performed in which detachment will be sought at low pedestal collisionality. This method of operation might be obtained with improved divertor closure, such as with the upgraded upper SAS divertor. High performance pedestal regimes, such as hybrid or Super-H discharges, will also be used for these tests.

Other mechanisms for pedestal degradation that will be tested include losses due to increased neutral density in the pedestal and increased turbulence due to higher collisionality. The measurement upgrades discussed for goal 1 will be important to evaluate the neutral density. Measurements of turbulence will make use of upgrades to fluctuation measurements, including the pedestal/SOL DBS system. The installation of a pedestal current diagnostic will provide a very important capability for studies of pedestal MHD stability and will enable stringent tests of models for bootstrap current, peeling-ballooning stability and pedestal turbulence.

**Challenge 2: Understand How Individual Pedestal Profiles Are Determined By Transport and Sources**

**Current progress.** During the past 5 years, DIII-D and other machines have made significant progress in understanding physics processes that may limit some pedestal profiles. Moreover, there has been mounting evidence that different profiles show different behaviors, suggesting that they are limited by different phenomena. There are measurements in DIII-D (Diallo 2015A) and AUG (Laggner 2016), which show that the electron density gradient saturates within a few milliseconds during recovery from an ELM crash whereas the  $T_e$  gradient usually saturates somewhat later in recovery phase. C-Mod also has similar results (Diallo 2015B). In all 3 cases, the saturation of  $T_e$  fluctuations is observed to be correlated with the onset and saturation of magnetic fluctuations, as shown for example in Fig. 4-12 for DIII-D. In addition, AUG (Laggner 2016) has reported that the saturation of the density gradient is correlated with the onset of magnetic fluctuations also, but at a different frequency than those correlated with  $T_e$  fluctuations. These results are consistent with the idea that pedestal  $T_e$  and  $n_e$

profiles are limited by critical gradient phenomena and that different phenomena limit each gradient.

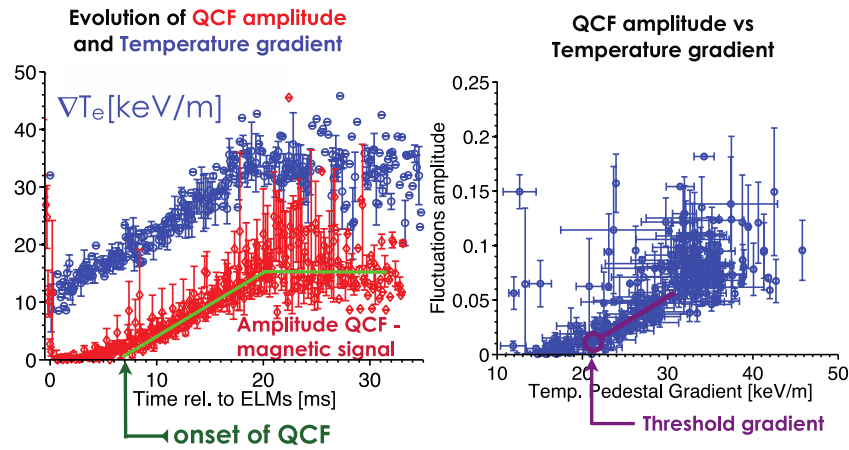


Fig. 4-12. During recovery from ELM, electron temperature gradient saturates at same time as saturation in magnetic fluctuations from a Quasi-Coherent Fluctuation (QCF) (A. Diallo et al., PoP 22 (2015) 056111)

Another important result in the past 5 years was an experiment in which the pedestal profiles were studied with different divertor geometries. Experiments showed that the pedestal neutral density was reduced with increased divertor closure (Fig. 4-13) [Leonard 2016], validating modeling results; pedestal density profile structure is observed to change significantly with a change in the source. With reduced ionization, the pedestal density and its gradient were both decreased. Transport modeling, using a purely diffusive particle flux, showed that observed changes in the density pedestal were consistent with changes in the neutral source and no changes in the density transport. Research will build on these results to develop a more complete picture of how the neutral source affects the density pedestal, identify and develop a projectable understanding of the physics processes that limit the pedestal profiles.

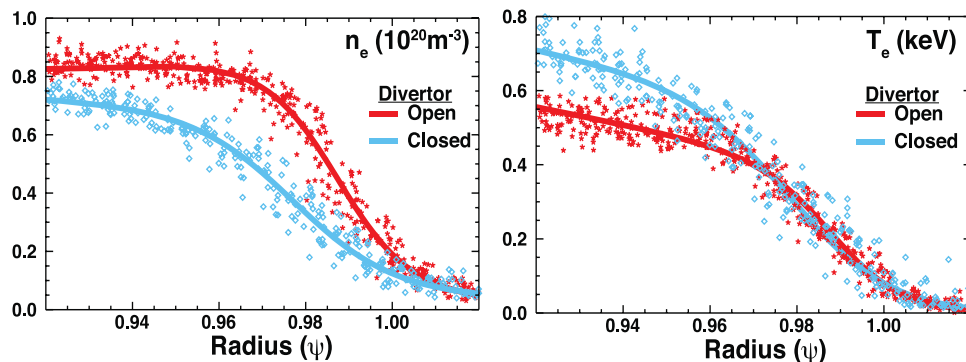


Fig. 4-13. More closed divertor (blue) shows broader and less steep  $n_e$  profile compared to more open divertor (red).  $T_e$  pedestal is higher with more closed divertor. (A.W. Leonard et al., 2016 IAEA-FEC, preprint0581.pdf)

**Goal 1: Validate models of turbulent fluctuations and other physics processes that control transport of individual pedestal profiles.**

Research will be performed to identify the processes that control transport in individual density and temperature profiles. The key goal will be to identify some of the important transport mechanisms. A vital element will be the characterization of turbulent transport mechanisms utilizing DIII-D's extensive fluctuation diagnostic suite, further extended in this plan. An important further part of this work is to develop an improved capability for evaluating sources in the pedestal. This includes the determination of the neutral particle source, discussed previously, and improved evaluation of electron and ion heat fluxes through the pedestal. Improved measurements of heat fluxes will be enabled by using measurements of main ions to evaluate  $T_i$  and  $n_i$  and by using the upgraded tangential Thomson system to better align electron and ion measurements at the outer midplane. These advances will significantly improve our knowledge of heat sources in the pedestal, which is required for quantitative comparisons with theoretical transport models.

As a prelude to identifying physics processes that control pedestal transport, experiments will be performed to vary sources and other actuators (heat, particle, ExB shear, gas puffing, etc.) to look for responses in various pedestal profiles. These experiments can be considered the pedestal analog of perturbative experiments that were performed in the core 10-20 years ago. Transient transport experiments will also be performed by using ELMs, a technique that has already been employed in pedestal studies (Diallo 2015A, Diallo 2015B, Laggner 2016). The goal is to determine how profiles respond to sources and to see if gradients reach limiting values. As part of these experiments, fluctuation behavior will be examined to determine if there is correlation between the amplitude of fluctuations and saturation of gradients. This class of experiments will have improved capability with planned BES upgrades in ~2019 and ECEI/MIR upgrades in ~2022. With the availability of current density measurements in ~2022, experiments will directly measure the response of the pedestal to variations of the edge current.

Linear theoretical modeling of the results from these experiments will be performed to explain the observed limitations on gradients or other pedestal parameters. This work will be carried out with codes such as CGYRO, BOUT++, TGLF, GENE and GEM to study fluctuation-driven transport. Codes such as NEO and XGC0 will also be used to look for evidence of neoclassical behavior, particularly in the ion thermal transport. This modeling work will be used to form hypotheses for the physics processes that control profiles of  $T_e$ ,  $n_e$  and  $T_i$ . This work will also be used to identify the important plasma parameters (such as gradients of temperature, density, and pressure) that control these physics processes. This information will be used to design a class of experiments that explore the hypotheses in more detail. Toward the end of the

2019-2024 five-year plan, it is anticipated that quantitative tests of proposed physics processes will be made with non-linear pedestal simulations. These simulations will require experiments that provide good measurements of heat fluxes through the pedestal, of the neutral source in the pedestal and of fluctuation quantities, including absolute fluctuation levels and spectral-resolved information. The output of this research will be the development of a predictive understanding of the physics processes that control pedestal transport and significant benchmarking of theoretical modeling codes in the pedestal.

### Challenge 3: Manipulate Pedestal/SOL/DIV Coupling to Raise Core Performance

In recent years various improvements to performance have been identified through pedestal manipulation. For example, the so-called Quiescent H mode (QH-mode) regime has demonstrated improved confinement in low rotation plasmas due to widening of the pedestal and reduced transport in the vicinity of the edge (Chen 2017). Modifications to rotation shear appear to play a role here, as shown in Fig. 4-14. It has also been possible to tune the pedestal to reach points of optimal performance and meta-stable regions of elevated pressure, termed ‘super H mode’. This regime was predicted by theory (Snyder 2015), and subsequently achieved in experiment (Fig. 4-15) (Solomon 2014). The Super-H regime offers the prospect of a high density pedestal that helps resolve compatibility of a high performance core with the divertor (see also Sections 2.1.2). A regime of improved pedestal performance has also been obtained in hybrid discharges with high power heating and gas puffing through similar benefits in pedestal stability [Petrie 2017]. Research in the 2019-2024 five-year plan will seek to explore the physics and to develop these regimes further, through use of upgraded and more flexible heating and current drive tools, new divertors, as well as new 3D field and shaping capabilities to control profiles and raise pedestal stability.

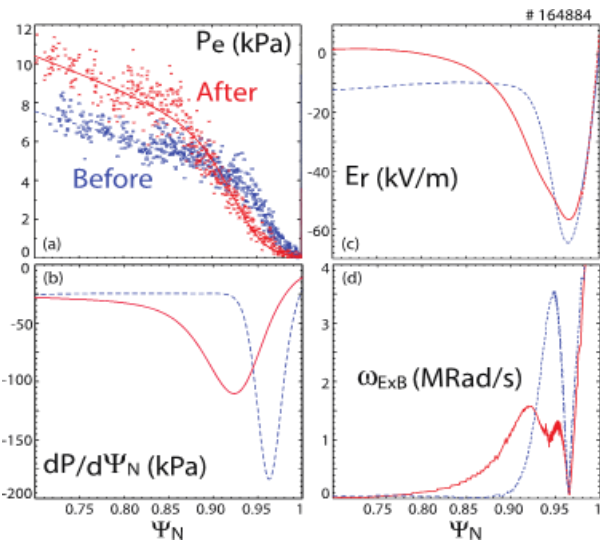


Fig. 4-14. Comparison of QH-mode in EHO phase (Before-blue) and in wide pedestal phase (After-red)

#### Goal 1: Develop understanding and techniques to achieve high, wide pedestals.

Experiments will be performed to understand how to optimize the pedestal height. These studies will test a number of actuators to determine if they can be used to improve pedestal performance in promising regimes of very good confinement. These regimes include the Super-

H-mode, wide pedestal QH-mode and the high-power hybrid regime. Actuators include torque control, low Z impurities, shape, ECH, and Resonant Magnetic Perturbation (RMP) fields. In addition to the parameter expansions these actuators confer, research discussed below must also explore the underlying physical mechanisms of their action, discussed in this pedestal research section, and also in Sections 2.1.2 (steady state), 2.2.2 (stability & 3D response), 2.3.1 (transport), 2.3.2 (rotation), 3.2.1 (SAS divertor).

These experiments will benefit from a number of planned facility improvements. Increased ECH and 3D capabilities provide better prospects for density control to access the super-H mode valley. Increased shaping (though enhanced power supplies) is predicted to raise pedestal height. Higher NTV torque enabled by the 2<sup>nd</sup> ASIPP 3D power supply (~2022) and increased flexibility of 3D spectra enabled by the M-coil upgrade (~2022) will be used in experiments to induce rotational shear, expected to improve performance of the wide pedestal QH-regime and possibly other discharge conditions.

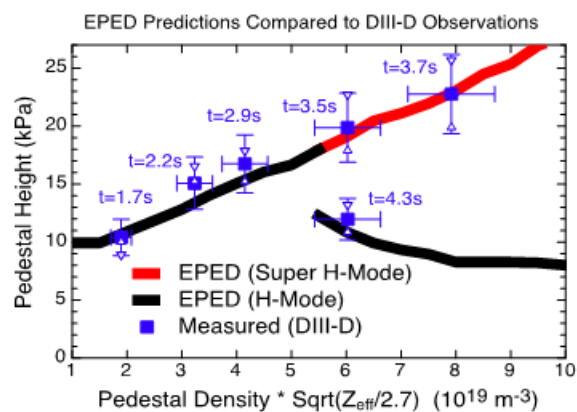


Fig. 4-15. Data points shows that experiment has achieved the predicted Super-H regime

Experiments will be performed to determine how recycling neutrals affect the pedestal height. The ionization source in the pedestal will be characterized. Recycling neutrals will be controlled with improved gas valves and divertor closure, available with various divertor geometries including the SAS 1 and SAS 2 divertors, and the response of the pedestal height will be measured. Experiments will be performed to understand how wall coatings, such as from boronization or siliconization (if it is employed) improve plasma performance.

The installation of the highly closed SAS 2U divertor (~2021), which will provide pumping and handle high power, will be tested to see if it allows improved Super H-mode or other regime performance. If helicon, Lower Hybrid inner wall launch or vertical EC launch systems are successfully developed, they are projected to enable high density, high beta operation with a significant fraction of non-inductive current drive (see modeling in Section 2.1.2). This raises the exciting prospect of overcoming the tension in DIII-D between a dissipative divertor and high performance core to explore directly reactor-relevant integrated solutions.

### 4.1.2.3 Improvements in Capabilities

The research described in this section will benefit from a number of planned hardware and diagnostic upgrades, listed in Table 4-6 and Table 4-7. Much of the work described here will benefit from improved control of recycling neutrals, which will be enabled by the various slot divertor implementations mentioned in Table 4-6 and by proposed upgrades to gas injectors to provide improved fueling efficiency.

**Table 4-6**  
**Hardware Improvements for DivSOL–Pedestal Coupling Studies**

<b>Hardware Capability</b>	<b>New Physics</b>
SAS-II Upper	Full-power AT scenarios with optimized divertor for detachment and pumping for particle control
SAS-II Lower	Pumped SAS divertor capable of high power operation in LSN discharges
3D supply #2	Additional current capability for using 3D coils as actuators for use in pedestal performance studies
M-Coil	Increased 3D spectral control for experiments to study 3D fields for pedestal optimization
Upgraded gas injectors	Improved control of recycling

Key diagnostic enhancements will provide measurements of neutrals, measurements of pedestal current density and Thomson scattering measurements of  $n_e$  and  $T_e$  at the outer midplane, which will improve our understanding of the separatrix location and improve mapping of Thomson and CER data into magnetic flux coordinates. A number of diagnostic upgrades will provide improved capability to study fluctuations in the pedestal and SOL, including ECEI/MIR upgrades, expanded/upgraded BES and magnetics upgrades. Some upgrades will enable us to examine the effects of 3D physics on pedestal transport and these include the upgraded midplane TS system as well as the 2<sup>nd</sup> toroidally displaced DBS system.

Much of the proposed pedestal research requires theoretical simulations to help interpret experimental results and these codes are listed in Table 4-8. Codes such as OEDGE, SOLPS and UEDGE will be required to help provide neutral densities and ionization sources in the pedestal. A number of codes will be used to help interpret experimental measurements in order to provide understanding of pedestal transport. These codes include CGYRO, TGLF, BOUT++, GENE, ELITE and NEO. Issues of 3D transport will be studied with TRIP3D, M3D-C1 and EMC3-EIRENE. Reduced models will be used to study pedestal structure (EPED) and integrated core, pedestal and SOL coupling (CESOL).

**Table 4-7.**  
**Diagnostic Improvements for DivSOL–Pedestal Coupling Studies**

<b>Scientific Objective</b>	<b>Physics Measurement</b>	<b>Diagnostic Technique</b>
Neutral trapping in SAS divertors	Neutral pressure	ASDEX Gauges
Physical processes impacting changes to divertor closure/pumping and SOL on pedestal neutral fueling	VUV spectroscopy, Deuterium Ly-alpha emission	Divertor SPRED, Ly-alpha arrays, Ly-alpha divertor camera (lower and possible upper views)
Pedestal impurity screening with optimized divertor	VUV/VIS spectroscopy, radiated power	Divertor SPRED, MDS, additional spectroscopy, Upper Bolometer to view SAS divertor
Limits on divertor detachment without pedestal degradation	Divertor density, temperature, heat flux, radiated power	Upper DTS, 2D DTS, IR/VIS in Upper Divertor, Upper Bolometer, Upgraded lower bolometer, Divertor Ti, Fast Thermocouples
Source for pedestal density	Neutral density	Divertor SPRED, Ly-alpha arrays, Ly-alpha divertor camera, pressure gauges, wall probes
Particle fluxes to walls	Image D and C fluxes, including during ELMS	Fast visible cameras, wall probes
Non-linear ELM structure	ELM filaments	Tile probes
ELM energy losses	Heat loads to divertor, including during ELMS	Fast IR Cameras
Pedestal/SOL turbulent transport	Density fluctuations	ECEI/MIR upgrades. Expanded/upgraded BES, magnetics upgrades
Improved magnetic equilibria	Te and ne at outer midplane	Tangential TS
Edge MHD stability	Pedestal current density	Imaging MSE, lithium polarimetry
Importance of 3D effects	Te and ne at multiple locations	2 <sup>nd</sup> DBS system, 2 <sup>nd</sup> ECE radiometer, 2 <sup>nd</sup> radial CO2 chord

**Table 4-8.**  
**Simulation Codes Used**

<b>Code</b>	<b>Purpose</b>
CESOL	Core (1.5D FASTRAN) – Edge (EPED) – SOL (SOLPS) coupling
OMFIT	Integrated modeling and experimental data analysis
OEDGE	Interpretive divertor/SOL modeling, ionization source
SOLPS	Divertor/SOL fluid transport, ionization source
UEDGE	Divertor/SOL fluid transport, ionization source
EPED	Reduced pedestal model
STRAHL	1D core impurity transport
EMC3-EIRENE	3D edge fluid code
CGYRO	Pedestal transport modeling
TGLF	Pedestal transport modeling
GENE	Pedestal transport modeling
BOUT++	Pedestal/DIVSOL transport and MHD modeling
ELITE	Peeling-ballooning stability
NEO	Neoclassical transport
TRIP3D	3D field line tracing code
M3D-C1	Non-linear extended MHD code

### 4.1.3 L-H Physics

*Physics Leads: L. Schmitz (UCLA), J. Boedo (UCSD), G. McKee (UW), T. Rhodes (UCLA), Z. Yan (UW), L. Zeng (UCLA), C.S. Chang (PPPL), P. Diamond (UCSD), X.Q. Xu (LLNL), P. Gohil (GA), D. Eldon (GA)*

H-mode operation is desired in future burning plasma experiments to achieve economical fusion energy production. This operating regime entails a narrow region of strongly reduced transport near the edge of a tokamak plasma, leading to a so-called ‘pedestal’ (sec 4.1.2) that roughly doubles energy confinement. Predicting the required auxiliary heating power to reliably access H-mode in burning plasma experiments is crucial; the path to access H-mode in various operating scenarios in ITER must be understood and improved upon, while the prediction is fundamental to the design of a future power plant or nuclear test facility, where a balance must be struck between radiation to reduce divertor heat fluxes and good H-mode access. Presently, an empirical scaling for the required threshold power  $P_{th}$  is used, based on a multi-machine database [Martin 2008]. This scaling does not reflect many known parameter dependences of  $P_{th}$  and fails to predict the experimentally observed low-density threshold behavior or isotope dependence of  $P_{th}$ . A physics-based transition model is therefore clearly needed to predict the power threshold and to confidently extrapolate auxiliary heating requirements for ITER and future burning plasma experiments.

Recent research at DIII-D and other facilities has focused on the coupling of L-mode edge turbulence and turbulence-driven shear flows. Several measurements have been presented which support the picture that increased turbulence-driven shear flow triggers the L-H transition. On DIII-D, an acceleration in the poloidal ion flow of the main ions has been directly observed preceding the L-H transition and the acceleration had been found to be quantitatively consistent with Reynolds-stress-driven shear flow amplification. Fluctuation measurements in DIII-D provide evidence that the isotope dependence of the L-H threshold may be related to a larger Reynolds stress in deuterium than in hydrogen due to higher density fluctuation levels in deuterium plasmas compared to comparable hydrogen discharges. Motivated by this progress, the challenge now is to develop a quantitative validated predictive capability of the L-H power threshold based on these turbulence-flow interactions, and to identify improved paths and actuators to aid H mode access at lower edge power flux.

#### 4.1.3.1 Challenges and Impact

The goal of the DIII-D L-H physics research program is to develop a physics-based model for the power thresholds for the L-H and H-L transitions so that these transitions can be reliably and safely achieved in future machines. To accomplish this goal, the L-H physics program is focused on three key challenges (Table 4-9). The first challenge is to develop a reliable prediction of the L-H transition threshold power. The experiment will address this challenge by developing an improved understanding of the important L-mode turbulence modes at high and low plasma density/collisionality. Appropriate code validation will be needed with simulations that properly treat the “L-mode pedestal” region adjacent to the last closed flux surface, which has relatively steep gradients in the kinetic plasma profiles and large parameter variations.

The second challenge is to ensure H-mode access and avoidance of the first ELM with application of RMP fields during the L-mode. This challenge is motivated by concerns that applied magnetic perturbations to prevent ELMs may increase the L-H threshold power in ITER [Gohil 2011]. Experiments will be performed to determine if the increase in threshold power can be mitigated with careful control of the RMP spectrum. Novel techniques to explore improved H-mode access will be tested, such as use of pellets or particular plasma geometries. The third challenge addresses the need to control the rate of release of plasma energy at the H-L transition, motivated by concerns for the safety of future large machines. A number of tools, including gradual reduction of heating power, pellet injection, steady-state or modulated 3-D fields, or inducing limit cycle oscillations near the H-L back-transition threshold, will be tested for the purpose of developing a safe shut-down strategy.

This research will help develop safe and reliable L-H and H-L transition scenarios in ITER and future large machines. A validated, predictive model of the L-H transition will allow the optimization of L-mode parameters to minimize the auxiliary heating power requirements for accessing H-mode confinement in ITER. This research will also identify tools for an integrated approach for safe energy release during the H-L back-transition in ITER plasmas.

#### 4.1.3.2 Research Plan Overview

The research plan for L-H physics will focus on the challenges and goals shown in Table 4-9. A timeline for addressing these challenges and providing needed facility upgrades is shown in Fig. 4-16. This roadmap benefits from considerable improvement of diagnostics for pedestal turbulence and structure early in the plan, as well as improved 3-D flexibility and new divertor geometries implemented through the plan.

**Table 4-9.**  
**Challenges, Approach, and Improvements for L-H Transition**

Challenge	Goals	Key Capability Improvements
<p>Develop reliable predictive capability for the L-H transition threshold power <math>P_{th}</math></p> <p><i>Use predictive capability to assess how to achieve resilient H-mode access for ITER/other burning plasma experiments (and to lower <math>P_{th}</math> via novel techniques)</i></p>	<ul style="list-style-type: none"> <li>• Identify turbulence modes leading up to L-H transition: RBM (high collisionality) vs. TEM/ITG (low collisionality)</li> <li>• Validate fluid/GK EM models of ITER-relevant L-mode, comparing plasmas with clearly differentiated <math>P_{th}</math></li> </ul>	<p><b>Hardware Upgrades</b></p> <ul style="list-style-type: none"> <li>• SAS Divertor (variable closure)</li> <li>• Upgraded 3-D coil set (n=1-6)</li> </ul> <p><b>Diagnostic Upgrades</b></p> <ul style="list-style-type: none"> <li>• High-<math>k</math> backscattering and upgraded PCI for <math>\tilde{n}(k_\theta)</math></li> <li>• CECE upgrade for intermediate-<math>k</math> <math>\tilde{T}_e</math></li> <li>• UF-CHERS for <math>\tilde{T}_i</math></li> <li>• 3-D turbulence diagnostics for <math>\tilde{n}, B_r</math> via toroidally/poloidally spaced modular DBS/CPS</li> </ul>
<p>Ensure H-mode access and safe avoidance of first ELM with RMP applied before the L-H transition</p>	<ul style="list-style-type: none"> <li>• Improve H-mode access with predictive capability and novel experimental techniques</li> <li>• Ensure safe avoidance of first ELM with RMP applied before the L-H transition</li> </ul>	<ul style="list-style-type: none"> <li>• Parallel wavenumber spectrum/correlation via DBS/CPS</li> <li>• Reciprocating probe head for <math>\tilde{B}_\theta, \tilde{B}_\phi</math></li> <li>• High-resolution 2D BES</li> </ul>
<p>Ensure safe ramp-down and controlled release of plasma stored energy across the H-L back-transition</p>	<ul style="list-style-type: none"> <li>• Optimize ramp-down and mitigate energy release during H-L back-transition</li> </ul>	<p><b>Code Development</b></p> <ul style="list-style-type: none"> <li>• Adapt and validate GK/full-f EM codes (Gene, XGC, BOUT++) for L-mode edge analysis (coupled core/SOL)</li> <li>• Develop/validate GK codes for 3-D modeling based on 3-D profile and turbulence data</li> <li>• Develop improved predictive capability for <math>P_{th}</math> based on multi-parameter conditional or neural-net based analysis of present multi-machine database of L-H-transition data</li> </ul>

Challenge	FY19-20	FY21	FY22	FY23	FY24
Develop reliable predictive capability for the L-H threshold power for ITER/burning plasma experiments	Achieve qualitative understanding of trigger physics in D, He, H				
	Characterize L-mode $\tilde{n}(k)$ spectrum, $\tilde{T}_e, \tilde{T}_i$ and electromagnetic turbulence contributions at low/high collisionality				
	Quantify role of Reynolds stress, bulk viscosity and thermal orbit loss in ISS plasmas vs. $n, M_i, T_e/T_i$ , and ion collisionality				
	Unravel L-mode turbulence/flow interactions in low torque ISS plasmas via validated fluid- and GK modeling				
	Quantify effect of divertor closure, neutral particle physics, and x-pt. geometry on $P_{th}$ in ITER-similar plasmas				
	Develop quantitative predictive capability for $P_{th}$ via advanced global nonlinear gyrokinetic simulations and reduced models				
Using predictive capability and novel exp. techniques, reduce L-H power threshold; optimize H-mode access via predictive modeling and via novel experimental techniques	Using this predictive capability, optimize H-mode access with D/He/Li pellet injection, control of divertor neutrals and shape and x-pnt control				
Ensure H-mode access and safe avoidance of first ELM with RMP applied before the L-H transition	Quantify parameter dependence of $P_{th}$ in low-torque ITER-relevant (ISS) plasmas with applied $n=2,3$ RMP				
	Stimulate/validate GK modeling of 3-D edge transport barriers via advanced turbulence/kinetic profile data; test theoretical models of RMP modification of flows, flow damping, shear layer topology				
Ensure safe ramp-down and controlled release of stored energy $W(t)$	Optimize H-mode access in ISS plasmas with RMP spectrum control via upgraded 3-D coils				
Improvements	Attempt control of $W(t)$ via slow ramp-down of $P_{aux}$ , shape control, applied 3-D fields, and via induced LCO				
	Test mitigation strategies to control energy release during H-L transitions (modulated 3-D fields; control of shape and divertor geometry/closure)				
	Develop integrated approach for safe ramp-down				
	Upgraded DBS, CPS, PCI, CECE, UF CHERS, BES-X    Upgraded 3-D coil set    Variable divertor closure    Increased ECH power for L-H transition				

Fig. 4-16. Research Plan Overview for L-H physics

## Challenge 1: Determine Role of Reynolds Stress, Bulk Viscosity, Orbit Loss in the Production of $E_r$ and Unravel Critical Trigger Physics

**Current progress; Reynolds stress/ nonlinear energy transfer driving transient  $E \times B$  flow:** Detailed analysis of L- to H-mode transition data has focused on the coupling of L-mode edge turbulence and turbulence-driven shear flows [Yan 2014, McKee 2009, Yan 2013, Conway 2011, Estrada 2011, Schmitz 2012, Schmitz 2014A, Xu 2011, Manz 2012, Tynan 2013, Shesterikov 2013, Cziegler 2015]. Measurements of long-wave length ( $k_{\perp} \rho_i$ ) turbulent eddy dynamics, characteristics, flows and flow shear from Beam Emission Spectroscopy (BES) in the near edge region of DIII-D plasmas have been obtained in a set of experiments during an ion gyro-radius scan and density scan in a favorable magnetic geometry in order to investigate the underlying physics that influence the macroscopic L-H transition power threshold scaling relations and the trigger mechanisms. Immediately before the transition turbulence amplitudes, Reynolds stress gradient and flow shear increase rapidly. New analysis on the nonlinear energy transfer between the fluctuations and shear flow during the L-H transition has been performed (Fig. 4-17). The calculation of the energy production term  $R_{\wedge} = \langle \bar{v}_r \bar{v}_q \rangle \frac{\partial V_{ZF}}{\partial t}$ , which is an energy source of the shear flow, shows a rapid increase just before the transition, and this change is localized in the pedestal region. This analysis is consistent with the picture that the increased shear flow generated from fluctuations becomes an energy sink for turbulence, reduces turbulence, and thus triggers the transition.

**Flow Acceleration via Turbulence-Flow Coupling:** A strong jet flow just inside the last closed flux surface (LCFS) at the transition to high confinement mode is considered to be the crucial ingredient that allows the H-mode edge transport barrier to form. Poloidal ion flow acceleration preceding the L-H transition has been measured in DIII-D via main ion Charge Exchange Recombination Spectroscopy (CER). The acceleration was found to be quantitatively consistent with Reynolds-stress-driven shear flow amplification across the entire L-mode edge plasma layer (Fig. 4-18). Theory [Rozhansky 1992] predicts that the poloidal flow acceleration is the sum of the radial gradient of the perpendicular turbulent Reynolds stress  $\partial \langle \tilde{v}_r \tilde{v}_\theta \rangle / \partial r$  (acting as a momentum source) and poloidal flow damping attributed to collisions. As illustrated in Fig. 4-18, evaluation of all terms of the ion flow equation from DIII-D data show that the theory quantitatively matches the experiment [Schmitz 2014B, Schmitz 2015]. Fig. 4-18 displays the measured poloidal flow acceleration (red squares), the measured Reynolds stress gradient (blue triangles) as well as the sum of the flow acceleration and damping (green circles) where poloidal damping is calculated from theory [Kim 1991], across the edge region. As predicted by theory [Rozhansky 1992], the sum of flow acceleration and flow damping matches the Reynolds stress

drive in sign and magnitude. The comparison reported here has been carried out in a helium plasma near the minimum power threshold.

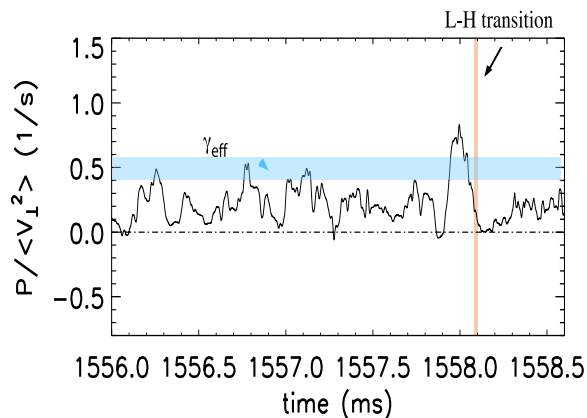


Fig. 4-17. Nonlinear energy transfer rate from turbulence ( $k_{\theta}\rho_s \leq 1$ ) to low frequency  $\mathbf{E} \times \mathbf{B}$  flow across the L-H transition; also shown is the ambient turbulence decorrelation rate.

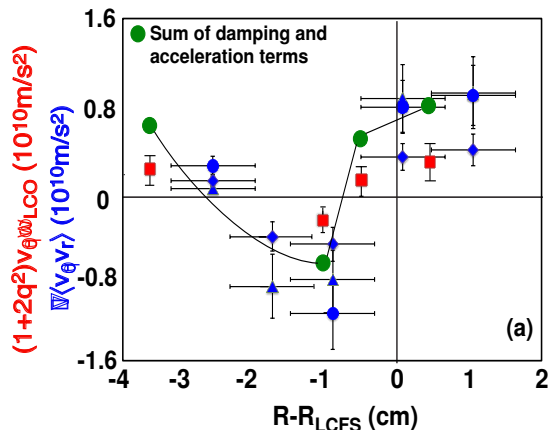


Fig. 4-18. Ion flow acceleration (from CER data, in red) and measured Reynolds stress gradients from BES (in blue), and the sum of the acceleration term and the calculated poloidal flow damping term according to Rozhansky 1992 (green circles), versus radius.

**Turbulence structure in Deuterium and Hydrogen plasmas:** Significant progress has also been made regarding the isotope scaling of the L-H threshold power. Fig. 4-19 shows the L-H threshold power in ISS deuterium and hydrogen plasmas in DIII-D, indicating a significantly higher threshold in hydrogen at medium and low plasma density [Yan 2017]. Examination of the microscopic turbulence dynamics revealed that deuterium and hydrogen plasmas with low threshold exhibit a dual mode turbulence structure just inside the LCFS (Fig. 4-19, [Yan 2017]).

Higher density fluctuation levels have been observed in deuterium plasmas compared to hydrogen in otherwise similar ISS plasmas. One hypothesis for this effect is that the Reynolds stress (which depends on the turbulence intensity) would be larger in deuterium as compared to hydrogen plasmas. This has been confirmed experimentally [Yan 2017, Schmitz 2017]. In addition, turbulence dispersions  $\omega$  vs.  $k_{\theta}$  have been recorded via BES and show two branches corresponding to electron and ion modes in cases where the threshold power is minimal. In contrast, cases with high threshold power exhibit single-mode structure. These results demonstrate clearly that the turbulence mode structure is directly coupled to the trigger process, shear flow amplification and the power threshold.

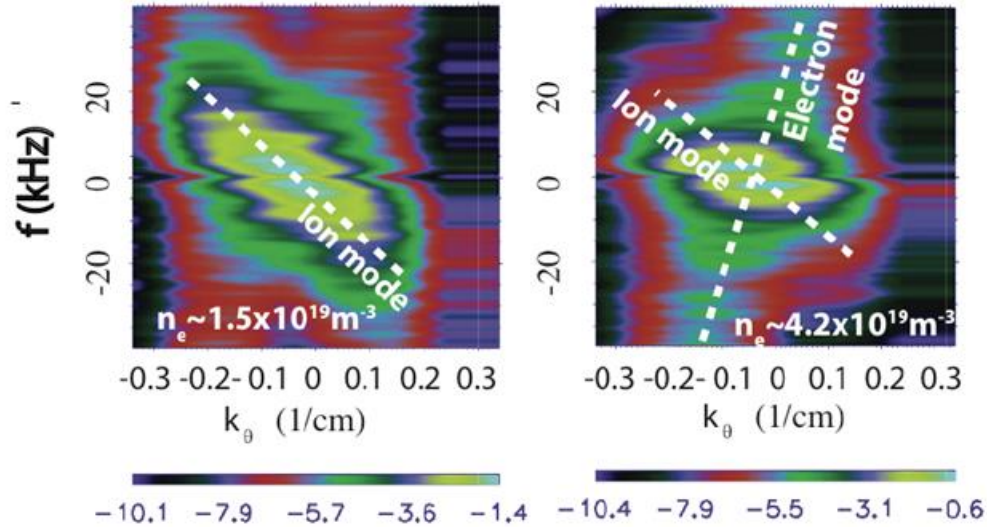


Fig. 4-19. Turbulence wavenumber spectrum (BES) for hydrogen plasmas at (a) low and (b) medium density, showing a clear dual-mode structure at medium density where the L-H threshold power is low.

### Goal 1: Identify turbulence modes leading up to L-H transition.

Research will emphasize the identification of the edge L-mode turbulence that is dramatically reduced at the L-H transition. The pronounced density dependence of the L-H power threshold, with a broad minimum observed at intermediate density, may provide a clue to the turbulence properties. One goal of the proposed work is to uncover potential differences in L-mode turbulence properties at low and high plasma density, and their effect on axisymmetric flows across the L-H transition. A working hypothesis is that Resistive Ballooning Mode (RBM) turbulence is important at high collisionality (high density) and that ITG or TEM modes are important at low collisionality (low density). Electromagnetic effects may play a role for RBMs, and thus localized internal measurements of the fluctuating magnetic field will be made very close to the LCFS. These measurements will be made with the recently added multi-channel Cross-polarization Scattering system, which provides measurements of radial magnetic field fluctuations. 2D BES and multichannel DBS will be used to reconstruct the wavenumber spectrum of density fluctuations, which will be instrumental for mode identification at lower collisionality in conjunction with linear stability analysis (e.g. distinguishing ITG vs. TEM modes). Research will compare conditions with known large differentials in the threshold power, which will allow for distinguishing systematic vs. incidental trends, since large differences are most suitable for validating nonlinear gyrokinetic simulations. These contrasting conditions include favorable/unfavorable grad-B drift direction, deuterium vs. hydrogen plasmas at low collisionality, and large differences in  $T_e/T_i$ . Of key interest will be identifying the characteristics

and dynamics of edge turbulence that drive and trigger the transition, comparing conditions on the verge of a transition with those far away from a transition.

**Goal 2: Validate fluid/GK EM models of ITER-relevant L-mode, comparing plasmas with clearly differentiated  $P_{th}$ .**

Studies will systematically investigate the link of trigger physics and power threshold scaling, across a wider parameter range than has been studied so far. A crucial element of the proposed research is the link to appropriate theoretical simulations with codes such as BOUT++, GENE, XGC-1, which are useful for understanding the dominant L-mode instability drive, the saturated L-mode turbulence spectra, radially sheared flows, and how their interaction triggers the L-H transition. Systematic code validation via comparison with measured turbulence properties is required and the simulations must be able to adequately treat an edge region that is characterized by steep gradients and substantial radial parameter variations. Global, non-linear simulations that can include both the outer core and the scrape-off layer (with appropriate sheath boundary condition) may address the important physics. The numerical simulation community will be engaged in this effort and data sets with widely varying power thresholds, as noted for goal 1, will be made available for this research. This work is an important step towards development of a validated physics-based L-H transition model.

**Challenge 2: Ensure H-Mode Access and Safe Avoidance of the First ELM with RMP Applied Before the L-H Transition**

**Current progress.** The H-mode power threshold cannot be predicted for ITER from a first principles model at present and thus there cannot be certainty that ITER can achieve the H-mode in all desired scenarios. Moreover, resonant magnetic perturbations may have to be initiated in ITER in advance of the L-H transition to safely avoid the first ELM. However, RMPs are known to increase  $P_{th}$ , in particular for higher toroidal mode number  $n$  [Scannell 2015]. Thus, identifying options to reduce the H-mode power threshold and to mitigate the effect of RMP fields on the threshold power would provide ITER with additional flexibility in designing its scenarios.

**Goal 1: Improve H-mode access with predictive capability and novel experimental techniques.**

Research will test ways to reduce the heating power required to obtain the H-mode transition. This research will generally rely on testing control parameters, which are known to modify the transition but are not accommodated in power threshold scalings. This research will also rely on testing new ideas. It is well known that there are a number of effects that can substantially affect

the H-mode power threshold but are not taken into account in the standard power threshold scalings. For instance, the power threshold depends sensitively on SOL geometry, such as the X-point height; thus, shape control of the divertor plasma will be explored to optimize H-mode access. The effect of divertor closure and detachment has not been systematically investigated previously and it will be tested in this research. This work will make use of various divertor geometries in DIII-D, including the SAS configuration, to test effect of divertor closure on the power threshold. The injection of shallow fuel pellets has shown promise in the past in DIII-D, and more work will be performed to unambiguously determine the underlying mechanism. Supersonic Molecular Beam Injection (SMBI) has been shown to lower the H-mode power threshold in the KSTAR tokamak and will be considered as a possible further capability for DIII-D. Finally, understanding from the simulation developed in Challenge 1 will be applied to identify optimal discharge trajectories.

**Goal 2: Ensure safe avoidance of first ELM with RMP applied before the L-H transition.**

RMPs are known to increase  $P_{th}$ , in particular for higher toroidal mode number  $n$  [Scannell 2015]. Hence, the effect on the power threshold must be mitigated as much as possible. Research will be conducted in DIII-D to understand the effect of RMPs on the power threshold and ways will be sought to mitigate this effect. Fluctuation and profile diagnostics in DIII-D will provide 3-D information on the modification of kinetic profiles,  $E \times B$  shear, and turbulence properties via  $n=2$  phase rotation or  $n=3$  phase flips. Theoretical hypotheses, such as modified stability thresholds and/or increased flow damping in the presence of RMP, will be tested. Finally, the planned RMP coil upgrade, which will allow spectrum control for  $n=1-4$ , offers expanded opportunities to optimize the RMP spectrum and will be used in a program to mitigate the effects on  $P_{th}$  as much as possible. This work will also test and stimulate theoretical models by exploring the dependence of threshold increase on electron/ion flow damping and  $E \times B$  shear layer modification.

**Challenge 3: Ensure Safe Ramp-Down and Controlled Release of Plasma Stored Energy across the H-L Back-Transition**

**Current progress.** It is well known that the H-L back transition typically occurs rapidly and therefore the energy of the plasma changes by a large amount in a short time, requiring significant changes in control currents. This pulse of energy is a concern for the safe operation of ITER and other future burning plasma plasmas due to stresses on the poloidal coil system and associated power supplies. In the past 5 years, research on DIII-D to study the back transition

concluded that the transition was not caused by ideal peeling-ballooning modes; rather, resistive MHD modes emerged as a candidate [Eldon 2015].

**Goal:** Research will be performed to explore several options that can potentially extend the time interval over which the stored energy is released during the H-L back-transition. These options include controlling the back-transition timescale by a slow ramp-down of the auxiliary heating power, reducing toroidal rotation in the co-current direction, radiative power dissipation via controlled impurity injection, or by inducing limit cycle oscillations during the back-transition. Proper modulation of the auxiliary heating power might allow incremental stored energy release within a safe limit of  $\partial W(t)/\partial t$ . Additionally, shape (triangularity) control modifies the peeling/ballooning as well as resistive ballooning stability limits and could be used to induce controlled back-transitions. Finally, applied RMP fields, with spectrum control available via the planned I-coil upgrade, may be used to limit the energy released in back-transition precursors or to control back-transition time evolution. These options also exploit the hysteresis (differential in threshold power) between L-H and H-L transitions, and will be systematically explored in DIII-D ITER-relevant plasmas. The goal of this work is to develop an integrated approach for controlling back-transition energy release.

#### 4.1.3.3 Improvements in Capabilities

The research described above benefits directly from several proposed improvements in hardware and diagnostic capability (Table 4-10 and Table 4-11). Increased ECH power and SAS divertor enhancements will allow studies to reduce the H-mode power threshold. Increased ECH power will enable new tests of the power threshold dependencies on plasma parameters, particularly when evaluating the low-density branch. A number of diagnostic upgrades will provide key information on turbulence properties in the L-mode and help enable an identification of the physics driving L-mode turbulence, placing DIII-D in a unique position to address the local (microscopic) physics of the L-H transition to validate advanced fluid, gyrokinetic and kinetic simulations of the L-H transition. Obtaining an understanding of the physics involved in the L-H transition and a predictive capability for the L-H power threshold will use and advance state of the art theoretical simulations (Table 4-12).

**Table 4-10.  
Hardware Improvements for L-H Transition Studies**

<b>Hardware Capability</b>	<b>New Physics</b>
SAS Divertor	Determine dependence of $P_{LH}$ on divertor closure
Increased ECH power	Determine how $P_{LH}$ depends on $T_e/T_i$
Upgraded 3-D Coil set	Mitigate increase of $P_{LH}$ with RMP/optimize H-mode access with $n=2-4$ RMP

**Table 4-11.**  
**Diagnostic Improvements for L-H Transition Studies**

<b>Scientific objective</b>	<b>Physics measurement</b>	<b>Diagnostic Technique</b>
Crucial ingredients for a physics-based transition model; validate GK modeling	Parallel turbulence correlation; toroidal and poloidal flow correlations; wavenumber spectrum $\tilde{n}(k)$	Dual DBS, Upgraded PCI
Determine role of EM turbulence in L-H transition dynamics; GK and kinetic code validation	Magnetic fluctuations ( $B_r$ ), high radial resolution 2D density fluctuations	Dual CPS Reciprocating probe head for $\tilde{B}$ BES-X
Identify dominant L-mode turbulence modes in different regimes; validate GK modeling	$\tilde{T}_e, \tilde{T}_i$	Upgraded CECE, UF CHERS

**Table 4-12.**  
**Simulation Codes Used**

<b>Code</b>	<b>Purpose</b>
BOUT++	L-mode edge turbulence characterization and L-H transition modeling at intermediate/higher collisionality (D, H, He plasmas)
XGC-1	Global kinetic H-mode transition modeling and predictive modeling of $P_{th}$ for ITER and future experiments
GENE	Gyrokinetic analysis of D, H, He L-mode plasma turbulence and flow generation; calculation of transport fluxes

## 4.2 CORE-EDGE

Burning plasma experiments such as ITER and DEMO require the simultaneous achievement of a high performance core plasma and a highly dissipative boundary plasma. The core plasma must have sufficient fuel density and temperature for the plasma to produce the desired fusion power. Heating and current-drive technologies may require specific ranges of density and temperature. For the protection of plasma facing components (PFCs), the boundary plasma must greatly reduce the heat flux and particle energies at limiting surfaces, such as divertor strike points, spreading the heat more diffusely via radiation or flux expansion. PFCs must be made of materials that can survive in the harsh environment of high heat and neutron fluxes and these materials must have low tritium retention. The heat fluxes from impulsive events, such as ELMs, must be eliminated or reduced to levels that will not damage or cause rapid erosion of PFCs.

In current machines, core and boundary performance are often optimized separately and the techniques for optimizing the core are often not optimal for optimizing the boundary and vice

versa. For instance, a core designed to have RF current drive may need to operate at a low density that is not compatible with densities required for obtaining a detached divertor. The use of high-Z metals for suitable PFCs often leads to unacceptable accumulation of radiating high-Z charge states in the core. These and many other examples show that the core and boundary are a strongly coupled system and they must be optimized together to achieve future acceptable burning plasma scenarios. This optimization requires simultaneous integration of the core, pedestal and boundary and is often called “core-edge integration” for short.

Throughout the 2014-2018 research plan, the DIII-D program put significant effort into core-edge integration. Research has been performed to combine radiative divertors with high performance core scenarios. ELM control techniques have been applied to high performance scenarios. The impact of a high-Z material on high performance plasmas was studied with installation of two W-coated rows of divertor tiles in the lower divertor. Recently, a task force has been formed to identify integration issues and to lead experiments to study them.

In the 2019-2024 five-year plan, DIII-D will significantly increase its effort on core-edge integration. The general thrust of the research is to develop the knowledge base to simultaneously optimize core and boundary performance. Major lines of research will focus on understanding the compatibility of the fusion core with reactor relevant wall materials (4.2.1), on studying the effect of plasma shape and boundary configurations on integrated solutions (4.2.2) and on integrating power and particle control strategies with high performance plasmas (4.2.3). Neither DIII-D nor any other existing device can simultaneously reproduce the core and boundary parameters expected in ITER and other burning plasma devices. Therefore, a strong focus of the proposed research is to develop validated physics models of the coupling of core, pedestal, and boundary regions, and a plan for this will be discussed later. The plan to develop these models includes strategies to include a range of wall materials, including metal in the models. The three research areas noted here will be briefly discussed below:

1. **Reactor relevant wall:** The objective of the DIII-D program on the compatibility of the fusion core with reactor relevant wall materials is to understand the source and transport of impurities, and to develop techniques to control impurities in the plasma core. This work will be done for a range of impurities for medium-Z to high-Z. The over-riding goal is to obtain a predictive model that describes the impurity content in the plasma for a specific choice of material and plasma properties. The planned research is divided into three themes: 1) develop a validated model for control of impurity transport in reactor-relevant regimes; 2) develop a validated model for pedestal and SOL impurity transport; 3) identify the origin of impurity wall and divertor sources for reactor relevant materials. This research plan will address two crucial issues for a reactor with a high-Z wall: the

transport and the source of the high-Z impurities. For transport studies, a range of impurities, including tungsten, will be introduced into the plasma via a laser blow-off system. This work will be used to develop models for core transport of high-Z impurities over a range of plasma conditions, and these models will be checked in two campaigns in which rows of W tiles are installed in divertor structures to produce a large W source. These latter experiments will also be used to study the source and transport of W in the SOL, research that will inform development of predictive models for high-Z influxes across the separatrix. The remainder of the PFCs will be graphite, which is an asset for these studies since the source of W will be highly localized. Key planned hardware upgrades include W divertors, a wall interaction test station (WITS) and increased ECH power. Later in the plan, implementation of siliconization and SiC tile arrays in key areas will enable further tests with reduced carbon induced erosion to isolate critical physics. Key enabling diagnostic enhancements include several improvements to provide spatially and temporally resolved measurements of a range of impurities, collector probes, and diagnostics for WITS. The proposed research plan is discussed in Section 4.2.1.

2. **Configuration:** The central aim of the DIII-D research program on plasma shape and boundary configuration is to study how plasma shape and divertor configuration affect physics process required for good core performance and good dissipative divertor conditions, and to develop a basis for a viable solution that meets all of the competing requirements in a fusion reactor. A given change in shape or divertor configuration might have a positive effect on core performance but a negative effect on divertor performance or vice versa. This research will study the trade-off of shape and divertor configurations to obtain optimum overall performance. The research plan will be structured to address three key challenges: 1) predict the trade-offs between SND and DND operation for integrated plasma performance; 2) predict the optimal elongation, triangularity, and squareness for integrated plasma performance; 3) predict the optimal baffling and divertor flux expansion strategies for power and particle exhaust and recycling control in high performance plasmas. Key enabling hardware upgrades include installation of the SAS 2 upper and lower divertors, installation of W divertor tiles for two tungsten campaigns, NBI and EC heating upgrades, helicon and/or lower hybrid installation for current drive, power supplies for advanced shape and divertor shape control and an upgraded gas injection system. Some of the key diagnostic upgrades include measurements of the pedestal ionization source, measurements of the pedestal current density, upgrades to the tangential Thomson system to provide edge midplane data and a

number of enhancements to diagnose the divertors. The proposed research plan is discussed in Section 4.2.2.

3. **Power and particle control:** the goal here will be to understand the use of radiating impurities to dissipate heat, the transport of impurities, and the interactions of divertor geometry, detachment, pedestal and core to establish the physics basis for the design of an integrated core-edge solution. The research plan will be structured to address four key challenges: 1) understand how impurity species influence pedestal and core performance to provide strong dissipation of heat and maximize core performance; 2) test and develop a projectable model for helium exhaust with a detached divertor; 3) establish the compatibility of ELM mitigation techniques with exhaust of gaseous impurities (radiators including high-Z, helium); 4) identify and understand the density limit, MARFEs, and operation close the H-L back transition threshold. Key hardware upgrades that will enable this research include installation of the SAS 2 upper and lower divertors that will be capable of handling high power, installation of W divertor tiles for two tungsten campaigns, increased EC power for current drive and heating and a steerable neutral beam for optimizing steady-state scenarios. Planned siliconization and SiC tile arrays will enable key further tests of radiative mantle physics with reduced carbon radiators. Key diagnostic upgrades include divertor and core spectroscopy for monitoring impurity sources and transport as well as measurements of pressures of various species in the divertor. The proposed research plan is discussed in Section 4.2.3.

There is a strong inter-relation between these three research areas and much of the work will be performed with jointly designed experiments; some of the work will also be performed jointly with research discussed in Section 4.1 on pedestal and ELMs. The research here will also make use of advancements in high performance core scenarios, discussed in Section 2.1 on robust plasma scenarios for future reactors and in Section 3 on the scientific basis for a fusion boundary solution. The other research areas mentioned here will develop the physics basis of specific aspects of tokamak performance. The work of the core-edge integration team is to perform research that couples work performed in two or more areas.

All three of the research areas are strongly focused on developing predictive models with a view towards developing predictions to optimize a fusion reactor. In particular, the research will seek to validate state of the art models that provide coupling of the core, pedestal and SOL regions. A desired goal of this research would be the ability to use reduced models to compute heat and particle sources and transport from the core to plasma limiting surfaces in order to predict temperature and density profiles in the confined plasma as well as in the SOL. These models will include effects from a range of wall materials including high-Z. Much but not all of

this modeling can now be done with the CESOL code, which is operated in the OMFIT framework, being developed by the AToM SciDAC project. CESOL can compute sources from beams, RF heating and edge neutrals and it couples core, pedestal and SOL models to compute temperature and density profiles. Core transport is obtained from TGLF, the pedestal is modeled with EPED and the C2 transport model is used to compute 2D transport in the SOL. Enhancements required to obtain the desired modeling ability are physics-based models for individual profiles of temperature and density in the pedestal and for transport in the SOL. For instance, at present, the user must specify the separatrix density to obtain temperature and density profiles in the pedestal from the EPED model, while SOL transport is obtained from user-specified particle diffusion and thermal diffusivity transport coefficients. Efforts in this five year plan aim to improve models in both areas. Another important enhancement would be the addition of a divertor model to CESOL. A solution that is being considered is to couple SOLPS to CESOL via the OMFIT framework. Thus, the AToM project provides powerful capability to model core-edge integration and this capability will improve with future upgrades. This modeling capability combined with the increased physics understanding and model resolutions possible from the DIII-D research, set out in this Five Year Plan, will provide the basis to develop predictive capability for integrated core-edge solutions in future fusion reactors.

#### **4.2.1 Compatibility of the Fusion Core with Reactor Relevant Wall Materials**

*Physics Leads: N. Howard (MIT), T. Abrams (GA), B. Grierson (PPPL), S. Haskey (PPPL), A. Jarvinen (LLNL), B. Victor (LLNL)*

It is widely accepted that the influx of medium and high-Z impurities into the tokamak core can produce unacceptable levels of core radiation when accumulation occurs. However future fusion reactors may require medium or high Z walls to avoid issues with unacceptably high levels of tritium retention in the wall. Research on novel materials such as ceramics (e.g., SiC) could potentially provide solutions with lower-Z materials. The choice of material, and development of compatible scenarios remain important open questions, with concerns over impurity accumulation with metal walls and power handling of lower Z surfaces. The key challenges for wall compatibility logically separate by the impurity path from the wall to magnetic axis. These are the appropriate choice of wall material [Tungsten (W), SiC, etc...], the influx of the wall material into the main plasma (via sputtering, SOL and pedestal transport), and impurity transport and control properties in the plasma core (turbulent/ neoclassical transport and control via external heating).

Research on metallic impurities has been performed primarily by the metal-walled tokamaks, JET, ASDEX-U and C-Mod. However, DIII-D, with its non-metallic wall, provides an

opportunity to study impurities perturbatively, to identify sources and mechanisms, without the presence of an unknown background source. Thus, DIII-D has assessed material erosion and migration properties using tile sample test facilities. And during FY16, two rows of tungsten-coated tiles were inserted in the lower divertor on DIII-D for a campaign to study the source and transport of W. Time resolved measurements were made of the W source in the divertor and the inter-ELM W erosion rate could be modeled arising from carbon sputtering of the W tiles [Abrams 2017A]. Core W accumulation was observed in some discharge scenarios; however, in near-steady-state hybrid discharges with strong on-axis EC power, W accumulation was not observed [Victor 2017]. This result is consistent with results from tokamaks worldwide (JET [Puiatti 2006], ASDEX-U [Dux 2003] and C-Mod [Loarte 2015], which have established that accumulation of high-Z impurities can be mitigated through the application of on-axis electron heating. Research on DIII-D has also studied the exhaust rate of the injected low-Z impurity fluorine in RMP-ELM suppressed and QH-mode discharges, which had no ELMs. Analysis showed that the injected fluorine transport across the edge barrier is comparable to that obtained in ELMing plasmas with ELM frequencies near 40 Hz [Grierson 2015]. Experiments with injection of low-Z impurities into the carbon-walled DIII-D device have seen little effect of the impurities on the pedestal height, in contrast to some results from the metal-walled JET and ASDEX machines, which saw increased pedestal pressures.

#### 4.2.1.1 Challenges and Impact

The goal of the DIII-D materials compatibility program is to develop models to understand and predict the transport and source of low and high Z impurities in a tokamak and to devise techniques to mitigate problems caused by impurities, should they arise. To achieve this goal, DIII-D research will focus on three challenges, as listed in Table 4-13. The first challenge is to develop a validated model for control of impurity transport in reactor-relevant regimes. Upgrades to DIII-D that enable the injection of impurities with a wide range of Z, combined with upgraded diagnostics to follow their transport will be used in conjunction with control solutions, such as ECH. An important open question is how the control solutions flush impurities and thus a further part of this challenge is to validate impurity transport models in the plasma core. The second challenge is to understand and tailor pedestal impurity transport. Currently, there is a large degree of uncertainty in the physics basis for this transport. It is assumed that in present devices the neoclassical impurity pinch is strong in the pedestal, but at reactor conditions the balance may tip towards impurity screening. Thus, an essential element of the challenge is to obtain an understanding of the structure of the density and temperature profiles in the pedestal at reactor SOL neutral opacity, and the possible role of turbulence in impurity transport. The required research will use existing profile and turbulence diagnostics as well as new diagnostic capability

to detect a range of impurities in the pedestal. The third challenge will be to identify the origin of impurity wall and divertor sources for reactor relevant materials. The interactions of relevant plasmas with the walls, and the resulting transport of materials in the scrape-off layer and divertor need to be understood to determine impurity flows into the plasma, and to evaluate proposed techniques to mitigate them. The effects of divertor screening, closure and detachment need to be understood here, as well as main chamber erosion.

**Table 4-13.  
Challenges for Core-Wall Compatibility**

<b>Challenge</b>	<b>Goals/deliverables</b>	<b>Key Capability Improvements</b>
Develop validated model for control of impurity transport in reactor-relevant regimes	<ul style="list-style-type: none"> <li>• Systematically test effect of actuators (NBI, ECH H&amp;CD, torque) on impurity transport to determine optimum control techniques</li> <li>• Validate impurity transport models in the plasma core</li> </ul>	<p><i>Hardware upgrades</i></p> <ul style="list-style-type: none"> <li>• Laser blow-off impurity injector</li> <li>• Localized gas puffing</li> <li>• Siliconization</li> <li>• Wall Interaction Tile Station (WITS)</li> <li>• SAS 1 W rings, SAS 2U W rings</li> <li>• Toroidal limiters of new material (optional)</li> <li>• Increased ECH power</li> <li>• Impurity powder dropper</li> </ul>
Develop validated model for pedestal and SOL impurity transport	<ul style="list-style-type: none"> <li>• Probe the nature of pedestal impurity transport and structure to resolve underlying physical mechanisms</li> <li>• Determine interplay of neoclassical and turbulent transport for impurities</li> </ul>	<p><i>Diagnostic Upgrades</i></p> <ul style="list-style-type: none"> <li>• Spatially resolved VUV spectrometer</li> <li>• Energy-resolved SXR measurement</li> <li>• Hydrogen sensors (main chamber CX)</li> <li>• DiMES imaging and heating, in-situ Thermal Desorption Spectroscopy)</li> <li>• Improved Langmuir probe placement and dynamic range</li> <li>• UV/VUV spectroscopy and imaging</li> <li>• Collector probes</li> <li>• Improved MDS time response</li> <li>• WITS diagnostics</li> <li>• Additional targeted filterscopes.</li> </ul>
Identify origin of impurity wall and divertor sources for reactor relevant materials	<ul style="list-style-type: none"> <li>• Develop empirical understanding of spatial origin of impurities</li> <li>• Develop Predictive Model of Reactor Impurities Based on Validated Impurity Source and Transport Models</li> </ul>	<p><i>Code Development</i></p> <ul style="list-style-type: none"> <li>• Integrate analysis of core/edge impurity transport codes into OMFIT for whole device modeling</li> <li>• Incorporate NEO for impurity transport coefficients in OMFIT</li> <li>• Test and begin using reduced models of core impurity transport for time-dependent impurity accumulation predictions</li> <li>• Begin using WALLDYN for edge studies</li> <li>• Expand ERO/OEDGE utility for constraining impurity sourcing, including due to transients</li> <li>• Couple DIVIMP to ERO and WALLDYN</li> </ul>

This research will develop the capability to both understand and model the effect of an arbitrary wall material on the performance of the fusion core. Despite not being a metal-walled

machine, DIII-D is well equipped to perform this research. Studies will be performed to perturb, measure and control transport of a wide range of impurities with a goal of predicting and mitigating problems from wall materials in future machines. The specific background wall material is not important for these studies. Research will also be performed to understand the sourcing and transport of high-Z impurities (W) in the SOL. This work will be done primarily in two different campaigns in which rows of W tiles are temporarily installed in a divertor structure for campaigns to study metal effects. The normal absence of W in DIII-D is an asset for these campaigns since the location of the W source will be highly localized and well known. The addition of siliconization will enhance studies by providing data without carbon as a strong impurity source. A strong modeling program will accompany these experiments and will be used to develop predictive capability for sourcing and transport of medium and high Z impurities in future machines.

A further goal of this research is to develop predictive capability to inform the choice of wall material for fusion reactor designs and to identify actuators and understanding that can be used to flush impurities from the core. Current thinking about wall materials is based primarily on results from the current generation of machines. ITER and reactors will operate with plasma parameters that are not achieved in current devices and impurity behavior might be significantly different than observed in today's machines. For instance, tungsten accumulation might not be a problem due to adequate transport and/or pedestal screening which does not occur in present day machines. If other materials are identified that have promising properties for handling heat and neutron fluxes in a reactor, this predictive capability could be used to evaluate their compatibility with core performance. For example, SiC plasma-facing components might be installed in DIII-D; if so they would enable studies of the impact of lower-Z advanced materials on the core plasma. If modeling shows that tungsten or other chosen materials pose a threat for core performance, then the understanding of how actuators work can be used to determine if the impurity problems can be mitigated.

This research will also be highly important to the identification of workable concepts for radiating mantles, which will be needed in DEMO-class machines. The ultimate goal of the research is to develop a predictive capability that allows for a reliable, physics-based extrapolation of impurity core concentrations in next-generation machines, scenario design, and informs decisions for wall materials in these devices. The research plan here will overlap with and be coordinated with research in other areas, particularly sections 3.3.1 and 4.2.3.

**4.2.1.2 Research Plan**

The materials compatibility research plan is organized according to the challenges and goals in Table 4-13. Fig. 4-20 gives the timeline for each challenge and the capability improvements necessary to achieve them.

Challenge	FY19-20	FY21	FY22	FY23	FY24
Develop validated model for control of impurity transport in reactor-relevant regimes	-----Validation of core/pedestal/edge models against experiments-----				
Develop validated model for pedestal and SOL impurity transport	Experiments probing the role of actuators (heating, current drive, fueling) on core, and pedestal impurity transport (W and Si from LBO)		Assess effect on performance of core & pedestal from edge sources of various Z materials, using upgraded divertor/edge diagnostics	Build off actuator studies and Edge sourcing studies to establish optimized, reactor-relevant scenarios	
Identify origin of impurity wall and divertor sources for reactor relevant materials				Integration of validated core/pedestal/edge models of impurity sources/transport for evaluation of wall/core compatibility	
Capability improvements	Installation of pedestal/core SXR arrays Installation of title station Divertor Ti measurement High res. divertor bolo/ 2-D divertor imaging / Increased IR coverage----- Hydrogen sensors (main chamber CX) DiMES imaging and heating, in-situ TDS) Improved Langmuir probe placement and dynamic range UV/VUV spectroscopy and imaging collector probes Upgraded edge spectroscopy (GPI, CX neutral diagnostics) Addition of XICS Addition of spatial resolved VUV SAS 1 W rings SAS 2U W rings				

Fig. 4-20. Research Plan Overview

**Challenge 1: Develop Validated Model for Control of Impurity Transport in Reactor-Relevant Regimes**

**Current progress.** During the past five years, DIII-D has identified sourcing and demonstrated control of high-Z impurities during a metal rings campaign with candidate steady state scenarios in which two rows of W-coated tiles were installed in the lower divertor. W

accumulation was observed in the core in some scenarios. However, in high power hybrid discharges with strong on-axis EC heating power, W accumulation was not observed, as shown in Fig. 4-21 [Victor 2017]. Panels f) and g) of the figure show no evidence of W in the core despite a significant W divertor source (panel e). In comparison with a reference discharge obtained prior to the installation of the W tiles,  $\beta_N$  and H98y2 were essentially identical.

In experiments with the standard graphite divertor, strong expulsion of highly ionized nickel from the core has been observed with the injection of lithium granules [Bortolon 2016] or deuterium pellets for ELM pacing. Low-Z impurity transport has been studied in ELM-controlled regimes with fluorine injected into RMP-ELM suppressed and QH-mode discharges. The transport of injected fluorine across the edge barrier was comparable to that obtained in ELMing plasmas with ELM frequencies near 40Hz [Grierson 2015], a highly encouraging development for ELM control methods in ITER.

**Goal 1: Establish methods for control of impurity transport in reactor-relevant regimes.**

As a first step in challenge one, DIII-D will establish heating scenarios that alleviate impurity accumulation and optimize reactor performance. Upgrades to DIII-D’s ECH capabilities will be important as will co and counter neutral beams (noting recent work predicting a strong effect of rotation [Casson 2014]) and ECCD. These actuators will all be used to modify local transport and tailor impurity transport profiles to reduce or eliminate impurity accumulation. Experiments early in the FY19-24 time period will focus on scenarios, such as QH-mode and the low torque ITER baseline scenario, that have projected relevance to ITER and future devices. High quality measurements of kinetic profiles and of turbulent fluctuations over a wide range of spatial scales and fields will complement the planned upgrades to spectroscopic capabilities for studying core impurity transport. Due to their promise as first wall materials, experimental emphasis will be placed on assessing core impurity transport and accumulation of W and Si. However, the installation of the new DIII-D laser blow-off (LBO) will allow for exploration of a wide range of impurity Z (~60 elements from Li to W can be studied) via controlled, trace impurity injection. Existing

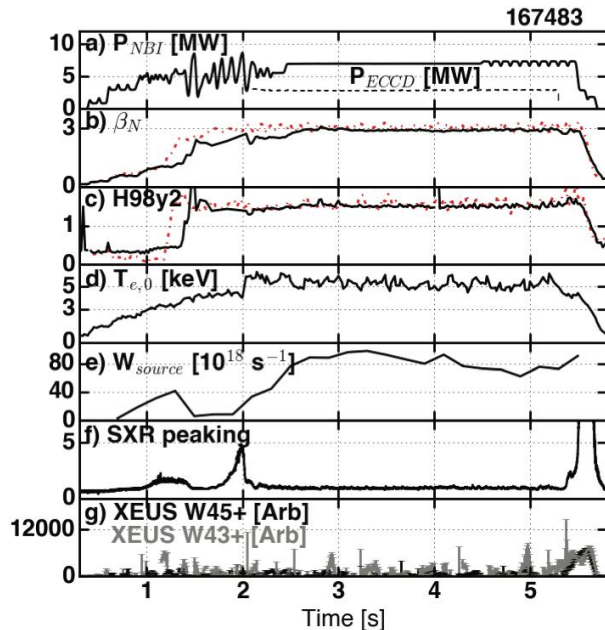


Fig. 4-21. Comparison of discharge with metal rings (black lines) and reference discharge (b and c only) without metal rings (dotted red)

spectroscopic capabilities provided by filterscopes (for diagnosing LBO source at edge), poloidal SXR arrays and CER will be bolstered by the installation of a multi-energy SXR camera, additional SXR arrays and an optional X-ray Imaging Crystal Spectrometer (XICS), during the FY19-24 time frame which will allow for a robust determination of impurity emission and impurity density. The combined trace introduction of impurities with upgraded spectroscopic abilities will allow for accurate determination of impurity transport coefficients over a wide range of plasma conditions with the goal of assessing the local modification of the kinetic profiles and impurity transport coefficients resulting from local heating and current drive. Measured changes in turbulent fluctuations and local gradients will be directly correlated with changes in measured impurity transport coefficients providing a never-before-acquired insight into the origin of the impurity transport changes.

**Goal 2: Validate impurity transport models in the plasma core.** This goal focuses on understanding and interpreting the physical processes that regulate accumulation, and developing a validated model to predict impurity transport in the core. The close interaction of the DIII-D experimental program with plasma theory and computation staff will allow for full exploitation of experimental upgrades (e.g., additional ECH power) and measurements (multi-energy SXR camera, pedestal SXR arrays, divertor SPRED, etc.). Neoclassical, gyrofluid, gyrokinetic, and MHD models all represent strong strengths of the GA theory group and will be used for the interpretation of experimental results [Howard 2014]. Validation of these models will provide a more concrete understanding of the physical origin of impurity transport and will provide a clear path toward the development of optimized reactor scenarios. Ultimately, it should be possible to move beyond a simple control room understanding of impurity control to a physics-based understanding, which will be used to develop and project “recipes” for mitigation of impurity accumulation in reactor-relevant scenarios.

**Challenge 2: Develop Validated Model for Pedestal and SOL Impurity Transport**

**Current progress.** A major DIII-D upgrade in the past 5 years was the installation of a 16 channel edge CER system that provides  $T_i$ , density and rotation  $V_{rot}$  of the main deuterium ions, providing the first measurement of this type anywhere [Haskey 2016]. Comparisons of main ion and C6+ measurements show that pedestal temperature and toroidal rotation of the two species differ and that the steep gradient region of C6+ is shifted slightly

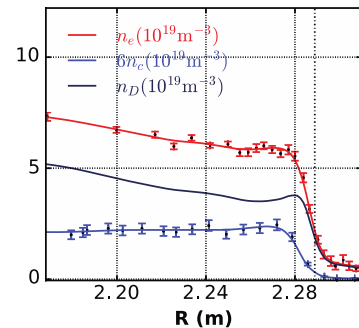
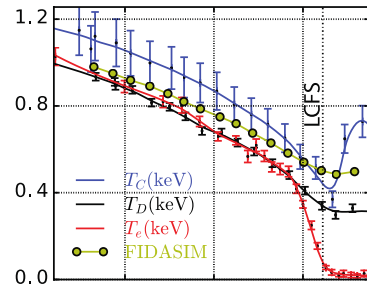


Fig. 4-22. Temperature and density profiles for electrons, D+ and C6+

inwards from that for D+ (Fig. 4-22). These measurements have implications for impurity transport and these results can be partially explained by neoclassical theory. However, a full assessment remains to be done.

In support of efforts to understand how nitrogen seeding has improved the pedestal height in the metal-walled machines JET [Giroud 2016] and AUG [Dunne 2017], DIII-D has performed seeding experiments with nitrogen, neon and lithium. DIII-D, a carbon-walled machine, has not seen the improvements in pedestal height with low-Z impurity seeding that have been observed in metal-walled devices. However, other experiments in DIII-D [Osborne 2015] and NSTX [Kugel 2008, Canik 2011] have achieved increased pedestal heights via the injection of lithium powder. In both cases, the confinement improvement can be attributed to changes in the pedestal pressure profile, leading to improved MHD stability. In NSTX, the improved MHD stability occurred because the pedestal pressure gradient was reduced and shifted inwards with large amounts of lithium. In DIII-D, the data support a model in which the injection of the lithium increases the amplitude of a density fluctuation (called BCM) very near the separatrix, leading to a flattening of the pressure gradient near the separatrix and thus improved MHD stability [Osborne 2015].

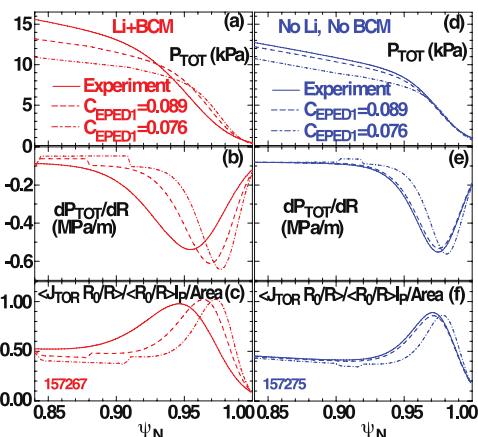


Fig. 4-23. Pressure gradient and bootstrap current move inward with Li and BCM

**Goal 1: Probe the nature of pedestal impurity transport and structure.** The research program for understanding and extrapolating pedestal impurity transport will advance the physics basis by using injected impurities and high-speed, high-resolution impurity and main-ion profile measurements. This research relies strongly on upgrades to provide spatially resolved impurity profiles in the pedestal. In collaboration with research in Section 4.1.2, trace impurities for a range of ion charge Z will be injected (via LBO) and their density will be measured with SXR diagnostics. The magnitude of the impurity particle pinch will be determined for two key parameter variations. First, studies will focus on contrasting conditions with high  $n_{e,Ped}/n_{e,Sep}$  where the neoclassical pinch is expected to be strong vs. conditions possessing a low  $n_{e,Ped}/n_{e,Sep}$  where the pinch is expected to be weaker. Second, the collisionality scaling will be determined. The impurity transport diffusion and pinch velocity will be determined experimentally using STRAHL simulations and compared to theoretical models. Local neoclassical transport will be computed with NEO and the impact of kinetic neoclassical physics will be determined with XGC. Coupled simulations using TGYRO+EPED+STRAHL will be used to explore

optimization schemes for achieving high performance pedestals with the assumption of neoclassical pedestal transport. This approach should provide a useful set of validated tools that can be used for experimental design.

**Goal 2: Determine interplay of neoclassical and turbulent transport for impurities.**

At reactor parameters the ExB shear in the pedestal might be decreased and turbulent transport would therefore become important [Hatch NF 2017]. This turbulent transport is expected to weaken the impurity pinch by producing high levels of impurity diffusion. A critical study of the pedestal turbulence in such regimes as wide pedestal QH-mode and pedestals exhibiting turbulent modes (i.e., Li-enhanced pedestal) will be explored with impurity injections. Both the nature of the pedestal turbulence (wavenumber range, and scaling with dimensionless parameters) measured by DIII-D fluctuation diagnostics, as well as the impact of the turbulence on the impurity transport, will be assessed by using STRAHL coupled with emerging gyrokinetic and gyrofluid models of the steep gradient region. With validated models of the pedestal turbulence, meaningful projections to reactor relevant conditions will be made.

**Challenge 3: Identify Origin of Impurity Wall and Divertor Sources for Reactor-Relevant Materials**

**Current Progress:** During the past five years, DIII-D studied sourcing, transport and accumulation of tungsten in a campaign where two rows of W-coated tiles, each row with a different isotope of W, were installed in the lower divertor. Spectroscopic measurements provided temporally resolved source rates of W from the divertor [Abrams 2017B], as illustrated in Fig. 4-24, providing important results regarding sourcing. In H-mode, large ELMs and disruptions were the main causes of unipolar arcing, and the W sputtering profile was driven by the carbon flux, ELM size and ExB drifts. A collector probe at the outer midplane used isotopic detection to quantify the source locations of W fluxes in the main SOL [Donovan 2017], as shown in Fig. 4-25. Deposition at the collector probe was consistent with simulation projections of an accumulation of tungsten near the upper (non-active) X point. Accumulation of W was observed in the core but high frequency ELMs were effective in flushing W from the core and high-power on-axis ECH prevented W build-up on axis in hybrid scenarios, although more off axis ECH deposition required to form more advanced profiles for the high  $q_{\min}$  scenario were subject to accumulation.

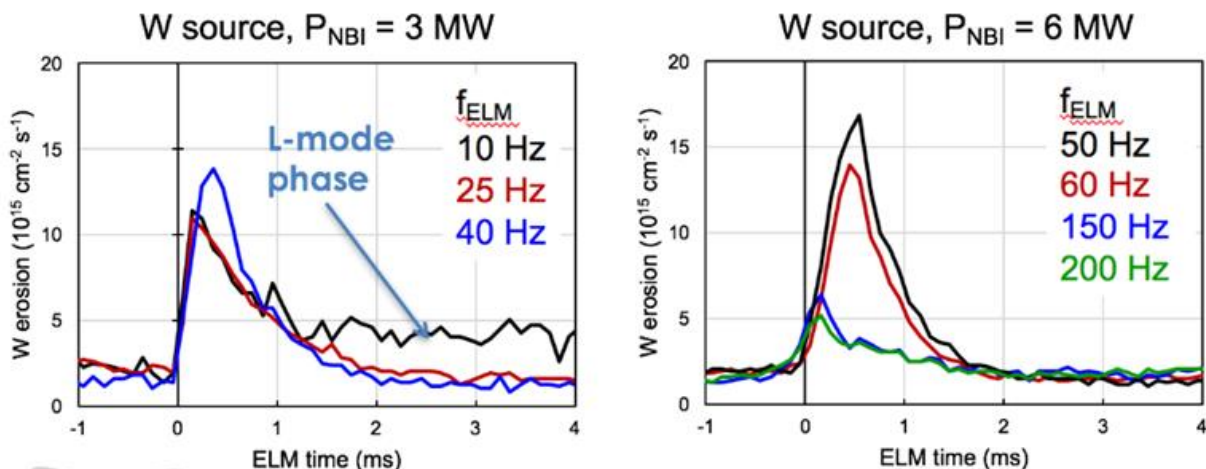


Fig. 4-24. Tungsten erosion rates for (a) 3 MW and (b) 6 MW cases, showing dependence on ELM frequency.

**Goal 1: Develop empirical understanding of spatial origin of impurities.** Important diagnostic upgrades will be made to understand the origin of impurities. These include the addition of extensive divertor measurements (Ti, bolometry, and upgraded IR measurement) as well as measurements such as GPI and CX neutral diagnostics. Emphasis will be on studying the effects of tungsten, which is seen as the leading high Z candidate target material for FNSF. Should SiC components be installed in DIII-D, these will enable studies of silicon as well. Planned core W and Si studies will utilize trace impurity injection via laser blow-off. Key studies will occur in 2020, when two rows of W-coated tiles are installed in the SAS 1 divertor, and in 2022, when 6 rows of W-coated tiles are installed in the SAS 2U divertor. The FY21 addition of the DIII-D Wall Interactions Tile Station will extend analysis of these wall reactor-relevant materials to the edge. Both dedicated and piggyback experiments will be used to understand the physical origins of impurity sources and to monitor overall impurity inventory spanning campaigns. Insights gained from experimental campaigns focused on plasma wall interaction/impurity sources will be used to optimize the reactor-scenarios developed as part of the experiments probing core actuators.

A clear understanding of the relevance of

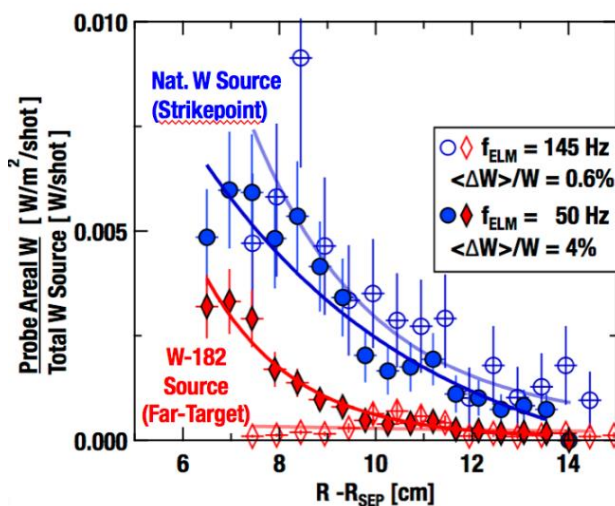


Fig. 4-25. Tungsten density profiles from collector probe, normalized to integrated tungsten source strength, for two different ELM parameters

impurity sources requires good modeling in conjunction with adequate measurements to constrain and validate the appropriate codes. Local erosion and re-deposition will be modeled with the ERO and REDEP/WBC codes. The DiMES system will be used for exposures of candidate materials, and OEDGE/DIVIMP modeling will be constrained by an extensive edge diagnostic set to provide plasma boundary conditions for the erosion modeling. The predicted gross erosion rates will be compared to experimental values, obtained with WI spectroscopy [Abrams 2017].

These measurements will be extended to the main chamber through the development of WITS, capable of exposing samples while simultaneously characterizing the main chamber particle and heat fluxes with the appropriate embedded diagnostics (see Sec 3.3). The migration of impurities through the scrape-off layer will be performed in the experiments with W-coated divertor tiles through a combination of collector probes, isotopically distinct ring materials, and isotopically sensitive ex-situ analysis techniques such as ICP-MS to quantify the time-integrated material transport in the SOL for various conditions.

**Goal 2: Develop predictive model of reactor impurities based on validated impurity source and transport models.** By the final year of the five-year research period, an integrated impurity model will be developed which will leverage the experimental and modeling results obtained in the FY19-FY24 time period. Using the OMFIT framework developed at General Atomics, the leading models will be integrated together to seamlessly pass impurities source rates from wall and divertor interactions to the SOL/pedestal models which can generate influx rates to core neoclassical, gyrofluid, and gyrokinetic models. Composed of validated physical models, this OMFIT integrated model will be used to more reliably assess the compatibility of wall material choices in ITER and future fusion devices and will represent a major advance in our understanding and prediction of impurities expected to be present in reactor conditions.

#### 4.2.1.3 Capability Enhancements

Key hardware upgrades (Table 4-14) that enable this research include increased ECH power to allow probing of electron-heated regimes. The installation of W tiles in two different divertors will enable studies of the physics controlling the source of W impurities and W transport in the SOL as well as the main plasma. The W tile campaigns will also enable tests of control strategies to mitigate impurity accumulation. Additional developments might include siliconization and SiC plasma-facing components in order to further assess impurity dynamics and also provide a low carbon background to further studies. Key diagnostic upgrades (Table 4-15) include the capability to measure spatial profiles of a range of impurities in the core and pedestal and diagnostics to make source measurements, including a system to study main chamber sources

(WITS). Coupling of a number of codes is required for prediction of impurity density sources and profiles (Table 4-16).

**Table 4-14.**  
**Hardware Improvements for Transport Studies**

<b>Hardware Capability</b>	<b>New Physics</b>
ECH upgrades	Ability to probe low-collisionality, electron-heated regimes relevant for reactor-like impurity transport. Also, additional actuator for control of core impurity accumulation.
Wall upgrades	Ability to increase power range on wall, different sputtering yields for given edge plasma parameters. W tiles on SAS 1 and SAS 2U divertors. Novel materials for global migration studies, back effects on main plasma, quantitative changes in main chamber recycling
Wall Interactions Tile Station (WITS)	Ability to study main-chamber contribution to impurity sourcing

**Table 4-15.**  
**Diagnostic Improvements for Transport Studies**

<b>Scientific Objective</b>	<b>Physics Measurement</b>	<b>Diagnostic Technique</b>
Understanding core and edge impurity transport in reactor-like regimes	Spatially and spectrally resolved, soft x-ray line emission from highly ionized charge states. ( $n_z, T_i, V_\phi$ )	X-ray Imaging Crystal Spectroscopy (XICS)
	Filtered SXR emission from core and pedestal regions of the plasma. Determination of edge and core $n_z$ along with impurity asymmetries.	Core and pedestal viewing SXR arrays with Be filters
	Spatially resolved Vacuum Ultra-violet (VUV) emission (for plasma edge) and constraint of edge $n_z$	Spatially resolved XEUS-like spectrometer
Understand effects of edge sourcing of impurities on pedestal	Spatial and partially energy resolved measurement of SXR emission. Determination of core $n_z$ particularly for high-Z materials	Multi-Energy SXR Camera
	Main chamber edge parameters, intensity of wall and divertor sources including due to transients	New spectroscopy, fast TCs, CX neutral diagnostics, Si sourcing and core concentration measurements
Modify main chamber impurity influx	Relative importance of impurity source from main chamber versus divertor for edge/pedestal/core contamination	Siliconization, Toroidal limiters (optional)
Understand radiation balance in divertor, local effect and time behavior of impurities.	Spatially localized VUV emission from divertor region to quantify time behavior of main divertor radiating species	Divertor SPRED

**Table 4-16.**  
**Simulation Codes Used**

<b>Code</b>	<b>Purpose</b>
Integrated version of TGYRO + EPED + STRAHL + UEDGE into whole device OMFIT Modeling	The coupling of edge (UEDGE) and core (STRAHL) impurity transport codes with plasma models provided by TGYRO and EPED will allow for prediction of impurity profiles and thus the prediction of radiated power, etc. in a whole device model.
ERO/DIVIMP/WALLDYN/GITR	Development of a model interface to span the present gap between PMI codes and boundary plasma codes, with the eventual goal of constraining wall impurity source values, and eventually plasma back reactions, in an eventual whole device model.

#### 4.2.2 Plasma Shape and Boundary Configuration

*Physics Leads: A. Jarvinen (LLNL), B. Grierson (PPPL), T. Petrie (GA), A. Leonard (GA), A. Moser (GA), M. Shafer (ORNL), A. Bortolon (PPPL)*

Tokamak reactor design activities have to address various trade-offs when deciding on the plasma configuration [Wenninger 2017, Kim 2015, Wan 2017, Najmabadi 2006, Chan 2010, Kessel 2015]. Reactor design must account for plasma current drive, transport, stability, boundary physics, and technological areas as an integrated whole [Luce 2011]. The decision on plasma shape is made very early in the design process and has a direct impact on most of these areas. Furthermore, the tension between core performance, current drive, and dissipative divertor conditions requires advanced boundary plasma solutions, which also need to be compatible with the plasma shape and scenario. However, since the physics processes involved in each of the requirements depend either explicitly or implicitly on the plasma shape and configuration, an optimal shape for one of the areas may be far from optimal or may even rule out reactor relevant operation for another area. Therefore, experimental research on a core-edge integrated approach is required to address the impact of plasma shape on the integrated performance of the system and to identify the configurations that meet all of the competing requirements in a fusion reactor.

With flexibility for making a wide range of plasma shapes and several different configurations, DIII-D is ideally suited to study many of these integration issues and has been performing relevant research for a long time. In the past five years, experiments have been performed on DIII-D to study pedestal performance in very nearly DND configurations. Very good performance is achieved in these, as expected from the EPED model. Experiments with high internal inductance discharges in DND shape have been used to obtain very high values of  $\beta_N$ . A “wide-pedestal” QH-mode regime, which operates reliably at very low torque, was discovered in DIII-D in a very nearly DND shape. In stark contrast to these benefits of high positive triangularity, an L-mode discharge with very good core confinement has been

demonstrated at negative triangularity. Experiments have been conducted at moderate triangularity to study the affect of closure on detachment. In addition, a new divertor called SAS (Small Angle Slot) was designed and installed in DIII-D. Nevertheless, the challenge remains to understand the full optimization of plasma shape.

#### **4.2.2.1 Challenges and Impact**

The goal of the DIII-D research program on configuration is to develop a systematic scientific database and model validation to address and understand the trade-off questions related to plasma shape and divertor configuration when extrapolating plasma operation to reactor scale. This section has connection with some other sections of the 5-year plan, and the research described here will be conducted in close collaboration with the other research areas. To accomplish this goal, the research on configuration will address following three key challenges (as listed in Table 4-17):

1. The first challenge is to determine the trade-offs between SND and DND operation for integrated plasma performance. In high performance plasma scenarios, the planned research will compare the effects of DND and highly elongated SND configurations on operational limits, especially the  $\beta_N$ -limit, assessing their impact on stability, configuration controllability, and disruption severity as well as the value of DND relative to SND on boundary power and particle exhaust capability.
2. The second challenge is to determine the optimal elongation, triangularity and squareness for integrated plasma performance with tolerable boundary loads. The planned research will study the impact of shaping on divertor heat flux control, particularly the role of triangularity. It will also assess the impact of shape on ELM control as well as the impact of a metal divertor (W). This research plan will be carried out in various DIII-D scenarios with an emphasis on high performance regimes.
3. The third challenge is to determine the optimal baffling and divertor flux expansion strategies for power and particle exhaust, and for recycling control. The effect of tungsten vs carbon divertor on heat flux control will also be studied. For this challenge, the impact and interplay of divertor baffling, closure and flux expansion will be studied in high performance plasmas.

The plasma shape and configuration affect many design choices of a tokamak reactor. These requirements include the choice of one divertor vs two, the optimal elongation, triangularity and squareness, the control stability requirements, how to optimize divertor baffling and divertor flux expansion, and the limits of integrated predictive capability to describe the interaction between the core, pedestal, and boundary. The goal of this research is to provide recommendations for

these design choices related to choice of plasma shape and divertor configuration in a reactor as well as to develop numerical and analytical predictive capability to provide confidence for the extrapolations to next step devices.

**Table 4-17.**  
**Shape and Boundary Configuration Challenges and Goals**

Challenge	Goals/Deliverables	Key Capability Improvements
<p>1. <i>Predict the trade-offs between SND and DND operation for integrated plasma performance</i></p>	<ul style="list-style-type: none"> <li>• Use lower SND and upper SND variations to understand how <math>\beta_N</math> optimizes with divertor configuration</li> <li>• Vary divertor configuration to optimize operational limits</li> <li>• Use LSN and USN variations to manipulate power and particle exhaust performance</li> </ul>	<p><b>Hardware Upgrades</b></p> <ul style="list-style-type: none"> <li>• Heating and current drive: NBI power to 23 MW, Increased off-axis NBI power, Increased balanced torque NBI power, Increased EC power, Helicon current drive, LH-current drive</li> <li>• Advanced shape control with the new 2D/3D power supply, including VFI-less operation</li> <li>• Advanced divertor control with the new 2D/3D power supply</li> <li>• Divertor upgrades: SAS 2U/L, power limits, pumping, baffled DND</li> <li>• Gas injection: more toroidal and poloidal gas valve locations</li> </ul>
<p>2. <i>Predict the optimal elongation, triangularity, and squareness for integrated plasma performance</i></p>	<ul style="list-style-type: none"> <li>• Test confinement models by varying shape in various scenarios and measuring plasma performance</li> <li>• Develop models to understand shape dependence of ELM mitigation strategies</li> </ul>	<p><b>Diagnostic Upgrades</b></p> <ul style="list-style-type: none"> <li>• Pedestal ionization source</li> <li>• Pedestal current density</li> <li>• Tangential midplane Thomson</li> <li>• Pedestal/SOL DBS</li> <li>• Fast IR</li> <li>• Fast camera upgrades</li> <li>• ASDEX gauges</li> <li>• Fast thermocouples</li> <li>• IR and visible imaging in upper divertor</li> </ul>
<p>3. <i>Predict the optimal baffling and divertor flux expansion strategies for power and particle exhaust and recycling control in high performance plasmas</i></p>	<ul style="list-style-type: none"> <li>• Determine trade-offs between divertor closure (baffling) and flux expansion strategies for integrated plasma performance</li> <li>• Develop predictive capability for extrapolating to reactor scale</li> </ul>	<ul style="list-style-type: none"> <li>• Langmuir Probes (SAS 2)</li> <li>• Wall Langmuir Probes</li> <li>• Divertor bolometer arrays</li> <li>• Divertor SPRED (VUV spectroscopy)</li> <li>• Main ion temperature in the pedestal, SOL, and divertor</li> </ul> <p><b>Code Development</b></p> <p>Comprehensive core-edge modeling capability including codes relevant from core transport to SOL physics:</p> <ul style="list-style-type: none"> <li>• CESOL, JINTRAC, SOLPS, UEDGE, OEDGE, STRAHL, CGYRO, TGLF, BOUT++, ELITE, EPED, NEO, TRIP3D, M3D-C1</li> </ul> <p>Development of reduced models and neural network approaches for faster physics analysis throughput.</p>

### 4.2.2.2 Research Plan

The research plan for configuration studies is organized according to the challenges and goals in Table 4-17. The timeline for each challenge, associated research tasks and the facility improvements necessary to achieve them are set out in Fig. 4-26. Of note, the additional power supply will enable fully independent control of all PF coils, enabling fully control of divertor and highly shaped core configurations to facilitate these studies.

Challenge	FY19-20	FY21	FY22	FY23	FY24
<b>1. Predict the trade-offs between SND and DND operation for integrated plasma performance</b>	Experiments documenting SND and DND operation for stability limits, controllability, core and pedestal performance, and power exhaust and pumping capability Validation and further development of physics understanding for predictive capability towards next step devices Systematic further experimental and theoretical assessment of various ‘go-nogo’ features of SND and DND configurations Extrapolation to reactor scale with recommendations of SND vs. DND				
<b>2. Predict the optimal elongation, triangularity, and squareness for integrated plasma performance</b>	Experiments documenting impact of elongation, triangularity, and squareness, for stability limits, controllability, core and pedestal performance, and power exhaust and pumping Assess the optimal plasma shape for DIII-D Document the impact of ELM control requirements on the pedestal and core performance in various configurations Extrapolate to reactor scale				
<b>3. Predict the optimal baffling and divertor flux expansion strategies for power and particle exhaust and recycling control in high performance plasmas</b>	Impact of baffling and flux expansion on the divertor heat flux challenge Assess the role of divertor volume / leg length on divertor performance Assess the trade-off between shaping (triangularity) and divertor heat flux Extrapolate to reactors Impact of baffling and flux expansion on recycling control and pumping Assess the pumping requirements for various DIII-D plasma scenarios Assess the up/down closure needs for DND plasmas Extrapolate to reactors				
<b>4. Diagnostic Enhancements</b>	Improved neutral diagnostics Edge current density / imaging MSE High resolution divertor bolometry Divertor neutral pressure measurements (ASDEX Gauge) Increased IRTV coverage for wall heat fluxes Upgraded 2D Divertor Imaging Improved fluctuation diagnostics Gas puff imaging Divertor T <sub>i</sub> measurement				
<b>5. Hardware Upgrades</b>	NB 19 MW 2 <sup>nd</sup> Off-Axis NBI Additional EC power New upper divertor (SAS 2), power limit/pumping 2D/3D supply #2 B-coil Switch, Helicon/LH Upgraded gas injection capability NB 20 MW 3D coils upgrade VFI-less Inside wall LH/Helicon NB 23 MW New lower divertor				
<b>6. Simulation tools</b>	Integrated whole plasma modeling with integrated codes CESOL and JINTRAC Development of reduced models and neural networks for faster modeling throughput Comprehensive core-edge modeling capability including several codes relevant from core transport to SOL physics				

Fig. 4-26. Timeline for the Shape and Boundary Configuration studies

## Challenge 1: Predict the Trade-Offs Between SND and DND Operation for Integrated Plasma Performance

**Current progress.** In the past five years, several experiments have studied performance in DND discharges in DIII-D. Research in both the Super-H regime [Solomon 2014, Snyder 2015] and in high power hybrid discharges [Petrie 2017] has provided more evidence that operation at high triangularity and near a double null divertor (DND) configuration is an excellent technique for optimizing the pedestal height and the plasma performance. The work in the Super-H regime was motivated by predictions of the EPED model [Snyder 2011] and the positive results show that theory provides good guidance for optimizing the pedestal height. Modeling of the high power hybrid discharges shows that operation near DND is helpful in eliminating the pedestal MHD ballooning limit, enabling improved pedestal performance. Experiments with high internal inductance discharges have obtained  $\beta_N \sim 5$  in a DND shape [Ferron 2015]. These experiments were consistent with earlier results showing that the maximum achievable  $\beta_N$  increased with shaping as shown in Fig. 4-27 [Ferron 2005]. A “wide-pedestal” QH-mode regime, which operates reliably at very low torque, was discovered in DIII-D in a very nearly DND shape [Burrell 2016, Chen 2017]; subsequently, the regime has been extended to a moderate range of lower and upper SND shapes. These results support the DND shape as good for plasma performance. A number of other issues related to the choice of SND vs DND are also important, but not as well studied. These include the vertical stability of highly shaped plasmas as well as the compatibility of the plasma shape with a divertor geometry that provides acceptable heat and power handling. Important research results for the latter point are illustrated in Fig. 4-28, which shows that the power and heat flux sharing between upper and lower divertors can be adjusted by varying the discharge shape from lower SND to DND to upper SND [Fenstermacher 2000].

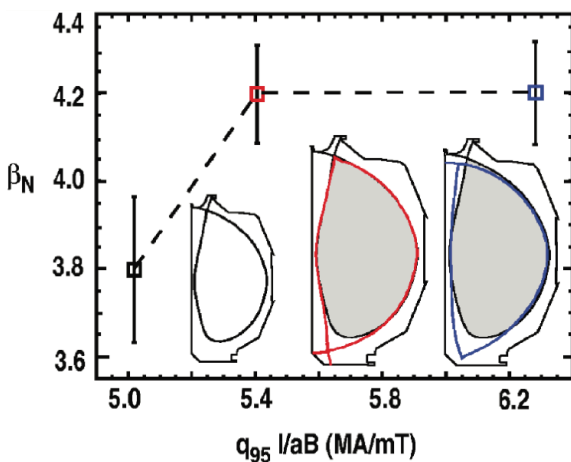


Fig. 4-27. Maximum achieved  $\beta_N$  increases with shaping.

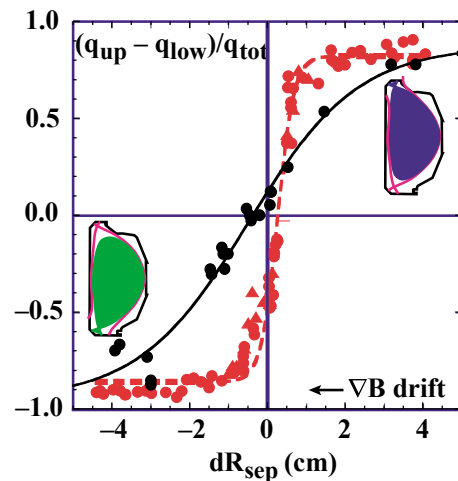


Fig. 4-28. Heat (red) and particle (black) flux sharing as magnetic balance is varied

**Goal 1: Use lower SND and upper SND variations to understand how  $\beta_N$  optimizes with shape.** As already discussed, previous experiments at DIII-D have shown that plasmas operating at balanced DND obtain higher  $\beta_N$  than those operating in SND. However, the relative impact of DND vs SND configurations on plasma performance is expected to depend on the plasma scenario. Therefore, experiments will be performed to investigate the relation between divertor configuration, plasma configuration and the maximum  $\beta_N$ . This research will be conducted in collaboration with the research performed in Section 2.1.2 “Fully Non inductive Scenarios for Steady State Fusion”. For these experiments, the scenarios are grouped into high and low  $q_{\min}$  branches and each branch is further divided into two separate scenarios: “high  $q_{\min}$ ” vs. “high  $\beta_p$ ” and “steady-state hybrid” vs. “high  $\ell_i$ ”. For each configuration and each scenario, experiments will be performed to measure the operational limits in  $\beta_N$ ,  $n/n_{GW}$  and  $I_p$  for SND and DND discharges. Experiments will probe stability and pedestal behavior to compare with simulation and help develop validated models. These studies will benefit strongly from facility upgrades to provide increased heating capability to explore higher power density conditions, balanced NBI injection at higher heating power for low net NBI torque conditions, off-axis NBI for broader plasma heating and current drive profiles as well as EC heating for dominant electron heating conditions.

**Goal 2: Vary divertor configuration to optimize operational limits.** The configuration variations discussed in goal 1 will also be extended to address a second issue of magnetic controllability: vertical stability and disruption severity. This issue must be resolved prior to ITER high power operation. Studies will explore limits in this regard and resilience of the plasma to perturbations. This research will be conducted in close collaboration with the research described in Section 2.2.3, including comparison to relevant control physics models, and their improvement.

**Goal 3: Use lower SND to upper SND variations to manipulate power and particle exhaust performance.** Further to the above work, such scans will also be used to evaluate the additional value of a DND relative to a SND for boundary power and particle exhaust capability. As shown in Fig. 4-27. Maximum achieved  $\beta_N$  increases with shaping. , varying  $dR_{\text{sep}}$ , the separation of the primary and secondary separatrices at the outer mid-plane, can vary the ratio of particle and heat fluxes to the lower and upper divertors. Experiments will be performed in which  $dR_{\text{sep}}$  is varied to adjust the magnetic configuration from upper SND to DND to lower SND and the power and particle fluxes to each divertor will be measured. These will be used to test models for the power split. Important parameters in the model will include ballooning cross-field transport, flux surface compression and geometric properties of tokamak plasmas. This

research will be performed in close connection with the research conducted within Section 3.1.2 on “Magnetic configuration”.

## Challenge 2: Predict the Optimal Elongation, Triangularity, and Squareness for Integrated Plasma Performance

**Current Progress:** Several experiments have shown that increasing triangularity and reducing squareness increases pedestal and core performance [Osborne 2000, Saibene 2002, Kallenbach 2002, Holcomb 2009]. Recently, a high performance, high density H-mode regime, called Super H-mode, has been theoretically predicted and experimentally demonstrated in highly shaped plasmas in DIII-D [Solomon 2014, Snyder 2015]. This regime operates at the kink-peeling boundary of the peeling ballooning diagram, as shown in Fig. 4-29.

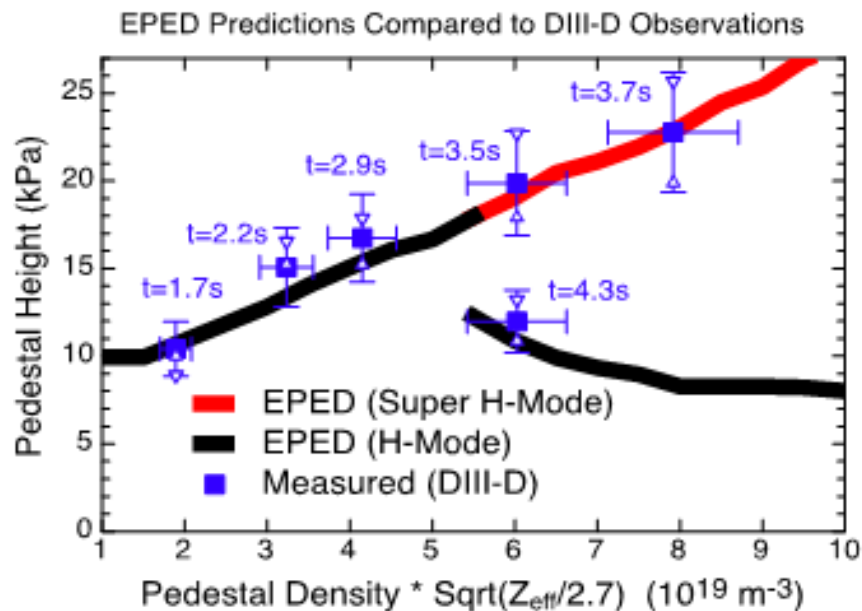


Fig. 4-29. Experiment (Blue squares) reaches Super-H boundary (red line) predicted by EPED model.

DIII-D experiments have also shown that RMP ELM suppression has dependencies on shape. For instance, joint experiments between DIII-D and ASDEX-U have shown that the threshold for RMP ELM suppression was reduced as triangularity was increased with other parameters constant. In DIII-D, RMP ELM suppression has been obtained so far only in SND configurations; several experiments have attempted to obtain suppression in a DND configuration but have failed to do so. Other experiments have shown rather subtle shape effects with a difference in threshold observed between the ISS (ITER similar shape) and IBS (ITER baseline shape) shapes in DIII-D, which are not very different from one another. Recent studies on negative triangularity operation have shown promising results of the impact of negative

triangularity on core and pedestal transport, stability, and ELM scaling [Medvedev 2015, Pochelon 2012]. Negative triangularity discharges have also been obtained in DIII-D L-mode discharges and these have exhibited very good confinement [Austin 2017]. This scenario provides valuable tests of underlying physics, and negative triangularity discharges will be studied if H-mode can be obtained in this shape.

**Goal 1: Test confinement models by varying shape in various scenarios and measuring plasma performance.**

To address this goal, experiments will be performed to fill gaps in systematic datasets towards understanding the impact of plasma shape parameters squareness, triangularity, elongation on density and temperature as well as on  $\beta_N$  and operational limits in  $n/n_G$  and  $I_p$ . This work will be performed in several DIII-D scenarios including AT, Super H-mode and QH-mode. A subset of these experiments will also be performed during campaigns in which tungsten tiles are installed in DIII-D divertors; the impact of a metal divertor on confinement in high performance scenarios will be measured and compared to results with a carbon divertor. Results from these experiments will be used to test integrated models of core and pedestal performance to determine if they have predictive power for the effect of shape on plasma confinement in these scenarios. In connection with these studies, the impact of triangularity on the divertor heat flux challenge will also be documented and understood. The optimal triangularity for plasma performance is a critical question that must be addressed very early in the five-year plan since this impacts directly the radial location and baffling decisions of the upgraded divertor structures, SAS 2U and SAS 2L. If tight fitting baffling structures are installed, flexibility in plasma triangularity might require additional modifications. Numerical simulations will be conducted for physics interpretation with several codes, such as EPED, ELITE, CGYRO, NEO, TGLF, BOUT++, GENE, M3D-C1, as well as SOL codes UEDGE, SOLPS, and OEDGE to study the interaction of SOL boundary conditions on pedestal and core performance. Integrated modeling with integrated code packages such as CESOL will be conducted for selected cases.

**Goal 2: Develop models to understand shape dependence of ELM mitigation strategies.**

The application and impact of ELM control strategies (discussed in 4.1.1) on the optimal plasma shape decision will be investigated to guide the trade-offs between optimized pedestal and core performance and acceptable ELM properties. ELM control methods that will be studied include RMP ELM control, QH-mode and pacing of ELMs via deuterium pellets or impurity granules. These experiments will determine whether a given ELM control technique works for a specific shape and scenario, the reduction of ELM heat flux to the divertor that can be achieved and the effect on the plasma confinement. Appropriate models will be tested with the goal of

attempting to predict whether a technique will produce ELM mitigation, thereby also testing underlying physical mechanisms. This model development will be performed with codes such as EPED, ELITE, M3D-C1 and NIMROD.

### Challenge 3: Predict the Optimal Baffling and Divertor Flux Expansion Strategies for Power and Particle Exhaust and Recycling Control in High-Performance Plasmas

The boundary plasma solution needs to be able to simultaneously exhaust the power flowing towards the wall without exceeding the engineering temperature and erosion limits of the wall materials as well as control plasma density and helium exhaust through pumping. Divertor strategies that can be used to optimize particle and heat control include magnetic balance of a DND configuration, poloidal flux expansion of divertor legs and baffling in the divertor. New divertor topologies, such as snowflake and X-divertor [Kotschenreuther 2013, Soukhanovskii 2012], have been proposed to provide heat flux reduction through flux expansion. The snowflake configuration has been achieved in TCV, NSTX and DIII-D and DIII-D has performed initial investigations with long outer divertor legs. An initial comparison has been performed in DIII-D of the performance of three very different divertor geometries: magnetically unbalanced double-null divertor plasmas, double-null “snowflake” plasmas, and single-null H-mode plasmas with a long outer divertor leg, as shown in Fig. 4-30 [Petrie 2015].

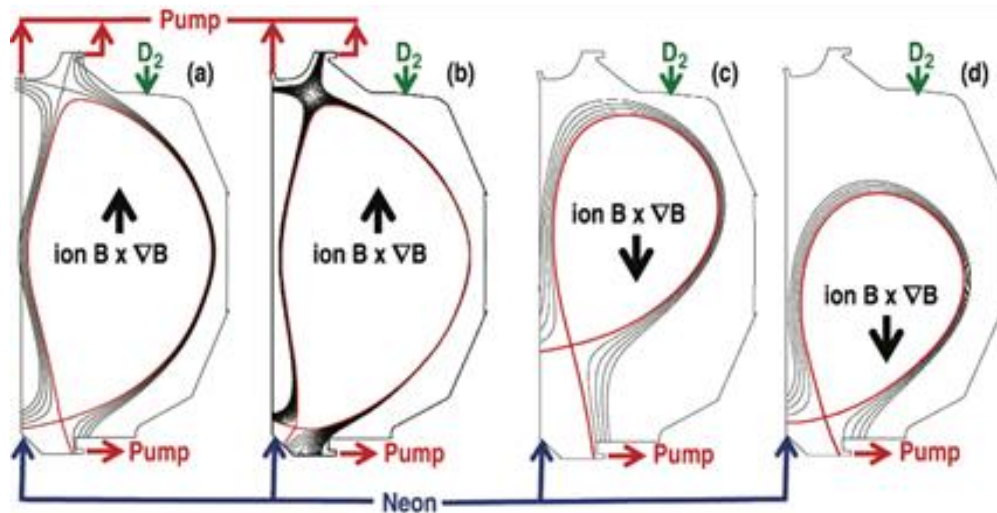


Fig. 4-30. Configurations studied in comparison of divertor geometries for heat flux control.

These studies showed that all 3 concepts achieved divertor heat flux reduction and maintained good H-mode confinement. The rather different upper and lower divertor structures in DIII-D have also been exploited to vary divertor closure, and experiments show that detachment is generally obtained with increased closure. SOLPS modeling has also been used to develop a concept for a type of slot divertor called SAS (Small Angle Slot) [Sang 2017, Guo

2017]. A test version of the SAS divertor with relatively low power handling capability has been installed in DIII-D for the FY16 run campaign. Initial tests have verified some important modeling predictions, and several SAS upgrades are proposed for the 5-year plan. The planned SAS-2 upper and lower divertors, compatible with high power fluxes, will enable much of the research proposed here.

**Goal 1: Determine trade-offs between divertor closure (baffling) and flux expansion strategies for integrated plasma performance.** This research begins by systematically addressing the impact of shaping decisions on divertor heat flux by investigating the impact of plasma triangularity, divertor volume, and magnetic balance on the heat dissipation physics, tightly connected to research in Section 3.1. Furthermore, the role of baffling will be studied by comparing the more closed upper divertor (pre-SAS 2) with the open lower divertor. These studies will also aim to address the pumping capability and needs for various DIII-D scenarios to provide reference to understand the impact of upgraded divertors on the pumping and density control capability of DIII-D. These will be followed with studies integrating magnetic flux expansion methods into the lower divertor plasmas, and utilizing the advanced plasma shaping capabilities provided by the new power supplies installed in the end of FY20, also connected to research in Section 3.2. The upper divertor plasmas will continue the investigations of baffling structures after the installation of the new SAS 2U, which will be pumped and capable for high heat flux operation. Following these studies, the pumping requirements for the lower divertor needed for various scenarios will be determined to provide information for baffling requirements and design of a new lower divertor for DIII-D, which is planned for installation in FY23. Experiments will also be performed during campaigns in which tungsten tiles are installed in the SAS 1 and SAS 2U divertors to determine how a metal divertor affects heat flux control in discharges which have previously demonstrated good heat flux control in a carbon divertor.

**Goal 2: Develop predictive capability for extrapolating to reactor scale.** Validation and development of predictive tools will be conducted throughout the five-year plan. Simulations with the 2D SOL fluid codes, such as SOLPS and UEDGE, will be conducted and compared to experimental measurements to validate the models as well as to predict the impact of these magnetic flux expansion strategies on the divertor heat and pump fluxes and on the pedestal ionization sources. Towards the end of the five-year plan, the focus will shift to building extrapolations towards reactor-scale plasmas, including poloidal flux expansion methods, pumping requirements, optimized baffling, optimal magnetic balance, and divertor volume extrapolations.

### 4.2.2.3 Capability Enhancements

The research described in this section will benefit from many hardware upgrades, as listed in Table 4-18. One of the primary upgrades for the configuration studies is the addition of power supplies (FY20 – FY21) that enable improved control of pertinent magnetic configurations. Divertor upgrades will provide access to enhanced main plasma density and divertor detachment control. Additional gas valves will enable more innovative gas injection strategies for simultaneous core density, divertor detachment, and radiative divertor control. Improved heating and current drive capabilities will enable higher power density control, pushing the SOL plasma closer to reactor-relevant power density values, as well as improved capability for development of advanced, high powered, non-inductive core scenarios.

**Table 4-18.  
Hardware Improvements for Shape and Boundary Configuration Studies**

<b>Hardware Capability</b>	<b>New Physics</b>
Heating and current drive	Extend plasma and divertor scenarios towards higher power density and push the limits of non-inductive scenarios
Advanced shape control by additional power supplies	Extend the controllability vs. shape studies towards more challenging scenarios, including controlled scans of dRsep.
Advanced divertor control by additional power supplies	Explore advanced divertor configurations (poloidal flux expansion) with advanced core scenarios
SAS 2 (power/pumped)	Closed divertor with pumping for higher power plasma. Dissipation at lower core density.
Gas injection: more toroidal and poloidal gas valve locations	Control fuel and impurity particle sources and flows.

The research plan will benefit from several planned diagnostic upgrades (listed in Table 4-19). Improved coverage of ASDEX pressure gauges together with improved neutral ionization measurements in the pedestal will enable determination of the effectiveness of divertor baffling in compressing recycling neutrals and reducing pedestal ionization sources. Improved VUV capabilities enable species resolved radiated power measurements. Particle flux measurements to the main chamber wall will enable studies of main chamber recycling. Improved fluctuation and transport measurement and pedestal current density measurements will enable improved testing of core and pedestal transport models. Divertor detachment diagnostics enable unambiguous characterization of divertor conditions and their connection to the main plasma performance in various configurations.

**Table 4-19.  
Diagnostic Improvements for Shape and Boundary Configuration Studies**

<b>Scientific Objective</b>	<b>Physics Measurement</b>	<b>Diagnostic Technique</b>
Neutral pressures in the divertor, pump fluxes, neutral compression	Neutral pressure	ASDEX Gauges
Species resolved divertor radiation	VUV spectroscopy	Divertor SPRED
Pedestal impurity screening with radiative divertor	VUV/VIS spectroscopy, radiated power	Divertor SPRED, MDS, additional spectroscopy, Upgraded bolometer
Divertor detachment and connection to core and pedestal performance	Divertor density, temperature, heat flux, radiated power	Upper DTS, 2D DTS, IR/VIS in Upper Divertor, Upper Bolometer, Divertor Ti, Fast Thermocouples
Neutral ionization distribution at the edge	Neutral density	Ly-alpha arrays, Ly-alpha divertor camera, pressure gauges, wall probes
Improved magnetic equilibria	Te and ne at outer midplane	Tangential TS

Simulations with various tools, listed in Table 4-20, will be performed throughout this five-year plan. The primary goal of these simulation efforts is to (1) enable detailed physics interpretation of the observed experimental phenomena as well as to (2) develop and validate the simulation tools for predictions for next step devices. A very important aspect of this work is the use of integrated simulations of the core, edge and boundary with the CESOL package including FASTRAN core (TGLF+EPED) and C2/GTNEUT SOL solver.

**Table 4-20.  
Simulation Codes Used for Shape and Boundary Configuration Studies**

<b>Code</b>	<b>Purpose</b>
CESOL	Core (1.5D FASTRAN) – Edge (EPED) – SOL (SOLPS) coupling
OMFIT	Integrated modeling and experimental data analysis
OEDGE	Interpretive divertor/SOL modeling, ionization source
SOLPS	Divertor/SOL fluid transport, ionization source
UEDGE	Divertor/SOL fluid transport, ionization source
EPED	Reduced pedestal model
CGYRO	Pedestal transport modeling
TGLF	Pedestal transport modeling
ELITE	Peeling-ballooning stability
NEO	Neoclassical transport

### 4.2.3 Integrated Power and Particle Control

*Physics Leads: B. Grierson (PPPL), A. Jarvinen (LLNL), T. Petrie (GA), N. Howard (MIT), S. Mordjick (W&M).*

A fusion reactor must maintain a high performance plasma core while simultaneously having sufficient exhaust of helium and tolerable levels of heat and particle fluxes to the divertor [Kukushkin 2013]. This is an important challenge because it is not guaranteed that these conditions can be simultaneously achieved. Means of reducing the heat flux, such as impurity seeding and radiative mantle are needed, but these could lead to unacceptable levels of dilution of the main plasma fuel if not well implemented, as well as radiation that may trigger an H-L back transition [Kallenbach 2013] or degrade pedestal performance. Main-plasma fueling and exhaust of impurities, both helium ash [Wade 1995] and seeded impurities, must be kept high when operating with a detached divertor. This is truly a global challenge as seeded impurities in the divertor can migrate to the magnetic axis, and helium ash that is produced at the axis must be exhausted through a detached divertor. A validated predictive capability is necessary to design the future fusion reactors and scenarios to satisfy these requirements.

The DIII-D team has made strong progress in addressing several of these physics issues during the past five years. Divertor detachment has been obtained and studied in several divertor geometries, including lower single null (LSN), upper single null (USN) and in a range of divertor closures. A new small angle slot closed divertor is found to be compatible with low upstream density and good pedestal performance. Radiative divertor operation has been extended to high core performance and fully non-inductive regimes, with favorable pedestal performance found in some cases. Acceptable low-Z impurity exhaust has been measured in some ELM-controlled regimes such as RMP and QH-mode, with good flushing of impurities. The exhaust of helium, seeded at the plasma edge, has been measured and found to be enhanced by the application of RMP fields. Compatibility of advanced core plasma configurations with tungsten divertor tiles has also been found, with techniques to control core impurity accumulation demonstrated. These are positive results but much work remains to obtain the scientific understanding for acceptable integration of core and boundary plasmas in a fusion reactor.

#### 4.2.3.1 Challenges and Impact

The goal of this research area is to understand the use of radiators to dissipate heat, the transport of particles, and the interactions of divertor geometry, detachment, pedestal and core to establish the physics basis for the design of an integrated core-edge solution from a particle dynamic perspective. To accomplish this, the research plan is focused on the four key challenges listed in Table 4-21. Challenge 1 focuses on understanding how impurity species influence

pedestal and core performance to provide strong dissipation of heat while good core performance is maintained. For this purpose, research will use DIII-D’s flexibility to test how the interplay between core performance and a radiative divertor is affected by plasma and divertor geometry. Experiments will make use of both single (SND) and double null (DND) divertor shapes and variations in magnetic balance as well as the various degrees of divertor closure that can be obtained in a variety of DIII-D divertor geometries, including the SAS-2 upgrade which will provide a slot divertor capable of accepting high heat fluxes. The research will test a range of radiators (such as nitrogen, neon and argon) introduced through different impurity injection geometries, including injection into the main chamber, divertor and private flux regions. Compatibility and differences with Tungsten divertor tiles will be assessed. Research will target high performance fully non-inductive scenarios such as the hybrid and high  $q_{min}$  regimes (2.1.2). Studies will explore both low collisionality cores, using electron cyclotron current drive and off axis neutral beams, and high density, exploiting new helicon and high field side lower hybrid current drive tools, as well as advanced pedestal techniques such as super-H mode.

**Table 4-21.**  
**Integrated Power and Particle Control Challenges**

<b>Challenge</b>	<b>Goals/Approaches</b>	<b>Key Capability Improvements</b>
Understand how impurity species influence pedestal and core performance to provide strong dissipation of heat and maximize core performance.	<ul style="list-style-type: none"> <li>• Develop heat flux control with high performance core</li> <li>• Test role of divertor closure for heat flux control</li> </ul>	<p><i>Hardware Upgrades</i></p> <ul style="list-style-type: none"> <li>• Increased power for electron heating (ECH) and current-drive (ECCD)</li> <li>• Steerable NBI for steady-state scenario and rotation control</li> <li>• Laser blow-off impurity injection</li> <li>• Flexible gas injection</li> <li>• Argon frosting of cyro pumps</li> <li>• Helium neutral beam injection</li> <li>• New SAS divertors &amp; temporary tungsten tile arrays in them.</li> </ul>
Test and develop projectable model for helium exhaust with a detached divertor	<ul style="list-style-type: none"> <li>• Develop model of global helium confinement in detached conditions</li> </ul>	<ul style="list-style-type: none"> <li>• Siliconization</li> <li>• Helicon and HFS LHCD</li> </ul> <p><i>Diagnostic Upgrades</i></p> <ul style="list-style-type: none"> <li>• Divertor impurity spectroscopy</li> <li>• Divertor pressure gauges</li> <li>• Penning gauges</li> <li>• Core impurity spectroscopy</li> <li>• SOL flows</li> </ul>
Establish the compatibility of ELM mitigation techniques with exhaust of gaseous impurities (radiators, helium)	<ul style="list-style-type: none"> <li>• Develop models of impurity transport in various ELM-mitigated regimes</li> </ul>	<p><i>Code Development</i></p> <p>TGYRO, STRAHL, SOLPS UEDGE, TRANSP</p> <p>Core-edge-SOL modeling capability with first-principles-based models and reduced models will be performed through OMFIT.</p>
Identify and understand density limit, MARFEs, and operation close to the H-L back transition threshold.	<ul style="list-style-type: none"> <li>• Develop feedback control to enable detached divertor near H-L threshold</li> </ul>	

The second challenge focuses on testing and developing a projectable model for helium exhaust with a detached divertor. This research will use DIII-D’s capabilities to frost cryo-pumps with argon in order to pump helium, to mimic helium ash through the use of helium neutral beams, and to puff helium gas from the plasma edge. The exhaust of helium injected from the core and from the edge will be measured in both attached and detached conditions in open and closed divertor configurations available in DIII-D. The third challenge will be to establish the compatibility of ELM mitigation techniques with the exhaust of impurities; both radiators and helium. These studies will use DIII-D’s capabilities to inject core helium, edge gaseous impurities and a wide range of high-Z impurities, including tungsten, with laser blow-off. The research will also use DIII-D’s capabilities to mitigate or eliminate ELM’s via RMP fields, the QH-regime or ELM pacing with pellets or impurity granules. The fourth challenge is to identify and understand the density limit, MARFEs, and operation close to the H-L back transition threshold. The research for this challenge will make use of DIII-D’s capability to perform real time feedback in order to control radiation from seeded impurities, its range of divertor closures available with different divertor geometries and an upgraded diagnostic suite to make temporally and spatially resolved measurements of impurity radiators.

This research will provide the physics basis to confidently extrapolate the expected impurity exhaust for core, pedestal and SOL transport processes to future machines. This knowledge will inform the strategy for choice and location of seeded impurity for power control, magnetic balance, and pumping efficiency with divertor closure in future machines. The research will answer the key question of whether a double-null configuration can be used for the dual purpose of heat flux and particle control, with one divertor focused on pumping and one on peak heat flux reduction. The operational space bounded by the H-L back transition, high fusion gain, and divertor detachment will be re-assessed in light of the experiments and integrated modeling of power and particle control on DIII-D. This research will provide the basis to develop integrated radiative scenarios for future fusion devices that adequately mitigate divertor heat loads, while ensuring high performance and good heat exhaust and particle control.

#### **4.2.3.2 Research Plan**

The integrated power and particle control research is organized according to the challenges and goals in Table 4-21. The timeline for each challenge, associated research tasks and the facility improvement necessary to achieve them are set out in Fig 4-31. The research plan for power and particle control will focus on seed impurities, helium, and the impact of ELM control techniques on radiation and particle transport. Key drivers for activities in this area are the upgrades of the DIII-D heating and current drive systems, divertors and diagnostics, which will each have an accompanying power and particle control experimental program that integrates the

core and edge solutions, but each with unique capabilities. These are described in the following sub-sections.

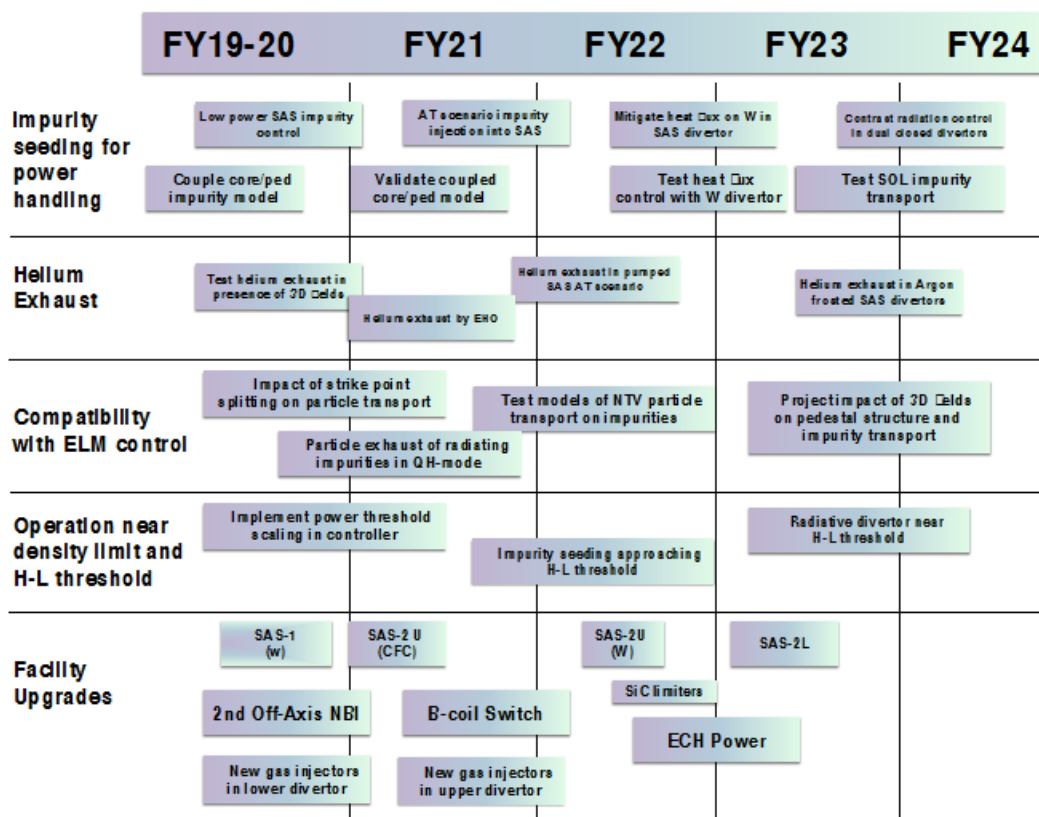


Fig. 4-31. Integrated Power and Particle Control Timeline

### Challenge 1: Understand How Impurity Species Influence Pedestal and Core Performance to Provide Strong Dissipation of Heat and Maximize Core Performance

**Current progress.** Historically, DIII-D has had a strong program of detachment studies in standard ELMing H-mode scenarios. During the past 5 years, research has been initiated to obtain a radiative divertor in high performance regimes that have significant non-inductive current drive with the aim of obtaining detachment in a steady state scenario. Good progress was made in obtaining a radiative divertor in high density, high power hybrid discharges which have significant non-inductive bootstrap-driven current [Petrie 2017]. Radiation in the divertor and in the periphery of the main plasma has been increased with both deuterium gas puffing and impurity injection, but full detachment has not yet been obtained. A major positive result from this research was that the pedestal performance improved with strong deuterium gas puffing for heating powers above 14 MW. As shown in Fig 4-32, MHD stability analysis of these discharges indicates that the double null shape was instrumental in eliminating the ballooning limit in the operating space, thus enabling high pedestal pressures. Another contributing factor was that

contrary to typical behavior, the density pedestal did not contract in width with increasing power and gas puffing. This behavior is not understood.

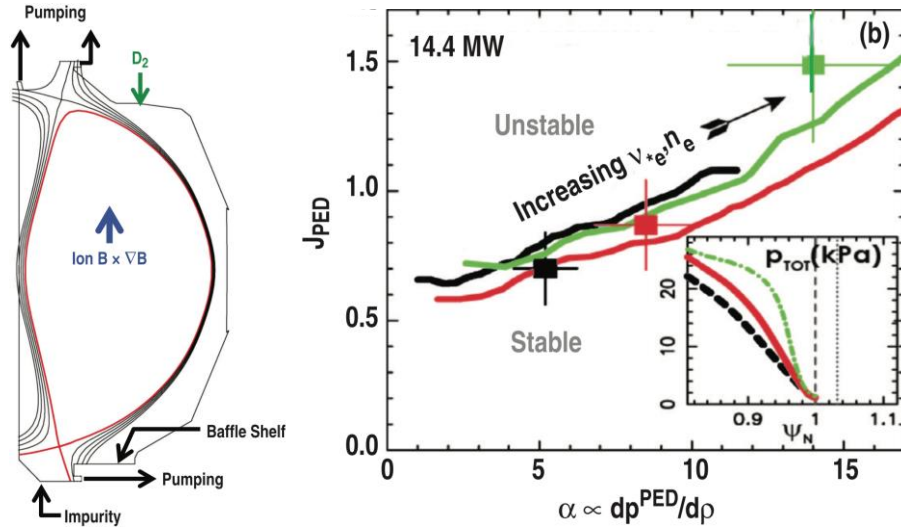


Fig. 4-32. (a) Near DND configuration for high power with impurity injection. (b) MHD stability analysis shows no ballooning limit at high power and density

The main approach of DIII-D’s advanced tokamak (AT) scenario, with a goal of obtaining a steady state discharge, is to use current drive tools that typically require densities below the level at which detachment is obtained in DIII-D. Thus, the AT scenarios have not been compatible with a radiative divertor. However, in the past 5 years, a form of slot divertor, called SAS (Small Angle Slot) [Guo 2017] has been designed and SOLPS modeling predicted that this divertor should be able to detach at low enough densities to be compatible with AT operation. A low power version of SAS was installed in DIII-D and initial characterization has been done. For the 2019-2024 five-year plan, a series of SAS upgrades are planned, culminating in a SAS-2 upper divertor which will be compatible with high heating power and which will be tested to determine if it is compatible with the AT regime of operation. In addition, new heating and current drive actuators are planned which will enable the extension of AT scenarios to higher core density. Furthermore, the compatibility of seeding impurities with the AT regime in the presence of a high-Z wall will be studied with the high-Z SAS-2U.

**Goal 1: Develop heat flux control with high performance core.** Early in the research plan we will use high pedestal and high confinement regimes to assess compatibility with private flux impurity seeding for power handling and overall performance. These conditions include the super-H pedestal and high beta steady state scenarios. Emerging capabilities in core-pedestal-SOL modeling using TGYRO, EPED and STRAHL will be used to interpret these experimental results and simulate the expectations at reactor conditions. Later in the research plan, improved capabilities for physics studies using the B-coil reversing switch, new divertors, and advanced

time-dependent modeling with upgraded TRANSP core/pedestal/SOL models will be used for validation and projection to reactor conditions.

DIII-D will test the physics of particle transport in high pedestal operation with seeded impurities to assess core compatibility. Early in the research plan the newly discovered high power high confinement hybrid scenario [Petrie 2017] will be tested for radiative impurity compatibility, paying specific attention to core impurity accumulation and heating scenario. Compatibility with more advanced “high  $q_{\min}$ ” scenarios will also be studied. Operation with puff-and-pump divertor and grad-B drift opposite to the X-point (unfavorable) will be explored with neon and argon injected into the private flux region and contrasted with previous studies with main-chamber impurity injection. Improved gas manifolds will enable optimal impurity seeding in this configuration. Physics of core impurity transport and impurity accumulation will be tested with physics-based transport models to balance the benefits of heat flux reduction against fuel dilution (see also 4.2.1). With successful development of planned helicon or high field side Lower Hybrid Current Drive (LHCD) techniques, high density and  $\beta_N$  advanced tokamak configurations will be used to project further toward reactor relevant edges. This behavior will be used to validate and help develop simulation capabilities.

**Goal 2: Test role of divertor closure for heat flux control.** In preparation for divertor upgrades enabling high power AT operation, the present SAS-1 divertor (un-pumped) will be used to change the pedestal structure via closure and examine the intrinsic carbon density profile gradients. These intrinsic impurity density profile gradients will be tested against local neoclassical theory (NEO) and turbulence theory (TGLF) to assess the stationary impurity peaking factor (pinch / diffusion) and project expectation for heat flux control from increased closure operation.

The second SAS divertor (SAS-2 CFC) is the first opportunity to operate high power AT with a closed divertor on DIII-D. The increased divertor pressure is expected to improve the efficiency of puff-and-pump impurity entrainment, and conditions will be studied with ion grad(B) down and impurity injection into the upper SAS-2 divertor. An upgrade of the toroidal field coil switch will enable between-shot comparisons with the same plasma wall conditions, enabling the contrasting of closed upper and open lower divertor experiments in the same day or between shots. Simulations with the STRAHL impurity transport code will determine the exhaust time constants and divertor impurity enrichment, constrained by core impurity density and SOL impurity pressure gauge measurements. Temporary installation of tungsten divertor tile arrays, combined with siliconization will also be used to assess possible influxes from the divertor and changes in radiative mantle and divertor behavior with reduced carbon radiation.

## **Challenge 2: Test and Develop Projectable Model for Helium Exhaust with a Detached Divertor**

**Current progress.** While previous studies of helium exhaust from a core source in DIII-D have shown sufficient pumping for fusion power operation, the implications of detached operation have not been explored. The detachment front acts as a virtual target, and the exhaust of helium through this virtual target into the pump has not been examined experimentally. This research will be initiated in the 2019-2024 five-year plan.

**Goal: Test model of global helium confinement in detached conditions.** DIII-D will assess the compatibility of helium exhaust in a detached divertor by performing experiments that inject core helium through NBI while pumping helium through argon frosted cryo panels. Divertor detachment will be obtained in both open (lower) and closed (upper SAS-2) configurations with optimized pumping. The global helium confinement,  $\tau_{\text{HP}}^*$  will be assessed in attached vs. detached and open vs. closed divertors in a 4x4 matrix. Penning gauges and core and divertor spectroscopy will monitor the core and divertor concentrations and deduce the impact of detachment and pumping on helium exhaust. Behavior will be compared with transport models to aid in their development.

## **Challenge 3: Establish the Compatibility of ELM Mitigation Techniques with the Exhaust of Gaseous Impurities (Radiators, Helium)**

**Current Progress:** Research performed in the past five years has studied the transport of fluorine ( $Z=9$ ) in RMP-ELM suppressed and QH-mode discharges, which had no ELMs [Grierson 2015]. Analysis shows that the injected fluorine transport across the edge barrier is comparable to that obtained in ELMing plasmas with ELM frequencies near 40Hz (Fig. 4-33). These exhaust rates are much faster than the ITER baseline demonstration discharges on DIII-D and appear favorable for medium  $Z$  impurity control in a fusion reactor in ELM suppressed regimes. Recent DIII-D experiments have also shown that helium injected from an edge valve is exhausted from the plasma faster when ELMs are suppressed with RMPs than during reference ELMing discharges in which RMPs are not applied [Hinson 2017]. In discharges with ELMs mitigated by injection of lithium granules [Bortolon 2016], a substantial reduction of core metal impurities (Ni XXV) has been observed, also a favorable result for the compatibility of this ELM mitigation technique with the exhaust of high- $Z$  impurities.

**Goal: Develop models of impurity transport in various ELM-mitigated regimes.**

The impact of 3D fields, EHO and ergodic regions for screening seeded impurities and helium will be tested with dedicated experiments that utilize laser blow off (LBO) of impurities, core helium neutral beam injection and upgraded penning gauges. As theoretical models for EHO and RMP-induced main-plasma and impurity transport emerge, they will be compared with the experimental observations. Later in the research plan, closed divertor geometries and localized gas injection into the upgraded SAS divertor will be leveraged for high power operation with increased pumping pressures. RMP ELM suppression in the more closed SAS-2 upper and lower divertors will be used to study the effect of the RMP induced particle transport and grad(B) drift direction on impurity screening. With stronger pumping, RMP ELM-suppressed conditions are expected to achieve better impurity control in contrast with previous studies [Petrie 2011].

An important possible further element is that the improved particle control with the closed SAS divertor may enable access to detachment with sufficiently low pedestal density to enable suppression mechanism such as RMP or QH mode to be applied successfully. This would be highly significant, providing deeper understanding and model validation in detached regimes without ELMs, as well as further insight into the interaction of ELMs with radiative techniques.

An important possible further element is that the improved particle control with the closed SAS divertor may enable access to detachment with sufficiently low pedestal density to enable suppression mechanism such as RMP or QH mode to be applied successfully. This would be highly significant, providing deeper understanding and model validation in detached regimes without ELMs, as well as further insight into the interaction of ELMs with radiative techniques.

**Challenge 4: Identify and Understand Density Limit, Marfes, and Operation Close to the H-L Back Transition Threshold**

**Current Progress:** ITER is expected to operate at heating powers slightly above the threshold to achieve H-mode and there are a number of operational concerns about its ability to operate there. This is also an important constraint (on desired core radiation) for future steady state reactors. Experiments in DIII-D and other devices show that a rising plasma density at heating powers only slightly above the H-mode threshold can often lead to an H-L back transition when the density rises to the density limit for maintaining H-mode. Radiated power is often a contributing factor to these back transitions. When the heating power is maintained

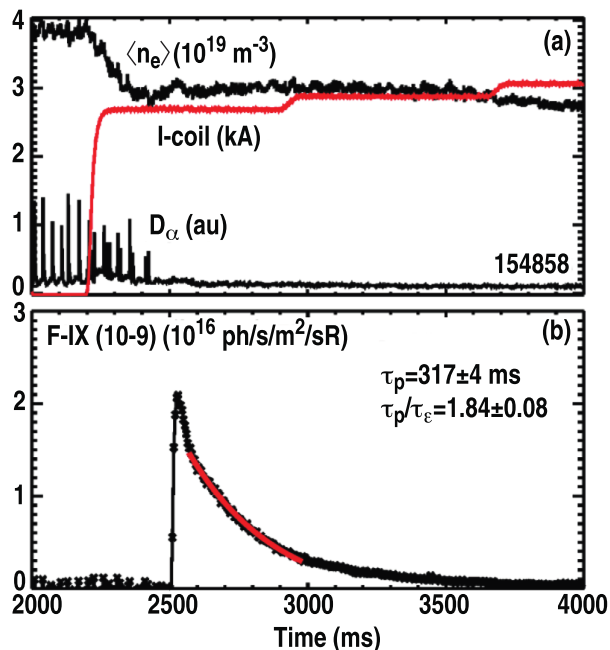


Fig. 4-33. Rapid pumpout of fluorine during RMP ELM suppression

constant in these discharges, the plasma often oscillates between the L and H mode states. Experiments also show that H-mode discharges with low heating power (slightly above the L-H threshold) are also susceptible to MARFE formation when strong gas puffing is applied to obtain detachment. Research will be performed in DIII-D to use feedback control as a technique to understand and prevent MARFE formation and H-L transitions at low heating powers.

**Goal: Develop feedback control to enable detached divertor near H-L threshold.** Proximity to the H-L transition, MARFEs, and the new capabilities with low density detachment will be explored to understand the density limit and closure effects on operation near the H-L threshold, extending previous DIII-D experience with an open divertor [Maingi 2005]. The first activity will be to upgrade the feedback control algorithm that maintains the heating power near the threshold power for stable, low frequency type-I ELM operation. This controller will be tested early in the experimental program without impurity injection. In the middle of the research program, feed-forward studies of the ELM behavior will be performed to understand the changes in pedestal stability and pressure as radiating impurities are introduced in high density pedestals near the density limit and H-L power threshold. Finally, using this controller, dedicated studies of impurity seeding and the plasma response will be performed to understand the stability of the pedestal and reaction to the modified plasma composition. The performance of the upper (closed) and lower (open) divertors for effective impurity exhaust will be contrasted to assess the expected advantages of a more closed divertor configuration.

#### 4.2.3.3 Capability Enhancements

Planned research for integration goals will use a number of hardware enhancements to the DIII-D facility as shown in Table 4-22. These include the installation of upper and lower SAS divertors that can handle high heat flux that will be used in research throughout this plan for power and particle handling studies and detachment studies at low density. Increases in ECH heating power will enable studies of core impurity transport with dominant electron heating. A 2<sup>nd</sup> off-axis neutral beam will improve access to advanced tokamak regimes. A Laser Blowoff system will provide seed impurities for transport studies over a wider range of Z, while tungsten tile arrays in the divertor will assess interaction and influxes from this region. This research will also be enabled by a number of diagnostic improvements, as listed in Table 4-23. These enhancements are primarily related to improving the ability of DIII-D to measure sources and inventories of particles over a wide range of ion charge. These measurements are crucial for performing the transport studies required to develop models of impurity transport.

This research plan has a strong focus on developing models (Table 4-24) for a variety of physics processes and is bolstered by in-progress and planned improvements in the modeling capabilities towards “whole device modeling”, including the role of global particle balance and

transport (core, pedestal) of seeded impurities and helium ash, shown in Fig. 4-34. A schematic multi-chamber model has been used, with effective particle fluxes and pumping rates. As improved physics models emerge, timescales and effective chambers will be replaced by transport models and plasma and neutral profiles. Specifically, the core/pedestal chambers will be replaced by the TGLF and NEO transport models and EPED pedestal, while the SOL is modeled by onion-skin models or 2D plasma models rather than a black box.

**Table 4-22.**  
**Hardware Improvements for Integrated Power and Particle Control**

<b>Hardware Capability</b>	<b>New Physics</b>
2 <sup>nd</sup> Off-axis NBI	High pressure weak magnetic shear steady-state regime
Increased ECH power	Dominant electron heating to test core impurity transport and accumulation
Laser Blowoff	Trace impurity injection
SAS divertor	Increased closure for neutral and impurity exhaust, and low density detachment
SAS divertor Tungsten Tile arrays (temporary)	Assess impact of mitigated plasmas on divertor tiles and effects of any resulting tungsten influxes
Siliconization.	Reduced carbon contribution to radiation and particle sourcing

**Table 4-23.**  
**Diagnostic Improvements for Integrated Power and Particle Control**

<b>Scientific Objective</b>	<b>Physics Measurement</b>	<b>Diagnostic Technique</b>
Measure low charge states of impurities in divertor	Photoemission spanning visible and ultraviolet	SPRED
Determine fuel gas pumping efficiency	Neutral pressure in main chamber and divertor	ASDEX gauges
Determine impurity pumping efficiency	Impurity partial pressure	Penning gauges
Core impurity density of low-Z ions	Charge exchange emission	Active charge exchange spectroscopy (CER)
Core impurity density of medium and high-Z ions	X-ray emission	Multi-energy soft x-ray cameras and x-ray pinhole cameras

**Table 4-24.**  
**Simulation Codes Used**

<b>Code</b>	<b>Purpose</b>
STRAHL	Impurity transport and radiation
TGYRO	Core turbulent and neoclassical transport
TGLF & NEO	Core transport
EPED	Pedestal prediction
SOLPS/UEDGE	Scrape-off layer transport
OMFIT	Integrated modeling framework
CESOL	Integrated core-edge modeling suite

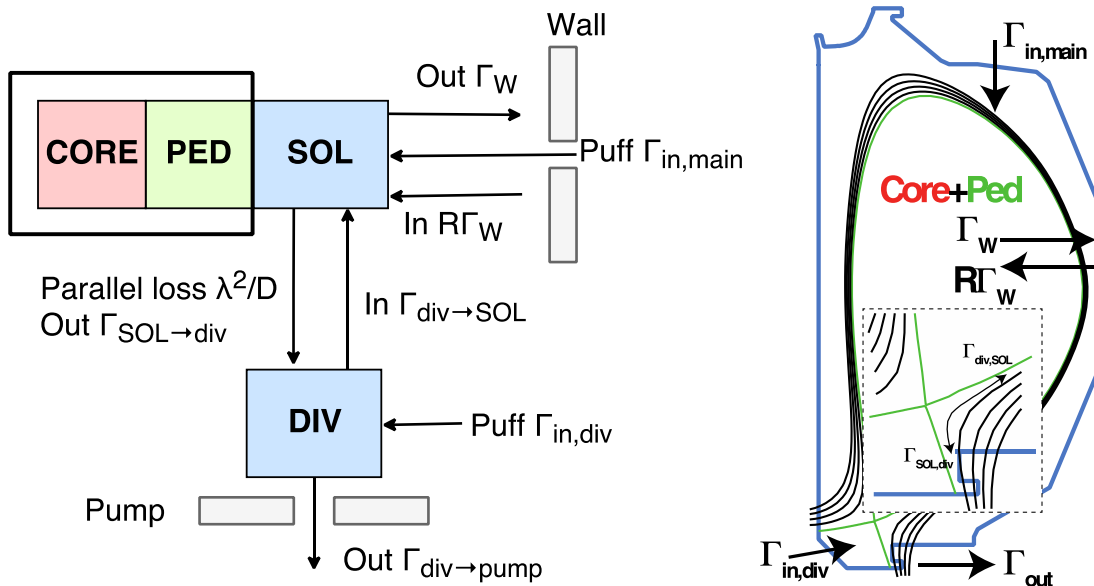


Fig. 4-34. Schematic (adapted from [Dux 1996]) and physical layout of global particle balanced used to interpret fueling and impurity studies

## References

- [Abrams 2017A] T. Abrams et al, Nucl. Fusion **57** (2017) 056034
- [Abrams 2017B] T. Abrams et al., "Understanding tungsten divertor sourcing and transport in DIII-D high performance discharges," SOFE-27 (2017) R.OP2.
- [Austin 2017] M. Austin et al., 2017 APS-DPP, Milwaukee, WI
- [Biedler 2017] M. Biedler et al, Phys. Plasmas **24** 052508 (2017)
- [Bortolon 2016] A Bortolon et al., "High frequency pacing of edge localized modes by injection of lithium granules in DIII-D H-mode discharges", Nucl. Fusion **56** (2016) 056008
- [Bortolon 2016] A. Bortolon et al, Nucl. Fusion **56** 056008 (2016)
- [Bortolon 2016] A. Bortolon et al., Nucl. Fusion **56** (2016) 056008
- [Burrell 2016] K.H. Burrell et al., Phys. Plasmas **23**, (2016) 056103
- [Burrell 2016] K.H. Burrell et al., Physics of Plasmas **23** (2016) 056103
- [Callen 2016] J.D. Callen et al, UW CPTC Report 16-4 (2016)
- [Canik 2011] J.M. Canik et al., Phys Plasmas **18** (2011) 056118
- [Casson 2014] F J Casson, Plas. Physics. Control. Fus. **57** (2014) 140031.
- [Chan 2010] V.S. Chan, et al. Fus. Sci. Tech. **57** (2010) 66-93
- [Chen 2016] X. Chen et al. Nucl. Fusion, Volume **56** 076011 (2016)

- [Chen 2017] X. Chen et al, Nucl. Fusion *57* 022007 (2017)
- [Chen 2017] X. Chen, et al. Nucl. Fusion **57** (2017) 022007
- [Chen 2017] Xi Chen et al, Nucl. Fusion **57** (2017) 022007
- [Conway 2011] G.D. Conway *et al Phys. Rev. Lett.* **106** (2011) 06500
- [Cziegler 2015] I. Cziegler et al *Nucl. Fusion* **55** (2015) 083007
- [Diallo 2015A] A. Diallo et al., Physics of Plasmas **22** (2015) 056111
- [Diallo 2015B] A. Diallo et al., Nucl. Fusion **55** (2015) 053003
- [Donovan 2017] D.C. Donovan SOFE Conference (2017)
- [Dunne 2017] M.G. Dunne 2017 Nucl. Fusion **57** (2017) 025002
- [Dux 1996] R Dux, “Measurement and modelling of neon radiation profiles in radiating boundary discharges in ASDEX Upgrade “, Plasma Phys. Control. Fusion 38 (1996) 989–999
- [Dux 2003] R. Dux et al. Plasma Phys. Control. Fusion **45** (2003) 1815-1825
- [Eldon 2015] D. Eldon et al Phys. Plasmas **22** (2015) 052109
- [Ernst 2016] D. Ernst et al, Phys. Plasmas 23 056112 (2016)
- [Estrada 2011] T. Estrada *et al Phys. Rev. Lett.* **107** (2011) 245004
- [Evans 2017] T. Evans et al, Nucl. Fusion 57 086016 (2017)
- [Fenstermacher 2000] M.E. Fenstermacher, et al. 18<sup>th</sup> International Atomic Energy Agency, Fusion Energy Conference, 4 – 10 October 2000, Sorrento, Italy, EX2/4
- [Ferron 2005] J.R. Ferron, et al. Phys. Plasmas **12** (2005) 056126
- [Ferron 2015] J.R. Ferron, et al. Nucl. Fusion **55** (2015) 073030
- [Futatani 2014] Nucl.Fus. 54 730008 (2014).
- [Futatani 2014] S. Futatani et al, Nucl. Fusion 54 073008 (2014)
- [Giroud 2016] C. Giroud et al., Nucl. Fusion **53** (2013) 113025
- [Gohil 2011] P. Gohil, T.E. Evans, M. Fenstermacher *et al* Nucl. Fusion **51** (2011) 103020
- [Grierson 2015] B. A. Grierson et al., "Impurity confinement and transport in high confinement regimes without edge localized modes on DIII-D", Physics of Plasmas 22 (2015) 055901
- [Grierson 2015] B. A. Grierson et al., Physics of Plasmas **22** (2015) 055901
- [Grierson 2015] B. Grierson et al, Phys. Plasmas 22 055901 (2015)
- [Guo 2017] “An Innovative Small Angle Slot Divertor Concept for Long Pulse Advanced Tokamaks”, H. Y. Guo et al., submitted to Phys. Plasmas (2017).
- [Guo 2017] H.Y. Guo et al, “Small angle slot divertor concept for long pulse advanced tokamaks” Nucl. Fusion **57** (2017) 044001
- [Guo 2017] H.Y. Guo et al, Nucl. Fusion **57** (2017) 044001

- [Haskey 2016] S.R. Haskey et al., *Rev. Sci. Instr.* **87** (2016) 11E553
- [Hatch 2017] D. Hatch et al., *Nucl. Fusion* **57** 036020 (2017)
- [Hinson 2017] E.T. Hinson et al., “Enhancement of He Exhaust During RMP ELM Suppression at DIII-D”, presented at 2017 APS-DPP meeting in Milwaukee, WI
- [Holcomb 2009] C.T. Holcomb, et al. *Phys. Plasmas* **16** (2009) 056116
- [Holod 2017] I. Holod et al, *Nucl. Fusion* 57 016005 (2017)
- [Howard 2014] N.T Howard et al., *Plasma Phys. Control. Fusion* **56** (2014) 124004
- [Hughes 2018 “Access to ITER-like pedestal pressure in the high magnetic field tokamak Alcator C-Mod”, J.W. Hughes et al., submitted to *Nuclear Fusion* 2017.
- [Kallenbach 2002] A. Kallenbach, et al. *Nucl. Fusion* **42** (2002) 1184
- [Kallenbach 2013] A Kallenbach, et al., “Impurity seeding for tokamak power exhaust: from present devices via ITER to DEMO “, *Plasma Phys. Control. Fusion* **55** (2013) 124041
- [Kessel 2015] C.E. Kessel, et al. *Fus. Sci. Tech.* **67** (2015) 1-21
- [Kim 1991] Y.B. Kim, P.H. Diamond, and R. Groebner *Phys. Fluids* **B3** (1991) 2050-2060
- [Kim 2015] K. Kim, et al. *Nucl. Fusion* **55** (2015) 053027
- [King 2015] *Physics of Plasmas* **22**, 072501 (2015).
- [King 2017] J.R. King et al, *Phys. Plasmas* 24 055902 (2017)
- [King 2017] J.R. King et al, *Phys. Plasmas* 24 055902 (2017).
- [Komm 2017] M. Komm et al, *Nucl. Fusion* 57 056041 (2017).
- [Kotschenreuther 2013] M. Kotschenreuther, et al. *Phys. Plasmas* **20** (2013) 102507
- [Kugel 2008] H.W. Kugel et al., *Phys. Plasmas* **15** (2008) 056118
- [Kukushkin 2013] A.S. Kukushkin, et al., “Consequences of a reduction of the upstream power SOL width in ITER” *Journal of Nuclear Materials* 438 (2013) S203–S207
- [Laggner 2016] F.M. Laggner et al., *Nucl. Fusion* **58** (2016) 065005
- [Leonard 2015] A.W. Leonard et al., *J. Nucl Mat*, **463**, (2015) Page 519
- [Leonard 2016] A.W. Leonard et al., 2016 IAEA-FEC, preprint0581.pdf
- [Leonard 2017] A.W. Leonard et al., *Nucl. Fusion* **57** (2017) 086033
- [Liu 2012] Y.Q. Liu et al, *Plasma Phys. Contrl. Fusion* 54 124013 (2012)
- [Liu 2017] F. Liu et al, *Plasma Phys. Contrl. Fusion* (2017, in press).
- [Liu 2017] F. Liu et al, *Plasma Phys. Contrl. Fusion* (2017, in press)
- [Loarte 2014] A. Loarte et al, *Nucl. Fusion* 54 033007 (2014)
- [Loarte 2015] A. Loarte et al., *Phys. of Plasmas* **22**, 056117 (2015)
- [Luce 2011] T.C. Luce, et al. *Phys. Plasmas* **18** (2011) 030501
- [Lyons 2017] B. Lyons et al, *Plasma Phys. Contrl. Fusion* 59 044001 (2017)

- [Maingi 2005] R. Maingi and M.A. Mahdavi, “Review of DIII-D H-mode Density Limit Studies”, *Fus. Sci. and Tech.* **48** (2005)
- [Manz 2012] P. Manz *et al Phys. Plasmas* **19** (2012) 072311
- [Marinoni 2015] A. Marinoni et al, *Nucl. Fusion* **55** 093019 (2015)
- [Martin 2008] Y.R. Martin and T. Takizuka *J. Phys.: Conf. Ser.* **123** (2008) 012033
- [McKee 2009] G.R. McKee *et al (2009) Nucl. Fusion* **49** (2009) 115016
- [McKee 2013] G. McKee et al, *Nucl. Fusion* **53** 113011 (2013)
- [Medvedev 2015] S.Yu. Medvedev, et al. *Nucl. Fusion* **55** (2015) 063013
- [Moyer 2017] R. Moyer et al, *Phys. Plasmas* **24** 102501 (2017)
- [Najmabadi 2006] F. Najmabadi, et al. *Fus. Eng. Design* **80** (2006) 3-23
- [Nazikian 2015] R. Nazikian et al, *Phys. Rev. Lett.* **114** 105002 (2015).
- [Nazikian 2015] R. Nazikian et al, *Phys. Rev. Lett.* **114** 105002 (2015)
- [Osborne 2000] T.H. Osborne, et al. *Plasma Phys. Control. Fusion* **42** (2000) A175
- [Osborne 2015] T.H. Osborne et al., *Nucl. Fusion* **55** (2015) 063018
- [Park 2017] J.-K. Park et al, *Phys. Plasmas* **24** 032505 (2017)
- [Paz-Soldan 2015] C. Paz-Soldan et al, *Phys. Rev. Lett.* **114** 105001 (2015)
- [PazSoldan 2015] C. Paz-Soldan et al, *Phys. Rev. Lett.* **114** 105001 (2015)
- [Petrie 2011] T.W. Petrie, et al., “Results from radiating divertor experiments with RMP ELM suppression and mitigation”, *Nucl. Fusion* **51** (2011) 073003
- [Petrie 2015] T.W. Petrie et al., *J. Nucl. Materials* **463** (2015) 1225
- [Petrie 2017] T.W. Petrie et al., *Nucl. Fusion* **57** (2017) 086004
- [Petrie 2017] T.W. Petrie, et al., “Improved confinement in highly powered high performance scenarios on DIII-D”, *Nucl. Fusion* **57** (2017) 086004
- [Petrie 2017] T.W. Petrie, et al., *Nucl. Fusion* **57** (2017) 086004
- [Petty 2017] C. Petty et al, *Nucl. Fusion* **57** 116057 (2017)
- [Pochelon 2012] A. Pochelon, et al. *Plasma and Fusion Research* **7** (2012) 2502148
- [Puiatti 2006] M.E. Puiatti et al., *Phys. of Plasmas* **13**, 042501 (2006)
- [Rozhansky 1992] V. Rozhansky *and M. Tendler*, *Physics of Plasmas* **4** (1992) 1877
- [Saibene 2002] G. Saibene, et al. *Plasma Phys. Control. Fusion* **44** (2002) 1769
- [Sang 2017] C.F. Sang et al., *Plasma Phys. Control Fusion* **59** (2017) 025009
- [Scannell 2015] R. Scannell et al, *Plasma Phys. Control. Fusion* **57** (2015) 075013
- [Schmitz 2012] L. Schmitz *et al Phys. Rev. Lett.* **108** (2012) 155002
- [Schmitz 2014A] L. Schmitz, L. Zeng, T.L. Rhodes *et al Nucl. Fusion* **54** (2014) 073012

- [Schmitz 2014B] L. Schmitz, *Proceedings 25<sup>th</sup> IAEA Fusion Energy Conference*, St. Petersburg, Russian Federation, Oct. 13-18, 2014, [http://www-naweb.iaea.org/napc/physics/FEC/FEC2014/fec\\_sourcebook\\_online.pdf](http://www-naweb.iaea.org/napc/physics/FEC/FEC2014/fec_sourcebook_online.pdf)
- [Schmitz 2015] L. Schmitz *et al* 2015 *Proceedings 42<sup>th</sup> EPS Conference on Plasma Physics*, Lisbon, Portugal, June 22-26, 2015. <http://ocs.ciemat.es/EPS2015PAP/pdf/P5.166.pdf>
- [Schmitz 2017] L. Schmitz *et al* 2017 *Proceedings 44<sup>th</sup> EPS Conference on Plasma Physics*, Belfast, NI, June 22-26, 2017 <http://ocs.ciemat.es/EPS2017PAP/pdf/O2.105.pdf>
- [Shesterikov 2013] Shesterikov I. *et al Phys. Rev. Lett.* **111** (2013) 055006
- [Snyder 2011] P.B. Snyder *et al.*, *Nucl. Fusion* **51** (2011) 103016
- [Snyder 2011] P.B. Snyder, *et al.* *Nucl. Fusion* **51** (2011) 103016
- [Snyder 2011] P.B. Snyder, *et al.* *Nucl. Fusion* 51 (2011) 103016.
- [Snyder 2015] P.B. Snyder *et al.*, *Nucl. Fusion* **55** (2015) 083026
- [Snyder 2015] P.B. Snyder *et al.*, *Nucl. Fusion* 55 (2015) 083026.
- [Snyder 2015] P.B. Snyder, *et al.* *Nucl. Fusion* **55** (2015) 083026
- [Solomon 2014] W. M. Solomon *et al.*, *Phys. Rev. Lett.* **113** (2014) 135001
- [Solomon 2014] W. Solomon *et al*, *Phys. Rev. Lett.* 113 135001 (2014)
- [Solomon 2014] W. M. Solomon, P. B. Snyder, K. H. Burrell, M. E. Fenstermacher, A. M. Garofalo, B. A. Grierson, A. Loarte, G. R. McKee, R. Nazikian, and T. H. Osborne, *Phys. Rev. Lett.* 113, 135001.
- [Solomon 2014] W.M. Solomon, *et al.* *Phys. Rev. Lett.* **113** (2014) 135001
- [Soukhanovskii 2012] V.A. Soukhanovskii, *et al.* *Phys. Plasmas* **19** (2012) 082504
- [Sun] Y.Sun *et al.*, “Dynamic Divertor Control Using Resonant Mixed Toroidal Harmonic Magnetic Fields During ELM Suppression in DIII-D”, submitted to *Phys. Plasmas* 2017.
- [Sung 2017] C. Sung *et al*, *Phys. Plasmas* 24 112305 (2017)
- [Tynan 2013] G.R. Tynan *et al Nucl. Fusion* **53** (2013) 073053
- [Victor 2017] B.S. Victor *et al.*, to be submitted to *Nucl. Fusion*
- [Wade 1995] M. R. Wade, *et al.*, “Helium transport and exhaust studies in enhanced confinement regimes in DIII-D”, *Phys. Plasmas* **2**, 2357 (1995)
- [Wan 2017] Y. Wan, *et al.* *Nucl. Fusion* **57** (2017) 102009
- [Wenninger 2017] R. Wenninger, *et al.* *Nucl. Fusion* **57** (2017) 016011
- [Xu 2011] G.S. Xu *et al Phys. Rev. Lett.* **107** (2011) 125001
- [Yan 2013] Z. Yan, G.R. McKee, J. Boedo *et al Nucl. Fusion* **53** (2013) 113028
- [Yan 2014] Z. Yan, G.R. McKee, R. Fonck *et al Phys. Rev. Lett.* **112** (2014) 125002
- [Yan 2017] Z. Yan *et al Nucl. Fusion*, **57** (2017) 126015



## 5. THE DIII-D NATIONAL FUSION FACILITY – OPERATION AND ENHANCEMENTS

The DIII-D National Fusion Facility is a world-class facility capable of carrying out a wide range of experiments to explore high-performance tokamak discharges as well as fundamental fusion science. In this section, we describe device operation and enhancements to the device hardware and infrastructure that will enable steady research advances while maintaining high system availability. The section is subdivided into DIII-D Operations and Maintenance (5.1), Sustaining Engineering (5.2), and Facility Capability Improvements (5.3).

Fig. 5-1 provides a high-level summary of the operation and improvements proposed in the next five years. For the years FY19-FY23, DIII-D will be operated for 12, 16, 16, 16, and 12 weeks, respectively. Major system enhancements will be performed in each of the years during 4-6 month shutdowns and the fourth Long Torus Opening of one year will be performed in the FY23-24 years. Major upgrades will include significant increases in the EC and NB heating and current-drive power and pulse length, completion of a high-power Helicon current-drive system, introduction of a new high-field-side lower hybrid current-drive system, a second co-counter NB system, a more flexible coil and power system for 3D field control, upgrades to the upper and lower divertor structures, an expanded materials program including a new materials sample system and tungsten use in the divertor, an upgraded vessel armor system compatible with higher power and longer pulse operation, and upgrades to the disruption avoidance and mitigation systems. An extensive expansion of the diagnostic systems will accompany this new hardware to improve understanding of the plasmas in the new regimes.

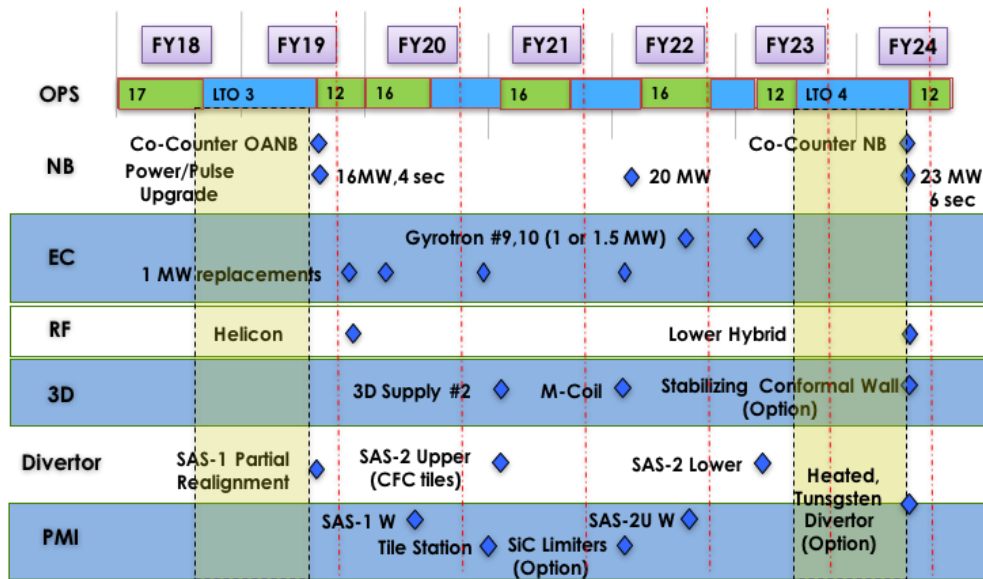


Fig. 5-1. Proposed Major Enhancements FY18-FY24. The vertical red lines indicate year 0 – year 5 of the plan.

At the heart of the facility is the DIII-D tokamak, which is renowned for its operational flexibility, enabling a wide range of research in highly shaped limiter and divertor plasma configurations. Substantial plasma heating and current-drive capability is available from 19 MW of neutral-beam heating and 2.8 MW (injected) of EC power. A 4 MW (source) FW heating and current-drive system consisting of two antennas and transmitters is presently mothballed. The DIII-D diagnostics set provides over 50 diagnostic systems capable of making definitive measurements of plasma parameters in the core, edge, and boundary regions of the plasma. A summary of all major non-heating systems is shown in Table 5-1.

**Table 5-1.**  
**Summary of All Major Non-Heating Systems**

<b>System</b>	<b>Description</b>
Poloidal field	7.5 V-s OH transformer Eighteen independently controllable field-shaping coils Fourteen phase-controlled dc supplies, 36 switching current regulators (2.5 kA)
Toroidal field	2.2 T on axis (1.695 m) for 5 s
3-D field	
C-coil	Six external coils on midplane, $B_{m=2/n=1} \sim 5$ G on $q=2$ surface Five phase-controlled dc supplies (7 kA); Four switching current regulators (4.5 kA); Six current regulators (2.7 kA, 450 V)
I-coil	Twelve internal coils above and below midplane, $B_{m=2/n=1} \sim 5$ G on $q=2$ 24 amplifiers (190 A, 0–20 kHz)
Vessel/first wall	Water-cooled inconel vessel, 90% graphite coverage
Vessel conditioning	350°C induction bake system for vessel walls Boronization, He glow cleaning
Fueling/disruption mitigation	Gas-puffing/pellets <ul style="list-style-type: none"> <li>— Eleven valves, 19 inlet locations, at 1–200 Torr-l/s each valve</li> <li>— Two fast valve arrays for massive gas injection — each at 2,000 Torr-l/s in 1–2 ms</li> <li>— Pneumatic pellet injector — 3 barrels at 30 Hz each</li> <li>— Two Shattered pellet injectors – SP1@400 Torr-liter, SP2@1,500 Torr-liter</li> <li>— Argon pellet injector - 20 Torr-liter</li> <li>— Large shell pellet injector</li> <li>— Lithium/impurity granular injector</li> <li>— Lithium dropper</li> </ul>
Pumping	Two turbopumps at 5,000 l/s each, two turbopumps at 1,500 l/s each Three in-vessel cryopumps — one at 37,000 l/s, two at 20,000 ls
Air/Water	Four deionized water-cooling systems for HV supplies (low pressure, deoxygenated), DIII-D vessel and coils (medium pressure), ECH gyrotrons (high pressure de-oxygenated) and NB ion sources (high pressure de-oxygenated); Clean dry air system for valve and switch actuation and equipment cooling
Prime power	Motor generator — 2.25 GJ at 525 MVA 138 kV Xfmr — 20 MVA(CW), 110 MVA (10 s)
Computers	Primarily Linux based, 30 GB raw data/shot, 330 TB total data storage
Cryogenics	150 l/h He liquifier, 11,000 gal LN <sub>2</sub> tank, 3,000 gal LN <sub>2</sub> tank, 1,000 gal He Dewar

The DIII-D tokamak uses conventional water-cooled copper coils to provide the magnetic field configuration (Fig. 5-2). The coil systems are designed to operate in a pulsed mode with the joule heat stored in the coil mass during the discharge and removed in the ten-minute interval between discharges. DIII-D operates at 2.2 T toroidal field and up to 2.5 MA plasma current with a discharge flattop duration of 5 s. Operation for longer duration at lower field and plasma current is also possible. Eighteen independently controlled poloidal field shaping coils provide a wide range of highly shaped, noncircular plasma cross sections. A set of six external picture-frame coils (C-coils) corrects small magnetic imperfections arising from non-axisymmetries in the coil systems and provides the capability to stabilize MHD instabilities. A set of 12 water-cooled internal picture-frame coils (I-coils) mounted on the interior vessel surface (six above and six below the midplane) provides improved error field correction, and improved instability control, allowing control of the Resistive Wall Mode (RWM) and Edge Localized Modes (ELM). The plasma control system provides state-of-the-art high-speed digital control of the magnetic configuration and other key plasma parameters. The system is capable of fully integrated control of plasma shape, density, pressure, current profile, energy, and toroidal rotation as well as performing feedback stabilization on the neoclassical tearing mode (NTM) and RWM.

Graphite tiles cover more than 90% of the interior plasma-facing surface. The tiles absorb heat during the discharge and are cooled by water channels in the vessel wall in the period between discharges. In the high heat flux areas of the upper and lower divertor regions and the centerpost, the edge-to-edge tile misalignment and tile gaps are less than 0.25 mm to reduce erosion and provide axisymmetry. Wall conditioning techniques include high-temperature baking to 350°C, boronization (deposition of a thin boron layer during high-temperature bake) prior to each operating period, and helium glow cleaning between discharges. These techniques enable rapid recovery of good plasma discharges following vents with personnel activity in the vessel and robust operation following plasma disruptions.

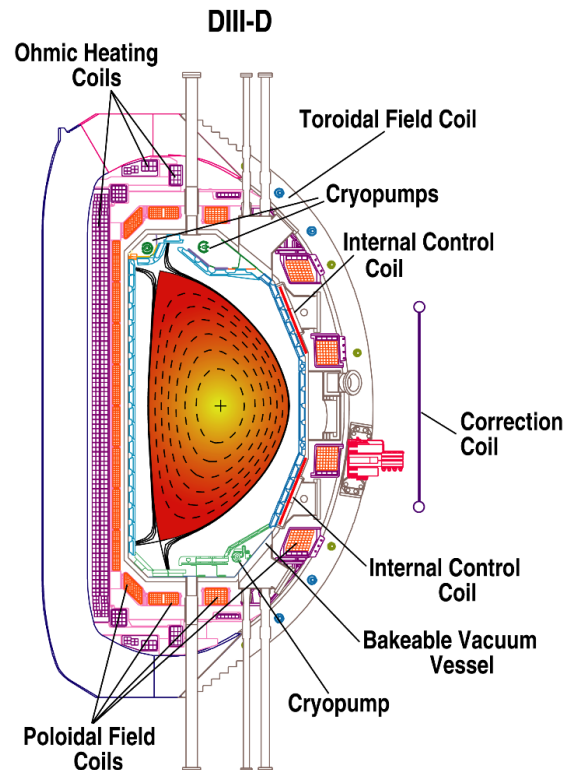


*Fig. 5-2. DIII-D capabilities allow a wide range of research and technology issues to be addressed.*

An extensive gas-puff system and pellet injector provide the tools for plasma fueling. The gas-puff system permits independent edge fueling with up to five different gases from more than 19 locations around the plasma including the inner wall and the upper and lower divertor regions. Three independent 30 Hz pneumatic pellet injectors provide ITER-relevant edge fueling as well as ELM mitigation via pellet pacing technique. Injection locations are either on the high-field side, low-field side near the midplane or the x-point. Two massive gas-puff systems at different toroidal/poloidal locations used for disruption mitigation experiments are provided by multi-valve injectors in which each of six high-speed valves are independently controllable and are designed to deliver fast rise time gas puffs. Four separate pellet systems are available for disruption studies: two shattered pellet injectors at different toroidal/poloidal locations provide deeper impurity penetration for more effective disruption mitigation, a pneumatic system is capable of injecting custom-designed shell pellets filled with chosen impurities, and an Argon pellet injector is available for triggering runaway electrons. A Lithium dropper system and an impurity granular injector for injecting various impurities at higher speeds are also available for control of ELMs and edge conditioning.

Three in-vessel baffled, cryopumps provide pumping of neutral gas in both the upper and lower divertor regions. The two pumps in the upper divertor regions separately pump both the inner and outer strikepoints ( $S \sim 20,000$  l/s and  $37,000$  l/s respectively for  $D_2$ ) of high triangularity upper single null or double null discharges. The geometry of the lower divertor was modified in 2005–2006 to pump the edge of high triangularity, single or double null divertor discharges ( $S \sim 20,000$  l/s for  $D_2$ ), thus improving the density control in high triangularity Advanced Tokamak discharges. The new geometry consists of a water-cooled shelf extending from the pump aperture to the outer baffle plate and permits the operation of lower triangularity divertor discharges at high power with the strikepoint(s) located on the top of the shelf. The pumps operate at liquid helium temperatures and actively pump both the  $D_2$  fuel and all volatile impurities during the discharge. An argon frosting technique has been used to provide effective pumping of He.

The present capabilities of the Neutral Beam and Electron Cyclotron heating and current-drive systems are summarized in Table 5-2. The eight neutral beams are capable of delivering 16 MW for 4 s or 19 MW for 3.0 s and are routinely used in most experiments for the primary source of heating and as a critical part of key diagnostic systems: charge exchange recombination as ion temperature, rotation speed, and impurity concentrations; beam emission spectroscopy for fluctuation measurements; and motional Stark effect for current profile and radial electric field measurements. Six of the sources are injected in the normal direction of the plasma current (“co-” sources) and two sources are injected in the counter direction. By reversing the direction of the plasma current, experiments can be performed with a full range of co- and counter-injection. Two

of the co-sources are capable of being tilted up to 16.5 degrees so that they can be aimed nearly 40 cm below the plasma axis to provide off-axis current drive. The electron cyclotron system presently consists of eight gyrotrons: five 1-MW class non-depressed collector gyrotrons (three are operational, one is presently under repair and one is scheduled for replacement), two 1-MW class depressed collector tubes, and one 1.5-MW class depressed collector tube that is presently being commissioned. Support systems for each of the gyrotrons (transmission lines, sockets, water, controls, power supplies, and launchers) are fully installed and operational. The power levels for the proposed Helicon and Lower Hybrid rf systems are also shown in the table. All power and pulse extensions are discussed in Section 5.3.

**Table 5-2.**  
**Auxiliary heating system power**

<b>System</b>	<b>Power (MW) FY18</b>	<b>Pulse (s)</b>	<b>Proposed Power (MW)</b>	<b>Pulse (s)</b>
Neutral Beam	16	4	23	4.5-6
• Co/Counter injection	12/4	4	23/12	6
• Balanced injection	8	4	22	6
Electron Cyclotron (Injected)	2.8	5	8.5	10
Radio Frequency				
• Helicon			1.0	10
• Lower Hybrid			1.0	10

A substantial number of other support systems are necessary to operate the facility. Prime power for the heating systems is taken directly off the utility grid while a 525 MVA motor generator supplies the power for the coil system. A second, smaller 260 MVA motor generator is presently mothballed. The coils are powered by a set of fourteen phase-controlled power supplies. In the case of the shaping coils, there are high-speed switching current regulators (choppers) in series with each; the non-axisymmetric coils utilize a combination of switching current regulators (0–1 kHz) and higher bandwidth amplifiers (0–20 kHz).

The computer systems for the facility are generally LINUX-based systems. The Fusion site is a node on ESnet operating at 10 Gb/s. DIII-D’s main computing center has a 10 Gb/s backbone with the network fanning out to 1 Gb/s connections to most offices. There is a dual 20 Gb/s link between the DIII-D facility and the main computing center with 10 Gb/s connections for key data-acquisition systems. The data-acquisition system routinely acquires approximately 30 GB per shot (all sizes compressed) and a new 330 TB storage array (220 TB used) permits all present and historical DIII-D data to be available for rapid access. Total raw data size anticipated to be acquired this fiscal year is 50 TB. Total managed storage (raw data, camera data, analyzed data, user files)

is approximately 325 TB. See Section 7 for more details about the computer system and proposed upgrades.

A closed loop, cryogenic system comprised of a 150 l/hr helium liquefier and two compressors provides liquid helium (LHe) needed to support operation of the neutral beamlines and in-vessel cryopumps. The LHe used for the EC superconducting magnets and the D<sub>2</sub> pellet injector is produced by a helium liquefier, but is used in a once-through system and is not recovered. The LN<sub>2</sub> used for the beamlines and in-vessel cryopumps is purchased and is stored in an 11,000 gallon tank and a 3,000 gallon tank. A set of water conditioning systems provides high purity, low conductivity, deoxygenated water to cool the DIII-D vessel, coils, neutral beams, gyrotrons, power supplies, diagnostics, and other systems.

## **5.1 OPERATIONS AND MAINTENANCE**

The scope of this subtask is the operation, maintenance, and routine repairs of the DIII-D device and facility. The research programs described in this plan depend on the safe, efficient, and reliable operation of the facility. This effort has become more demanding due to the increasing complexity and capability of the facility. To achieve this goal, a highly skilled operations staff has been assembled and a comprehensive preventive maintenance program has been developed that has enabled the DIII-D facility to become one of the most productive tokamak facilities in the world. To assure a high level of safety, a comprehensive safety program with continuous personnel training is fully integrated into all tasks and across all organizational boundaries within the DIII-D program. In order to maintain high reliability and availability of the facility, an inventory of spare equipment is maintained to enable rapid repairs or ‘hot spares’ are installed when feasible that can either be switched in automatically or rapidly brought on-line. A comprehensive program of ongoing proactive refurbishment, modernization, and minor system enhancements to improve productivity and enhance facility capability are described in the following section on Sustaining Engineering, Section 5.2.

The number of operating weeks for research in each year of the proposal is 25, 16, 16, 12, and 4 for a total of 73 weeks (an operating week is 5 days of single shift, 8 hours/day). The number of operating weeks is low in the final year because most of the year is associated with an extended opening for facility enhancements (see Section 5.3). Because of the misalignment of the contract period and the fiscal year, the five years of the proposal extend across six fiscal years (FY19-FY24) and the number of operating weeks in each of the six associated fiscal years is a more uniform 12, 16, 16, 16, 12, and 12 weeks respectively. Three weeks in the first year and eight weeks in the final year are not funded within this proposal. The remainder of the time each year will be used for system testing and commissioning, equipment maintenance and repair, diagnostic calibration, baking and boronization, and the facility upgrades and improvements outlined in this

proposal. A 70% increase in operating time is also proposed as an option obtained by running extended hours on each day (8:30 AM – 11:00 PM instead of 8:30 AM – 5:00 PM) while maintaining the same number and schedule of calendar weeks and other activities contained in this proposal.

Operation of the tokamak with deuterium fuel results in significant neutron production. Radiation levels at the site boundary are limited to 100 mrem/yr by state of California regulations and internally to 80 mrem/yr by DIII-D procedures. Radiation levels for staff are limited to 5,000 mrem/yr by state of California regulations and internally to 3,200 mrem/yr (800 mrem/qtr) by DIII-D procedures. An active ALARA program keeps radiation doses from facility operation As Low As Reasonably Achievable.

Presently, the radiation dose at the site boundary for a typical week of operation is approximately 1.2 millirem (less than a typical dental X-ray exposure), based on the 2017 experimental campaign. If the balance in the experimental program between high-performance discharges producing high-radiation dose and lower dose discharges remains the same, an extension of the typical pulse length by 50% and a doubling of our auxiliary power heating capability would increase the typical weekly dose by a factor of approximately 2.5, resulting in a weekly dose to 3.0 mrem. Thus, the facility can be operated for roughly 26 weeks without exceeding our DIII-D procedures or 33 weeks within all legal limits. To accommodate the higher weekly dose and the proposed operations schedule in which most operations are performed in two quarters, it is likely that our internal procedures will need to be modified to allow increased quarterly dose while staying within the annual legal limits. This is particularly true for the proposed option for extended days where the weekly dose could approach 5 mrem.

In a typical operating year, the 16 weeks are performed during 27 calendar weeks with alternating periods of 3-4 weeks of experimental operations followed by 2 weeks of maintenance. These short maintenance periods are extremely important since they provide time for on-going maintenance and repairs to maintain high availability, provide opportunities for installation and testing of new systems throughout the year, and allow modification of existing systems to respond to changing experimental needs. This operating schedule is a cornerstone of the flexibility of the DIII-D program in that it enables new systems to be installed and/or modified throughout the year to accommodate research schedules for participating scientists or in response to new research results.

Following the completion of the experimental program each year, there is typically an extended maintenance period of four to five months to enable the performance of longer maintenance and refurbishment tasks, and permit modest upgrades and new system installation and commissioning, both in-vessel and ex-vessel. The annual vessel openings are also used to perform routine

diagnostic calibrations and alignments. There is typically a one-month “cooldown” period prior to the start of any extended in-vessel work in order to allow radiation levels to decay to levels that will permit useful work periods within the constraints of our radiation guidelines.

At the end of an extended maintenance/upgrade period involving significant in-vessel work or facility modifications, there is a five- to six-week startup period. This includes a three-week period that includes leak checking, high-temperature baking, system testing and checkout, and new system commissioning. This is followed by two weeks of plasma cleaning operation and one week for diagnostic calibrations that require plasma operation. Excluding experimental operating weeks and the extended in-vessel work period, the device is typically operated with magnetic fields and/or plasma for an additional 60 days per year for system testing, diagnostic calibration, baking, boronization, plasma conditioning, and new system commissioning. Conditioning of the EC and NB systems are performed on an as-needed basis throughout the year.

In recent years, two new modes of operation and upgrade schedules have been utilized. The first involves a weekly two-hour shift from 5-7 PM to provide for testing and development of new plasma configurations, control algorithms, or other new system commissioning that requires plasma operation. Testing of systems without plasma is typically performed during the two-week maintenance periods on second shift. A second variant on the ‘typical’ operating year is a short vessel opening (1 day – 2 weeks) for performance of a specific task or tasks that are targeted at a dedicated run campaign immediately following the opening. If the in-vessel work duration is kept short, the required radiation cooldown time between the end of operations and the start of the in-vessel work is shorter. In addition, by limiting the in-vessel work scope and restricting ex-vessel work on other operations systems, the recovery and startup time following the vent has been shortened to as little as 2 weeks. This enables a dedicated, task-specific vent during the normal operating year without significant loss of calendar time. This has been performed for installation of tungsten tiles in 2016, installation of upper divertor diagnostics in 2017, and a one-day vent is planned for FY18 to install a lower hybrid mockup on the centerpost.

DIII-D utilizes a comprehensive preventive and corrective maintenance program that tracks and schedules maintenance activities, and provides written procedures for the work. More than 620 pieces of equipment are maintained and 912 work orders for preventive maintenance were completed in 2017. New initiatives are also planned to expand ‘health-driven’ maintenance activities in which system performance and key parameters are monitored to better determine when maintenance is required. Examples of this include vibration monitoring in pumps and motors, heat transfer coefficients in heat exchangers, and ground current leakage for motors.

The success of the DIII-D operations systems, maintenance and refurbishment program is evidenced by the sustainment of high facility availability during the period of this past contract

performance. During the period of 2014-2017, the average availability has been 78.5% with two years exceeding 80% (83% and 82% in FY14 and FY16 respectively). The availability is shown in Figure 5.3.

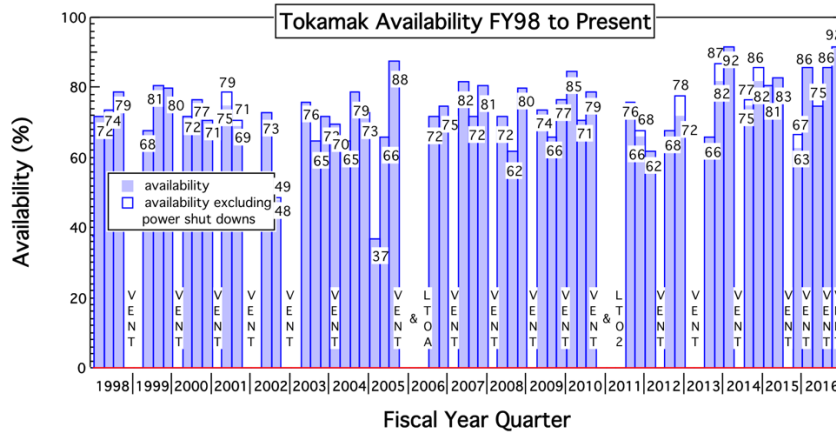


Fig. 5-3. Availability by quarter for the period of FY1998 – 2016. Availability is a measure of the fraction of time the DIII-D device and operating systems are available to achieve the goals of the scheduled experiment.

## 5.2 SUSTAINING ENGINEERING

In conjunction with GA’s DIII-D Preventive Maintenance program, GA is now pursuing a program of sustaining engineering best practices designed to address a variety of issues relating to equipment longevity. These include: identification of, and evaluation of, remaining useful life (RUL) of critical, long-lived systems and components; issues and sources of reliability/availability degradation; impending issues related to obsolescence and technology advancement; and, opportunities to improve operational efficiency. Failure to proactively address these issues in a timely manner can result in a reduction in system availability, reduced operational efficiency, and, ultimately, increased operating costs.

A recent comprehensive study was performed of the risk to DIII-D Operations of failure of operations-related systems. The risk to the program was evaluated as a combination of the probability of failure and the impact of failure, where the impact was a combination of schedule, technical, budget, and safety impacts. This risk was then used to develop a set of non-routine refurbishments, replacements, or modernizations of the facility to maintain reliable performance. As a result of the latest assessment conducted in 2016, GA has identified ten (10) sustaining engineering projects designed to maintain a high level of availability. The top three areas identified were motor generator (MG) cooling, MG power distribution, and gyrotron replacement. The full set of proposed projects with the major items associated with each is shown below. The timing of the projects is determined by the level of the risk and the compatibility of the work duration with the DIII-D operating schedule. The MG cooling refurbishment consisting of piping, valves, pumps,

and heat exchangers had the highest risk severity and is being performed during the Long Torus Opening period in the final year of the existing 2014-2018 five-year plan.

- Gyrotron Sustaining Engineering
  - Replace the four remaining oldest gyrotrons (Model 8110 - 1 MW non-depressed collector) that are now more than 15 years old. Three gyrotrons will be replaced with an upgraded 8110A with upgraded collector material (CuCrZr vs OFHC) and one gyrotron will be replaced with a new 1.5 MW depressed collector tube.
- MG2 Power Distribution Sustaining Engineering
  - Motor Generator cable testing and replacement.
- Neutral-Beam Components & Subsystems Sustaining Engineering
  - Replace source filaments, filament plates, and gas-valve drivers.
- Neutral-Beam Power System Sustaining Engineering
  - Replace 150 kV coax, 13.5kV fuses, and control cards.
- Cryogenic & Vacuum System Sustaining Engineering
  - Purchase two (2) 2000 l/sec turbopumps, controllers, and mechanical pump.
- Power Systems Sustaining Engineering
  - Replace 13.8 kV circuit breakers, disconnects for HV2 and D2 supplies, switchgear and circuit breakers for T5 transformer (main house power), 480 V cabling for pumps/cooling towers, and HV oil-processor equipment
  - Rebuild a step-up transformer for auxiliary heating systems.
- Water Systems Sustaining Engineering
  - Replace all metal-oxide varistors in X and HX choppers and all capacitors in high-temperature baking power supply,
  - Replace and modernize the control system for the Poloidal Field power supplies.
- Facility Services Sustaining Engineering
  - Replace water hoses for coils, power supplies, gyrotrons, and neutral beams,
  - Replace three ECH pumps with totally enclosed pumps and motors,
  - Refurbish one clean dry air compressor and manifold with newer, higher capacity pump and manifold.
- Operations Systems Enhancements
  - Design and install toroidal field reversing switch,
  - Install flexible multi-valve injector gas-puffing system for upper and lower divertors,

- Install supersonic molecular beam injector (SMBI),
- Upgrade torus hall access control system,
- Increase duration of uninterruptible power supply for computers,
- Implement backup diesel power for PF-coil water pumps.

### 5.3 FACILITY CAPABILITY IMPROVEMENTS

The productivity and long-term viability of a research program is closely tied to its ability to continually provide new capabilities to the scientific staff to pursue scientific challenges and address new questions that arise from on-going research. The DIII-D National Fusion Facility has a history of continual facility improvements that have enabled it to explore and resolve these questions and provide scientific leadership in the world fusion community. In particular, the facility is capable of carrying out a wide range of experiments to explore high-performance tokamak discharges as well as fundamental fusion science. This section describes improvements to the device hardware and infrastructure that will enable steady research advances in the areas identified by our research staff and offer opportunities for new discoveries. Table 5.3 summarizes the improvements proposed in the next five years and the research elements that are driving the changes. Major upgrades will include significant increases in the heating and current-drive power and pulse length (EC and NB), new rf systems for more efficient current drive, a more flexible coil and power system for ELM control and 3D physics, an upgraded vessel armor system compatible with higher input energy, innovative new divertor upgrades for improved power handling, and a materials test station and high Z wall armor for an expanded Plasma Materials Interaction research program.

The proposed schedule (Fig. 5-1) shows the pace of adding new capabilities to the research program throughout the five-year period. Most of the enhancements will be performed during the annual maintenance periods; however, the modification of the second beam line for co-counter injection beginning in FY23 will require a non-operating period longer than the typical periods described above. Fig. 5-1 shows the long torus opening (LTO 4) bridging FY23 and FY24. This will be modeled after the 2010/11 and 2018/19 schedules; a slightly shorter experimental schedule will be executed in FY23 and FY24 (12 weeks vs 16 weeks) before and after the LTO.

**Table 5-3.  
Major Hardware Upgrades**

<b>New Capability</b>	<b>Hardware Upgrades</b>	<b>Research Elements</b>	<b>Section</b>
Electron cyclotron (EC): Increase injected power from 2.8 MW to 8.5 MW  Improved EC launch efficiency	3–1.5 MW gyrotrons; Replacement 1 MW gyrotrons; High-voltage PS#5; 2 transmission lines, launcher Top-launch EC	$J(\rho)$ , NTM, $T_e \sim T_i$	5.3.1
Neutral beam (NB): Increase balanced power from 8 to 22 MW  Increase total power from 16 to 23 MW  Increase injected energy from 60 MJ to 180 MJ	Second co-counter beamline  Increase beam voltage to 93 kV  Improve power handling of internal beam collimators	$J(\rho)$ , energetic particles, toroidal/poloidal rotation; Long-pulse Advanced Tokamak (AT) High beta, low rotation studies	5.3.2  5.3.3  5.3.7.1
Reduced error field	30 deg TF feed modification	Low rotation physics	5.3.2.3
Improved divertor operation	Upper and lower small-angle slot pumped divertors	Detachment, divertor physics	5.3.4.1 5.3.4.2
More flexible control of 3D fields	12-element (1x12) in-vessel outer midplane coil (M-coil)	ELM control, heat and particle control	5.3.5
Improved operation of resonant magnetic perturbation (RMP) and multi-mode error correction	1 Power supply (16 kA, 500V) with 6 switching amplifiers ( $\pm 2.7$ kA, $\pm 450$ V)	Integrated scenario operation, 3D physics	5.3.6
180 MJ heat removal (75 MJ present)	Vessel armor upgrade – CFC tiles	Long-pulse AT	5.3.7.1
High-Z divertor	Tungsten tiles in divertor regions	High-Z divertor physics: source and transport	5.3.7.2
Improved Disruption Mitigation	Cryogenic shell pellet injector Room temp diamond shell pellets	Mitigation physics	5.3.8
Radio Frequency (rf): Higher efficiency current drive using Helicon rf power  Higher efficiency current drive using high-field-side Lower Hybrid	476 MHz, 1.0 MW Klystron, antenna, waveguide, HV supply,  4.6 GHz, 4 x 8 launcher on centerpost, waveguide, HV supply, water system	$J(\rho)$ , Long-pulse AT	5.3.9  5.3.10
Improved plasma stability	Conformal wall – 60° prototype (option)	Long-pulse AT	5.3.11

The proposed upgrades are described in the following sections.

### 5.3.1 EC System Power Upgrade

The research program for the next five-year period requires continued growth in gyrotron power and pulse length. The proposed hardware plan takes advantage of the worldwide progress in higher power gyrotrons and will increase the injected power from 2.8 MW to almost 9 MW. Pursuing the higher-power gyrotron is a more cost-effective path to higher system power than increasing the number of existing 1-MW gyrotron systems because it minimizes the need for additional HV power supplies, gyrotron sockets, transmission lines, launchers, and DIII-D ports. Using 1.5-MW higher efficiency gyrotrons, only one additional HV supply, two gyrotron sockets, two transmission lines, and one dual launcher are required.

Fig. 5-4 shows the plan for this five-year period to expand the EC system from the current eight-gyrotron EC system, which includes a 1.2-MW gyrotron that was made available to the DIII-D program by the National Aeronautics and Space Administration (NASA). One of the existing 1-MW gyrotrons (*aka* Han) recently suffered a vacuum failure, and the gyrotron from NASA replaced this failed gyrotron. The failed 1 MW gyrotron is being repaired and at the same time its collector is being upgraded to a CuCrZr collector, as on the 1.5-MW gyrotron, to improve the lifetime for cyclic thermal fatigue. This gyrotron should be ready to support operations early in the five-year period. Procurement of three 1-MW gyrotrons with upgraded collectors will begin in FY18 for operation in FY20 and FY21 to replace three existing 1-MW gyrotrons.

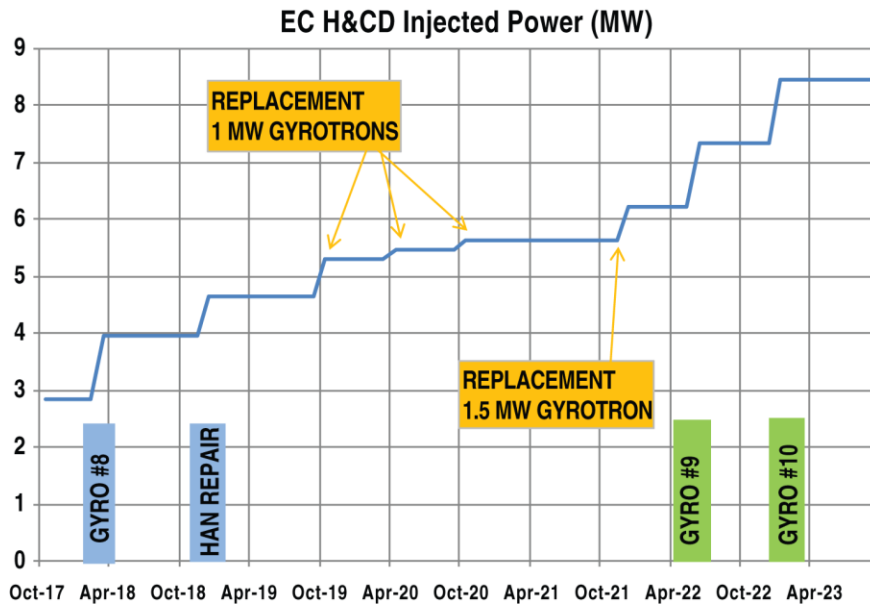


Fig. 5-4. Plan to increase the EC system power to almost 9 MW.

The first of the 1.5 MW tubes was delivered in mid-FY17 and two additional 1.5-MW gyrotrons will be procured in FY21 and FY22 after the first unit demonstrates good performance during the FY18 physics campaign. One additional 1.5 MW unit will be procured as a replacement,

as the 1 MW units are phased out. At the end of the five-year period, the system will consist of four 1 MW tubes, two 1.2 MW tubes, and four 1.5 MW tubes.

**5.3.1.1 Gyrotrons.** GA led the development of a higher power (1.5 MW), higher efficiency depressed collector gyrotron that is focused on the reliable support of physics. The first 1.5-MW gyrotron, gyrotron #8, was built and successfully tested at the factory, and is now being tested at GA (Fig. 5-5). Upon satisfactory demonstration of the gyrotron performance, two more 1.5-MW gyrotrons (#9, #10) will be procured. A cryogen-free superconducting magnet and its associated power supplies will be procured with each new gyrotron.

A failed 1-MW gyrotron is being repaired and should be ready to support operations early in the five-year period. Concurrent with the repair, the collector is being upgraded to a CuCrZr collector.

In this five-year period, the existing 1-MW gyrotrons will be replaced, some of which will be over 15 years old by 2018. Three new 1 MW gyrotrons with upgraded collectors will begin procurement in FY18 and FY19 and be ready for operation in FY20 and FY21. This is a lower cost option compared to procuring more replacement 1.5-MW depressed collector gyrotrons because the sockets do not have to be modified and the power supplies do not need to be upgraded as they would for the higher operating current of the 1.5-MW gyrotrons. To complete the replacement of the existing 1-MW gyrotrons, an additional 1.5-MW gyrotron will be procured late in this five-year period. Because the existing superconducting magnets are compatible with the 1.5-MW gyrotron, a new magnet need not be procured, and the power supply that will operate this gyrotron is already capable of higher operating current. The 1 MW gyrotron socket will be adapted for this depressed collector gyrotron.



*Fig. 5-5. The first 1.5 MW gyrotron was delivered and installed in its socket in mid FY17.*

**5.3.1.2 Sockets and Transmission Lines.** Each socket has an HV tank, water-cooling manifold, and a gyrotron instrumentation and control subsystem, all of which will be essentially copied from the existing DIII-D EC system. The instrumentation and controls for the test socket and two new gyrotron sockets will be located in the new building extension.

Two new transmission lines will be fabricated and installed to route the radio frequency (rf) power from the new gyrotrons to the fifth dual launcher to be installed on DIII-D. These lines will use the same components as the existing lines that are capable of safely transporting 1.5 MW.

**5.3.1.3 Water Upgrade.** The ECH high-pressure water cooling system will be expanded by adding two more high-pressure pumps to increase the total capacity of the system. The water cooling of the collectors of the new gyrotrons requires a higher inlet pressure and a boost pump per gyrotron will be installed as currently done for the two 1.2-MW and new 1.5-MW gyrotrons.

**5.3.1.4 Launcher.** A fifth dual launcher will be provided by PPPL and installed into its assigned port. This launcher will have the same functionality as the current launchers to remotely control the mirrors in order to vary the poloidal and toroidal injection angles of the rf beamline.

**5.3.1.5 Building Modification.** An extension to the North end of the building will be added to house the two new gyrotrons as well as a potential future gyrotron test socket, as shown in Fig. 5-6, on the second floor in the north ECH vault. The second floor will also house the instrumentation and controls for the new sockets in an expanded electronics room. The ground floor will have the enclosure for the modulator regulators of ECHPS#5 and house the boost pumps for the new gyrotrons.

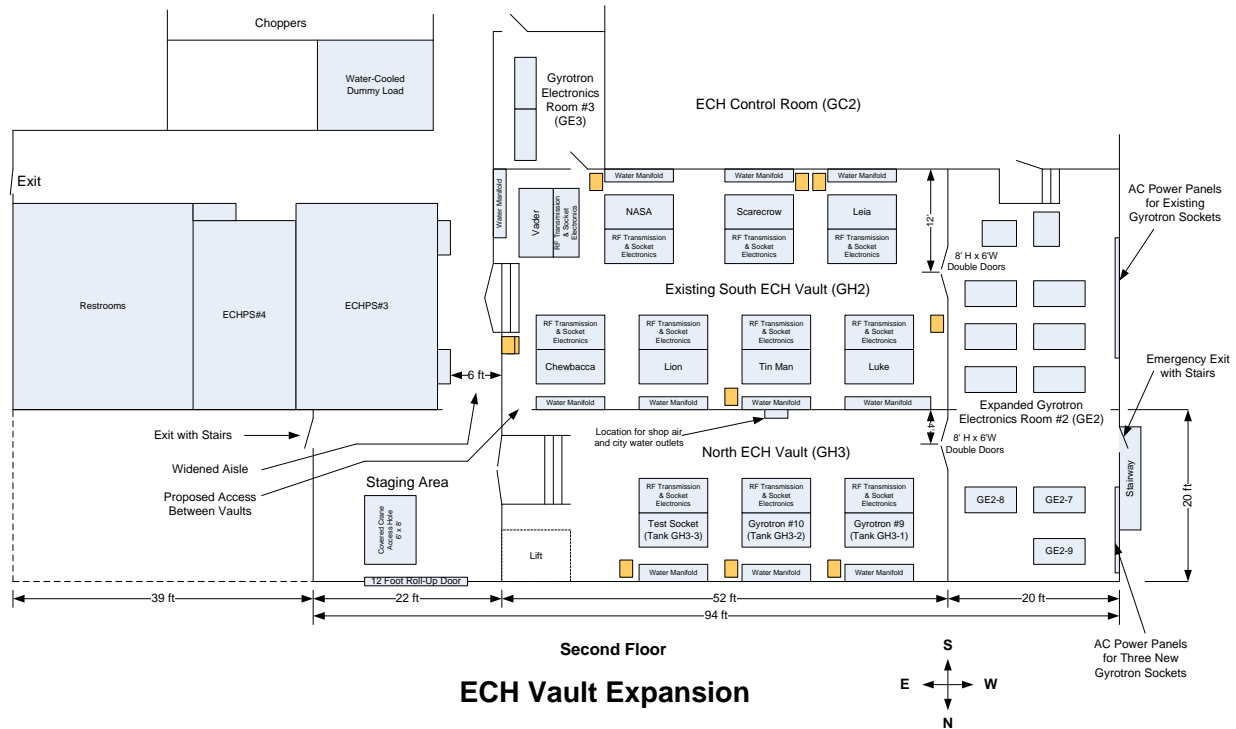


Fig. 5-6. Upgrading EC system towards 10 MW with only 10 gyrotrons. Only one additional power supply, ECPS#5 is required.

**5.3.1.6 ECHPS#5.** The current EC H&CD system has four EC power supplies, one of which has three tetrode-based 80 kV, 50 A modulator-regulators in it. A fifth EC power supply, which will have two modulator-regulators as in ECPS#4, will be built and installed in the ground floor of

the building extension. It will use one of the onsite neutral-beam power supplies obtained from the Lawrence Livermore National Laboratory (LLNL) Mirror Fusion Test Facility (MFTF) program for the HV dc input to the modulator regulators.

### 5.3.1.7 EC Top Launch

Recent projections (see Section 2.3.4) have shown that the EC current-drive efficiency can be significantly improved when the waves are launched directly above the plasma (top launch). The top-launch project is designed to demonstrate these projections compared to the traditional ECH launch scheme from above the midplane at the outer wall. As a first step, the angle of injection will be fixed in the toroidal direction, with a ~60 degree angle from vertical.

The first launcher will use access from an available upper port, coupled through an existing penetration in the upper divertor plate. The system will be able to carry up to 1 MW of power at either 110 or 117.5 GHz, with limited impact on other existing in-vessel components. The access port is adjacent to existing transmission lines that feed the outer-wall launcher. A microwave switch will be used to direct the power from either system, enabling a direct comparison between the two approaches and limiting the needs for a new transmission line to be installed. Fig. 5-7 shows a conceptual implementation of the approach in DIII-D, where the microwave power (shown in green) is directed from a corrugated waveguide to the mirror and then to the plasma.

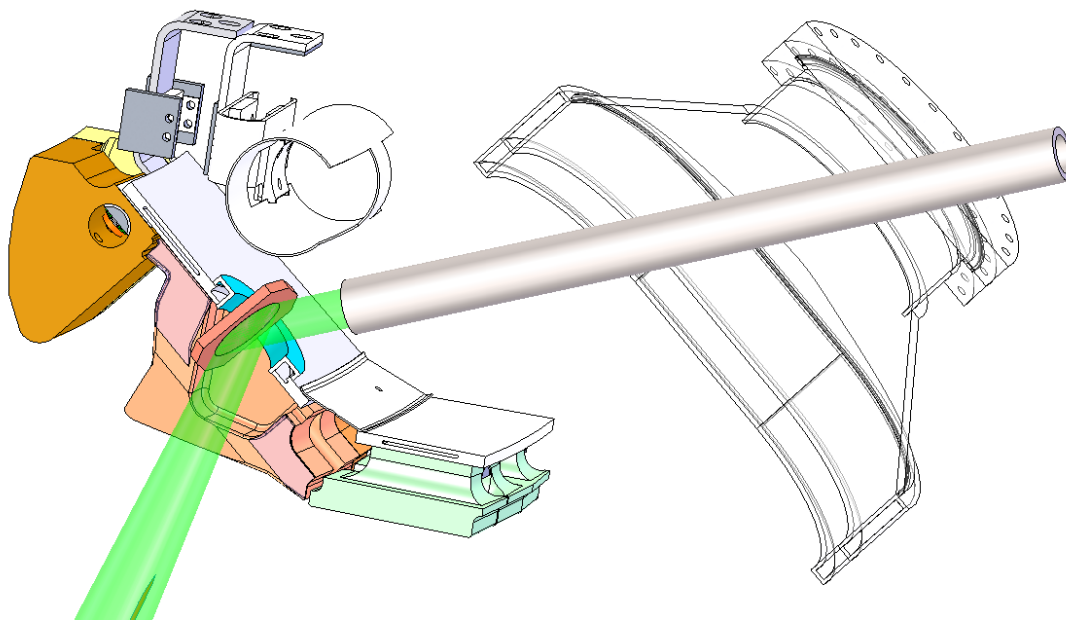


*Fig. 5-7. ECH top launch system conceptual design, located at the 300 degree upper port sector. The EC power is reflected by a fixed mirror through an existing penetration in the upper divertor.*

### 5.3.2 Co-Counter NB-30 Degrees (CCNB30)

The present neutral-beam system on DIII-D comprises four beamlines, specified by their toroidal location in degrees, each with two sources, left (L) and right (R). Three of the beamlines (NB30, NB330, and NB150) inject in the same direction as the normal plasma current, the “co-direction” ( $19.5^\circ \pm 4^\circ$  for the Left and Right sources relative to radial injection) and one beamline (NB210) injects in the counter direction. In FY18-19, this counter beam will be modified to be rotatable to either co- or counter-injection. With each beamline delivering approximately 4 MW (4 sec) and 3 N-m of torque at the nominal voltage of 75 kV, the new system will be capable of delivering from 16 MW of co-injected power to 4 MW of counter-injection and at the maximum power of 19 MW (3 sec), providing a net co-injection torque of 6-12 N-m. Balanced injection with zero injected torque can be provided but only with half of the total NB power. This limits the plasma pressure or beta that is achievable at low rotation, more ITER-like discharges. In order to provide the flexibility to study both high-rotation, high-beta advanced tokamak discharges and high-beta, low-rotation, more reactor-like discharges, NB30 will be modified to have the similar co-counter rotation ability as NB210. NB30 will remain horizontal, however, and inject *on axis*, but will be *rotatable* to allow operation in either the co- or counter-injection orientation. The modification is planned during a fourth Long Torus Opening (LTO4) scheduled for FY23-24.

#### 5.3.2.1 CCNB30 Beamline

The design for the NB30 co-/counter-injection beamline (CCNB30) will be similar in some aspects to the NB210 design, but will have many unique design features and challenges. The rotational rail system will be the same and the injection angles will be either  $+19.5^\circ$  or  $-19.5^\circ$  (relative to pure radial injection), similar to the 210 deg. beam. However, the rotational drive system and the beamline stand must be smaller than NB210 because the NB30 beamline is closer to the floor (the beam injects through the top part of the beamline instead of the bottom [see Fig. 5-8.]).

A major simplification is afforded by the fact that the NB210 beamline is permanently off-axis, while the NB30 beamline will be permanently on-axis, thus avoiding the need for hydraulic lifting pistons, etc. The two ion sources

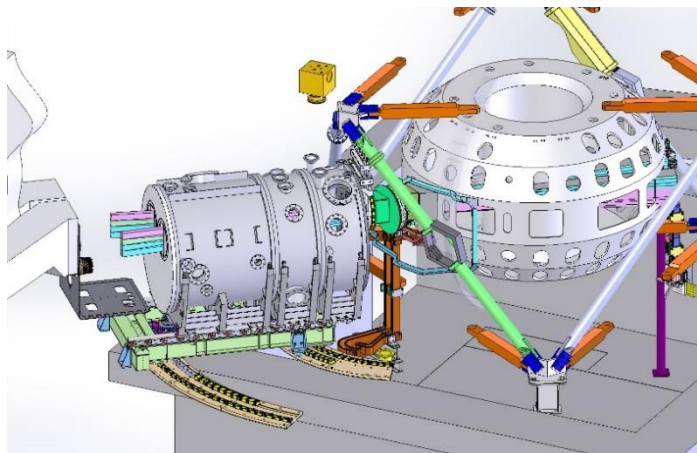


Fig. 5-8. 30 deg. co-/counter-injection beamline (CCNB30) design.

for NB30 will be full-aperture, normal focus sources. Some of the most significant engineering issues for co-counter NB30 system include:

- Beamline moving and support structures, including the rotation-control system.
- Lower profile beamline stand to fit on rotation carriage structure.
- Relocation of interfering poloidal field coil power cables running under the existing beamline stand.
- Relocation and/or redesign of affected tokamak diagnostic systems and in particular, diagnostics using NB30 beam paths through plasma (MSE, CER, etc.)
- Support of the front part of the beamline over the lower pit; relocation or accommodation of existing items in the lower pit, such as buswork feeding toroidal field coil.
- Design new beamline flexible connections as necessary, including ion source transmission lines, cryo lines, vacuum pipes, water-cooling lines, and gas feeds.
- Vessel interface – fabricate new drift duct, bellows assembly, and co- and counter-adaptors.
- Fabricate replacement internal beamline components, including collimators, bending magnet pole shields, and calorimeters, to accommodate longer pulse and higher energy beam (unchanged from 210 design)
- Appropriate in-vessel modifications – install pyrometers and armor tiles instrumented with thermocouples for shine-through protection.

### 5.3.2.2 CCNB30 Diagnostics

With the upgrade planned for the 30NB, two important diagnostics will require modifications and enhancements. Presently, the main parts of the CER and MSE systems are using the NB30L beam. When the beam will be in the counter position, CER measurements in the core of the plasma will not be directly accessible. In order to retain this essential diagnostic, the viewing chords will be moved to the stationary NB330 beam. The new system will be installed at a nearby midplane port, essentially flipping the view from 30NB to 330NB.

The MSE system will be relocated at the 255 midplane port, offering an optimized view of the 330NB. A new vacuum interface will be required, but this will also offer an opportunity to implement the promising technique of Imaging MSE (see section 6.1). The imaging approach will be tested prior to the work on the 30NB. This will enable optimizing the approach between the standard polarization measurement or imaging techniques.

This task also includes resolving some minor impacts on other diagnostics that will be encountered on the project near or at the 30° location.

### 5.3.2.3 Reduced Error Field from TF Feed Point

Magnetic error fields can negatively impact plasma performance by reducing confinement, slowing plasma rotation, destabilizing the plasma, and restricting low-density operation. On DIII-D the primary sources of error fields are due to non-axisymmetries in F7A and F6A field shaping coils and the 30° TF current feed point, one of the two TF-current feed points. The planned modification of the 30° beamline described above requires its removal from the machine hall and this provides access to the feed point and the opportunity to modify the feed point conductors and significantly reduce the associated error field.

The TF feed point at 210° was redesigned during 2005–2006 and reduced the error field by a factor of ten (Fig. 5-9). This has brought significant benefits to the research program: the region of stable low-density operation without locked modes was extended from  $n_L = 1.2$  to  $0.85 \cdot 10^{19} \text{ m}^{-3}$ , a 30% reduction, and a reduction of external torque has enabled steady plasma rotation at low torque input and, thus, low velocity. A similar amplitude field error remains at the 30° TF feed point. Unlike other sources of error fields from the F and TF coils, the feed point is spatially localized, and so it has a slowly decaying spectrum of higher- $n$  Fourier harmonics. If the TF-coil 30° feed error was reduced several-fold, then the remaining DIII-D intrinsic error would be predominantly  $n=1$  and  $n=2$  from coil alignment and spacing errors. Such an intrinsic error is amenable to good correction by the C-coil alone.

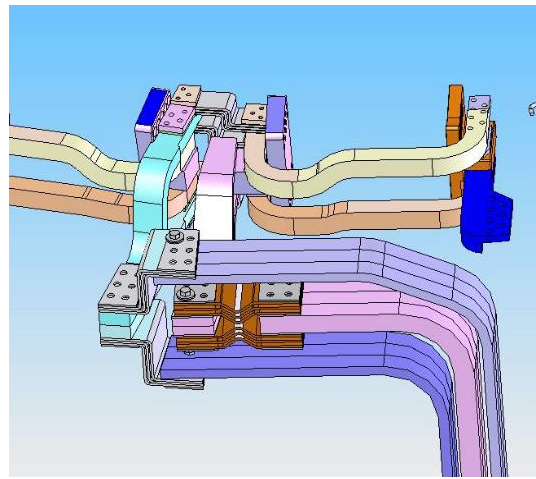


*Fig. 5-9. Modified TF feedpoint at 210 deg. reduced magnetic error field by a factor of 10.*

Analysis shows that a relatively simple modification to the buswork can provide significant error-field reduction. The conductors in the vertical section of the buswork are spaced widely apart in a dipole configuration that contributes approximately half of the error field from the feed. This section is amenable to correction by redesigning the buswork with reduced spacing between conductors and changing from a dipole to a quadrupole configuration. The lower section of the feed consists of elaborate buswork that extends from the vertical conductor to the output of the TF-supply coax, and this contributes the other half of the error field. This section is not amenable to any simple realignment of conductors, but the possibility that it may be correctable using a bucking coil is being explored.

### 5.3.3 Raise NBI Energy (Power Increase and Pulse Extension)

DIII-D continues to expand the boundaries of research into high-beta, advanced tokamak plasma physics regimes and continuing that trend is aided significantly by increasing the capabilities of the neutral-beam heating system. To accomplish this, the neutral-beam power and the pulse lengths will be increased from the current levels of 75 kV, 4 sec to higher levels of 93 kV, 6 sec. The desired outcome is an increase in the energy delivered from all types of beam-heating systems with different geometries, including co-injection, counter-injection, on-axis, and off-axis beams. The modifications of the NB210 and NB30 beamlines planned for the next two LTOs provide the capability to inject several beams with a selectable combination of those geometries. Increasing the energy of those beams, however, requires the upgrade of several subsystems. The design of the upgraded components for the internal beamline components and the ion source modification required for higher energy throughput have been completed and implemented on some of the beamlines already. Required changes for any beamline to reliably achieve 93 kV, 6 second operation include:

- Internal beamline components – beam collimators, bending magnet pole shields, and beam dump calorimeters must be upgraded to handle higher energy. New designs have been created for all needed components and some systems have already deployed upgraded components (150 collimators installed and 330 pole shields installed)
- Ion sources – in order to maximize pole shield lifetime, some ion sources were modified in the past to become Reduced Aperture Masking Plate (RAMP) sources (10 cm vs 12 cm width); however, this resulted in a reduction in beam power. With the successful redesign of pole shields for both higher power and pulse length in 2015, these ion sources can be “un-RAMPed,” thus increasing the output power (30L and 330L and R sources have already been un-RAMPed; NB150 geometry is not compatible with full aperture sources).
- High-voltage equipment – to obtain reliable operation at higher voltages, a number of changes are required:
  - Improve DC voltage regulation to obtain better control of the overhead voltage on the tetrode-based control system to prevent overdissipation and breakdown across the tetrode.
  - Upgrade the tetrode bias voltages regulation to more precisely regulate the gain.
  - Upgrade the isolation for the arc power supplies for the UVC systems (30, 330). The Transrex systems (210, 150) have sufficient isolation.
  - Improve voltage isolation between the HV cables and source housing (210 to be upgraded in LTO3).

The schedule to complete the necessary upgrades to beamline internal components and ion sources is shown schematically in Fig. 5-10. The first beamline to be completely upgraded will be the NB210 system during the upcoming LTO3 (FY18-19). The required HV system upgrades will be the pacing item for the 210 system in order to provide time for design and testing of the new controls. The HV upgrades on the remaining system will be scheduled to match the beamline upgrades, resulting in a steadily increasing power from 16 MW up to 23 MW, accompanied by increases in pulse length.

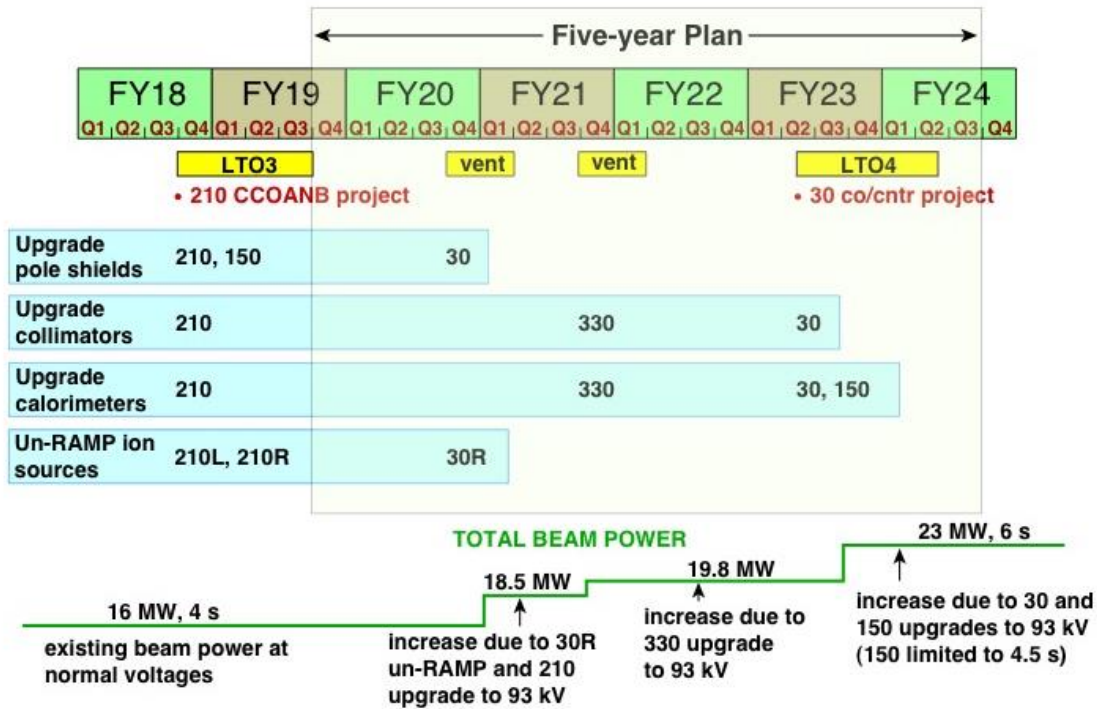


Fig. 5-10. Upgrade plan for the beamline internal components and ion sources.

### 5.3.4 Divertor Upgrade

#### 5.3.4.1 Upper Small-Angle Slot (SAS-2U) Divertor

The configuration flexibility of the DIII-D tokamak provides a unique opportunity to explore and quantify key divertor design parameters controlling divertor detachment and energy dissipation and to validate models for extrapolation to reactor conditions. In early FY17, an unpumped small-angle slot (SAS-1U) divertor was installed in the upper divertor region on the outboard side of the existing water-cooled divertor structure. This enabled a test of the SAS concept without impacting the performance of the pumped upper divertors. Based on the success of the SAS-1U divertor, the upper main divertor will be converted into a pumped-SAS in 2020 to improve control of plasma density and impurities via pumping and gas injection into the slot, and to examine compatibility with high-performance plasma scenarios.

This SAS-2U will incorporate a small-angle slot located on the current DIII-D ceiling tile and will incorporate new tile geometries to seven other upper toroidal tile rows (Fig. 5-11). Four new water-cooled panels will be designed and installed to support the new tile rows. These cooled panels and tiles will be designed to enable the SAS-2U to be ready to adequately manage the planned enhanced thermal input capability of DIII-D (30 MW for 6 sec, see Section 5.3.7.1). The major change to the panels will be increased water flow achieved using multiple in-vessel water circuits for each toroidal ring. The position of the SAS-2U slot will also allow for particle control via cryo-pumping.

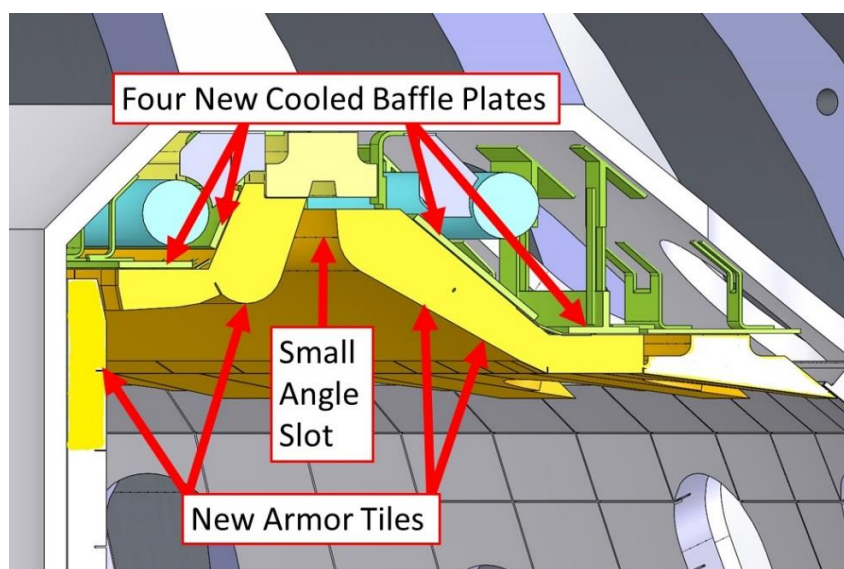


*Fig. 5-11. New tile geometries will be incorporated to upper toroidal tile rows to provide a small-angle slot with a pumping aperture. The existing cryopumps (blue) will remain unchanged.*

#### 5.3.4.2 Lower Small-Angle Slot (SAS-2L) Divertor

In FY22-23, based on model optimization and the SAS-2U experiments with enhanced diagnostics in the slot, the lower divertor will be upgraded for use with advanced tokamaks for core-edge integration with a double null SAS. This SAS-2L will incorporate a small-angle slot located in the region of the current outer floor tile and will also incorporate a new inner floor water-cooled panel structure (Fig. 5-12). Pumping capability will be maintained using the outer cryopump. Tile geometries/materials for five lower toroidal tile rows will be modified to maximize thermal performance and to allow for the SAS-2L to be ready to adequately manage the planned enhanced thermal input capability of DIII-D.

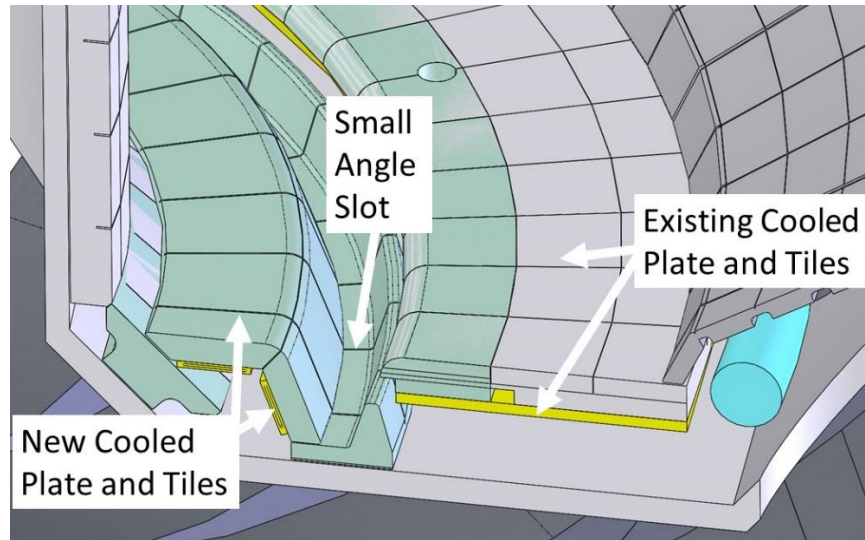


*Fig. 5-12. The lower SAS-II will incorporate a small-angle slot on the current outer floor tile and a new inner floor cooled panel structure.*

## SAS-2 Upper and Lower Diagnostic Impact

Both SAS-2U and -2L divertors will be equipped with a comprehensive set of diagnostics needed to understand the physical mechanisms at play. Presently, both upper and lower divertors are well covered with an existing set of measurements, both at the first wall and in the plasma found at the boundary. Many of these diagnostics will be relocated and refurbished with the implementation of the SAS-2U, L divertors.

In both implementations, the magnetic probes will be relocated, first to allow for the new geometry, and new probes will be added as needed to fine tune the equilibrium reconstructions required for target control. Langmuir probes will be installed, drawing from the extensive set already in place. Fast thermocouples, including recently developed surface-eroding thermocouples (see section 6) will be reinstalled at key locations. Filterscope, spectrometer and divertor bolometer viewing chords will be adjusted and augmented as needed. Other new measurements, such as neutral density, ion temperature, and extended divertor Thomson scattering will be added in parallel with the changes to the divertor geometry.

### 5.3.5 Advanced 3D Coils

#### 5.3.5.1 Advanced 3D Coils

A new in-vessel non-axisymmetric coil array is proposed to augment the existing DIII-D capability to study 3D physics. Presently, the C-coils (6 external coils on the vessel midplane) and the I-coils (2x6 array of in-vessel coils above and below the midplane) are used for correction or enhancement of magnetic error fields, feedback stabilization of the Resistive Wall Mode (RWM), and the creation of a Resonant Magnetic Perturbation (RMP) for ELM stabilization.

A midplane coil, the M-coil, (1x12 array of in-vessel coils on the outer midplane) is proposed to improve the effectiveness of controlling ELMs, error fields, and the rotation profile, while maintaining the ability to perform RWM stabilization and error field correction with the existing coil arrays (Fig. 5-13). Key design goals include the ability to create field configurations of  $n=1-6$ , control of poloidal mode spectrum for  $n=1-3$ , and rigid rotation capability for  $n=1-4$  structures.

The proposed coils will have four turns with a current/turn of 2.7 kA. Compared to the I-coils, the value of the product NAI (turns x area x current/turn) is ~20% higher for this new coil set. The increase in the turns and reduction in the current/turn matches the power supply capability while still keeping the coil inductance below the external cabling inductance. Existing R&D has provided confidence that these coils can be wound in-vessel with minimal in-vessel joints. This fabrication method will result in a design that is significantly more robust, less costly, and faster to install than the existing I-coils. Work has begun with a vendor on the development of an in-vessel winding tool. The cabling for the coils will be fabricated by swaging stainless steel tubing over MgO onto water-cooled copper tubing. Preliminary layout studies have indicated that the 12 coils can be designed and located to have uniform areas to better than 0.01%. A new patch panel, cables, interlocks, data acquisition and control, water-cooling, and armor tiles are required. To make room for the 2 x 2 cable pack, the armor tiles will need to be re-designed for the outer midplane (R0 plane) of the vessel. The M-coil is scheduled for installation in the FY21/22 vessel entry and will be ready for the FY22 campaign. The new power supply described in Section 5.3.6 will be installed in the prior year and will allow for the full utilization of the new M-coils.

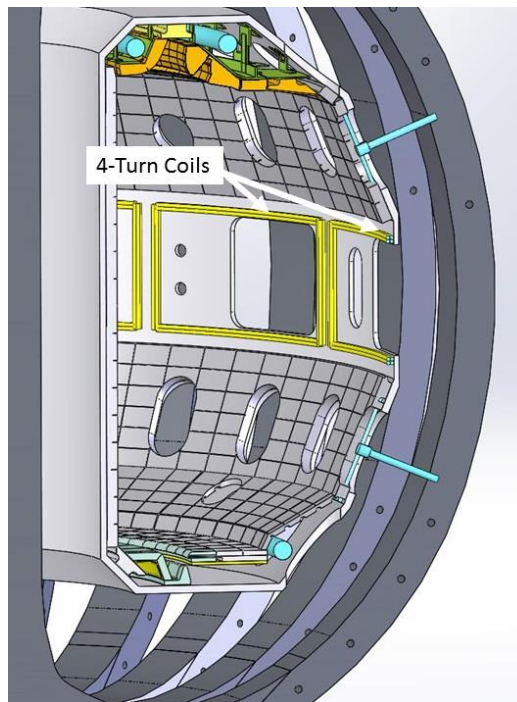


*Fig. 5-13. A midplane coil, the M-coil, (1x12 array of in-vessel coils on the outer midplane) is proposed.*

The M-coil is scheduled for installation in the FY21/22 vessel entry and will be ready for the FY22 campaign. The new power supply described in Section 5.3.6 will be installed in the prior year and will allow for the full utilization of the new M-coils.

### 5.3.5.2 Advanced 3D-Coil Diagnostics

The implementation of the M-coils will be accompanied by a significant upgrade of the magnetics diagnostics. The scope of this upgrade is similar to the one completed in 2013. That task, so-called 3D magnetics, saw an increase in magnetic probes (>100), with a focus on high-field-side measurements. With the M-coils, another set of probes would be added (~100), that

would enable measurements of  $n \leq 6$  to be performed. These probes will necessitate additional integrators and digitizers. However, the design of the new probes has been previously completed (see section 6.2) and only minor modifications are envisioned, mostly to fit specific locations.

This task also includes some minor modifications to other diagnostics that will be displaced or directly impacted, especially by the planned additions of the current feeds for the M-coils themselves.

### 5.3.6 Power Supplies for 3D Coils and PF Shaping Coils

On DIII-D, the existing 3D coils (2x6 I-coil and 1x6 C-coil) are used for a variety of applications including error field correction, stabilization of resistive wall modes, ELM stabilization using  $n=2$  and  $n=3$  RMPs, and magnetic braking experiments. The proposed M-coil upgrade would significantly enhance the ability to create different mode structures, and in particular, it would enable studying configurations up to  $n=6$  with the ability to rotate both  $n=2$  and  $n=3$  structures. This extensive set of applications for our 3D coils requires a highly flexible set of power supplies and patch panels, since practical budgets do not permit having dedicated full-current, 4-quadrant power supplies on each of the 30 3D coils (18 existing coils + 12 proposed M-coils). However, both the existing 3D coil arrays and the new coil array would benefit from an expanded set of power supplies with similar operational characteristics to the existing dc-supply and inverter combination, but with higher operating voltage and current. In addition, similar supplies would enhance the capability of our PF-coil shaping system by providing sufficient power to control all 18 coils rather than the 14 coils typically controlled for a double null configuration. We propose to augment the recently installed Super SPA (4-quadrant switching supply) with an additional supply of the same type and manufacturer.

Table 5-4 summarizes the specifications of both the existing and proposed supplies.

**Table 5-4.**  
**Specifications of Both the Existing and Proposed Supplies**

<b>Name</b>	<b>Status</b>	<b>Quantity</b>	<b>Type</b>	<b>Current, Voltage</b>
C Supply	Existing	5	dc	7 kA, 350 V
SPA	Existing	4	4-Quadrant switching amplifier	$\pm 4.5$ kA, $\pm 300$ V
	Existing	12	Sub-SPA mode (3 per SPA)	$\pm 1.5$ kA, $\pm 300$ V
Super SPA#1	Existing	1	4-Quadrant switching IGBT	$\pm 16$ kA, $\pm 450$ V
		6	Sub-SPA mode (6 per SSPA)	$\pm 2.6$ kA, $\pm 450$ V
Super SPA#2	Proposed	1	4-Quadrant switching IGBT	$\pm 16$ kA, $\pm 450$ V
		6	Sub-SPA mode (6 per SSPA)	$\pm 2.6$ kA, $\pm 450$ V

The first of these Super SPAs (4-quadrant switching power supplies) was provided by ASIPP and has already been installed and supported the FY17 physics campaign. Each of the Super SPAs can be operated as six independent modules of  $\pm 2.6$  kA,  $\pm 450$  V capability or with subsets of the modules in parallel up to a total of 16 kA for the full Super SPA. We propose to augment this supply with an additional supply of the same type and manufacturer to be operational for the FY21 campaign. With the addition of a second Super SPA, the number of independently controllable coils at the 2.6 kA level will increase from the current 10 to 16 in FY21 and beyond.

The new supply will get its ac power from a dedicated feed off of the Motor Generator #2 (MG2) distribution bus after being stepped down from the 13.8 kV (nominal MG2 output voltage) to the supply's 480 Vac. The step-down transformer (supplied by ASIPP) has already been installed but the switchgear and cabling support need to be added. The feed to the transformer will incorporate a line reactor and fused disconnects for system protection and personnel safety. The existing MG2 distribution bussing has already been extended as part of the infrastructure improvement needed for the first Super SPA. In addition, the second power supply will require a building modification and expansion to be built by GA, and will be available by 4<sup>th</sup> quarter of FY20. In summary, the new equipment required includes:

- Switchgear
- Cabling support
- Line reactor
- Fused disconnects
- Patch panel expansion
- Building modification

### **5.3.7 First Wall/Divertor**

#### **5.3.7.1 Thermal Upgrade**

As the DIII-D research program pushes to higher beta, longer pulses, and fully integrated core/divertor solutions, it is necessary to upgrade the divertor and first wall to handle both higher peak power (30 MW) and total energy (180 MJ) consistent with full-power pulses for six seconds. This thermal upgrade will be done in stages that are consistent with the proposed increase in power and pulse length (Section 5.3.3) and divertor upgrades (Section 5.3.4). The lower divertor region will be ready for the increased power levels at the beginning of the five-year plan. The upper divertor region will be ready for the increased power levels at the end of the SAS-2U upgrade at the end of 2020. The centerpost region will be ready for the increased power levels after the completion of centerpost thermal upgrade at the end of 2021.

The engineering requirements assume an energy deposition pattern based on 30% radiation of the input power, with the remaining 70% conducted to the first wall, typically the divertor region. The conducted power is assumed to be distributed 60%/40% to the outer/inner strike points for single-null plasmas and 90%/10% to the outer/inner strike points for double-null plasmas, with a 20% up/down asymmetry assumed for the double-null configurations. The power deposited on the tiles is assumed to be a triangular deposition over the full height of the tile. The majority of the approximately 3,000 tiles on the inner and outer walls will still be acceptable and will remain ATJ™. At the strike point areas, thermal analysis shows that at higher energy loadings, the existing design ATJ™ tiles have limitations based on peak surface temperatures and thermally induced stresses. To avoid these limits, improvements will be required in plasma-facing tile thermal conductivity and material tensile strength. It is expected that carbon-carbon (C-C) composite materials will be required in the high heat flux areas and new tile designs may be required in the highest heat flux areas. The basic water-cooling system for the DIII-D vessel and the lower divertor shelf is adequate to remove 180 MJ between shots. However, the upper divertor cooling water flow is significantly lower than the flow in the lower divertor or vessel walls and modifications to the flow circuits are required in order to avoid boiling the cooling water. The cooling flow to the upper divertors will be improved when the SAS-2U is installed in 2020. The centerpost tiles presently have flat surfaces and will be contoured to match the field lines to decrease the edge erosion and symmetrize the heat flux to the centerpost.

### 5.3.7.2 High Z

The scope of this subtask is to provide high-Z material targets into the existing (Phase 1) and future (Phase 2) upper divertor geometry, facilitating study of high-Z material interaction and performance. The high-Z material is planned to be tungsten-coated TZM inserts in graphite tiles. This work is very similar to the high-Z campaign that was successfully completed by DIII-D in 2016 during which two rows of tungsten coated TZM were inserted into the lower divertor graphite tiles. This subtask is divided into two phases. Phase 1 consists of two toroidal rows of inserts in the existing SAS-1 region to be tested in 2020. Phase 2 will consist of six toroidal rows of inserts in the planned SAS-2U region to be tested in 2022. Coating of the TZM using different isotopes of tungsten will be employed to enable localization of the tungsten sources. For the 2016 high-Z campaign, the TZM inserts were coated using two different methods: chemical vapor deposition (CVD) was used for coating with natural tungsten and e-beam evaporative coating was developed and used by ORNL for the W-182 isotope. Tests of ion deposition directly onto the graphite tiles were conducted showing the latter to be a very robust coating and may be used instead of the CVD-coated inserts for the locations where natural tungsten is desired and the inserts might pose

structural problems. The e-beam method will again be used for the pure isotope coating because it uses very little tungsten compared to the other methods.

An option is also proposed to design, fabricate and install a heated ( $\leq 600^\circ\text{C}$ ), full tungsten target upper Small-angle Slot divertor. The heated surface would prevent carbon deposition and provide a clean environment in which to study the metal SAS performance.

### **5.3.7.3 Silicon Carbide Belt Limiter**

An option is proposed to design, fabricate, and install four toroidal rows of SiC belt-limiters to decrease the overall wall carbon source, substituting silicon for carbon. This option would include two rows of SiC-coated graphite tiles in the upper and lower divertor regions and two additional rows just above and below the outer midplane.

### **5.3.8 Fueling and Disruption Mitigators**

The DIII-D disruption mitigation program will be focused on developing new approaches for the study and remediation of runaway electron (RE) generation and dissipation. A new tangential EUV camera (see Section 6.2) will aim to image the formation of RE seed. On the mitigation side, a new technique will be developed that consists of a cryogenic shell pellet injector that will launch cold metallic shells filled with impurity “dust.” These pellets are expected to have improved penetration and deliver their payloads closer to the core of the discharge. Room-temperature shell pellet injection, using specially designed diamond shells, will be compared to the cryogenic counter-parts. Modifications to the existing shattered pellet injector are planned, in order to optimize the shattering mechanism.

### **5.3.9 Helicon Current Drive**

The use of Helicons (also known as “whistlers” or very high harmonic fast waves) has been proposed as a high-efficiency method of driving off-axis current drive in future devices such as the Fusion Nuclear Science Facility (FNSF) or demonstration power plant (DEMO). The high electron beta in DIII-D AT discharges provides an excellent platform to test this proposal. The proposed system will utilize a 1.2 MW 476 MHz klystron which is available for transfer from the Stanford Linear Accelerator (SLAC) to DIII-D. A klystron high-voltage power supply (HVPS), circulator, and associated klystron hardware will also be transferred to DIII-D from SLAC.

A low-power helicon traveling wave antenna was installed in DIII-D (see Fig. 5-14) in FY16 and successfully tested. The design of the high-power system is underway; a single prototype high-power module of the antenna was assembled and tuned (see Fig. 5-15), achieving the proper resonant RF frequency with low loss.

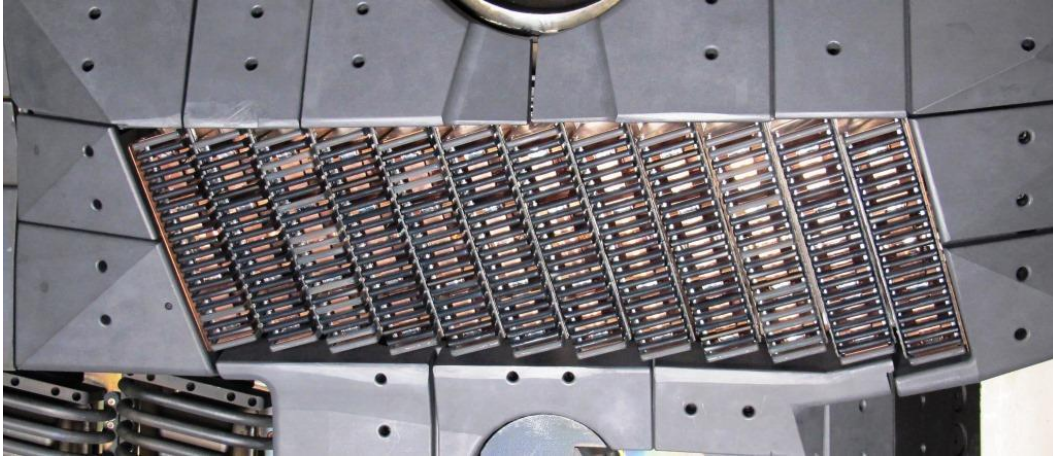


*Fig. 5-14. Photograph of low-power Helicon antenna installed in DIII-D. The 12-module antenna was located above the midplane and was positioned 1 mm behind the surrounding graphite tiles.*

By the end of the 2014-2018 five-year plan, the design and fabrication of the in-vessel RF system will be completed and installed during LTO3. The designs of the klystron system, RF transmission system, and the concrete pad for high-voltage power supply will be completed, with procurements and fabrication underway. The Work for Others Agreement (WFOA) between SLAC and GA will be in place for preparing the klystron system for shipment to DIII-D and providing support during the installation, check-out, and start-up of the system at DIII-D. The klystron system will have been delivered to DIII-D prior to the end of the current five-year plan, but no installation or testing will be performed.

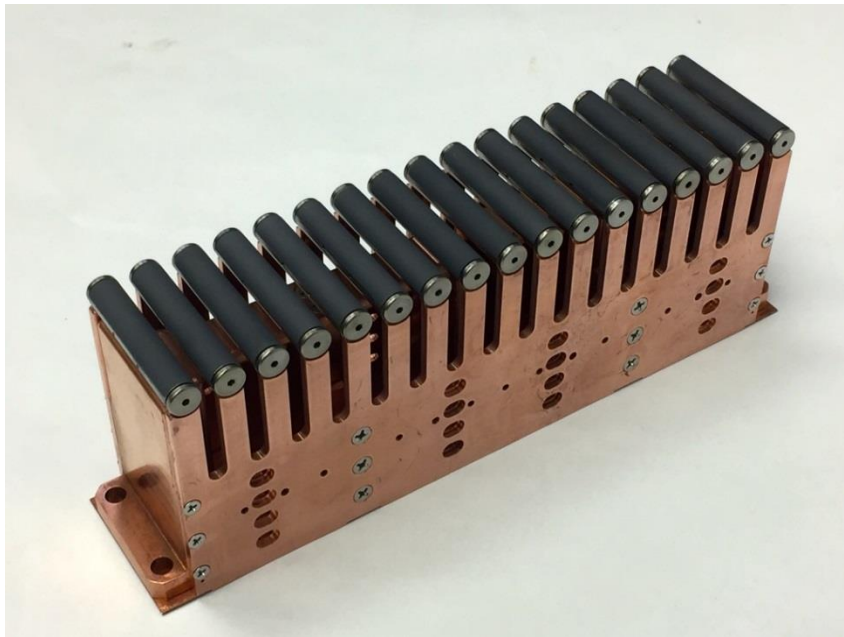


*Fig. 5-15. Brazed prototype high-power Helicon antenna module. The darker rods on the top of the module are boron carbide coated TZM Molybdenum Faraday shields. The high power will consist of 30 modules.*

In the new five-year plan, all remaining ex-vessel work on the project will be performed. The klystron system will be installed and the ex-vessel RF transmission system will be routed from the klystron to the DIII-D vessel and connected to the feeds of the antenna. The klystron HVPS will be connected to the site 12.47 kVAC primary power and the output high-voltage coaxial cable and the control cables will be routed to the klystron system in the DIII-D building. The Helicon system will be checked out and then started up with RF power.

### **5.3.10 High-Field-Side Lower Hybrid**

The proposed Lower Hybrid launcher drives plasma current from the high-field side, providing a higher proportion of current drive per megawatt input than coupling from the low-field side. The operating frequency is 4.6 GHz and is driven by (8) 250 kW klystrons that are coupled in parallel driving a phased-array waveguide launcher for 1 MW launched power. The launcher is located on the centerpost in DIII-D just below mid-plane. The system installation at DIII-D is split between MIT, providing the system components previously used on C-MOD, and GA, providing the facility installation interfaces and accommodations. There are two phases of installation: 1 MW through the 0° R-1 port and 1 MW through 30° R-2. Highlights of the first system are presented below followed by a list outlining institutional responsibilities.

#### **5.3.10.1 Launcher**

The 4 row by 8 channel launcher is mounted to the vessel wall nominally 2 mm behind the surrounding protective tiles. They are driven by eight waveguides that are routed beneath the wall tiles, from the launcher to the 0° R-1 vessel port. The protective tiles on the centerpost will need to be raised approximately 1 in. and thinned to accommodate the nominally 2-in. waveguide underneath and require water cooling to prevent thermal ratcheting (Fig. 5-16). Similarly, the design of the floor tiles will need to be modified to accommodate the routing of the waveguide from the ports on the outer wall to the centerpost. The waveguides on the floor and the lower section of the centerpost will be rotated so that their height off the floor and/or wall is less than the section near the launcher. This will reduce the impact on the floor tiles and should allow the limiting floor surface to remain at the same height off the vessel wall and not affect the space available for the plasma. An experiment is planned in mid-FY18 to evaluate whether the close proximity of the copper launcher assembly on the centerpost has any detrimental effect on plasma performance and to determine the heat load on the proposed launcher structure.

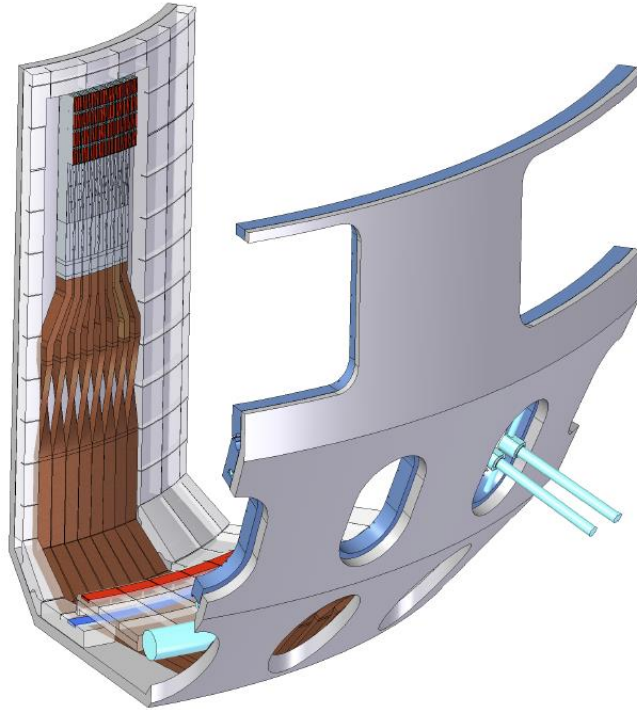


*Fig. 5-16. Inside Launcher mounted on the centerpost below vessel midplane. The waveguide is fed from a 0°R-1 port and the “twist” from lower to higher profile of the rectangular waveguide is located on the lower centerpost.*

### 5.3.10.2 Transmission Line and Klystrons

The ex-vessel transmission line will connect the klystrons that are located in the old ECH vault. This area is presently filled with the Fast Wave antenna tuning elements. The tuners will have to be removed and the vault cleared to attain the shortest line to the vessel to minimize losses. The klystrons require: water cooling, 3-phase AC power, gaseous nitrogen for the waveguides, and a high-voltage feed (50 kV).

### 5.3.10.3 Water System

The water feed for the klystrons is already routed to the north wall of the old ECH vault. The water will be fed from a new pad that will be located on the west side of Building 34, adjacent to existing pump skids that provide low-pressure water cooling. An expansion of the pad is required along with new pumps, tanks, resin beds, and controls. The new system will use existing headers to connect the pump skid to the ECH vault.

### 5.3.10.4 High-Voltage Power Supply

The 50-kV DC high-voltage feed will originate in the existing RF (ABB) power yard. The high-voltage DC power supply will be provided by MIT and will use the 3-phase 12.47 kV power that presently feeds the ABB units.

As noted above, this project will be led by MIT with joint engineering efforts by MIT and GA. The major institutional responsibilities are shown below:

## GA

- Vessel tiles (floor, centerpost)
- Vessel feedthrough for waveguides (port modification, in-vessel support)
- Water cooling pad (pumps, tank, ac power, resin beds, piping)
- HV cabling (50 kV cables, 480 Vac)
- DC power supply site, prep (6 MW breakers, cabling, concrete pad).

## MIT

- High-voltage (50 kV) power supply
- Eight klystrons (phase 1) and eight klystrons (phase 2)
- Controls for klystrons
- Waveguide transmission line from klystrons to vessel
- All in-vessel hardware associated with transmission line installation.

### 5.3.11 Conformal Wall

A close fitting, conformal conducting surface is a key tool for providing stable access to fully non-inductive conditions at high plasma pressure. With the addition of divertor hardware in both the upper and lower regions of the DIII-D vessel, the stabilizing impact of the DIII-D conducting wall has been reduced. Even with limited poloidal extent, a closer fitting conducting wall on the low-field side of the vessel would provide an important margin of stability at high plasma beta (more detail is in Sec. 2.1.2). A more conformal, conducting surface is proposed as an option to be installed inside the DIII-D vessel on the R+1 and R-1 planes as represented in the Fig. 5-17.

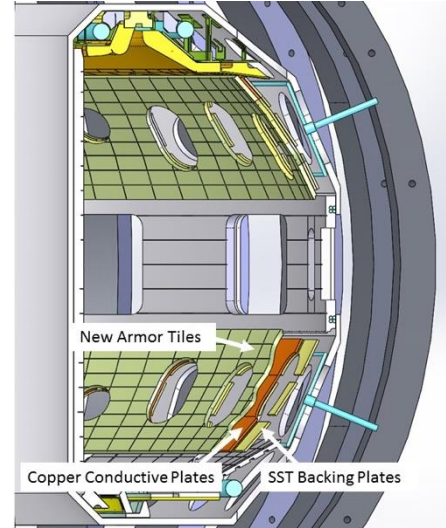


*Fig. 5-17. Construction and installation of a more conformal, conducting surface inside the DIII-D vessel on the R+1 and R-1 planes is proposed.*

The central element of this project is the design and fabrication of two toroidal rows of copper plates that are shaped to provide a conformal conducting surface close to the low-field side plasma boundary. As presently modeled, the copper plates would have three poloidal facets in order to better conform to the outer plasma boundary. In order to allow for installation in the vessel, the plates would be built in toroidal

sections of between  $15^\circ$  and  $60^\circ$  mounted on water-cooled stainless-steel structures that are attached to the vessel walls. The tiles currently in place on the R+1 and R-1 surfaces would be removed and replaced with lower profile graphite tiles to shield the copper plates while allowing the plasma a closer approach to the conducting copper structure. To minimize the impact of the conformal wall on the remaining in-vessel hardware, the extent of the plates is limited from the top (bottom) of the R0 plane to the bottom (top) of the R+2 (R-2) plane and would interface smoothly with the new divertor hardware that is proposed in this plan.

The full project is envisioned as a three-year effort, proposed as an option starting in FY21-22. In Year 1 of the project, a prototype  $60^\circ$  sector would be designed and built consisting of the SS backing plate, conducting copper plates and armor tiles. The purpose of this prototype is to evaluate fabrication methods. In Year 2 (FY22-23), the detailed design of the full set of plates would be performed, including the significant impacts that such a close-fitting wall would have on diagnostic views. Fabrication and installation would be performed in Year 3 (full installation during the FY-23-24 Long Torus Opening).



## 6. DIAGNOSTICS – PLASMA MEASUREMENTS

Diagnostic measurements are the key enabler of progress in scientific understanding and plasma control, as recognized in the Plasma 2010 report for the National Research Council (NRC):

***“The required progress in [...] key areas will not be possible without significant expansion of our plasma diagnostic capabilities. Quite simply, we cannot understand what we cannot measure.”***

The Plasma 2010 panel recommends in their report that a new initiative in diagnostic development be formulated at the DOE-OFES level. That recommendation was echoed in the FES Ten-Year Perspective (2015-2025) strategy, which stresses the importance of state-of-the-art diagnostic measurements. DIII-D is presently equipped with the most comprehensive diagnostic set of any magnetic fusion facility, providing a unique perspective for identifying improvements in diagnostic systems capable of leading to transformative results in the areas of fusion development and control.

The ability to accurately measure the relevant parameters in fusion plasmas is an essential component in bringing about predictive understanding and validating theories and models. To adequately test theories, a comprehensive set of diagnostics is required which not only measures all relevant equilibrium parameters (i.e.,  $T_i(\rho)$ ,  $T_e(\rho)$ ,  $n_e(\rho)$ ,  $V(\rho)$ ,  $J(\rho)$ , ...) with appropriate spatial and temporal resolution, but also measures fluctuating parameters in order to identify plasma behaviors that affect transport and stability. Measurements are needed in the plasma core, the scrape-off layer, the divertor region, and on the first wall material interface. Comprehensive measurements are also required for control of the plasma shape, equilibrium profiles, and magnetohydrodynamic (MHD) stability.

The diagnostic set assembled on DIII-D is the result of many fruitful collaborations with national and international partners. Developing and fielding a diagnostic on DIII-D remains a key involvement for many research groups, especially from universities, and offers the capability to participate directly in experiments and scientific discoveries, and opens a particularly engaging and formative path for students. This large involvement and integration is particularly evident in Table 6-1, which summarizes the diagnostics presently found on DIII-D. In addition, the operation, development, and maintenance of these diagnostics largely extend across institutional boundaries, with well over 100 diagnosticians (too many to list by name) working through integrated teams.

Table 6-1 also shows (in blue) the systems which were added or significantly upgraded in the last five years. Separately, shown in Fig. 6-1, is a view of the interior of the tokamak (outer wall) showing some of the diagnostics and their very good port access. Presently, more than 180 access ports are available, with the majority dedicated to diagnostic use. Of that large number of ports, a

sufficient fraction remains available to cover the proposed systems described in the following sections.

Successful fusion research at DIII-D required the pursuit of three important aspects related to diagnostics:

- QUALITY measurements, accurate, precisely calibrated.
- RELIABILITY of the measurement to support experiments.
- COMPLETENESS of the set (in coverage, resolution, and/or parameters).

**Table 6-1.**  
**Summary of Current DIII-D Diagnostics (Updated 10/12/2017)**  
 (Blue text indicates systems that were added or significantly upgraded in the last five years)

<b>Electron Temperature and Density</b>		<b>Lead Institution</b>
Thomson scattering	12 lasers, 78 chords	GA
ECE Michelson interferometer	Horizontal midplane	U Texas
ECE radiometer	Horizontal midplane, 48 channels	U Texas
CO2 interferometer	3 vertical chords, 1 radial chord	GA
Density profile reflectometer	Full radial profile into SOL	UCLA
ECE Imaging	2D ECE emission, 2 areas, 320 channels	UC Davis
<b>Ion Temperature, Velocity, and Density</b>		
Charge exchange recombination spectroscopy (CER)	32 vertical, 48 tangential	GA
Main Ion CER	32 tangential chords	PPPL
Fast ion density profile (FIDA)	2 vertical, 12 oblique views, imaging	UCI
<b>Core Impurity Concentration</b>		
VUV survey spectrometer (SPRED)	Radial midplane view	GA
Visible Bremsstrahlung array	Radial profile at midplane, 16 channels	ORNL
<b>Radiated Power</b>		
Bolometer arrays	4 poloidal arrays, 112 channels	GA
Fast bolometers	3 poloidal arrays, 106 channels	UCSD
<b>Boundary Diagnostics</b>		
Visible spectrometer	12 channels, upper and lower divertor	ORNL
Divertor survey spectrometer	Vertical view of lower divertor	LLNL
Ly-alpha X-pt imaging	Tangential view, 2 cameras	ORNL
Coherence Imaging (CIS)	2 cameras: tangential and lower divertor	LLNL
Infrared cameras	3 camera views	LLNL
Main chamber periscope	Infra-red and visible	LLNL
UV-enhanced imaging	Lower divertor view	GA
Fast neutral pressure gauges	7 locations, 4 in divertors, 1 main chamber 2 in SAS divertor	ORNL
Penning gauges	Under divertor baffle (upper and lower)	GA/U Wisc.
Baratron gauge	Under divertor baffle	GA/U Wisc.
Langmuir probes	32 in lower divertor, 40 in upper divertor	SNL
Moveable scanning probes	Vertically scanning, lower divertor	UCSD
Tile current monitors	10 lower divertor	GA
Fast Thermocouple array	20 in lower divertor	GA/SNL
Surface Eroding Thermocouples (SETC)	2 in SAS divertor	UTK
DiMES, MiMES	Lower divertor, outer midplane	GA/UCSD

Plasma TV	4 cameras	GA/LLNL
Fast framing camera	2 tangential views	UCSD
IR camera	Inner, outer wall and ceiling, floor views	LLNL
<a href="#">Visible filterscopes</a>	<a href="#">24 locations</a>	<a href="#">ORNL</a>
Swing Langmuir probes	Centerpost, 2 poloidal locations	UT/GA
<b>Magnetic Properties</b>		
Plasma current Rogowski loops	3 toroidal locations	GA
Flux/voltage loops	44 poloidal locations	GA
$B_\theta$ probes	135 probes	GA
Diamagnetic loops	2 toroidal locations	GA
External $B_r$ loops	4 arrays, 36 loops	GA
Internal $B_r$ loops	64 loops	GA
Internal $B_T$ loops	4 toroidal locations	GA
Coil current Rogowski loops	52 loops on 40 coil circuits	GA
<b>Fluctuations/Wave Activities</b>		
Beam emission spectroscopy	2-D, 64 channels	U Wisc
Phase contrast imaging (PCI)	Vertical view, 32 channels	MIT
<a href="#">PCI Interferometer</a>	<a href="#">Vertical view, 1 chord</a>	<a href="#">MIT</a>
<a href="#">Correlation ECE (CECE)</a>	<a href="#">8 radial channels</a>	<a href="#">UCLA</a>
UF-CHERS	1 radial position	U Wisc
<a href="#">Cross-polarization scattering (CPS)</a>	<a href="#">8 radial channels</a>	<a href="#">UCLA</a>
Doppler Backscattering (DBS)	8 radial channels	UCLA
Mirnov coils	Toroidal, poloidal, and radial arrays, 60 coils	GA
High-frequency Mirnov array	1 toroidal location, 5 coils	GA
<a href="#">Polarimeter</a>	<a href="#">3 radial chords</a>	<a href="#">UCLA</a>
X-ray imaging system	100 channels, 5 arrays	UCSD
Ion Cyclotron Emission (ICE)	5 plasma-facing antennae, 6 recessed loops	GA
Scanning probes	Outer midplane, lower X-point	UCSD
mm-Wave Imaging Reflectometry (MIR)		UC Davis
<b>Particle Diagnostics</b>		
Fast neutron scintillation counters	4 channels	UCI
Beam ion loss detector (BILD)	2 toroidal locations	UCI
Fast ion loss detector (FILD)	2 poloidal locations	GA
Neutron detectors	4 channels	UCI
DT neutron counters	2 locations	UCI
Neutral Particle Analyzers	3 channels	UCI
<a href="#">Imaging neutral particle analyzer (INPA)</a>	<a href="#">Radial profile</a>	<a href="#">UCI</a>
<b>Plasma Current Profiles</b>		
Motional Stark polarimeter	3 views, 40 channels, full radial coverage	LLNL
Li beam injector (edge current profile)	Radial beam with 32 vertical viewing channels	GA
<a href="#">Polarimeter</a>	<a href="#">3 radial chords</a>	<a href="#">UCLA</a>
<b>X-ray / Gamma Ray</b>		
<a href="#">Gamma Ray Imager</a>	<a href="#">Midplane tangential view, 55 channels</a>	<a href="#">GA</a>
Hard x-ray monitors	4 toroidal locations	GA
Hard x-ray scintillator array	16 locations	UCSD
X-ray Spectrometer	1 chord	LLNL
<a href="#">Soft X-ray Imaging (SXRI)</a>	<a href="#">1 tangential view</a>	<a href="#">ORNL</a>
X-ray imaging system	100 channels, 5 arrays	UCSD

---



The scientific goals set in Sections 2-4 are bringing additional challenges in the required coverage (spatial, temporal, and spectral). New and upgraded diagnostics are thus required to meet these new challenges beyond simply adding chords to existing designs. When it comes to reliability, there is an even bigger question than the simple availability for physics analysis. The program is moving toward a fully controlled system, where sensors (i.e., diagnostics) are called upon to control actuators (power, fields, fueling, etc.) in an increasingly complex way in order to control and sustain performance. Physics control needs are described in Section 2.2.3 and the inputs to the Plasma Control System are summarized in Section 7.2.1. Reliability will become a major issue in a successful reactor, where systems have to be regularly available for high duty factors. Finally, the need for completeness is crucial when one contemplates the interconnections between particles and fields in a multi-dimensional system (space, velocity, and time).

Significant progress in our scientific understanding of fusion plasmas will require the development of new diagnostic techniques. For the DIII-D program, this includes:

- A concerted and collaborative effort between facilities, at the national and international levels
  - Small lab development and testing (e.g., universities, small business)
  - Sharing of experience, engineering design capability, and proof of validity
  - Testing and exploitation on larger devices, such as DIII-D
- A continuous thrust into the introduction of new technologies
  - Small scale, increased sensitivity and ultra-fast detectors
  - Upgrading data-acquisition systems for dynamic range, speed, and reliability
  - New imaging techniques

For each scientific objective described in Sections 2 through 4, physics measurements have been identified, and a series of proposed diagnostic techniques associated with these needs. In some cases, well-known techniques can be applied. In others, the development of a new technique will be required. The overall plans for the implementation of these new or upgraded measurements are shown in Fig. 6-2. In each subsection, the items are arranged by priority (top: high priority). Detailed design and available resources will affect the details of the timeline. Triangles indicate planned systems whereas circles indicate options. These needs are further detailed in the next sections arranged by topical areas.

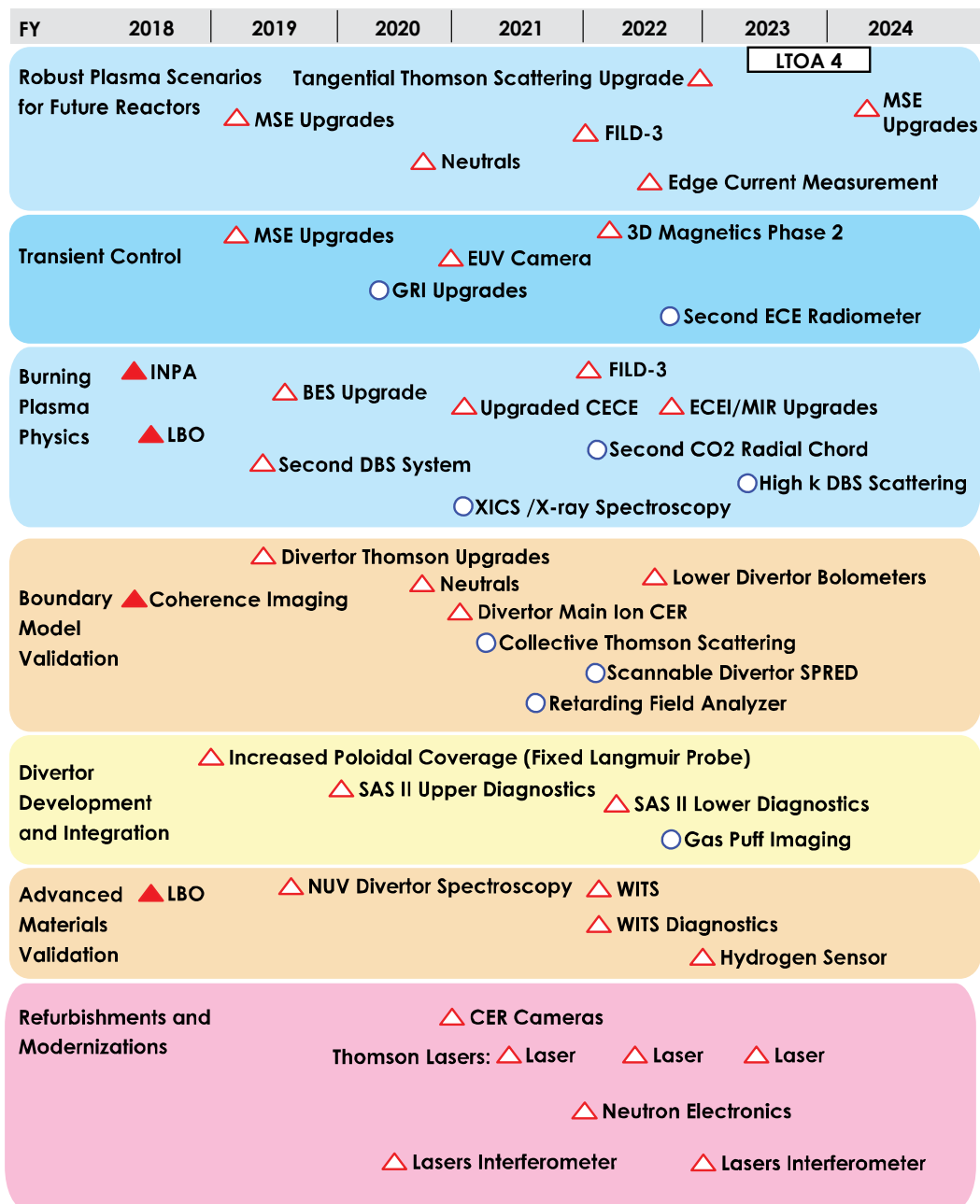


Fig. 6-2. Planned timeline for the implementation of new or upgraded systems. Within each subsection, the priority runs from high (top) to lower (bottom). Triangles indicate completed (filled) or planned (open) systems, circles indicate an option.

## 6.1 DIAGNOSTICS FOR ROBUST PLASMA SCENARIOS IN FUTURE REACTORS (SECTIONS 2.1 AND 4)

The development of the best operating scenarios for ITER and other next-step devices requires a detailed understanding of the underlying physical mechanisms, creating the physics basis for extrapolating conditions from existing tokamaks to these devices. Of particular interest is a careful characterization of the performance and physical mechanisms in the core of the plasma (see

Section 2.1) with sufficient resolution and accuracy. With recent advances in scientific understanding and technical tools, one of the goals is to develop plasmas compatible with steady-state operation, and to develop active means of full stability control, which will require appropriate sensors. The required additional measurements are summarized in Table 6-2, with optional systems shown in italics.

**Table 6-2.  
Robust Plasma Scenarios Measurement Needs**

<b>Scientific Objective</b>	<b>Physics Measurement</b>	<b>Proposed Diagnostic Technique</b>
Characterize scenario performance and stability	Improved electron density and temperature profiles	Redesigned tangential Thomson scattering system
	High precision core current profile measurement	Additional motional Stark effect (MSE) chords (core), near $q=2$ , and the edge or through Imaging MSE (IMSE)
Characterize fast-ion confinement	Escaping fast ions	Fast-Ion Loss Detector (FILD-3) for reverse $B_r$ operation
Identify role of neutrals in edge dynamics	Measure neutral (D) density and ionization rate	Lyman alpha arrays and imaging, <i>scattering techniques, stimulated ionization</i>

- **Redesigned tangential Thomson scattering:** This consists of reversing the laser beam direction (thus enhancing the scattering angle sensitivity at higher electron temperature) and enlarging the collection optics for these chords. The system will also be expanded to reach the pedestal region, complementing the existing high-resolution edge Thomson scattering and reducing uncertainties in profiles due to view locations mapping.
- **MSE:** The addition of a new system at the equatorial port at 255 degrees, viewing the 330 NB, will serve two purposes. The first one will supply the core MSE measurements when the 30 NB is changed to a co-counter system. It will add chords near the core where additional resolution is needed (e.g., near  $q\sim 2$ ). An Imaging MSE (IMSE) approach is presently being tested and may prove to be superior to the standard approach and would be implemented as a full-profile system, including the edge.
- **Edge current measurement:** In addition to the planned MSE upgrade described above, new dedicated systems are being evaluated for measuring edge currents beyond the capability of the lithium beam polarization technique. Following the recent success in polarimetry, the plan is to implement an edge polarimeter, with an edge vertical view,

starting with one chord (with plasma sweeps), and, if successful, switching to an imaging approach.

- **FILD-3:** The array of fast ion loss detectors will be augmented by adding a third detector, to be located near the equatorial midplane. The detector will use the standard scheme (see Fig. 6.4) where escaping fast ions are dispersed onto a scintillator according to their pitch-angle and energy (gyroradius). The system will be oriented to perform in a reverse  $B_T$  configuration, a configuration not covered by the existing two systems.
- **Neutral density measurements:** see Section 6.4

## 6.2 MEASUREMENTS FOR TRANSIENT CONTROL (SECTIONS 2.2 AND 4)

Transients in high-performance burning plasma devices need to be avoided, and, in the last resort, mitigated. Transients encompass very fast time scales, localized interactions, and difficult environmental conditions and therefore require dedicated diagnostics. A focus of the DIII-D research plan (see Section 2.2.1) includes the understanding of runaway electron generation and the physics understanding associated with an efficient avoidance scheme (Section 2.2.2).

The establishment of the scientific basis for understanding and predicting limits to macroscopic stability of magnetically confined plasmas has many control implications. A large part of the research (see Section 2.3) is aimed at investigating and validating basic MHD stability physics. A substantial improvement in tokamak operating regimes can be achieved by making use of DIII-D's extensive set of diagnostics for precise, detailed measurements of the pressure and current-density profiles, along with details of the internal structure of MHD modes. In fact, stability research includes critical issues for both conventional and Advanced Tokamak (AT) plasmas.

Other transients include the suppression, or at least mitigation, of ELMs (see Section 4.1.1). Many diagnostics are needed to understand the plasma response to external perturbations through RMP or pellet pacing.

The proposed improved capability is described in Table 6-3 (options shown in *italics*).

**Table 6-3.  
Transient Measurement Needs**

Scientific Objective	Physics Measurement	Proposed Diagnostic Technique
<b>Disruption Mitigation</b>		
Characterize runaway formation	Current channel width, energy of runaways	EUV camera, <i>GRI upgrades</i>
Characterize magnetic structure	Halo currents	<i>Increased tile current monitor and halo sensor coverage</i>
<b>Disruption Avoidance</b>		
Characterize NTM, RWM and TAE radial mode structure	ECE ( $T_e$ ) measurements, line integrated density ( $n_e$ ) measurements	<i>Second ECE radiometer, second CO2 radial chord</i>
Characterize error field, NTM and RWM poloidal and toroidal mode structure	Magnetics (first wall)	Additional magnetics coverage (3D) phase 2, (n=6 and/or rotating mode/structure)
	High-precision core current profile measurement	Additional motional Stark effect (MSE) chords (core), near q=2, and the edge or through Imaging MSE (IMSE)
<b>ELM Mitigation</b>		
Characterize plasma response to 3D fields	Magnetics (first wall)	Additional magnetics coverage (3D) phase 2, (n=6 and/or rotating mode/structure)

- **Second ECE radiometer:** A second radiometer will be installed giving the temperature profile at a second toroidal location. The system will use the existing microwave access of the Michelson interferometer.
- **EUV camera:** The proposed system uses multi-layer reflective optics to image DIII-D plasmas in the EUV (~100 eV) energy range. High-precision reflective optics enables high reflectivity (>50% at normal incidence) achieving very high light throughput. This is expected to achieve very fast (10 kHz+) imaging with high spatial resolution. An equatorial tangential view will enable the greatest cross section view of the plasma and enable study of poloidal asymmetries.
- **MSE:** See section 6.1.

- **Additional magnetics coverage (3D) phase 2:** The installation of the new internal 3D coils will require the further addition of internal magnetic probes (both poloidal and radial, see Fig. 6-3), with an  $n=6$  resolution and high poloidal number  $m$ , and capability to identify rotating modes.



*Fig. 6-3. a) Poloidal magnetic probe. b) Radial field saddle loop c) Compact combined poloidal and radial magnetic probes.*

### 6.3 BURNING PLASMA SCIENCE RESEARCH (SECTIONS 2.3 AND 4)

In the last few years, significant progress has been made in the study of the different roles of the turbulent mechanisms in heat transport (ion-temperature gradient [ITG], trapped electron mode [TEM], electron temperature gradient [ETG], etc.). With this progress, the selection of the next generation of key measurements is now targeting parameters and parameter range that will enable validation of the current models. This model validation (see Sections 2.3.1, 2.3.2, and 2.3.3) is required for design and operation of next-step devices. In particular, a renewed focus is being developed for the study of particle transport, a natural complement to heat and momentum transport studies already well underway. Attention is being given to fully diagnose and understand the mechanisms leading to an L-mode to H-mode (L-H) transition, with attention to turbulence generation and suppression, and including effects due to neutrals. Many new diagnostics have been commissioned (e.g., main ion CER) for the study of plasma rotation (Section 2.3.2) in the current 2014-2018 five-year period, with torque-free measurements (e.g., ECH only) being needed through X-ray spectroscopy.

It has long been recognized that energetic particles bring new challenges (and opportunities) in reaching the needed conditions for a burning plasma. The confinement of these particles is particularly important, and their impact on plasma instabilities, such as Alfvén instabilities, is critical. Recent success in energetic particle dynamics research has been possible with the capability enabled by new and upgraded diagnostics such as the fast interferometer, scattering techniques, ECE and ECEI/MIR, beam emission spectroscopy (BES), fast-ion D-alpha (FIDA), fast-ion loss detectors (FILD), and more recently by the successful implementation of the Imaging NPA (INPA). However, measurement needs remain, especially in terms of mode identification

(high  $n$  numbers) and diagnosis in reverse magnetic field configuration, which affects fast-ion orbits (see details in Section 2.3.3).

The proposed additional and/or upgraded capability is described in Table 6-4 (options shown in *italics*).

**Table 6-4.  
Burning Plasma Physics Measurement Needs**

<b>Scientific Objective</b>	<b>Physics Measurement</b>	<b>Proposed Diagnostic Technique</b>
<b>Transport/LH physics</b>		
Understand role of turbulence	$T_e$ fluctuations	Upgraded CECE
	Density turbulence	Expanded BES, second DBS
	High $k$ density turbulence	<i>Additional receiver location/scattering angle (high-<math>k</math> DBS scattering)</i>
	Ion temperature and velocity fluctuations	<i>UF-CHERS upgrade</i>
	Neutral density and ionization rate	Lyman alpha arrays and imaging, <i>Rayleigh scattering techniques, Photoionization technique, TALIF</i>
	Particle transport (impurities)	Impurity X-ray diagnostics
<b>Energetic Particles</b>		
Understand mode structure	Measure toroidal mode number	<i>Second ECE radiometer, Second CO2 radial chord</i>
	Measure mode structure	BES upgrade
Understand interaction of mode with fast ions	Measure loss of fast particles	Additional Fast-Ion Loss Detector (FILD-3)
<b>Rotation</b>		
Understand evolution and role of rotation	Impurity ion temperature and velocity without torque injection	<i>X-ray crystal spectrometers (XCS)</i>

- Upgraded and extended BES:** The BES diagnostic system that measures low-wavenumber density fluctuations in the radial-poloidal plane will be upgraded and expanded. The goal is to radially expand the 2D viewing capability from 64 to 96 channels to better understand the nonlinear interactions between low- $k$  turbulence and mesoscale instabilities. In parallel, a separate high radial-resolution pedestal fluctuation diagnostic

will be developed to measure predicted pedestal instabilities such as kinetic ballooning modes, micro tearing modes, etc. This more specialized diagnostic should achieve radial resolution of 0.3-0.5 cm, compared to 1.0-1.2 cm for conventional BES measurements, and will also be capable of 2D radial-poloidal pedestal fluctuation measurements. Options also include additional measurements to discern the toroidal n-number for fluctuations arising from Alfvén modes, zonal flows, GAMs, and 3D perturbations.

- **Impurity X-ray diagnostics:** A variety of X-ray systems will be deployed to measure the spatial distributions (mostly radial) in the core and edge plasmas. High spatial resolution systems using spectral binning will be complemented with high spectral resolutions. Multiple systems are also envisioned to cover the necessary spectral ranges, covering given impurities and local temperatures (core/edge).
- **Second DBS system:** A second DBS system will serve multiple purposes. When combined with the first system, it will enable measurements of non-axisymmetric perturbations, including information on their n-numbers. In addition, when positioned at different radial scattering areas, such as the pedestal, it will offer a wider profile picture of the fluctuations and their interaction. This second system will take advantage of existing microwave access to the equatorial region of the plasma.
- **Upgraded CECE:** This upgrade will provide eight spatial channels of localized temperature turbulence measurements. New optical system will increase the poloidal wavenumber range from the current 0-1  $\text{cm}^{-1}$  to 0-3  $\text{cm}^{-1}$ . The new design will be internal to the vacuum vessel and based upon a dichroic lens scheme. This upgrade will significantly expand the wavenumber range, thereby providing access to TEM turbulence relevant scales (e.g.,  $k^*\rho_s \sim 1.5$ ).
- **High k DBS scattering:** This system will provide up to eight channels of spatially localized density turbulence and flow measurements. The probe frequencies will be in the range of 80-100 GHz with detected poloidal wavenumbers from 16-30  $\text{cm}^{-1}$ . This represents a significant increase in wavenumber range with  $k^*\rho_s = 8-15$  – deep into the ETG turbulence scales, a currently inaccessible region. A port either above or below the midplane will provide the angular access required for this scattering geometry.
- **FILD 3:** see section 6.1
- **Second CO<sub>2</sub> radial chord:** DIII-D is presently equipped with a midplane radial chord. Plans are to add a second chord with a small toroidal separation; the combination of the two radial chords will yield information of the n number of core modes (such as Alfvén modes), with high numbers (up to 20). Since the second chord aims at looking mostly at fluctuations, or MHD activity, no vibration compensation is necessary.

- **Neutrals:** see Section 6.4

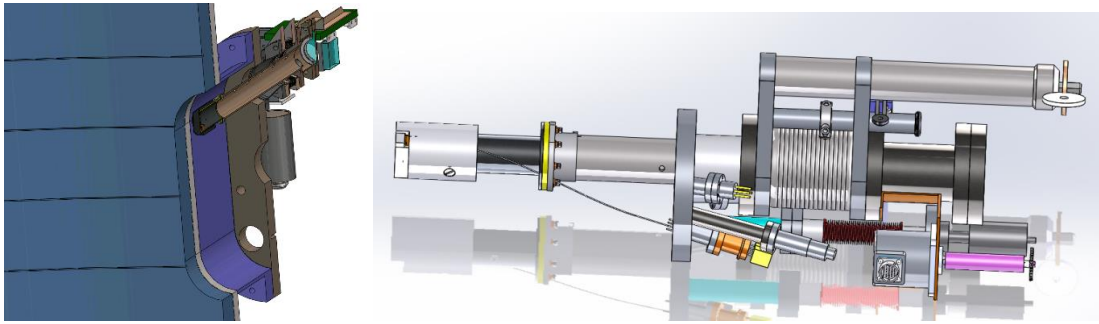


Fig. 6-4. Conceptual design of the third Fast-Ion Loss Detector, to be located near the midplane for use in reverse  $B_T$  operation.

#### 6.4 MEASUREMENT NEEDS FOR BOUNDARY MODEL VALIDATION, DIVERTOR DEVELOPMENT AND INTEGRATION (SECTIONS 3.1, 3.2 AND 4)

One of the greatest challenges in magnetically confined plasmas is associated with the development of a scientific and technological solution to the heat and particle handling in the divertor. The boundary layer found in the divertor encompasses vastly different conditions over a small physical scale. Temperatures on the order of kilo-electron-volts and high densities are found just inside the last closed flux surface (e.g., pedestal), whereas much lower temperatures are encountered at the plasma-wall interface. This wide contrast and the presence of severe background issues present a difficult challenge in diagnosing this region. Several underlying physical issues complicate our attempt to understand boundary physics. Transport, MHD stability, and atomic physics all play a role in controlling the conditions encountered in that region. The boundary plasmas have strong two-dimensional character due to poloidal asymmetries, the presence of an X-point, and strong radial dependencies. The interaction of the hot plasma with the first-wall material and the impact of any eroded material on the plasma core are important and relevant issues for understanding boundary physics. In support of this research, the proposed measurement improvements are described in Table 6-5 (options shown in *italics*).

**Table 6-5.**  
**Boundary Model Validation, Divertor Development and Integration Measurement Needs**

Scientific Objective	Physics Measurement	Proposed Diagnostic Technique
Understand particle transport in SOL	Local electron density and temperature	Advanced DTS, <i>Helium emission line ratio (GPI)</i>
	Flow velocities	Spectroscopy (coherence imaging)
	Neutral density and ionization rate	Lyman alpha arrays and imaging, <i>Rayleigh scattering techniques, Photoionization technique, TALIF</i>
Understand and control heat flux to divertor plates	Heat flux	IR camera upgrades, Surface Eroding Thermocouples (SETC)
	Ion heat transport	Divertor main ion CER, coherence imaging, <i>Collective Thomson Scattering (CTS)</i> , increased fixed Langmuir probe coverage, divertor bolometers, <i>retarding field analyzer (RFA)</i>
Characterize edge turbulence	Density, electric field fluctuations	<i>Gas-puff imaging (GPI)</i> , Fast probe ( $T_e$ ) measurements

- **Advanced Divertor Thomson Scattering (DTS):** The divertor Thomson scattering will undergo multiple enhancements to increase the coverage of the system. The lower divertor system will be augmented in the number of laser chords to allow simultaneous 2D imaging, and to cover a range of plasma configurations. In addition, the system will be expanded in the upper divertor to cover the various SAS configurations (see Figures 6.5 and 6.6).
- **Ion Temperature Measurements:** One of the key parameters presently undiagnosed in the divertor and/SOL areas is the (main) ion temperature. A few candidates are being evaluated and planned for development and implementation. They are:
  - **Coherence Imaging:** Spectrographic information of emitted line radiation (e.g., carbon) can be stored through interferogram techniques directly onto a camera (video) image. Line shifts will give the local flow speed, and its width the local ion temperature. This technique is being applied to both upper and lower divertor through tangential views. With successful flow measurements already performed, separate systems will be devoted to ion temperature measurements.
  - **Upgraded Main Ion CER (Divertor Main Ion CER):** The main ion CER system has been very successful in measuring the deuterium velocity and temperature in the core and pedestal plasmas, presently with 32 chords. The system will be expanded to the lower divertor SOL, by taking advantage of both 150 and 210 heating beams aimed in an off-axis position. These will require new views, using available lower ports (so called R-1 ports).

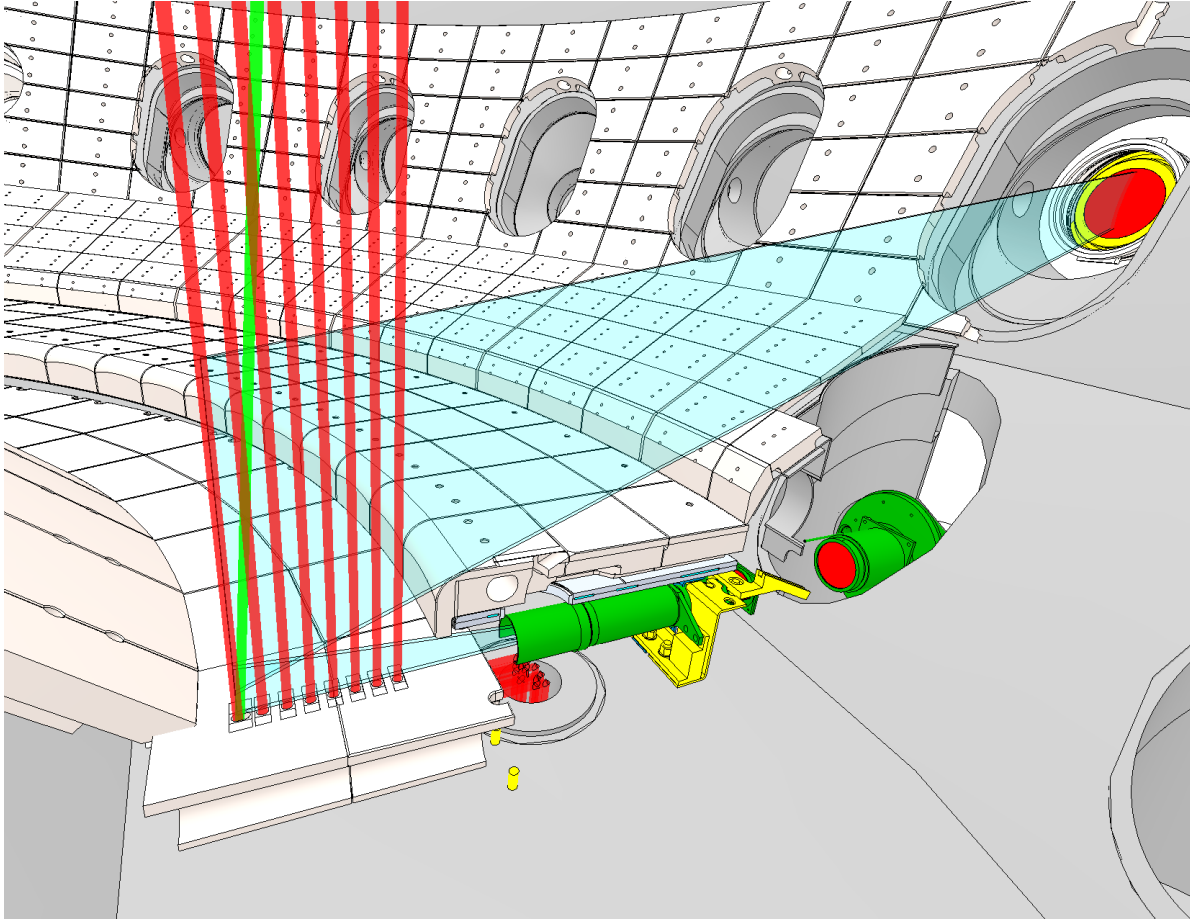


*Fig. 6-5. Advanced 2D Divertor Thomson Scattering Imaging System with high triangularity plasma capability (red lines are the selectable laser beam paths, the green line is the path for the upper SAS II slot).*

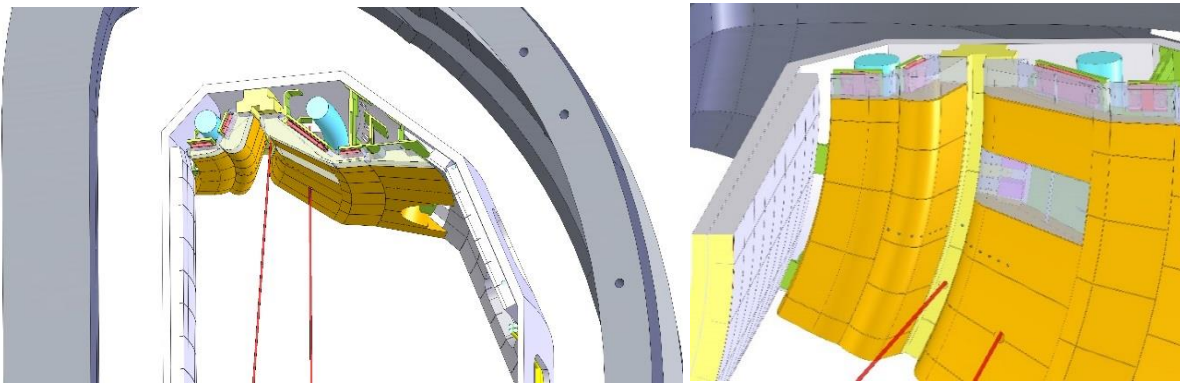


*Fig. 6-6. SAS II upper divertor diagnostic set. Shown through (upper tiles) are the magnetic probes underneath the tiles and the ASDEX gauges. The red lines are the laser beams for the upper divertor Thomson scattering system.*

- **Collective Thomson Scattering (CTS):** The technique exploits Thomson scattering to probe the spectrum of Doppler-shifted radiation, yielding information on the velocity distribution of electrons and ions. For long enough probe wavelengths, the so-called collective Thomson scattering (CTS) diagnostic technique can be used to make measurements of the main-ion temperature ( $T_i$ ) profile. The new approach builds on a novel optical design enabling sufficient dynamic range and resolution to resolve the so-called ion feature. This technique will result in first-ever localized multi-point  $T_i$  measurements in the divertor and scrape-off layer regions.
- **Retarding field analyzer:** The system consists of a series of biased grids installed on a probe head which can analyze the ion distribution function locally. The first unit is planned for the lower divertor.
- **Neutrals:** Since measuring the density and ionization rate of neutrals ( $D$ ) is particularly difficult in tokamaks, and since the measurements must be done in several areas (including pedestal, SOL, and divertor areas), a variety of complementary techniques are proposed. These techniques are at different levels of readiness and laboratory testing is presently ongoing to prepare them for implementation on DIII-D during the 2019-2024 period.
  - **Lyman alpha arrays and imaging:** In-vessel filtered photodiodes are proposed to be used to detect Deuterium Lyman emission at specific locations. This will be complemented by imaging the emission through filtered scintillators using standard visible cameras.
  - **Rayleigh scattering:** a new approach is being evaluated using Rayleigh scattering measurements on neutral population.
  - **Photoionization:** options are being evaluated using photo-ionization as a means to probe the neutral population, using available pulsed-laser beams and ultra-fast detection schemes.
  - **TALIF (laser induced fluorescence):** A two-photon (laser) fluorescence scheme is proposed to measure the local neutral deuterium density. The laser beams aim at the lower divertor through a vertical port, and the emission is captured by collection optics sharing the same lower vertical port.
- **Increased poloidal coverage (fixed Langmuir probe):** A series of fixed Langmuir probes at key locations on the first wall will be added, especially on the low-field side. The design will be based on the existing design.

- **Helium emission line ratio (GPI):** The injection of a small amount of helium through a set of nozzles will enable the local measurement of electron temperature and density based on the ratio of two (or more) known emission lines. First measurements will be done near the outer midplane. The measurements will be performed using filterscope-type views (ORNL) and using a camera, which will yield 2D coverage. Local turbulence measurements will also be available with the camera view (UCSD).
- **Surface Eroding Thermocouples (SETC):** SETCs utilize a “self-renewing” thermocouple junction that is capable of continuous measurement while the surface erodes. They are designed to measure surface temperatures while in direct contact with the divertor plasma. First developed for extreme heat flux applications like rocket nozzles, SETCs are capable of ultrafast temperature measurements limited primarily by the data-acquisition hardware (>1 kHz), greatly improving their response time over embedded thermocouples and on par with IR thermography. SETCs have been tested at the DIII-D divertor on DiMES in the 2017 campaign and have shown agreement with IR thermography and Langmuir probes, while demonstrating a capability of distinguishing ELMs. They are particularly suited for shadowed regions where IR thermography has no line-of-sight, making them a powerful tool to add to DIII-D’s heat-flux diagnostic capabilities. Prototypes have been installed in upper SAS and will be fully tested during the FY18 campaign.
- **High-resolution bolometers:** The bolometer system will be augmented to allow high spatial resolution measurements in both divertors, including new SAS configurations (see example in Fig. 6.7).

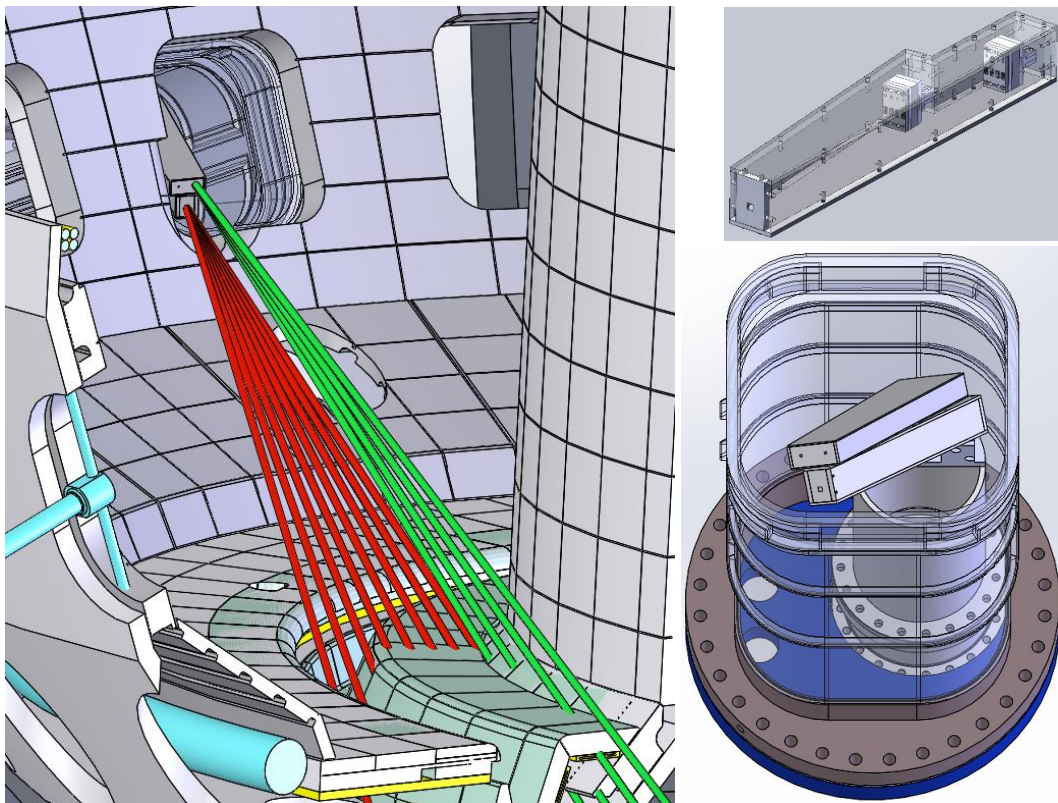


*Fig. 6-7. (Left): Lower divertor bolometer assembly. (Top right): Bolometer detector assembly. (Bottom right): Conceptual assembly of the two bolometer cameras within the lower port.*

## 6.5 ADVANCED MATERIALS EVALUATION (SECTION 3.3)

A remaining challenge for burning plasma experiments and next-step devices is the development of a fully integrated and compatible plasma-material solution. The study of interaction of plasmas and first wall material requires a set of dedicated diagnostics, both from the point of view of plasma conditions, but also in situ characterization of the wall components (tiles, divertors, etc.). The diagnosis of these conditions also requires additional facility capability for handling, accessing and modifying local conditions. These needs are summarized in Table 6-6 (options shown in *italics*).

**Table 6-6.**  
**Advanced Materials Validation Measurement Needs**

Scientific Objective	Physics Measurement	Proposed Diagnostic Technique
Characterize surface conditions	In situ measurement erosion and deposition	Wall Interaction Test Station (WITS), <i>LIBS</i> , <i>upper collector probes</i>
	Impurity source	NUV spectroscopy, WITS diagnostics (Langmuir probes, thermocouples, <i>filterscope views</i> , <i>spectroscopic views</i> )
	Hydrogen retention	Hydrogen sensor
	Core impurity accumulation	X-ray spectroscopy

**WITS:** The Wall Interaction Tile Station (WITS) system is a large, moveable limiter, ~50 cm in both linear dimensions. With ~15 cm of linear travel, WITS will be capable of sufficient radial motion to become the primary limiting plasma-facing surface in relevant magnetic configurations. Inside the “bulk” portion of WITS will be a smaller, removable sample exposure probe, ~10 cm in diameter, similar in functionality to DiMES, but with larger sample capability and improved flexibility. The larger area will also allow tile-scale testing of main-chamber PFCs at heated and ambient temperature conditions.

- **WITS diagnostics:** The WITS system will have diagnostics built into the station such as Langmuir probes, thermocouples, and surface monitors. Diagnostics will also be added to view the surface from adjacent ports, including filterscopes, pyrometers, spectrometers and viewing systems.
- **Hydrogen Sensor:** Following a successful testing on DiMES, the sensor (see Fig. 6-9) will be added to an access point located within the lower divertor.

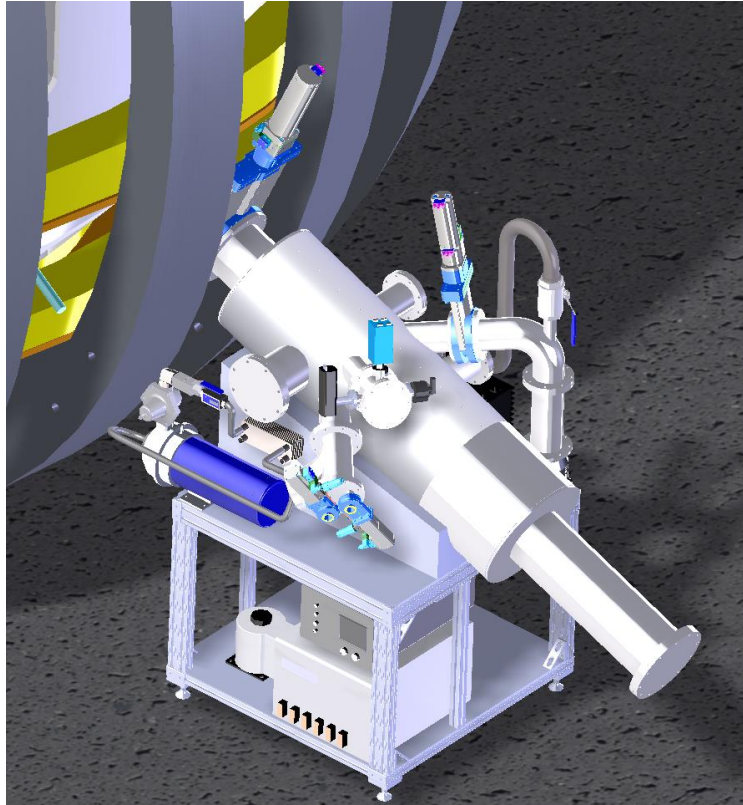


Fig. 6-8. Conceptual design of the remote handling system WITS. A second option has also been developed for an equatorial port.

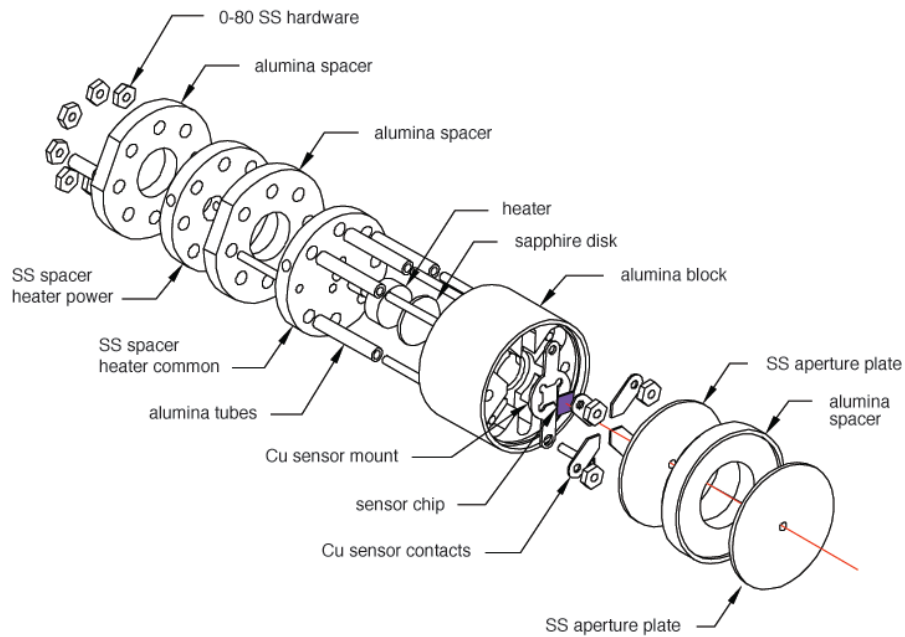


Fig. 6-9. Schematic of an in-vessel hydrogen sensor.

## 6.6 INTEGRATE DEVELOPMENT OF DIAGNOSTICS FOR BURNING PLASMA EXPERIMENTS (BPX)

Diagnostic development for a burning plasma experiment (ITER, FNSF, DEMO, CFETR, etc.) is also sorely needed. In a BPX, the application of standard techniques and the fielding of specialized diagnostics are facing challenges, including environmental issues (e.g., radiation), access, long pulse, etc. Additional measurement requirements (e.g., alpha particles) are particularly difficult to meet. The development of these new or alternate techniques presently lacks extensive testing capability in an existing tokamak. The development of burning plasma diagnostics and related technology requires a coordinated effort with the US Burning Plasma Organization (USBPO), US ITER Project Office (USIPO), the International Tokamak Physics Activities (ITPA) and ITER Organization (IO). The DIII-D program aims at contributing efforts wherever possible to address long-term needs in this area.

Specifically, these activities aim to address the following questions/issues:

- The development of a new technique where needed
- The test of a new technique in a large tokamak with relevant parameters
- Development of alternative techniques for problematic measurements
- Complete test of control techniques (reliability, versatility)
- Continued study of erosion and deposition (for eventual input to diagnostic design, e.g., first mirrors)
- Continued evaluation of measurement requirements for a BPX, in regard to profile, divertor and/or control-associated needs

It is anticipated that, in the timeframe covered by this proposal, the DIII-D program will continue to support testing prototypes to verify proposed designs for the U.S.-procured systems to ITER. That list includes the tangential interferometer and polarimeter (TIP), ECE, MSE, viewing systems (infrared [IR] and visible), reflectometer, and possibly X-ray crystal spectrometers (XCS).

Additionally proposed is the development of alternate techniques that may be required for ITER and/or other BPX, including but not limited to FNSF, CFETR, and DEMO.

They include such techniques as:

- Demonstration of fast-Alfvén reflectometry for isotope mix ratio measurement and applications of Ion Cyclotron Emission (ICE)
- CER, coherence imaging, and microwave-based measurements for  $q$  profile reconstruction, including pedestal regions
- CER based measurement of fast ion population losses
- New soft X-ray detection concepts (in high-radiation environment)

- New concepts in polarimetry and interferometry, including imaging techniques

## **6.7 SPECIFIC DIAGNOSTIC REFURBISHMENTS**

While periodic maintenance on diagnostic systems aims at ensuring their reliability, the refurbishment and/or modernization of many systems is often a necessary step for the long-term sustainment of DIII-D's capability. In virtually all these cases, the refurbishment was accompanied by a significant upgrade in measurement capability, greatly benefiting the program. In the current 2014-2018 five-year period, Thomson scattering, CER, filterscopes, neutrons, BES, and magnetics systems have undergone significant modernization efforts. The electronics, data acquisition, collection lens assembly, fiber optics, and laser systems for the Thomson scattering diagnostics have been redesigned, rebuilt, and commissioned. Other planned refurbishments include the gradual replacement of the CER cameras (~10), interferometer lasers (4), SXR systems (2 more systems out of 5), and completion of the refurbishment of all neutron diagnostic electronics. The refurbishment of data-acquisition systems is also planned and details can be found in Section 7.11.

## 7. COMPUTER SYSTEMS AND SCIENCE

The DIII-D National Fusion Facility requires a flexible computing infrastructure that can rapidly adapt to the changing research needs while at the same time provide a dependable and secure environment. DIII-D's Computer Systems and Science includes: 1) the data acquisition, instrumentation, and controls systems unique to the facility's operation, 2) the underlying computer infrastructure encompassing user-support services, computing, networking, and data storage, 3) support for effective and efficient data analysis, and 4) cybersecurity.

The core team, led by David Schissel, successfully designed, implemented, and controlled the evolution of DIII-D's computing infrastructure over the past decade, and this team remains intact for this proposal. Staff additions during the current five-year plan in the areas of cybersecurity, networking, and high-performance computing have further strengthened the team. The breadth of knowledge and experience of the staff combined with active collaborations with other magnetic fusion research facilities worldwide creates a group that can architect and deploy the varied solutions discussed in this Section.

### 7.1 OVERVIEW

Successful operation of the DIII-D facility requires the coordinated activity of a diverse set of computers and software applications. There are numerous systems dedicated to experimental operations that support real-time plasma control, data acquisition, and plant operation functions that rely heavily upon custom, in-house developed computing solutions in order to fulfill the many unique requirements of the research program.

The underlying computer infrastructure that supports the entire DIII-D program includes the general-purpose computational systems, the numerous large storage disk arrays, the tape backup systems, DIII-D control room computers, operational services, the entire network infrastructure, and the overarching cyber-security program.

Providing an infrastructure that allows for the effective and efficient analysis of data is both critical and fundamental to the DIII-D scientific mission. The term data analysis is used in the broadest sense and includes a body of methods that help to describe facts, detect patterns, develop explanations, and test hypotheses. DIII-D's analysis infrastructure is layered on top of the general computer infrastructure.

## 7.2 DIII-D EXPERIMENT SUPPORT

*Lead Personnel: B. Penaflor (GA), R. Johnson (GA), D. Piglowski (GA), C. Parker (GA), F. Garcia (GA), C. Liu (GA), D. Kaplan (GA)*

### 7.2.1 Plasma Control System

The DIII-D Plasma Control System (PCS) is a real-time data acquisition and feedback control system that provides a structured yet flexible framework for rapid development and deployment. Recent upgrades have been made to replace older 32-bit computer systems along with the obsolete 2.1 Gb/s Myrinet real-time networking hardware. The present system operates on 12 64-bit Linux-based multi-processor computers running in parallel with 40 Gb/s InfiniBand network connectivity. Real-time data acquisition is performed by D-TACQ acq196 hardware consisting of over 100 analog output channels, 800 analog input channels, and 256 digital input/outputs (Table 7-1). Throughout the past 20 years, the DIII-D PCS implementation has continually evolved to meet the control needs for all DIII-D experiments. This evolution will continue in the proposed five-year plan with important hardware and software updates being implemented to support advanced control scenarios and to keep current with the latest hardware technology. Updating to newer hardware will reduce risks of failure and improve I/O performance which would benefit and enhance DIII-D's control capabilities.

**Table 7-1.**  
**Diagnostics and the Number of Channels Presently Acquired by the DIII-D PCS as Well as Those New Systems to be Added during the Proposed Five-Year Plan**

<b>PCS Diagnostic Signal</b>	<b>Number of Channels Present</b>	<b>Number of Channels by 2024</b>	<b>Description/Usage</b>
Coil currents	55	67	Shape control
Power supply voltages	52	58	Trouble-shooting feedback control
Rogowskis	2	2	Plasma current feedback control
Magnetics	180	180	RTEFIT shape control
MSE	160	160	RTEFIT profile control
CER	16	32	Rotation, Ti feedback control
ECE	64	64	Te feedback control
Density	8	8	Density control
Gas flow	12	12	Density control
Neutral-beam data	16	16	Neutral-beam power feedback
ECH data	8	8	ECH gyrotron power feedback
Thomson	54	74	Te, ne profile feedback control
Bolometers	12	28	Radiation feedback control
Filterscopes	2	18	Real-time scope display
Langmuir probes	0	24	Detachment control
SPRED	0	2	Radiated power control
Mirnov probes	12	12	MHD control
Misc	147	179	Tokamak monitoring, RT scopes
<b>Total</b>	<b>800</b>	<b>944</b>	

Upgrades (Table 7-1) to existing PCS real-time computing systems will continue at a rate of two computers per year so that the PCS can take advantage of the ever-increasing raw processing power for time-critical algorithms that will support new types of control scenarios. Additional very high-performance computational hardware, including a mix of Xeon-Phi, GPU, and FPGA augmented systems, will be investigated to improve real-time kinetic magnetic equilibrium reconstructions and real-time MHD stability analysis. A kinetic reconstruction that converges sufficiently well to be useful in a stability analysis typically requires more than 100 iterations from EFIT, and requires a higher density computational grid than normally used in real-time or between pulses. Increasing the grid resolution can be facilitated through a processor that does matrix/vector algebra rapidly, since that is where the computation time increases most noticeably with the grid density.

DIII-D is uniquely suited to study divertor control strategies due to its impressive suite of diagnostics, but more data from those diagnostics are needed in real time. Bolometers are used to measure radiated power and have been used by several facilities [Kallenbach 1995, Wu 2017] in feedback control schemes to manage heat loads. Currently, 12 out of 48 bolometer channels are available in real-time.

Because these channels have been instrumental in technical progress [Eldon 2017], more powerful control algorithms will be developed to take advantage of the full set. A planned upgrade to the bolometer diagnostic will add 16 new channels to the upper divertor and future upgrades will add a similar number to the lower divertor. The plan is to digitize the new bolometer channels in the PCS and avoid the need for a separate digitizer.

New connections to existing DIII-D diagnostics will be added (such as Langmuir probe data) and will require new InfiniBand networking hardware and real-time data-acquisition hardware. Langmuir probes have been used in a detachment control scheme at JET [Guillemaut 2017]. The plan is to digitize DIII-D's Langmuir probes in real time and implement a new detachment control algorithm based on probe data. This will augment existing Divertor Thomson Scattering (DTS) data already being collected by the PCS and provide an alternative means of performing detachment control. Such an algorithm will be used in a much wider variety of plasma shapes and also make DIII-D's PCS more valuable to other facilities that have probes but not DTS. To accomplish this plan, more digitizers will be added to both gather data in real time for the PCS and also provide post-pulse data for more probes.

CER data are needed to measure ion temperature and density profiles for use as inputs to kinetic equilibrium reconstructions. With 16 CER channels currently available in real-time, profile analysis is possible in the PCS now, and having more channels would improve fit quality.

The SPRED diagnostic is used to measure the intensity of emission lines from various elements and track impurities in the plasma. The main SPRED system monitors the core plasma, and there is a new divertor SPRED system being installed. It is planned to have SPRED data available in real-time to improve radiated power control techniques that operate by impurity seeding. Knowledge of which impurities are present and with what relative quantities will be especially helpful when more than one gas is simultaneously introduced, as has been proposed to separately control divertor and core radiation.

Real time detection of ELMs using filterscope data has allowed DTS measurements taken during ELMs to be rejected so that DIII-D's detachment control system can function in H-mode [Eldon DOI:10.1088]. It is currently possible to connect two filterscope channels to the PCS at once. However, offline analysis has shown that a more robust ELM detector is achieved by averaging the signals from several (4-8+) filterscope channels together before running the detection algorithm. Another benefit to having more filterscope data digitized in real time is that it would not be necessary to alter hardware connections to provide appropriate ELM detection signals for different plasma shapes. This would be generally useful, but could be especially helpful for strike point sweeps, which are common in divertor physics experiments.

Improvements to the real-time PCS display capabilities are planned to expand the amount of information shown in the control room and extend this data to users outside of the DIII-D building complex. Improvements to data sharing between PCS processes, both within the same computer and from different computers, are planned to aid in the development of more advanced control algorithms that require extensive data exchanges between a large number of parallel processes.

### **7.2.2 Data Acquisition**

DIII-D's diagnostic set requires a robust and efficient data-acquisition environment that minimizes the time from the end of the plasma until data is available for automatic processing or visualization by the scientific team. At present, there are over two dozen distinct Linux-based data-acquisition systems used for control, monitoring, neutral-beam injection, and diagnostic data that store their data for long-term preservation in DIII-D's PTDATA format (raw data). A quarter of these systems have been upgraded within the past two years to increase local storage capacity, expand network bandwidth, and migrate from 32-bit to 64-bit operating systems. In addition, there are numerous data-acquisition systems that are maintained by the collaborating institution that manages the diagnostic. Outside of PTDATA, there are a number of computers associated with camera diagnostics that store data in the camera's native format.

Upgrades to data acquisition hardware are expected to continue at a rate of two to three computers per year in order to bring the oldest of these systems up to date and increase overall reliability and performance. The set of analog-to-digital conversion (ADC) data acquisition

hardware used in converting the raw analog signals to digital format at frequencies ranging from 1 kHz to 200 MHz are also planned for annually upgrade to replace aging systems and keep up with increasing diagnostic needs. These include a large number of D-TACQ ACQ196 cPCI digitizers that are used for close to half of all DIII-D data acquisition. Among the digitizers scheduled for upgrade during the five-year plan are the ones used for audio amp acquisition, I-Coil acquisition, bottom thermocouple acquisition, as well as parts of the NBI acquisition. New digitizers are required to increase the total number of channels acquired on existing diagnostics including Ion Cyclotron Emission (ICE) data, Gamma Ray Imaging, and Bolometer data. For the Reciprocating Probes diagnostic, a higher acquisition frequency has been desired, which will require upgrades to the digitizers used in acquiring this data.

### 7.2.3 DIII-D Control Room

The DIII-D control room is critical to the success of DIII-D’s mission (Fig. 7-1). Recent upgrades have been made to provide remote collaborators with access to status display content previously available only to users in the control room. Further upgrades are planned for the DIII-D control room terminal stations that are used to provide users with access to DIII-D networked computer systems during operations. The large control room displays are used to show real-time machine status information, and the smaller displays underneath show live tokamak control and plasma control data. These systems will be upgraded to the latest display technology as part of the proposed five-year plan.



*Fig. 7-1. The DIII-D control room with real-time displays for the scientific staff.*

Good progress has been made in the last five-year plan to upgrade the computing infrastructure, providing centralized ZFS-based file storage, user login access, and plant data sharing for the DIII-D Linux-based computer control and data-acquisition systems. Expansion of the file storage server along with refurbishments to the supporting computing infrastructure are planned for the next five-

year plan. This work includes expanding the availability of general plant data through a dedicated in-memory Redis database that resides outside of the secure DIII-D control and operations network.

### **7.3 COMPUTER INFRASTRUCTURE**

*Lead Personnel: D. Schissel (GA), D. Miller (GA), F Garcia (GA), D. Piglowski (GA), C. Parker (GA), S. Flanagan (GA), K. Greene (GA), B. Penaflor (GA), R. Johnson (GA), M. Margo (GA)*

#### **7.3.1 Data Storage**

The majority of data storage at DIII-D is comprised of raw data (PTDATA and object storage), analyzed data (MDSplus), associated metadata (relational databases), and user files (ZFS-based). These mass storage systems are all located in the main data center.

Out of all of DIII-D's data repositories, PTDATA is the largest (214 TB compressed), and growing (Fig. 7-2) at the fastest absolute rate per fiscal year (48 TB compressed acquired in FY17). From a percentage standpoint, PTDATA growth has averaged 25% year-over-year since FY10 with the largest single year-over-year growth of 50% (FY16). This growth is driven by the addition of new diagnostics and the enhancement (more channels, faster digitization) of existing systems. All major enhancements to existing systems and new diagnostics undergo a design review that includes data-acquisition requirements to ensure that the proper amount of data is being preserved, along with an assessment of the impact on the existing PTDATA repository.

DIII-D's philosophy has been, and will continue to be, that the entire PTDATA dataset will be available on disk for rapid access. Predictions for the total size of DIII-D's PTDATA repository at the end of FY24 range from 1.2 PB (25% growth) to 2.6 PB (50% growth). The existing PTDATA system, Athena, will reach full capacity early in FY20. A new system will be put into production and will continue to use a ZFS-based file system with the benefits of native compression as well as replication. The new system will have a flexible design so that additional storage can be added as required to handle either the 25% or 50% growth rate.

DIII-D's MDSplus repository contains approximately 23 TB of compressed data, with an anticipated yearly growth rate on the order of 15%, yielding approximately 50 TB of data in 2024. As with Athena, the existing MDSplus system (Atlas) will reach full capacity during the proposed five-year plan. Therefore, a new system will be put into production, which will continue to use a ZFS-based file system and have a flexible design allowing additional storage to be added if the 15% growth trend is significantly exceeded.

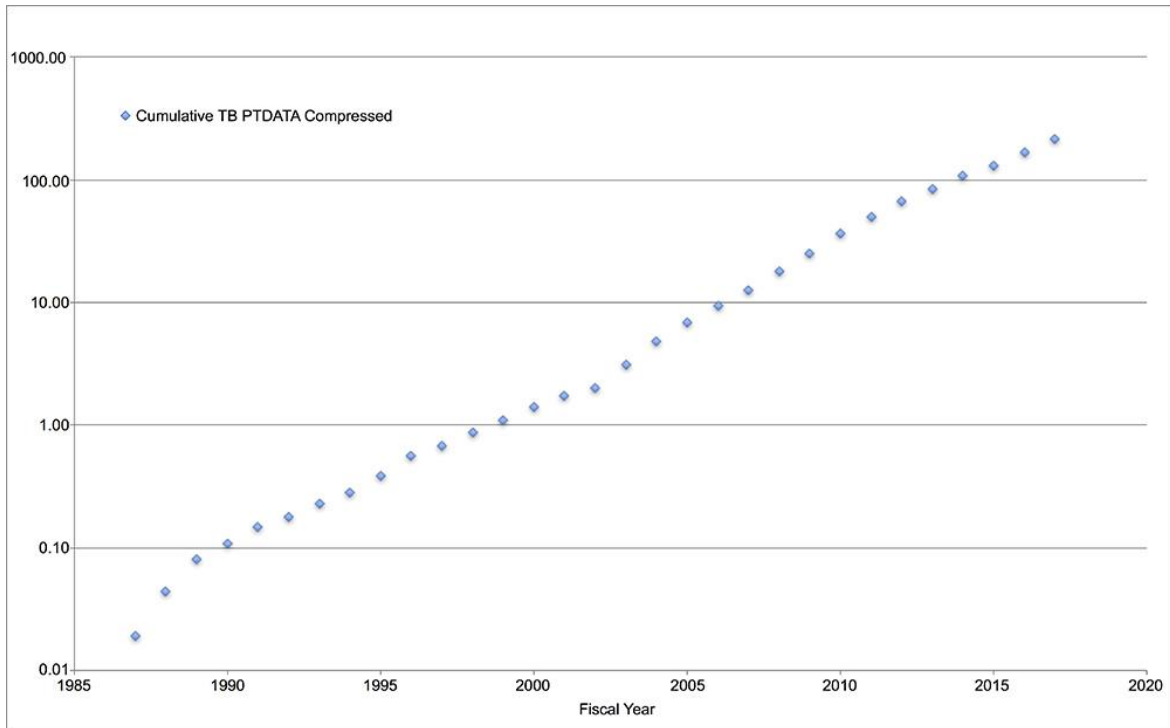


*Fig. 7-2. DIII-D’s raw data repository (PTDATA) has had year-over-year growth rates between 25% and 50% with an anticipated total size at the end of the proposed five-year plan between 1.2 PB and 2.6 PB.*

Previously, the storage of DIII-D’s camera diagnostic data was transitioned to an object storage repository rather than storage on the same file system used for user files. The two primary benefits of this storage methodology are a reduced cost per TB of storage compared to the user file system and that camera data can be accessed via a client-server system using the S3 (Simple Storage Service) API (application program interface) from any approved computer without the need for mounting a file system. This methodology will be continued in the present five-year plan. The total camera data repository is at about 40 TB and is increasing at about the same rate as PTDATA. However, like Athena and Atlas, the object storage hardware will reach full capacity during the proposed five-year plan. Therefore, it will be replaced and its capacity increased to accommodate the increasing size of the camera data.

It should be noted that a policy change was previously enacted whereby two spinning copies of both PTDATA and MDSplus are retained in the data center allowing for rapid recovery if the primary system fails. This policy will continue and the object storage will continue to be used as the location of the second spinning copy of PTDATA. The new Atlas system for MDSplus will continue to have two distinct spinning copies contained within the overall system.

Previously, the storage of user files was transitioned to a ZFS-based file system. Given the large amount of ASCII files, a space savings of 1.5x was observed due to compression yielding a

total repository size of approximately 40 TB. As was done for PTDATA and MDSplus, a second spinning copy of the user file system is also maintained. Given the recent dramatic increase in computational power available to the scientific staff (see next section) it is hard to predict the growth of the user file system but based on recent trends, a growth rate of 10 TB per year would not be unexpected. This growth rate will not exceed the capacity of the present system, but in keeping with our philosophy of replacing critical computer hardware by at least the five-year mark, the hardware will be upgraded during the proposed five-year plan.

For additional data protection against catastrophic failure, a tape backup system will continue to be used for all data. Four tapes are written; two each of PTDATA and camera data with one copy of each stored permanently off-site for disaster recovery (DR). Since PTDATA and camera data are write-once data, tape storage only needs to handle the incremental increase. In contrast, the write-many data of MDSplus and user data is incrementally backed up nightly and a full backup is done monthly and also stored off-site. All systems (~100) are also routinely backed up for recovery purposes. To keep pace with the increasing volume of MDSplus and user data, the tape system that includes a backup server, a large (~300 TB) hard disk staging area, tape drives, and tape robots will be routinely upgraded.

Although a second spinning copy of critical data is presently maintained for rapid recovery in the event of device failure, they both reside in the same data center and, thus, there is no geographical separation of these two copies. When data repositories reach 100s of TBs or even PBs, recovery from standard tape systems takes too long (months) to allow reasonable business continuity. Therefore, as part of this five-year plan, an off-site ZFS replication of the MDSplus and user file repositories will be accomplished by contracting with a third-party data center. The built-in replication that is inherent to ZFS is perfectly suited for automatic synchronization of these read-write repositories. The replication of PTDATA could be accomplished in an identical fashion, but since it is a write-once system, it presently makes greater budgetary sense to accomplish geographical replication in a different manner. Several paths will be investigated and one includes using the high-speed tape system (HPSS-High-Performance Storage System) at NERSC. Although tape based, this system is very high performance, such that just a few of their tape drives can saturate DIII-D's 10 Gb/s network connection resulting in a data recovery on par with reading from a local high-performance disk array.

### **7.3.2 Computational Systems**

Previously, a transition was made to a new computational environment yielding more computational power and a better overall file organization system. The old Venus cluster that ran Sun Grid Engine for its queuing system was replaced by the Iris cluster running the Slurm workload manager. The old mix of /u/ and /data/ for all codes, libraries, and user files was replaced

with the more structured `/home/`, `/usc/`, and `/project/` environment. For the proposed five-year plan, the same workload manager, directory structure, and architecture of interactive and worker nodes will be maintained, yet the Iris computational cluster will need to be refreshed. Included in the work will be the transition of the operating system to version 8 of Red Hat Enterprise Linux. In addition, system enhancements will be aligned relative to the mix of DIII-D codes running at that time. For example, an increase in GPU processing power may be beneficial or the introduction of InfiniBand networking in conjunction with 10 Gb/s Ethernet may be beneficial depending on the software demands.

The other large computational capability utilized by the DIII-D program are the computers that perform all of the automated between-pulse data analysis. More than 100 analysis codes run after every pulse that compute simple scalar quantities such as total beam power, the complete time history of kinetic profiles such as  $n_e$ ,  $T_e$ ,  $T_i$ ,  $V_r$ ,  $P_{rad}$ , and  $Z_{eff}$  as well as perform a time-independent power balance. Presently, three computer systems are utilized for between-pulse analysis and they will be refreshed during the five-year plan. Part of that refresh will be an examination of the codes that are running and those that are anticipated relative to current CPU demands to be sure that there is enough computational headroom to grow as data analysis is added. GPUs will also be added if there are analysis codes that can take advantage of these hardware systems. For between-pulse analysis tasks that require significantly greater computational resources than are available on-site, success has been obtained running between-pulse codes at remote large computational centers [Kostuk 2017]. As the between-pulse computational needs of DIII-D continue to grow, off-site resources will be pursued as required.

### 7.3.3 Networking

The DIII-D project is connected to the Internet at 10 Gb/s via the Energy Sciences Network (ESnet). A diverse-path backup network connection is provided at 1 Gb/s. For this proposal, the DIII-D network will remain connected to ESnet and an upgrade of the backup network to 10 Gb/s, that is presently being investigated, will be completed. Besides allowing fail-over with no loss of network speed, a backup network at 10 Gb/s can be used in conjunction with the main network to double the Fusion network's connectivity to ESnet. This would be very valuable if the remote operation of other tokamaks (e.g., EAST) becomes routine and puts a strain on the Fusion network's existing 10 Gb/s connectivity. The ESnet Site Coordinators Committee (ESCC) provides a forum for DIII-D's network site coordinator to interact with ESnet staff, as well as site coordinators from other laboratories. Participation in the ESCC has previously proven very valuable to the DIII-D project and will be continued in the proposed five-year plan.

Substantial progress was made upgrading the Fusion network infrastructure during the current five-year plan with all core and edge networking switches replaced, as well as the extension of 10

Gb/s networking deeper into the DIII-D experimental facility. In addition, a new next-generation firewall was put into production and significantly improved DIII-D’s cybersecurity posture by combining traditional firewall technology with other network device filtering functionalities, such as an intrusion prevention system (IPS) and URL filtering.

Upgrades planned for the Fusion network include the full deployment of Network Access Control (NAC) as well as complete segmentation of the network. The complete refurbishment of the underlying network hardware allows these two large steps to now be pursued. Deployment of NAC yields much tighter control of new devices added to the Fusion network as well as devices that physically move around the network. Segmentation of the Fusion network allows the grouping of systems and services into appropriate enclaves yielding reduced congestion (better performance) and improved security.

A Fusion wireless network will be deployed during the proposed five-year plan. This new wireless network combined with NAC and segmentation allow the DIII-D scientific team to be mobile within the DIII-D complex (offices, conference rooms, experimental facility) yet obtain the same level of performance with appropriate security as with the wired network.

## **7.4 DATA ANALYSIS AND REMOTE PARTICIPATION**

*Lead Personnel: D. Schissel (GA), B. Penaflor (GA), D. Piglowski (GA), S. Flanagan (GA), R. Johnson (GA), D. Miller (GA), M. Kostuk (GA), B. Sammulu (GA), C. Parker (GA), K. Greene (GA), L. Coviello (GA), F. Garcia (GA), M. Margo (GA)*

### **7.4.1 Analysis Infrastructure**

In today’s world, a scientific data analysis infrastructure, by necessity, consists of a broad range of Information Technology components that include data management, scientific visualization, high-performance computing, analysis algorithms, web technology, monitoring, software regression testing, and advanced collaborative environments. As always, the overarching goal is to allow faster, more secure, easier access to all analyzed data, data analysis codes, and visualization applications on a 24/7 basis. For DIII-D, data analysis needs to be accomplished on three timescales, each having its own unique challenges. Real-time computing was discussed earlier under Plasma Control. The between pulse time-scale of ~15 minutes is critical for data analysis that informs effective decision making during an experiment [Schissel 2010]. The long timescale includes the periods prior to and after the experiment; this data analysis is critical to developing effective experimental plans, post-experimental understanding, and subsequent publication of results.

Substantial progress was made previously with the transition to the new computing environment (e.g., Iris for computing and /home/, /usc/, /project/ for storage), which has been used

for both between-pulse and longer-term data analysis. The newer environment provides for greater computational power, a more centralized location for general libraries and routines, and easier exploration of software availability. During the transition, substantial effort was dedicated to reducing name pollution on codes and routines, general efficiency enhancements, and the usage of Git, which is a software version control system for tracking changes in multiple computer files amongst a distributed development team. Between-shot analysis codes were similarly transitioned, and in some cases restructured, resulting in speed improvements and data availability up to four minutes earlier.

For the proposed five-year plan, a working group will apply advanced high-performance computing methods to existing DIII-D data analysis and simulation routines in an effort to modernize their performance and increase the efficiency of scientific research and discovery. Some benefits have already been observed with large user codes (e.g., SURFMN achieved ~20x single processor speedup) and it is anticipated that there are a large number of additional legacy codes that will also see a reduction in computation time. The optimization methods include relying upon MPI for proper parallelism, while reducing MPI overhead and overlapping communication with computation, increasing the usage of OpenMP vectorization and cache-alignment, streamlining data formats, and reducing file system input/output with direct data access to and from the MDSplus and PTDATA data repositories (Fig. 7-3). Improving existing codes in this way generates more scientific productivity by directly reducing the time to solution, and increasing the resolutions, numerical stability, and physics fidelity of simulation results. It also enhances the efficiency of the computational and human resources that are required to use the analysis tools, and improves future code maintenance through integration with modern software libraries.

Another area of modernization will be the transition, where appropriate, from IDL-based codes to Python. Such a change has the benefit of not requiring a commercial software license, relaxing a constraint on where the code can run; this is of particular importance when sharing analyses with our collaborating partners. In general, many of the legacy workflows can be modernized for efficiency and this includes supporting the broader adoption of OMFIT as a general workflow engine for data analysis.

The support for analyzed data storage in MDSplus and metadata in the relational database D3DRDB will continue. Administrative maintenance includes applying the normal software updates as well as the transition to new hardware when it becomes available. As new diagnostics are added and new analysis codes are written, user support will be provided with new data storage within MDSplus and D3DRDB. Enhancements to metadata storage at DIII-D that follow the path initiated by the MPO project [Schissel 2014] will be pursued to better track data provenance. The MPO (metadata, provenance, ontology) software system can automate the documentation of

scientific workflows and associated information. Tracking data provenance has the benefit of understanding data reliability and quality (e.g., automated analysis with no human examination) and also allowing for its reproducibility. It also provides a way to rapidly determine when an analysis change requires dataset recomputation. By implementing such an infrastructure, it affords the DIII-D facility the added benefit of having a historical record of all workflows and, therefore, an easy methodology to understand what analysis has been done on any particular shot. As the team grows and is more geographically dispersed, this will be an excellent way for results to be discovered and shared, thereby eliminating unnecessary duplication of analysis.

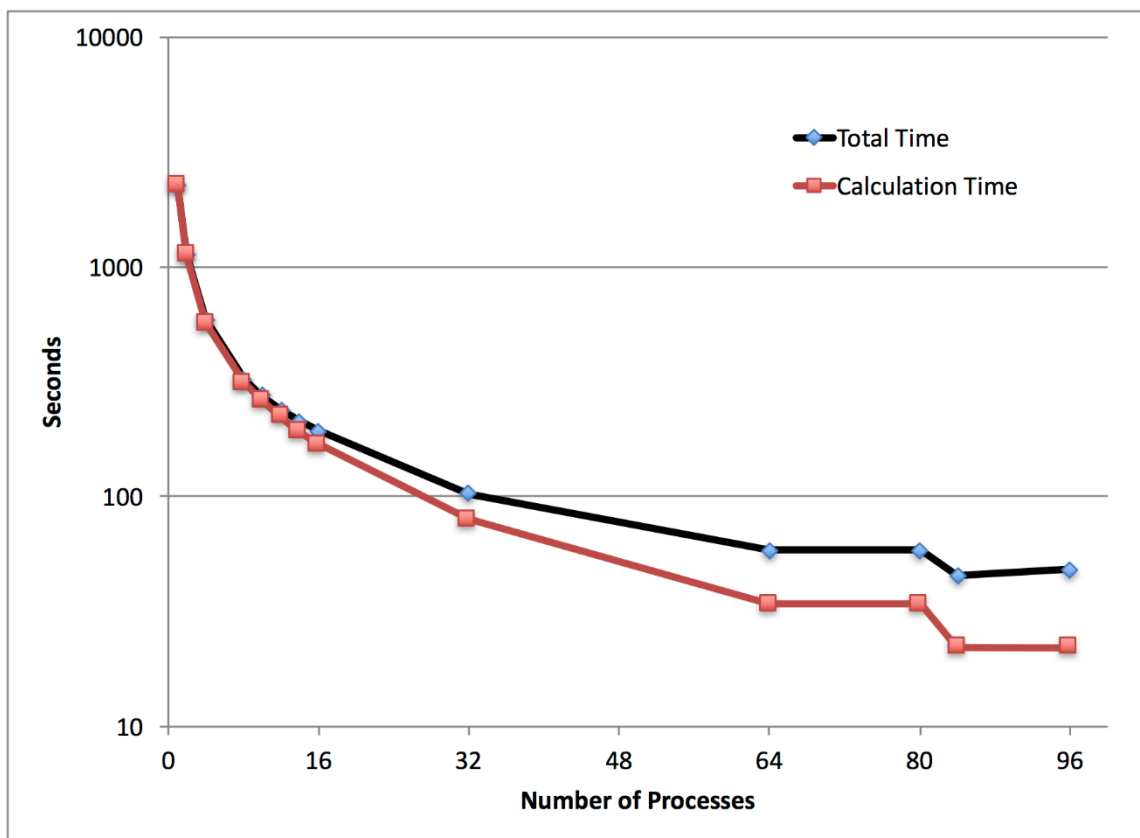


*Fig. 7-3. In addition to a 20x single process speedup for SURFMN, parallelizing with MPI allows strong scaling over many cores for even more dramatic reduction in time to solution.*

Visualization is an important component of the data analysis workflow, and in the five-year plan, existing core tools (e.g., ReviewPlus, EFITViewer) will be supported, new ones developed as required, and legacy applications retired. Although, for many years IDL has been the preferred language for graphics at DIII-D, the use of the Python programming language by the scientific staff has increased, and new tools will be targeted for Python. This transition to Python has the

added benefit of being a more widely-known language in comparison to IDL, thereby lowering the barrier for new staff and collaborators to be rapidly productive at DIII-D.

Another component of the data analysis infrastructure is the software codes that actually perform the analysis. To better monitor software quality, a dedicated system for software regression testing that leverages the Jenkins/Git infrastructure will be pursued. Jenkins is an open-source automation server for the non-human part of the software development process (executable building, regression testing, etc.) For DIII-D, the intent of regression testing is to ensure that a code change has not introduced a defect that results in an incorrect answer. For very large codes, regression testing is an excellent method to determine whether a change in one part of the software affects other parts of the software and therefore the code's output.

#### **7.4.2 Web Technology**

The usage of web technology has continued to grow at DIII-D with a 50% increase in the number of web accounts to ~770 over the past five years. The ability of the scientific staff to contribute to DIII-D's wiki-based web site has proven to be a valuable collaboration tool with ~2,500 pages and ~8,200 uploaded files. Web-based applications have also expanded in their scope and their usage remains fundamental to DIII-D's ability to meet its scientific mission. For example, the research opportunities forum website holds ~4,000 ideas submitted by internal and external users which are reviewed by an internal coordinator. The mini-proposal website has collected ~900 proposals which have gone through multiple levels of approval process and planning meetings (~3,100 mini-proposal reviewer comments and planning meeting entries). These mini-proposals have been scheduled into ~1,800 experiment entries in the schedule application. During operations, the electronic logbook is heavily used and currently holds ~312,000 entries.

The software technology refresh that was previously initiated will be continued during the five-year plan with an aim of increased efficiency, reduced duplication, ease-of-maintenance, and enhanced cybersecurity. Particular attention will be paid to existing web applications as the transition to an updated architecture will be completed with new frameworks and libraries. Current web applications' interactions with the internal systems and data stores will be reviewed and more secure and standardized methods will be implemented (e.g., RESTful API) to address the various access needs. Newer web applications, such as those for remote collaboration, will be expanded to meet the needs of the DIII-D community (Fig. 7-4). The ability to rapidly read data from any of DIII-D's data stores as well as perform interactive graphics via the D3 library allows a tremendous amount of scientific functionality to be made available via web applications. Under the new architecture and design, existing and new applications will be integrated to provide a seamless experience to the users.

The increase in complexity of DIII-D’s environment requires a concurrent increase in both data and code documentation. It is envisioned that this documentation will include the traditional text form and possibly tutorial-like videos. The latter will be viewed directly in the web browser via the DIII-D website. Although this capability will be new for DIII-D, it has been successfully used for online education and it should translate well as a how-to for less complex information for the scientific staff. Along with more documentation can come the difficulty in locating the relevant information. Given the substantial growth of the DIII-D website, its design will be examined and, if required, a new structure and layout will be deployed to enhance usability.

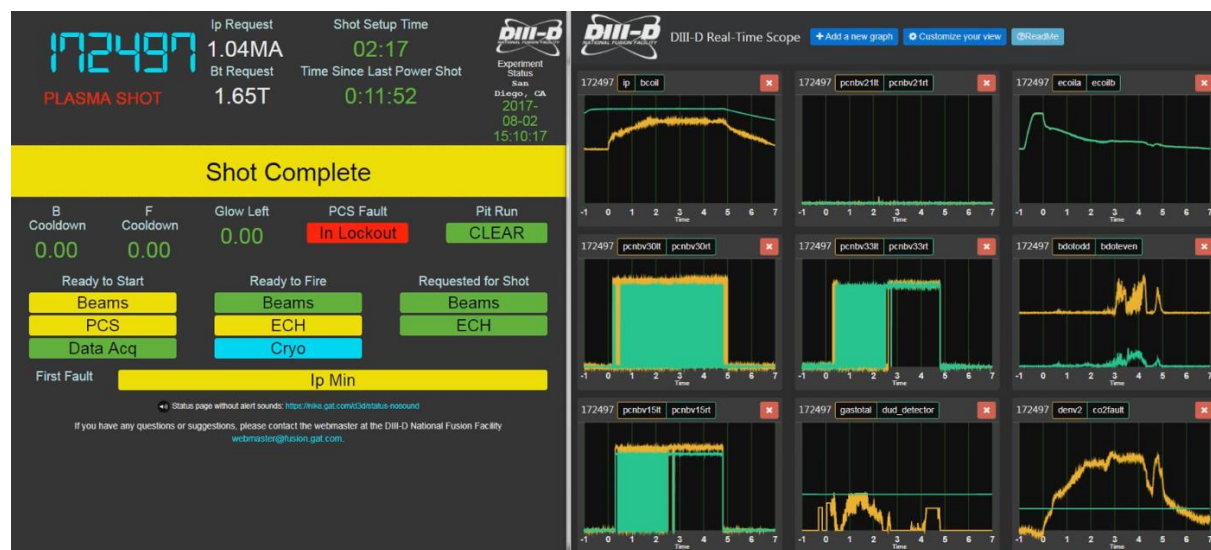


Fig. 7-4. Web applications have been deployed that allow monitoring of the DIII-D shot cycle as well as real-time plasma control data visualization for scientists not physically located in the DIII-D control room.

Finally, the public-facing nature of DIII-D’s websites means that they are often targets for attempted security breaches. The footprint of DIII-D’s public facing website will be reduced in scope, and the underlying software significantly hardened for enhanced cybersecurity. As part of the overall DIII-D cybersecurity plan, all DIII-D websites are maintained with security updates and will be internally scanned on a regular basis to search for new vulnerabilities, and if found, they will be mitigated. To better monitor and manage information made public via the web, a retention policy and content publishing process will be periodically reviewed and updated as required. Finally, dedicated hardware will be upgraded as required.

### 7.4.3 Remote Participation

Previously, the DIII-D project transitioned from using ESnet’s audio-video bridging services to a commercial solution provided by Zoom Video Communications to support remote meetings. The Zoom solution (Mac, PC, tablet, phone) for audio, video, and screen sharing has proven very

successful and will be continued for meetings, as well as for collaboration with the DIII-D control room during operations.

Enhancements to remote participation in DIII-D operations will include greater availability of real-time data as well as audio from the control room. Real-time data includes read-only information from the PCS as well as general status information from the tokamak control computers which will be made available using web applications in conjunction with enhancements mentioned above. Remotely available control room audio, shared via Zoom, will be augmented with automatically generated audio from the tokamak control computers that specify the steps in the pulse cycle (e.g., “annex cleared,” “ready to fire,” “pulse in progress”). Joining the automated audio on Zoom will be the audio announcements that the Session Leader makes over the control room’s PA system. Taken as a whole (real-time data, status data, enhanced audio), the ability to effectively remotely participate in DIII-D’s operation will be greatly enhanced.

## 7.5 CYBERSECURITY

*Lead Personnel: T. Waddell (GA), D. Miller (GA), L. Coviello (GA)*

DIII-D Cybersecurity’s objective is to protect data resources from internal and external cybersecurity-related threats by implementing industry-accepted security best practices in cyber planning, implementation, management, and operations, focusing on the following initiatives:

- Devising techniques for cost-effective security measures that appropriately safeguard the DIII-D network, information systems, and information system resources.
- Developing programs that validate information security in systems and services, which in turn form the basis for continuous improvement initiatives.
- Continuous monitoring and improvement of situational awareness for all DIII-D information systems as needed to maintain a safe cyber environment.

The overall objective is to provide situational cyber awareness for management to make informed decisions before, during, and after an incident.

### 7.5.1 Training

It is essential to educate the DIII-D user community concerning cyber risks, vulnerabilities, and protection requirements, particularly as new and emerging technologies are employed. There is a need for the ability to collect metrics to measure the progress of the cyber awareness training of the DIII-D user environment. Providing metrics by monitoring the progress of Cyber Security Training will help in gauging the level of the effectiveness of the cybersecurity training program. This may require a third-party service to provide a view that is unbiased of users’ cybersecurity program training levels. This should occur annually, allowing for annual adjustment of the

program for the evolving threats. Using security awareness training and phishing security tests can be effective tools to reduce unintentional insider threats. However, if robust metrics are not put in place, phishing tests can create organizational social engineering blind spots.

### **7.5.2 Privilege Access Management**

Separation of duties, user, and admin privilege, access, and password management is planned for implementation by FY20. The implementation of these technical management processes follows DOE best practices, ensuring each user account is notified and required to change their password within the password cycle requirement specifications. Late FY19 is the target time for test and initial implementation. This may also be accomplished using Mutli-Factor access methods, thereby eliminating the use of passwords altogether.

### **7.5.3 Patch Management**

Maintaining patch management requires enhancements to the current monitoring system. This will ensure that the system meets the required patching level for the system/resources being monitored. By FY22, patch management system for the various operating systems (OS) should be enhanced for improvement and analytics.

### **7.5.4 Continuous Monitoring**

Better ways to monitor and analyze machine-to-machine communications will be a big step for continuous monitoring. This will be an ongoing annual update/enhancement task to review the current tool and evaluate new developing tools that work with industry best practices for continuous monitoring of analytic data. Enhancement to the Network monitoring services is another layer of protection used to manage the cyber risk of the DIII-D network. Maintaining and enhancing existing tools, such as web scanners like Netsparker and vulnerability scanners like Nessus, used for vulnerability scanning internal resources, will be an ongoing annual occurrence. Enhancing monitoring tools will also add a layer of mitigation for emerging threats and vulnerabilities.

As Active Directory (AD) is introduced into the DIII-D network infrastructure, certificate management must be carefully maintained and monitored. This will require a major training/education effort for the staff, and will go a very long way in reducing the risk of loss of certificates. It will be a major contributing factor in the situational awareness of the DIII-D network. With the implementation of Active Directory (AD) in the NAC environment, protections for certificate management will be needed by FY22-FY23. This is a major step in mitigating cyber risk, by maintaining best practices in configuration management and access control, and providing continuous monitoring of Enterprise keys and certificates adding to the overall situational awareness and security.

Refurbishing and enhancing the cyber environment processes and security will be a constant, ongoing task to keep in step with the ever-changing and evolving cyber threats. This requires the use of industry’s best practices and tools to successfully manage and mitigate cyber risk.

Network Access Control (NAC) and network segmentation will provide additional layers of risk-reducing protection against unauthorized access of the network, providing ease of isolation of network cyber threats, reduction in the propagation of cyber threats, and mitigation of the risk of cyber intrusions.

Refurbishing and enhancing the firewall will provide next-generation monitoring and protection to the traffic on the DIII-D network. This will take place during FY23-FY24. Refurbishing, managing, and enhancing the VPN and SSL access will be used to manage and mitigate the risk encountered by enabling offsite network access for users. FY23-FY24 will be the next cycle of refurbishment for VPN, and will introduce enhanced multi-factor authentication processes.

## References

- [Kallenbach 1995] A. Kallenbach, et al., H mode discharges with feedback controlled radiative boundary in the ASDEX upgrade tokamak, *Nucl. Fusion* 35 (1995) 1231, DOI:0029-5515/35/10/I07.
- [Wu 2017] K. Wu, et al., Radiative feedback for divertor heat spread on EAST, *Fusion Engineering and Design*, submitted (2017).
- [Eldon 2017] D. Eldon, et al., Divertor control development at DIII-D and implications for ITER, submitted to *Fusion Eng. Des.* (2017).
- [Guillemaut 2017] C. Guillemaut, et al., Real-time control of divertor detachment in H-mode with impurity seeding using langmuir probe feedback in JET-ITER-like wall, *Plasma Phys. Control. Fusion* 59 (2017) 045001, DOI:10.1088/1361-6587/aa5951.
- [Eldon DOI:10.1088] D. Eldon, et al., Controlling marginally detached divertor plasmas, *Nucl. Fusion*; DOI:10.1088/1741-4326/aa6b16.
- [Kostuk 2017] M. Kostuk, et al., Automated between-pulse analysis of DIII-D experimental data performed remotely on a supercomputer at Argonne Leadership Computing Facility, accepted for publication in *Fusion Science & Technology* (2017).
- [Schissel 2010] D.P. Schissel et al., *Fusion Sci. Technol.* 58, 720 (2010).
- [Schissel 2014] D.P. Schissel, et al., “Automated Metadata, Provenance Cataloging, and Navigable Interfaces: Ensuring the Usefulness of Extreme-Scale Data,” *Fusion Engineering and Design* 89, 745-749 (2014).



## 8. THE COLLABORATIVE NATIONAL PROGRAM

The DIII-D National Fusion Program is a highly collaborative multi-institutional research endeavor with 637 professional scientific users from 106 institutions worldwide. The DIII-D research program derives its strength from the diversity and capabilities of its national and international collaborating institutions and associated individuals. GA has the largest number of directly funded scientific staff (full time equivalents) of any participating institution, but GA scientists comprise less than half the total scientific staff. Collaborating institutions and scientific collaborators have significant roles at all levels of the program. Consequently, the DIII-D program has and will continue to invest significant resources to grow and maintain supportive and effective collaborations.

University participation is critically important to the US Fusion Energy Sciences Program and to DIII-D. DIII-D facility users include 80 graduate students and 71 post docs (as of Q1 FY17), with 35 post docs and 24 graduate students conducting the bulk of their research on site at GA. University partners carry out highly visible and significant research in support of Fusion Energy Science and the DIII-D program. We continually seek to improve the research experience for these visiting scholars. The proposed facility investments laid out in this proposal will sustain a leading-edge research environment conducive to expanded university participation which will provide excellent preparation for next generation fusion scientists to enable the US to realize the full benefit of our participation in ITER.

The DIII-D National Fusion Program maintains close linkage to key elements of the broader US and international fusion science communities as part of its DOE FES mission. The DIII-D program is strongly coupled to the US Theory Program and to the growing number of topical centers in the US. The DIII-D Program also coordinates its research with other US and international fusion facilities through both formal and informal bilateral and multiparty agreements, including the US Fusion Facilities Coordinating Committee, the US Burning Plasma Organization (USBPO), the International Tokamak Physics Activity (ITPA), and the International Energy Agency (IEA) Technology Collaboration Programme for Co-operation on Tokamak Programmes (CTP). Specific international collaborations that receive funding separate from the DIII-D program (e.g., for EAST and KSTAR collaborations) are covered in separate proposals.

The DIII-D program actively participates in the ITER project on many levels, and DIII-D research addresses issues critical to the success of ITER. Each year the ITER Organization Central Team (IO-CT) is invited to propose experiments and participate in the DIII-D experimental planning process. The DIII-D program routinely supports testing of prototype

diagnostics, hardware, and physics concepts for ITER, often involving direct participation of members of the IO-CT. The USBPO coordinates US research in support of ITER and potential next-step experiments. Many DIII-D scientists serve in leadership positions within the USBPO, including Dr. Charles Greenfield, who serves as Director.

## 8.1 SCOPE OF THE DIII-D FUSION PROGRAM

Collaboration has been a signature feature of the fusion effort at GA since its inception. The present DIII-D National Program supports and benefits from a large number of diverse collaborations spanning the nation and the globe, as indicated in Fig. 8-1. These collaborations carry out the integrated DIII-D program mission. GA provides most of the operations support for onsite collaborators and, through data management systems and remote participation infrastructure, for national and international partners.



**Engaging and training a future generation of fusion scientists**

Fig. 8-1. National and international collaborations in support of the DIII-D research program.

In the present DIII-D National Fusion Program about 60% of the scientific staff (full time equivalents) are from collaborating institutions. There are a total of 637 users of the facility (data taken from facility user database), 77 from GA and another 560 from:

- 21 national laboratories (US [7], Europe [8], Korea [3], Japan, India, and Argentina);
- 67 universities (US [28], Europe [18], China [9], Japan [4], Russia [2], Australia, Brazil, Canada, India, Peru, and Turkey); and
- 15 domestic industrial companies (US [13], Europe [2])

- 3 others (ITER Organization, American Physical Society, Oak Ridge Institute for Science Education)

### 8.1.1 The DIII-D National Team

The core of the DIII-D National Team consists of about 90 operating staff and ~90 research scientists (details provided in Appendix E of this document). GA is responsible for facility operations and safety, though ~10% of the full-time employees (FTEs) are employed by collaborating institutions. The operating staff is responsible for the DIII-D tokamak and its major heating and current drive systems, as well as design, fabrication, and execution of major facility improvements. More recently, the larger collaborating institutions have assumed responsibility for providing key hardware systems for DIII-D, such as ECH launchers, neutral beam components, pellet fueling systems, and controls for major heating systems. These institutions have personnel onsite to assist with operation and maintenance of specific tokamak systems or larger diagnostic systems.

The team ranges from undergraduates to senior scientists with more than three decades of experience in fusion research. The presently active staff of DIII-D includes over 40 Fellows of the American Physical Society (APS) and 17 winners of the APS John Dawson Excellence in Plasma Physics Award (almost all based on research conducted at DIII-D). One of the research team members is a winner of the Maxwell Prize for Plasma Physics (M. Porkolab), two have won the Rosenbluth Award for outstanding doctoral theses, and three have won the Landau-Spitzer Award in 2014 (2) and 2016 (1). One team member recently won the Katherine Weimer Award for Women in Plasma Science.

Many of the DIII-D scientists provide broad operations support for the research program in the form of diagnostic development, operation and data analysis, as well as experimental program planning. Table 8-1 shows the programmatic roles of the larger collaborating institutions. GA often provides additional diagnostic support to collaborating scientists in the form of engineering design, infrastructure hardware, installation assistance, data acquisition hardware, and system maintenance. These collaborative efforts have increased the diagnostic capability of DIII-D dramatically, enabling comprehensive measurements of plasma profiles, magnetohydrodynamic (MHD) modes, and plasma turbulence and transport. These measurements are being compared against numerical simulation in unprecedented detail.

In addition to GA, there are 11 major collaborating institutions that have broad programmatic responsibilities on multiple topics. Major collaborating institutions join with GA to form an Executive Committee to guide the program's strategic and near-term directions. The programmatic responsibilities of these DIII-D collaborators are given in Table 8-1. Many other

collaborations involve both universities and national and international laboratories and institutes. University collaborations will be covered more fully in Section 8.3.

**Table 8-1. Programmatic Responsibilities for Collaborating Institutions with Representation on the DIII-D Executive Committee 2017-18**

---

**MIT**

Multi-channel, multi-scale core transport  
Efficient RF tools for off-axis current drive  
Disruption database for prediction/warning  
Naturally ELM-suppressed stationary regimes

**PPPL**

Core predictive transport in advanced regimes  
Impurity and main-ion transport  
NB, ECH and Helicon system support  
ELM & pedestal control: RMP & IGI  
Radiation and boundary configuration control  
Fast-ion transport in advanced regimes

**LLNL**

Advanced Tokamak development  
MSE current profile measurements  
DIII-D Experiment Coordination  
Div/SOL flow, spectroscopy  
Divertor Thomson & IRTV, IR/VIS periscope  
Div/SOL modeling (UEDGE)  
BOUT++ modeling of ELMS and QH mode

**ORNL**

Pellet ELM pacing hardware and experiments  
Diagnostics and modeling for 3D physics studies including RMP ELM control  
Disruption mitigation experiments: MGI, SPI  
Integrated modeling for advanced tokamak scenarios  
Boundary and PMI physics diagnostics and modeling

**SNL**

Characterization of Div/SOL conditions and determination of particle/heat flux  
Divertor erosion/redeposition measurements for coupled plasma-material models  
Surface analysis of wall materials  
Material transport, hydrogen retention, and plasma-induced changes to surface morphology  
Edge diagnostics (e.g. charge-exchange neutrals)  
Thermal Modeling of experiments

**UC Irvine**

Fast-ion physics  
Fast-ion diagnostics  
Alfvén eigenmode stability

**Columbia U.**

Leading role in resistive wall mode control  
Advanced tokamak development  
3D field physics  
Stability of the low torque ITER Baseline Scenario

**UCLA**

ITPA membership: Diagnostics TG  
Physics of anomalous thermal and particle transport, LH-transition, core turbulence, turbulent  $E_r$  and multi-scale turbulence and NTM coupling  
ITER reflectometer density profile system tests, monostatic, real-time FPGA phase processing, etc.  
ITER prototype microwave diagnostics  
Advanced diagnostics: turbulence/fluctuations of localized magnetic,  $n_e$ ,  $T_e$ ,  $E_r$ ; profiles of density, flows, and  $E_r$

**UCSD**

Disruption mitigation, disruption and quiescent runaway electron dissipation  
ELM control and 3D magnetic perturbation experiments and modeling  
Core transport model validation and experiments  
SOL transport and flows  
Plasma-surface interactions and dust physics  
3D MHD disruption and ELM modeling

**U. Texas**

Transport experiments and modeling  
Fine-scale (spatial, temporal) ECE  $T_e$  measurements  
Advanced Divertor Studies

**U. Wisconsin**

L-H transition physics, pedestal, 3D and core turbulence, in collaboration with NSTX-U & Pegasus  
Turbulent transport model testing and validation, 3D and pedestal transport modeling  
BES and UF CHERS fluctuation diagnostics  
Zonal flows and neoclassical MHD research  
3D effects in the pedestal, SOL, and divertor

---

**8.1.2 International Collaborations**

The DOE Fusion Energy Sciences Program is placing increased emphasis on international collaborations to prepare for participation in ITER and to exploit the capabilities of the existing and new superconducting tokamak experiments in Asia (EAST in China, KSTAR in Korea, SST-

1 in India, and JT60-SA in Japan). The DIII-D program continues engagement with a number of tokamak programs in Europe, as well. The guiding principle for DIII-D international collaborations is to seek out mutually beneficial partnerships that enhance the value of the DIII-D research program to the US fusion program and DOE through a combination of detailed exchanges of scientific information with foreign researchers and participation in complementary/confirmatory experiments on other fusion facilities. Collaborations are closely related to the research areas of prime interest to DOE and on DIII-D. Overall, the DIII-D program derives great benefit from its international collaborations. Further details on these international collaborations follows in Chapter 9.

## 8.2 NATIONAL LEADERSHIP ROLE AND PROGRAM LINKAGES

A key element of this DIII-D Program Plan is to provide national program leadership arising from the DIII-D mission: *optimization of the tokamak approach to fusion energy*. The US Department of Energy Office of Science Fusion Energy Sciences program (DOE FES) has put together a 10-Year Perspective to articulate its strategic plan. FES is now organized under two broad areas: Burning Plasma Science and Discovery Science. US tokamak research is supported under three sub-elements of Burning Plasma Science:

- **Foundations** — Focusing on domestic capabilities; major facilities and universities in partnership, targeting key scientific issues. Theory and computation focus on questions central to understanding the burning plasma state.  
*Challenge:* Understand the fundamentals of transport, macro-stability, wave-particle physics, and plasma-wall interactions.
- **Long Pulse** — Building on domestic capabilities and furthered by international partnership.  
*Challenge:* Establish the basis for indefinitely maintaining the burning plasma state including: maintaining magnetic field structure to enable burning plasma confinement and developing the materials to endure and function in this environment.
- **High Power** — ITER is the keystone as it strives to integrate foundational burning plasma science with the science and technology girding long-pulse, sustained operations.  
*Challenge:* Establishing the scientific basis for attractive, robust control of the self-heated, burning plasma state.

The DIII-D program seeks to be a recognized positive influence for US fusion research on many levels spanning all of these areas and, particularly, in research supporting a successful ITER program. Collaborations between DIII-D and other facilities and research groups are well-

aligned with the research activities within the Foundations and Long-pulse research areas as described in the language of the FY17 Presidential budget request (February 2016):

### **Foundations**

- Research at major experimental facilities aimed at resolving fundamental advanced tokamak and spherical torus science issues, including developing the predictive understanding needed for ITER operations and providing solutions to high-priority ITER concerns.
- Research on small-scale magnetic confinement experiments to elucidate physics principles underlying toroidal confinement and to validate theoretical models and simulation codes.
- Theoretical work on the fundamental description of magnetically confined plasmas and the development of advanced simulation codes on current and emerging high-performance computers.
- Research on technologies needed to support the continued improvement of the experimental program and facilities.
- Support for infrastructure improvements at Office of Science laboratories conducting fusion research.

### **Long Pulse: Tokamak**

- US research teams will be supported to work on the long-pulse international tokamaks that are coming online either now or in the near future. These teams will build on the experience gained from US fusion facilities to conduct long-pulse research on the international tokamaks. Long plasma pulse research will enable the exploration of new plasma physics regimes, and allow the US fusion program to gain the knowledge needed to operate long plasma discharges in ITER and other fusion energy devices.

The connections between the DIII-D program and other FES program elements under the Foundations and Long-Pulse topical areas will be described in the following sections, beginning with DIII-D research in support of ITER. Participation in ITER is the central element of the US fusion program, as “ITER represents an extraordinary commitment of funding and effort,” according to former FES Associate Director Dr. Edward Synakowski. Ensuring the success of ITER is seen as enabling for future steps toward fusion energy, and so remains the highest priority of the DIII-D program.

The possibility of providing the capabilities of DIII-D to a broader community for studies that are not directly targeted at fusion goals is being explored. In 2017, DIII-D was made available to the Discovery Science community through a one-week university-led non-fusion campaign that led to several important scientific results and a post-deadline invited talk at the 2017 APS-DPP Conference. DIII-D can offer new capabilities to the US Plasma Science community that leverage the investments already made to support DIII-D’s programmatic goals, and this segment of the program could grow in the future.

### **8.2.1 DIII-D Research in Support of ITER**

The DIII-D National Fusion Program is committed to the success of the ITER research program and to enabling the US ITER Project Office to fulfill its commitments to the international ITER project. The DIII-D National Fusion Program is addressing key issues related to the design, construction, and operation of ITER. DIII-D capabilities allow researchers to simulate many aspects of ITER operation; research on DIII-D has led to expansion of ITER capabilities. ITER-related experiments are the largest single component of the experimental program — using approximately half the run time to address urgent issues such as pedestal structure, edge-localized mode (ELM) control and pellet pacing, disruption mitigation, divertor and first-wall heat load management, and scenario development (e.g., Q=10 operation with an emphasis on low rotation, NTM control, and high-performance hybrid plasmas).

Members of the DIII-D National Team are actively engaged with the international fusion community in conducting ITER-related R&D. These collaborations leverage the capabilities of the DIII-D facility in significant ways: e.g., US research teams gain experienced international experts who bring fresh perspectives and new ideas with them, DIII-D data can be integrated into international databases more effectively, and US scientists gain access to international facilities with the corresponding ability to conduct more comprehensive experiments. In addition to individual international collaborations related to ITER, DIII-D team members are active in the International Tokamak Physics Activity (ITPA) and often lead or co-lead topical groups (see Table 8-2). The DIII-D program is well represented at the biennial ITPA topical group meetings and experimental proposals are developed that are aligned with ITPA research goals.

Every year, the DIII-D program creates a special session during its Research Opportunities Forum for the ITER Science and Operations Department to submit proposals for run time to address ITER-urgent issues. Members of the ITER science team regularly travel to San Diego to work with the DIII-D team and participate in experiments. The ITER team is also invited to comment on the DIII-D experimental program, both directly in meeting with the DIII-D Director, and as part of the DIII-D Program Advisory Committee, providing further input as to which proposed experiments might have the largest impact on the ITER project. Results from

such experiments are often reported during webinars organized by the USBPO, as well as at regularly scheduled ITPA meetings.

**Table 8-2. DIII-D Staff Participating in the ITPA Topical Groups as Members (approximately 55 more serve as official experts)**

<b>Coordinating Committee</b> C. Greenfield	<b>MHD, Disruptions, and Control</b> N. Eidietis R. Granetz J. Harris (Stellarator Rep) R. La Haye E. Strait
<b>Diagnostics</b> R. Boivin D. Hillis C. Lasnier	<b>Pedestal and Edge Physics</b> M. Fenstermacher (Vice Chair) J. Hughes R. Maingi T. Rognlén P. Snyder
<b>Energetic Particle Physics</b> W. Heidbrink M. Van Zeeland	<b>Scrape-Off-Layer and Divertor</b> H. Guo (representing China) R. Doerner A. Leonard P. Stangeby
<b>Integrated Operation Scenarios</b> J.-M. Park E. Schuster J. Ferron	<b>Transport and Confinement</b> G. McKee S. Mordijck C. Petty G. Staebler

As expected, ITER’s needs are shifting from design-related issues to operational issues. DIII-D has already contributed to development of operating scenarios, preparation for hydrogen and helium operation, and simulated operation of the ITER control system. Hydrogen and helium operation are important because the ITER research plan includes two non-activated operational phases with these as the working gases, whereas all high-power, high-performance tokamaks have operated exclusively in deuterium for the past 20 years. As a result of these R&D activities in support of ITER, the DIII-D facility will provide excellent training for the next generation fusion scientists in the US who will assume responsibility for conducting fusion experiments on ITER.

### 8.2.2 DIII-D Support for the US Burning Plasma Organization

The US Burning Plasma Organization (USBPO) was created in FY06 to coordinate relevant US fusion research with broad community participation “to advance the scientific understand of burning plasma and ensure the greatest benefit from a burning plasma experiment.” DIII-D

scientists were instrumental in setting up the organization. Dr. T.S. Taylor, former DIII-D Program Director, served as the first Deputy Director of the USBPO.

Dr. Charles Greenfield of GA serves as Director of the USBPO, and Drs. David Pace and Gary Staebler of GA serve on the USBPO Council. Other DIII-D scientists serve as topical group leaders or deputy leaders:

Max Austin (Texas)	Diagnostics (Leader)
Eric Bass (UCSD)	Energetic Particles (Leader)
Dan Boyer (PPPL)	Operations and Control (Deputy Leader)
Cami Collins (GA)	Energetic Particles (Deputy Leader)
Luis Delgado-Aparicio (PPPL)	Diagnostics (Deputy Leader)
Jerry Hughes (MIT)	Pedestal and Divertor/SOL (Deputy Leader)
Lang Lao (General Atomics)	Modeling and Simulation (Leader)
Saskia Mordijck (William & Mary)	Confinement and Transport (Leader)
Carlos Paz-Soldan (General Atomics)	MHD, Macroscopic Plasma Physics (Deputy)
Eugenio Schuster (Lehigh)	Operations and Control (Deputy Leader)
Francesca Turco (Columbia)	Integrated Scenarios (Deputy Leader)

### 8.2.3 DIII-D Research and US Theory Program

The DIII-D program prominently features close interactions between theorists and experimentalists both within the US and worldwide. Theory motivates and guides formulation of experimental proposals and, conversely, DIII-D experimental observations are often used to guide development of theory and computational tools. DIII-D, with its comprehensive diagnostics, provides key data for testing theories of confinement, stability, energetic particles, and rf heating and current drive. Theorists are included in DIII-D near-term and long-term program planning and serve on the DIII-D Research Council. They are actively involved in the planning, execution and analysis of DIII-D experiments. This interaction, together with systematic validation of theoretical predictions with experiments, has led to the identification of a great deal of important new physics.

The GA Theory Group is uniquely placed in facilitating community involvement in DIII-D. The GA Theory Group hosts visitors and enables remote collaboration with numerous US and worldwide theory programs, assists in training graduate students and postdocs, and develops and supports a well-integrated set of numerical tools (including TGYRO, GYRO, NEO, TGLF, GATO, ELITE, EFIT, ONETWO) and the OMFIT integrated modeling framework, which are used by an extensive group of users at DIII-D and around the world. The GA Theory Group and its collaborators focus on six areas of research:

- Macroscopic Stability,
- Confinement and Transport,

- Boundary Physics,
- Plasma Heating and Non-inductive Current Drive,
- Energetic Particles, and
- Integrated Modeling.

Six members of the GA Theory Group are APS fellows, two have won the General Atomics Marshall N. Rosenbluth Award for Fusion Theory, and two have been awarded the American Physical Society John Dawson Award for Excellence in Plasma Physics Research.

Through its interactions with the GA Theory program and its onsite collaborators, the DIII-D program maintains close connection to the US Scientific Discovery through Advanced Computing (SciDAC) program and other FES Theory program initiatives. SciDAC projects and theory and simulation initiatives which feature strong connections to the DIII-D program include: Center for the Study of Plasma Microturbulence (CSPM), Gyro-kinetic Simulation of Energetic Particle Turbulence and Transport (GSEP), Edge Simulation Laboratory (ESL), Center for Edge Physics Simulation (EPSI), Center for Simulation of Wave-Plasma Interactions (CSWPI), Center for Extended MHD Modeling (CEMM), Plasma Surface Interactions (PSI): Bridging from the Surface to the Micron Frontier through Leadership Class Computing (PSI SciDAC), and Advanced Tokamak Modeling (AToM), and Simulation Center for Runaway Electron Avoidance and Mitigation (SCREAM).

In the following, a brief description of the relationships between DIII-D and some of these projects is given:

- In connection with CSPM, benchmarking and validation exercises related to core and pedestal drift wave instabilities and transport are ongoing using data from DIII-D experiments.
- Through the GSEP project, GYRO was applied to simulate reversed-shear Alfvén eigenmodes and toroidal Alfvén eigenmodes in DIII-D and local energetic-particle turbulent transport. An energetic-particle density transport code, ALPHA, was recently developed and has been applied to validate a critical-gradient energetic-particle driven Alfvén eigenmode transport model with data from the DIII-D tilted beam experiments. A new kinetic energetic-particle transport code, EPtran, was also developed and successfully applied to simulate a DIII-D tilted NBI discharge.
- Through the ESL project, the NEO drift-kinetic neoclassical transport code was developed and is being applied to study neoclassical flows and transport in DIII-D experiments. Integration of NEO into the TGYRO code improves DIII-D steady-state gyro-kinetic transport studies. NEO has been extended to 3D and has been applied to

study 3D effects on neoclassical transport and bootstrap current in DIII-D geometry. ESL is also engaged on the development of a new gyro-kinetic code CGYRO to enable more extensive gyro-kinetic studies near the edge of DIII-D.

- The GA Theory group, working with the CEMM project, put a large effort into linear and nonlinear ELM simulations and ELM mitigation by resonant magnetic perturbations (RMPs). M3D-C1 is being extensively applied to simulate plasma response to RMP fields and their effects on ELMs. In addition, a resistive-wall model has been implemented in M3D-C1. This new capability is being used to model a number of effects in DIII-D, including RMP plasma response with improved boundary conditions and VDEs during the current quench phase of disruptions.
- In direct collaboration with the CEMM effort, NIMROD has been applied to simulate mitigated and unmitigated disruptions using improved radiation, runaway electron, and pellet/gas-jet penetration models, including the effects of plasma rotation. In addition, NIMROD has also been applied to simulations of disruption mitigation and RE confinement.
- The AToM SciDAC project is led by GA Theory in collaboration with UCSD, ORNL, LLNL and the FastMath (Frameworks, Algorithms and Scalable Technologies for Mathematics) and Super (Sustained Performance, Energy and Resilience) SciDAC institutes. The goal of the AToM project is to enhance and extend the best existing integrated, predictive modeling capabilities. In the short-term, AToM targets integration of core and edge simulations and workflows, and in the longer-term seeks to also incorporate scrape-off layer physics workflows with both SOLPS and COGENT. The key component in this effort is the OMFIT framework, which has been expanded to include BOUT, NIMROD, COGENT, SOLPS, and EPED modules. A recent showcase workflow has been developed that couples the TGYRO and EPED modules to carry out transport simulations with a dynamically evolving pedestal. New reduced pedestal and transport models based on smoothed neural-net representation to allow fast prediction have been developed and tested. Ongoing validation of this new capability with DIII-D data is underway.
- In connection with the SCREAM SciDAC project, benchmarking and validation exercises related to runaway electron generation and evolution and scenarios for avoidance are ongoing using data from DIII-D experiments.

Serving in its role as a national fusion facility, DIII-D data is made available to theorists worldwide via a number of collaborations targeting some of the most challenging issues confronting fusion energy science. The GA Theory group and its collaborators are uniquely

placed in this regard with its past history of leadership in this area. Both the theorists onsite and the experimental research staff are committed to helping collaborators in the US Theory Program with access to the data for validation of theory. Infrastructures have been set up to facilitate this interaction, which produce a continuous dialogue between theory and experiment.

Close theory interactions occur throughout the DIII-D research program. Five areas are of particular interest.

**Turbulence and Transport:** Turbulence and transport studies on DIII-D have improved physics understanding and identified new challenges. The theory group at GA approaches the problem of transport in tokamak plasmas using full gyro-kinetic simulations and computationally more efficient theory-based transport models accurately fitted to these simulations to predict self-consistent plasma profiles with sources. This work is greatly enhanced by the close relationship between Theory and the DIII-D National Tokamak Program, including extensive engagement in the planning and analysis of turbulence and transport experiments. An existence of multiple transport states due to Shafranov-shift stabilization was recently demonstrated for the DIII-D high- $\beta_p$  regime discharges using TGLF that has very promising implications for improved energy confinement in a high-bootstrap fraction reactor operating regime. A new predict-first initiative focusses on using predictive simulations and models before an experiment is being conducted to aid in planning of experiments as well as uncertainty quantification and validation of models.

**Pedestal Physics and Control of Edge Localized Modes (ELMs):** The GA Theory group has made important breakthroughs in physics understanding of ELMs, ELM-free operation, and ELM mitigation over the past few years. In particular, the ELITE code and EPED pedestal height and width model, pioneered by GA in collaboration with the University of York, has continued to be quantified, elaborated, and extensively and successfully tested against experimental data from DIII-D and other tokamaks. The ELITE MHD code has recently been extended to treat low- $n$  modes, which enables it to efficiently study the full range of MHD modes limiting the pedestal, including lower  $n$  ( $n = 1,2,3$ ) edge modes that can be limiting in low collisionality regimes such as QH mode.

**3D Fields for ELM and Rotation Control and Transport:** Significant new capabilities for 3D modeling have been developed in the past few years, and will play a greater role in theory and analysis going forward. M3D-C1 has been extensively applied to analyze DIII-D experiments, particularly those involving the application of external 3D magnetic fields. Recent M3D-C1 simulations of plasma responses driven at rotation zero-crossings find that the change to the resonant field as the zero-crossing approaches a rational surface have a significant impact on the external perturbed magnetic field, and the quasi-linear torque of the plasma response may

play an important role in bifurcations into ELM suppression. Continued applications of M3D-C1 to calculate the extended MHD plasma response to these applied fields are planned.

**Disruption Mitigation and RE Physics:** NIMROD modeling of disruption mitigation in DIII-D has led to an increased understanding of the role played by MHD in MPI experiments, particularly in producing radiation asymmetry. Recent NIMROD simulations of shell-pellet injection show that the thermal quench time can be tailored by varying the payload composition. The unified theory of pellet ablation for arbitrary atomic number  $Z$  has been extended to include multi-species pellets such as mixtures of deuterium and neon, and polyatomic (molecular) pellets for DIII-D applications.

**Integrated Modeling:** The OMFIT framework has been specifically developed to provide a modern infrastructure to support DIII-D integrated modeling and to facilitate DIII-D theory-experiment comparison. A large number of physics workflows have been developed and validated against DIII-D data. Significant improvements to the OMFIT framework and progress on a broad range of its physics modules were made in a recent OMFIT code-camp. Validation of a new OMFIT workflow that enables profile prediction using core transport coupled to a dynamic pedestal model shows that the experimental profiles can be predicted with high fidelity for a DIII-D ITER baseline scenario discharge. Two highly efficient numerical tools for predicting tokamak pedestal height and width and transport fluxes that are capable of real time application have also been developed based on the smooth neural-net method. An updated OMFIT coupled core-pedestal workflow that is capable of using the full TGLF transport model or its smooth neural-net representation has been successfully benchmarked against data from a DIII-D ion-stiffness experimental database.

#### 8.2.4 Role of DIII-D Research for Enabling Technologies, Contributions, and Needs

Progress in fusion has been closely coupled to advances in enabling technology. DIII-D will continue to participate in developing enabling technologies critical to the future of the tokamak in burning plasma experiments (e.g., ECH systems, RF systems, and innovative plasma-facing materials and advanced divertor development). DIII-D participation in the Virtual Laboratory for Technology (VLT) features strong connections to the materials development and modeling community including SciDAC-PSI. The DiMES/MiMES materials evaluation and ALPS PMI modeling programs are part of the VLT program activities with broad national and international collaborations in this critical area. In addition, DIII-D plays a leading role in the development of advanced divertor configurations to address heat exhaust and erosion issues facing PFMs for the steady-state operation of advanced tokamaks.

A key DIII-D enabling technology need is for reliable, long-pulse high-power ( $P_{\text{tube}} \geq 1.5$  MW) gyrotrons at 117.5 GHz. Long pulses are essential to control the current-density profiles

due to the long current diffusion times of the plasma. Using internal research and development funds, GA supported the design of a second-generation depressed collector tube by Communications Power Industries (CPI). The DIII-D program supported the gyrotron fabrication, testing, and subsequent R&D program to address the voltage standoff problem of the prototype gyrotron, rebuild of the tube, and the ongoing installation and commissioning of the remanufactured tube to high power and long pulse. In the future, 1.5 MW tubes will save money on ECH systems since fewer power supplies and control systems will be needed. The Advanced Tokamak program directly benefits from development of improved launchers to allow fast tracking for MHD mode control.

Plasma control and operations research is essential to the development of fusion energy in order to convert advances in tokamak physics to operational solutions. Control mathematics and related approaches to design of effective real-time algorithms are themselves critical enabling technologies for successful experiments and a successful fusion power plant. Enormous strides have been made at DIII-D in these areas, including model-based design of controllers for current profiles, divertor operation, off-normal and fault responses, development of real-time identification of potentially disruptive states, and faster than real-time plasma state evolution codes. These advances must be extended, and new potentially transformational algorithmic and computational technologies must be applied to fusion problems. Machine learning methods, artificial intelligence advances, and real-time parallel processing algorithms should be increasingly exploited to enable both extraction of unperceived physics knowledge from the large DIII-D database, and design of controllers with unprecedented internal logic complexity, performance, and reliability.

Continuing advancement in the DIII-D experimental program requires consistent development of powerful control algorithms that make possible the identification and elucidation of new physics understanding. Increasing focus at DIII-D on highly precise and sustained advanced tokamak plasma regimes requires continuing progress in active control to maintain desired current density and pressure profiles, with integrated regulation of divertor and boundary characteristics. Active regulation of MHD instabilities and fast particle-driven modes will require advances in real-time analysis of plasma stability and algorithms capable of maintaining distance from stability boundaries. New DIII-D actuators, including additional off-axis neutral beams, new RF current drive and heating systems, and additional power supplies, will enable both achievement and regulated sustainment of high-performance plasma regimes.

The DIII-D group continually develops, tests, and applies new control systems as a necessary part of its research program. The DIII-D Plasma Control System (PCS) itself has been exported to nearly a dozen devices over the last two decades, and continues to be the most widely-used

PCS in the world. Highly effective DIII-D collaborations in scenarios and control on devices sharing the DIII-D PCS, including EAST and KSTAR, will continue to advance understanding of sustained long-pulse operating scenarios in superconducting tokamaks.

Disruption avoidance and mitigation is also needed on next-generation experiments such as ITER. DIII-D is presently working with the fusion community to advance disruption-effects-mitigation techniques, such as shattered pellet injection and shell pellet injection. Recent experiments that seek to safely dissipate disruption-induced runaway electrons continue to benefit from regular interaction with the ITER Organization.

The plasma-materials interface will be key to development of fusion energy over the long term. Over the last five-year period, the DiMES program has performed detailed scientific investigations of plasma-material interaction in DIII-D, in particular, focusing on the understanding of local erosion and redeposition of different solid wall materials in the divertor, and developing active means to control erosion sourcing by local gas injection and electrical biasing. In addition, the DiMES program has been performing experiments in response to ITPA technical needs, for example, the study of dust and evaluation of divertor tile-edge power loading, and validation of reactor-relevant materials. Significant progress has also been made on the PMI modeling front with the ALPS program, leveraging the unique experimental capability of DiMES and MiMES in DIII-D. The importance of the sheath potential and the background distribution of the low-Z impurity flux to accurately predict high-Z PFM (W, Mo) erosion has been demonstrated. Important modeling support for the recent metal rings campaign on DIII-D with two toroidally symmetric rings of different isotopically enriched tungsten tiles in the lower divertor to study W sourcing and migration in a mixed materials environment has been provided.

The need for advanced divertor solutions to efficiently dissipate heat from fusion reactors is critical because the maximum steady-state power load for envisioned plasma-facing components (PFC) is limited to  $q_t \leq 10 \text{ MW/m}^2$  on PFC surfaces, whether solid or liquid, while the undissipated power loads will be an order of magnitude higher. A small angle slot (SAS) divertor concept has been proposed to address the challenge of efficient divertor heat dispersal compatible with non-inductive current drive in future tokamaks, and it is expected that this can be achieved with minimized divertor volume without internal magnetic coils, thereby maximizing the plasma volume for fusion energy production. A prototype SAS divertor is being evaluated on DIII-D and has produced promising results. This divertor concept will be further optimized and validated in the next five years to bring this new technology to a higher Technology Readiness Level (TRL3-4) for application in next-step fusion devices.

### 8.2.5 Collaboration with other US Fusion Experiments

To serve the US Fusion Program more fully, and benefit from the breadth of US fusion research, the DIII-D program maintains active collaborations with the two other large magnetic confinement experiments in the US program. Each year the NSTX-U, DIII-D, and Alcator C-Mod programs have conducted joint experiments on specific topics of particular interest to DOE; efforts in 2016 examined approaches to predict, avoid, and mitigate tokamak disruptions, of critical importance for ITER and subsequent tokamaks. These experiments used a variety of diagnostic measurements and actuators to forecast and avoid disruptive states, as well as both Massive-Gas Injection (MGI) and Shattered-Pellet Injection (SPI), to mitigate unavoidable disruptions. Joint experiments in FY17 have conducted research on the effects of configuration on dissipative divertor operating space. Although DIII-D is currently the only major operating tokamak in the US, work on the Joint Research Targets will continue to involve all three (C-Mod, DIII-D, and NSTX-U) experimental teams working collaboratively. Collaborations with the NSTX-U and Alcator C-Mod Teams are briefly described here.

**National Spherical Torus Experiment Upgrade (NSTX-U)** is a large spherical tokamak (ST) at PPPL. NSTX-U's mission is to investigate scientific issues for the ST in relation to possibilities for a future FNSF. Scientists from NSTX-U collaborate with the DIII-D program to study fast-ion physics, resistive wall mode (RWM) stabilization, boundary physics, and MHD stability. During the shutdown, NSTX-U scientists are participating in the DIII-D research program and two weeks of dedicated experimental time on DIII-D will be used to support NSTX-U programmatic research. When operations resume at NSTX-U, DIII-D will resume joint experiments to address current profile effects, confinement, MHD-stability, and divertor physics, as well as specific topics in support of ITER.

**Alcator C-Mod** was located at the Massachusetts Institute of Technology (MIT). Operation of C-Mod has been terminated, and the MIT staff have begun carrying out active collaborations with DIII-D and NSTX-U through subcontracts with GA and PPPL, respectively. Beginning in FY17, the MIT staff received significant funding from DOE to directly participate in both DIII-D and NSTX-U programs. On DIII-D, the funding allows MIT to participate at a level comparable to the larger national lab collaborators. The DIII-D program looks forward to continuing high-impact collaborations with MIT on disruption characterization and mitigation, ELMs and pedestal physics, ELM-free operating modes, divertor detachment, plasma-material interactions, and plasma rotation.

**The Fusion Facilities Coordinating Committee (FFCC)** was established in 1998 to facilitate improved coordination between the then-three major US magnetic fusion facilities (DIII-D, NSTX, and C-Mod) as well as between the major US facilities and major international

facilities. Representative program leaders from the US facilities meet together via teleconference with the relevant DOE program managers, the corresponding facility Program Advisory Committee (PAC) chairs, USBPO representatives, and ITER managers. Topics for discussion include operating schedules, research goals, national and international collaboration activities, and ITER-related research activities. Other FFCC meetings take place either by phone or in person throughout the year as needed. Each year the FFCC works with the DOE FES program managers to identify Joint Research Targets which utilize the unique capabilities of the three major US tokamaks to conduct a coordinated research program addressing important topics in fusion science.

**Joint Research Targets (Level 1 DOE FES fusion program milestones).** The DOE FES program has established the practice of identifying one high-level milestone each year for conducting coordinated research among the three major US facilities: DIII-D, NSTX, and C-Mod. Each year, the FFCC holds meetings to discuss potential research topics that could best provide important high-visibility results in a timely manner through coordinated research activities. Topics and quarterly targets are developed and chosen that reflect expected facility capabilities and FES/facility research priorities. Each program then adjusts its programmatic milestones to support the joint milestone and allocates sufficient resources (run time and scientific staff) to complete the work. The list of recent and proposed Joint Research Targets appears in Table 8-3.

**Table 8-3.**  
**FES Joint Research Targets FY08–FY18**

<b>Fiscal Year</b>	<b>Title or Subject Area</b>	<b>Lead Program</b>
2008	Plasma rotation and momentum transport, impact on plasma stability and confinement	DIII-D
2009	Particle control and hydrogenic retention	C-Mod
2010	Thermal transport in the SOL plasma	NSTX
2011	Pedestal structure: experiment and theory	FFCC chair
2012	Core transport	C-Mod
2013	Stationary enhanced confinement regimes without large ELMs	DIII-D
2014	Plasma response to applied 3D magnetic fields in tokamaks	DIII-D
2015	Current profile effects on confinement and stability	NSTX-U
2016	Detect/minimize consequences of disruptions in tokamaks	MIT
2017	Effect of Configuration on Dissipative Divertor Operating Space	DIII-D
2018	Test predictive models of fast-ion transport by multiple Alfvén eigenmodes	NSTX-U

### **8.2.6 Collaborations with the Transport Task Force and the Broader Science Community**

The DIII-D program performs research that addresses and advances foundational fusion science and integrates graduate students, post-doctoral researchers, and scientists from national and international universities and other research institutions. Many onsite and offsite team members work for universities and national laboratories, and numerous graduate students perform their primary dissertation research on DIII-D.

The US Transport Task Force (TTF) seeks to advance our understanding of turbulent transport in magnetized plasmas, which ultimately determines global energy confinement and fusion energy production. The long-term goal of the TTF is to develop “a predictive understanding of plasma transport leading to transport control.” Recent emphasis within the TTF has been placed on the study and understanding of the underlying plasma turbulence; particle, heat, momentum and impurity transport; and of profile stiffness. Transport in the pedestal is a critical area that determines pedestal pressure height, ELM onset and sets the boundary conditions for core transport. Turbulence studies have been made possible by dramatic improvements in the ability to control and measure internal profiles and multi-scale, multi-field turbulence properties. Demonstrating our understanding requires multiple, successful, quantitative tests of theory, simulation, and modeling using experiments in fusion-relevant plasmas. Research has also focused on direct and indirect impact of wall, PMI and scrape-off-layer effects on impurity generation, transport and corresponding core performance, and core impurity control.

A more complete understanding of plasma transport has been achieved by integrating theory and experiment, which is often accomplished by comprehensive comparisons of experimental data with the predictions of theory-based simulation codes. DIII-D now has extensive capability for simultaneously measuring a number of important fundamental plasma and turbulence properties, allowing comparisons with theory and simulation to unprecedented detail. Turbulence diagnostics are continually being expanded, enhanced and implemented to measure new fields. Recent developments include measurement of magnetic field, ion temperature and toroidal velocity fluctuations, and new diagnostics are being designed, tested, and deployed. Experiments planned for FY19-23 include understanding of impurity transport and control in a range of operational scenarios by exploiting the new laser blow-off system; understanding underlying mechanisms for transport near unity ion-to-electron temperature ratio; collisionality effects; particle transport; effects of resonant magnetic perturbations on transport; understanding the L-H trigger transition and power threshold scaling properties; intrinsic rotation, pedestal transport, identifying the mechanisms behind the isotope effect on confinement; and multi scale effects

behind energetic particle transport. These topics are also central to the TTF mission and will continue to be highlighted by TTF.

The DIII-D program continues to provide strong support for the TTF, as it has since its inception. The work of the TTF requires the integration of many individuals, groups, and machines, spread among a large number of institutions. The main vehicle for this integration is the annual meeting of the TTF at which participants present results, identify issues and discuss future plans. In recent years, an average of about ten DIII-D scientists have attended the yearly TTF meeting. More recently, the US and EU Transport Task Forces hold joint meetings, alternating between US and EU venues, and in the future will hold joint meetings with the newly formed Asian TTF. DIII-D intends to maintain ongoing participation in, and support for, the US TTF. The Turbulence and Transport, L-H Physics, Rotation and Energetic Particle groups, within the Burning Plasma Physics topical science area, contribute directly to the TTF mission.

### **8.3 UNIVERSITY PARTICIPATION: TRAINING SCIENTISTS FOR FUSION RESEARCH IN THE ITER ERA**

The DIII-D team takes seriously its role as a steward of plasma physics, its responsibility to maintain a world-class scientific research facility, and its duty to help recruit and train tomorrow's fusion scientists. The DIII-D program supports scientific education and training at four levels:

- Undergraduate education at colleges and universities through the Science Undergraduate Laboratory Internship program (10 summer students each at GA in FY15 and FY16; 12 in FY17)
- Graduate education leading to the Ph.D. (80 Graduate student facility users in FY17)
- Professional training through post-doctoral fellowships (FY17 Q1 facility users include 71 post-doctoral fellows)
- Faculty and research scientists from a wide range of academic institutions participate in ongoing research using DIII-D, often spending summers or taking academic leave to be onsite for experiments.

University participation broadens and maximizes the scientific output from operating the DIII-D facility, thereby advancing fusion science across a broad front. The DIII-D program welcomes inquiries from university faculty and research staff regarding starting new or expanding existing collaborations on DIII-D.

DIII-D facility users in FY16 Q1 represent more than 54 institutions of higher learning from the US (28) and around the world (26). More than 40% of the facility's 637 users are affiliated with universities or institutes whose primary mission is one of education, with 80 graduate

students and 71 post docs among them (FY17 Q1). US universities that participate in the DIII-D program are funded by one or more of the following:

- Peer-reviewed direct grants from DOE FES in response to open calls for research proposals;
- Direct grants from DOE awarded through a special-topic peer review process (e.g., diagnostic awards and calls for international collaborations);
- Subcontracts from GA and other DIII-D collaborators receiving DOE funding.

University participation adds breadth to the DIII-D research program that would be unobtainable otherwise, and it strengthens university programs by providing exciting research opportunities for students and faculty. Table 8-4 lists ongoing North American university collaborations at DIII-D and their primary research interests. New ideas for collaboration are welcome from university programs across a broad range of topics.

**Table 8-4 Primary Research Interests of University Collaborators in North America (2017)**

<b>School</b>	<b>Primary Research Emphasis</b>
Auburn University (AL)	3D field physics and 3D plasma equilibrium and effect on confinement
CIPS, University of Colorado Boulder	Plasma transport simulation, magnetic perturbations, plasma-shaping effects
The College of William and Mary (VA)	ELM control, 3D magnetic perturbations, simulations and analysis
Columbia University (NY)	Resistive wall mode control, plasma response to 3D magnetic fields, high-beta plasmas, steady-state and ITER scenarios
Georgia Institute of Technology (Atlanta)	MHD theory, transport theory, particle transport and flows, pedestal structure
Lehigh University (Lancaster, PA)	Plasma control algorithms, current and pressure profile evolution and control, ITER control algorithms
Massachusetts Institute of Technology (Cambridge)	Phase contrast imaging diagnostic, short wavelength plasma turbulence, rf heating and current drive, edge plasma physics, ELM-free H-modes
Palomar College (San Marcos, CA)	High-speed data acquisition for fusion research
Princeton University (NJ)	Nonlinear MHD, resistive MHD simulations, energetic particle effects, flow shear, and two-fluid effects on stability
UC Davis	Microwave imaging diagnostic development, 2D mode structure of MHD instabilities
UC Irvine	Fast-ion stability and transport, energetic particle diagnostics, TAE and RSAE mode structure and stability
UC Los Angeles	Plasma transport, plasma turbulence, L-H transition physics, ITER scenario development, wave profile, and turbulence diagnostics
UC San Diego	Disruption mitigation, runaway electron dissipation, edge probes, SOL flows and turbulent transport, L-H transition physics, surface erosion, and analysis, dust generation & transport (DiMES, MiMES)
U. Maryland	Microwave measurements, ITER ECE diagnostic prototyping
U. Tennessee (Knoxville)	Metal rings analysis, PMI diagnostic development
U. Texas (Austin)	ECE electron temperature profile measurements, ITER ECE development, internal transport barriers
U. Toronto	Plasma surface interactions, impurity transport, SOL profiles, plasma detachment, edge flows, SOL Langmuir probes
U. Washington	Disruption mitigation experiments
U. Wisconsin (Madison)	Beam emission spectroscopy diagnostic, turbulent flows, L-H transition physics, RMP ELM suppression effects

### 8.3.1 Opportunities for Training Students

Universities that participate in the DIII-D program use the facility as a training ground for graduate students. More than 20 graduate students receive direct support from DOE as part of the DIII-D National Fusion Program. Other graduate students use DIII-D data but receive DOE-FES funding under other budget categories, while others (in particular, those enrolled in foreign universities) may use DIII-D data even though their research is supported with separate, non-DOE funding. Table 8-5 lists present (FY17-Q2) graduate students working most closely with members of the DIII-D team. Table 8-6 lists past graduate students. The DIII-D facility user database, generated from annual cyberaccess requests, shows a total of 80 graduate students seeking a PhD degree (self-identified when they last renewed cyberaccess); ~30% are onsite users. Taking a snapshot of student users is always somewhat imprecise, as they often return to their home institution well before completing their degree and there is little incentive for them to inform their DIII-D host when they finally complete their project and graduate.

**Table 8-5.**  
**Present (Second Quarter FY17) Graduate Students**  
**with Main Focus on DIII-D Data**

	<b>Graduate Student</b>	<b>Affiliation</b>	<b>Topic</b>
1.	J. Barton	Lehigh U.	Current profile control
2.	D. Boyer	Lehigh U.	Kinetic/burn control
3.	M. Brookman	U. Texas	ECE studies of electron transport
4.	J. Cabrera	Columbia U.	SOL current dynamics in disruptions
5.	C. Chrobak	UCSD	Plasma-material interactions and erosion
6.	M. Clement	UCSD	GPU-based feedback control of RWMs
7.	E. Davis	MIT	Phase contrast imaging studies
8.	B. Fitzpatrick	U. Toronto	Hydrogenic retention
9.	M. Hill	Georgia Tech	Burn control methods
10.	W. Hu	ASIPP	Control of energetic particles
11.	K. Kim	Seoul National U.	Scenario modeling
12.	R. King	Georgia Tech.	Analysis of rotation measurements
13.	M. Knoelker	LMU Munich	Nonlinear phase of ELMs
14.	H. Lan	ASIPP	Effect of impurities on H-mode pedestal
15.	N. Piper	Georgia Tech.	Analysis of L-H transitions in DIII-D
16.	J. Ross	Georgia Tech	Analysis of H-L back transition in DIII-D
17.	J. Rovetto	Georgia Tech	Transport in pedestal region of DIII-D
18.	W. Shi	Lehigh U.	Data-driven model-based control on DIII-D
19.	L. Stagner	UC Irvine	Bayesian inference of fast-ion distribution
20.	S. Tang	UCLA	Energetic particle modes on NSTX and DIII-D
21.	D. Truong	U. Wisconsin	Multifield turbulence and GAM structure
22.	W. Wehner	Lehigh U.	Control of poloidal flux profile for AT scenarios in DIII-D
23.	G. Xu	ASIPP	High-Z impurity sources and transport modeling
24.	P. Zhang	ASIPP	High-Z impurity sources and transport modeling

A number of graduate students work full time at the DIII-D site designing, installing, and using diagnostic systems or analyzing DIII-D data, such as those shown in Fig. 8-2. Others may work at their university writing analysis codes or developing theories, explaining plasma phenomena observed on DIII-D. All students are encouraged to present their work at science meetings.

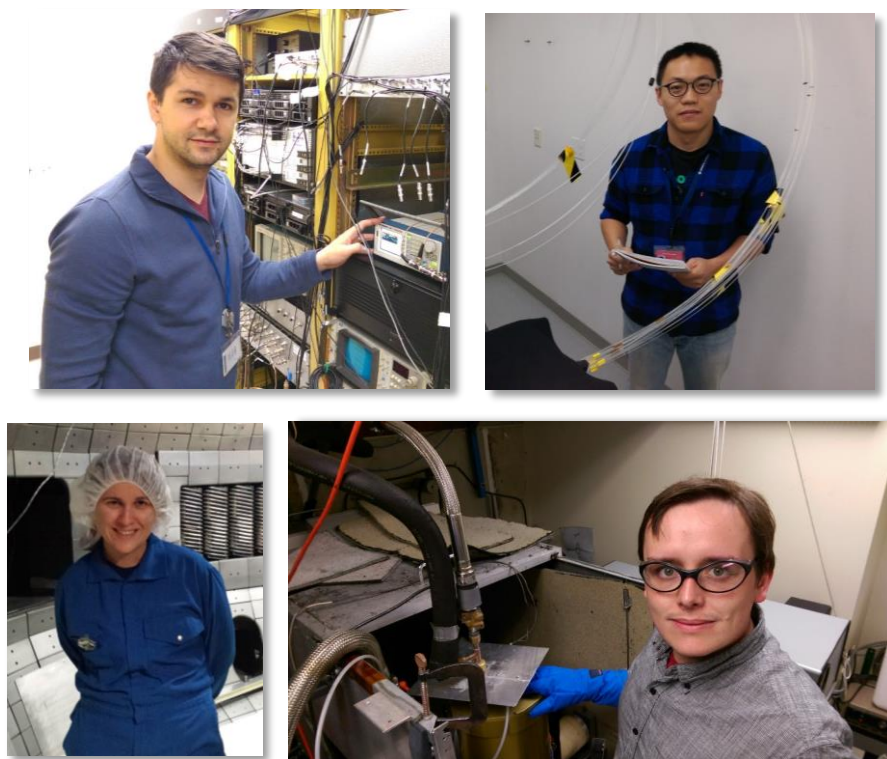


*Fig. 8-2. DIII-D hosts many students and postdocs, providing a wide range of research experiences. Clockwise from upper left: Oak Ridge Associated Universities postdoc and recent UCLA (DIII-D) graduate Lazlo Bardoczi; UC Irvine postdoc Xiaodi Du; University of Texas graduate student Michael Brookman, and Oak Ridge Associated Universities postdoc Kathreen Thome.*

### **8.3.2 Opportunities for Post-Doctoral Fellowships**

Postdoctoral fellowships provide important opportunities for developing future leaders in fusion research. Funding for postdoctoral fellowships (as with graduate students) is provided in several ways: directly to the university as part of the total DIII-D program funding, indirectly through subcontracts with the largest DIII-D program partners (GA and National Labs), or through grants that are outside the scope of the DIII-D program (i.e., DOE Theory, ASCR, NSF, or through international collaborations). Overall, the situation with postdoctoral fellows (as with graduate students) is quite fluid due to the variety of institutional funding arrangements, temporary nature of the appointments, and evolving personal ambitions/interests of the postdocs themselves.

Thirty-five post-doctoral fellows are conducting research onsite at the DIII-D facility (Table 8-7 lists those who are regularly onsite and Table 8-8 lists previous DIII-D postdoctoral fellows). Altogether, 71 postdocs are using data from the DIII-D facility in their research. All post-doctoral fellows are offered the opportunity to fully participate in all areas of the DIII-D program, with activities ranging from diagnostic development and numerical simulation to serving as a DIII-D tokamak physics operator. Postdocs propose experiments and the run time priority of such experiments are carefully considered as part of DIII-D’s commitment to their success. Scientists holding post-doctoral fellowships at universities have also furthered their scientific training at the GA fusion facility. Most of those completing fellowships at DIII-D have remained in the US fusion program.

**Table 8-6.**  
**Past Graduate Students at DIII-D**

	<b>Graduate Student</b>	<b>Affiliation</b>	<b>Topic</b>
1.	S. Angelini	MIT	Disruption modeling
2.	N. Antoniuk-Pablant	UCSD	B-Stark diagnostic
3.	C. Bae	Georgia Tech	Theoretical model for plasma rotation
4.	L. Bardoczi	UCLA	Turbulence, flows, and neoclassical tearing modes
5.	N. Bolte	UCI	Passive FIDA measurements of fast-ion loss
6.	Q. Boney	Hampton University	Divertor impurity diagnostic
7.	E. Carolipio	UCI	TAE mode studies
8.	W. Choi	Columbia U.	Locked modes
9.	C. Chrystal	UCSD	Investigation of poloidal rotation
10.	S. Coda	MIT	CO <sub>2</sub> phase image interferometer
11.	T. Collart	Georgia Tech.	Investigation of neoclassical rotation model
12.	K. Comer	U. Wisconsin	MHD studies
13.	D. Content	Johns Hopkins	Bolometers and visible bremsstrahlung
14.	R. Deranian	U. Wales	Plasma control
15.	M. Donales	Hampton University	Divertor impurity diagnostic
16.	J. Dorris	MIT	Phase contrast imaging
17.	H. Duong	UCI	Fast-ion bursts
18.	D. Elder	U. Toronto	OEDGE modeling of C13 experiments
19.	D. Eldon	UCSD	Edge pedestal Thomson scattering
20.	C. Estrada-Mila	UCSD	Turbulent transport simulations
21.	D. Finkenthal	UCB	He transport
22.	J. Fitzpatrick	UCB	TAE mode analysis
23.	B. Fitzpatrick	U. Toronto	Hydrogenic retention (oxygen bake)
24.	J.P. Floyd	Georgia Tech.	Evolution of edge pedestal profiles between ELMs
25.	C. Fransson	Chalmers U.	Plasma control
26.	H. Frerichs	FZ Jülich	3D fluid modeling of RMP
27.	Z. Friis	Georgia Tech.	Thermal instabilities
28.	R. Gatto	UCB	Heat pinch modeling
29.	B. Grierson	Columbia	Interchange turbulence in dipole plasma
30.	W. Guo	ASIPP	Integrated modeling
31.	S. Harrison	U. Wisconsin	Plasma-surface interactions
32.	J. Hillesheim	UCLA	Multi-frequency Doppler reflectometry
33.	W. Howl	UCSD	MHD reconstruction
34.	D. Hua	UCB	ITG modes and energy confinements
35.	M. Jakubowski	U. Wisconsin	Beam-emission diagnostics
36.	A. James	UCSD	Disruption-induced runaway electrons
37.	S. Janz	U. Maryland	ECE diagnostic bolometers

	<b>Graduate Student</b>	<b>Affiliation</b>	<b>Topic</b>
38.	O. Katsuro-Hopkins	Columbia U.	RWM feedback control modeling
39.	F. Kelly	Georgia Tech	Radiation modeling
40.	K.W. Kim	UCLA	Fast density profiles reflectometry
41.	J. King	UCB (LLNL)	Fast response, digital MSE
42.	S. Kruger	U. Wisconsin	Flow shear effects on MHD
43.	R. Laengner	FZ Jülich	Divertor material migration with RMP
44.	M. Lanctot	Columbia U.	RWM feedback control
45.	T. Le Hecka	UCLA	Microwave reflectometry
46.	J.H. Lee	UCLA	Fast wave studies
47.	B. Leslie	U. Wisconsin	Beam emission spectroscopy
48.	N. Logan	Princeton U.	Application of the ideal perturbed equilibrium code to DIII-D magnetic diagnostic upgrade designs
49.	Y. Luo	UCI	Beam ion studies
50.	A. McLean	U. Toronto	Plasma surface interactions
51.	B. Modi	UCB	Turbulence modeling
52.	S. Mordijck	UCSD	2D modeling of edge transport
53.	Y. Mu	U. Toronto	Hydrocarbon fragmentation modeling
54.	C. Muscatello	UCI	Fast-ion transport
55.	E. Nardon	CCFE-MAST	ELM control by stochastic fields
56.	Q. Nguyen	UCB	UEDGE development
57.	M. Ohno	NIFS/U. Wisc.	Edge turbulence and QH-mode
58.	C. Pan	ASIPP	Integrated modeling
59.	Y-S. Park	Seoul National U.	NTM detection and control
60.	M. Perry	Johns Hopkins	Impurity transport
61.	D. Pretty	Australia National U.	Stochastic edge mag. field studies
62.	Chuang Ren	U. Wisconsin	Plasma rotation
63.	Q. Ren	ASIPP	Integrated modeling
64.	X. Ren	UCD	MIR
65.	C. Rettig	UCLA	Microturbulence studies
66.	R. Rubilar	Georgia Tech	Radiation modeling
67.	G. Sager	U. Illinois	Data analysis program
68.	M. Sayer	Georgia Tech.	Evolution of edge pedestal profiles over the L-H transition
69.	M. Shafer	U. Wisconsin	Turbulence & flow during ITB formation
70.	P. Shriwise	U. Wisconsin	Velocimetry of 2D BES data and relation to electrostatic fluctuations
71.	R. Stockdale	Princeton U.	Perturbative transport experiments
72.	H. Stoschus	FZ Jülich	Electron transport with rotating RMP
73.	R. Sweeney	Columbia U.	Locked modes
74.	D. Thompson	U. Wisconsin	BES – detector development
75.	B. Tobias	UCD	ECE imaging
76.	C. Tsui	U. Toronto	Oxygen bake, C13 experiments
77.	W. Wang	UCI	Neoclassical transport studies
78.	G. Watson	UCI	ICRF Studies
79.	A. White	UCLA	Te fluctuation diagnostic
80.	T. Wilks	Georgia Tech.	Interpretative modeling of RMP effect on edge pedestal transport
81.	L. Yu	UCD	Characterization of intense bursts of mm-wave emission using new RF spectrometer on the DIII-D tokamak
82.	Q. Yuan	ASIPP	Plasma control and operations
83.	B. Zaniol	U. Padova	Impurity ion flow in divertor
84.	S. Zemedkun	U. Colorado	ECE Imaging of Temperature Fluctuations and Drift waves in DIII-D plasmas
85.	J. Zhang	UCLA	Magnetic Fluctuation Polarimetry
86.	Y. Zhao	Souchow U/U. Wisconsin	BES fluctuation studies
87.	A. Zwicker	Johns Hopkins	Multi-layer mirror spectrometer

**Table 8-7.**  
**Present (FY17) Post-Doctoral Fellows at DIII-D**

	<b>Postdoctoral Fellow</b>	<b>Affiliation</b>	<b>Topic</b>
1.	A. Ashourvan	PPPL	Angular momentum transport studies
2.	K. Barada	UCLA	Cross-polarization scattering
3.	L. Bardoczi	UCLA	Turbulence, flows, and neoclassical tearing modes
4.	J. Barr	ORAU	Disruption studies
5.	J. Barton	Sandia	Langmuir probes
6.	I. Bykov	UCSD	Divertor physics
7.	L. Casali	ORAU	Divertor modeling
8.	J. Chen	UCLA	Polarimetry/interferometry
9.	L. Cui	PPPL	TRANSP studies of DIII-D and EAST discharges
10.	X. Du	UC Irvine	Imaging neutral particle analyzer, other energetic particle studies
11.	J. Guterl	ORAU	Plasma-facing components and erosion
12.	J. Herfindal	ORAU	Disruption studies
13.	E. Hinson	U. Wisconsin	Boundary physics
14.	N. Howard	ORAU	Gyrokinetic simulations
15.	A. Jarvinen	LLNL	Divertor modeling
16.	C. Luo	UC Davis	MIR, ECE imaging
17.	A. Lvovskiy	ORAU	Gamma ray imaging diagnostic
18.	B. Lyons	ORAU	Extended MHD theory
19.	J. McClenaghan	ORAU	Transport modelling of ITER steady-state
20.	S. Munaretto	ORAU	3D MHD studies
21.	C. Rea	MIT	Machine learning algorithm for disruption prediction
22.	J. Ren	U Tennessee Knoxville	Fast thermocouples
23.	C. Samuel	LLNL	Coherence Imaging of Plasma Flows
24.	C. Sang	ORAU	Divertor modeling
25.	C. Sung	UCLA	Correlation ECE
26.	Z. Taylor	ORAU	Tearing mode physics
27.	K. Thome	ORAU	Transport and scenario studies
28.	G. Trevisan	ORAU	3D equilibrium reconstruction
29.	B. Victor	LLNL	Motional Stark effect diagnostic
30.	H. Wang	ORAU	Pedestal and divertor physics
31.	R. Wilcox	ORNL	Transport effects of applied 3D fields
32.	T. Wilks	MIT	Pedestal modeling and analysis, particularly in ELM-free regimes
33.	D. Zhao	ORAU	CFETR studies
34.	H. Zhao	U. Texas	ECE systems on DIII-D
35.	Y. Zhu	UC Davis	ECEI diagnostic, operate ECEI/MIR for edge plasma measurements

**Table 8-8.**  
**Past Post-Doctoral Fellows at DIII-D**

	<b>Postdoctoral Fellow</b>	<b>Affiliation</b>	<b>Topic</b>
1.	T. Abrams	ORAU	Plasma/materials interactions
2.	M. Austin	U. Maryland	ECE diagnostics
3.	E. Bass	ORISE	Gyrokinetic code for energetic particles
4.	D. Battaglia	PPPL	3D magnetics and particle transport
5.	E. Belli	ORISE	Edge gyrokinetic simulations
6.	D. Brennan	ORISE	MHD
7.	A. Briesemeister	ORNL	Edge/divertor physics
8.	A. Brizard	UCB	Transport analysis
9.	X. Chen	ORISE	Integrated model of pedestal profiles for stability research
10.	C. Chrystal	ORAU	Pedestal physics
11.	A. Cole	U. Wisconsin	Non-resonant field error effects
12.	C. Collins	UCI	EP instabilities using FIDA
13.	N. Commaux	ORAU (ORNL)	Pellet injection
14.	C. Cooper	ORAU	Fast particle diagnostics
15.	B. Covele	U. Texas	Divertor detachment/X-divertor configuration
16.	J. Cutherbertson	SNLA	Divertor Langmuir probe measurements
17.	J. Dorris	MIT	Phase Contrast Imaging
18.	N. Eidietis	ORISE	Plasma control
19.	D. Eldon	PPPL	Boundary physics and control
20.	D. Ernst	Princeton	Transport studies
21.	N. Farraro	ORISE/DOE	Resistive MHD-edge
22.	C. Fenzi	France/U. Wisconsin	Beam emission spectroscopy
23.	T. Fouquet	ORISE	Integrated modeling
24.	H. Frerichs	FZ Juelich	3D edge transport modeling
25.	A. Garofalo	Columbia U.	Wall stabilization
26.	G. Garstka	U. Maryland	ECE diagnostics
27.	T. Gianakon	U. Wisconsin	MHD theory and modeling
28.	D. Gray	UCSD	Disruption and coherent mode studies
29.	B. Grierson	PPPL	Main-ion rotation measurements
30.	M. Groth	LLNL	Boundary physics
31.	W. Guo	ASIPP	Plasma simulation
32.	D. Gupta	U. Wisconsin	Beam emission spectroscopy
33.	J. Hanson	Columbia U.	MHD mode control
34.	S. Haskey	PPPL	Charge exchange recombination spectroscopy
35.	C. Holcomb	LLNL	MSE diagnostic
36.	C. Holland	ORISE/UCSD	Turbulence studies
37.	E. Hollmann	UCSD	Disruption and coherent mode studies
38.	B. Hudson	ORISE	Edge current measurement
39.	Y. Jeon	ORISE	Integrated modeling
40.	I. Joseph	UCSD	RMP ELM control
41.	O. Katsuro-Hopkins	Columbia U.	RWM Feedback Control Modeling
42.	J. King	ORISE	3D magnetics
43.	J. Kinsey	Lehigh	Transport modeling
44.	M. Kissick	U. Wisconsin	Heat pulse propagation
45.	S. Kruger	U. Wisconsin	MHD studies
46.	K. Kupfer	ORISE	RF current drive
47.	T. Kurki-Suonio	UCB	Transport analysis
48.	M. Lanctot	LLNL	3D field effects, MSE, and current profile control

	<b>Postdoctoral Fellow</b>	<b>Affiliation</b>	<b>Topic</b>
49.	R. Lehmer	UCSD	Divertor physics and turbulence
50.	E. Li	U. Texas	Electron cyclotron emission
51.	G. Li	ASIPP	Integrated modeling
52.	D. Liu	UCI	FIDA analysis
53.	Z. Liu	LLNL	Pedestal modeling
54.	N. Logan	PPPL	3D MHD stability physics, NTV torque
55.	R. Maingi	ORISE	Divertor physics
56.	A. Marinoni	MIT	Phase contrast imaging
57.	G. McKee	ORNL	Divertor spectroscopy
58.	A. McLean	ORNL	Hydrogenic retention
59.	O. Meneghini	ORISE	Integrated modeling
60.	O. Meyer	CEA Cadarache	Charge exchange recombination spectroscopy
61.	S. Mueller	UCSD	Momentum transport and intrinsic rotation
62.	J. Munoz	ORISE	Divertor spectroscopy
63.	C. Muscatello	UCD	MIR
64.	P. O'Shea	MIT	Phase contrast imaging
65.	E. Olofsson	ORAU	Current profile control
66.	D. Orlov	UCSD	3D fields and ELM control modeling
67.	D. Pace	UCI	Energetic Particle Research
68.	J.M. Park	ORNL	Integrated modeling
69.	C. Paz-Soldan	ORISE	3D magnetic field effects
70.	D. Ponce	ORISE	Thomson scattering
71.	H. Reimerdes	Columbia	Resistive wall mode stabilization
72.	Q. Ren	ASIPP	Integrated modeling
73.	C. Rost	MIT	Phase contrast imaging
74.	D. Rudakov	UCSD	Edge turbulence and transport studies
75.	O. Schmitz	FZ Julich	Divertor DiMES camera
76.	M. Shafer	ORISE	Divertor spectroscopy and ELM control
77.	D. Shiraki	ORNL	Pellets and disruption mitigation
78.	W. Solomon	PPPL	CER diagnostics
79.	A. Sontag	ORNL	MHD studies
80.	J. Squire	ORISE	X-ray diagnostic
81.	R. Srinivasan	IPR-India	Integrated modeling
82.	H. Stoschus	ORISE	Edge current measurement with Li beam
83.	B. Tobias	PPPL	ECE imaging
84.	F. Turko	ORISE	Resistive MHD in AT scenarios
85.	Z. Unterberg	ORNL	Edge spectroscopy
86.	I. Uzun-Kaynak	U. Wisconsin	UFIT
87.	M. VanZeeland	ORISE	CO2 interferometer
88.	F. Volpe	ORISE	Structure of magnetic islands
89.	M. Wade	ORISE	Helium transport
90.	G. Wang	UCLA	Transport studies/diagnostics
91.	T. Weber	LLNL	Edge plasma flows
92.	A. White	ORISE	Validation of Gyrokinetic Transport Codes
93.	D. Whyte	CCFM/Canada/UCSD	Divertor physics
94.	A. Wingen	ORAU	3D fields and synthetic SXR diagnostics
95.	Z. Yan	U. Wisconsin	Beam emission spectroscopy
96.	Z. Yang	Huazhong U. Sci. Tech/U. Texas	High resolution ECE
97.	J. Yu	UCSD	Disruption studies
98.	L. Zeng	UCLA	Transport studies/diagnostics

### 8.3.3 Opportunities for Expanded University Partnerships

New opportunities for expanded university partnerships arise regularly, often through annual FES Funding Opportunity Announcements (FOA). The DIII-D program welcomes new ideas from university programs across a broad range of topics. Each year at the APS-DPP Conference, the DIII-D program advertises opportunities for collaborative research and makes available a contact list to encourage collaboration; a sample flier appears in Fig. 8-3. Research proposals are collected each year in a Research Opportunities Forum, which is an open forum to present and discuss ideas for DIII-D experiments.

Each year the DIII-D program also invites experimental proposals for the Torkil Jensen Award. The prize is experimental time on the DIII-D tokamak to conduct innovative experiments. Torkil was an internationally recognized Theoretical Physicist at GA known for his creative thinking on a wide range of plasma physics topics related to magnetic confinement fusion. The Torkil Jensen Award is open to both US and international grad students, post-doctoral fellows, and staff scientists at universities, industry, and national laboratories. Proposers need not be formally affiliated with the DIII-D program, but are encouraged to partner with program scientists. Now in its tenth year, many proposals have been received and evaluated, with one or two run days awarded to the winners each year. There are three criteria for the award:

1. Potential for transformational new results
2. Potential for producing high visibility, high-impact science
3. Collaborative effort (national or international partners)

The selection committee consists of a mix of onsite and collaborating DIII-D scientists. Travel funding for university participants is made available on a case-by-case basis.

<https://fusion.gat.com/global/DIII-D>



**OPPORTUNITIES FOR COLLABORATION & RESEARCH PROPOSALS for DIII-D in 2017-9**

The DIII-D National Fusion Facility is inviting collaboration in its 2017-9 program commencing in the Fall. This is a nationally and internationally collaborative research program amongst ~90 institutions. Collaborators manage elements of the program, generate ideas and innovations, lead experiments, build and operate diagnostics and other equipment, analyze data, provide theory and modeling support, and report and publish results world wide. Opportunities also exist for graduate and undergraduate students.

The overall goal of the DIII-D program is to establish the scientific basis for the optimization of the tokamak approach to fusion energy. Research covers a broad spectrum of important foundational scientific work, but in 2018 will include particular focus on developing the basis for Q=10 in ITER, ELM control, rotation projection and divertor development, as well as a new Core-Edge Integration Task Force and support for long pulse development in collaboration with the EAST facility. The 2019 program will turn to the development of fully non-inductive plasmas, benefiting from a major heating upgrade.

Experiments in the coming year will benefit from developments in electron cyclotron heating, improved disruption mitigation systems, a recent power supply upgraded from ASIPP China for enhanced 2-D/3-D field capabilities, and the new SAS divertor and increased closure main upper divertor, as well as improved diagnostics such as gamma ray and ECE imaging, and divertor measurements. In 2019, neutral beam injectors will be reoriented to double off axis current drive and increase co-direction heating power. A hallmark of the DIII-D program is its emphasis on model validation enabled by a world-leading diagnostic set, which benefits from many high resolution 1D, 2D and 3D diagnostics, and extensive arrays of magnetic diagnostics, as well as additional visible and infra-red imaging systems.

Experiments for the imminent 2017-18 campaign have now been determined, though opportunities remain for scientific engagement and analysis with these studies, plus a limited number of additional days to be defined, including an expected Frontiers Science campaign week. A further call will be issued next year for new experiment proposals for 2019. See the above link to get engaged!

*We look forward to your participation.*



*Fig. 8-3. Flier encouraging participation in the DIII-D research program and the Research Opportunities Forum distributed annually at the APS-DPP meeting*

Table 8-9 defines three broad categories of university participation and lists needs representative of those that could be addressed by new or expanded formal university collaborations. The list is meant to be suggestive of possible topical areas and is neither exclusive nor all-inclusive.

**Table 8-9.**  
**Areas of Potential Additional University Collaboration**

Activity	Needs/Opportunities
Diagnostic Instrumentation	<ul style="list-style-type: none"> <li>• SOL/Divertor Neutral density and ionization measurements</li> <li>• 3D field effects</li> <li>• Disruption-induced runaway electrons</li> <li>• High resolution internal magnetic field measurements</li> <li>• Turbulence and magnetic fluctuation measurements</li> <li>• SOL/Divertor ion temperature and flow</li> <li>• Divertor radiation loss and detachment</li> <li>• In-situ surface temperature measurements</li> <li>• Erosion/Redeposition</li> <li>• Plasma rotation (impurity and main ion)</li> <li>• Main chamber particle fluxes to first wall</li> <li>• High-resolution impurity spectroscopy</li> </ul>
Experiment and Analysis	<ul style="list-style-type: none"> <li>• Core-edge integration</li> <li>• Pedestal width</li> <li>• Pedestal turbulence</li> <li>• Pedestal/SOL neutral and flow dynamics</li> <li>• Main ion particle transport</li> <li>• Disruption heat loads</li> <li>• Disruption mitigator particle assimilation</li> <li>• Disruption-induced runaway electron dissipation</li> <li>• ELM losses</li> <li>• 3D field effects</li> <li>• Divertor detachment</li> <li>• Wall/divertor material migration</li> </ul>
Theory and Modeling	<ul style="list-style-type: none"> <li>• Synthetic diagnostic development</li> <li>• Intrinsic rotation</li> <li>• Error field screening effects</li> <li>• Scenario modeling</li> <li>• SOL/divertor conditions</li> <li>• Extended MHD</li> <li>• Pedestal width and core/edge coupling</li> <li>• ELM losses</li> <li>• Wall/divertor material migration</li> <li>• Advanced divertor modeling</li> </ul>



## 9. INTERNATIONAL PARTNERSHIPS

The DIII-D program continues to provide compelling and essential progress toward the scientific basis for fusion energy. However, we also recognize that DIII-D is an important part of the world's fusion portfolio (Fig. 9-1), with a high degree of complementarity between DIII-D and its international partners. The main premise of the international collaboration program at DIII-D is to advance the science of fusion plasma physics through interaction with these partners in such a manner as to accelerate the progress toward fusion energy realization. Areas of collaboration include (a) the validation of fusion plasma physics through joint experiments; (b) testing and advancing the capabilities of plasma control techniques through applications on multiple machines; (c) broadening the knowledge base and experience of the research staff aimed toward further innovation in fusion physics. These collaborative exchanges provide the building blocks for advancing fusion energy science worldwide, particularly in preparing for and supporting international next-step experiments starting with ITER. The range of scientific exchanges is very broad and covers a large number of plasma physics topics (Section 9.4). A major objective of DIII-D's collaborative efforts is to ensure the success of ITER through joint research organized through the International Tokamak Physics Activity (ITPA), as well as targeted areas identified through direct interaction with the ITER Organization Central Team. DIII-D Team members also interface with ITER through participation in its advisory committees and design reviews.

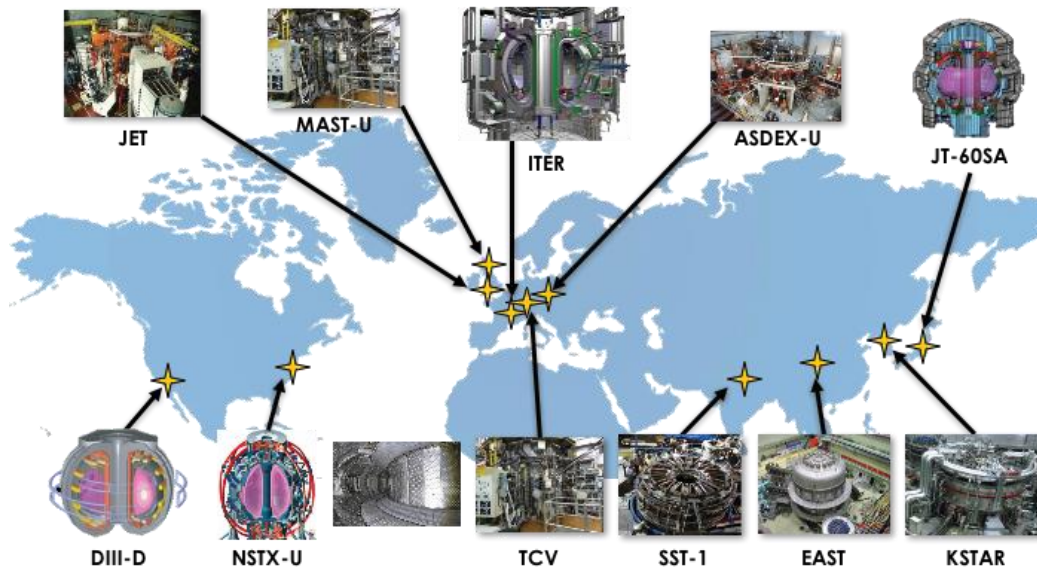


*Fig. 9-1. DIII-D is an important element of the world fusion portfolio, working together to prepare for a successful ITER research program and to establish the basis for operation of future burning plasma devices that will be central to the development of fusion energy.*

Present and future activities planned in the DIII-D international collaboration program are detailed in this chapter and are highlighted in Table 9-1. This list covers a broad range of topics, including personnel exchanges to prepare and perform joint experiments; the development of software and hardware components for specific applications, such as plasma control and auxiliary heating systems; the development of remote participation capabilities; the development of tools for data analysis and modeling; and work on technical and advisory committees.

**Table 9-1.**  
**Collaborative Activities Described in this Chapter**

<b>Section</b>	<b>Collaborative Activity</b>	<b>Status and Plans</b>
<b>9.2</b>	<b>Collaboration with other tokamak facilities</b>	<ul style="list-style-type: none"> <li>• <b>Scientific personnel exchanges for performing joint experiments data analysis and modeling</b></li> <li>• <b>Remote participation in joint experiments at foreign facilities</b></li> <li>• <b>Hardware and diagnostic development of prime areas of research</b></li> </ul>
	<b>9.2.1 EAST</b>	<ul style="list-style-type: none"> <li>— Plasma control</li> <li>— Long-pulse operating scenarios</li> <li>— In-kind hardware improvements to DIII-D</li> </ul>
	<b>9.2.2 KSTAR</b>	<ul style="list-style-type: none"> <li>— Plasma control</li> <li>— Long-pulse operating scenarios</li> <li>— H-mode physics</li> </ul>
	<b>9.2.3 QST/JT-60U/JT-60SA</b>	<ul style="list-style-type: none"> <li>— Long-pulse operating scenarios</li> <li>— MHD stability</li> <li>— Transport</li> </ul>
	<b>9.2.4 EFDA-JET</b>	<ul style="list-style-type: none"> <li>— ITER-Like Wall studies</li> <li>— Joint experiments on high-performance steady-state plasmas, NTM and RWM studies, hybrid plasma development, real-time profile control and ITB studies</li> </ul>
	<b>9.2.5 ASDEX-U</b>	<ul style="list-style-type: none"> <li>— Energetic particle physics</li> <li>— Joint experiments on RWM ELM control, energetic particle physics, pedestal studies and divertor/scrape off layer (SOL) studies</li> </ul>
	<b>9.2.6 MAST</b>	<ul style="list-style-type: none"> <li>— RWM ELM control</li> <li>— 3D physics</li> <li>— Diagnostic Development</li> </ul>
	<b>9.2.7 ADITYA/SST-1</b>	<ul style="list-style-type: none"> <li>— Participation in DIII-D experiments</li> <li>— Long-pulse operating scenarios</li> </ul>
<b>9.3</b>	<b>International tokamak physics activity (ITPA)</b>	<ul style="list-style-type: none"> <li>• <b>Active involvement of DIII-D personnel in ITPA topical groups</b></li> <li>— Propose and execute joint experiments with other fusion facilities</li> <li>— Perform data analysis and prepare reports of scientific results</li> </ul>
<b>9.4</b>	<b>International Cooperative Agreements</b>	<ul style="list-style-type: none"> <li>• <b>Develop framework for carrying out collaborative activities</b></li> </ul>
<b>9.5</b>	<b>International Investment in DIII-D</b>	<ul style="list-style-type: none"> <li>• <b>Scientific exchanges</b></li> <li>• <b>Direct investment in DIII-D capabilities by international partners</b></li> </ul>
<b>9.6</b>	<b>Web access to the DIII-D facility</b>	<ul style="list-style-type: none"> <li>• <b>Develop and enhance capabilities for interaction with the DIII-D research program through web-based tools</b></li> </ul>

These collaborations will continue to expand on activities with long-established fusion facilities, such as EFDA-JET and ASDEX-U, as well as the maturing generation of superconducting, long-pulse, tokamaks such as EAST and KSTAR.

High priority within this international program is focused on a continuing Long-Pulse, High-Performance (LPHP) Initiative. This initiative synergistically combines DIII-D’s world-leading capabilities in scenario development and plasma control and the burgeoning capability worldwide for steady-state operations (via superconducting devices such as EAST, KSTAR, JT-60SA, and SST-1) to demonstrate the promise of steady-state, high-performance operation. This approach has been very successful in advancing fusion energy science during the last several years, and has built strong connections between the DIII-D team and its counterparts in China and Korea.

## **9.1 COLLABORATION WITH OTHER TOKAMAK FACILITIES**

Below are described some of the activities to be carried out jointly with international partners. Many of these activities fall under a general theme of long-pulse, high-performance tokamak, which are proposed as an international initiative aiming to demonstrate the promise of these modes of operation as a basis for future devices including ITER’s steady-state mission and, ultimately, DEMO and power plant devices.

Within the international LPHP initiative, DIII-D will develop appropriate operating scenarios, including both inductive and steady-state. DIII-D’s part in this would include plasma control techniques, studies of the applicability of various actuators (heating and current drive, shaping, 3D fields, etc.), and full scenario demonstrations sustained for a few resistive times. The most promising scenarios could be exported on superconducting devices such as EAST, KSTAR, JT-60SA, and SST-1 for extension to long-pulse operation and assessments of the scenarios’ compatibility with PFC limitations. At the same time, JET and ASDEX-U would be able to evaluate the scenarios’ viability with metal walls.

Although DIII-D does not have the long-pulse capabilities of its partners, the facility will, for the foreseeable future, maintain a level of flexibility that is unmatched in the world program. This will enable the team to bring the results of tests in superconducting devices back to DIII-D as a guide for further development. Also, this effort is envisioned as carried out by multi-institutional and multi-national teams, so these efforts will deliver valuable experience to the US FES community that are hoped to eventually be applied to development of a DEMO program with major US involvement.

The collaborations described here are carried out both by personnel exchanges and via remote collaboration. To support this, a “remote control room” was built and outfitted at GA

(Fig. 9-2). This capability, which can serve as a model for international efforts such as ITER, has been extensively exploited, to the point of remotely executing third-shift experiments on EAST, and will continue to be one of our essential tools for international collaboration.

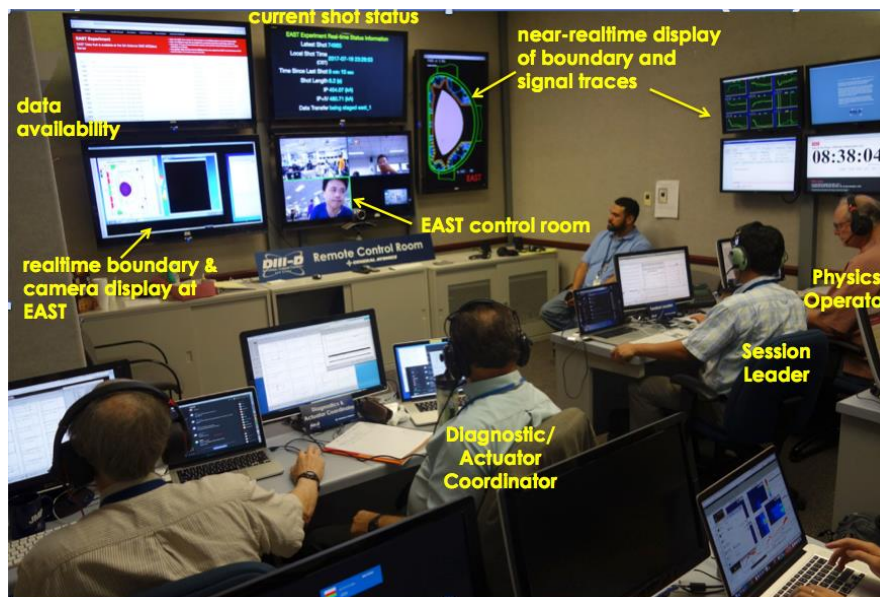


*Fig. 9-2. Experiments were recently carried out remotely on EAST by a team in the GA remote control room. The photo shows the GA team leading experiments during “third shift” (overnight) operation. In this instance, four experiments were carried out over five such shifts in a week. Access to EAST without traveling is valuable to DIII-D staff, but also helps ASIPP increase the utilization of their facility while operating with minimum onsite staff.*

Below are described some of the proposed joint activities to be carried out with international partners. A Long-Pulse, High-Performance (LPHP) Initiative has been proposed as a major theme of DIII-D’s international collaborations with superconducting tokamaks in Asia (EAST, KSTAR, JT-60SA, and SST-1). The LPHP initiative addresses the challenge of demonstrating that high-performance plasmas can be maintained for times long compared to characteristic discharge times, such as the current redistribution time and plasma-wall equilibration time. DIII-D has world-leading capabilities in plasma control and scenario development, and a comprehensive diagnostic set to evaluate and understand the complex interaction of the profiles. Joint experimental teams are demonstrating access to steady-state high-performance regimes on DIII-D, then incorporating and extending these scenarios to long pulse on the superconducting devices. In FY13, a joint EAST/DIII-D team developed and tested a startup-ramp-up high-performance scenario suitable for implementation on EAST in 2014. In FY14, further joint experiments on DIII-D improved the physics understanding of this scenario, enabling enhanced performance by up to 30% in beta. In FY15, confinement in this scenario was found relatively insensitive to reductions in plasma rotation and  $q_{95}$ , and an inductive extension

of the scenario at higher plasma current was developed. In FY16, a high  $\beta_P$  scenario, similar to one previously developed on DIII-D, was extended to long-pulse operation on EAST. The experiments in both DIII-D and EAST were reported in a pair of talks at the 2016 IAEA Fusion Energy Conference (FEC) in Kyoto, Japan.

### 9.1.1 EAST

Collaboration with the Chinese Academy of Science Institute of Plasma Physics (ASIPP) in Hefei, China, has been the most rapidly growing active international collaboration with DIII-D over the past several years. ASIPP is the host institution for the EAST tokamak. EAST is a superconducting tokamak, representing a major advance in both the Chinese and world fusion programs. DIII-D and GA have provided extensive assistance in plasma control, heating systems, and the benefit of long experience with tokamak physics, which has helped to bring success to the EAST program. In return, DIII-D has received in-kind delivery of various important hardware elements, including the lower divertor shelf installed in DIII-D and more recently a 4-quadrant switching supply (Super SPA), and has been able to perform extensive research in superconducting and long-pulse plasma control. The collaboration has expanded recently (FY13 and renewed in FY17) through a separately funded multi-institutional DOE award that involves scientific exchanges focused on control and scenario physics. This multi-institutional project, entitled “Control and Extension of High-performance Scenarios to Long Pulse,” involves efforts to adapt discharge scenarios from US devices to EAST and KSTAR in order to study control and scenario physics in superconducting long-pulse execution. In addition to, and in support of, the scenario and control science focus, the project includes collaborations in diagnostic development and implementation, heating and current drive physics, scenario and actuator effects simulations, and remote experimental participation and operations.

There are now two major components of the broad bi-lateral collaborative effort between DIII-D and ASIPP/EAST:

**Joint experiments:** Scientists from EAST regularly travel to DIII-D for extended visits, during which they support the DIII-D program through work on EFIT, OMFIT, and control-related research. Similarly, scientists from DIII-D regularly travel to EAST to participate in experiments. Dr. Andrea Garofalo (GA) has an appointment as a “visiting research scientist” and facilitates joint experiments on both DIII-D and EAST. Typically, experienced staff work with visiting ASIPP scientists to develop scenarios on DIII-D that can be implemented on EAST, thereby accelerating progress on EAST. Remote participation in experiments from one site to the other is now in routine use. Notable experiments carried out by remote participation in FY15 included an SOL similarity experiment and a set of scenario development transport experiments.

**Direct ASIPP investment in the DIII-D tokamak facility:** ASIPP recently provided a large reconfigurable, fast-responding poloidal field power supply which has now been installed and is in routine use, making contributions across a broad swath of the DIII-D research program. Other areas of investment are also being evaluated.

The DIII-D program also supports and benefits from a growing collaboration with the Southwestern Institute of Physics (SWIP) in Chengdu, China. SWIPP is the host institution for the HL-2A tokamak and is now building a new device (HL-2M) that will be similar in size to DIII-D.

During the next several years, this collaboration is expected to continue and expand. EAST and KSTAR (below) are currently the only major superconducting tokamaks operating in the world. Each of these devices has reached a point in their development where the teams have begun testing the long-pulse scenarios that were initially developed and characterized on DIII-D; the next phase of the aforementioned LPHP Initiative.

This plan leverages the EAST collaboration by envisioning their contributing additional hardware to the DIII-D program, which will be extremely valuable in meeting the goals described in other chapters of this plan. Areas of concentration for these in-kind contributions may include bipolar power supplies and additional 3D coils to enhance our 3D physics efforts and support efforts to provide a physics basis for RMP ELM control in ITER. Also under discussion are additional power supplies and transformers that will enable DIII-D to increase its heating and current-drive capabilities (neutral beams and ECH).

### **9.1.2 KSTAR**

The National Fusion Research Institute (NFRI) in Daejeon, South Korea, operates the KSTAR tokamak. KSTAR is the other currently operating major superconducting tokamak. It has demonstrated several important milestones, including 70-second H-mode and  $n=2$  RMP ELM suppression. The DIII-D Plasma Control group has played an instrumental role in KSTAR plasma operation through both onsite visits and, more recently, increased remote participation.

Much of what was said about EAST above applies equally to KSTAR. The DIII-D Plasma Control group has enabled KSTAR to make important contributions to the world fusion program, and this collaboration has expanded with KSTAR's capabilities. As the capabilities increase further, it is anticipated that KSTAR will be a major participant in the LPHP Initiative.

### **9.1.3 QST/JT-60U/JT-60SA**

The collaboration with the Japan Atomic Energy Agency (JAEA), formerly known as the Japan Atomic Energy Research Institute (JAERI), has been the longest and most extensive in the history of the DIII-D research program. The collaborative agreement started in 1978 during the

first year of operations on Doublet III. For nearly the last 30 years, the agreement has provided a source of both financial contributions and scientific manpower that has significantly enhanced the DIII-D research program. With the advent of the JT-60U fusion facility, the areas of collaboration with DIII-D were greatly increased, particularly in the fields of Advanced Tokamak (AT) science and steady-state, integrated performance optimization. With the termination of the JT-60U program, the collaboration has continued at a slower pace, with JAEA participation in a wide range of scientific areas on DIII-D.

The National Institutes for Quantum and Radiological Science and Technology (QST) took over Japan’s fusion energy research programs from the Japan Atomic Energy Agency (JAEA) during FY16. QST is focused on construction of JT-60SA, a superconducting tokamak being built in collaboration with the European Union (EU) as part of their “Broader Approach.” The US is currently not a party in JT-60SA, and so there is little formal participation. JT-60SA’s first plasma is anticipated in 2019.

Several QST scientists have visited DIII-D to participate in our research program during the past several years. Dr. Maiko Yoshida’s work was a recent highlight as she visited several times to work with DIII-D scientists on experiments that demonstrated that internal transport barrier discharges with negative central shear do not exhibit confinement degradation with the application of electron-cyclotron heating. Her work was also presented orally at the IAEA FEC.

The possibility of future formal participation of the US in JT-60SA is unknown at this time. However, there is significant alignment in the DIII-D team’s interests and those of their QST colleagues, and significant complementarity between the capabilities of the DIII-D facility and the focus of the JT-60SA on long-pulse, high-performance, and steady-state operation. As opportunities arise, JT-60SA is expected to become an important partner in the LPHP initiative and a target for other areas of potential collaboration.

#### **9.1.4 EFDA-JET**

The JET fusion device is organized under EUROfusion and is operated primarily as a user facility for member associations within EFDA. Since installing their “ITER-Like Wall” (ILW), the JET program has focused on operational issues providing data to the ITER program on the behavior of tokamaks with a tungsten divertor and beryllium wall. Many collaborative activities between DIII-D and JET are centered on performing joint experiments at both facilities which take advantage of large difference in  $\rho^*$  between the two devices. For example, data from JET and DIII-D helped anchor the edge database that determined the  $1/B_{\text{pol}}$  SOL heat flux-width scaling (“Eich scaling”) that is now in common use. More recently, DIII-D scientists have participated in other experiments that have addressed L-H transition physics and confinement, as

well as scenario development (e.g., hybrid discharges) and current-profile effects. These experiments are helping to prepare for D-T experiments in 2019.

As JET has many similarities with DIII-D, other than its larger dimensions and first-wall materials, ITER will benefit strongly from the continuation of a variety of paired studies between the two devices. In particular, disruption mitigation and operating scenario development are two areas where our collaboration may make an important contribution. Also, JET is foreseen as a partner in the LPHP Initiative, providing a test bed for determining the resilience of operating scenarios to changes in first-wall material.

### **9.1.5 ASDEX-U**

ASDEX Upgrade, in Garching, Germany, operates with a tungsten coating on its walls, and is carrying out a broad physics program studying H-mode access, ELM mitigation, disruption mitigation, and energetic particle physics, to name a few prominent areas. Collaboration between DIII-D and ASDEX-U is focused on RMP ELM control, assessment of the effect of impurities on the H-mode pedestal, and energetic particle physics. In the latter area, scientists from GA (David Pace and Mike Van Zeeland) shared the Landau-Spitzer Prize in 2014 for outstanding theoretical, experimental, or technical contribution(s) in plasma physics, and for “advancing the collaboration and unity between the European Union (EU) and the United States of America (USA) by joint research, or research that advances knowledge which benefits the EU and USA communities in a unique way.” In FY16, a joint DIII-D/ASDEX-U team demonstrated for the first time complete RMP ELM suppression in ASDEX-U using a “recipe” developed in DIII-D. The results of these experiments were reported in a post-deadline talk at the 2016 IAEA FEC.

Comparative studies between DIII-D (an all-carbon PFC device) and ASDEX-U in the above-named research areas will endeavor to resolve the virtues of the various PFC materials used. This collaboration will continue as part of the LPHP Initiative. We also anticipate continuation of the highly successful collaboration on energetic particle physics between the two devices.

### **9.1.6 MAST**

Collaboration with the MAST experiment (Mega-Ampere Spherical Tokamak), hosted by the Culham Center for Fusion Energy (CCFE) in Culham, UK, focuses on ELM control and pedestal physics, as well as plasma control. The tokamak has undergone a major upgrade to modify its divertor to study the Super-X configuration. MAST-Upgrade also will have increased heating power (from 5 MW to 12.5 MW ultimately), longer pulse lengths (0.5 s to 4-5 s), higher current (1.3 MA to 2.0 MA), higher toroidal field (0.55 T to 0.84 T), and improved capability for RMP

ELM control with the addition of upgrades to its internal coil system. Operation is scheduled to resume presently.

### **9.1.7 ADITYA/SST-1**

The DIII-D program supports and benefits from an ongoing collaboration with the Institute for Plasma Research (IPR) near Ahmedabad, India. The IPR hosts the Steady-State Tokamak (SST-1) superconducting tokamak and the smaller ADITYA conventional tokamak. SST-1 is aimed at developing the tools for long pulse, steady-state operation primarily in the areas of plasma control and operation, the development and assessment of divertor concepts and PFC material research, and developing codes for integrated modeling. Two beam engineers worked with the DIII-D beam group from October 2014 - January 2015, one vacuum/gas feed engineer worked with the vacuum group from October 2014 - July 2015, one scientist worked together with DIII-D scientists on developing 3D field codes from October 2014 - September 2015, and one ECH engineer worked with the ECH group from July 2015 - October 2015. GA provides support for living expenses (an apartment) for the visiting scientists. This collaboration, which does not fall under the umbrella of the IEA Cooperation on Tokamak Programmes (CTP) Implementing Agreement, has been on hold due to administrative obstacles within India that have made it difficult for their scientists to visit DIII-D. The DIII-D team continues to reach out to IPR in hopes of increasing the activity within this collaboration.

### **9.1.8 Other Fusion Devices**

The DIII-D research program is actively engaged with many other fusion programs around the world, which cannot all be mentioned in detail here. Most of this engagement takes place through the International Tokamak Physics Activity (ITPA, section 9.3). Opportunities for mutually beneficial collaborations with the international fusion community will continue to be sought. For example, two devices in Europe may present opportunities in the future; these are the Wendelstein 7X Stellarator in Greifswald, Germany, and the WEST Tokamak in Cadarache, France.

## **9.2 INTERNATIONAL TOKAMAK PHYSICS ACTIVITY**

The DIII-D research program is actively engaged with the workings and plans of the International Tokamak Physics Activity (ITPA). The ITPA is presently under the auspices of the ITER Organization and is a joint activity of fusion programs in US, EU, Japan, Korea, China, India, Russia, and Australia. The ITPA aims to provide cooperation on the tokamak physics R&D activities in order to develop the physics basis for burning tokamak plasmas. The internationally coordinated research activities within the ITPA are separated into topical physics groups and are performed on a voluntary basis. The purpose of these topical groups is to: (a)

propose joint experiments to advance the understanding of fusion plasma physics; (b) assimilate data from these experiments and coordinate the analysis and prepare reports on the results; (c) organize, manage, and update qualified databases in the different areas of fusion physics; (d) develop theoretical models and simulation codes to explain and reproduce experimental results; (e) integrate the R&D results toward improving the plasma performance and developing the operational scenarios for burning plasmas; (f) identify and resolve the key diagnostics issues associated with the control and analysis of burning plasma experiments.

The DIII-D research program is closely involved with the ITPA and makes strong contributions on many ITPA tasks, particularly with regard to the proposal and execution of ITPA joint experiments. For the DIII-D experimental program for 2017, out of the 51 experiments performed, roughly 33 were allocated for ITPA-related experiments. Table 9-2 shows the breakdown of the experiments according to the research topics. The close involvement with the ITPA is also reflected in the US membership of the ITPA topical groups and leadership, which is shown in Table 9-3. The names highlighted in red are closely involved with the DIII-D program and reflect the strong contribution of the DIII-D program to this important international activity.

The DIII-D program will continue to place a high emphasis on performing ITPA tasks within its research program and further adapt to the high priority tasks, as well as the evolution of the ITPA organization itself, in light of the greater requirements and influence of the ITER organization.

**Table 9-2.**  
**General and ITPA-Related Experiments Performed on DIII-D in 2017**

<b>Thrust or Topical Science Area</b>	<b>Total Experiments</b>	<b>ITPA Experiments</b>
ELM Control: 3D Field induced transport	6	4
Burning Plasma Physics	10	6
Dynamics and Control	20	16
Boundary and Pedestal Physics	13	7
Torkil Jensen Award	<u>2</u>	<u>0</u>
<b>Total</b>	<b>51</b>	<b>33</b>

**Table 9-3.  
US Members of the ITPA Topical Groups**

Coordinating Committee	J. Van Dam C. Greenfield R. Hawryluk	MHD, Disruptions, & Control	N. Eidielis R. Granetz J. Harris (Stellarator Rep) S. Jardin R. La Haye S. Sabbagh E. Strait F. Waelbroeck
Diagnostics	R. Boivin D. Brower (chair) L. Delgado-Aparicio E. Doyle D. Hillis C. Lasnier J. Terry	Pedestal & Edge Physics	C.S. Chang M. Fenstermacher J. Hughes R. Maingi (Chair) A. Pankin P. Snyder X. Xu
Energetic Particle Physics	B. Breizman E. Fredrickson N. Gorelenkov W. Heidbrink D. Spong (Deputy Chair) M. Van Zeeland S. Wukitch	Scrape-Off-Layer & Divertor	R. Doerner H. Guo (Chair, PRC) M. Jaworski B. LaBombard A. Leonard P. Stangeby M. Umansky
Integrated Operation Scenarios	P. Bonoli J. Ferron Y. Lin T. Luce (Chair) J.-M. Park F. Poli E. Schuster	Transport & Confinement	W. Guttenfelder G. McKee D. Mikkelsen S. Mordijck C. Petty J. Rice G. Staebler

### 9.3 INTERNATIONAL COOPERATIVE AGREEMENTS

DIII-D and most of its collaborators are party to the IEA Cooperation on Tokamak Programmes (CTP), which includes all of the ITER parties, with the exception of Russia, and ITER itself. In addition, there are bilateral agreements between the US and Europe, Japan, Korea, and China. The majority of DIII-D’s international collaborations fall under the auspices of one or more of these agreements.

### 9.4 INTERNATIONAL INVESTMENT IN DIII-D

Our international partners demonstrate their enthusiasm for participating in the DIII-D research program through their investments, both in scientific exchanges and direct investment in device capabilities. These investments are a way of leveraging the program’s support by DOE.

Many beneficial scientific exchanges have been and continue to be carried out under the auspices of the ITPA and CTP, as well as through bilateral agreements. Table 9-4 lists recent exchanges from the beginning of FY 2016 through the present, indicating collaborative activity in many different topical areas. Table 9-5 shows the full current list of international collaborating institutions.

**Table 9-4.  
A Broad Range of Personnel Exchanges Enhance International Collaborations and Joint Experiments  
(FY2016 and FY2017)**

<b>To DIII-D</b>		<b>From DIII-D</b>	
<p><b>Divertor Development</b> M. Groth (Aalto U) D. Ennis (U Toronto) J. Chen (ASIPP) H. Si (ASIPP) H. Du (Dalian U) D. Carralero (IPP Garching) J. Le (Qinzhou U)</p> <p><b>Plasma-Material Interactions</b> G. Xu (ASIPP/USTC) P. Zhang (ASIPP/USTC) J. Allcockb (Durham U) C. Clauser Bariloche (Atomic Center, Argentina) N. Ashikawa (NIFS)</p> <p><b>KSTAR Scenarios and Control</b> H. Park (NFRI) Y-K. Oh (NFRI) S.H. Hahn (NFRI) H. Kim (NFRI) K.I. You (NFRI) L. Jung (NFRI)</p> <p><b>EAST Scenarios and Control</b> B. Xiao (ASIPP) Q.P. Yuan (ASIPP) Z.P. Luo (ASIPP) J.P. Qian (ASIPP) X. Gong (ASIPP) S. Ding (ASIPP) W. Hu (ASIPP) Q. Ren (ASIPP) J. Huang (ASIPP) S. Ding (ASIPP) G. Xu (ASIPP)</p>	<p><b>IPS/FASTRAN Simulation</b> K. Kim (SNU) C. Byun (SNU)</p> <p><b>KSTAR MSE Collaboration</b> J. Ko (NFRI) W. Hanmin (NFRI)</p> <p><b>EAST MSE Collaboration</b> J. Fu (ASIPP)</p> <p><b>Profile Control</b> T. Vu (EPFL)</p> <p><b>Fusion Big Data</b> T.W. Park (S. Korea Ministry of Information Technology)</p> <p><b>Disruption Prediction</b> J. Vega (CIEMAT) R. Castro (CIEMAT)</p> <p><b>ITER Science and Operations</b> A. Winter (ITER IO)</p> <p><b>HL-2A/HL-2M Control</b> B. Li (SWIP) J. Zhou (SWIP) X. Song (SWIP)</p> <p><b>3D Physics</b> Y. Sun (ASIPP) H. Wang (ASIPP)</p> <p><b>RF Physics/Helicon CD</b> X. Zhang (ASIPP) Y. Zhao (ASIPP) Q. Chengming (ASIPP)</p> <p><b>Super-Supply Installation</b> X. Li (ASIPP) Z. Sheng (ASIPP) F. Zhang (ASIPP) J. Zhang (ASIPP) Xi'An (Actionpower)</p>	<p><b>Divertor Development (EAST)</b> T. Leonard (GA) H. Guo (GA) D. Thomas (GA)</p> <p><b>Divertor Development (IPP Garching)</b> D. Rudakov (UCSD)</p> <p><b>Divertor Development (IPP Greifswald)</b> C. Samuel (LLNL)</p> <p><b>KSTAR Scenarios and Control</b> M. Walker (GA) J. Barr (ORAU) N. Eidielis (GA) M. Lanctot (GA) J.M. Park (ORNL)</p> <p><b>Pedestal Experiments (EAST)</b> T. Osborne (GA)</p> <p><b>3D Physics</b> C. Paz-Soldan (GA) L. Cui (PPPL) R. Nazikian (PPPL)</p>	<p><b>EAST Scenarios and Control</b> D. Humphreys (GA) A. Garofalo (GA) T. Osborne (GA) A. Leonard (GA) C. Holcomb (LLNL) R. Nazikian (PPPL) M. Lanctot (GA) B. Sammuli (GA) D. Eldon (GA) B. Penaflo (GA) I. Anyonetu (GA) D. Piglowski (GA)</p> <p><b>ITER Science and Operations</b> M. Walker (GA) D. Humphreys (GA) D. Schissel (GA)</p> <p><b>ASDEX-U Control</b> M. Walker (GA) D. Humphreys (GA)</p>

**Table 9-5.**  
**DIII-D maintains a large number of active international collaborations (2017)**

Europe & Russia	Asia
Aalto University (Finland)	ASIPP (China)
CEA Cadarache (France)	Dalian University of Technology, China
Chalmers University of Technology (Sweden)	Graduate University for Advanced Study (Japan)
Ciemat (Spain)	Huazhong University of Science and Technology (China)
Consorzio RFX (Italy)	Institute for Plasma Research (India)
Cosylab (Slovenia)	Ishikawa National College of Technology (Japan)
D-TACQ Solutions Ltd (UK)	ITER-India
Durham University	Korea National Fusion Research Center
Ecole Polytechnique (France)	METU - Middle East Technical University (Turkey)
Eindhoven University (Netherlands)	Ministry of Science, ICT and Future Planning
ENEA C.R. Frascati (Italy)	National Fusion Research Institute (Korea)
EPFL (Lausanne, Switzerland)	National Institute for Fusion Science (Japan)
IFP - Consiglio Nazionale delle Ricerche (Italy)	National Institute of Technology, Gifu College (Japan)
Inst. of Control Sciences (Russia)	QST (Japan)
Institute for Nuclear Research (Ukraine)	Peking University
Institute of Plasma Physics AS (Czech Republic)	Seoul National University
Instituto Superior Tecnico, Lisboa, Portugal	Soochow University (China)
ITER Organization	Southwestern Institute of Physics (China)
Kungliga Tekniska Hogskolan (Sweden)	Tsinghua University (China)
Max-Planck Institute for Plasma Physics	University of Science and Technology (China)
Politecnico di Torino (Italy)	
RRC Kurchatov Institute	Australia
Technical University of Denmark	Australian National University
United Kingdom Atomic Energy Authority (CCFE)	
Universita degli Studi di Padova (Italy)	
Universita' degli Studi di Napoli Federico II (Italy)	
University of Nice (Italy)	
University of Seville	
University of Strathclyde	
University of York	
VTT Technical Research Centre (Finland)	

## 9.5 WEB ACCESS TO THE DIII-D FACILITY

The website of the DIII-D National Fusion Facility (<http://fusion.gat.com/>) is a critical tool for successfully conducting the program's mission by a geographically dispersed research team. Traditionally, this tool has been used for communication and as an historical information archive. From the daily experimental plan to the publications repository, the web has allowed for rapid worldwide communication. The evolution of web-related technology has been rapid and the DIII-D web site will take advantage of new capabilities to better serve the scientific community and to improve the interaction of international collaborators with DIII-D.

To allow for easier web authoring by the DIII-D national team, the DIII-D internal website is based on a Wiki that allows editing by the scientific staff. This capability allows more scientists to add web content and to do so faster by eliminating the need to learn HTML and by eliminating the bottleneck of waiting for a web master to make required changes. To ease access, web-

related security such as viewing access, Wiki editing, Bugzilla, and web-based applications are unified to present a single security interface to the international DIII-D team.

Given the ubiquity of web browser clients on all operating systems, some client software has been transitioned away from custom applications to web-based systems. Moving to a web interface provides easier access, is more reliable, and can allow for usage by a DIII-D team member located worldwide, including our international colleagues. Details on security and web-based applications are provided in Chapter 7.

## 10. DIII-D GOVERNANCE

Effective governance is an essential component of the DIII-D National Fusion Program, both for efficient management and for supporting a world-class multi-institutional fusion energy research program. Governance includes defining overall roles and responsibilities, establishing an open program planning process that nurtures both efficiency and innovation, coordinating research activities among the partners, and reporting and publication of results. Professional development is an important consideration here, since the strength of the DIII-D program resides in the motivated creativeness of the participants.

The structures, linkages, and processes described here provide a snapshot of a dynamic organization that began with the Doublet-III project, which featured a major collaboration with JAERI in Japan. DIII-D participants provide continuous feedback and suggestions for improvement in what is a very open and collaborative environment. The present way of doing business builds upon this past experience and reflects the broad-based input provided by team members.

### 10.1 ROLES AND RESPONSIBILITIES

**General Atomics** is the host institution for the DIII-D National Fusion Facility. The Director of the DIII-D National Fusion Program is an employee of GA and is responsible for safe operation of the facility and for oversight of the DIII-D National Fusion Program. The present Deputy Director and Assistant Director are both GA employees, as well. The Director of the DIII-D Experimental Science Division is responsible for the execution of the DIII-D research program.

**The DIII-D Team.** The DIII-D program is an open program with extensive national and international collaborations. The DIII-D national team consists of US collaborations among 7 national laboratories, 28 universities, and 13 industrial companies. International collaborations are conducted with 14 national laboratories, 39 universities and 2 industrial companies. Presently, the near full time scientific staff consists of approximately 40% GA scientists and 60% collaborating scientists.

**DIII-D Executive Committee (DEC).** The DIII-D Executive Committee generally meets quarterly to advise the DIII-D Director on a broad range of programmatic issues such as long-range program planning. The DEC also addresses institutional issues related to managing the DIII-D team, such as invited talks at major conferences, operational scheduling, and budgets. DEC membership consists of 31 senior representatives (or their alternates) from GA and the major collaborators, including, Princeton Plasma Physics Laboratory, Lawrence Livermore

National Laboratory, Oak Ridge National Laboratory, Sandia National Laboratory, Massachusetts Institute of Technology, Columbia University, University of Texas, the University of California at Los Angeles, the University of California at San Diego, University of California at Irvine, and the University of Wisconsin. Many members participate by video or teleconference to reduce travel expenses.

**DIII-D Program Advisory Committee (PAC).** The DIII-D Program Advisory Committee is composed of 15 experts in the field not directly involved in the DIII-D program. It reports to the GA vice-president of Magnetic Fusion Energy (MFE). The PAC meets openly at least once per year, responding to specific charges, which generally seek their comments on the Experimental Plan for the coming year and other issues prominent at the time (e.g., they were asked to comment on this five-year program plan during its development). Formally, their report is given to the vice-president of MFE and to DOE, though it is broadly distributed to members of the DIII-D team.

**Research Council.** The Research Council (RC) is a small multi-institutional advisory group (12 members for FY18) chaired by the DIII-D Deputy Program Director and with rotating membership. It is composed of scientists at all levels representing the various research areas, program management structures, and major collaborators. Its principal role is to advise and assist the DIII-D Director and his staff on matters relating to development and execution of the experimental program, such as goals and objectives, relative research and hardware priorities, topical balance, and run-time allocations. Table 10-1 lists the members of the FY 2018 Research Council.

**Table 10-1**  
**FY18 Research Council Members and Affiliations**

<b>Chair:</b> Wayne Solomon (GA)	<b>Vice Chair:</b> Max Fenstermacher (LLNL)	
Richard Buttery (GA)	Houyang Guo (GA)	Tony Leonard (GA)
John Canik (ORNL)	William Heidbrink (UC Irvine)	Francesca Turco (Columbia)
Charles Greenfield (GA)	Valerie Izzo (UCSD)	
Brian Grierson (PPPL)	Arnie Kellman (GA)	

The DIII-D Scientific Program is carried out by the **Experimental Science (ES) Division** and the **Boundary and PMI Center (BPMIC)**. Together, ES and BPMIC are organized to support DIII-D’s long-range research objectives, which are well-aligned with DOE FES research needs as described in the 2015 FES Ten-Year Perspective. The scientific content and expertise within these groups is broad topically and institutionally, so each is divided into Topical Area

Working Groups. All scientists and students participating in onsite research are associated with at least one of these topical areas.

**Experimental Science Division.** The Experimental Science Division is responsible for developing and executing the overall DIII-D Research Plan. This division is composed of three physics groups:

- Dynamics and Control
- Pedestal and ELM
- Burning Plasma Physics

The **Dynamics and Control Group** is responsible for developing the physics basis for integrated operating scenarios for ITER and subsequent fusion devices. This integration includes research in the areas of scenario development, plasma control, stability, disruptions, and heating/current drive. This group also coordinates the physics operators supporting DIII-D experiments.

The **Pedestal and ELM Control Physics Group** is responsible for developing an improved physics basis and control solutions for the pedestal and ELMs. Activities of this group include experiments at DIII-D to identify and understand the physics processes controlling the H-mode pedestal structure, to develop ELM control strategies and understand the physics of these regimes and to use the knowledge gained to develop improved pedestal solutions. A focus of the group is to work toward predictive capability by testing and evaluating theoretical models for pedestal structure and ELM control.

The **Burning Plasma Physics Group** is responsible for advancing the predictive capability of critical physics phenomena in burning plasmas. Activities of the group include core transport and turbulence, L-H transition physics, and energetic particle research. Validation of comprehensive physics models in the areas of transport and energetic particles will be a key focus of this group.

The mission of the **DIII-D Boundary and PMI Center** is to develop optimized boundary/PMI solutions for application to burning plasma devices. The Center includes three physics groups:

- Advanced Materials Validation
- Divertor Optimization
- Integrated Modeling

The **Advanced Material Validation Group** is responsible for validating models and provision of data under realistic fusion environments to the community on PMI, and studying advanced wall material alternatives to carbon and tungsten, including coatings, for post-ITER devices.

The **Divertor Optimization Group** works to compare experiment with theory and models to validate divertor/boundary codes for divertor optimization, develop an understanding of core-edge integration, and, ultimately, to identify a viable divertor/boundary solution compatible with high core performance.

The **Integrated Modeling Group** works to adapt and optimize codes and computational tools for developing a new divertor concept in DIII-D, optimizing ITER scenarios and designing next-step fusion devices, and provide relevant data for realistic fusion environments to the PMI community.

Specific research activities are organized and executed by **Topical Area Working Groups** and by **Task Forces**. Topical Area Working Groups are organized within each of the six physics groups, but may draw participants from across the organization (including the GA Theory group). Task Forces address near-term high-priority research that is cross-cutting in nature, which is best managed by a team of experts specifically assembled for the task at hand. Both types of groups are responsible for experimental planning, execution, and data analysis. Working group leaders report to their physics group leader, while the Task Forces report directly to the appropriate division director. Leadership of Task Forces and working groups constitutes a significant programmatic responsibility, which often leads to increased leadership opportunities for DIII-D program scientists, including those from universities and other collaborating institutions. Fig. 10-1 shows the Topical Area Working Group and Task Force structure for FY 2018.

**DIII-D Operations Division.** This group is responsible for the safe and efficient operation and maintenance of the DIII-D facility. They oversee all the major hardware systems on DIII-D, including the auxiliary heating and current drive systems, the DIII-D vessel and coil systems, all major power supplies, vacuum systems, water systems, and cryogenic systems. The Operations Division is responsible for modifications and upgrades to these systems. This division is organized into six groups: Tokamak Operations, Project Engineering, Neutral Beam Systems, Electron-Cyclotron Systems, Mechanical Systems, and Electrical Engineering Systems. Staff from major collaborators (PPPL, LLNL, and ORNL) are responsible for a number of significant hardware systems and serve in key positions within the Operations Division.

**Theory Division within the Energy Group at GA.** The DIII-D program relies on and benefits from close connection to theory. DIII-D scientists participate in a broad range of collaborations with theorists from around the US and abroad. The DIII-D program provides data for validating new theory and models; conversely, theory motivates and guides planning for many DIII-D experiments. The theory group at GA includes scientists from other institutions (e.g., UCSD) who spend a majority of their year onsite at GA. The theorists work closely with the DIII-D program, providing not only general theory support, but also extending key data analysis codes such as EFIT and the ONETWO profile analysis codes, as well as simulation tools such as the NIMROD resistive MHD and XGC0 PIC edge plasma codes. Members of the theory group (both GA and non-GA staff) serve on both the DEC and the Research Council.

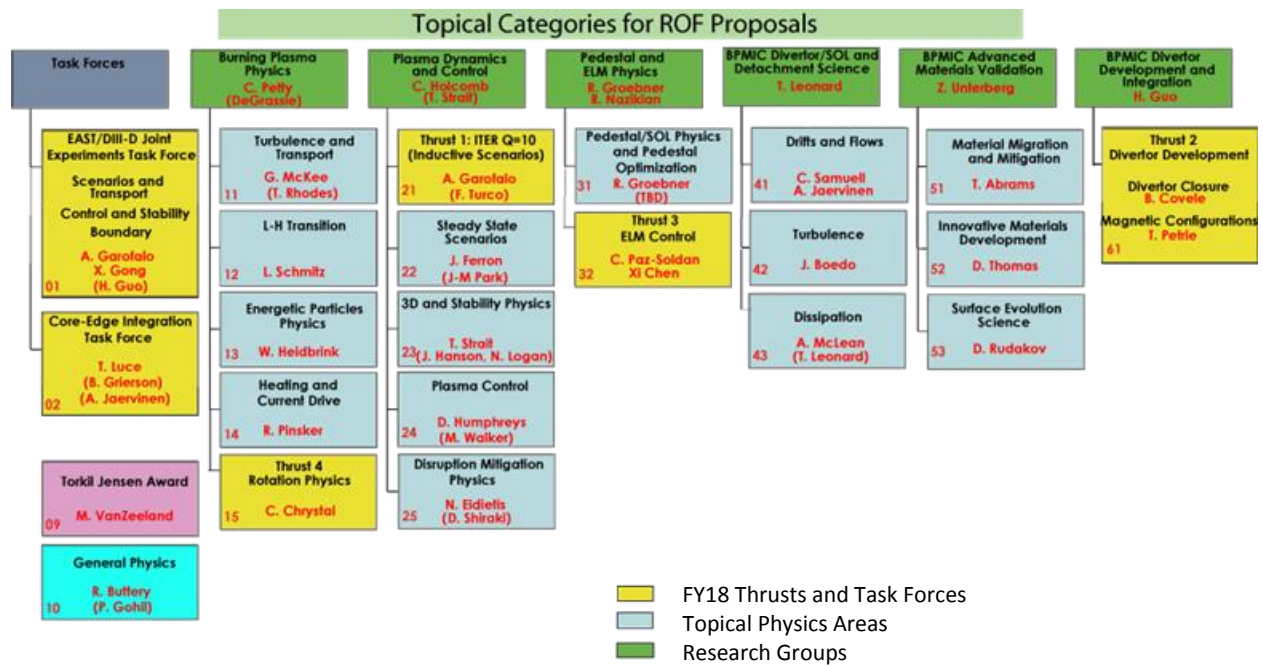


Fig. 10-1. Organization of experimental science task forces and working groups for 2018 DIII-D research operation.

## 10.2 PROGRAM PLANNING

Planning for the DIII-D National Program is carried out in partnership with DIII-D management, DIII-D collaborators, and DOE FES, with input provided by the broader (national and international) fusion community. Program plans range from daily experiments to this five-year program plan. Both GA and its DIII-D collaborators provide regular reporting to DOE. In this section, the planning process for these various program plans is outlined, starting from the longer-term perspective.

1. A **Five-Year Program Plan** is prepared every five years through open interaction of the DIII-D team with the US and international fusion communities and the DOE FES Program:
  - a. The process begins with a Long Range Planning Workshop, where the scientific team can propose research directions, areas of emphasis and hardware upgrades to be considered.
  - b. A draft Five-Year Plan is prepared by the DIII-D national team. Multi-institutional teams are formed to develop various possible program elements for inclusion in the Five-Year Plan.
  - c. The draft plan is presented to the DIII-Program Advisory Committee for their consideration. Feedback may lead to changes in the proposed plan.
  - d. GA proposes the five-year research program to DOE FES. In parallel, major collaborators develop their own plan to complement the overall DIII-D Five-Year Plan. In the past, companion documents from the major collaborators were submitted together with the GA proposal to provide a complete view of the DIII-D National Program to the FES program management. For 2019-2024, national lab partners will submit costed proposals directly and will be independently peer-reviewed.
  - e. A formal GA proposal for a cooperative agreement, with content based on the Five-Year Plan, is reviewed by a panel appointed by FES.
  - f. Once in place, the Cooperative Agreement between GA and the DOE may be updated to make it consistent with evolution of national program priorities and technical developments in the international fusion effort.
  
2. An **Annual Experimental Plan** is prepared as follows:
  - a. A review of the previous year's results is typically presented in a DIII-D Year-End Review (although other forums, including the annual American Physical Society Division of Plasma Physics (DPP) meeting and the International Atomic Energy Agency (IAEA) Fusion Energy Conference (FEC), are often utilized) provides the technical basis to begin developing the experimental plan for next fiscal year's operation.
  - b. High-level research goals covering the next 1-3 years are put forward for consideration by the DIII-D Research Council and the full research team.
  - c. Following the initial discussion of possible research goals, the DIII-D Director works with the staff to identify high priority research topics (thrusts) and then provides initial guidance for allocating 80% of experimental time among the research topics. Special Task Forces may be created to address a particular topic. The remaining 20%

- of the run time is reserved for allocation in mid-year following an evaluation of progress on achieving research goals.
- d. An international Research Opportunities Forum provides an opportunity for the community to propose experiments within the thrust and topical areas. Remote interactive participation is provided via the Internet.
  - e. Based on the proposals, Task Force and Working Group leaders work with groups interested in the specific research area to prepare detailed experimental plans. These plans are presented to the Research Council for final review of the overall program balance.
  - f. The DIII-D Executive Committee (Section 10.1) and the international DIII-D Advisory Committee (Section 10.1) also review the draft experimental plan.
  - g. The annual Experimental Plan is reviewed on a monthly basis, taking into account changing hardware availability and DIII-D or national program priorities, as provided by the OFES, the USBPO, or the ITER Project Office.
3. Monthly and Daily Experimental Planning is managed by the DIII-D Experiment Coordinator in consultation with the directors of DIII-D Operations, the Experimental Science Division, the Boundary and PMI Center, and program scientists.

### 10.3 FUNDING OF RESEARCH ON DIII-D

- The major participating laboratories in the DIII-D team (GA, PPPL, LLNL, ORNL, SNLA, MIT) receive their funding directly from the DOE-FES program.
- Existing university participants in DIII-D (UCSD, Texas, Columbia, Wisconsin, Auburn, Princeton University, Tennessee) also receive their funding directly from DOE through specific calls for proposals that occur through an annual DOE Funding Opportunity Announcement (FOA).
- GA subcontracts with some universities and industries for specialized diagnostics and technical services.
- Investigators who make proposals at the annual research opportunities forum meetings can apply to DOE for funding if their proposals are included in the experimental plan.
- Universities, laboratories, and private industry may (and have) apply for DOE or NSF funding to conduct research at the DIII-D facility in response to specific calls for proposals that occur on a regular basis (e.g., FOA, SBIR, diagnostic competitions, joint projects between DOE and other government agencies, and various awards such as Young Investigator Awards or Faculty Startup awards).

## 10.4 REPORTING DIII-D PROGRAM ACTIVITIES

- DIII-D issues weekly highlights to the broader fusion research community on program activities. These highlights are available on the Web at <https://diii-d.gat.com/diii-d/Weekly>.
- DOE conducts quarterly reviews of the program. GA and major collaborators report on facility operations, technical accomplishments, budgets, safety matters, and outstanding issues.
- The annual Experiment Plan is submitted to DOE.
- The DIII-D program activities are discussed at the Fusion Facilities Coordinating Committee (FFCC) meetings for coordination with other major US facilities such as NSTX-U.
- The DIII-D program planning is reported each March to DOE FES program managers at a meeting at Germantown.
- DIII-D program activities are discussed extensively at meetings of the USBPO. Often, DIII-D results form the core technical content of USBPO reports and recommendations.
- DIII-D is a major contributor to national and international fusion and plasma physics meetings and conferences, including APS, EPS, IAEA, PSI, and many special workshops.
- DIII-D research results are reviewed and published in many scientific, technical, and engineering journals. An extensive bibliography of DIII-D publications resulting from the previous five-year cooperative agreement appears in Section 15 at the end of this document.
- The GA DIII-D Website at <https://fusion.gat.com/global/DIII-D> provides a collection of public information about the DIII-D program.

## 10.5 SAFETY

DIII-D Management is committed to maintaining an Environmental, Health, and Safety program that places high value on ensuring the protection of life, the environment, and the facility. The utmost regard is placed on personnel, collaborators, visitors, and contractors working onsite. In order to maintain a level of excellence for onsite personnel, specific programs have been implemented.

- The facility complies with federal, state, and local regulations governing safety and environmental stewardship practices. Regulations have been incorporated in training, documents, and work practices.

- Safety training classes are assigned for all job classifications. After completion of the classes, new personnel (GA and collaborators) are escorted by trained personnel until their supervisor is confident that they have incorporated safety policies and procedures in the DIII-D work environment.
- Collaborators are assigned a GA host who acts as the onsite supervisor. The onsite supervisor, Safety Officer, and representatives from the home institution, will ensure that the appropriate training to perform the assigned work is completed.
- Safety controls, such as administrative, engineering, and good work practices, are designed to minimize and eliminate accidents.
- A reporting and tracking system ensures that all concerns are addressed in a timely manner. Progress is measured to make continual and necessary improvements.

## **10.6 MANAGEMENT OF THE COLLABORATIVE NATIONAL TEAM**

### **10.6.1 General Principles of Collaboration**

The following principles serve as guidelines for conducting institutional collaboration on the DIII-D program:

- Advancement of the DIII-D program is held by all participating institutions to be essential for advancement of US fusion energy science and to be in the interests of all DIII-D program participants.
- Collaborators will accord high priority to their DIII-D commitments, both in the use of resources and in the assignment of personnel. GA will recognize that some collaborating personnel assigned to DIII-D activities may have additional responsibilities in their home programs.
- In support of the DIII-D program objectives, collaborators will be accorded lead responsibilities in defined areas and participation in other areas as spelled out in institutional Memoranda of Understanding (MOU). “Lead responsibility” does not imply sole responsibility. In those areas where it does not hold a lead, a party may elect to retain significant minority participation sufficient to develop and sustain expertise in the area. These lead or support roles will be based on consensus assessments of capability and party needs by the program leadership and the DIII-D Executive Committee. Individuals or groups which wish to collaborate on DIII-D should negotiate with the institution that has lead task responsibility. Cases of disagreement should be called to the attention of the Director and the Executive Committee. Institutions having lead responsibility for a task are not to delegate responsibility to another party without approval of the Director.

- GA will have sole responsibility for operating the DIII-D tokamak, though it counts on support from collaborating institutions. If a collaborator has a lead role involving an auxiliary hardware system on DIII-D, they may undertake the responsibility to operate that system. The scope of the collaborators' responsibility in design, construction, and operation of systems will be defined in the individual MOU between GA and collaborating institutions.
- In order that the DIII-D program accomplish its programmatic objectives and the individual researchers have the opportunity to pursue rewarding research, it is generally expected that the participants will spend roughly half of their time carrying out program-related support tasks (e.g., leading research topics, operating a diagnostic, analyzing data, or engaged in research planning) and spend the other half of their time pursuing an agreed-upon research program.
- All data, raw or analyzed, will be considered the property of the DIII-D program and will be accessible to others in the program. The rights of first authorship and lead responsibility will be respected. It is expected that GA staff and collaborators operating diagnostics or doing specialized analysis will provide data into defined DIII-D databases on a routine basis and to other members of the program when requested.
- Subject to DOE's technical data rights and patent rights, all data and results from the DIII-D program will be freely shared and acknowledged between the collaborating parties. In general, all publications or reports must go through the standard GA DIII-D review cycle. However, in the case that the work reported on is principally done by collaborating personnel using collaborators' equipment and codes, the publication or report may be submitted through the collaborating institution's review process. In such cases, a copy must be provided for timely courtesy review by the responsible DIII-D research area coordinator and division director. DIII-D division directors will make the determination of the appropriate review channel. Publications and reports will clearly identify that the work was done on the DIII-D tokamak and acknowledge DOE funding support. Detailed requirements for presentation formats, use of logos, and issues related to invited talks and papers will be managed by the DIII-D Program Director with review by the DIII-D Executive Committee.
- DOE data and patent rights as specified in GA's contract with DOE will take precedence in all work done on, or derived from, DIII-D.
- All GA data, which GA identifies as proprietary, will be protected by individual collaborators and collaborators' institutions.
- Collaborating institutions are expected to participate in all DIII-D related DOE and community reviews.

### 10.6.2 Documents Governing Active Collaborations

MOUs are written between GA and major collaborators. MOUs generally cover the historical background that has led to the collaboration, the institutional goals and requirements of both parties for participating in the collaboration, the principles and agreed-upon procedures for the collaboration, and a definition of lead and participatory roles for the collaborator. The MOU is signed by the program leaders of GA and the collaborating institution.

### 10.6.3 Approval Process for Project Activities

A graded approach is used for Project Management involving the DIII-D facility. All DIII-D participants, as well as outside technical specialists, may review project plans and provide advice. Progress, costs, and schedules for special projects are reported at DOE Quarterly Reviews. DIII-D Program tasks for both GA and collaborators are summarized in common master schedules and milestones. A manual describing the work procedures for DIII-D tasks and projects is available for all DIII-D personnel and collaborators. It describes a sequence of procedures (WP-01 through WP-14) which establish a uniform approach to developing and maintaining new capabilities at DIII-D including designing, engineering, fabricating, installing, and maintaining hardware and equipment on the DIII-D tokamak or any of its related systems. Procedures are also included to guide the performance of work in the machine pit and within the facility. Depending on the complexity of the proposed task, the review and approval process may include a:

- Physics Validation Review describing research need and proposed actions to address the need
- Conceptual Design Review to lay out the proposed technical approach
- Preliminary Design Review to assess design features and overall plan at an early stage
- Final Design Review to assess all elements of the design prior to beginning work
- Operational Readiness Review to assess status of all systems, controls, and training prior to commissioning the system

These work procedures undergo periodic review and updating. They are available on the DIII-D local web at [https://diii-d.gat.com/d3d-wiki/images/7/77/D3WP\\_tofc.pdf](https://diii-d.gat.com/d3d-wiki/images/7/77/D3WP_tofc.pdf)

### 10.6.4 Budget Planning for DIII-D Projects

Budgets for program tasks are generated by all task managers working with the DIII-D Planning and Control Group and submitted to the DIII-D program director for distribution to the Executive Committee and the DOE. Task priorities are set by the DIII-D program director in consultation with the DIII-D Executive Committee and in accordance with GA's contractual

requirements with the DOE. Resource disbursements are made with input from collaborating DIII-D program leaders. The Executive Committee will also make recommendations on the priorities of collaborators budgets. Disagreements between parties will be arbitrated by DOE when they cannot be resolved by the Institutional Leadership.

#### **10.6.5 Program Reporting**

GA will submit all required plans and reports identified in its contract with the DOE. GA will prepare a DIII-D Experimental Plan each year that details all planned experiments for that year, including those to be performed by collaborators. It will be reviewed quarterly in conjunction with the DOE Quarterly Contract Review and updated as needed. The plan will be prepared by the DIII-D Research Council, which includes representatives from the major collaborators as well as GA. Before submission to DOE for approval, it will be reviewed by the Executive Committee and approved by the DIII-D program Director.

Technical program reports will be submitted quarterly as part of the DOE Quarterly Review or as needed. An Annual Technical Report and Final Contract Technical Report will also be submitted. An overall Management Plan will be submitted after contract award. At the beginning of the contract and on a quarterly basis thereafter, GA will submit management status and summary reports. Annually, GA will submit a milestone schedule plan, cost plan, and milestone schedule status report.

## 11. ACCOMPLISHMENTS AND HISTORY OF THE DIII-D PROGRAM

### 11.1 OVERVIEW

The DIII-D National Fusion Program is recognized as one of the most productive fusion research programs in the world as measured in impact of results, uncovering fundamental phenomena, and the overall number of publications, citations, and awards. These contributions have been made over a wide range in plasma science and fusion technology. The DIII-D results have had a large impact on the direction of international magnetic fusion research and progress toward fusion energy. An essential ingredient in this success has been the integration of contributions from a wide range of collaborators from around the world, together with the participation of DIII-D staff in research at other facilities. Currently, the DIII-D program is strengthened by collaborations from 106 US and foreign institutions. DIII-D's results have influenced the designs of several operating tokamaks, including the Mega-Ampere Spherical Tokamak (MAST), the National Spherical Torus Experiment Upgrade (NSTX-U), the Korean Superconducting Tokamak Advanced Research (KSTAR), and China's Experimental Advanced Superconducting Tokamak (EAST), and in the design of ITER.

Work in the 2014-2018 five-year program continued this high-level of productivity — enabled by new hardware and diagnostic capabilities that have come on line during this period. In this section, some of the past DIII-D accomplishments are highlighted as a prologue to future DIII-D success in fusion research and in the program's capability to deliver on the proposals and plans detailed in this document.

### 11.2 DIII-D ACCOMPLISHMENTS

The DIII-D tokamak program at GA has made many scientific contributions to the worldwide fusion effort. The prescient pursuit of shaped plasmas drove the pioneering shape control techniques that were rewarded in record plasma beta values and reactor-relevant fusion triple products ( $nT\tau$ ), demonstrating that a stable reactor core can exist. The mission of the DIII-D Research Program implies integration of magnetic fusion-focused scientific research and advanced plasma control techniques into new operating scenarios aimed at optimizing the tokamak, providing improved regimes for ITER, and developing high-performance scenarios for an advanced tokamak (AT). In the 2014-2018 five-year plan, the DIII-D program had a significant focus on validating the physics basis for a number of key issues to ensure ITER's success. These contributions are detailed in Section 11.7.

Table 11-1 lists significant DIII-D contributions to burning plasma research. Many of these results are now the basis of everyday experimental operation at DIII-D, while others continue to

be refined and developed further because of their importance for ITER and the design of subsequent fusion devices.

Operational hallmarks of the DIII-D program over the years have been reliability, flexibility, and adaptability. DIII-D was designed to be highly flexible in experimental capability, having excellent diagnostic access and the ability to access a wide range of plasma shapes. The DIII-D plasma shape can be programmed to emulate the shape of virtually any existing or planned tokamak. In collaboration with other devices, this capability has enabled numerous “wind tunnel” comparisons that elucidate dependences of plasma behavior on design and operating parameters.

**Table 11-1.**  
**Major DIII-D Contributions to Tokamak Plasma Research**

- 
- Combined an understanding of the roles of plasma shape and internal profiles for stability to demonstrate discharges that satisfy the high-gain goals of burning plasma conditions.
  - Optimized plasma shaping for simultaneous high plasma performance and divertor control of the heat and particle flux.
  - Exported the DIII-D-developed digital plasma control system to fusion experiments (both tokamak and non-tokamak) throughout the world.
  - Developed magnetohydrodynamic (MHD) equilibrium analysis for non-circular plasmas based on magnetic measurements, the pressure profile, the current profile, and rotation. The DIII-D equilibrium code “EFIT” is now used by institutions throughout the world for shaped tokamaks.
  - Developed a predictive theoretical model for H-mode pedestal stability, validated by a very large body of DIII-D experimental results.
  - Used ECCD to suppress and control deleterious neoclassical tearing modes as predicted by theory.
  - Stabilized resistive wall modes (RWMs) with feedback controlled non-axisymmetric magnetic perturbation coils, thereby increasing the accessible plasma  $\beta$ .
  - Identified and characterized Alfvén eigenmodes and their role in transporting fast-ion energy out of the plasma. Experiments validated a critical gradient model of fast-ion transport by Alfvén eigenmodes (AE).
  - Discovered that edge localized modes (ELMs) in several H-mode-based operating scenarios can be stabilized by the application of small non-axisymmetric resonant magnetic perturbations (RMPs), providing the basis for ITER’s ELM control coils.
  - Demonstrated that rapid injection of frozen deuterium pellets can trigger more rapid smaller ELMs and reduce the resulting pulsed heat load to tolerable levels for ITER.
  - Discovered the QH-mode of operation, having no ELMs, and demonstrated its compatibility with capabilities of future burning plasma devices.
  - Demonstrated effective techniques for avoiding and mitigating disruptions, providing the basis for ITER’s Disruption Mitigation System.
  - Developed and demonstrated active divertor plasma pumping to allow control of the particle inventory.
  - Strong toroidal field direction dependence of divertor in-out asymmetries of measured temperature and density profiles are qualitatively reproduced by UEDGE with  $E \times B$  Drifts.
  - Pioneered the use of non-dimensional transport scaling experiments for plasma characterization, thereby providing a scientifically sound basis for projecting present results to future burning plasmas.
-

- 
- Demonstrated fast wave radio frequency current drive and validated theory.
  - Experimentally verified the role of  $E \times B$  velocity shear in stabilizing turbulence, creating transport barriers, and thereby increasing plasma confinement.
  - Pioneered millimeter wave gyrotron system implementation and launching technology.
  - Demonstrated electron cyclotron heating and current drive and validated theory.
  - Measured peaked edge main ion rotation at plasma edge, showing intrinsic plasma rotation.
  - Developed and demonstrated several high-performance operating scenarios by combining advances in equilibrium, stability, heating, and boundary control; in particular the VH-mode and Negative Central Shear regimes.
  - Identified, motivated, and demonstrated the value of the Advanced Tokamak concept for enhancing the attractiveness of a power-producing tokamak reactor.
  - Fully noninductive conditions developed and demonstrated for a range of operating scenarios.
  - RMP ELM suppression was obtained in fully non-inductive hybrid plasma with minimal impact on performance.
- 

The adaptability of the program is demonstrated by recent examples where DIII-D performed experiments to respond to urgent ITER requests for scientific input. These included a demonstration of RMP ELM suppression in helium plasmas, requested by the ITER Organization (IO) for input into ITER’s Pre-Fusion Power Operation (PFPO) phases, and an experiment to vary RMP coil currents to spread out RMP-produced asymmetries divertor heat load, also requested by the IO, to address concerns of asymmetries created in the divertor heat loads by RMP fields. The program’s adaptability and community leadership is also shown by the recent addition of national campaigns, where tokamak run-time was provided for scientists from C-Mod and NSTX-U, and a Frontier Science Campaign, to provide DIII-D and all of its capabilities as a resource to plasma scientists performing basic research.

### **11.3 SCIENTIFIC ACCOMPLISHMENTS DURING THE CURRENT COOPERATIVE AGREEMENT 2014–2019 AND PROJECTIONS TO 2019–2024**

Some recent accomplishments are highlighted that apply directly to the major technical objectives for the new 2019–2024 period. Topical areas with significant results are indicated as bold bullets and those underlined indicate the major thrusts for the 2014–2018 Program Plan.

#### **Develop and qualify ELM control solutions for ITER**

*ELMs have always been observed during H-mode in tokamaks and stellarators, but as device size and energy content approaches that of ITER, their repetitive heat pulses can threaten the integrity of plasma-facing materials in the divertor. DIII-D has pioneered several methods to avoid this damage.*

- ELM suppression and mitigation with Resonant Magnetic Perturbations (RMP) was first developed in DIII-D, and DIII-D’s results form the basis for ITER’s ELM coils. Recent

experiments have begun to reveal the physics basis for RMP ELM suppression and to broaden the parameter space where it is observed.

- RMP ELM control experiments varied the  $n=2$  field structure and used new 3D magnetics to show that resonant field penetration may be the key to RMP suppression of ELMs. [Nazikian 2015]
- Identification of dual mode response helps determine the path to optimize RMP ELM suppression. The low-field side sees a pressure-driven kink with amplitude that changes with  $\beta_N$ . The high-field side sees a current-driven kink correlated with ELM suppression. [Paz-Soldan 2016]
- DIII-D RMP ELM suppression was extended to the ASDEX Upgrade (AUG) shape, leading to the first demonstration of ELM suppression at low collisionality in AUG. [Nazikian 2016]
- ELM pacing, where ELMs are triggered by injection of small fuel or impurity pellets, is aimed at increasing the ELM frequency while proportionally decreasing the peak heat flux.
  - ELM pacing with deuterium pellets was demonstrated in ITER-similar conditions on DIII-D, with an order-of-magnitude increase in ELM frequency and concomitant decrease in peak heat flux. [Baylor 2013]
  - ELM triggering with Li granules (0.7 mm) was successfully demonstrated ( $3\times$  increase in ELM frequency), with nearly 100% trigger fraction during the entire duration of the current flattop. [Bortolon 2016]
- QH-mode is a naturally ELM-free operating scenario, first identified in DIII-D in 1999 with strong counter NBI. It provides an extremely attractive operating point for a reactor, with the main challenge being elimination of the need for externally applied torque.
  - The QH-mode edge is regulated by MHD activity that takes the place of ELMs in expelling impurities from the core. M3D-C1 simulations showed that rotation shear drives low- $n$  Edge Harmonic Oscillation (EHO) seen in most QH-mode plasmas. [Chen 2016]
  - QH-mode has been maintained with low or zero torque without the torque from 3D fields. Zero torque leads to reduced  $E\times B$  shear, raising edge turbulence, resulting in a broader, higher pedestal while maintaining ELM-stable operation. Efforts continue to access the QH-mode without an initial phase of increased torque. [Burrell 2016]
- Experiments were performed during the DIII-D Helium campaign to study Type-I ELMs and the pedestal in low collisionality plasmas in support of the Pre Fusion Power Operations phases in ITER.
  - RMP ELM suppression was obtained in a helium plasma. [Evans 2017]

## Develop and qualify disruption control solutions for ITER

*Disruptions that release most or all of the device's energy present a major challenge to the tokamak as a reactor concept. Research in DIII-D is addressing the prediction, avoidance, and mitigation of disruptions in order to manage the risk.*

- DIII-D has tested both Massive Gas Injection (MGI) and Shattered Pellet Injection (SPI) as techniques for introducing large quantities of material to safely radiate the plasma's energy. Based on DIII-D's unique experience, ITER has selected SPI for its Disruption Mitigation System.
  - SPI was shown to provide faster response and larger impurity assimilation than MGI [Commaux 2016].
  - Control of SPI neon fraction was shown to tune disruption mitigation metrics to meet scaled ITER requirements, including: 1) High-Z needed to radiate 90% thermal energy, 2) current quench cannot be too fast or mechanical damage can occur [Shiraki 2016a].
  - Toroidal radiation asymmetries during (MGI) were quantified and magneto-hydrodynamic activity was identified as a key contributor to those asymmetries [Commaux 2014, Izzo 2015, Shiraki 2015].
  - Poloidal radiation asymmetries were found to be highly dependent upon the poloidal location of the MGI, but within acceptable ITER limits except under very conservative assumptions [Eidietis 2017].
  - Experiments where impurities were injected into plasmas with large pre-existing MHD modes (as expected in ITER) found that mitigation effectiveness remains unaffected by the pre-disruption MHD activity [Shiraki 2016b].
  - Mitigation of vertical displacement events (VDE's) was found to be insensitive to the poloidal location of the injector relative to the direction of motion, but highly sensitive to timing [Hollmann 2015a].
  - Neon SPI into the early-current quench may successfully suppress the formation of a population of superthermal “runaway” electrons (RE) [Eidietis 2014].
  - A novel tangential Gamma Ray Imager (GRI) was developed to provide spatially resolved measurements of RE energy spectra from bremsstrahlung emission [Cooper 2016].
  - Measurements from the GRI and other diagnostics identified key RE dissipation mechanisms and revealed discrepancies with existing models, especially at low RE energy [Hollmann 2015b, Paz-Soldan 2017].

- The first direct measurements of RE-seed generation rates were made, revealing discrepancies with existing models [Hollmann 2017].

### **Core Stability Control for Disruption-Free Operation**

*DIII-D stability research is aimed at ensuring reliable, disruption-free operation of ITER and future fusion devices. This goal requires investigation of the underlying physics of MHD stability in tokamaks, as well as the development of methods to optimize the 2D and 3D configuration of the plasma for stability, and the prediction and control of instabilities.*

- DIII-D research has made significant advances in developing both passive stability and active control of the tearing modes that are the chief performance-limiting instability in discharges simulating ITER’s Q=10 baseline scenario. Methods to predict the onset of tearing modes are also being developed.
  - Critical details of the current density near the  $q=2$  surface associated with tearing instabilities have been identified [Turco 2016], and tailoring the current density profile early in the discharge enables stable discharges with  $\beta_N$  and  $q_{95}$  values of ITER’s baseline scenario, and zero net neutral beam torque [Turco 2017].
  - Preemptive stabilization of the 2/1 mode with electron-cyclotron current drive and/or heating has been demonstrated in low-torque, low-rotation ITER baseline scenario discharges, using real-time tracking of the  $q=2$  location [LaHaye 2017].
  - Forced rotation of large magnetic islands using resonant magnetic perturbations (RMP) avoids wall-locking and disruption [Choi 2017, Okabayashi 2017].
  - Active MHD spectroscopy for direct measurement of tearing mode stability in ITER-like plasmas has shown promising initial results [Turco 2016, LaHaye 2016].
  - Sophisticated “machine learning” techniques are under development for prediction of disruptions [Rea 2017 Kleijwegt 2017 Parsons 2016]. Offline analysis has yielded disruption predictions with better than 90% accuracy.
- DIII-D research is developing the physics basis for both passive stability and active stabilization of kink modes, in the high-beta regime needed for steady-state operation with a large bootstrap current fraction and high fusion power density.
  - Modeling and experiments in discharges compatible with steady-state operation show that kinetic effects enable passive stability with beta values well above the no-wall kink stability limit [Hanson 2017]. Resonant interactions with fast ions from neutral beam injection may be important for passive stability [Turco 2015].

- Feedback stabilization with internal control coils enables steady-state-compatible discharges to reach beta values approaching the ideal-wall kink stability limit [Hanson 2017]. Initial tests of a model-based controller and external control coils show stabilization comparable to that of internal coils [Clement 2017].
- DIII-D has been a pioneer in understanding the importance of small non-axisymmetric “3D” magnetic fields in a nominally axisymmetric tokamak plasma. Recent research has provided detailed comparisons with MHD theory and expanded the repertoire of techniques for optimizing 3D fields.
  - New magnetic diagnostics have shown that the plasma’s magnetic response to external  $n=1$  perturbations is in good agreement with linear, ideal MHD models [King 2015]. In plasmas with moderate beta, the plasma response is well described by a single stable mode [Paz-Soldan 2014, Lanctot 2017].
  - With  $n=2$  fields, a multi-modal response is seen, again in good agreement with MHD models [Paz-Soldan 2015, Munaretto 2017]. A new paradigm of “reluctance eigenmodes” explains the complexities of the plasma response in terms of a strong response by very stable modes as well as by weakly stable ones [Logan 2016].
  - Minimization of rotation braking provides a new path to real-time optimization of single-mode  $n=1$  error field correction that may be useful for ITER [Lanctot 2016].
  - A recent empirical scaling study suggests that “intrinsic torque” in ITER, including neoclassical toroidal viscosity (NTV) torque caused by 3D magnetic fields, could be comparable to ITER’s expected neutral beam torque [Chrystal 2017a].

### **Transport and confinement**

*DIII-D’s comprehensive diagnostic set has been brought to bear on a wide range of studies aimed at developing a basic understanding of the processes governing the transport of particles, energy, and momentum in the tokamak plasma. These efforts greatly benefit from a partnership with the theory and modeling community, and an emphasis on designing experiments and diagnostics with a goal of validating theory-based predictions.*

- Measured intrinsic plasma rotation behavior crossing the scrape-off-layer into the pedestal across the separatrix, has been successfully replicated by the XGC1 ion orbit loss model [Seo 2014]
- Projection to ITER from dimensionless empirical scaling shows modest intrinsic toroidal rotation. [Chrystal 2017b]

- The large energy confinement reductions typically seen in conventional scenarios with positive magnetic shear as  $T_e/T_i$  approaches unity was observed to be a significantly smaller effect (confinement not reduced as much) in plasmas with negative magnetic shear. [Yoshida 2017]
- Application of ECH to QH-mode plasmas results in local density flattening as  $T_e/T_i$  increases. Here, trapped electron modes (TEMs) are directly observed as a band of discrete mode numbers, whilst GYRO simulation results simultaneously match flux and density fluctuation spectra, both with and without ECH. The results indicate that density gradient driven TEM turbulence during strong ECH increases particle transport. [Ernst 2016]
- First observation of localized modulation of turbulent density fluctuations by neoclassical tearing modes showed that magnetic islands exhibit reduction in turbulence predicted to lead to faster NTM growth. [Bardóczi 2016]
- An experiment to test the recent Eich model of ELM heat-flux density as a function of pedestal parameters including collisionality, was done as part of a PhD thesis.

### **Energetic Particle Physics**

*A burning DT plasma will produce a population of energetic alpha particles which is, in turn, expected to heat the thermal plasma as the alphas thermalize. Although present-day fusion experiments do not produce these alphas, energetic ions injected by neutral beams are a proxy for studies of the behavior of superthermal ions and the Alfvén eigenmode (AE) instabilities that can cause losses from the plasma. Experiments in DIII-D are validating theories explaining these losses and suggesting techniques for their control.*

- Experiments validated the critical gradient model of fast-ion transport by AE with improved spatial resolution and multiple diagnostics. [Collins 2016]
- The onset threshold of AE) induced fast-ion transport is delayed when reversed-shear AE (RSAE) are suppressed. Suppression was achieved by adjusting the current profile to place  $q_{\min}$  away from the position of maximum fast-ion gradient, validating theoretical predictions. [Kramer 2017]
- RSAE suppression with ECH has been understood to result from a narrowing of the frequency range for RSAE existence due to an increase in  $T_e$  and gradient in  $T_e$ . [Van Zeeland 2016]
- In simulation, for the first time, a first-principles code reproduced experimental AE amplitudes and fast-ion transport. [Todo 2016]

- The effect of ECH on AE stability was explained and a new actuator, variable beam perveance, was developed and tested. [Pace 2017]

### Long pulse steady-state research

*The Advanced Tokamak (AT), combining high fusion performance with steady-state operation, is the embodiment of DIII-D’s mission to establish the scientific basis for the optimization of the tokamak approach to fusion energy production.*

- Fully noninductive, steady-state hybrid plasmas were sustained at ~80% of the ideal stability limit with either on- or off-axis NBI. [Turco 2015, Petty 2016]
- Confinement degradation observed in steady-state high- $\beta_p$  discharges at high  $q_{\min}$  ( $>2$ ) was found to be a consequence of AEs appearing when the fast-ion gradient  $\nabla\beta_{\text{fast}}$  exceeds a critical value. Improved performance was achieved by tuning the discharges to limit  $\nabla\beta_{\text{fast}}$  below that critical value. [Holcomb 2015]
- RMP ELM suppression over a relatively wide  $q_{95}$  range from 6-7.5 was achieved in a  $I_p \approx 1$  MA fully non-inductive hybrid plasma with minimal impact (~5%) on performance [Petty 2017]
- DIII-D/EAST joint experiment developed a fully-noninductive high- $\beta_p$  scenario with  $q_{95} \sim 10$ ,  $q_{\min} \sim 3$  and very high confinement ( $H_{98y2} \geq 1.5$ ) due to a large-radius ITB [Garofalo 2015, Ren 2016].
- The internal transport barrier (ITB) and high confinement in the high  $\beta_p$  scenario are insensitive to plasma rotation, and have been extended to more reactor-relevant lower rotation and  $q_{95}$ , with Shafranov shift stabilization key to maintaining the ITB. [Garofalo 2017]
- An improved confinement regime called the “Super H-mode” was produced and sustained [Solomon 2014] as predicted by the EPED model.
- Lithium injection led to a pedestal bifurcation with enhanced electron pedestal pressures and  $2\times$  larger pedestal widths. [Pace 2015]

### Divertor detachment

*Most of the power flowing out of a tokamak plasma will be brought to the divertor, where unchecked, a large energy flux could be focused on a small region of the plasma-facing components, inevitably resulting in melting or other damage. ITER and subsequent tokamaks are envisioned to employ a partially or fully detached divertor, in which power reaching the divertor region is radiated away before striking the solid surface. DIII-D is working to develop a physics basis for a detached divertor compatible with a high-performance fusion core plasma.*

- Improved divertor temperature measurements from the upgraded divertor Thomson scattering diagnostic indicate a sharp reduction in temperature, to  $<1$  eV, at detachment. [McLean 2015]
- The observed strong toroidal field direction dependence of divertor in-out asymmetries has been qualitatively reproduced by UEDGE with  $E \times B$  Drifts. Changes in asymmetry of the inner vs. outer divertor leg densities and temperatures are consistent with the directions of radial and poloidal  $E \times B$  drifts for normal and reversed  $B_T$ . [Rognlien 2017]
- The UEDGE 2D fluid code predicts a rapid onset of detachment when drifts are included. As upstream density increases,  $E \times B$  drifts drive increasing amounts of ionization source from the outer strike point (low-field side) to the inner strike point (high-field side). [Jaervinen 2016]
- The “radiation shortfall” in predicted radiated power from both the SOLPS and UEDGE fluid codes can be largely accounted for by using measured divertor densities from divertor Thomson scattering and elimination of uncertainties in the atomic/molecular reaction rates by using helium plasmas. [Canik 2017]

### **Divertor geometries**

*The ability to obtain a detached divertor can be very sensitive to the magnetic geometry and the geometry of the wall. Research in DIII-D is working to identify configurations that are particularly amenable to obtaining detachment.*

- Initial experiments with the modified upper divertor featuring a novel “small angle slot” (SAS) geometry have confirmed the trends predicted by the original modeling study using SOLPS [Guo 2017a, Guo 2017b].
- An unexpectedly simple correlation has been discovered in SOLPS code divertor analysis between the electron temperature at the divertor target and the corresponding molecular density, for temperatures less than 10 eV and extending over two orders of magnitude. This may imply that achievement of low target temperature reduces essentially to identifying the divertor baffle geometry which achieves the highest gas density near the target [Stangeby 2017].
- Experiments compared detachment onset in the upper (more closed) and lower (more open) divertors to study the effects of divertor closure. A comparison of three divertor configurations shows that the pedestal density required for divertor detachment decreases with increasing divertor closure, with a 20-30% reduction in pedestal density  $n_{e,ped}$  from the most open geometry to the most closed. This result was consistent with SOLPS simulations [Moser 2016].

- Detachment density was shown to be reduced, compared to a standard divertor configuration, by an X-divertor configuration applied to both high- and low-triangularity plasmas [Covele 2017].

### **Divertor materials**

*Experiments to determine the behavior of metallic first-wall materials benefit from DIII-D's comprehensive diagnostic set and the carbon wall, which allows more direct observation of impurity behavior.*

- ELM-resolved tungsten (W) sputtering measurements using DiMEs have shown that maximum W sputtering is highly dependent on the outer strike-point (OSP) location, as well as time within the ELM cycle. Inter-ELM spatial profiles of the gross W sputtering show a peaking at the OSP, in contrast to the intra-ELM profile, which exhibits sputtering minimized at the OSP and rising monotonically into the common flux region. [Abrams 2016, Abrams 2017]
- Tungsten nanostructures (W-fuzz) prepared in the PISCES-A linear device have been found to survive direct exposure to divertor plasmas in DIII-D using DiMES, with little obvious damage except in the areas where unipolar arcing occurred. Arcing is effective in W-fuzz removal, and it appears that surfaces covered with W-fuzz can be more prone to arcing than smooth W surfaces. [Rudakov 2016]
- The sheath potential and background impurities are found to directly impact high-Z material erosion. The 3D Monte Carlo code ERO predicted that decreasing the sheath potential can suppress net erosion by reducing the sputtering yield due to lower incident energy, which was experimentally confirmed with a biased sample of molybdenum. [Ding 2016]
- Experiments with the tungsten rings and isotopic analysis of collector probes have shown that divertor leakage can be dominated by strike-point location. With the OSP on the inner ring, there is little contribution from the far SOL in high-powered H-mode, even after normalizing for the source rate. [Unterberg 2016]

## **11.4 FACILITY OPERATION AND DEVELOPMENT**

The 2014-2018 five-year plan laid out an ambitious plan for increasing the scientific and operational capabilities of the DIII-D facility. The plan requested funding for 14 weeks of operation each year, with a 12-month shutdown straddling FY15 and FY16 for the installation of a second off-axis neutral beam. The actual funding profile was somewhat different with the approved operational targets for each year of 18, 15, 15, 17, and 17 weeks in the years FY14 – FY18 respectively. DIII-D successfully operated at 104% of the commitment for the period

through FY17, with a total of 67.5 weeks of operation over four years. As of December 2017, six weeks of operation have been obtained with a target of 17 weeks for FY18. The extended shutdown or Long Torus Opening (LTO3) was moved to FY18-19 and 17 and 12 weeks of operation are scheduled for the fiscal years before and after this period. The operations statistics, including device availability for each of the years from FY03 – FY17, is shown in Table 11.2. The availability for the period of FY14 – FY18 averaged 78.5%, which is slightly higher than the average of the last 15 years of 76.5%. It should be noted that the deficit of 1.3 weeks of operation in FY15 below the target of 15 weeks is the first time in over 20 years that DIII-D failed to achieve its operational goal, although the 13.7 weeks of operation represents 91% of the target. The major causes of lost time in FY15 include an underground cable failure in a 4160V main power feed, an arc flash incident on the main Motor Generator 13.8 kV distribution bus, a blockage in the cryogenic system following maintenance on one of the He compressors, and three days of power shutdowns due to hot weather and loads on the regional utility grid. The underground cabling failure and 13.8 kV bus failure highlighted that the end-of-life considerations for basic infrastructure needed to be addressed more systematically and proactively. This was addressed in the response to these specific events and a more comprehensive evaluation and plan for addressing these issues has been undertaken and is part of this proposal (Section 5.2).

**Table 11-2.**  
**Operations Statistics by Fiscal Year**

<b>Fiscal Year</b>	<b>DOE Target (weeks)</b>	<b>Achieved (weeks)</b>	<b>Availability</b>	<b>Shots Achieved</b>
<b>FY03</b>	14	14.5	72%	2156
<b>FY04</b>	18	18.2	78%	2663
<b>FY05</b>	14	15.6	68%	2196
<b>FY06</b>	12	12.7	74%	1794
<b>FY07</b>	12	12.8	80%	1812
<b>FY08</b>	18	19.0	76%	2674
<b>FY09</b>	13	16.0	77%	2284
<b>FY10</b>	14	18.2	81%	3162
<b>FY11</b>	14	14.5	71%	2191
<b>FY12</b>	13	15.2	72%	2828
<b>FY13</b>	12	13.2	85%	1979
<b>FY14</b>	18	18.9	83%	3153
<b>FY15</b>	15	13.7	76%	2388
<b>FY16</b>	15	17.3	82%	2772
<b>FY17</b>	17	17.6	73%	2919
<b>FY18</b>	17	7.1 (as of 12/31/17)		972 (as of 12/31/17)

Throughout the contract period, the DIII-D facility has continued to evolve through a combination of major upgrades, repairs, refurbishments, and modernizations. These areas are described below.

**Major upgrades** - completed or scheduled for completion within the period of performance of the 2013-2018 five-year plan include:

- ASIPP Power Supply – Installed new power supply and all associated systems (six power supply modules (450 V, 2.6 kA each), transformer, patch panel, switchgear, control system interface, and data acquisition). Successfully commissioned new supply and the supply is in routine operation (FY15 – FY17)
- Helicon Wave System – Designed, fabricated, and installed a low-power Helicon wave system (antenna, protective tiles, and diagnostics) in DIII-D. Performed lower power experiments and confirmed good coupling into target plasma and compatibility with DIII-D plasma conditions (completed FY16-Q1). Design of a high-power 1-MW system began in FY16-Q1 but was put on hold in FY16-Q3 to shift priorities to other areas. The design was restarted in FY17-Q3 and the full system (antenna, tiles, coax, klystron, HV supply, and diagnostics) is planned to be installed by the end of the long torus opening LTO3 (FY19-Q3).
- High-Z tiles – Performed research on tungsten coating on graphite and molybdenum. Designed, fabricated, and installed two rows of tiles with tungsten-coated inserts in graphite tiles in the lower divertor region. These were installed in a short vent in May 2016 and successfully used in dedicated experiments in June/July 2016.
- Small Angle Slot Upper Divertor (SAS-1U) – Designed, fabricated, and installed two rows of tiles (38 tile designs) into the Upper Divertor region of DIII-D, including 120 tiles, Langmuir probes and thermocouple array, magnetic probes, and gas-puff valves (FY16 – FY17). Installed additional diagnostics (Langmuir probe, ASDEX pressure gauges, surface eroding thermocouples) in slot region in a two-week vent in September 2017.
- Variable Beam Voltage – A new capability for real-time modulation of the NB energy by +/- 10 kV was developed and is in routine use. This has many novel and exciting applications in the research program, such as avoiding fast-ion driven Alfvén instabilities.
- Electron Cyclotron System Expansion (Final buildout is planned at 10 gyrotrons) –
  - 7<sup>th</sup> Gyrotron System (Depressed Collector Gyrotron *aka* NASA gyrotron) – A full gyrotron system (gyrotron, launcher, waveguides, socket, and controls) was fully commissioned (FY14-Q4) and is in routine operation in the DIII-D system.

- 1.5 MW Depressed Collector Gyrotron – A 1.5 MW depressed collector was developed with gyrotron vendor CPI during 2012-2014. The tube delivered 1.8 MW short pulse (2 msec) but failed to produce longer pulses. An R&D effort was coordinated with CPI to investigate and correct the cause of the failure. A series of seven tests were performed at CPI resulting in a modified gyrotron that successfully holds off the required voltages for long pulses, and produced greater than 1.5 MW short pulse and over 700 kW for five second pulses at CPI (this is the limit of their testing capability). The rebuilt gyrotron is now installed at DIII-D and is undergoing higher-power, long-pulse commissioning with a schedule for use in DIII-D in spring of 2018. If successful, this gyrotron will be the basis for future expansion of the system from 8 to 10 gyrotrons for a final injected power of 8-9 MW.
- Co-Counter Off-Axis Beam (210 CCOANB) – The design of a toroidally rotatable co-counter neutral beam that is injected at a fixed off-axis (poloidally) position has been performed and is over 95% complete. Fabrication is in progress and installation is scheduled for the long torus opening LTO3 from May 2018 – April 2019. The full system should be operable for experiments in the FY19 campaign.
- Increased NB pulse length – To increase the power and pulse length of the NB sources a number of improvements are needed both on the HV power supplies and the beamline component heat-handling capability. Three steps have been completed on this project:
  - Bending magnet pole shield (PPPL/GA) – this is the weakest component thermally and was redesigned with removable TZM Moly inserts that are capable of handling the full power and pulse length required (3.2 MW, 6 second). The first set of these new shields was installed in the 330L and 330R beamlines and have performed well for two years. Installation in the 150 beamline and 210 CCOANB is scheduled for LTO3. Replacement in 30 NB is proposed in 2023.
  - As part of 210 CCOANB project, the internal collimators of the beamline are being upgraded to handle higher power and longer pulse operation during LTO3. The 150 NB was previously upgraded.
  - TZM moly shields for protection against reionization were installed in the drift ducts between the beamline and the vessel in all four beamlines (FY 15 – FY 17).
- Lithium Granular Injector (PPPL) – A dedicated injector capable for lithium granules was installed and in use on DIII-D (FY 14-FY 15). The system has been upgraded for operation with boron and carbon granules (FY 16).
- New/upgraded diagnostics

- Design, fabrication, and installation of new divertor Thomson scattering (FY 15/16)
- Multichord divertor Thomson scattering (FY17)
- Cross-polarization scattering (UCLA) (FY16)
- Gamma ray imager (spectroscopy) (FY15/16)
- Polarimeter (UCLA) (FY15/16)
- Main Ion CER upgrade (PPPL/GA) (FY15)
- ECE radiometer upgrade (UT) (FY16)
- Impurity spectrometer, camera, and collector probes for the high-Z tile experiments (with GA, LLNL, ORNL) (FY16)
- Diagnostics for new SAS divertor (Langmuir probes, Thomson scattering, spectroscopic views, ASDEX neutral gauge, thermocouples) (with GA, ORNL, UTK, and SNL) (FY17)
- 2<sup>nd</sup> X-point SXR camera at different toroidal location (ORNL/NIFS) (FY16/17)
- 2<sup>nd</sup> Shattered cryogenic pellet injector at different location (ORNL) (FY16/17)
- New Imaging Neutral Particle Analyzer (FY16/17)
- New Divertor SPRED for impurity monitoring (LLNL/GA) (FY17/18)
- Laser blow-off (MIT/GA – FY17/18)
- High-resolution upper divertor bolometer array (FY18)
- New/upgraded computer/data systems
  - PCS hardware upgrade to 64-bit and Myrinet retirement (FY17)
  - New ZFS-based user file storage along with new file structure (FY15/16)
  - New DIII-D computational cluster (Iris) (FY15/16)
  - New Object Storage system for DIII-D’s raw camera diagnostic data (FY16)
  - Upgraded storage of DIII-D’s raw and analyzed data (FY15/16)
  - New fusion network core and edge switch hardware (FY16/17)
  - Implementation of Fusion Wireless Network with NAC (FY17)
  - Complete retirement of CAMAC (FY18)

### **Refurbishments/Modernizations**

- NB System: Strong progress on NB grid replacement
- Instrumentation and Control: NB Local Control Stations (LCS) - LCS #8 modernized (FY16), LCS #5 and #6 – scheduled for FY18 installation; CAMAC replacement (continuous, > 95% complete)

- Air/Water System: MG water cooling refurbishment Phase 1 (FY15); MG water cooling Phase 2 (scheduled for FY18); replace AWCS in-line electric heater; replace AWCS compressors (scheduled for FY18)
- EC Systems: Refurbishment/redesign of failed Han/Lion gyrotrons into a hybrid gyrotron with improved collector design (in progress); refurbishment of all ECH launchers; refurbish EC collector thermal mapping system
- HV/Power Systems: Refurbish aging switchgear for PF supplies HV1, D1, T1, T2; Rebuilt HV step-up transformer; replaced four HV tetrodes in NB and EC HV supplies
- Diagnostic Refurbishments CER/FIDA cameras (GA/PPPL), Thomson fibers/lenses, neutrons electronics, BES fibers/lens (UW/PPPL), neutron diagnostic electronics, CO2 interferometer laser and alignment system, BES, FILD1

### **Operation System Productivity/Reliability Enhancements**

- ECH compressor water chiller for EC compressors to extend compressor life
- ‘Hot spares’ - ECH high-pressure pump, clean dry air compressor
- Achieved higher speed motion for EC mirrors (GA/PPPL)
- ECH gyrotron “restart after fault” capability for higher reliability
- Dedicated diagnostic air-cooling system
- 2<sup>nd</sup> external absorber for cryogenic He system
- Artificial Intelligence system developed for verifying proper placement of patch panel pins

## **11.5 HISTORY OF THE DIII-D PROGRAM**

The GA Tokamak Program has a history of creative concept development. The program began in 1968 with the Doublet I device, the first tokamak with a highly noncircular cross section, using solid copper walls to shape the plasma. Experiments on this device showed the doublet configuration to be magnetically and dynamically stable. These successes led in 1971 to the larger Doublet II device, also with solid copper walls. Doublet II was reconfigured in 1974 to use external coils to replace the copper walls. The new device was named Doublet IIA, and it pioneered the use of external coils to shape a wide range of highly noncircular plasmas and maintain them in nondecaying magnetic configurations.

The success of these experiments led to construction of the Doublet III device, completed in 1978. In the first years of operation, it was the largest operating tokamak in the world and attained the highest plasma current levels recorded at that time (2.2 MA). Experiments with a broad range of plasma configurations demonstrated the importance of elongation and shape

control. Dee-shaped plasmas proved easiest to form and maintain and were predicted to be stable at high  $\beta$  values adequate for viable power plants. Diverted dee-shaped plasmas were also effective in achieving reduced impurity levels and enhanced confinement.

These successes led to the reconstruction of the Doublet III tokamak into a large dee-shaped cross section capable of a wide range of plasma shapes and divertor configurations. The upgraded device was renamed DIII-D in 1986. DIII-D rapidly reached currents of over 3 MA and achieved superior levels of confinement and  $\beta$ . DIII-D set and still holds the record of 13% beta for a conventional aspect ratio tokamak. Another significant numerical achievement was reaching a value of the fusion triple product  $nT\tau$  of  $7 \times 10^{20}$  keV-s/m<sup>3</sup> corresponding to an equivalent fusion gain of 0.3.

In the late 1980s and early 1990s, DIII-D contributed, with other world tokamaks, to developing an empirical understanding of routine tokamak performance that projected to a successful burning plasma experiment. The main parametric dependences of plasma confinement were found to be common among the various tokamaks, allowing the development of confinement scaling laws which implied a common underlying physics for the results and which allowed empirical extrapolation to burning plasma experiments. The limits to the stable operating space were identified and the empirical beta limit was in accord with Troyon scaling and also in agreement with theory. These developments allowed the definition of the standard tokamak operating space as given by an H factor of 2 (confinement time twice as good as the L-mode, for which the first empirical scaling relations were determined) for conventional ELMing H-mode operation and a normalized beta of 2 for the beta limit.

However, the DIII-D team realized that the tokamak as a magnetic confinement configuration had potentially much more to offer than this nominal performance. In the early 1990s, modes of enhanced confinement considerably above the nominal H=2 scaling were being achieved. Theory calculations implied that normalized beta values up to perhaps 6 might be possible with wall stabilization, strong shaping, and broad pressure profiles. The DIII-D team coined the term “Advanced Tokamak” to capture that package of scenario characteristics aimed at finding out just what the limits of the tokamak configuration could be as a magnetic confinement device. Since that time a major emphasis of the DIII-D program has been Advanced Tokamak physics. With the stabilization of the resistive wall mode, operation above the free boundary limit has been realized. Advanced Tokamak research is also closely aligned with the requirements for steady state, since a high bootstrap current fraction requires a high normalized beta and enhanced confinement at lower plasma current than is given by H=2. Discharges with 100% non-inductive current have been obtained that project to the long-pulse Q=5 goal in ITER, and 90% noninductive discharges have been obtained for approximately a current redistribution

time of 2 s. It is expected that sustaining these “steady-state” discharge conditions at 100% non-inductive plasma current for several current redistribution times can be accomplished with additional co-injected neutral beam injection (NBI), off-axis neutral beam injection (OANBI) current drive, and ECCD. Advanced Tokamak research is now a major effort in many of the world’s tokamaks, and is the basis for several collaborations combining DIII-D’s flexibility and the long-pulse capabilities of super-conducting tokamaks, including EAST (China, first plasma 2006), KSTAR (Korea, first plasma 2008), and JT60-SA (Japan) with first plasma expected around 2020).

Ensuring the successful construction and operation of ITER continues to be a high priority within the DIII-D program. Over the years, the emphasis has evolved from design issues (although a few remain and continue to be addressed on DIII-D) to operational issues. DIII-D provided the basis for ITER's capabilities to manage transients, in particular the ELM coils and the Disruption Mitigation System (DMS). DIII-D has qualified ITER's capability to control ELMs with less than its full set of internal coils and provided data on the need to rotate the RMP perturbation to spread out asymmetries in the divertor heat load. Also, DIII-D remains the only device to have tested Shattered Pellet Injection as a disruption mitigator, and is currently performing research (soon in collaboration with JET) to answer the last few questions for a final design review of ITER's DMS. DIII-D has also been highly responsive to requests from ITER for research on a host of issues including error field compensation, hydrogen and helium operation, and demonstration of both baseline and more advanced operating scenarios for ITER.

## **11.6 THE US FUSION PROGRAM COMMITS TO BURNING PLASMAS**

The US magnetic fusion program is moving into a new era of burning plasmas. This commitment and vision have given an even greater focus to DIII-D research and technological developments in support of this new paradigm. In this and following sections we describe how the DIII-D program has adapted accordingly, recent results in support of ITER, and how work in the present cooperative agreement (2014-2018) is the basis for the forward-looking Five-Year Plan presented in the earlier sections of this document.

ITER is a US Presidential Initiative. ITER is the most important element of the US fusion effort, and the success of ITER is a high priority of the DIII-D Program. The US and six other international parties have agreed to build ITER, an international Tokamak “to demonstrate the scientific and technological feasibility of fusion energy.” The intent for the US to move forward with ITER came in 2003, and the ITER Organization became a legal entity in November 2007. ITER construction is now a reality, and this is the most significant change in the US Fusion Program over the last decade. The US ITER Project Office was formed at Oak Ridge National Laboratory (ORNL) to be responsible for US contributions to ITER construction. The USBPO

was formed to advance burning plasma science and provide the coordination of the US scientific efforts for ITER and burning plasmas. The DIII-D Program maintains close ties with these US organizations.

Relatively soon after the ITER Agreement, a Fusion Energy Science Advisory Committee (FESAC) report identified significant gaps beyond ITER in being able to harness fusion power. At this time, GA was actively involved in developing a strategy for a Fusion Development Facility (FDF) that specifically addressed many of the gaps identified. It was recognized that the physics basis needed for FDF included development of the basis for steady-state AT scenarios. Thus, the 2009–2013 DIII-D program maintained a vigorous effort in AT physics supporting the Fusion Development Facility/Fusion Nuclear Science Facility Advanced Tokamak (FDF/FNSF-AT) concept.

Again, in short order (2009), the DIII-D program was honed as a result of the US program’s Research Needs Workshop (ReNeW), held to survey the issues identified in previous studies and begin to identify research thrusts to make fusion a practical energy source. The resulting ReNeW report divided the program into 4 themes and 18 thrusts, the themes being: (1) Burning Plasmas in ITER, (2) Creating Predictable, High-Performance Steady-State Plasmas, (3) Taming the Plasma-Material Interface, and (4) Harnessing Fusion Power. It was realized that the DIII-D program could address the first three themes, while an FDF is required for the fourth. DIII-D program plans began to conform accordingly. The step to FDF-AT also became a US priority. In 2010, FES (E. Synakowski) presented an “Emergent FES Vision,” in which he described the future program referring specifically to these four themes and articulating an urgent need for a Fusion Nuclear Science Facility Advanced Tokamak.

Additionally, plasma operation is well underway in two superconducting tokamaks in ITER-partner countries, EAST (China), 2006, and KSTAR (South Korea), 2008. The capabilities of these devices are rapidly advancing. DIII-D has had a long and productive cooperative scientific program with both facilities. There is an opportunity in the near future for making rapid progress in demonstrating burning plasma relevant very long-pulse high-performance discharges. Together with China’s Academy of Sciences Institute of Plasma Physics (ASIPP), DIII-D has begun a *long-pulse initiative* where joint teams focus on accessing and developing an understanding of high-performance discharges on DIII-D and then extending them to 100s of seconds on EAST. This provides an opportunity to accelerate progress on steady-state discharges and provides a firm basis for continued partnership between DIII-D and EAST/ASIPP.

More recently, DOE-FES restated its main priorities as Burning Plasma Science: Foundations, Burning Plasma Science: Long Pulse, Burning Plasma Science: High Power and Discovery Plasma Science. These priorities very explicitly demonstrate a strong US commitment

to achieving burning plasmas. In the same time frame, DOE-FES charged FESAC to develop a 10-year strategic plan and FESAC responded with a set of recommendations delivered in a report in late 2014. Based partly on this report, DOE-FES identified four high-level strategic initiatives to be a significant focus of its program. These initiatives were: Integrated Simulations, Plasma-Materials Interactions, Transients, and Plasma Science Frontiers. The first three of these foci impact directly on burning plasma issues. A series of workshops was commissioned in 2015 with considerable community engagement, resulting in the identification of research opportunities described in reports to DOE-FES. The DIII-D program has had, and will continue to have, strong programs in transients and plasma-materials interactions. Integrated simulation goals are supported through detailed model validation efforts on DIII-D, leveraging DIII-D's comprehensive diagnostic set and working together with the theory and modeling community. In particular, a recently initiated “predict-first initiative” is helping to bring about a culture of addressing model validation across the DIII-D research program.

## 11.7 CONTINUITY OF THE DIII-D MISSION

The DIII-D program mission adopted in this new five-year plan is

*To establish the scientific basis for the optimization of the tokamak approach to fusion energy production.*

This is the same mission statement as in the current 2014–2018 program plan. This statement captures the essence of the DIII-D program intent, maintaining a strong focus on excellent science, focusing on innovation and optimization—all brought to bear on the goal of an attractive fusion power plant. Our primary goal is to maintain a strong effort in ensuring progress and success in the pursuit of fusion energy: this often translates into pursuing research to answer a specific research and development (R&D) question needed for ITER. Our focus on science is two-fold. First, addressing a research objective based on solid scientific principles and background is the most effective process to resolve the R&D issues and make progress toward fusion energy. Second, the most effective way (often the only way) to translate the knowledge gained on DIII-D to future devices is through scientific understanding and validated models. In this quest for fusion power, our aim is to do excellent science. The focus upon an energy goal determines the proper high-impact science to pursue.

While focusing on achieving energy production, at the same time the program continues to seek opportunities to improve the tokamak concept. DIII-D's past contributions in increased beta and performance with plasma shape, stable sustained operation above the free-boundary kink limit, development of advanced performance scenarios with profile and shape, understanding of improved transport and stability with plasma rotation, and suppression of ELMs with resonant

magnetic perturbations are excellent examples of transformational research that has improved the tokamak concept as a fusion energy device.

For the 2019-2024 Five-Year plan, two major overarching objectives will be pursued:

- Ensure success of ITER and,
- Identify a credible path to a fusion power plant.

These objectives are buttressed by two cross-cutting sub-themes:

- Develop the scientific basis for fusion energy through experimental validations of theoretical models and,
- Performing research to simultaneously integrate core, edge, and wall solutions.

The DIII-D program focus will continue to be heavily influenced by the research needs of ITER. The first of these goals recognizes the importance of the success of ITER in the US and international program, and also recognizes that the time for impact on ITER design choices is drawing to a close and that preparing for research operation of ITER will become increasingly important. Thus, the near-term DIII-D program will continue to focus on finding and optimizing solutions for disruptions on ITER and ELM control. For example, DIII-D remains the only device to have tested Shattered Pellet Injection as a disruption mitigator and is currently performing research (soon in collaboration with JET) to answer the last few questions for a final design review of ITER's DMS. However, developing and understanding operational scenarios under ITER-like conditions will become increasingly important in the DIII-D research efforts. ITER-like conditions will include, ITER shape,  $q_{95} \sim 3$ ,  $T_e/T_i \sim 1$ ,  $n_e^* \sim 0.02$ ,  $\beta_N \sim 2$ , low neutral beam (NB) input torque, ELM control, and a radiative divertor.

The second DIII-D theme is aimed at developing the physics basis for advanced tokamak scenarios suitable for steady-state fusion reactors. This includes a strong research program to develop scenarios with full non-inductive current drive, high beta, and good confinement. In addition, this will include addressing other high priority issues, such as developing solutions compatible with high heat flux. Implementing advanced divertor geometries and developing a radiative boundary are elements of this research plan. This second goal also includes developing the physics basis for AT operation in DEMO.

Building on a sound and tested scientific foundation is the most reliable and effective way to advance fusion energy. This embodies doing “science with a purpose.” Continuing to advance fundamental understanding and predictive capability of fusion science is the foundation for making progress toward fusion energy and succeeding in our two major objectives. The DIII-D program also recognizes the need in reactors for high-performance core solutions to be

compatible with high-performance dissipative divertors. To address this need, the program will have a significant focus on issues of “core-edge integration.”

## References

- [Abrams 2016] T. Abrams et al., "Impact of ELMs on the tungsten source distribution near the DIII-D outer strike point," PSI-22 O29 (2016)
- [Abrams 2017] T. Abrams et al., Nucl. Fusion 57, 056034 (2017)
- [Bardóczi 2016] PRL 116, 215001 (2016) "Modulation of core turbulent density fluctuations by large-scale neoclassical tearing mode islands in the DIII-D tokamak", L Bardóczi, TL Rhodes, TA Carter, A Banon Navarro, WA Peebles, F Jenko, G McKee  
[<https://journals.aps.org/prl/abstract/10.1103/PhysRevLett.116.215001>]
- [Baylor 2013] L.R. Baylor et al, Lett., 110, 245001 (2013)
- [Bortolon 2016] A. Bortolon et al, Fusion 56, 056008 (2016)
- [Burrell 2016] K.H. Burrell et al, of Plasmas 23, 056103 (2016)
- [Canik 2017] Canik J.M. et al 2017 Phys. Plasmas 24 056116
- [Chen 2016] X. Chen et al, Fusion 56, 076011 (2016)
- [Choi 2017] W. Choi, et al., “Feedforward and feedback control of locked mode phase and rotation in DIII D with application to modulated ECCD experiments,” submitted to Nuclear Fusion (2017)
- [Chrystal 2017a] C. Chrystal, et al., Phys. Plasmas 24, 042501 (2017)
- [Chrystal 2017b] C. Chrystal et al, Phys. Plasmas 24, 056113 (2017)
- [Clement 2017] M. Clement, et al., Control Engineering Practice 68, 15 (2017)
- [Collins 2016] C.S. Collins, et.al., Phys. Rev. Lett. 116, 095001 (2016)
- [Commaux 2014] N. Commaux et al., Phys. Plasmas 21 (2014) 102510
- [Commaux 2016] N. Commaux et al., Nucl. Fusion 56 (2016) 046007
- [Cooper 2016] C.M. Cooper et al., Rev. Sci. Instrum. 87 (2016) 11E602
- [Covele 2017] B. Covele et al 2017 Nucl. Fusion 57 086017
- [Ding 2016] R. Ding et al., Nucl. Fusion 56, 016021 (2016)
- [Eidietis 2014] N.W. Eidietis et al., 25th IAEA Fusion Energy Conference (St. Petersburg, Russia) post-deadline selection (2016)
- [Eidietis 2017] N. Eidietis et al., Phys. Plasmas 24 (2017) 102504
- [Ernst 2016] D. R. Ernst, K. H. Burrell, W. Guttenfelder, T. L. Rhodes, A. M. Dimits, R. Bravenec, B. A. Grierson, C. Holland, J. Lohr, A. Marinoni, G. R. McKee, C. C. Petty, J. C. Rost, L. Schmitz, G. Wang, S. Zemedkun, L. Zeng, and the DIII-D Team,

- "Role of density gradient driven trapped electron mode turbulence in the H-mode inner core with electron heating" PHYSICS OF PLASMAS 23, 056112 (2016)
- [Evans 2017] T.E. Evans et al, Fusion 57, 086016 (2017)
- [Garofalo 2015] A.M. Garofalo et al., Nucl. Fusion **55** (2015) 123025
- [Garofalo 2017] Garofalo A.M. et al., "Joint DIII-D/EAST research on the development of a high poloidal beta scenario for the steady-state missions of ITER and CFETR", accepted for publication in Plasma Physics Controlled Fusion, 2017
- [Guo 2017a] H.Y. Guo et al 2017 Nucl. Fusion 57 044001
- [Guo 2017b] Guo. H.Y. et al., "First Results from Small Angle Slot Divertor in DIII-D", Paper YI2 6, Bull. Am. Phys. 2017 (<http://meetings.aps.org/Meeting/DPP17/Session/YI2.6>)
- [Hanson 2017] J.M. Hanson, et al., Nucl. Fusion 57, 056009 (2017)
- [Holcomb 2015] Holcomb, C.T. *et al.* 2015 Physics of Plasmas **22**, 055904
- [Hollmann 2015a] E.M. Hollmann et al., Phys. Plasmas 22 (2015) 102506
- [Hollmann 2015b] E.M. Hollmann et al., Phys. Plasmas 22 (2015) 056108
- [Hollmann 2017] E.M. Hollmann et al., Nucl. Fusion 57 (2017) 016008
- [Izzo 2015] V.A. Izzo et al., Nucl. Fusion 55 (2015) 073032
- [Jaervinen 2016] Jaervinen A.E. et al 2016 "Investigations of the impact of cross-field drifts on divertor detachment in DIII-D with UEDGE" Proc. of the 36 EPS conf. on fusion energy
- [King 2015] J.D. King, et al., Phys. Plasmas 22, 072501 (2015)
- [Kleijwegt 2017] K. Kleijwegt, et al., "Disruption prediction using machine learning algorithms for DIII D," to be submitted to Nuclear Fusion (2017).
- [Kramer 2017] G.J. Kramer et al 2017 Nucl. Fusion 57 056024
- [LaHaye 2016] R.J. La Haye, et al, Proc. 43rd EPS Conf. on Plasma Physics, (Leuven, Belgium, July 4-8, 2016), Europhysics Conference Abstracts 40A, P5.026 (2016).
- [LaHaye 2017] R.J. La Haye, "Forecasting electron cyclotron current drive stabilization of neoclassical tearing modes in ITER," Proceedings of the 22nd Topical Conference on RF Power in Plasmas (Aix en Provence, France, May 30-June 2, 2017).
- [Lanctot 2016] M.J. Lanctot, et al., Nucl. Fusion 56, 076003 (2016).
- [Lanctot 2017] M.J. Lanctot, et al., Nucl. Fusion 57, 036004 (2017). [McLean 2015] McLean A.G. et al 2015 Jour. Nucl. Mater. 463 533
- [Logan 2016] N.C. Logan, et al., Phys. Plasmas 23, 056110 (2016).
- [Moser 2016] A. M. Moser et al. "Effect of divertor closure on pedestal fueling and divertor detachment onset in DIII-D", presented at the 22nd International Conference on

- Plasma Surface Interactions in Controlled Fusion Devices, Rome, Italy, May 30-June 3, 2016
- [Munaretto 2017] S. Munaretto, et al., “Modal analysis of the full poloidal structure of the plasma response to n=2 magnetic perturbations,” to be submitted to *Phys. Plasmas* (2017).
- [Nazikian 2015] R. Nazikian et al, 114 105002 (2015)
- [Nazikian 2016] R. Nazikian et al, Proceedings 2016 IAEA-FEC conference, Kyoto
- [Okabayashi 2017] M. Okabayashi, et al., *Nucl. Fusion* 57, 016035 (2017).
- [Pace 2015] Osborne, T. *et al.* *Nucl. Fusion* 55 (2015) 063018
- [Pace 2017] D.C. Pace, et al, 2017 *Nucl. Fusion* 57 014001
- [Parsons 2016] M. Parsons, et al., “Application of the Disruption Predictor Feature Developer to developing a machine-portable disruption predictor,” *Bull. Am. Phys. Soc.*
- [Paz-Soldan 2014] C. Paz-Soldan, et al., *Phys. Plasmas* 21, 072503 (2014).
- [Paz-Soldan 2015] C. Paz-Soldan, et al., *Phys. Rev. Lett.* 114, 105001 (2015).
- [Paz-Soldan 2016] C. Paz-Soldan et al, *Fusion* 56 056001 (2016)
- [Paz-Soldan 2017] C. Paz-Soldan et al., *Phys. Rev. Lett.* 118 (2017) 255002
- [Petty 2016] C.C. Petty et al., *Nucl. Fusion* 56, 016016 (2016)
- [Petty 2017] C.C. Petty et al., *Nucl. Fusion* 57, 116057 (2017)
- [Rea 2017] C. Rea and R. Granetz, “Exploratory Machine Learning studies for disruption prediction using large databases on DIII-D,” submitted to *Fus. Sci. Technology* (2017).
- [Ren 2016] Q. Ren, et al., *Phys. Plasmas* 23, 062511 (2016)
- [Rognlien 2017] Rognlien T.D. et al 2017 *Nucl. Mater. Energy* 12 44
- [Rudakov 2016] D.L. Rudakov *Scr. T167*, 014055 (2016)
- [Seo 2014] J. Seo et al, *Phys. Plasmas* 21, 092501 (2014)
- [Shiraki 2015] D. Shiraki et al., *Nucl. Fusion* 55 (2015) 073029
- [Shiraki 2016a] D. Shiraki et al., *Phys. Plasmas* 23 (2016) 062516
- [Shiraki 2016b] D. Shiraki et al., 26th IAEA Fusion Energy Conference (Kyoto, Japan) EX/P3-20 (2016)
- [Solomon 2014] Solomon W.M. *et al.* 2014 *Phys. Rev. Lett.* **113** 135001
- [Stangeby 2017] Stangeby P.C. and Sang CF 2017 *Nucl. Fusion* 57 056007
- [Todo 2016] Y. Todo et al 2016 *Nucl. Fusion* 56 112008
- [Turco 2015] F. Turco et al., *Phys. Plasmas* 22, 056113 (2015)

- [Turco 2016] F. Turco, et al., 2016 IAEA Fusion Energy Conf. (Kyoto, Japan, 17–22 October 2016), paper EX/P3-14.
- [Turco2017] F. Turco, “Understanding the stability of the low torque ITER Baseline Scenario in DIII-D,” abstract of invited talk at the 59th Annual Meeting of the APS Division of Plasma Physics (Milwaukee, Oct. 23-27, 2017).
- [Unterberg 2016] E.A. Unterberg et al., “Characterization of Different Divertor Tungsten Sources, Migration and Impact on the Core in DIII-D ELM-y H-mode Conditions”, IAEA-FEC 2016 PDP-6 (2016)
- [Van Zeeland 2016] M.A. Van Zeeland et al 2016 Nucl. Fusion 56 112007
- [Yoshida 2017] M. Yoshida et al., Nucl. Fusion **57** 056027 (2017).



## 12. BIBLIOGRAPHY

### (FY13 THROUGH FY17)

#### 12.1 PUBLICATIONS FOR FY13

- Austin, M., Bass, E., Budny, R., Heidbrink, W., Hillesheim, J., & Holcomb, C. et al. (2013). Energetic ion transport by microturbulence is insignificant in tokamaks. *Physics Of Plasmas*, **20**(5), 056108. <http://dx.doi.org/10.1063/1.4803930>
- Bae, C., Stacey, W., & Solomon, W. (2013). Extension of neoclassical rotation theory for tokamaks to realistically account for the geometry of magnetic flux surfaces. *Nuclear Fusion*, **53**(4), 043011. <http://dx.doi.org/10.1088/0029-5515/53/4/043011>
- Baylor, L., Commaux, N., Jernigan, T., Brooks, N., Combs, S., & Evans, T. et al. (2013). Reduction of Edge-Localized Mode Intensity Using High-Repetition-Rate Pellet Injection in TokamakH-Mode Plasmas. *Physical Review Letters*, **110**(24). <http://dx.doi.org/10.1103/physrevlett.110.245001>
- Boyer, M., Barton, J., Schuster, E., Luce, T., Ferron, J., & Walker, M. et al. (2013). First-principles-driven model-based current profile control for the DIII-D tokamak via LQI optimal control. *Plasma Physics And Controlled Fusion*, **55**(10), 105007. <http://dx.doi.org/10.1088/0741-3335/55/10/105007>
- Boyer, M., Barton, J., Schuster, E., Walker, M., Luce, T., & Ferron, J. et al. (2014). Backstepping Control of the Toroidal Plasma Current Profile in the DIII-D Tokamak. *IEEE Transactions On Control Systems Technology*, **22**(5), 1725-1739. <http://dx.doi.org/10.1109/tcst.2013.2296493>
- Burrell, K., Garofalo, A., Solomon, W., Fenstermacher, M., Orlov, D., & Osborne, T. et al. (2013). Quiescent H-mode operation using torque from non-axisymmetric, non-resonant magnetic fields. *Nuclear Fusion*, **53**(7), 073038. <http://dx.doi.org/10.1088/0029-5515/53/7/073038>
- Buttery, R. J., Eidietis, N., Holcomb, C., Haye, R. J. L., Leonard, A., Nazikian, R., ... Jackson, G. (2013). DIII-D accomplishments and plans in support of fusion next steps. In 2013 IEEE 25th Symposium on Fusion Engineering (SOFE). IEEE. <https://doi.org/10.1109/sofe.2013.6635483>
- Candy, J. (2013). Turbulent energy exchange: Calculation and relevance for profile prediction. *Physics Of Plasmas*, **20**(8), 082503. <http://dx.doi.org/10.1063/1.4817820>
- Chapman, I., Graves, J., Sauter, O., Zucca, C., Asunta, O., & Buttery, R. et al. (2013). Power requirements for electron cyclotron current drive and ion cyclotron resonance heating for sawtooth control in ITER. *Nuclear Fusion*, **53**(6), 066001. <http://dx.doi.org/10.1088/0029-5515/53/6/066001>
- Chen, X., Austin, M., Fisher, R., Heidbrink, W., Kramer, G., & Nazikian, R. et al. (2013). Enhanced Localized Energetic-Ion Losses Resulting from Single-Pass Interactions with Alfvén Eigenmodes. *Physical Review Letters*, **110**(6). <http://dx.doi.org/10.1103/physrevlett.110.065004>
- Cooper, W., Chapman, I., Schmitz, O., Turnbull, A., Tobias, B., & Lazarus, E. et al. (2013). Bifurcated helical core equilibrium states in tokamaks. *Nuclear Fusion*, **53**(7), 073021. <http://dx.doi.org/10.1088/0029-5515/53/7/073021>
- Diem, S., Fehling, D., Hillis, D., Horton, A., Nagy, A., Pinsker, R., & Unterberg, E. (2013). Initial Testing of Optical Arc Detector inside 285/300 Fast Wave Antenna Box on DIII-D. *Fusion Science And Technology*, **64**(3), 530-532. <http://dx.doi.org/10.13182/fst13-a19147>

- Evans, T., Orlov, D., Wingen, A., Wu, W., Loarte, A., & Casper, T. et al. (2013). 3D vacuum magnetic field modelling of the ITER ELM control coil during standard operating scenarios. *Nuclear Fusion*, **53**(9), 093029. <http://dx.doi.org/10.1088/0029-5515/53/9/093029>
- Ferraro, N., Evans, T., Lao, L., Moyer, R., Nazikian, R., & Orlov, D. et al. (2013). Role of plasma response in displacements of the tokamak edge due to applied non-axisymmetric fields. *Nuclear Fusion*, **53**(7), 073042. <http://dx.doi.org/10.1088/0029-5515/53/7/073042>
- Ferron, J., Holcomb, C., Luce, T., Park, J., Politzer, P., & Turco, F. et al. (2013). Progress toward fully noninductive discharge operation in DIII-D using off-axis neutral beam injection. *Physics Of Plasmas*, **20**(9), 092504. <http://dx.doi.org/10.1063/1.4821072>
- Garcia-Munoz, M., Äkäslompolo, S., Asunta, O., Boom, J., Chen, X., & Classen, I. et al. (2013). Fast-ion redistribution and loss due to edge perturbations in the ASDEX Upgrade, DIII-D and KSTAR tokamaks. *Nuclear Fusion*, **53**(12), 123008. <http://dx.doi.org/10.1088/0029-5515/53/12/123008>
- Grierson, B., Burrell, K., Solomon, W., Budny, R., & Candy, J. (2013). Collisionality scaling of main-ion toroidal and poloidal rotation in low torque DIII-D plasmas. *Nuclear Fusion*, **53**(6), 063010. <http://dx.doi.org/10.1088/0029-5515/53/6/063010>
- Groebner, R., Chang, C., Hughes, J., Maingi, R., Snyder, P., & Xu, X. et al. (2013). Improved understanding of physics processes in pedestal structure, leading to improved predictive capability for ITER. *Nuclear Fusion*, **53**(9), 093024. <http://dx.doi.org/10.1088/0029-5515/53/9/093024>
- Heidbrink, W., Van Zeeland, M., Austin, M., Bass, E., Ghantous, K., & Gorelenkov, N. et al. (2013). The effect of the fast-ion profile on Alfvén eigenmode stability. *Nuclear Fusion*, **53**(9), 093006. <http://dx.doi.org/10.1088/0029-5515/53/9/093006>
- Hill, D. (2013). DIII-D research towards resolving key issues for ITER and steady-state tokamaks. *Nuclear Fusion*, **53**(10), 104001. <http://dx.doi.org/10.1088/0029-5515/53/10/104001>
- Hillesheim, J., DeBoo, J., Peebles, W., Carter, T., Wang, G., & Rhodes, T. et al. (2013). Experimental characterization of multiscale and multifield turbulence as a critical gradient threshold is surpassed in the DIII-D tokamak. *Physics Of Plasmas*, **20**(5), 056115. <http://dx.doi.org/10.1063/1.4807123>
- Holland, C., Kinsey, J., DeBoo, J., Burrell, K., Luce, T., & Smith, S. et al. (2013). Validation studies of gyrofluid and gyrokinetic predictions of transport and turbulence stiffness using the DIII-D tokamak. *Nuclear Fusion*, **53**(8), 083027. <http://dx.doi.org/10.1088/0029-5515/53/8/083027>
- Hollmann, E., Austin, M., Boedo, J., Brooks, N., Commaux, N., & Eidietis, N. et al. (2013). Control and dissipation of runaway electron beams created during rapid shutdown experiments in DIII-D. *Nuclear Fusion*, **53**(8), 083004. <http://dx.doi.org/10.1088/0029-5515/53/8/083004>
- Hollmann, E., Commaux, N., Eidietis, N., Humphreys, D., Jernigan, T., & Lasnier, C. et al. (2013). Characterization of heat loads from mitigated and unmitigated vertical displacement events in DIII-D. *Physics Of Plasmas*, **20**(6), 062501. <http://dx.doi.org/10.1063/1.4810792>
- Izzo, V. (2013). Impurity mixing and radiation asymmetry in massive gas injection simulations of DIII-D. *Physics Of Plasmas*, **20**(5), 056107. <http://dx.doi.org/10.1063/1.4803896>
- Kolemen, E., Ellis, R., La Haye, R., Humphreys, D., Lohr, J., & Noraky, S. et al. (2013). Real-time mirror steering for improved closed loop neoclassical tearing mode suppression by electron cyclotron current drive in DIII-D. *Fusion Engineering And Design*, **88**(11), 2757-2760. <http://dx.doi.org/10.1016/j.fusengdes.2013.02.168>

- Kramer, G., Budny, R., Bortolon, A., Fredrickson, E., Fu, G., & Heidbrink, W. et al. (2013). A description of the full-particle-orbit-following SPIRAL code for simulating fast-ion experiments in tokamaks. *Plasma Physics And Controlled Fusion*, **55**(2), 025013. <http://dx.doi.org/10.1088/0741-3335/55/2/025013>
- Kramer, G., McLean, A., Brooks, N., Budny, R., Chen, X., & Heidbrink, W. et al. (2013). Simulation of localized fast-ion heat loads in test blanket module simulation experiments on DIII-D. *Nuclear Fusion*, **53**(12), 123018. <http://dx.doi.org/10.1088/0029-5515/53/12/123018>
- Luce, T. (2013). An analytic functional form for characterization and generation of axisymmetric plasma boundaries. *Plasma Physics And Controlled Fusion*, **55**(9), 095009. <http://dx.doi.org/10.1088/0741-3335/55/9/095009>
- Luce, T. (2013). Corrigendum: An analytic functional form for characterization and generation of axisymmetric plasma boundaries. *Plasma Physics And Controlled Fusion*, **55**(11), 119501. <http://dx.doi.org/10.1088/0741-3335/55/11/119501>
- Matsunaga, G., Okabayashi, M., Aiba, N., Boedo, J., Ferron, J., & Hanson, J. et al. (2013). Dynamics of energetic particle driven modes and MHD modes in wall-stabilized high- $\beta$  plasmas on JT-60U and DIII-D. *Nuclear Fusion*, **53**(12), 123022. <http://dx.doi.org/10.1088/0029-5515/53/12/123022>
- McKee, G., Yan, Z., Holland, C., Buttery, R., Evans, T., & Moyer, R. et al. (2013). Increase of turbulence and transport with resonant magnetic perturbations in ELM-suppressed plasmas on DIII-D. *Nuclear Fusion*, **53**(11), 113011. <http://dx.doi.org/10.1088/0029-5515/53/11/113011>
- Meneghini, O., & Lao, L. (2013). Integrated Modeling of Tokamak Experiments with OMFIT. *Plasma And Fusion Research*, **8**(0), 2403009-2403009. <http://dx.doi.org/10.1585/pfr.8.2403009>
- Moreau, D., Walker, M., Ferron, J., Liu, F., Schuster, E., & Barton, J. et al. (2013). Integrated magnetic and kinetic control of advanced tokamak plasmas on DIII-D based on data-driven models. *Nuclear Fusion*, **53**(6), 063020. <http://dx.doi.org/10.1088/0029-5515/53/6/063020>
- Petrie, T., Canik, J., Lasnier, C., Leonard, A., Mahdavi, M., & Watkins, J. et al. (2013). Effect of changes in separatrix magnetic geometry on divertor behaviour in DIII-D. *Nuclear Fusion*, **53**(11), 113024. <http://dx.doi.org/10.1088/0029-5515/53/11/113024>
- Petrie, T., Canik, J., Lasnier, C., Leonard, A., Mahdavi, M., & Watkins, J. et al. (2013). Effect of changes in separatrix magnetic geometry on divertor behaviour in DIII-D. *Nuclear Fusion*, **53**(11), 113024. <http://dx.doi.org/10.1088/0029-5515/53/11/113024>
- Solomon, W. M., Politzer, P. A., Buttery, R. J., Holcomb, C. T., Ferron, J. R., Garofalo, A. M., ... Welander, A. S. (2013). Access to high beta advanced inductive plasmas at low injected torque. *Nuclear Fusion*, **53**(9), 93033. <https://doi.org/10.1088/0029-5515/53/9/093033>
- Spong, D. (2013). Simulation of Alfvén frequency cascade modes in reversed shear-discharges using a Landau-closure model. *Nuclear Fusion*, **53**(5), 053008. <http://dx.doi.org/10.1088/0029-5515/53/5/053008>
- Stacey, W. (2013). Effect of ion orbit loss on the structure in the H-mode tokamak edge pedestal profiles of rotation velocity, radial electric field, density, and temperature. *Physics Of Plasmas*, **20**(9), 092508. <http://dx.doi.org/10.1063/1.4820954>
- Stacey, W., Sayer, M., Floyd, J., & Groebner, R. (2013). Interpretation of changes in diffusive and non-diffusive transport in the edge plasma during pedestal buildup following a low-high transition in DIII-D. *Physics Of Plasmas*, **20**(1), 012509. <http://dx.doi.org/10.1063/1.4775601>

- Staebler, G., Candy, J., Waltz, R., Kinsey, J., & Solomon, W. (2013). A new paradigm for  $E \times B$  velocity shear suppression of gyro-kinetic turbulence and the momentum pinch. *Nuclear Fusion*, **53**(11), 113017. <http://dx.doi.org/10.1088/0029-5515/53/11/113017>
- Stoschus, H., Thomas, D., Hudson, B., Watkins, M., Finkenthal, D., Moyer, R., & Osborne, T. (2013). Status and characterization of the lithium beam diagnostic on DIII-D. *Review Of Scientific Instruments*, **84**(8), 083503. <http://dx.doi.org/10.1063/1.4816824>
- Tobias, B., Yu, L., Domier, C., Luhmann, N., Austin, M., & Paz-Soldan, C. et al. (2013). Boundary perturbations coupled to core  $3/2$  tearing modes on the DIII-D tokamak. *Plasma Physics And Controlled Fusion*, **55**(9), 095006. <http://dx.doi.org/10.1088/0741-3335/55/9/095006>
- Tooker, J., Huynh, P., Felch, K., Blank, M., Borchardt, P., & Cauffman, S. (2013). Gyrotron and power supply development for upgrading the electron cyclotron heating system on DIII-D. *Fusion Engineering And Design*, **88**(6-8), 521-524. <http://dx.doi.org/10.1016/j.fusengdes.2013.01.079>
- Wade, M., Nazikian, R., deGrassie, J., Evans, T., Ferraro, N., & Moyer, R. et al. (2015). Advances in the physics understanding of ELM suppression using resonant magnetic perturbations in DIII-D. *Nuclear Fusion*, **55**(2), 023002. <http://dx.doi.org/10.1088/0029-5515/55/2/023002>
- Waltz, R., Bass, E., & Staebler, G. (2013). Quasilinear model for energetic particle diffusion in radial and velocity space. *Physics Of Plasmas*, **20**(4), 042510. <http://dx.doi.org/10.1063/1.4802808>
- Wilks, T., Stacey, W., & Evans, T. (2013). Analysis of toroidal phasing of resonant magnetic perturbation effects on edge transport in the DIII-D tokamak. *Physics Of Plasmas*, **20**(5), 052505. <http://dx.doi.org/10.1063/1.4804350>
- Wong, C., Abdou, M., Katoh, Y., Kurtz, R., Lumsdaine, A., & Marriott, E. et al. (2013). Progress on DCLL Blanket Concept. *Fusion Science And Technology*, **64**(3), 623-630. <http://dx.doi.org/10.13182/fst13-a19161>
- Wong, S., & Chan, V. (2013). Electron perpendicular viscosity in Braginskii's equations. *Physics Of Plasmas*, **20**(7), 074502. <http://dx.doi.org/10.1063/1.4813250>
- Yan, Z., McKee, G., Boedo, J., Rudakov, D., Schmitz, L., & Diamond, P. et al. (2013). Relating the L–H power threshold scaling to edge turbulence dynamics. *Nuclear Fusion*, **53**(11), 113038. <http://dx.doi.org/10.1088/0029-5515/53/11/113038>

## 12.2 PUBLICATIONS FOR FY14

- Chrystal, C., Burrell, K. H., Grierson, B. A., Lao, L. L., & Pace, D. C. (2014). A method for determining poloidal rotation from poloidal asymmetry in toroidal rotation (invited). *Review of Scientific Instruments*, **85**(11), 11E302. <https://doi.org/10.1063/1.4891601>
- Battaglia, D. J., Burrell, K. H., Chang, C. S., Ku, S., deGrassie, J. S., & Grierson, B. A. (2014). Kinetic neoclassical transport in the H-mode pedestal. *Physics of Plasmas*, **21**(7), 72508. <https://doi.org/10.1063/1.4886803>
- Belli, E. A., Candy, J., & Angioni, C. (2014). Pfirsch–Schlüter neoclassical heavy impurity transport in a rotating plasma. *Plasma Physics and Controlled Fusion*, **56**(12), 124002. <https://doi.org/10.1088/0741-3335/56/12/124002>
- Burrell, K. H., & Chrystal, C. (2014). Functional form for plasma velocity in a rapidly rotating tokamak discharge. *Physics of Plasmas*, **21**(7), 72316. <https://doi.org/10.1063/1.4891351>

- Burrell, K. H., Grierson, B. A., Solomon, W. M., & Belli, E. A. (2014). Comparison of measured impurity poloidal rotation in DIII-D with neoclassical predictions under low toroidal field conditions. *Nuclear Fusion*, **54**(8), 83020. <https://doi.org/10.1088/0029-5515/54/8/083020>
- Cengher, M., Lohr, J., Gorelov, Y. A., Ellis, R., Kolemen, E., Ponce, D., ... Moeller, C. P. (2014). Performance and Upgrades for the Electron Cyclotron Heating System on DIII-D. *IEEE Transactions on Plasma Science*, **42**(7), 1964–1970. <https://doi.org/10.1109/tps.2013.2292299>
- Chen, X., Heidbrink, W. W., Kramer, G. J., Van Zeeland, M. A., Pace, D. C., Petty, C. C., ... Podesta, M. (2014). Enhanced localized energetic ion losses resulting from first-orbit linear and non-linear interactions with Alfvén eigenmodes in DIII-D. *Physics of Plasmas*, **21**(8), 82503. <https://doi.org/10.1063/1.4891442>
- Chen, X., Heidbrink, W. W., Van Zeeland, M. A., Kramer, G. J., Pace, D. C., Petty, C. C., ... Zeng, L. (2014). Using neutral beams as a light ion beam probe (invited). *Review of Scientific Instruments*, **85**(11), 11E701. <https://doi.org/10.1063/1.4889733>
- Chen, X., Kramer, G. J., Heidbrink, W. W., Fisher, R. K., Pace, D. C., Petty, C. C., ... Van Zeeland, M. A. (2014). Non-linear wave-particle interactions and fast ion loss induced by multiple Alfvén eigenmodes in the DIII-D tokamak. *Nuclear Fusion*, **54**(8), 83005. <https://doi.org/10.1088/0029-5515/54/8/083005>
- Chrystal, C., Burrell, K. H., Grierson, B. A., Staebler, G. M., Solomon, W. M., Wang, W. X., ... Meneghini, O. (2014). Testing neoclassical and turbulent effects on poloidal rotation in the core of DIII-D. *Physics of Plasmas*, **21**(7), 72504. <https://doi.org/10.1063/1.4887296>
- Commaux, N., Baylor, L. R., Jernigan, T. C., Hollmann, E. M., Humphreys, D. A., Wesley, J. C., ... Meitner, S. J. (2014). Radiation asymmetries during disruptions on DIII-D caused by massive gas injection. *Physics of Plasmas*, **21**(10), 102510. <https://doi.org/10.1063/1.4896721>
- Grierson, B. A., Burrell, K. H., Crowley, B., Grisham, L., & Scoville, J. T. (2014). High speed measurements of neutral beam turn-on and impact of beam modulation on measurements of ion density. *Review of Scientific Instruments*, **85**(10), 103502. <https://doi.org/10.1063/1.4896514>
- Grierson, B. A., Burrell, K. H., Garofalo, A. M., Solomon, W. M., Diallo, A., & O'Mullane, M. (2014). Response of impurity particle confinement time to external actuators in QH-mode plasmas on DIII-D. *Nuclear Fusion*, **54**(11), 114011. <https://doi.org/10.1088/0029-5515/54/11/114011>
- Hanson, J. M., Bialek, J. M., Baruzzo, M., Bolzonella, T., Hyatt, A. W., Jackson, G. L., ... Zanca, P. (2014). Feedback-assisted extension of the tokamak operating space to low safety factor. *Physics of Plasmas*, **21**(7), 72107. <https://doi.org/10.1063/1.4886796>
- Haskey, S. R., Lanctot, M. J., Liu, Y. Q., Hanson, J. M., Blackwell, B. D., & Nazikian, R. (2014). Linear ideal MHD predictions for  $n=2$  non-axisymmetric magnetic perturbations on DIII-D. *Plasma Physics and Controlled Fusion*, **56**(3), 35005. <https://doi.org/10.1088/0741-3335/56/3/035005>
- Heidbrink, W. W., Ferron, J. R., Holcomb, C. T., Van Zeeland, M. A., Chen, X., Collins, C. M., ... Zhu, Y. (2014). Confinement degradation by Alfvén-eigenmode induced fast-ion transport in steady-state scenario discharges. *Plasma Physics and Controlled Fusion*, **56**(9), 95030. <https://doi.org/10.1088/0741-3335/56/9/095030>
- Holcomb, C. T., Ferron, J. R., Luce, T. C., Petrie, T. W., Park, J. M., Turco, F., ... Lanctot, M. J. (2014). Steady state scenario development with elevated minimum safety factor on DIII-D. *Nuclear Fusion*, **54**(9), 93009. <https://doi.org/10.1088/0029-5515/54/9/093009>
- King, J. D., Strait, E. J., Boivin, R. L., Taussig, D., Watkins, M. G., Hanson, J. M., ... Bak, J. G. (2014). An upgrade of the magnetic diagnostic system of the DIII-D tokamak for non-axisymmetric measurements. *Review of Scientific Instruments*, **85**(8), 83503. <https://doi.org/10.1063/1.4891817>

- Kolemen, E., Welander, A. S., La Haye, R. J., Eidietis, N. W., Humphreys, D. A., Lohr, J., ... Turco, F. (2014). State-of-the-art neoclassical tearing mode control in DIII-D using real-time steerable electron cyclotron current drive launchers. *Nuclear Fusion*, **54**(7), 73020. <https://doi.org/10.1088/0029-5515/54/7/073020>
- Lasnier, C. J., Allen, S. L., Ellis, R. E., Fenstermacher, M. E., McLean, A. G., Meyer, W. H., ... Van Zeeland, M. A. (2014). Wide-angle ITER-prototype tangential infrared and visible viewing system for DIII-D. *Review of Scientific Instruments*, **85**(11), 11D855. <https://doi.org/10.1063/1.4892897>
- Leonard, A. W. (2014). Edge-localized-modes in tokamaks. *Physics of Plasmas*, **21**(9), 90501. <https://doi.org/10.1063/1.4894742>
- Luce, T. C., Humphreys, D. A., Jackson, G. L., & Solomon, W. M. (2014). Inductive flux usage and its optimization in tokamak operation. *Nuclear Fusion*, **54**(9), 93005. <https://doi.org/10.1088/0029-5515/54/9/093005>
- Meneghini, O., Luna, C. J., Smith, S. P., & Lao, L. L. (2014). Modeling of transport phenomena in tokamak plasmas with neural networks. *Physics of Plasmas*, **21**(6), 60702. <https://doi.org/10.1063/1.4885343>
- Mordijck, S., Moyer, R. A., Ferraro, N. M., Wade, M. R., & Osborne, T. H. (2014). The radial electric field as a measure for field penetration of resonant magnetic perturbations. *Nuclear Fusion*, **54**(8), 82003. <https://doi.org/10.1088/0029-5515/54/8/082003>
- Muscatello, C. M., Domier, C. W., Hu, X., Kramer, G. J., Luhmann, N. C., Jr., Ren, X., ... Yu, L. (2014). Technical overview of the millimeter-wave imaging reflectometer on the DIII-D tokamak (invited). *Review of Scientific Instruments*, **85**(11), 11D702. <https://doi.org/10.1063/1.4889735>
- Orlov, D. M., Moyer, R. A., Evans, T. E., Wingen, A., Buttery, R. J., Ferraro, N. M., ... Nazikian, R. (2014). Comparison of the numerical modelling and experimental measurements of DIII-D separatrix displacements during H-modes with resonant magnetic perturbations. *Nuclear Fusion*, **54**(9), 93008. <https://doi.org/10.1088/0029-5515/54/9/093008>
- Paz-Soldan, C., Eidietis, N. W., Granetz, R., Hollmann, E. M., Moyer, R. A., Wesley, J. C., ... Zhu, Y. (2014). Growth and decay of runaway electrons above the critical electric field under quiescent conditions. *Physics of Plasmas*, **21**(2), 22514. <https://doi.org/10.1063/1.4866912>
- Paz-Soldan, C., Lanctot, M. J., Logan, N. C., Shiraki, D., Buttery, R. J., Hanson, J. M., ... Strait, E. J. (2014). The importance of matched poloidal spectra to error field correction in DIII-D. *Physics of Plasmas*, **21**(7), 72503. <https://doi.org/10.1063/1.4886795>
- Pigarov, A. Y., Krasheninnikov, S. I., Rognlien, T. D., Hollmann, E. M., Lasnier, C. J., & Unterberg, E. (2014). Multi-fluid transport code modeling of time-dependent recycling in ELMy H-mode. *Physics of Plasmas*, **21**(6), 62514. <https://doi.org/10.1063/1.4885346>
- Piovesan, P., Hanson, J. M., Martin, P., Navratil, G. A., Turco, F., Bialek, J., ... Shiraki, D. (2014). Tokamak Operation with Safety Factor  $q_{95} < 2$  via Control of MHD Stability. *Physical Review Letters*, **113**(4). <https://doi.org/10.1103/physrevlett.113.045003>
- Pipes, R., Fisher, R. K., & Van Zeeland, M. A. (2014). Mapping and uncertainty analysis of energy and pitch angle phase space in the DIII-D fast ion loss detector. *Review of Scientific Instruments*, **85**(11), 11D841. <https://doi.org/10.1063/1.4891596>
- Prater, R., Moeller, C. P., Pinsker, R. I., Porkolab, M., Meneghini, O., & Vdovin, V. L. (2014). Application of very high harmonic fast waves for off-axis current drive in the DIII-D and FNSF-AT tokamaks. *Nuclear Fusion*, **54**(8), 83024. <https://doi.org/10.1088/0029-5515/54/8/083024>

- Rhodes, T. L., Peebles, W. A., Crocker, N. A., & Nguyen, X. (2014). Development of a cross-polarization scattering system for the measurement of internal magnetic fluctuations in the DIII-D tokamak. *Review of Scientific Instruments*, **85**(11), 11D838. <https://doi.org/10.1063/1.4887276>
- Rost, J. C., Porkolab, M., Dorris, J., & Burrell, K. H. (2014). Short wavelength turbulence generated by shear in the quiescent H-mode edge on DIII-D. *Physics of Plasmas*, **21**(6), 62306. <https://doi.org/10.1063/1.4883135>
- Rudakov, D. L., Stangeby, P. C., Wampler, W. R., Brooks, J. N., Brooks, N. H., Elder, J. D., ... Wong, C. P. C. (2014). Net versus gross erosion of high-Z materials in the divertor of DIII-D. *Physica Scripta*, T159, 14030. <https://doi.org/10.1088/0031-8949/2014/t159/014030>
- Schissel, D. P., Abla, G., Flanagan, S. M., Greenwald, M., Lee, X., Romosan, A., ... Wright, J. (2014). Automated metadata, provenance cataloging and navigable interfaces: Ensuring the usefulness of extreme-scale data. *Fusion Engineering and Design*, **89**(5), 745–749. <https://doi.org/10.1016/j.fusengdes.2014.01.053>
- Schmitz, L., Zeng, L., Rhodes, T. L., Hillesheim, J. C., Peebles, W. A., Groebner, R. J., ... Wang, G. (2014). The role of zonal flows and predator–prey oscillations in triggering the formation of edge and core transport barriers. *Nuclear Fusion*, **54**(7), 73012. <https://doi.org/10.1088/0029-5515/54/7/073012>
- Shiraki, D., La Haye, R., Logan, N., Strait, E., & Volpe, F. (2014). Error field detection in DIII-D by magnetic steering of locked modes. *Nuclear Fusion*, **54**(3), 033006. <http://dx.doi.org/10.1088/0029-5515/54/3/033006>
- Solomon, W. M., Snyder, P. B., Burrell, K. H., Fenstermacher, M. E., Garofalo, A. M., Grierson, B. A., ... Osborne, T. H. (2014). Access to a New Plasma Edge State with High Density and Pressures using the Quiescent H Mode. *Physical Review Letters*, **113**(13). <https://doi.org/10.1103/physrevlett.113.135001>
- Staebler, G. M., & Groebner, R. J. (2014). H-mode transitions and limit cycle oscillations from mean field transport equations. *Plasma Physics and Controlled Fusion*, **57**(1), 14025. <https://doi.org/10.1088/0741-3335/57/1/014025>
- Staebler, G. M., Kinsey, J. E., Belli, E. A., Candy, J., Waltz, R. E., Greenfield, C. M., ... Chrystal, C. (2014). Resolving the mystery of transport within internal transport barriers. *Physics of Plasmas*, **21**(5), 55902. <https://doi.org/10.1063/1.4875334>
- Strait, E. J., Buttery, R. J., Casper, T. A., Chu, M. S., Hanson, J. M., Garofalo, A. M., ... Volpe, F. A. (2014). Measurement of tokamak error fields using plasma response and its applicability to ITER. *Nuclear Fusion*, **54**(7), 73004. <https://doi.org/10.1088/0029-5515/54/7/073004>
- Tobias, B., Grierson, B. A., Muscatello, C. M., Ren, X., Domier, C. W., Luhmann, N. C., Jr., ... Classen, I. G. J. (2014). Phase-locking of magnetic islands diagnosed by ECE-imaging. *Review of Scientific Instruments*, **85**(11), 11D847. <https://doi.org/10.1063/1.4892438>
- Truong, D. D., & Austin, M. E. (2014). High spatial resolution upgrade of the electron cyclotron emission radiometer for the DIII-D tokamak. *Review of Scientific Instruments*, **85**(11), 11D814. <https://doi.org/10.1063/1.4889737>
- Wingen, A., Schmitz, O., Evans, T. E., & Spatschek, K. H. (2014). Heat flux modeling using ion drift effects in DIII-D H-mode plasmas with resonant magnetic perturbations. *Physics of Plasmas*, **21**(1), 12509. <https://doi.org/10.1063/1.4862034>
- Zeng, L., Peebles, W. A., Doyle, E. J., Rhodes, T. L., Crocker, N., Nguyen, X., ... Wang, G. (2014). Performance and data analysis aspects of the new DIII-D monostatic profile reflectometer system. *Review of Scientific Instruments*, **85**(11), 11D843. <https://doi.org/10.1063/1.4889775>

### 12.3 PUBLICATIONS FOR FY15

- Barton, J. E., Boyer, M. D., Shi, W., Wehner, W. P., Schuster, E., Ferron, J. R., ... Johnson, R. D. (2015). Physics-model-based nonlinear actuator trajectory optimization and safety factor profile feedback control for advanced scenario development in DIII-D. *Nuclear Fusion*, **55**(9), 93005. <https://doi.org/10.1088/0029-5515/55/9/093005>
- Baylor, L. R., Lang, P. T., Allen, S. L., Combs, S. K., Commaux, N., Evans, T. E., ... Osborne, T. H. (2015). ELM mitigation with pellet ELM triggering and implications for PFCs and plasma performance in ITER. *Journal of Nuclear Materials*, **463**, 104–108. <https://doi.org/10.1016/j.jnucmat.2014.09.070>
- Belli, E. A., & Candy, J. (2015). Neoclassical transport in toroidal plasmas with nonaxisymmetric flux surfaces. *Plasma Physics and Controlled Fusion*, **57**(5), 54012. <https://doi.org/10.1088/0741-3335/57/5/054012>
- Briesemeister, A. R., Isler, R. C., Allen, S. L., Ahn, J.-W., McLean, A. G., Unterberg, E. A., ... Meyer, W. H. (2015). Impurity ion flow and temperature measured in a detached divertor with externally applied non-axisymmetric fields on DIII-D. *Journal of Nuclear Materials*, **463**, 524–527. <https://doi.org/10.1016/j.jnucmat.2014.11.031>
- Brooks, J. N., Elder, J. D., McLean, A. G., Rudakov, D. L., Stangeby, P. C., & Wampler, W. R. (2015). Analysis of a tungsten sputtering experiment in DIII-D and code/data validation of high redeposition/reduced erosion. *Fusion Engineering and Design*, **94**, 67–71. <https://doi.org/10.1016/j.fusengdes.2015.03.022>
- Buttery, R. J. (2015). DIII-D research to address key challenges for ITER and fusion energy. *Nuclear Fusion*, **55**(10), 104017. <https://doi.org/10.1088/0029-5515/55/10/104017>
- Candy, J., & Belli, E. A. (2015). Non-axisymmetric local magnetostatic equilibrium. *Journal of Plasma Physics*, **81**(3). <https://doi.org/10.1017/s0022377815000264>
- Canik, J. M., Briesemeister, A. R., Lasnier, C. J., Leonard, A. W., Lore, J. D., McLean, A. G., & Watkins, J. G. (2015). Modeling of detachment experiments at DIII-D. *Journal of Nuclear Materials*, **463**, 569–572. <https://doi.org/10.1016/j.jnucmat.2014.11.077>
- Chan, V. S., Costley, A. E., Wan, B. N., Garofalo, A. M., & Leuer, J. A. (2015). Evaluation of CFETR as a Fusion Nuclear Science Facility using multiple system codes. *Nuclear Fusion*, **55**(2), 23017. <https://doi.org/10.1088/0029-5515/55/2/023017>
- Chrobak, C., Stangeby, P. C., Leonard, A. W., Rudakov, D. L., Wong, C. P. C., McLean, A. G., ... Tynan, G. R. (2015). Measurements of gross erosion of Al in the DIII-D divertor. *Journal of Nuclear Materials*, **463**, 810–813. <https://doi.org/10.1016/j.jnucmat.2014.11.003>
- Chrystal, C., Burrell, K. H., Grierson, B. A., & Pace, D. C. (2015). Spatial calibration of a tokamak neutral beam diagnostic using in situ neutral beam emission. *Review of Scientific Instruments*, **86**(10), 103509. <https://doi.org/10.1063/1.4933337>
- deGrassie, J. S., Boedo, J. A., & Grierson, B. A. (2015). Thermal ion orbit loss and radial electric field in DIII-D. *Physics of Plasmas*, **22**(8), 80701. <https://doi.org/10.1063/1.4928558>
- Diallo, A., Groebner, R. J., Rhodes, T. L., Battaglia, D. J., Smith, D. R., Osborne, T. H., ... Snyder, P. B. (2015). Correlations between quasi-coherent fluctuations and the pedestal evolution during the inter-edge localized modes phase on DIII-Da). *Physics of Plasmas*, **22**(5), 56111. <https://doi.org/10.1063/1.4921148>

- Ding, R., Stangeby, P. C., Rudakov, D. L., Elder, J. D., Tskhakaya, D., Wampler, W. R., ... Snyder, P. B. (2015). Simulation of gross and net erosion of high-Z materials in the DIII-D divertor. *Nuclear Fusion*, **56**(1), 16021. <https://doi.org/10.1088/0029-5515/56/1/016021>
- Doane, J., Anderson, J., Grunloh, H., & Wu, W. (2015). Power monitor miter bends for high-power microwave transmission. *Fusion Engineering and Design*, **93**, 1–8. <https://doi.org/10.1016/j.fusengdes.2015.01.012>
- Eidietis, N. W., Gerhardt, S. P., Granetz, R. S., Kawano, Y., Lehnen, M., ... Lister, J. B. (2015). The ITPA disruption database. *Nuclear Fusion*, **55**(6), 63030. <https://doi.org/10.1088/0029-5515/55/6/063030>
- Elder, J. D., Stangeby, P. C., Bray, B. D., Brooks, N., Leonard, A. W., McLean, A. G., ... Watkins, J. G. (2015). OEDGE modeling of DIII-D density scan discharges leading to detachment. *Journal of Nuclear Materials*, **463**, 565–568. <https://doi.org/10.1016/j.jnucmat.2014.09.055>
- Eldon, D., Boivin, R. L., Chrystal, C., Groebner, R. J., McKee, G. R., Schmitz, L., ... Snyder, P. B. (2015). Evolution of  $E \times B$  shear and coherent fluctuations prior to H-L transitions in DIII-D and control strategies for H-L transitions. *Physics of Plasmas*, **22**(11), 112506. <https://doi.org/10.1063/1.4935919>
- Eldon, D., Boivin, R. L., Groebner, R. J., Osborne, T. H., Snyder, P. B., Turnbull, A. D., ... Wilson, H. R. (2015). Investigation of peeling-ballooning stability prior to transient outbursts accompanying transitions out of H-mode in DIII-D. *Physics of Plasmas*, **22**(5), 52109. <https://doi.org/10.1063/1.4919942>
- Evans, T. E. (2015). Resonant magnetic perturbations of edge-plasmas in toroidal confinement devices. *Plasma Physics and Controlled Fusion*, **57**(12), 123001. <https://doi.org/10.1088/0741-3335/57/12/123001>
- Ferron, J. R., Holcomb, C. T., Luce, T. C., Park, J. M., Kolemen, E., La Haye, R. J., ... Turco, F. (2015). High internal inductance for steady-state operation in ITER and a reactor. *Nuclear Fusion*, **55**(7), 73030. <https://doi.org/10.1088/0029-5515/55/7/073030>
- Garofalo, A. M., Burrell, K. H., Eldon, D., Grierson, B. A., Hanson, J. M., Holland, C., ... Zeng, L. (2015). The quiescent H-mode regime for high performance edge localized mode-stable operation in future burning plasmas. *Physics of Plasmas*, **22**(5), 56116. <https://doi.org/10.1063/1.4921406>
- Garofalo, A. M., Gong, X., Grierson, B. A., Ren, Q., Solomon, W. M., Strait, E. J., ... Xu, G. (2015). Compatibility of internal transport barrier with steady-state operation in the high bootstrap fraction regime on DIII-D. *Nuclear Fusion*, **55**(12), 123025. <https://doi.org/10.1088/0029-5515/55/12/123025>
- Grierson, B. A., Burrell, K. H., Nazikian, R. M., Solomon, W. M., Garofalo, A. M., ... Belli, E. A. (2015). Impurity confinement and transport in high confinement regimes without edge localized modes on DIII-Da. *Physics of Plasmas*, **22**(5), 55901. <https://doi.org/10.1063/1.4918359>
- Haskey, S. R., Lanctot, M. J., Liu, Y. Q., Paz-Soldan, C., King, J. D., Blackwell, B. D., & Schmitz, O. (2015). Effects of resistivity and rotation on the linear plasma response to non-axisymmetric magnetic perturbations on DIII-D. *Plasma Physics and Controlled Fusion*, **57**(2), 25015. <https://doi.org/10.1088/0741-3335/57/2/025015>
- Hawryluk, R. J., Eidietis, N. W., Grierson, B. A., Hyatt, A. W., Kolemen, E., Logan, N. C., ... Wolfe, S. (2015). Control of plasma stored energy for burn control using DIII-D in-vessel coils. *Nuclear Fusion*, **55**(5), 53001. <https://doi.org/10.1088/0029-5515/55/5/053001>

- Haye, R. J. L., Paz-Soldan, C., & Strait, E. J. (2015). Lack of dependence on resonant error field of locked mode island size in ohmic plasmas in DIII-D. *Nuclear Fusion*, **55**(2), 23011. <https://doi.org/10.1088/0029-5515/55/2/023011>
- Heidbrink, W. W., Austin, M. E., Collins, C. S., Gray, T., Grierson, B. A., Kramer, G. J., ... Mclean, A. G. (2015). Synergy between fast-ion transport by core MHD and test blanket module fields in DIII-D experiments. *Nuclear Fusion*, **55**(8), 83023. <https://doi.org/10.1088/0029-5515/55/8/083023>
- Heidbrink, W. W., Fu, G.-Y., & Van Zeeland, M. A. (2015). Ions lost on their first orbit can impact Alfvén eigenmode stability. *Physics of Plasmas*, **22**(8), 82507. <https://doi.org/10.1063/1.4928436>
- Holcomb, C. T., Heidbrink, W. W., Ferron, J. R., Van Zeeland, M. A., Garofalo, A. M., Solomon, W. M., ... Podesta, M. (2015). Fast-ion transport in  $q_{min} > 2$ , high- $\beta$  steady-state scenarios on DIII-Da). *Physics of Plasmas*, **22**(5), 55904. <https://doi.org/10.1063/1.4921152>
- Hollmann, E. M., Commaux, N., Eidietis, N. W., Lasnier, C. J., Moyer, R. A., Parks, P. B., & Shiraki, D. (2015). Mitigation of upward and downward vertical displacement event heat loads with upper or lower massive gas injection in DIII-D. *Physics of Plasmas*, **22**(10), 102506. <https://doi.org/10.1063/1.4932999>
- Hollmann, E. M., Parks, P. B., Commaux, N., Eidietis, N. W., Moyer, R. A., Shiraki, D., ... Rudakov, D. L. (2015). Measurement of runaway electron energy distribution function during high-Z gas injection into runaway electron plateaus in DIII-Da). *Physics of Plasmas*, **22**(5), 56108. <https://doi.org/10.1063/1.4921149>
- Humphreys, D., Ambrosino, G., de Vries, P., Felici, F., Kim, S. H., Jackson, G., ... Zabeo, L. (2015). Novel aspects of plasma control in ITER. *Physics of Plasmas*, **22**(2), 21806. <https://doi.org/10.1063/1.4907901>
- Ida, K., Kobayashi, T., Evans, T. E., Inagaki, S., Austin, M. E., Shafer, M. W., ... Itoh, K. (2015). Self-regulated oscillation of transport and topology of magnetic islands in toroidal plasmas. *Scientific Reports*, **5**(1). <https://doi.org/10.1038/srep16165>
- Izzo, V. A., Parks, P. B., Eidietis, N. W., Shiraki, D., Hollmann, E. M., Commaux, N., ... Strait, E. J. (2015). The role of MHD in 3D aspects of massive gas injection. *Nuclear Fusion*, **55**(7), 73032. <https://doi.org/10.1088/0029-5515/55/7/073032>
- Jackson, G. L., Chrobak, C. P., McLean, A. G., Maingi, R., Mansfield, D. K., Roquemore, A. L., ... Tripathi, J. (2015). Effect of lithium in the DIII-D SOL and plasma-facing surfaces. *Journal of Nuclear Materials*, **463**, 1160–1164. <https://doi.org/10.1016/j.jnucmat.2014.12.004>
- Jackson, G. L., Luce, T. C., Solomon, W. M., Turco, F., Buttery, R. J., Hyatt, A. W., ... Politzer, P. A. (2015). Long-pulse stability limits of the ITER baseline scenario. *Nuclear Fusion*, **55**(2), 23004. <https://doi.org/10.1088/0029-5515/55/2/023004>
- King, J. D., Strait, E. J., Ferraro, N. M., Hanson, J. M., Haskey, S. R., Lanctot, M. J., ... Turnbull, A. D. (2015). Landau resonant modification of multiple kink mode contributions to 3D tokamak equilibria. *Nuclear Fusion*, **56**(1), 14003. <https://doi.org/10.1088/0029-5515/56/1/014003>
- King, J. D., Strait, E. J., Lazerson, S. A., Ferraro, N. M., Logan, N. C., Haskey, S. R., ... Turnbull, A. D. (2015). Experimental tests of linear and nonlinear three-dimensional equilibrium models in DIII-D. *Physics of Plasmas*, **22**(7), 72501. <https://doi.org/10.1063/1.4923017>
- King, J. D., Strait, E. J., Nazikian, R., Paz-Soldan, C., Eldon, D., Fenstermacher, M. E., ... Turnbull, A. D. (2015). Three-dimensional equilibria and island energy transport due to resonant magnetic perturbation edge localized mode suppression on DIII-D. *Physics of Plasmas*, **22**(11), 112502. <https://doi.org/10.1063/1.4935486>

- Kinsey, J. E., Staebler, G. M., Candy, J., Petty, C. C., Rhodes, T. L., & Waltz, R. E. (2015). Predictions of the near edge transport shortfall in DIII-D L-mode plasmas using the trapped gyro-Landau-fluid model. *Physics of Plasmas*, **22**(1), 12507. <https://doi.org/10.1063/1.4905630>
- Kolemen, E., Allen, S. L., Bray, B. D., Fenstermacher, M. E., Humphreys, D. A., Hyatt, A. W., ... Unterberg, E. A. (2015). Heat flux management via advanced magnetic divertor configurations and divertor detachment. *Journal of Nuclear Materials*, **463**, 1186–1190. <https://doi.org/10.1016/j.jnucmat.2014.11.099>
- La Haye, R. (2015). A fresh look at electron cyclotron current drive power requirements for stabilization of tearing modes in ITER. Presented at the RADIO FREQUENCY POWER IN PLASMAS: Proceedings of the 21st Topical Conference, EURATOM. <https://doi.org/10.1063/1.4936483>
- Lasnier, C. J., ... Wingen, A. (2015). Fast ion transport during applied 3D magnetic perturbations on DIII-D. *Nuclear Fusion*, **55**(7), 73028. <https://doi.org/10.1088/0029-5515/55/7/073028>
- Leonard, A. W., Makowski, M. A., McLean, A. G., Osborne, T. H., & Snyder, P. B. (2015). Compatibility of detached divertor operation with robust edge pedestal performance. *Journal of Nuclear Materials*, **463**, 519–523. <https://doi.org/10.1016/j.jnucmat.2014.11.007>
- Lohr, J., Anderson, J., Brambila, R., Cengher, M., Chen, X., Ellis, R. A., ... Torrezan, A. C. (2015). The Multiple Gyrotron System on the DIII-D Tokamak. *Journal of Infrared, Millimeter, and Terahertz Waves*, **37**(1), 21–44. <https://doi.org/10.1007/s10762-015-0201-5>
- Maggs, J. E., Rhodes, T. L., & Morales, G. J. (2015). Chaotic density fluctuations in L-mode plasmas of the DIII-D tokamak. *Plasma Physics and Controlled Fusion*, **57**(4), 45004. <https://doi.org/10.1088/0741-3335/57/4/045004>
- Makowski, M. A., Lasnier, C. J., Leonard, A. W., Osborne, T. H., Umansky, M., Elder, J. D., ... Myra, J. R. (2015). Models of SOL transport and their relation to scaling of the divertor heat flux width in DIII-D. *Journal of Nuclear Materials*, **463**, 55–60. <https://doi.org/10.1016/j.jnucmat.2014.09.065>
- Marinoni, A., Rost, J. C., Porkolab, M., Hubbard, A. E., Osborne, T. H., White, A. E., ... Burrell, K. H. (2015). Characterization of density fluctuations during the search for an I-mode regime on the DIII-D tokamak. *Nuclear Fusion*, **55**(9), 93019. <https://doi.org/10.1088/0029-5515/55/9/093019>
- McLean, A. G., Leonard, A. W., Makowski, M. A., Groth, M., Allen, S. L., Boedo, J. A., ... Watkins, J. G. (2015). Electron pressure balance in the SOL through the transition to detachment. *Journal of Nuclear Materials*, **463**, 533–536. <https://doi.org/10.1016/j.jnucmat.2015.01.066>
- Meneghini, O., Smith, S. P., Lao, L. L., Izacard, O., Ren, Q., Park, J. M., ... Staebler, G. M. (2015). Integrated modeling applications for tokamak experiments with OMFIT. *Nuclear Fusion*, **55**(8), 83008. <https://doi.org/10.1088/0029-5515/55/8/083008>
- Mordijck, S., Rhodes, T. L., Zeng, L., Doyle, E. J., Schmitz, L., Chrystal, C., ... Moyer, R. A. (2015). Effects of resonant magnetic perturbations on turbulence and transport in DIII-D L-mode plasmas. *Plasma Physics and Controlled Fusion*, **58**(1), 14003. <https://doi.org/10.1088/0741-3335/58/1/014003>
- Mordijck, S., Wang, X., Doyle, E. J., Rhodes, T. L., Schmitz, L., Zeng, L., ... McKee, G. R. (2015). Particle transport in low-collisionality H-mode plasmas on DIII-D. *Nuclear Fusion*, **55**(11), 113025. <https://doi.org/10.1088/0029-5515/55/11/113025>
- Nazikian, R., Paz-Soldan, C., Callen, J. D., deGrassie, J. S., Eldon, D., Evans, T. E., ... Wade, M. R. (2015). Pedestal Bifurcation and Resonant Field Penetration at the Threshold of Edge-Localized Mode Suppression in the DIII-D Tokamak. *Physical Review Letters*, **114**(10). <https://doi.org/10.1103/physrevlett.114.105002>

- Osborne, T. H., Jackson, G. L., Yan, Z., Maingi, R., Mansfield, D. K., ... Grierson, B. A. (2015). Enhanced H-mode pedestals with lithium injection in DIII-D. *Nuclear Fusion*, **55**(6), 63018. <https://doi.org/10.1088/0029-5515/55/6/063018>
- Pace, D. C., Heidbrink, W. W., & Van Zeeland, M. A. (2015). Keeping fusion plasmas hot. *Physics Today*, **68**(10), 34–39. <https://doi.org/10.1063/pt.3.2946>
- Pace, D. C., Lanctot, M. J., Jackson, G. L., Sandorfi, A. M., Smith, S. P., & Wei, X. (2015). Controlling Fusion Yield in Tokamaks with Spin Polarized Fuel, and Feasibility Studies on the DIII-D Tokamak. *Journal of Fusion Energy*, **35**(1), 54–62. <https://doi.org/10.1007/s10894-015-0015-4>
- Parks, P. B., Alexander, N., Moeller, C., & Callis, R. (2015). Microwave-Induced Flash Vaporization of Volatile Media: A Preliminary Thrust Generation Study for the Waveguide Pellet Acceleration Concept. *Fusion Science and Technology*, **67**(4), 792–801. <https://doi.org/10.13182/fst14-834>
- Paz-Soldan, C., Logan, N. C., Lanctot, M. J., Hanson, J. M., King, J. D., La Haye, R. J., ... Strait, E. J. (2015). Decoupled recovery of energy and momentum with correction of  $n = 2$  error fields. *Nuclear Fusion*, **55**(8), 83012. <https://doi.org/10.1088/0029-5515/55/8/083012>
- Paz-Soldan, C., Nazikian, R., Haskey, S. R., Logan, N. C., Strait, E. J., Ferraro, N. M., ... Tobias, B. J. (2015). Observation of a Multimode Plasma Response and its Relationship to Density Pumpout and Edge-Localized Mode Suppression. *Physical Review Letters*, **114**(10). <https://doi.org/10.1103/physrevlett.114.105001>
- Petrie, T. W., Allen, S. L., Fenstermacher, M. E., Groebner, R. J., Holcomb, C. T., Kolemen, E., ... Watkins, J. G. (2015). Application of the radiating divertor approach to innovative tokamak divertor concepts. *Journal of Nuclear Materials*, **463**, 1225–1228. <https://doi.org/10.1016/j.jnucmat.2014.11.008>
- Pinsker, R. I. (2015). Whistlers, helicons, and lower hybrid waves: The physics of radio frequency wave propagation and absorption for current drive via Landau damping. *Physics of Plasmas*, **22**(9), 90901. <https://doi.org/10.1063/1.4930135>
- Ren, Q., Lao, L. L., Garofalo, A. M., Holcomb, C. T., Solomon, W. M., Belli, E. A., ... Xu, G. (2015). Test of bootstrap current models using high- $\beta$ pEAST-demonstration plasmas on DIII-D. *Plasma Physics and Controlled Fusion*, **57**(2), 25020. <https://doi.org/10.1088/0741-3335/57/2/025020>
- Rudakov, D. L., Stangeby, P. C., Wong, C. P. C., McLean, A. G., Wampler, W. R., Watkins, J. G., ... Moyer, R. A. (2015). Control of high-Z PFC erosion by local gas injection in DIII-D. *Journal of Nuclear Materials*, **463**, 605–610. <https://doi.org/10.1016/j.jnucmat.2014.10.056>
- Shiraki, D., Commaux, N., Baylor, L. R., Eidietis, N. W., Hollmann, E. M., Izzo, V. A., ... Paz-Soldan, C. (2015). Characterization of MHD activity and its influence on radiation asymmetries during massive gas injection in DIII-D. *Nuclear Fusion*, **55**(7), 73029. <https://doi.org/10.1088/0029-5515/55/7/073029>
- Shiraki, D., Paz-Soldan, C., Hanson, J. M., La Haye, R. J., Logan, N. C., Olofsson, K. E. J., ... Volpe, F. A. (2015). Measurements of the toroidal torque balance of error field penetration locked modes. *Plasma Physics and Controlled Fusion*, **57**(2), 25016. <https://doi.org/10.1088/0741-3335/57/2/025016>
- Smith, S. P., Petty, C. C., White, A. E., Holland, C., Bravenec, R., Austin, M. E., ... Meneghini, O. (2015). Electron temperature critical gradient and transport stiffness in DIII-D. *Nuclear Fusion*, **55**(8), 83011. <https://doi.org/10.1088/0029-5515/55/8/083011>

- Snyder, P. B., Solomon, W. M., Burrell, K. H., Garofalo, A. M., Grierson, B. A., Groebner, R. J., ... Wilson, H. R. (2015). Super H-mode: theoretical prediction and initial observations of a new high performance regime for tokamak operation. *Nuclear Fusion*, **55**(8), 83026. <https://doi.org/10.1088/0029-5515/55/8/083026>
- Solomon, W. M., Burrell, K. H., Fenstermacher, M. E., Garofalo, A. M., Grierson, B. A., Loarte, A., ... Snyder, P. B. (2015). Extending the physics basis of quiescent H-mode toward ITER relevant parameters. *Nuclear Fusion*, **55**(7), 73031. <https://doi.org/10.1088/0029-5515/55/7/073031>
- Soukhanovskii, V. A., Allen, S. L., Fenstermacher, M. E., Hill, D. N., Lasnier, C. J., Makowski, M. A., ... Petrie, T. W. (2015). Radiative snowflake divertor studies in DIII-D. *Journal of Nuclear Materials*, **463**, 1191–1195. <https://doi.org/10.1016/j.jnucmat.2014.12.052>
- Stangeby, P. C., Canik, J. M., Elder, J. D., Lasnier, C. J., Leonard, A. W., Eldon, D., ... Grierson, B. A. (2015). Identifying the location of the OMP separatrix in DIII-D using power accounting. *Nuclear Fusion*, **55**(9), 93014. <https://doi.org/10.1088/0029-5515/55/9/093014>
- Stangeby, P. C., Tsui, C. K., Lasnier, C. J., Boedo, J. A., Elder, J. D., Kocan, M., ... Rudakov, D. L. (2015). Power deposition on the DIII-D inner wall limiter. *Journal of Nuclear Materials*, **463**, 389–392. <https://doi.org/10.1016/j.jnucmat.2014.09.051>
- Strait, E. J. (2015). Magnetic control of magnetohydrodynamic instabilities in tokamaks. *Physics of Plasmas*, **22**(2), 21803. <https://doi.org/10.1063/1.4902126>
- Tooker, J. F., & Huynh, P. (2015). Final design and test results of a high voltage amplifier for a gyrotron body power supply. *Fusion Engineering and Design*, **96–97**, 607–610. <https://doi.org/10.1016/j.fusengdes.2015.06.183>
- Turco, F., Petty, C. C., Luce, T. C., Carlstrom, T. N., Van Zeeland, M. A., Heidbrink, W., ... Ferron, J. R. (2015). The high- $\beta_N$  hybrid scenario for ITER and FNSF steady-state missions. *Physics of Plasmas*, **22**(5), 56113. <https://doi.org/10.1063/1.4921161>
- Turco, F., Turnbull, A. D., Hanson, J. M., & Navratil, G. A. (2015). Modeling of fast neutral-beam-generated ion effects on MHD-spectroscopic observations of resistive wall mode stability in DIII-D plasmas. *Physics of Plasmas*, **22**(2), 22503. <https://doi.org/10.1063/1.4906885>
- Turco, F., Turnbull, A. D., Hanson, J. M., & Navratil, G. A. (2015). Modeling of fast neutral-beam-generated ions and rotation effects on RWM stability in DIII-D plasmas. *Nuclear Fusion*, **55**(11), 113034. <https://doi.org/10.1088/0029-5515/55/11/113034>
- Volpe, F. A., Hyatt, A., La Haye, R. J., Lanctot, M. J., Lohr, J., Prater, R., ... Welander, A. (2015). Avoiding Tokamak Disruptions by Applying Static Magnetic Fields That Align Locked Modes with Stabilizing Wave-Driven Currents. *Physical Review Letters*, **115**(17). <https://doi.org/10.1103/physrevlett.115.175002>
- Wade, M. R., Nazikian, R., deGrassie, J. S., Evans, T. E., Ferraro, N. M., Moyer, R. A., ... Zeng, L. (2015). Advances in the physics understanding of ELM suppression using resonant magnetic perturbations in DIII-D. *Nuclear Fusion*, **55**(2), 23002. <https://doi.org/10.1088/0029-5515/55/2/023002>
- Walker, M. L., Humphreys, D. A., Sammulu, B., Welander, A. S., Winter, A., Snipes, J., ... Rapson, C. (2015). Development environments for Tokamak plasma control. In 2015 IEEE 26th Symposium on Fusion Engineering (SOFE). IEEE. <https://doi.org/10.1109/sofe.2015.7482289>
- Waltz, R. E., Bass, E. M., Heidbrink, W. W., & VanZeeland, M. A. (2015). Development and validation of a critical gradient energetic particle driven Alfvén eigenmode transport model for DIII-D tilted neutral beam experiments. *Nuclear Fusion*, **55**(12), 123012. <https://doi.org/10.1088/0029-5515/55/12/123012>

- Wang, Z. R., Lanctot, M. J., Liu, Y. Q., Park, J.-K., & Menard, J. E. (2015). Three-Dimensional Drift Kinetic Response of High- $\beta$  Plasmas in the DIII-D Tokamak. *Physical Review Letters*, **114**(14). <https://doi.org/10.1103/physrevlett.114.1450050>
- Watkins, J. G., Labombard, B., Stangeby, P. C., Lasnier, C. J., McLean, A. G., Nygren, R. E., ... Rudakov, D. L. (2015). Recent sheath physics studies on DIII-D. *Journal of Nuclear Materials*, **463**, 436–439. <https://doi.org/10.1016/j.jnucmat.2014.12.109>
- Wingen, A., Ferraro, N. M., Shafer, M. W., Unterberg, E. A., Canik, J. M., Evans, T. E., ... Sontag, A. C. (2015). Connection between plasma response and resonant magnetic perturbation (RMP) edge localized mode (ELM) suppression in DIII-D. *Plasma Physics and Controlled Fusion*, **57**(10), 104006. <https://doi.org/10.1088/0741-3335/57/10/104006>
- Zemedkun, S. E., Che, S., Chen, Y., Domier, C. W., Luhmann, N. C., Jr., Munsat, T., ... Yu, L. (2015). Spatially resolved measurements of two-dimensional turbulent structures in DIII-D plasmas. *Physics of Plasmas*, **22**(12), 122508. <https://doi.org/10.1063/1.4938032>

## 12.4 PUBLICATIONS FOR FY16

- Abla, G., Coviello, E. N., Flanagan, S. M., Greenwald, M., Lee, X., Romosan, A., ... Wu, K. J. (2016). The MPO system for automatic workflow documentation. *Fusion Engineering and Design*, **112**, 1007–1013. <https://doi.org/10.1016/j.fusengdes.2016.04.023>
- Austin, M. E., Brookman, M. W., Rowan, W. L., Danani, S., Bryerton, E. W., & Dougherty, P. (2016). Design and first plasma measurements of the ITER-ECE prototype radiometer. *Review of Scientific Instruments*, **87**(11), 11E111. <https://doi.org/10.1063/1.4960163>
- Bardóczi, L., Rhodes, T. L., Carter, T. A., Bañón Navarro, A., Peebles, W. A., Jenko, F., & McKee, G. (2016). Modulation of Core Turbulent Density Fluctuations by Large-Scale Neoclassical Tearing Mode Islands in the DIII-D Tokamak. *Physical Review Letters*, **116**(21). <https://doi.org/10.1103/physrevlett.116.215001>
- Bardóczi, L., Rhodes, T. L., Carter, T. A., Crocker, N. A., Peebles, W. A., & Grierson, B. A. (2016). Non-perturbative measurement of cross-field thermal diffusivity reduction at the O-point of 2/1 neoclassical tearing mode islands in the DIII-D tokamak. *Physics of Plasmas*, **23**(5), 52507. <https://doi.org/10.1063/1.4948560>
- Battaglia, D. J., Burrell, K. H., Chang, C. S., deGrassie, J. S., Grierson, B. A., Groebner, R. J., & Hager, R. (2016). Improved kinetic neoclassical transport calculation for a low-collisionality QH-mode pedestal. *Plasma Physics and Controlled Fusion*, **58**(8), 85009. <https://doi.org/10.1088/0741-3335/58/8/085009>
- Boedo, J. A., deGrassie, J. S., Grierson, B., Stoltzfus-Dueck, T., Battaglia, D. J., ... Rudakov, D. L. (2016). Experimental evidence of edge intrinsic momentum source driven by kinetic ion loss and edge radial electric fields in tokamaks. *Physics of Plasmas*, **23**(9), 92506. <https://doi.org/10.1063/1.4962683>
- Bolte, N. G., Heidbrink, W. W., Pace, D., Van Zeeland, M., & Chen, X. (2016). Measurement and simulation of passive fast-ion D-alpha emission from the DIII-D tokamak. *Nuclear Fusion*, **56**(11), 112023. <https://doi.org/10.1088/0029-5515/56/11/112023>
- Bortolon, A., Maingi, R., Mansfield, D. K., Nagy, A., Roquemore, A. L., Baylor, L. R., ... Van Zeeland, M. A. (2016). High frequency pacing of edge localized modes by injection of lithium granules in DIII-D H-mode discharges. *Nuclear Fusion*, **56**(5), 56008. <https://doi.org/10.1088/0029-5515/56/5/056008>

- Brookman, M. W., Austin, M. E., McLean, A. G., Carlstrom, T. N., Hyatt, A. W., & Lohr, J. (2016). Improved cross-calibration of Thomson scattering and electron cyclotron emission with ECH on DIII-D. *Review of Scientific Instruments*, **87**(11), 11E517. <https://doi.org/10.1063/1.4959916>
- Burrell, K. H., Barada, K., Chen, X., Garofalo, A. M., Groebner, R. J., Muscatello, C. M., ... Zeng, L. (2016). Discovery of stationary operation of quiescent H-mode plasmas with net-zero neutral beam injection torque and high energy confinement on DIII-D. *Physics of Plasmas*, **23**(5), 56103. <https://doi.org/10.1063/1.4943521>
- Cengher, M., Lohr, J., Gorelov, Y., Torrezan, A., Ponce, D., Chen, X., & Moeller, C. (2016). DIII-D Electron Cyclotron Heating System Status and Upgrades. *IEEE Transactions on Plasma Science*, **44**(12), 3465–3470. <https://doi.org/10.1109/tps.2016.2571219>
- Chen, J., Ding, W. X., Brower, D. L., Finkenthal, D., Muscatello, C., Taussig, D., & Boivin, R. (2016). Faraday-effect polarimeter diagnostic for internal magnetic field fluctuation measurements in DIII-D. *Review of Scientific Instruments*, **87**(11), 11E108. <https://doi.org/10.1063/1.4960056>
- Chen, X., Burrell, K. H., Ferraro, N. M., Osborne, T. H., Austin, M. E., Garofalo, A. M., ... Yan, Z. (2016). Rotational shear effects on edge harmonic oscillations in DIII-D quiescent H-mode discharges. *Nuclear Fusion*, **56**(7), 76011. <https://doi.org/10.1088/0029-5515/56/7/076011>
- Chen, X., Burrell, K. H., Osborne, T. H., Solomon, W. M., Barada, K., ... Garofalo, A. M. (2016). Stationary QH-mode plasmas with high and wide pedestal at low rotation on DIII-D. *Nuclear Fusion*, **57**(2), 22007. <https://doi.org/10.1088/0029-5515/57/2/022007>
- Chrystal, C., Burrell, K. H., Grierson, B. A., Haskey, S. R., Groebner, R. J., Kaplan, D. H., & Briesemeister, A. (2016). Improved edge charge exchange recombination spectroscopy in DIII-D. *Review of Scientific Instruments*, **87**(11), 11E512. <https://doi.org/10.1063/1.4958915>
- Ciro, D., Evans, T. E., & Caldas, I. L. (2016). Modeling non-stationary, non-axisymmetric heat patterns in DIII-D tokamak. *Nuclear Fusion*, **57**(1), 16017. <https://doi.org/10.1088/0029-5515/57/1/016017>
- Collins, C. S., Heidbrink, W. W., Austin, M. E., Kramer, G. J., Pace, D. C., ... Petty, C. C. (2016). Observation of Critical-Gradient Behavior in Alfvén-Eigenmode-Induced Fast-Ion Transport. *Physical Review Letters*, **116**(9). <https://doi.org/10.1103/physrevlett.116.095001>
- Commaux, N., Shiraki, D., Baylor, L. R., Hollmann, E. M., Eidietis, N. W., Lasnier, C. J., ... Foust, C. R. (2016). First demonstration of rapid shutdown using neon shattered pellet injection for thermal quench mitigation on DIII-D. *Nuclear Fusion*, **56**(4), 46007. <https://doi.org/10.1088/0029-5515/56/4/046007>
- Cooper, C. M., Pace, D. C., Paz-Soldan, C., Commaux, N., Eidietis, N. W., Hollmann, E. M., & Shiraki, D. (2016). Applying the new gamma ray imager diagnostic to measurements of runaway electron Bremsstrahlung radiation in the DIII-D Tokamak (invited). *Review of Scientific Instruments*, **87**(11), 11E602. <https://doi.org/10.1063/1.4961288>
- Davis, E. M., Rost, J. C., Porkolab, M., Marinoni, A., & Van Zeeland, M. A. (2016). A phase contrast imaging–interferometer system for detection of multiscale electron density fluctuations on DIII-D. *Review of Scientific Instruments*, **87**(11), 11E117. <https://doi.org/10.1063/1.4960727>
- deGrassie, J. S., Solomon, W. M., Rice, J. E., & Noterdaeme, J.-M. (2016). Dimensionless size scaling of intrinsic rotation in DIII-D. *Physics of Plasmas*, **23**(8), 82501. <https://doi.org/10.1063/1.4960023>
- Ding, S., Xu, G. S., Wang, Q., Solomon, W. M., Zhao, Y., Gong, X., ... Wan, B. N. (2016). Scenario development for high- $\beta$ plow torque plasma with  $q_{min}$  above 2 and large-radius internal transport barrier in DIII-D. *Nuclear Fusion*, **57**(2), 22016. <https://doi.org/10.1088/0029-5515/57/2/022016>

- Doerner, R. P., Rudakov, D. L., Chrobak, C. P., Briesemeister, A. R., Corr, C., De Temmerman, G., ... Winters, V. (2016). Investigation of He–W interactions using DiMES on DIII-D. *Physica Scripta*, T167, 14054. <https://doi.org/10.1088/0031-8949/t167/1/014054>
- Ernst, D. R., Burrell, K. H., Guttenfelder, W., Rhodes, T. L., Dimits, A. M., ... Bravenec, R. (2016). Role of density gradient driven trapped electron mode turbulence in the H-mode inner core with electron heating. *Physics of Plasmas*, **23**(5), 56112. <https://doi.org/10.1063/1.4948723>
- Evans, T. E. (2016). Erratum: Resonant magnetic perturbations of edge-plasmas in toroidal confinement devices (2015 *Plasma Phys. Control. Fusion* 57123001). *Plasma Physics and Controlled Fusion*, **58**(4), 49601. <https://doi.org/10.1088/0741-3335/58/4/049601>
- Ferraro, N. M., Jardin, S. C., Lao, L. L., Shephard, M. S., & Zhang, F. (2016). Multi-region approach to free-boundary three-dimensional tokamak equilibria and resistive wall instabilities. *Physics of Plasmas*, **23** (5), 56114. <https://doi.org/10.1063/1.4948722>
- Glass, F., Carlstrom, T. N., Du, D., McLean, A. G., Taussig, D. A., & Boivin, R. L. (2016). Upgraded divertor Thomson scattering system on DIII-D. *Review of Scientific Instruments*, **87**(11), 11E508. <https://doi.org/10.1063/1.4955281>
- Gorelenkov, N. N., Heidbrink, W. W., Kramer, G. J., Lestz, J. B., Podesta, M., Van Zeeland, M. A., & White, R. B. (2016). Validating predictive models for fast ion profile relaxation in burning plasmas. *Nuclear Fusion*, **56**(11), 112015. <https://doi.org/10.1088/0029-5515/56/11/112015>
- Grierson, B. A., Burrell, K. H., Chrystal, C., Groebner, R. J., Haskey, S. R., & Kaplan, D. H. (2016). High resolution main-ion charge exchange spectroscopy in the DIII-D H-mode pedestal. *Review of Scientific Instruments*, **87**(11), 11E545. <https://doi.org/10.1063/1.4960604>
- Guo, H. Y., Hill, D. N., Leonard, A. W., Allen, S. L., Stangeby, P. C., Thomas, D., ... Watkins, J. G. (2016). Developing and validating advanced divertor solutions on DIII-D for next-step fusion devices. *Nuclear Fusion*, **56**(12), 126010. <https://doi.org/10.1088/0029-5515/56/12/126010>
- Halpern, F. D., & Ricci, P. (2016). Velocity shear, turbulent saturation, and steep plasma gradients in the scrape-off layer of inner-wall limited tokamaks. *Nuclear Fusion*, **57**(3), 34001. <https://doi.org/10.1088/1741-4326/aa4eb6>
- Hanson, J. M., Bialek, J., Turco, F., King, J., Navratil, G. A., Strait, E. J., & Turnbull, A. (2016). Validation of conducting wall models using magnetic measurements. *Nuclear Fusion*, **56**(10), 106022. <https://doi.org/10.1088/0029-5515/56/10/106022>
- Haskey, S. R., Grierson, B. A., Burrell, K. H., Chrystal, C., Groebner, R. J., Kaplan, D. H., ... Stagner, L. (2016). Measurement of deuterium density profiles in the H-mode steep gradient region using charge exchange recombination spectroscopy on DIII-D. *Review of Scientific Instruments*, **87**(11), 11E553. <https://doi.org/10.1063/1.4963148>
- Heidbrink, W. W., Collins, C. S., Stagner, L., Zhu, Y. B., Petty, C. C., & Van Zeeland, M. A. (2016). Interpretation of fast-ion signals during beam modulation experiments. *Nuclear Fusion*, **56**(11), 112011. <https://doi.org/10.1088/0029-5515/56/11/112011>
- Heidbrink, W. W., Persico, E. A. D., Austin, M. E., Chen, X., Pace, D. C., & Van Zeeland, M. A. (2016). Diverse wave-particle interactions for energetic ions that traverse Alfvén eigenmodes on their first full orbit. *Physics of Plasmas*, **23**(2), 22503. <https://doi.org/10.1063/1.4941587>
- Hollmann, E. M., Commaux, N., Moyer, R. A., Parks, P. B., Austin, M. E., Bykov, I., ... Shiraki, D. (2016). Use of Ar pellet ablation rate to estimate initial runaway electron seed population in DIII-D rapid shutdown experiments. *Nuclear Fusion*, **57**(1), 16008. <https://doi.org/10.1088/0029-5515/57/1/016008>

- Holod, I., Lin, Z., Taimourzadeh, S., Nazikian, R., Spong, D., & Wingen, A. (2016). Effect of resonant magnetic perturbations on microturbulence in DIII-D pedestal. *Nuclear Fusion*, **57**(1), 16005. <https://doi.org/10.1088/0029-5515/57/1/016005>
- King, J. R., Burrell, K. H., Garofalo, A. M., Groebner, R. J., Kruger, S. E., Pankin, A. Y., & Snyder, P. B. (2016). NIMROD modeling of quiescent H-mode: reconstruction considerations and saturation mechanism. *Nuclear Fusion*, **57**(2), 22002. <https://doi.org/10.1088/0029-5515/57/2/022002>
- La Haye, R. J., Paz-Soldan, C., & Liu, Y. Q. (2016). Effect of thick blanket modules on neoclassical tearing mode locking in ITER. *Nuclear Fusion*, **57**(1), 14004. <https://doi.org/10.1088/0029-5515/57/1/014004>
- Lanctot, M. J., Olofsson, K. E. J., Capella, M., Humphreys, D. A., Eidietis, N., Hanson, J. M., ... Walker, M. L. (2016). Error field optimization in DIII-D using extremum seeking control. *Nuclear Fusion*, **56**(7), 76003. <https://doi.org/10.1088/0029-5515/56/7/076003>
- Lanctot, M. J., Snipes, J. A., Reimerdes, H., Paz-Soldan, C., Logan, N., Hanson, J. M., ... Van Zeeland, M. A. (2016). A path to stable low-torque plasma operation in ITER with test blanket modules. *Nuclear Fusion*, **57**(3), 36004. <https://doi.org/10.1088/1741-4326/57/3/036004>
- Logan, N. C., Park, J.-K., Paz-Soldan, C., Lanctot, M. J., Smith, S. P., & Burrell, K. H. (2016). Dependence of neoclassical toroidal viscosity on the poloidal spectrum of applied nonaxisymmetric fields. *Nuclear Fusion*, **56**(3), 36008. <https://doi.org/10.1088/0029-5515/56/3/036008>
- Logan, N. C., Paz-Soldan, C., Park, J.-K., & Nazikian, R. (2016). Identification of multi-modal plasma responses to applied magnetic perturbations using the plasma reluctance. *Physics of Plasmas*, **23**(5), 56110. <https://doi.org/10.1063/1.4948281>
- Luce, T. C., Petty, C. C., Meyer, W. H., Holcomb, C. T., Burrell, K. H., & Bergsten, L. J. (2016). Method for correction of measured polarization angles from motional Stark effect spectroscopy for the effects of electric fields. *Plasma Physics and Controlled Fusion*, **58**(12), 125010. <https://doi.org/10.1088/0741-3335/58/12/125010>
- Lunsford, R., Bortolon, A., Roquemore, A. L., Mansfield, D. K., Nagy, A., Maingi, R., ... Chrobak, C. P. (2016). Lithium granule ablation and penetration during ELM pacing experiments at DIII-D. *Fusion Engineering and Design*, **112**, 621–627. <https://doi.org/10.1016/j.fusengdes.2016.04.041>
- Meneghini, O., & Volpe, F. A. (2016). Full-wave feasibility study of anti-radar diagnostic of magnetic field based on O-X mode conversion and oblique reflectometry imaging. *Review of Scientific Instruments*, **87**(11), 11E120. <https://doi.org/10.1063/1.4960538>
- Nishijima, D., Hollmann, E. M., Doerner, R. P., & Rudakov, D. L. (2016). Laser-induced breakdown spectroscopy analyses of tungsten surfaces. *Physica Scripta*, **T167**, 14032. <https://doi.org/10.1088/0031-8949/t167/1/014032>
- Okabayashi, M., Zanca, P., Strait, E. J., Garofalo, A. M., Hanson, J. M., ... In, Y. (2016). Avoidance of tearing mode locking with electro-magnetic torque introduced by feedback-based mode rotation control in DIII-D and RFX-mod. *Nuclear Fusion*, **57**(1), 16035. <https://doi.org/10.1088/1741-4326/57/1/016035>
- Olofsson, K. E. J., Choi, W., Humphreys, D. A., La Haye, R. J., Shiraki, D., Sweeney, R., ... Welander, A. S. (2016). Electromechanical modelling and design for phase control of locked modes in the DIII-D tokamak. *Plasma Physics and Controlled Fusion*, **58**(4), 45008. <https://doi.org/10.1088/0741-3335/58/4/045008>

- Orlov, D. M., Evans, T. E., Moyer, R. A., Lyons, B. C., Ferraro, N. M., & Park, G.-Y. (2016). Impact of resistive MHD plasma response on perturbation field sidebands. *Plasma Physics and Controlled Fusion*, **58**(7), 75009. <https://doi.org/10.1088/0741-3335/58/7/075009>
- Orlov, D. M., Moyer, R. A., Evans, T. E., Paz-Soldan, C., Ferraro, N. M., Nazikian, R., ... Wingen, A. (2016). Suppression of type-I ELMs with reduced RMP coil set on DIII-D. *Nuclear Fusion*, **56**(3), 36020. <https://doi.org/10.1088/0029-5515/56/3/036020>
- Pace, D. C., Collins, C. S., Crowley, B., Grierson, B. A., Heidbrink, W. W., ... Pawley, C. (2016). Control of power, torque, and instability drive using in-shot variable neutral beam energy in tokamaks. *Nuclear Fusion*, **57**(1), 14001. <https://doi.org/10.1088/0029-5515/57/1/014001>
- Pace, D. C., Cooper, C. M., Taussig, D., Eidietis, N. W., Hollmann, E. M., Riso, V., ... Watkins, M. (2016). Gamma ray imager on the DIII-D tokamak. *Review of Scientific Instruments*, **87**(4), 43507. <https://doi.org/10.1063/1.4945566>
- Pace, D. C., Van Zeeland, M. A., Fishler, B., & Murphy, C. (2016). Consideration of neutral beam prompt loss in the design of a tokamak helicon antenna. *Fusion Engineering and Design*, **112**, 14–20. <https://doi.org/10.1016/j.fusengdes.2016.07.018>
- Paz-Soldan, C., La Haye, R. J., Shiraki, D., Buttery, R. J., Eidietis, N. W., ... Hollmann, E. M. (2016). The non-thermal origin of the tokamak low-density stability limit. *Nuclear Fusion*, **56**(5), 56010. <https://doi.org/10.1088/0029-5515/56/5/056010>
- Paz-Soldan, C., Logan, N. C., Haskey, S. R., Nazikian, R., Strait, E. J., Chen, X., ... Park, J.-K. (2016). Equilibrium drives of the low and high field sides = 2 plasma response and impact on global confinement. *Nuclear Fusion*, **56**(5), 56001. <https://doi.org/10.1088/0029-5515/56/5/056001>
- Petrie, T. W., Fenstermacher, M. E., Holcomb, C. T., Osborne, T. H., Allen, S. L., Ferron, J. R., ... Watkins, J. G. (2016). Results from core-edge experiments in high Power, high performance plasmas on DIII-D. *Nuclear Materials and Energy*. <https://doi.org/10.1016/j.nme.2016.10.029>
- Piovesan, P., Igochine, V., Turco, F., Ryan, D. A., Cianciosa, M. R., ... Liu, Y. Q. (2016). Impact of ideal MHD stability limits on high-beta hybrid operation. *Plasma Physics and Controlled Fusion*, **59**(1), 14027. <https://doi.org/10.1088/0741-3335/59/1/014027>
- Piron, C., Martin, P., Bonfiglio, D., Hanson, J., Logan, N. C., Paz-Soldan, C., ... Turnbull, A. (2016). Interaction of external  $n = 1$  magnetic fields with the sawtooth instability in low-qRFX-mod and DIII-D tokamaks. *Nuclear Fusion*, **56**(10), 106012. <https://doi.org/10.1088/0029-5515/56/10/106012>
- Podestà, M., Gorelenkova, M., Fredrickson, E. D., Gorelenkov, N. N., & White, R. B. (2016). Effects of energetic particle phase space modifications by instabilities on integrated modeling. *Nuclear Fusion*, **56**(11), 112005. <https://doi.org/10.1088/0029-5515/56/11/112005>
- Ratynskaia, S., Toliás, P., Bykov, I., Rudakov, D., De Angeli, M., Vignitchouk, L., ... De Temmerman, G. (2016). Interaction of adhered metallic dust with transient plasma heat loads. *Nuclear Fusion*, **56**(6), 66010. <https://doi.org/10.1088/0029-5515/56/6/066010>
- Ren, Q. L., Garofalo, A. M., Gong, X. Z., Holcomb, C. T., Lao, L. L., McKee, G. R., ... Wan, B. N. (2016). Progress toward steady-state tokamak operation exploiting the high bootstrap current fraction regime. *Physics of Plasmas*, **23**(6), 62511. <https://doi.org/10.1063/1.4948724>
- Rudakov, D. L., Wong, C. P. C., Doerner, R. P., Wright, G. M., Abrams, T., Baldwin, M. J., ... Watkins, J. G. (2016). Exposures of tungsten nanostructures to divertor plasmas in DIII-D. *Physica Scripta*, **T167**, 14055. <https://doi.org/10.1088/0031-8949/t167/1/014055>

- Sang, C. F., Stangeby, P. C., Guo, H. Y., Leonard, A. W., Covele, B., Lao, L. L., ... Thomas, D. M. (2016). SOLPS modeling of the effect on plasma detachment of closing the lower divertor in DIII-D. *Plasma Physics and Controlled Fusion*, **59**(2), 25009. <https://doi.org/10.1088/1361-6587/59/2/025009>
- Shi, L., Valeo, E. J., Tobias, B. J., Kramer, G. J., Hausammann, L., Tang, W. M., & Chen, M. (2016). Synthetic diagnostics platform for fusion plasmas (invited). *Review of Scientific Instruments*, **87**(11), 11D303. <https://doi.org/10.1063/1.4961553>
- Shinya, T., Takase, Y., Yajima, S., Moeller, C., Yamazaki, H., & Tsujii, N. et al. (2016). Plasma current start-up experiments using outboard- and top-launch lower hybrid wave on the TST-2 spherical tokamak. *Nuclear Fusion*, **57**(3), 036006. <http://dx.doi.org/10.1088/1741-4326/57/3/036006>
- Shiraki, D., Commaux, N., Baylor, L. R., Eidietis, N. W., Hollmann, E. M., Lasnier, C. J., & Moyer, R. A. (2016). Thermal quench mitigation and current quench control by injection of mixed species shattered pellets in DIII-D. *Physics of Plasmas*, **23**(6), 62516. <https://doi.org/10.1063/1.4954389>
- Solomon, W. M., Snyder, P. B., Bortolon, A., Burrell, K. H., Garofalo, A. M., Grierson, B. A., ... Poli, F. (2016). Exploration of the Super H-mode regime on DIII-D and potential advantages for burning plasma devices. *Physics of Plasmas*, **23**(5), 56105. <https://doi.org/10.1063/1.4944822>
- Staebler, G. M., Candy, J., Howard, N. T., & Holland, C. (2016). The role of zonal flows in the saturation of multi-scale gyrokinetic turbulence. *Physics of Plasmas*, **23**(6), 62518. <https://doi.org/10.1063/1.4954905>
- Strait, E. J., King, J. D., Hanson, J. M., & Logan, N. C. (2016). Spatial and temporal analysis of DIII-D 3D magnetic diagnostic data. *Review of Scientific Instruments*, **87**(11), 11D423. <https://doi.org/10.1063/1.4960419>
- Sweeney, R., Choi, W., La Haye, R. J., Mao, S., Olofsson, K. E. J., & Volpe, F. A. (2016). Statistical analysis of  $m/n = 2/1$  locked and quasi-stationary modes with rotating precursors at DIII-D. *Nuclear Fusion*, **57**(1), 16019. <https://doi.org/10.1088/0029-5515/57/1/016019>
- Tobias, B., Chen, M., Classen, I. G. J., Domier, C. W., Fitzpatrick, R., Grierson, B. A., ... Paz-Soldan, C. (2016). Rotation profile flattening and toroidal flow shear reversal due to the coupling of magnetic islands in tokamaks. *Physics of Plasmas*, **23**(5), 56107. <https://doi.org/10.1063/1.4946026>
- Truong, D. D., Fonck, R. J., & McKee, G. R. (2016). Optimization and application of cooled avalanche photodiodes for spectroscopic fluctuation measurements with ultra-fast charge exchange recombination spectroscopy. *Review of Scientific Instruments*, **87**(11), 11E551. <https://doi.org/10.1063/1.4963147>
- Turnbull, A. D., Hanson, J. M., Turco, F., Ferraro, N. M., Lanctot, M. J., Lao, L. L., ... Martin, P. (2016). The external kink mode in diverted tokamaks. *Journal of Plasma Physics*, **82**(3). <https://doi.org/10.1017/s0022377816000568>
- Turnbull, A. D., Reiman, A. H., Lao, L. L., Cooper, W. A., Ferraro, N. M., & Buttery, R. J. (2016). Stabilization of the vertical instability by non-axisymmetric coils. *Nuclear Fusion*, **56**(8), 86006. <https://doi.org/10.1088/0029-5515/56/8/086006>
- Van Zeeland, M. A., Heidbrink, W. W., Sharapov, S. E., Spong, D., Cappa, A., Chen, X., ... Petty, C. (2016). Electron cyclotron heating can drastically alter reversed shear Alfvén eigenmode activity in DIII-D through finite pressure effects. *Nuclear Fusion*, **56**(11), 112007. <https://doi.org/10.1088/0029-5515/56/11/112007>

- Victor, B. S., Holcomb, C. T., Allen, S. L., Meyer, W. H., Makowski, M. A., & Thorman, A. (2016). Asymmetries in the motional Stark effect emission on the DIII-D tokamak. *Review of Scientific Instruments*, **87**(11), 11E126. <https://doi.org/10.1063/1.4961560>
- Wang, X., Mordijck, S., Zeng, L., Schmitz, L., Rhodes, T. L., Doyle, E. J., ... Smith, S. P. (2016). Turbulent particle transport as a function of toroidal rotation in DIII-D H-mode plasmas. *Plasma Physics and Controlled Fusion*, **58**(4), 45026. <https://doi.org/10.1088/0741-3335/58/4/045026>
- Wilcox, R. S., Shafer, M. W., Ferraro, N. M., McKee, G. R., Zeng, L., Rhodes, T. L., ... Unterberg, E. A. (2016). Evidence of Toroidally Localized Turbulence with Applied 3D Fields in the DIII-D Tokamak. *Physical Review Letters*, **117**(13). <https://doi.org/10.1103/physrevlett.117.135001>
- Wilks, T. M., & Stacey, W. M. (2016). Improvements to an ion orbit loss calculation in the tokamak edge. *Physics of Plasmas*, **23**(12), 122505. <https://doi.org/10.1063/1.4968219>
- Wingen, A., Wilcox, R. S., Cianciosa, M. R., Seal, S. K., Unterberg, E. A., Hanson, J. M., ... Shafer, M. W. (2016). Use of reconstructed 3D VMEC equilibria to match effects of toroidally rotating discharges in DIII-D. *Nuclear Fusion*, **57**(1), 16013. <https://doi.org/10.1088/0029-5515/57/1/016013>
- Xiao, W. W., Evans, T. E., Tynan, G. R., & Eldon, D. (2016). Location of the first plasma response to resonant magnetic perturbations in DIII-D H-mode plasmas. *Nuclear Fusion*, **56**(6), 64001. <https://doi.org/10.1088/0029-5515/56/6/064001>
- Zeng, L., Doyle, E. J., Rhodes, T. L., Wang, G., Sung, C., Peebles, W. A., & Bobrek, M. (2016). A novel technique for real-time estimation of edge pedestal density gradients via reflectometer time delay data. *Review of Scientific Instruments*, **87**(11), 11E719. <https://doi.org/10.1063/1.4961289>

## 12.5 PUBLICATIONS FOR FY17

- Abrams, T., Ding, R., Guo, H. Y., Thomas, D. M., Chrobak, C. P., Rudakov, D. L., ... Watkins, J. G. (2017). The inter-ELM tungsten erosion profile in DIII-D H-mode discharges and benchmarking with ERO+OEDGE modeling. *Nuclear Fusion*, **57**(5), 56034. <https://doi.org/10.1088/1741-4326/aa66b2>
- Abrams, T., Ding, R., Guo, H., Thomas, D., Chrobak, C., & Rudakov, D. et al. (2017). The inter-ELM tungsten erosion profile in DIII-D H-mode discharges and benchmarking with ERO+OEDGE modeling. *Nuclear Fusion*, **57**(5), 056034. <http://dx.doi.org/10.1088/1741-4326/aa66b2>
- Anderson, J. P., Doane, J. L., Grunloh, H. J., O'Neill, R. C., Ikeda, R., Oda, Y., ... Sakamoto, K. (2017). High power testing of water-cooled waveguide for ITER-like ECH transmission lines. *Nuclear Fusion*, **57**(5), 56030. <https://doi.org/10.1088/1741-4326/aa6414>
- Bardóczi, L., Rhodes, T. L., Bañón Navarro, A., Sung, C., Carter, T. A., La Haye, R. J., ... Jenko, F. (2017). Multi-field/-scale interactions of turbulence with neoclassical tearing mode magnetic islands in the DIII-D tokamak. *Physics of Plasmas*, **24**(5), 56106. <https://doi.org/10.1063/1.4977533>
- Bardóczi, L., Rhodes, T. L., Carter, T. A., La Haye, R. J., Bañón Navarro, A., & McKee, G. R. (2017). Shrinking of core neoclassical tearing mode magnetic islands due to edge localized modes and the role of ion-scale turbulence in island recovery in DIII-D. *Physics of Plasmas*, **24**(6), 62503. <https://doi.org/10.1063/1.4985078>

- Barton, J. L., Nygren, R. E., Unterberg, E. A., Watkins, J. G., Makowski, M. A., Moser, A., ... Buchenauer, D. (2017). Comparison of heat flux measurement techniques during the DIII-D metal ring campaign. *Physica Scripta*, T170, 14007. <https://doi.org/10.1088/1402-4896/aa878a>
- Boedo, J., & Rudakov, D. (2017). Estimation of plasma ion saturation current and reduced tip arcing using Langmuir probe harmonics. *Review Of Scientific Instruments*, **88**(3), 033505. <http://dx.doi.org/10.1063/1.4978453>
- Bortolon, A., Maingi, R., Mansfield, D. K., Nagy, A., Roquemore, A. L., Baylor, L. R., ... Shiraki, D. (2017). Mitigation of divertor heat flux by high-frequency ELM pacing with non-fuel pellet injection in DIII-D. *Nuclear Materials and Energy*, **12**, 1030–1036. <https://doi.org/10.1016/j.nme.2017.01.003>
- Canal, G. P., Ferraro, N. M., Evans, T. E., Osborne, T. H., Menard, J. E., Ahn, J.-W., ... Sabbagh, S. A. (2017). M3D-C1 simulations of the plasma response to RMPs in NSTX-U single-null and snowflake divertor configurations. *Nuclear Fusion*, **57**(7), 76007. <https://doi.org/10.1088/1741-4326/aa6e10>
- Canik, J. M., Briesemeister, A. R., McLean, A. G., Groth, M., Leonard, A. W., ... Lore, J. D. (2017). Testing the role of molecular physics in dissipative divertor operations through helium plasmas at DIII-D. *Physics of Plasmas*, **24**(5), 56116. <https://doi.org/10.1063/1.4982057>
- Cengher, M., Chen, X., Ellis, R., Gorelov, Y., Lohr, J., Moeller, C., ... Torrezan, A. (2017). Advances in technology and high power performance of the ECH system on DIII-D. *Fusion Engineering and Design*. <https://doi.org/10.1016/j.fusengdes.2017.05.022>
- Chen, X., Burrell, K. H., Osborne, T. H., Barada, K., Ferraro, N. M., ... Garofalo, A. M. (2017). Bifurcation of quiescent H-mode to a wide pedestal regime in DIII-D and advances in the understanding of edge harmonic oscillations. *Nuclear Fusion*, **57**(8), 86008. <https://doi.org/10.1088/1741-4326/aa7531>
- Choi, H., & Schleicher, R. W. (2017). The Energy Multiplier Module (EM2): Status of Conceptual Design. *Nuclear Technology*, **200**(2), 106–124. <https://doi.org/10.1080/00295450.2017.1364064>
- Chrobak, C. P., Doerner, R. P., Stangeby, P. C., Wampler, W. R., Rudakov, D. L., Wright, G. M., ... Tynan, G. R. (2017). Characterizing Low-Z erosion and deposition in the DIII-D divertor using aluminum. *Nuclear Materials and Energy*, **12**, 441–446. <https://doi.org/10.1016/j.nme.2016.11.033>
- Chrystal, C., Grierson, B. A., Staebler, G. M., Petty, C. C., Solomon, W. M., deGrassie, J. S., ... Salmi, A. (2017). Predicting rotation for ITER via studies of intrinsic torque and momentum transport in DIII-D. *Physics of Plasmas*, **24**(5), 56113. <https://doi.org/10.1063/1.4979194>
- Chrystal, C., Grierson, B., Solomon, W., Tala, T., deGrassie, J., & Petty, C. et al. (2017). Dependence of intrinsic torque and momentum confinement on normalized gyroradius and collisionality in the DIII-D tokamak. *Physics Of Plasmas*, **24**(4), 042501. <http://dx.doi.org/10.1063/1.4978563>
- Churchill, R. M., Canik, J. M., Chang, C. S., Hager, R., Leonard, A. W., Maingi, R., ... Stotler, D. P. (2017). Kinetic simulations of scrape-off layer physics in the DIII-D tokamak. *Nuclear Materials and Energy*, **12**, 978–983. <https://doi.org/10.1016/j.nme.2016.12.013>
- Churchill, R., Canik, J., Chang, C., Hager, R., Leonard, A., & Maingi, R. et al. (2017). Total fluid pressure imbalance in the scrape-off layer of tokamak plasmas. *Nuclear Fusion*, **57**(4), 046029. <http://dx.doi.org/10.1088/1741-4326/aa5fb1>
- Clement, M., Hanson, J., Bialek, J., & Navratil, G. (2017). GPU-based optimal control for RWM feedback in tokamaks. *Control Engineering Practice*, **68**, 15–22. <https://doi.org/10.1016/j.conengprac.2017.08.002>

- Collins, C. S., Heidbrink, W. W., Podestà, M., White, R. B., Kramer, G. J., ... Pace, D. C. (2017). Phase-space dependent critical gradient behavior of fast-ion transport due to Alfvén eigenmodes. *Nuclear Fusion*, **57**(8), 86005. <https://doi.org/10.1088/1741-4326/aa720c>
- Covele, B., Kotschenreuther, M., Mahajan, S., Valanju, P., Leonard, A., Watkins, J., ... Si, H. (2017). Increased heat dissipation with the X-divertor geometry facilitating detachment onset at lower density in DIII-D. *Nuclear Fusion*, **57**(8), 86017. <https://doi.org/10.1088/1741-4326/aa7644>
- Crowley, B., Rauch, J., Torreblanca, H., Liang, L., Xie, Y., & Scoville, J. T. (2017). Power and particle deposition modeling for DIII-D neutral beam system. *Fusion Engineering and Design*. <https://doi.org/10.1016/j.fusengdes.2017.02.006>
- Cui, L., Nazikian, R., Grierson, B. A., Belli, E. A., Evans, T. E., Logan, N. C., ... Snyder, P. B. (2017). The energy confinement response of DIII-D plasmas to resonant magnetic perturbations. *Nuclear Fusion*, **57**(11), 116030. <https://doi.org/10.1088/1741-4326/aa7efe>
- Ding, R., Rudakov, D. L., Stangeby, P. C., Wampler, W. R., Abrams, T., Brezinsek, S., ... Watkins, J. G. (2017). Advances in understanding of high-Z material erosion and re-deposition in low-Z wall environment in DIII-D. *Nuclear Fusion*, **57**(5), 56016. <https://doi.org/10.1088/1741-4326/aa6451>
- Ding, R., Rudakov, D. L., Stangeby, P. C., Wampler, W. R., Abrams, T., Brezinsek, S., ... Watkins, J. G. (2017). High-Z material erosion and its control in DIII-D carbon divertor. *Nuclear Materials and Energy*, **12**, 247–252. <https://doi.org/10.1016/j.nme.2017.03.012>
- Ding, S., Garofalo, A. M., Qian, J., Cui, L., McClenaghan, J. T., Pan, C., ... Wan, B. (2017). Confinement improvement in the high poloidal beta regime on DIII-D and application to steady-state H-mode on EAST. *Physics of Plasmas*, **24**(5), 56114. <https://doi.org/10.1063/1.4982058>
- Duarte, V. N., Berk, H. L., Gorelenkov, N. N., Heidbrink, W. W., Kramer, G. J., Nazikian, R., ... Van Zeeland, M. A. (2017). Prediction of nonlinear evolution character of energetic-particle-driven instabilities. *Nuclear Fusion*, **57**(5), 54001. <https://doi.org/10.1088/1741-4326/aa6232>
- Eldon, D., Kolemen, E., Barton, J. L., Briesemeister, A. R., Humphreys, D. A., Leonard, A. W., ... Stangeby, P. C. (2017). Controlling marginally detached divertor plasmas. *Nuclear Fusion*, **57**(6), 66039. <https://doi.org/10.1088/1741-4326/aa6b16>
- Evans, T. E., Loarte, A., Orlov, D. M., Grierson, B. A., Knölker, M. M., Lyons, B. C., ... Unterberg, E. A. (2017). ELM suppression in helium plasmas with 3D magnetic fields. *Nuclear Fusion*, **57**(8), 86016. <https://doi.org/10.1088/1741-4326/aa7530>
- Garofalo, A. M., Gong, X. Z., Qian, J., Chen, J., Li, G., Li, K., ... Wan, B. (2017). Development of high poloidal beta, steady-state scenario with ITER-like tungsten divertor on EAST. *Nuclear Fusion*, **57**(7), 76037. <https://doi.org/10.1088/1741-4326/aa7186>
- Grierson, B., Wang, W., Ethier, S., Staebler, G., Battaglia, D., & Boedo, J. et al. (2017). Main-Ion Intrinsic Toroidal Rotation Profile Driven by Residual Stress Torque from Ion Temperature Gradient Turbulence in the DIII-D Tokamak. *Physical Review Letters*, **118**(1). <http://dx.doi.org/10.1103/physrevlett.118.015002>
- Guo, H., Sang, C., Stangeby, P., Lao, L., Taylor, T., & Thomas, D. (2017). Small angle slot divertor concept for long pulse advanced tokamaks. *Nuclear Fusion*, **57**(4), 044001. <http://dx.doi.org/10.1088/1741-4326/aa5b46>
- Halpern, F. D., LaBombard, B., Terry, J. L., & Zweben, S. J. (2017). Outer midplane scrape-off layer profiles and turbulence in simulations of Alcator C-Mod inner-wall limited discharges. *Physics of Plasmas*, **24**(7), 72502. <https://doi.org/10.1063/1.4989705>

- Hanson, J. M., Berkery, J. W., Bialek, J., Clement, M., Ferron, J. R., Garofalo, A. M., ... Turnbull, A. D. (2017). Stability of DIII-D high-performance, negative central shear discharges. *Nuclear Fusion*, **57**(5), 56009. <https://doi.org/10.1088/1741-4326/aa6266>
- Heidbrink, W. W., Collins, C. S., Podestà, M., Kramer, G. J., Pace, D. C., Petty, C. C., ... Zhu, Y. B. (2017). Fast-ion transport by Alfvén eigenmodes above a critical gradient threshold. *Physics of Plasmas*, **24**(5), 56109. <https://doi.org/10.1063/1.4977535>
- Izzo, V. (2017). The effect of pre-existing islands on disruption mitigation in MHD simulations of DIII-D. *Physics Of Plasmas*, **24**(5), 056102. <http://dx.doi.org/10.1063/1.4977462>
- Izzo, V. A., & Parks, P. B. (2017). Modeling of rapid shutdown in the DIII-D tokamak by core deposition of high-Z material. *Physics of Plasmas*, **24**(6), 60705. <https://doi.org/10.1063/1.4990447>
- Jaervinen, A. E., Allen, S. L., Groth, M., McLean, A. G., Rognlien, T. D., Samuell, C. M., ... Porter, G. D. (2017). Interpretations of the impact of cross-field drifts on divertor flows in DIII-D with UEDGE. *Nuclear Materials and Energy*, **12**, 1136–1140. <https://doi.org/10.1016/j.nme.2016.11.014>
- King, J. R., Kruger, S. E., Groebner, R. J., Hanson, J. D., Hebert, J. D., Held, E. D., & Jepson, J. R. (2017). Effect of scrape-off-layer current on reconstructed tokamak equilibrium. *Physics of Plasmas*, **24**(1), 12504. <https://doi.org/10.1063/1.4972822>
- King, J., Kruger, S., Burrell, K., Chen, X., Garofalo, A., & Groebner, R. et al. (2017). MHD modeling of a DIII-D low-torque QH-mode discharge and comparison to observations. *Physics Of Plasmas*, **24**(5), 055902. <http://dx.doi.org/10.1063/1.4977467>
- Kramer, G., Podestà, M., Holcomb, C., Cui, L., Gorelenkov, N., & Grierson, B. et al. (2017). Improving fast-ion confinement in high-performance discharges by suppressing Alfvén eigenmodes. *Nuclear Fusion*, **57**(5), 056024. <http://dx.doi.org/10.1088/1741-4326/aa6456>
- Lanctot, M. J., Park, J.-K., Piovesan, P., Sun, Y., Buttery, R. J., ... Frassinetti, L. (2017). Impact of toroidal and poloidal mode spectra on the control of non-axisymmetric fields in tokamaks. *Physics of Plasmas*, **24**(5), 56117. <https://doi.org/10.1063/1.4982688>
- Leonard, A. W., McLean, A. G., Makowski, M. A., & Stangeby, P. C. (2017). Compatibility of separatrix density scaling for divertor detachment with H-mode pedestal operation in DIII-D. *Nuclear Fusion*, **57**(8), 86033. <https://doi.org/10.1088/1741-4326/aa778c>
- Li, E., Austin, M. E., White, R. B., & Taylor, G. (2017). The build-up of energetic electrons triggering electron cyclotron emission bursts due to a magnetohydrodynamic mode at the edge of tokamaks. *Physics of Plasmas*, **24**(9), 92509. <https://doi.org/10.1063/1.4999186>
- Lohr, J., Brambila, R., Cengher, M., Chen, X., Gorelov, Y., Grosnickle, W., ... Dormier, C. (2017). Protecting Against Damage from Refraction of High Power Microwaves in the DIII-D Tokamak. *EPJ Web of Conferences*, **147**, 3003. <https://doi.org/10.1051/epjconf/201714703003>
- Lore, J. D., Briesemeister, A. R., Ferraro, N. M., Frerichs, H., Lyons, B., McLean, A., ... Shafer, M. W. (2017). Pedestal-to-wall 3D fluid transport simulations on DIII-D. *Nuclear Fusion*, **57**(5), 56025. <https://doi.org/10.1088/1741-4326/aa64ad>
- Luce, T. (2017). A simplified analytic form for generation of axisymmetric plasma boundaries. *Plasma Physics And Controlled Fusion*, **59**(4), 042001. <http://dx.doi.org/10.1088/1361-6587/aa5393>
- Lyons, B. C., Ferraro, N. M., Paz-Soldan, C., Nazikian, R., & Wingen, A. (2017). Effect of rotation zero-crossing on single-fluid plasma response to three-dimensional magnetic perturbations. *Plasma Physics and Controlled Fusion*, **59**(4), 44001. <https://doi.org/10.1088/1361-6587/aa5860>

- Marinoni, A., Pinsker, R. I., Porkolab, M., Rost, J. C., Davis, E. M., ... Burrell, K. H. (2017). The effect of electron cyclotron heating on density fluctuations at ion and electron scales in ITER baseline scenario discharges on the DIII-D tokamak. *Nuclear Fusion*, **57**(12), 126014. <https://doi.org/10.1088/1741-4326/aa8333>
- McClenaghan, J., Garofalo, A. M., Meneghini, O., Smith, S. P., Leuer, J. A., Staebler, G. M., ... Qian, J. (2017). Transport modeling of the DIII-D high  $\beta_p$  scenario and extrapolations to ITER steady-state operation. *Nuclear Fusion*, **57**(11), 116019. <https://doi.org/10.1088/1741-4326/aa79ca>
- McKee, G. R., Austin, M., Boedo, J., Bravenec, R., Holland, C., Jackson, G., ... Zhao, Y. (2017). Turbulence evolution and transport behavior during current ramp-up in ITER-like plasmas on DIII-D. *Nuclear Fusion*, **57**(8), 86032. <https://doi.org/10.1088/1741-4326/aa78b8>
- Meier, E. T., Goldston, R. J., Kaveeva, E. G., Makowski, M. A., Mordijck, S., Rozhansky, V. A., ... Voskoboinikov, S. P. (2017). Drifts, currents, and power scrape-off width in SOLPS-ITER modeling of DIII-D. *Nuclear Materials and Energy*, **12**, 973–977. <https://doi.org/10.1016/j.nme.2016.12.016>
- Meneghini, O., Smith, S. P., Snyder, P. B., Staebler, G. M., Candy, J., Belli, E., ... Poli, F. (2017). Self-consistent core-pedestal transport simulations with neural network accelerated models. *Nuclear Fusion*, **57**(8), 86034. <https://doi.org/10.1088/1741-4326/aa7776>
- Nagy, A., deGrassie, J., Moeller, C., Hansink, M., Fishler, B., Murphy, C., ... Tooker, J. (2017). A High Power Helicon Antenna Design for DIII-D. *Fusion Science and Technology*, 1–5. <https://doi.org/10.1080/15361055.2017.1347459>
- Pan, C., Staebler, G. M., Lao, L. L., Garofalo, A. M., Gong, X., Ren, Q., ... Smith, S. P. (2017). Investigation of energy transport in DIII-D High- $\beta$ PEAST-demonstration discharges with the TGLF turbulent and NEO neoclassical transport models. *Nuclear Fusion*, **57**(3), 36018. <https://doi.org/10.1088/1741-4326/aa4ff8>
- Park, J. M., Murakami, M., St. John, H. E., Lao, L. L., Chu, M. S., & Prater, R. (2017). An efficient transport solver for tokamak plasmas. *Computer Physics Communications*, **214**, 1–5. <https://doi.org/10.1016/j.cpc.2016.12.018>
- Paz-Soldan, C., Cooper, C. M., Aleynikov, P., Pace, D. C., Eidietis, N. W., Brennan, D. P., ... Shiraki, D. (2017). Spatiotemporal Evolution of Runaway Electron Momentum Distributions in Tokamaks. *Physical Review Letters*, **118**(25). <https://doi.org/10.1103/physrevlett.118.255002>
- Petrie, T. W., Osborne, T., Fenstermacher, M. E., Ferron, J., Groebner, R., Grierson, B., ... Watkins, J. (2017). Improved confinement in highly powered high performance scenarios on DIII-D. *Nuclear Fusion*, **57**(8), 86004. <https://doi.org/10.1088/1741-4326/aa7399>
- Petty, C. C., Nazikian, R., Park, J. M., Turco, F., Chen, X., Cui, L., ... Zhu, Y. (2017). Advances in the steady-state hybrid regime in DIII-D—a fully non-inductive, ELM-suppressed scenario for ITER. *Nuclear Fusion*, **57**(11), 116057. <https://doi.org/10.1088/1741-4326/aa80ab>
- Pitts, R. A., Bardin, S., Bazylev, B., van den Berg, M. A., Bunting, P., Carpentier-Chouchana, S., ... Watkins, J. G. (2017). Physics conclusions in support of ITER W divertor monoblock shaping. *Nuclear Materials and Energy*, **12**, 60–74. <https://doi.org/10.1016/j.nme.2017.03.005>
- Qian, J., Garofalo, A., Gong, X., Ren, Q., Ding, S., & Solomon, W. et al. (2017). Advances in the high bootstrap fraction regime on DIII-D towards the  $Q = 5$  mission of ITER steady state. *Nuclear Fusion*, **57**(5), 056008. <http://dx.doi.org/10.1088/1741-4326/aa626a>

- Ratynskaia, S., Toliias, P., De Angeli, M., Weinzettl, V., Matejicek, J., Bykov, I., ... De Temmerman, G. (2017). Tungsten dust remobilization under steady-state and transient plasma conditions. *Nuclear Materials and Energy*, 12, 569–574. <https://doi.org/10.1016/j.nme.2016.10.021>
- Rognlien, T. D., McLean, A. G., Fenstermacher, M. E., Groth, M., Jaervinen, A. E., Joseph, I., ... Umansky, M. V. (2017). Comparison of 2D simulations of detached divertor plasmas with divertor Thomson measurements in the DIII-D tokamak. *Nuclear Materials and Energy*, 12, 44–50. <https://doi.org/10.1016/j.nme.2016.12.002>
- Rognlien, T. D., McLean, A. G., Fenstermacher, M. E., Groth, M., Jaervinen, A. E., Joseph, I., ... Umansky, M. V. (2017). Comparison of 2D simulations of detached divertor plasmas with divertor Thomson measurements in the DIII-D tokamak. *Nuclear Materials and Energy*, 12, 44–50. <https://doi.org/10.1016/j.nme.2016.12.002>
- Rudakov, D. L., Abrams, T., Ding, R., Guo, H. Y., Stangeby, P. C., Wampler, W. R., ... Wong, C. P. C. (2017). DiMES PMI research at DIII-D in support of ITER and beyond. *Fusion Engineering and Design*. <https://doi.org/10.1016/j.fusengdes.2017.03.007>
- Sang, C., Guo, H. Y., Stangeby, P. C., Lao, L. L., & Taylor, T. S. (2017). SOLPS analysis of neutral baffling for the design of a new divertor in DIII-D. *Nuclear Fusion*, 57(5), 56043. <https://doi.org/10.1088/1741-4326/aa6548>
- Schissel, D. P., Coviello, E., Eidietis, N., Flanagan, S., Garcia, F., Humphreys, D., ... Yuan, Q. (2017). Remote third shift EAST operation: a new paradigm. *Nuclear Fusion*, 57(5), 56032. <https://doi.org/10.1088/1741-4326/aa65a8>
- Schuster, E., Wehner, W. P., Barton, J. E., Boyer, M. D., Luce, T. C., Ferron, J. R., ... Johnson, R. D. (2017). Enhanced reproducibility of L-mode plasma discharges via physics-model-based q-profile feedback control in DIII-D. *Nuclear Fusion*, 57(11), 116026. <https://doi.org/10.1088/1741-4326/aa7cab>
- Sontag, A. C., Chen, X., Canik, J., Leonard, A., Lore, J. D., Moser, A. L., ... Petty, C. (2017). SOL effects on the pedestal structure in DIII-D discharges. *Nuclear Fusion*, 57(7), 76025. <https://doi.org/10.1088/1741-4326/aa6cb6>
- Stangeby, P. C., & Sang, C. (2017). Strong correlation between D2 density and electron temperature at the target of divertors found in SOLPS analysis. *Nuclear Fusion*, 57(5), 56007. <https://doi.org/10.1088/1741-4326/aa5e27>
- Stangeby, P. C., Elder, J. D., McLean, A. G., & Watkins, J. G. (2017). Experimentally-based ExB drifts in the DIII-D divertor and SOL calculated from integration of Ohm's law using Thomson scattering measurements of  $T_e$  and  $n_e$ . *Nuclear Materials and Energy*, 12, 876–881. <https://doi.org/10.1016/j.nme.2017.03.021>
- Stangeby, P. C., Tsui, C. K., Lasnier, C. J., Boedo, J. A., Elder, J. D., Kocan, M., ... Rudakov, D. L. (2015). Power deposition on the DIII-D inner wall limiter. *Journal of Nuclear Materials*, 463, 389–392. <https://doi.org/10.1016/j.jnucmat.2014.09.051>
- Victor, B. S., Allen, S. L., Beiersdorfer, P., & Magee, E. W. (2017). X-ray and extreme ultraviolet spectroscopy on DIII-D. *Journal of Instrumentation*, 12(6), C06011–C06011. <https://doi.org/10.1088/1748-0221/12/06/c06011>
- Wang, L., Makowski, M. A., Guo, H. Y., Leonard, A. W., Xu, G. S., Gong, X. Z., ... Wan, B. N. (2017). Effect of heating scheme on SOL width in DIII-D and EAST. *Nuclear Materials and Energy*, 12, 221–226. <https://doi.org/10.1016/j.nme.2017.01.024>

- Wang, W. X., Grierson, B. A., Ethier, S., Chen, J., Startsev, E., & Diamond, P. H. (2017). Understanding and predicting profile structure and parametric scaling of intrinsic rotation. *Physics of Plasmas*, **24**(9), 92501. <https://doi.org/10.1063/1.4997789>
- Wang, X., Mordijck, S., Doyle, E. J., Rhodes, T. L., Zeng, L., McKee, G. R., ... Smith, S. P. (2017). Understanding ECH density pump-out in DIII-D H-mode plasmas. *Nuclear Fusion*, **57**(11), 116046. <https://doi.org/10.1088/1741-4326/aa7f99>
- Wilcox, R. S., Wingen, A., Cianciosa, M. R., Ferraro, N. M., Hirshman, S. P., Paz-Soldan, C., ... Unterberg, E. A. (2017). Modeling of 3D magnetic equilibrium effects on edge turbulence stability during RMP ELM suppression in tokamaks. *Nuclear Fusion*, **57**(11), 116003. <https://doi.org/10.1088/1741-4326/aa7bad>
- Wilks, T. M., Stacey, W. M., & Evans, T. E. (2017). Calculation of the radial electric field from a modified Ohm's law. *Physics of Plasmas*, **24**(1), 12505. <https://doi.org/10.1063/1.4973599>
- Xu, G. S., Wan, B. N., Wang, Y. F., Wu, X. Q., Chen, X., Martin Peng, Y.-K., ... Li, J. (2017).  $E \times B$  flow shear drive of the linear low- $n$  modes of EHO in the QH-mode regime. *Nuclear Fusion*, **57**(8), 86047. <https://doi.org/10.1088/1741-4326/aa7975>
- Yan, Z., Gohil, P., McKee, G. R., Eldon, D., Grierson, B., Rhodes, T., & Petty, C. C. (2017). Turbulence and sheared flow structures behind the isotopic dependence of the L-H power threshold on DIII-D. *Nuclear Fusion*, **57**(12), 126015. <https://doi.org/10.1088/1741-4326/aa82c9>
- Yoshida, M., McKee, G. R., Murakami, M., Grierson, B. A., Nakata, M., Davis, E. M., ... Solomon, W. M. (2017). Magnetic shear effects on plasma transport and turbulence at high electron to ion temperature ratio in DIII-D and JT-60U plasmas. *Nuclear Fusion*, **57**(5), 56027. <https://doi.org/10.1088/1741-4326/aa611e>